

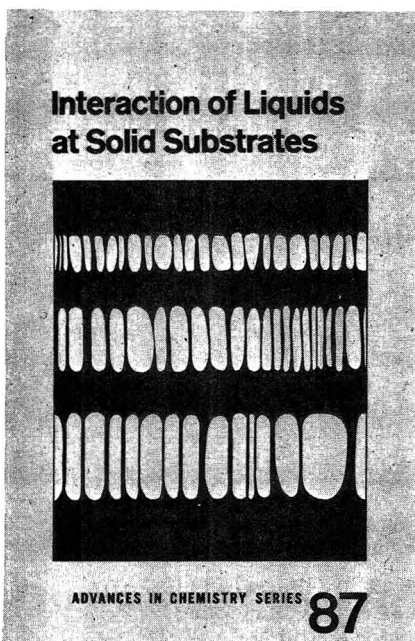
THE JOURNAL OF PHYSICAL CHEMISTRY

Volume 74, Number 9 April 30, 1970

Kinetics of Aqueous Indium(III) Perchlorate Dimerization.	Edward M. Eyring and Jeffrey D. Owen	1825
High Temperature Kinetics of the Oxidation and Nitridation of Pyrolytic Silicon Carbide in Dissociated Gases Daniel E. Rosner and H. Donald Allendorf		1829
A Comparative Study of the Cosolvent Effect in Ethyl Alcohol-Benzene and Isopropyl Alcohol-Benzene Solutions. The Solvolysis of <i>m</i> -Fluorobenzoyl Chloride, <i>m</i> -Trifluoromethylbenzoyl Chloride, and Anisoyl Chloride Thomas F. Fagley, Jonathan S. Bullock, and Dale W. Dycus		1840
Nuclear Magnetic Resonance Study of the Reaction of Methoxide Ion with Methyl Formate in Methanol Solution Dallas L. Rabenstein		1848
The Reaction of (³ P ₁) Oxygen Atoms with Cyclopropane	Alfred A. Scala and Woo-Tien Wu	1852
Isotope Effects in Recoil Tritium Reactions with Fluoroform and Deuteriofluoroform Thomas Smail and F. S. Rowland		1859
The Insertion Reactions of Mono- and Difluorocarbene with Hydrogen Halides Thomas Smail and F. S. Rowland		1866
Photochemical Formation of Free Radicals from Acetonitrile as Studied by Electron Spin Resonance P. Svejda and D. H. Volman		1872
Influence of pH upon the Photolysis of the Uranyl Oxalate Actinometer System Lawrence J. Heidt, George W. Tregay, and Frederick A. Middleton, Jr.		1876
Chemical Effects in Thin Films of 1-Hexene at 77°K Due to Low-Energy Electron Impact Linda M. Hunter, Toshiaki Matsushige, and William H. Hamill		1883
Further Studies on the Properties of Electrons Trapped in Glassy Hydrocarbons A. Ekstrom, R. Suenram, and J. E. Willard		1888
Excitation Transfer in the Pulse Radiolysis of Naphthalene and Benzophenone Solutions R. A. Holroyd, L. M. Theard, and F. C. Peterson		1895
Electron Spin Resonance Studies on γ -Irradiated Frozen Aqueous Solutions of Sodium Formate R. A. Nazhat, N. B. Nazhat, P. N. Moorthy, and J. J. Weiss		1901
Ultraviolet and Infrared Studies of Free Radicals in Irradiated Polyethylene.	D. C. Waterman and M. Dole	1906
The Radiation Chemistry of Polyethylene. X. Kinetics of the Conversion of Alkyl to Allyl Free Radicals D. C. Waterman and Malcolm Dole		1913
Line-Width Parameters for the ($1 \leq J \leq 8, K = 1$) Lines of the Inversion Spectrum of Ammonia James A. Roberts		1923
Solvation of Extracted Complex Metal Acids. VI. The Transfer of HFeCl ₄ to Bis(2-chloroethyl) Ether-Benzene Mixtures	R. L. McDonald and T. H. Hufen	1926
Activity Coefficients for the Systems Sodium Benzenesulfonate-Xylose-Water and Sodium Benzenesulfonate-Urea-Water at 25° from Isopiestic Measurements Hatsuho Uedaira and Hisashi Uedaira		1931
Acidity Measurements at Elevated Temperatures. IV. Apparent Dissociation Product of Water in 1 <i>m</i> Potassium Chloride up to 292°	R. E. Mesmer, C. F. Baes, Jr., and F. H. Sweeton	1937
Behavior of Electrolytes in Propylene Carbonate. II. Further Studies of Conductance and Viscosity Properties. Evaluation of Ion Conductances	L. M. Mukherjee, David P. Boden, and Richard Lindauer	1942
Heats of Transport of Gases. II. Thermoosmosis of Binary Gaseous Mixtures without Chemical Reaction R. P. Rastogi and H. P. Singh		1946
Interactions between Surface Hydroxyl Groups and Adsorbed Molecules. II. Infrared Spectroscopic Study of Benzene Adsorption	J. A. Cusumano and M. J. D. Low	1950

INTERACTION OF LIQUIDS AT SOLID SUBSTRATES

ADVANCES IN CHEMISTRY SERIES NO. 87



Papers from two symposia by the Division of Organic Coatings and Plastics Chemistry of the American Chemical Society.

This volume includes twelve papers comprising the symposium on "The Interaction of Liquids at Solid Substrates," chaired by Allen L. Alexander. These papers include work on "coupling agents," adhesion of polymers, organic/inorganic interfaces, and ultrasonic impedometry. Also included are four papers concerned with heparinized surfaces at the blood/material interface which were part of the symposium on "The Medical Applications of Plastics," chaired by R. I. Leininger.

212 pages with index Cloth (1968) \$9.50

Free set of L. C. cards with library orders upon request.

Other books in the **ADVANCES IN CHEMISTRY SERIES** in colloid chemistry include:

No. 86 Pesticidal Formulations Research: Physical and Colloidal Chemicals Aspects. Fifteen papers survey contact angle of surface active agents, transport through a membrane, vapor pressure of pesticides, role of surfactants in sprays, biological activity, evaporation, spray formation and drift, and several studies on specific pests and pesticides.

212 pages Cloth (1969) \$9.50

No. 84 Molecular Association in Biological and Related Systems. Nineteen articles survey and report new work on molecular association in fat digestion, in soap systems, in membrane constituents, and in mixed monolayers and membranes, include bile salt micelles, lipid monolayers and membranes, and a definitive review of biological membrane structure.

308 pages Cloth (1968) \$10.50

No. 79 Adsorption from Aqueous Solution. Fifteen papers discuss thermodynamic and kinetic aspects of adsorption phenomena and the results of studies on a variety of adsorbate-adsorbent systems.

212 pages Cloth (1968) \$10.00

No. 63 Ordered Fluids and Liquid Crystals. Twenty-two studies on characterization, properties, and occurrence of these phenomena in many substances such as tristearin, *p*-azoxyanisole, mono- and di-hydric alcohols, phospholipids, and polypeptides.

332 pages Cloth (1967) \$11.50

No. 43 Contact Angle, Wettability, and Adhesion. Surface chemistry studies. Relation of equilibrium contact angle to liquid and solid construction, contact angle as a thermodynamic property, surface energy estimation from contact angle. Contact angle hysteresis, relationship between wetting and adhesion.

389 pages Cloth (1964) \$10.50

No. 33 Solid Surfaces and the Gas-Solid Interface. Thirty-seven papers from the Kendall Award Symposium honoring Stephen Brunauer. Theory and techniques for studying surface phenomena.

381 pages Cloth (1961) \$12.00

No. 25 Physical Functions of Hydrocolloids. Treats six broad physical functions—production of viscosity or body, gelatin, stabilization of emulsions, stabilization of suspensions, stabilization of foams, control of crystal growth—with emphasis on food applications.

103 pages Paper (1960) \$5.00

No. 11 Natural Plant Hydrocolloids. The protective colloids or stabilizers, including calcium pectinate, agar, gum arabic, gum karaya, tragacanth, locust bean gum, alginates, Irish moss, and red seaweed.

103 pages Paper (1954) \$5.00

All books postpaid in U.S. and Canada; plus 30 cents in PUAS and elsewhere.

Order from:

**SPECIAL ISSUES SALES
AMERICAN CHEMICAL SOCIETY
1155 SIXTEENTH ST., N.W.
WASHINGTON, D.C. 20036**

Hydrogen Diffusion through (Palladium-Silver)-Tantalum-(Palladium-Silver) Composites	Gerhard L. Holleck	1957
Reflection of a Voltage Step from a Section of Transmission Line Filled with a Polar Dielectric	H. R. Fellner-Feldegg and E. F. Barnett	1962
Electron Spin Resonance Studies of Ion Association between Alkali Metal Ions and Hydrocarbon Radical Ions	Ira B. Goldberg and James R. Bolton	1965
A Semicontinuum Model for the Hydrated Electron	Kenji Fueki, Da-Fei Feng, and Larry Kevan	1976
The Extent of Self-Association of Trifluoroacetic Acid in Different Nonpolar Solvents	Wafaa S. Higazy and Ahmed A. Taha	1982
The Role of Hindered Rotation in the Physical Adsorption of Hydrogen Weight and Spin Isomers	P. L. Gant, K. Yang, M. S. Goldstein, M. P. Freeman, and A. I. Weiss	1985
Reactions Involving Electron Transfer at Semiconductor Surfaces. I. Dissociation of Nitrous Oxide over n-Type Semiconductors at 20°	Joseph Cunningham, John J. Kelly, and A. L. Penny	1992
Stokes' Principle of Reversion and the Optical Measurement of Soap Film Thickness	J. B. Rijnbout	2001
Electrokinetic Flow in Fine Capillary Channels	Douglas Hildreth	2006
The Ionization of Clusters. I. The Dicarboxylic Acids	S. L. Dygert, Giovanna Muzii, and H. A. Saroff	2016

NOTES

Nuclear Magnetic Resonance Studies of 2-Pyridones, 2-Pyridithiones, and 2-Thioalkylpyridines	W. E. Stewart and T. H. Siddall, III	2027
The Dimerization of the Tetracyanoethylene Anion Radical	Raymond Chang	2029

COMMUNICATIONS TO THE EDITOR

Proposed Temperature Effects on the Phosphorescence Lifetime of Benzene in Glasses at 77°K	T. E. Martin and A. H. Kalantar	2030
Comments on "Thermodynamics of Micellization of Some Zwitterionic N-Alkyl Betaines"	Kōzō Shinoda	2032
Entropy Changes Associated with Micellization	Richard E. Lindstrom and James Swarbrick	2033
Molecular Mobility in Simple Glasses	Gyan P. Johari and Martin Goldstein	2034
Dehydration and Polymerization of Barium Methacrylate Monohydrate	F. M. Costaschuk, D. F. R. Gilson, and L. E. St. Pierre	2035
Comment on "Electron Spin Resonance of Perfluorocyclobutanone Ketyl. Long-Range Fluorine Coupling," by J. A. Gerlock and E. G. Janzen. The Angular Dependence of β -Fluorine Hyperfine Splitting	E. Thomas Strom and Aaron L. Bluhm	2036
On the Angular Dependence of β -Fluorine Electron Spin Resonance Hyperfine Coupling in Fluoro-Substituted Nitroxide Radicals	Edward G. Janzen, Bruce R. Knauer, John L. Gerlock, and Kenneth J. Klabunde	2037
Electrical Conductivity of Bromine Trifluoride	Herbert H. Hyman, Terry Surles, Lloyd A. Quarterman, and Alexander Popov	2038
Electrical Conductivity of Bromine Trifluoride	Karl O. Christe	2039
The Kinetics of Spreading	Raymond V. Dyba	2040
Absorption Spectrum of the Pyrene Excimer	Chmouel R. Goldschmidt and Michael Ottolenghi	2041

AUTHOR INDEX

- | | | | | |
|---|--|---|---|--|
| <p>Allendorf, H. D., 1829
Baes, C. F., Jr., 1937
Barnett, E. F., 1962
Bluhm, A. L., 2036
Boden, D. P., 1942
Bolton, J. R., 1965
Bullock, J. S., 1840

Chang, R., 2029
Christe, K. O., 2039
Costaschuk, F. M., 2035
Cunningham, J., 1992
Cusumano, J. A., 1950

Dole, M., 1906, 1913
Dyba, R. V., 2040
Dycus, D. W., 1840
Dygert, S. L., 2016

Ekstrom, A., 1888
Eyring, E. M., 1825

Fagley, T. F., 1840
Fellner-Feldegg, H. R., 1962</p> | <p>Feng, D.-F., 1976
Freeman, M. P., 1985
Fueki, K., 1976

Gant, P. L., 1985
Gerlock, J. L., 2037
Gilson, D. F. R., 2035
Goldberg, I. B., 1965
Goldschmidt, C. R., 2041
Goldstein, M., 2034
Goldstein, M. S., 1985

Hamill, W. H., 1883
Heidt, L. J., 1876
Higazy, W. S., 1982
Hildreth, D., 2006
Holleck, G. L., 1957
Holroyd, R. A., 1895
Hufen, T. H., 1926
Hunter, L. M., 1883
Hyman, H. H., 2038

Janzen, E. G., 2037
Johari, G. P., 2034</p> | <p>Kalantar, A. H., 2030
Kelly, J. J., 1992
Kevan, L., 1976
Klabunde, K. J., 2037
Knauer, B. R., 2037

Lindauer, R., 1942
Lindstrom, R. E., 2033
Low, M. J. D., 1950

Martin, T. E., 2030
Matsushige, T., 1883
McDonald, R. L., 1926
Mesmer, R. E., 1937
Middleton, F. A., Jr., 1876
Moorthy, P. N., 1901
Mukherjee, L. M., 1942
Muzii, G., 2016

Nazhat, N. B., 1901
Nazhat, R. A., 1901

Ottolenghi, M., 2041
Owen, J. D., 1825</p> | <p>Penny, A. L., 1992
Peterson, F. C., 1895
Popov, A., 2038

Quarterman, L. A., 2038

Rabenstein, D. L., 1848
Rastogi, R. P., 1946
Rijnbout, J. B., 2001
Roberts, J. A., 1923
Rosner, D. E., 1829
Rowland, F. S., 1859, 1866

St. Pierre, L. E., 2035
Saroff, H. A., 2016
Scala, A. A., 1852
Shinoda, K., 2032
Siddall, T. H., III, 2027
Singh, H. P., 1946
Smail, T., 1859, 1866</p> | <p>Stewart, W. E., 2027
Strom, E. T., 2036
Suenram, R., 1888
Surles, T., 2038
Svedja, P., 1872
Swarbrick, J., 2033
Sweeton, F. H., 1937

Taha, A. A., 1982
Theard, L. M., 1895
Tregay, G. W., 1876

Uedaira, Hatsuho, 1931
Uedaira, Hisashi, 1931

Volman, D. H., 1872

Waterman, D. C., 1906, 1913
Weiss, A. I., 1985
Weiss, J. J., 1901
Willard, J. E., 1888
Wu, W.-T., 1852

Yang, K., 1985</p> |
|---|--|---|---|--|

ANNOUNCEMENT

Division of Industrial and Engineering Chemistry 37th Annual Chemical Engineering Symposium

The Division of Industrial and Engineering Chemistry announces the 37th Annual Chemical Engineering Symposium to be held at Tulane University in New Orleans, Louisiana, on December 14 and 15, 1970. The Symposium topic is "Recent Advances in Establishing the Physico-Chemical Bases for Chromatography." Professor Riki Kobayashi and Harry A. Deans, both of the Chemical Engineering Department at Rice University, Houston, Texas 77001, are acting as Cochairmen.

The objective of this 37th IEC "Christmas Symposium" is to allow presentation and discussions of recent advances in the physico-chemical bases for gas-liquid, gas-solid, and liquid-liquid chromatography. Quantification of these areas both in terms of new theories and experiments will be discussed. Primary interest will be in principles rather than in specific separations. The meeting will be designed to stimulate analytical chemists, physical chemists, and chemical engineers who are interested in some recent advances in our understanding of the principles underlying chromatographic separations.

Interested chemists and chemical engineers are invited as speakers or as members of the audience. Several outstanding invited speakers will be announced later. Those desiring consideration in being on the program should submit abstracts to the symposium chairman by June 1, 1970.

THE JOURNAL OF PHYSICAL CHEMISTRY

Registered in U. S. Patent Office © Copyright, 1970, by the American Chemical Society

VOLUME 74, NUMBER 9 APRIL 30, 1970

Kinetics of Aqueous Indium(III) Perchlorate Dimerization

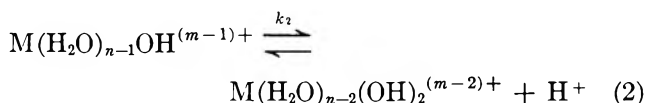
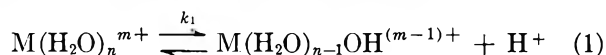
by Edward M. Eyring and Jeffrey D. Owen

Department of Chemistry, University of Utah, Salt Lake City, Utah 84112 (Received October 2, 1969)

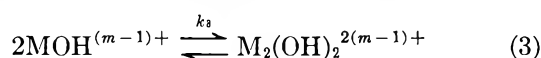
Temperature jump relaxation times observed in acidic, aqueous solutions of indium(III) perchlorate have been identified with the equilibrium $2\text{InOH}^{2+} \xrightleftharpoons{k_3} \text{In}_2(\text{OH})_2^{4+}$. The rate constant k_3 at 25° and 0.5 *M* ionic strength was found to be $4.1 \pm 0.4 \times 10^5 M^{-1} \text{sec}^{-1}$. A comparison of this result is made with earlier data on the complexation of InOH^{2+} to discover whether the rate-determining step in the dimerization is loss of an inner coordination sphere water molecule from an InOH^{2+} cation.

Introduction

Sillén and others¹ have provided equilibrium constants for the hydrolysis, dimerization, and further polymerization of cations of many metals including In(III). Hydrolysis reactions of the type



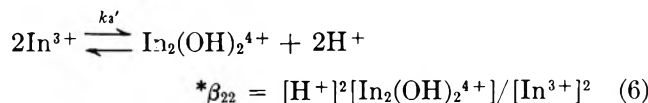
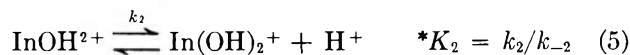
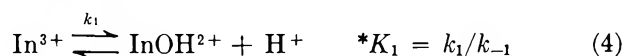
proceed very rapidly in aqueous solution with measured²⁻⁵ rate constants k_{-1} and k_{-2} generally equal to $10^9 M^{-1} \text{sec}^{-1}$ or greater. Such rate constants approach in magnitude the diffusion-limited values predicted by Debye.⁶ It is more difficult to predict a rate constant for the dimerization reaction



Here we have simplified our notation, as we will do hereafter, by omitting the first coordination sphere water molecules, *i.e.*, $\text{MOH}^{(m-1)+}$ denotes $\text{M}(\text{H}_2\text{O})_{n-1}\text{OH}^{(m-1)+}$, etc. The objective of the present study was to measure k_3 in aqueous indium(III) perchlorate solutions and then make comparisons with other kinetic

data to determine whether the rate-determining step in the dimerization is loss of a water molecule from the first coordination sphere of InOH^{2+} .

Biedermann^{7,8} reported the following indium(III) perchlorate hydrolysis and dimerization equilibrium constants at 25° in aqueous 3 *M* NaClO_4



(1) L. G. Sillén and A. E. Martell, "Stability Constants," The Chemical Society, London, 1964.

(2) D. L. Cole, E. M. Eyring, D. T. Rampton, A. Silzars, and R. P. Jensen, *J. Phys. Chem.*, **71**, 2771 (1967).

(3) L. P. Holmes, D. L. Cole, and E. M. Eyring, *ibid.*, **72**, 301 (1968).

(4) D. L. Cole, L. D. Rich, J. D. Owen, and E. M. Eyring, *Inorg. Chem.*, **8**, 682 (1969).

(5) E. M. Eyring and D. L. Cole in "Fast Reactions and Primary Processes in Chemical Kinetics," S. Claesson, Ed., Interscience Publishers, New York, N. Y., 1967, p 255.

(6) P. Debye, *Trans. Electrochem. Soc.*, **82**, 265 (1942).

(7) G. Biedermann, *Ark. Kemi*, **9**, 277 (1956).

(8) G. Biedermann, *Rec. Trav. Chim.*, **75**, 716 (1956).

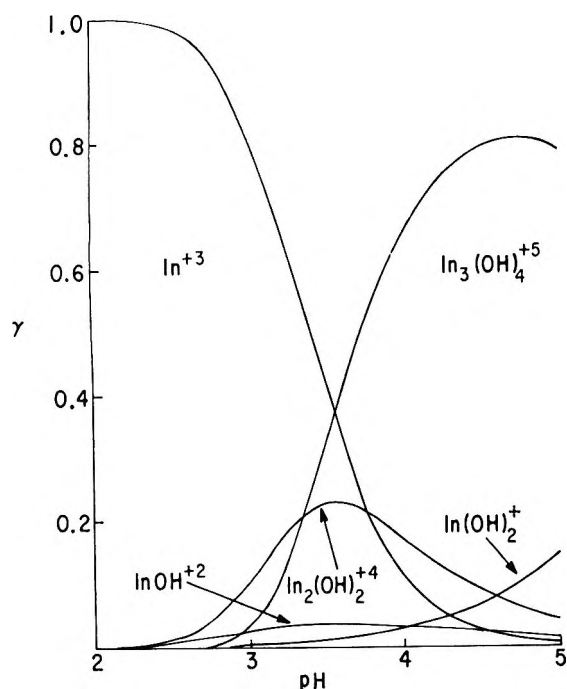
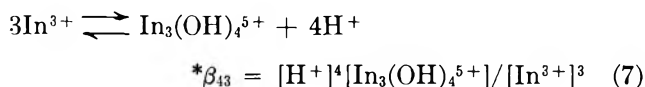


Figure 1. Distribution of indium(III) between different ions for total indium(III) perchlorate concentration $C_0 = 0.02 M$ and 25° calculated with Biedermann's equilibrium constants. At a given pH, the fraction γ of indium(III) present as a particular ion is represented by the length of a vertical line segment extended from the abscissa to the respective curve.



where $p^*K_1 = 4.42$, $p^*K_2 = 3.9$, $p^*\beta_{22} = 5.21$, and $p^*\beta_{43} = 9.90$. The relative importance of the concentration of the various aqueous indium(III) perchlorate species for pH 2-5 is depicted in Figure 1.

Experimental Section

Concentrations of aqueous stock solutions of G. F. Smith Co. reagent grade indium(III) perchlorate were determined by titrating with EDTA using Eriochrome Black T as an indicator.⁹ Sample solutions were made $2 \times 10^{-5} M$ in methyl orange to permit spectrophotometric measurements of the relaxation time τ at 520 nm and adjusted to $0.5 M$ with NaClO_4 to assure rapid heating ($\sim 5 \mu\text{sec}$) from 17 to $25 \pm 1^\circ$. The pH of each solution was measured with a Beckman 1019 pH meter. Our temperature jump apparatus closely resembles that of Hammes and Fasella¹⁰ modified for single beam operation.¹¹ Blank aqueous solutions containing only indicator and NaClO_4 were temperature jumped to verify that the exponential oscilloscope traces were caused by indium(III) perchlorate.

Results

Several alternative treatments of the kinetic data in Table I should be considered. The four equilibria, eq 4

through 7, as well as the methyl orange equilibrium



conceivably could account for the relaxation data. It would be reasonable to assume that equilibria 4, 5, and 8 are rapidly achieved compared to (6) and (7) and that (7) is so much slower than (6) that it may be neglected. The relaxation time corresponding to reaction 6 would then be

$$\tau^{-1} = \frac{4k_3}{\gamma} [\text{In}^{3+}] + k'_{-3}([\text{H}^+]^2 - \frac{4\beta}{\alpha\gamma} [\text{H}^+][\text{In}_2(\text{OH})_2^{4+}]) \quad (9)$$

where

$$\alpha \equiv 1 + \frac{[\text{A}^-]}{K_A + [\text{H}^+]} + \frac{[\text{In}(\text{OH}_2^+)]}{[\text{H}^+]} + \frac{^*K_2[\text{InOH}^{2+}]}{[\text{H}^+]^2}$$

$$\beta \equiv \frac{^*K_1^*K_2}{[\text{H}^+]^2} - 1$$

$$\gamma \equiv 1 + \frac{^*K_1}{[\text{H}^+]} + \frac{^*K_1^*K_2}{[\text{H}^+]^2} - \frac{\beta}{\alpha} \left(\frac{[\text{InOH}^{2+}]}{[\text{H}^+]} + \frac{^*K_2[\text{InOH}^{2+}]}{[\text{H}^+]^2} - [\text{In}(\text{OH})_2^+] \right)$$

The equilibrium concentrations of all species (see Table I) were calculated using $^*K_1 = 10^{-4.42}$, $^*K_2 = 10^{-3.9}$, $^*\beta_{22} = ^*\beta_{22}/^*K_1^2 = 10^{3.63}$, $^*\beta_{43} = 10^{-9.90}$, and a value of $K_A = 10^{-3.39}$ for methyl orange at $\mu = 0.5 M$ and 25° reported by Kolthoff.¹² $[\text{H}^+] = 10^{-\text{pH}}/0.77$ where the denominator is the activity coefficient for H^+ at 25° and $\mu = 0.5 M$.¹³ The use of $\mu = 3.0 M$ equilibrium constants with $\mu = 0.5 M$ kinetic data is a necessary approximation. It is difficult to operate a Joule heating temperature jump at ionic strengths much above $0.5 M$, and a complete set of equilibrium constants is not yet available for $\mu < 3.0 M$. The limited pH range of the kinetic data was imposed by precipitation at $\text{pH} > 3.4$ and by small relaxation amplitudes for $\text{pH} < 3.0$. A least-squares analysis of the data of Table I inserted in eq 9 yielded an impossible negative value of $k_{-3}' = -9.1 \times 10^7 M^{-2} \text{sec}^{-1}$ and $k_3' = 3.9 \times 10^4 M^{-1} \text{sec}^{-1}$. Thus the overall reaction of eq 6 does not satisfactorily account for the data.

The word "overall" should be emphasized throughout this discussion. The existence of In^{3+} , for example, as

(9) F. J. Welcher, "The Analytical Uses of Ethylenediaminetetraacetic Acid," D. Van Nostrand Co., Inc., Princeton, N. J., 1958, p 178.

(10) G. G. Hammes and P. Fasella, *J. Amer. Chem. Soc.*, **84**, 4644 (1962).

(11) G. G. Hammes and J. I. Steinfield, *ibid.*, **84**, 4639 (1962).

(12) I. M. Kolthoff, *J. Phys. Chem.*, **34**, 1466 (1930).

(13) R. A. Robinson and R. H. Stokes, "Electrolyte Solutions," 2nd ed, Butterworths, London, 1959, p 491.

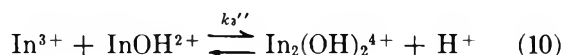
Table I: Experimental Chemical Relaxation Times and Calculated Indium(III) Perchlorate Equilibrium Concentrations at 25°

C_0^a $10^{-2} M$	pH ^b	τ^c msec	$[H^+]^d$ $10^{-4} M$	$[In^{3+}]^e$ $10^{-2} M$	$[InOH^{2+}]^e$ $10^{-3} M$	$[In(OH)_2^+]^e$ $10^{-4} M$	$[In_2(OH)_2^{4+}]^e$ $10^{-3} M$	$[In_2(OH)_4^{6+}]^e$ $10^{-3} M$	$[A^-]^e$ $10^{-3} M$
4.00	3.319	1.27	6.23	1.71	1.04	2.10	4.63	4.15	0.79
3.20	3.357	1.35	5.71	1.39	0.926	2.05	3.67	3.20	0.83
2.56	3.370	1.65	5.54	1.20	0.748	1.54	2.87	2.29	0.85
2.00	3.330	1.78	6.08	1.12	0.725	1.44	2.09	1.29	0.80
1.60	3.343	2.15	5.90	0.946	0.609	1.30	1.58	0.881	0.82
1.28	3.348	2.65	5.83	0.807	0.526	1.14	1.18	0.573	0.82
0.80	3.356	3.00	5.72	0.567	0.376	0.828	0.605	0.214	0.83
2.00	3.110	2.90	10.1	1.52	0.575	0.718	1.41	0.432	0.57
2.00	3.260	2.70	7.14	1.25	0.667	1.18	1.90	0.956	0.73
2.00	3.370	1.80	5.54	1.04	0.710	1.61	2.15	1.48	0.85

^a Total molar concentration of indium(III) perchlorate. ^b Glass electrode pH of the sample solution. ^c Average of six independent measurements of the chemical relaxation time at each concentration. Estimated error in each value of τ is approximately $\pm 10\%$. ^d Hydrogen ion concentration calculated from $[H^+] = 10^{-pH}/0.77$. ^e Molar concentrations calculated from a mass conservation relation and eq 4-7 in the text using $*K_1 = 10^{-4.42}$, $*K_2 = 10^{-3.9}$, $*\beta_{22} = 10^{-5.21}$, $*\beta_{43} = 10^{-9.90}$, and $K_A = 10^{-3.39}$.

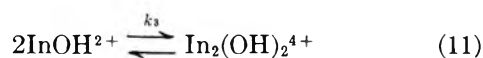
a separate entity in water is unlikely. It probably pairs with one or more anions to yield a composite, reacting entity of lower charge. Two such composite species would actually participate in the dimerization with a subsequent, perhaps rate-determining, splitting out of water of solvation and/or anions. The overall kinetics would be the same, but no implausible reactions between highly charged cations would be required.

Another overall reaction that might be substituted for eq 6 is



When this reaction is combined with eq 4, 5, 7, and 8 and a least-squares analysis of the data is made in terms of the consequent expression for the relaxation time, one obtains $k_3'' = 1.0 \times 10^5 M^{-1} sec^{-1}$ and $k_{-3}'' = 3.6 \times 10^4 M^{-1} sec^{-1}$. The multiple correlation coefficient = 0.321 is much less than unity indicating a poor fit of the data that is significant at only the 37% confidence level. Furthermore, the quotient $k_3''/k_{-3}'' = 2.8$ is in poor agreement with the thermodynamic $*\beta_{22}/*K_1 = 0.16$.

Finally, we can consider replacing eq 6 by the overall reaction



as the slow step in a reaction scheme that includes the rapid reactions 4, 5, and 8. The resulting expression for the relaxation time is

$$\tau^{-1} = 4k_3\alpha[InOH^{2+}] + k_{-3} \quad (12)$$

where

$$\frac{1}{\alpha} = 1 + \frac{[InOH^{2+}]\beta + [H^+]}{*K_1} + \frac{*K_2 - [In(OH)_2^+]\beta}{[H^+]}$$

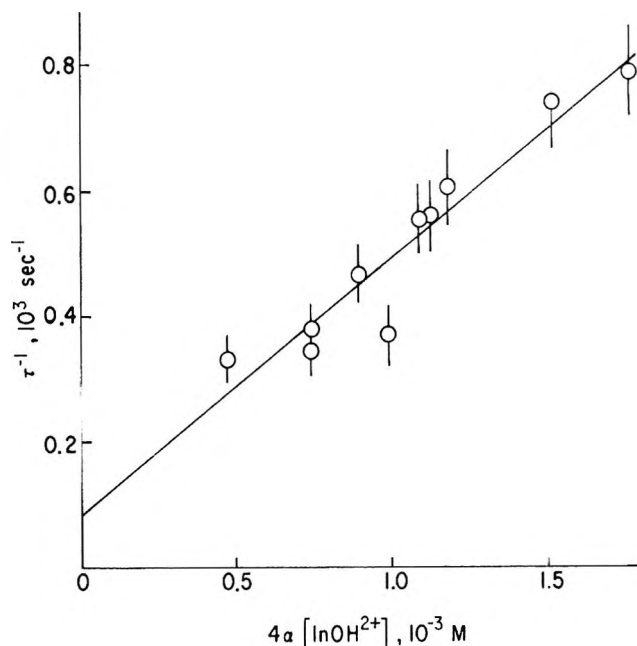


Figure 2. Plot of the reciprocal of the temperature jump relaxation time vs. the product $4\alpha[InOH^{2+}]$, where α is defined in connection with eq 12 of the text. The diagonal through the experimental points is a least-squares straight line of slope $k_3 = 4.1 \times 10^5 M^{-1} sec^{-1}$.

and

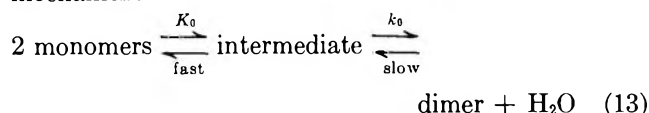
$$\beta = \frac{\frac{*K_2}{[H^+]} - \frac{[H^+]}{*K_1}}{1 + \frac{[A^-]}{K_A + [H^+]} + \frac{[InOH^{2+}]}{*K_1} + \frac{[In(OH)_2^+]}{[H^+]}}$$

the least-squares analysis of the data in terms of eq 12 yields $k_3 = 4.1 \times 10^5 M^{-1} sec^{-1}$ and $k_{-3} = 85 M^{-1} sec^{-1}$ with the very satisfactory fit shown in Figure 2. The agreement of $k_3/k_{-3} = 10^{5.68}$ with the thermodynamic $\dagger K_{22} = 10^{5.63}$ is excellent.

Discussion

That the rate-determining step in the formation of dimer from 2MOH^{2+} is the loss of a water molecule from the inner hydration sphere of one MOH^{2+} cation was first postulated by Eigen and Wilkins.¹⁴ Wendt¹⁵ ostensibly confirmed this expectation for FeOH^{2+} dimerization, as well as for the dimerization of the vanadyl monohydroxy cation VOOH^+ . The following discussion of our InOH^{2+} dimerization results follows closely Wendt's reasoning.¹⁵

The bimolecular formation of the dimer according to eq 11 may be expressed in terms of the Eigen reaction mechanism



The rate-determining inner coordination sphere water loss from the intermediate is preceded by a rapid (essentially diffusion controlled) equilibrium between free monohydroxy indium(III) cations and cations with inner coordination spheres in contact with one another. If the equilibrium constant for the formation of this contact complex is K_0 (M^{-1}) and the overall specific rate of dimerization at zero ionic strength is k_{03} ($M^{-1} \text{sec}^{-1}$), then the first-order specific rate of the rate-determining water loss k_0 (sec^{-1}) at zero ionic strength is given by

$$k_0 = k_{03}/K_0 \quad (14)$$

The value of k_{03} ($\mu = 0, 25^\circ$) can be deduced from $k_3 = 4.1 \times 10^5 M^{-1} \text{sec}^{-1}$ ($\mu = 0.5, 25^\circ$) using the Brønsted-Bjerrum relation¹⁶

$$\log k_{03} = \log k_3 - \log \frac{f_a f_b}{f_{\pm}} \quad (15)$$

Assuming that the activity coefficients f_a , f_b , and f_{\pm} are closely approximated by the Davies equation¹⁷

$$-\log f_{\pm} = 0.5 Z_a Z_b [\sqrt{\mu}/(1 + \sqrt{\mu}) - 0.3\mu] \quad (16)$$

it follows for 2InOH^{2+} where $Z_A = Z_B = +2$ and $\mu = 0.5 M$ that

$$\log k_{03} = \log (4.1 \times 10^5) - Z_a Z_b [\sqrt{\mu}/(1 + \sqrt{\mu}) - 0.3\mu] \quad (17)$$

or $k_{03} = 3.6 \times 10^4 M^{-1} \text{sec}^{-1}$.

The Fuoss theoretical equation¹⁸ for the contact pair association equilibrium constant is

$$K_0 = 2.524 \times 10^{-3} \bar{a}^3 \exp(b) \quad (18)$$

where \bar{a} is the ion-contact distance in ångströms. The exponent

$$b = -Z_a Z_b e_0^2 / a D k T \quad (19)$$

where $e_0 = 4.80 \times 10^{-10}$ esu, a is the ion-contact distance expressed in centimeters, the dielectric constant $D = 80$, $k = 1.38 \times 10^{-16}$ erg deg $^{-1}$, and $T = 298^\circ$. Equation 18 predicts that K_0 for the formation of a cation-cation pair will be much less than unity. This is qualitatively correct although Wendt's subsequent utilization¹⁵ of the numerical values of K_0 as if they had quantitative significance is speculative.

Following Wendt's argument we use the above equations to compare specific rates of water loss k_0 and k_0^* from InOH^{2+} in the course of dimerization and of complexation by SO_4^{2-} ion, respectively. We use Wendt's¹⁵ arbitrary value of $a = 5 \times 10^{-8}$ cm. For $Z_a = Z_b = +2$, eq 16 yields $K_0 = 1.2 \times 10^{-3} M^{-1}$. The specific rate of the rate-determining water loss from $\text{In}(\text{H}_2\text{O})_6\text{OH}^{2+}$ is thus $k_0 = (3.6 \times 10^4 M^{-1} \text{sec}^{-1})(1.2 \times 10^{-3} M^{-1})^{-1} = 3.0 \times 10^7 \text{sec}^{-1}$. This value of k_0 should be compared with the specific rate measured by Miceli and Stuehr¹⁹ for the reaction $\text{InOH}^{2+} + \text{SO}_4^{2-} \rightarrow \text{HOInSO}_4$, $k_{46} = 2.5 \times 10^7 M^{-1} \text{sec}^{-1}$ ($\mu = 0, 25^\circ$). For the case where $Z_a = +2$ and $Z_b = -2$, the Fuoss theory $K_0 = 84 M^{-1}$. Thus the first-order specific rate, $k_0^* = k_{46} K_0^{-1} = 3 \times 10^5 \text{sec}^{-1}$.

A value of unity for the quotient k_0/k_0^* would confirm the Eigen-Wilkins postulate.¹⁴ Wendt was satisfied with quotients of 4.4 and 3.3 for FeOH^{2+} and VOOH^+ , respectively. However, for InOH^{2+} we have found $k_0/k_0^* = 10^2$. A larger ion-contact distance $a = 7 \times 10^{-8}$ cm is required to achieve Wendt's standard of agreement for InOH^{2+} , i.e., $k_0/k_0^* = (3.6 \times 10^4)(1.6 \times 10^{-2})^{-1}/(2.5 \times 10^7)(48)^{-1} = 4.3$. It would be a mistake to misconstrue this as either evidence for a 7 Å ion-contact distance in the case of InOH^{2+} or as a proof or disproof of the Eigen-Wilkins postulate for indium(III) dimerization. The most likely explanation is that the Fuoss formalism, eq 18, underestimates the magnitude of K_0 for reaction 13, possibly because the associating cations carry anions with them and are hence less highly charged than Wendt has inferred.

Acknowledgment. This research was supported by the Directorate of Chemical Sciences, Air Force Office of Scientific Research, Grant AF-AFOSR-69-1717. We thank Professor Raymond M. Fuoss for an instructive letter reviewing ref 15.

(14) M. Eigen and R. G. Wilkins in "Mechanisms of Inorganic Reactions," Advances in Chemistry Series, No. 49, American Chemical Society, Washington, D. C., 1965, p 55.

(15) H. Wendt, *Inorg. Chem.*, **8**, 1527 (1969).

(16) K. J. Laidler, "Chemical Kinetics," 2nd ed, McGraw-Hill Book Co., New York, N. Y., 1965, pp 219-221.

(17) C. W. Davies, "Ion Association," Butterworths, London, 1962, p 41.

(18) R. M. Fuoss, *J. Amer. Chem. Soc.*, **80**, 5059 (1958).

(19) J. Miceli and J. Stuehr, *ibid.*, **90**, 6967 (1968).

High Temperature Kinetics of the Oxidation and Nitridation of Pyrolytic Silicon Carbide in Dissociated Gases¹

by Daniel E. Rosner² and H. Donald Allendorf

Department of Engineering and Applied Science, Yale University, New Haven, Connecticut 06520, and AeroChem Research Laboratories Inc., Division of Sybron Corporation, Princeton, New Jersey 08540 (Received August 22, 1969)

Microwave discharge, fast-flow vacuum system techniques, coupled with resistance heating of specimens in filament form, have been employed to study the true kinetics of silicon and carbon atom removal from pyrolytic silicon carbide attacked by O(g), O₂(g), N(g), and N₂(g) in the nominal temperature range 1750–2400°K, at reactant pressures above 10⁻⁴ Torr. Extremely high reaction probabilities ($\epsilon > 10^{-1}$) have been observed for the attack of bare polycrystalline SiC by O atoms, N atoms, or O₂ molecules; however, if the temperature level is low enough and/or the reactant pressure high enough, semi-protective reaction product layers (presumably SiO₂(c) and Si₃N₄(c)) are present causing Si atom and C atom removal rates to be determined by dissociative sublimation under the influence of imposed reactant fluxes. In this "passive" regime, which also corresponds to steady-state surface recession at a constant (time-independent) rate, the reaction probabilities for SiC attack by O, O₂, N, N₂ are low ($\epsilon < 10^{-2}$), sharply temperature dependent (with an activation energy exceeding the corresponding heats of sublimation), and, for O, O₂, and N, fall rapidly with increased reactant pressure (corresponding in extreme cases to *negative* reaction orders). Reactant dissociation considerably extends the reactant pressure/temperature domain characterized by the steady-state presence of semi-protective product films. For oxygen this effect far exceeds that expected on simple thermochemical grounds, and at 1800°K amounts to about a 100-fold reduction in the oxygen pressure at which the existence of a silica film becomes evident in the kinetic behavior. The implications of these macroscopic kinetic results with regard to the elementary steps of dissociative adsorption, product film formation, and dissociative sublimation are discussed in the light of available kinetic and thermochemical data for these, and related, gas-solid reactions.

1. Introduction

To further understand the reactivity of refractory solids in *dissociated* gases, we have recently extended our previous measurements on the (elemental) solids Mo,³⁻⁵ W,^{3,4} Re,⁶ C,^{7,8} B,^{4,9} to include the important binary compound SiC, with the results reported herein. In addition to intense industrial and aerospace interest in the chemical stability of polycrystalline silicon carbide¹⁰ in corrosive environments,^{11,12} the kinetic behavior of this material in dissociated oxygen and nitrogen at high temperatures and low pressures is of fundamental interest for the following reasons: (a) while SiC(s) sublimates silicon preferentially, forming a carbon-rich surface layer *in vacuo* (or in inert gases) its high temperature reactivity in atomic oxygen and nitrogen is likely to differ markedly from graphite, being dominated by the tendency to produce (and dissociatively sublime) semi-protective product films [SiO₂(c) and Si₃N₄(c), respectively]; (b) however, the *existence* of semi-protective condensed product films (being determined by competitive kinetic processes) is not assured at all reactant pressure/surface temperature combinations; indeed, reactant dissociation is likely to strongly modify the temperature level at which the kinetics ultimately reveal "bare surface" (low coverage) behavior. Additionally, the kinetic effects of reactant dissociation should differ markedly depending

(1) This research was supported by the Propulsion Division of the Office of Aerospace Research, U. S. Air Force Office of Scientific Research, under Contract AF 49(638) 1637. Revision of AeroChem TP-215.

(2) Associate Professor, Chemical Engineering Group; to whom inquiries concerning this paper should be sent.

(3) D. E. Rosner and H. D. Allendorf, *J. Electrochem. Soc.*, **114**, 305 (1967).

(4) D. E. Rosner and H. D. Allendorf, "Proceedings, Third International Symposium on High Temperature Technology," Butterworths and Co., Ltd., London, 1969, p 707.

(5) D. E. Rosner and H. D. Allendorf, *J. Phys. Chem.*, **69**, 4290 (1965).

(6) D. E. Rosner and H. D. Allendorf, *J. Chem. Phys.*, **49**, 5553 (1968).

(7) D. E. Rosner and H. D. Allendorf, *Carbon (Oxford)*, **3**, 153 (1965); *ibid.*, **7**, 515 (1969).

(8) D. E. Rosner and H. D. Allendorf, *AIAA J.*, **6**, 650 (1968).

(9) D. E. Rosner and H. D. Allendorf, *J. Phys. Chem.*, **72**, 4159 (1968).

(10) Crystalline silicon carbide is a covalently bonded "giant molecule" in which each silicon atom is tetrahedrally coordinated to four carbon atoms (and vice versa). In its cubic (β) modification the structure is that of diamond, with appropriate C \rightarrow Si-atom replacements, leading to successive layers of puckered sheets of C atoms and Si atoms.

(11) J. H. Westbrook and E. R. Stover, "High Temperature Materials and Technology," I. E. Campbell and E. M. Sherwood, Ed., John Wiley and Sons, New York, N. Y., 1967, p 379; E. G. Kendall, "Ceramics for Advanced Technologies," J. E. Hove and W. C. Riley, Ed., John Wiley and Sons, New York, N. Y., 1965, p 143.

(12) A. R. G. Brown, Technical Note Metallurgical Physics, No. 325, AD 249 685, Royal Aircraft Establishment, Farnborough-Ministry of Aviation, London, 1960; J. E. Antill and J. B. Warburton, "Oxidation of Silicon and Silicon Carbide at 1000–1300°C," 34th AGARD-NATO Propulsion and Energetics Panel Meeting Proceedings, AGARD Conference Proceedings No. 52, Feb 1970, Paper No. 10.

on the presence or absence of condensed product films, as we have already observed in the case of boron oxidation.⁴ However, the present case is rendered more interesting by the fact that the eligible condensed reaction products SiO₂(c) and Si₃N₄(c) sublime *dissociatively*,¹³ hence their sublimation rates can be influenced by the imposed reactant (atom or molecule) flux itself.

These considerations, coupled with a sparsity of experimental information on the response of refractory solids to well-defined *dissociated* oxidizing gases and the commercial availability of high purity, dense silicon carbide in filament form, prompted the macroscopic kinetic experiments described below. While our emphasis is on dissociation effects, it should be kept in mind that the reactions of SiC(s) with the *diatomic* gases O₂(g) and N₂(g) are far from having been completely explored,¹⁰⁻¹² particularly in the high temperature weight-loss ("linear") kinetic regime, where previous investigators¹⁴ have encountered reactant transport limitations on observed reaction rates (despite the subatmospheric pressures employed). It is anticipated that many of our findings will have implications vis a vis the use of silicide-protected materials^{15,16} in low pressure, dissociated gas environments (*e.g.*, high speed motion in the Earth's atmosphere).³

2. Experimental Section

The techniques used here are similar to those described in our earlier reports³⁻⁹ on heterogeneous reactions of atomic oxygen and atomic chlorine. In the present section we indicate our procedure for generating and monitoring atomic nitrogen and atomic oxygen in the absence of O₂(g) and describe the nature of the polycrystalline SiC specimens studied. Those details of the overall technique and equipment necessary to properly interpret the results below will also be reviewed.

Atom Production and Detection. Since our preliminary experiments showed that O and O₂ had comparable reactivity on high temperature SiC, while N₂ was comparatively unreactive, atomic oxygen was generated indirectly¹⁷ by first passing 3% N₂/97% Ar mixtures through a microwave discharge at ≈ 1 Torr, and then converting the resulting N atoms into O atoms by introducing nitric oxide immediately downstream of the discharge (*i.e.*, exploiting the rapid bimolecular exchange reaction $N + NO \rightarrow O + N_2$). Chemiluminescent reactions in this system provide a direct indication of the NO-flow rates corresponding to complete conversion of N into O, and, conveniently, a reliable titration method of determining absolute atom concentrations.¹⁸ For kinetic studies of heterogeneous reactions of N atoms, NO addition is simply omitted, except, of course, before and after a nitridation experiment to determine the absolute N-atom concentration. While ground state N atoms are known to be the main

chemically reactive component of microwave discharge-produced active nitrogen,¹⁸ nonnegligible contributions from metastable nitrogen molecules (*e.g.*, N₂(A³Σ⁺_u)) were ruled out in control experiments by introducing a 2-5-cm packing of Pyrex wool "quencher" immediately downstream of the discharge, and then verifying that the observed reaction rates on SiC were compatible with the (reduced) N-atom concentration and kinetic data obtained on SiC in the absence of the Pyrex wool. Most of the experiments reported below were carried out with the total pressure level at the specimen location maintained at 1 Torr, and the total flow rate maintained at 20 cc(STP)/sec. This corresponded to a linear velocity of approximately 2×10^4 cm/sec in the Vycor "discharge" tube, or a residence time of ≈ 1 msec between the microwave discharge cavity and SiC(s) specimen.

Materials. Our SiC specimens are ≈ 3 cm lengths of resistively heated filament (initially 0.102 mm in outer diameter) with the filament axis oriented perpendicular to the reactant gas flow. These specimens are cut from commercially available pyrolytic silicon carbide filament spools¹⁹ [produced by chemical vapor deposition (CVD) on a 0.0127 mm (0.5 mil) tungsten substrate] and mounted on a two-pronged, brass, current-carrying specimen holder, using silver conductive paint at the filament ends to facilitate electrical contact. Filament cross sections (see Figure 1a, b) before and after a 2-min O₂/Ar exposure at high temperature ($T \approx 2100^\circ\text{K}$) reveal no evidence for SiC/W interdiffusion and a reasonable degree of cylindrical symmetry even after extensive loss of material. The latter observation underlies our procedure for computing SiC reaction rates (see below) based on post-mortem average diameter measurements along the central 0.5-cm length of each specimen. Studies of the microstructure of CVD-pyrolytic silicon carbide²⁰ indicate

(13) Thermochemical data (used hereafter) for these condensed phases and their gaseous decomposition products have been taken from "JANAF Thermochemical Tables," The Dow Chemical Co., Midland, Mich., 1963, ASTIA AD 248 425, and "JANAF Thermochemical Tables—Addendum," 1966; available as Report PB 168 370-1 from the Clearinghouse for Federal Scientific and Technical Information.

(14) E. A. Gulbransen, K. A. Andrew, and F. A. Brassart, *J. Electrochem. Soc.*, **113**, 1311 (1966).

(15) C. A. Krier and J. M. Gunderson, paper presented at the Fall Meeting of the Electrochemical Society, Philadelphia, Pa., 1966; report available from Structures and Materials Technology Aerospace Group, The Boeing Co., Seattle, Wash.

(16) R. Wehrman, "High Temperature Materials and Technology," I. E. Campbell and E. M. Sherwood, Ed., John Wiley and Sons, New York, N. Y., 1967, p 399.

(17) J. E. Morgan, L. Elias, and H. I. Schiff, *J. Chem. Phys.*, **33**, 930 (1960).

(18) A. N. Wright and C. A. Winkler, "Active Nitrogen," Academic Press, Inc., New York, N. Y., 1968.

(19) Texaco Experiment Inc. (Richmond, Va.) supplier: Data Sheet TEI M-1020 (March 1967). While no longer available from this producer, an equivalent material can now be obtained from United Aircraft Corp.

(20) T. D. Gulden, *J. Amer. Ceram. Soc.*, **51**, 424 (1968).

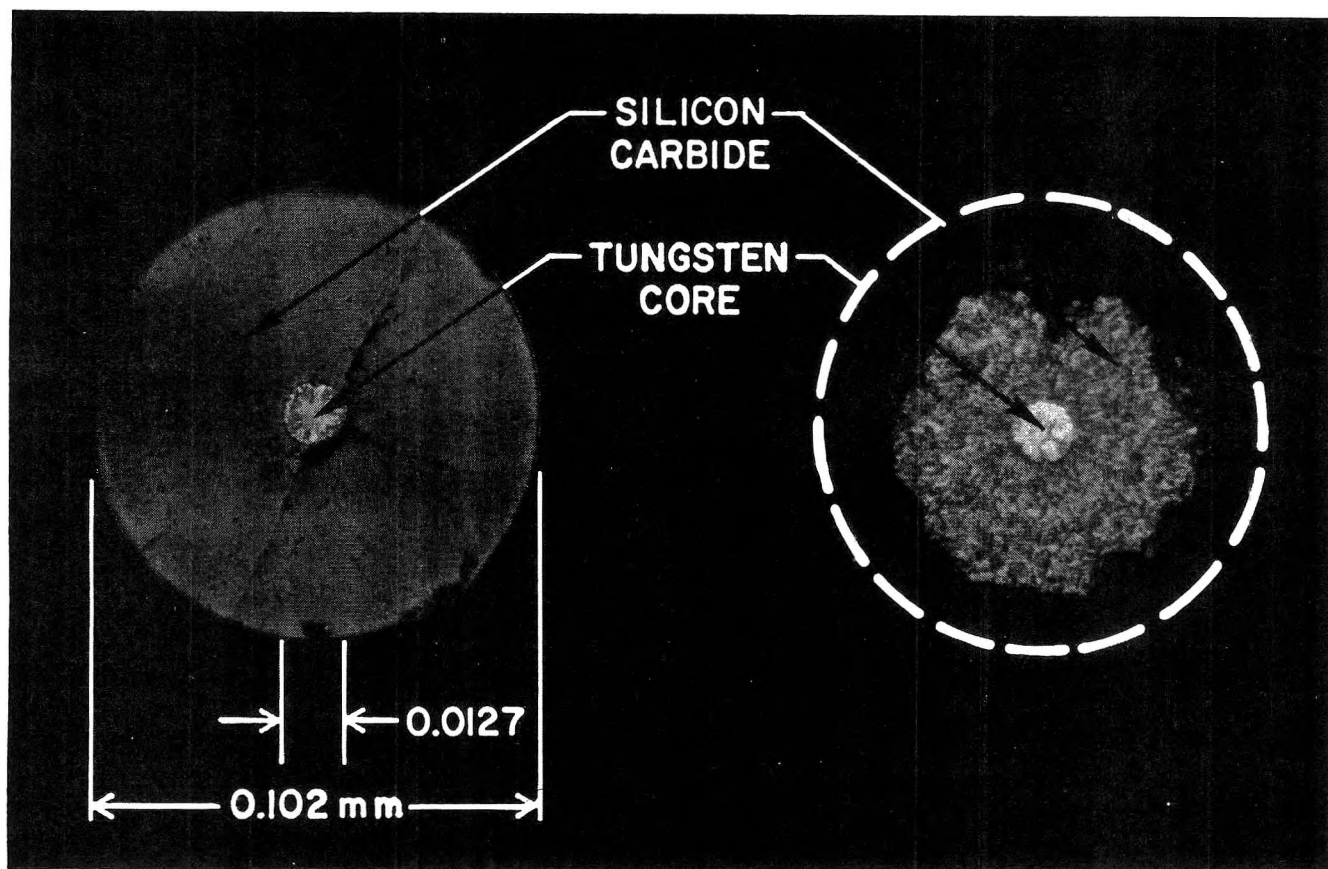


Figure 1. Silicon carbide filament cross sections; (a) as received, (b) following heating at 1 Torr in an O_2 -Ar mixture ($p_{O_2} = 10^{-2}$ Torr, $T = 2100^\circ K$) for 2 min.

the presence of columnar grains of predominantly β -SiC (the cubic modification) with preferential orientation, and a density close to the theoretical (X-ray) value of 3.21 g/cm^3 .

Extra dry grade (Linde) oxygen, high purity-dry grade nitrogen (Linde), high purity-dry grade argon (Linde), and technical grade nitric oxide (Matheson) were used without further treatment.

Reaction Rate. All measurements reported here pertain to reactant pressure/temperature conditions under which there is a steady-state rate of diameter reduction due to the formation-desorption of oxides and/or nitrides of silicon and/or carbon. Despite the continuous reduction in composite specimen cross-sectional area, the filament surface temperature is maintained constant during the course of an experiment by manually adjusting the electrical power dissipation in accord with the output of an optical pyrometer (Pyro Micro-Optical Pyrometer, Model 95 Lens E). Filament temperature levels reported are taken to be proportional to the observed brightness temperatures, corrected (to account for nonunity emittance and light absorption by intervening glass) using simultaneous observations on the melting of four pyrometric compounds²¹ in the temperature range 1366 – $1644^\circ K$. SiC removal per unit time and area was calculated from microscope determinations of the re-

duction in filament diameter after known duration exposures to nitrogen or oxygen-containing gas mixtures. The duration of the present experiments (typically $1 \leq \Delta t \leq 120$ min) far exceeds the duration of any initial transient associated with establishment of the steady-state adsorbed gas population or condensed product film thickness (*cf.* section 4). Accordingly, runs of different duration lead to calculated reaction rates which are constant (independent of duration) to within our experimental reproducibility. The element fluxes of silicon and carbon were therefore calculated using the observed mean rates of diameter reduction $\Delta d/\Delta t$ and the estimated density (3.1 g/cm^3) of the SiC. In all cases analyzed quantitatively the total fractional change in diameter was smaller than that shown in Figure 1b, and in no case was it allowed to exceed 25%.

To ensure that the observed reaction rates were not influenced by reactant access (diffusional) limitations,^{22,23} and to minimize (a) secondary surface reactions, (b) product escape limitations, and (c) O-atom and N-atom losses by termolecular (homogeneous) atom

(21) Produced by the Tempil Corp., New York, N. Y.

(22) D. E. Rosner, "Eleventh Symposium (International) on Combustion," Combustion Institute, Pittsburgh, Pa., 1967, p 181.

(23) D. E. Rosner, *AIAA J.*, 2, 593 (1964).

recombination, high flow velocities ($\approx 10^4$ cm/sec, directed normal to the filaments) and low total pressures (≈ 1 Torr) were employed. These conditions, coupled with the small specimen diameters, have enabled us to obtain chemical kinetic measurements for silicon carbide free of the intervention of gas phase diffusion phenomena²⁴ in the nominal range of conditions: $1750 \leq T \leq 2400^\circ\text{K}$, $10^{-4} \leq p_{\text{O}} \leq 5 \times 10^{-2}$ Torr, $3 \times 10^{-3} \leq p_{\text{O}_2} \leq 10^0$ Torr, $3 \times 10^{-4} \leq p_{\text{N}} \leq 10^{-2}$ Torr, $10^0 \leq p_{\text{N}_2} \leq 4 \times 10^2$ Torr.

To facilitate a comparison of the observed reaction rates with the theoretical maximum rates (under the imposed reactant fluxes) we have cast all reaction rate data in the form of a dimensionless *adsorbent atom removal probability*, ϵ , calculated as the ratio of the observed Si- or C-atom flux, $\dot{Z}''_{(\text{Si,C})}$, away from the filament (regardless of the chemical state of aggregation) to the impingement rate, \dot{Z}''_i , of reactant i (atoms or molecules) per unit area. Under the present conditions of gas density level, specimen size and flow rate, \dot{Z}''_i is calculated from the reactant partial pressure p_i and specimen temperature, T , using the Hertz-Knudsen equation

$$\dot{Z}''_i = \frac{1}{4} \frac{p_i}{kT} \left(\frac{8kT}{\pi m_i} \right)^{1/2} \quad (1)$$

where m_i is the mass of reactant species i ($i = \text{O}, \text{O}_2, \text{N}, \text{N}_2$) and k is the Boltzmann constant. Thus, ϵ as defined above, is simply the average number of Si atoms (or C atoms) removed from the filament per reactant atom (or molecule) strike under the reported p_i, T conditions; *no assumptions regarding product molecule identity enters its calculation*. As is customary, the temperature and reactant pressure dependence of the reaction can be described in terms of the apparent "activation energy," E , and reaction "order" n , which, in the present case, would be locally defined, respectively, by $-R d[\ln \dot{Z}''_{(\text{Si,C})}]/d[1/T]$ and $d[\ln \dot{Z}''_{(\text{Si,C})}]/d[\ln p_i]$ (where R is the universal gas constant). These conventional definitions reveal that (a) the activation energy calculated from a plot of $\ln \epsilon$ vs. $1/T$ will exceed that determined from $\ln \dot{Z}''_{(\text{Si,C})}$ vs. $1/T$ by the (usually negligible) amount $RT/2$ (1.987 kcal/mol at 2000°K) and (b) the local slope of a $\log \epsilon$ vs. $\log p_i$ plot will be $n - 1$, and, hence, zero for a first order [$\dot{Z}''_{(\text{Si,C})} \propto p_i$] process, and -1 for a zero-order [$\dot{Z}''_{(\text{Si,C})} \propto p_i^0$] process.

3. Results

The Silicon Carbide/Oxygen System. The results of our SiC oxidation rate measurements covering the nominal temperature range 1750 – 2400°K , at comparable reactant partial pressures, are presented in Figure 2. Under these low pressure conditions it is seen that the O and O_2 reaction probabilities are comparable and display similar trends with temperature. In particular, both reaction probabilities are quite high

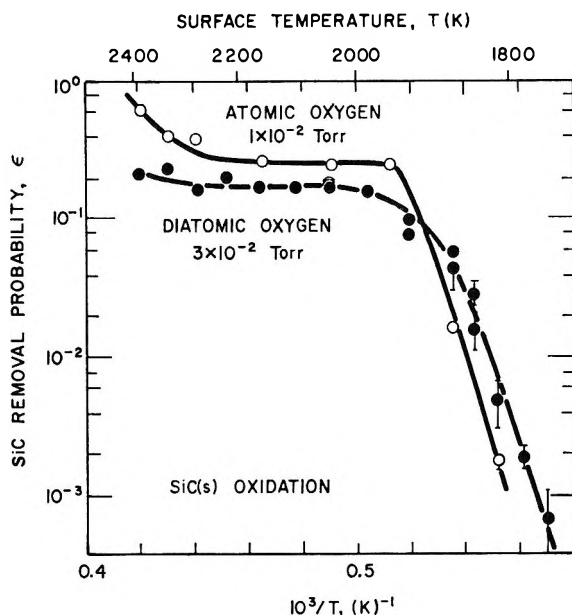


Figure 2. Temperature dependence of the oxidation probability of silicon carbide (O, atomic oxygen; ●, diatomic oxygen).

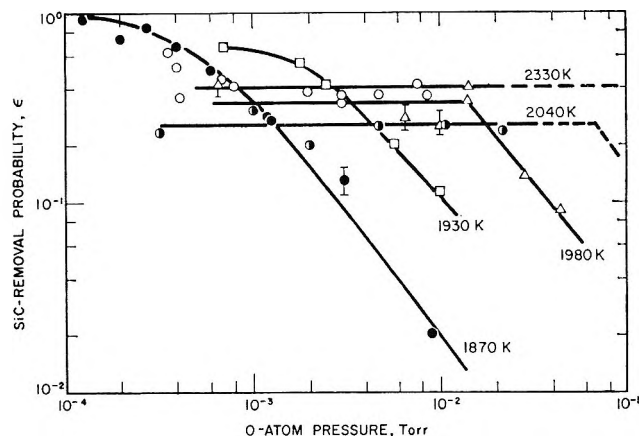


Figure 3. Dependence of silicon carbide oxidation probabilities on O-atom pressure.

($>10^{-1}$) above 1900°K , and only weakly temperature dependent over most of this high temperature range. However, below $\approx 1900^\circ\text{K}$ both reaction probabilities assume low values and are strongly temperature dependent (apparent activation energy, $E \approx 270$ kcal/mol), with the O_2 -reaction probability actually exceeding that for O atoms by an appreciable factor (≈ 7.5 , when corrected for the threefold difference in reactant pressure). At any particular temperature, transition behavior is also exhibited in the dependence of ϵ on reactant pressure. For atomic oxygen (see Figure 3) at each tem-

(24) Control experiments in which deliberate changes were effected in total flow rate and carrier gas identity demonstrate that the reaction rates reported pertain to the chemically controlled attack of SiC at the reported surface temperature. Chemical control is also indicated by the symmetry observed in the reacted specimen cross sections (cf. Figure 1b).

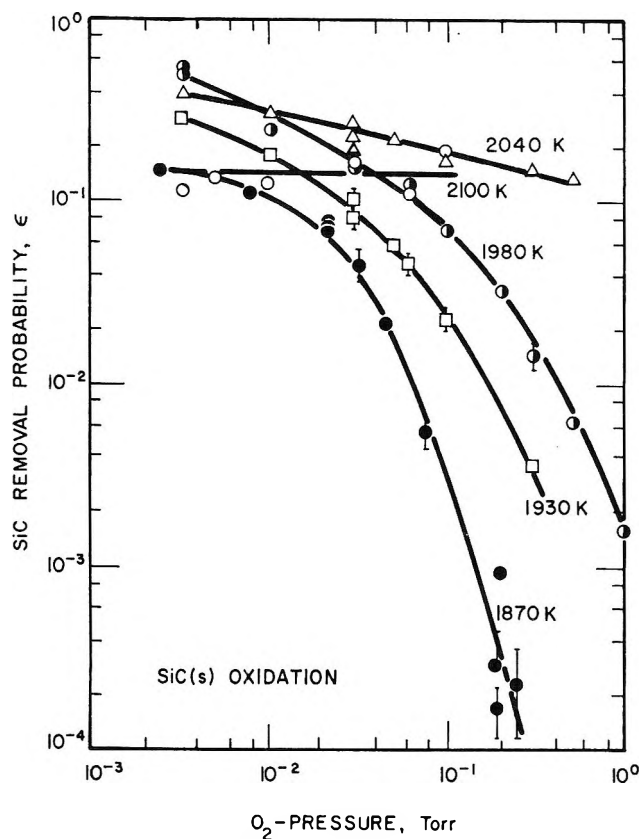


Figure 4. Dependence of silicon carbide oxidation probabilities on O_2 pressure.

perature level shown the reaction probability is high and p_{O_2} independent until a rather well-defined threshold O-atom concentration is achieved, above which ϵ drops almost inversely with p_{O_2} (corresponding to absolute Si-atom and C-atom fluxes that become nearly independent of O-atom pressure).²⁵ Qualitatively similar behavior is displayed for the $SiC(s) + O_2(g)$ reaction (see Figure 4) except that the above-mentioned transition behavior is more gradual, and ϵ falls off more steeply with increased reactant pressure (at sufficiently high reactant pressures). When translated into absolute Si-atom and C-atom fluxes, this high p_{O_2} behavior corresponds to element removal rates which ultimately decrease with increasing p_{O_2} [in accord with $\sim(p_{O_2})^{-2}$ for 1870°K at the highest pressures shown]. Thus, the absolute silicon carbide oxidation rate is actually a maximum at some intermediate O_2 pressure (where the local slope is -1 on each of the isotherms in Figure 4)—an interesting trend apparently anticipated in an earlier study of the $SiC(s) + O_2(g)$ reaction by Ervin.²⁶

The Silicon Carbide/Nitrogen System. In contrast to the corresponding oxidation case, we find that the reactivity of the parent molecule, N_2 , is negligible compared with that of N atoms under the present experimental conditions (see Figure 5). While this ϵ discrepancy effectively precluded kinetic studies at comparable reactant pressures, it is clear from Figure 5, and our ancillary results on the pressure dependence of ϵ

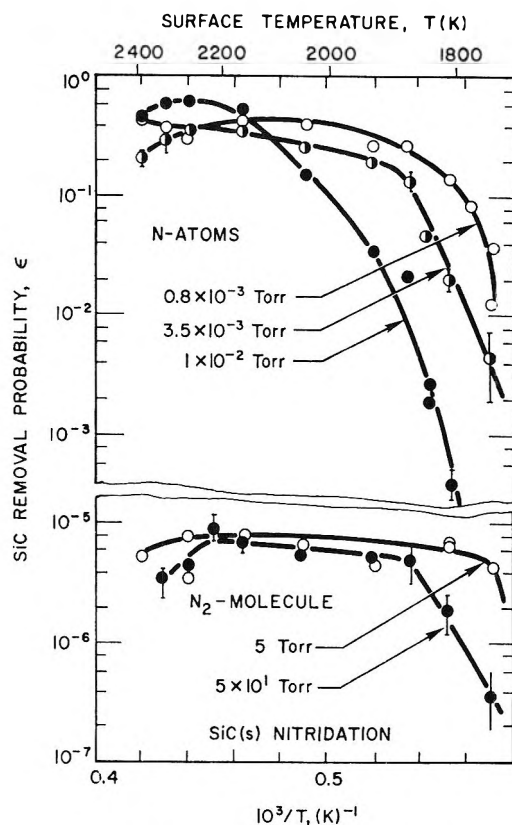


Figure 5. Temperature dependence of the nitridation probability of silicon carbide (top panel: atomic nitrogen; bottom panel: diatomic nitrogen).

(cf. Figures 6 and 7), that (a) the N-atom reaction remarkably efficient at sufficiently high temperatures, with ϵ exceeding the corresponding peak nitridation probabilities for N_2 by some 230-fold (when corrected for the large difference in reactant pressures); (b) when present in comparable concentrations, the N_2 contribution to the reactivity of an N- N_2 mixture can be neglected for $SiC(s)$ (a fact which greatly simplifies the treatment of SiC -nitridation data obtained in microwave discharged 3% N_2 /97% Ar mixtures, since only some 4.7% of the N_2 molecules are dissociated).²⁷ At any particular reactant pressure, both reactions reveal complex behavior on the Arrhenius ($\log \epsilon$ vs. $1/T$) plane, passing from low and sharply temperature dependent ϵ values at the lowest temperatures investi-

(25) Actually, the data seem to indicate a slightly negative reaction order, corresponding to a reaction rate which locally decreases with an increase in reactant concentration.

(26) G. Ervin, Jr., *J. Amer. Ceram. Soc.*, **41**, 347 (1958); see also G. Ervin, Jr., "Oxidation of Uranium Monocarbide at High Temperatures and Low Pressures" in Proceedings of the Third International Symposium on High Temperature Technology, Butterworths and Co., Ltd., London, 1969.

(27) As an important corollary, this result, together with Figure 2, reveals that in the O- N_2 mixture formed by titrating N atoms with NO (see section 2), the contribution of N_2 to the attack of silicon carbide is likewise negligible compared with that of O atoms. In contrast, Figure 2 also reveals that if O atoms were directly produced by the microwave dissociation of the parent molecule O_2 , one could not neglect the O₂ contribution to the reactivity of the resulting discharge products.

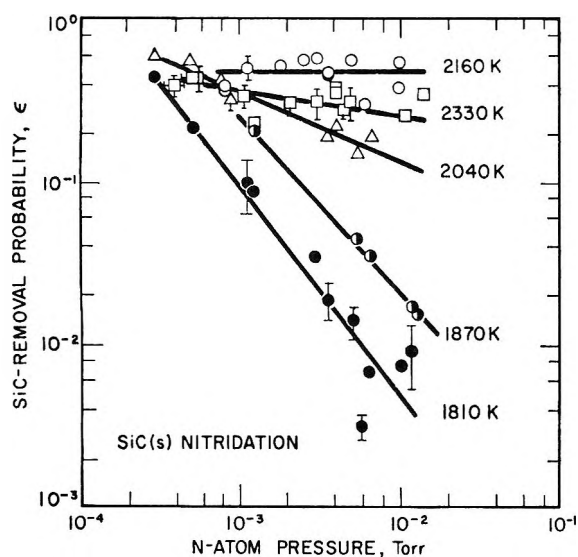


Figure 6. Dependence of silicon carbide nitridation probability on N-atom pressure.

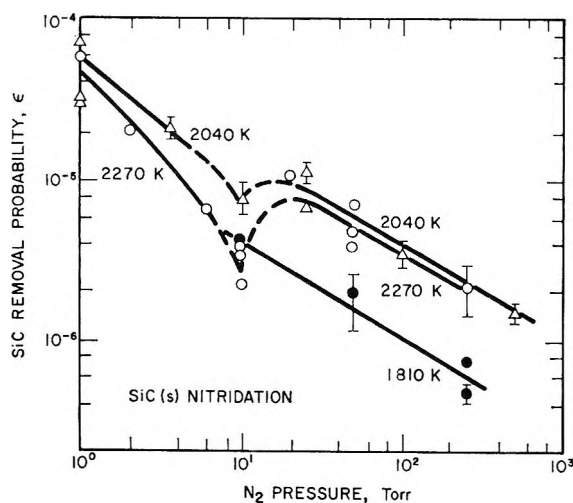


Figure 7. Dependence of silicon carbide nitridation probability on N_2 pressure.

gated (*e.g.*, $E \approx 200$ kcal/mol for $p_N = 3.5 \times 10^{-3}$ Torr, $1750 \leq T \leq 1850^\circ\text{K}$) to a weakly temperature dependent ϵ "plateau" at higher temperatures (1900 – 2200°K for $p_N = 3.5 \times 10^{-3}$, $p_{N_2} = 5 \times 10$ Torr) and finally to a region of $d\epsilon/dT < 0$ (negative E) at sufficiently high temperatures ($T \geq 2300^\circ\text{K}$, for the cases investigated). As will be discussed later on, it is probably significant that in the high E (low T) portion of the Arrhenius plots, while the ϵ values are widely disparate, the ϵp_i values ($i = N, N_2$) are comparable for the N and N_2 reactions, corresponding to similar absolute (Si, C)-atom removal rates despite the widely different reactant pressures employed. Turning to the dependence of nitridation probability on nitrogen pressure, our results for the $\text{SiC(s)} + \text{N(g)}$ reaction (*cf.* Figure 6) reveal a gradual transition from nearly zero-order behavior at 1810°K to first-order behavior at

2160°K . However, in contrast to the corresponding O-atom reaction (*cf.* Figure 3), there appears to be no identifiable and temperature-dependent threshold pressure delineating this reaction-order transition. The $\text{SiC(s)} + \text{N}_2(\text{g})$ reaction generally exhibited fractional order behavior²⁸ at all temperatures studied (*cf.* Figure 7).

4. Discussion

While supplementary data (*e.g.*, on product vapor distributions) should ultimately prove useful in understanding further details of the complex reaction mechanism, the present macroscopic kinetic data already provide information of immediate practical significance and valuable clues concerning microscopic events at the gas-solid interface. To be able to anticipate the effects of environmental conditions not explicitly studied here, or predict the kinetic behavior of related silicon-containing refractory materials in dissociated oxygen and/or nitrogen, it is useful to try to reconcile the observed behavior with available thermodynamic, structural, and kinetic data for Si-C-O-N and closely related chemical systems. In this way we also hope to define fruitful areas for future experimentation and kinetic analysis.

Relation to Previous Studies. Available free-energy data¹³ and Table I (itemizing bond energies in the

Table I: Matrix of Bond Dissociation Energies^a in the Si-C-O-N System

	Si	C	O	N
Si	79.7	103 ^b	184	104
C	103 ^b	142	256	165
O	184	256	118	150
N	104	165	150	225

^a Unless otherwise specified, each value tabulated is the dissociation energy D_0° , for the diatomic gas molecule (radical) in the gas phase (expressed in kcal/mol), as calculated from data given in ref 13. ^b D_0° taken from ref 29.

Si-C-O-N system) reveal that the oxidation of silicon carbide is thermodynamically favorable at all temperature levels considered here, for either $\text{O}_2(\text{g})$ or O(g) as the reactant. Most available data on the *rate* of the reaction between SiC and $\text{O}_2(\text{g})$ pertain to p_{O_2} - T conditions such that there was a continuous net weight *gain* of the (crystalline powder or sintered) specimen due to the formation-accumulation of thick silica surface layers^{26,30} outweighing the mass loss contribution due to CO(g) , $\text{CO}_2(\text{g})$ formation-evolution. In this regime the kinetics are frequently well described

(28) Except for anomalous behavior evident near $p_{N_2} = 10$ Torr, which will bear further investigation.

(29) See also, P. Grieveson and C. B. Alcock, "Special Ceramics," A. Popper, Ed., Academic Press, Inc., New York, N. Y., 1960, p 183.

(30) R. F. Adamsky, *J. Phys. Chem.*, **63**, 305 (1959).

by a film growth law of the simple "parabolic" form³¹: $\delta^2 = 2k_p(T; p_{O_2})t$ (where δ is the product film thickness at exposure time t , and k_p is the corresponding "parabolic rate constant"). However, in recent investigations covering the temperature range 1423–1673°K, Gulbransen, Andrew, and Brassart¹⁴ employed oxygen pressures low enough to enter a continuous weight loss regime, within which the silicon carbide surface was apparently considered free of an SiO₂(c) film, due to the rapid volatilization and removal of silicon oxides. Unfortunately, their weight loss data in this (so-called "active") regime revealed that the observed reaction rates were limited by vapor phase transport near the high temperature sample. Indeed, a modification of Wagner's theory of the active-passive transition in silicon-containing diffusion-limited systems³² (see below) was reported to be in approximate accord with the observed p_{O_2} - T locus of incipient weight loss. In sharp contrast, the present chemically controlled measurements for the SiC(s) + O₂(g) and SiC(s) + O(g) reactions in the weight loss regime will be used (below) to demonstrate that (a) the condition of quasi-steady weight diminution is *not* to be equated with the absence of condensed reaction product films; (b) *within* the weight loss regime there is a kinetic transition from "bare-surface" to condensed product film behavior which is, more aptly, the true "active-passive" transition; (c) *thermodynamic* considerations alone cannot provide even a reasonable first approximation to the p_i - T location of this transition ($i = O, O_2$); and, finally (d) its p_i - T location and the behavior of the true reaction probabilities, ϵ , within each p_i - T domain, are markedly influenced by the substitution of O(g) for O₂(g).

With respect to the nitridation of silicon carbide, the available literature is sparse indeed. In Brown's useful review¹² of the mechanical, electrical, and chemical properties of SiC one finds the statement that above 1673°K SiC(s) decomposes in N₂ ($p = 1$ atm?) to yield silicon nitrides and cyanogen, yet available thermochemical data¹³ reveal positive standard free-energy changes for this reactant-product combination in the temperature range of interest here. Similar estimates for the reactant atomic nitrogen reveal that this N₂ → N substitution makes the nitridation reaction thermodynamically favored ($\Delta F^\circ < 0$), especially for the case of simple product vapors (*e.g.*, SiN(g) + CN(g)).³³ In this chemical system the potential reaction product Si₃N₄(s) is itself a relatively stable refractory substance,³⁴ however its equilibrium dissociation pressure at the high temperature levels of interest here (1800–2400°K) becomes appreciable (in fact $p_{N_2,eq} = 1$ atm at $T \approx 2073^\circ\text{K}$). This overall situation, and the potential practical importance of SiC (s) reactions in dissociated air (or nitrogen), motivated the nitridation kinetic experiments³⁵ outlined in the previous section and discussed below.

Condensed Product Film Regime. Despite the fact that all of the present measurements pertain to the quasi-steady weight loss regime (constant rate of specimen diameter decrease), in the "low" T -high p_i conditions examined here we find kinetic evidence for the existence of steady-state product films, *viz.* low and extremely temperature-dependent reaction probabilities, and low (even negative) reaction orders. The principal features of such a regime can best be understood by considering the simplest case of a material which ordinarily forms a "scale" at the rate $(d\delta/dt)_{form} = k_p/\delta$ when evaporation (sublimation) of the scale is negligible, and at the net rate $d\delta/dt = (k_p/\delta) - (d\delta/dt)_{evap}$ when evaporation of the scale is appreciable (*e.g.*, at higher temperatures)[where $(d\delta/dt)_{evap}$ is the evaporative contribution (assumed below to be independent of the scale thickness itself)]. Under the latter conditions the differential equation for $\delta(t)$ reveals that a steady-state product-film thickness, $\delta_{ss} = k_p/(d\delta/dt)_{evap}$, would be approached after a time interval of the order of $k_p/(d\delta/dt)_{evap}^2 \equiv \tau$ (*e.g.*, when $t = \tau$, $\delta = 0.7\delta_{ss}$). Before this time has elapsed the specimen would initially grow in size, but, for $t \gg \tau$, $d\delta/dt \rightarrow 0$ and the overall specimen diameter would decrease at the constant rate $2(d\delta/dt)_{evap}$. It seems likely that this latter period is being observed in high E -low n kinetic regime encountered here (*e.g.*, for the oxidation of SiC(s)); hence, for this regime we write

$$(d\delta/dt)_{evap} = 1/2(\Delta d/\Delta t)_{obsd} = p_i^n A \exp(-E/RT) \quad (2)$$

where $A \approx$ constant. Therefore, if the parabolic rate constant measured under conditions of negligible scale evaporation can be extrapolated using the familiar form³¹

$$k_p = p_i^n A_p \exp\left(-\frac{E_p}{RT}\right) \quad (3)$$

it follows that for each data point in the "passive"

(31) See, *e.g.*, P. Kofstad, "High Temperature Oxidation of Metals," John Wiley and Sons, New York, N. Y., 1966. A discussion of the complicating effects of scale evaporation, similar to that presented below, has been given by C. E. Birchenall, "Kinetics of High Temperature Processes," W. D. Kingery, Ed., Technology Press, M.I.T., 1959, *cf.* Chapter 32.

(32) C. Wagner, *J. Appl. Phys.*, **29**, 1295 (1958).

(33) As noted below, one must also remain alert to the possible existence of as yet undiscovered or uncharacterized stable product molecules, especially in ternary systems (see below).

(34) J. M. Blocher, Jr., "High Temperature Materials and Technology," I. E. Campbell and E. M. Sherwood, Ed., John Wiley and Sons, New York, N. Y., 1967, p 379; see also, N. L. Parr and E. R. W. May, "Nuclear and Engineering Ceramics," Proceedings No. 7, British Ceramic Society, 1967, p 81.

(35) Studies of the nitridation kinetics of Si(s) (*cf. e.g.*, the experiments of J. W. Evans and S. K. Chatterji, *J. Phys. Chem.*, **62**, 1064 (1958), who worked at $p_{N_2} \approx 1.5$ Torr, $1481 \leq T \leq 1645^\circ\text{K}$, and R. G. Frieser, *J. Electrochem. Soc.*, **115**, No. 10, 1092 (1968), who worked at $p_{N_2} = 760$ Torr, $1423 \leq T \leq 1648^\circ\text{K}$) have revealed a strongly decelerating ("logarithmic") growth rate of dense Si₃N₄ films, which precludes the complete nitridation of large diameter silicon particles in a reasonable length of time.

regime one can assign a quasi-steady film thickness, δ_{ss} , and "induction time," τ , according to

$$\delta_{ss} = p_i^{(n_p - n)} (A_p/A) \exp[(E - E_p)/(RT)] \quad (4)$$

and³⁶

$$\tau = p_i^{(n_p - 2n)} (A_p/A^2) \exp[(2E - E_p)/(RT)] \quad (5)$$

In the usual case $n \leq 0 \leq n_p$ and $E \gg E_p$, hence, the steady-state product-film thickness would decrease sharply with increased temperature level, and increase with increased reactant pressure (as $p_i^{(n_p - n)}$). While these relations certainly oversimplify a more complex reality, they at least indicate the role of product film vaporization kinetics in governing the observed reaction rate (via specimen surface recession) and (when the parabolic kinetics assumption is relaxed) even suggest a correlation for the p_i - T locus separating product-film behavior (low ϵ , high E , low n) from bare surface behavior (see below).

At the present time it does not appear to be possible to quantitatively relate the observed values of ϵ , E , and n in the "passive" regime to independently determined kinetic parameters for the sublimation of any of the eligible condensed phases (*e.g.*, SiO_2 , Si_3N_4 , SiO_4C_4 , etc.).³⁷ Many qualitative features are in fact those expected for the dissociative sublimation of condensed phases³⁸—most notably the suppression in sublimation rate due to O_2 impingement.³⁹ Based on the behavior of simpler chemical systems one can speculate that the higher steady-state coverage of adsorbed oxygen in the presence of O-atom bombardment probably retards lattice bond breaking at defects in the product film surface, leading to the interesting reversal shown in Figure 2, *viz.* *SiC can react much more rapidly in $\text{O}_2(\text{g})$ than $\text{O}(\text{g})$ [below 1900°K at $p_i \approx 10^{-2}$ Torr, $i = \text{O}, \text{O}_2$].* Indeed similar "reversal" behavior would seem likely for other important silicon-containing refractory materials, an expectation which would be of practical as well as fundamental interest.

In one respect the present results are similar to our earlier results on the oxidation of boron,⁴ *viz.* low and sharply temperature-dependent apparent reaction probabilities are ultimately observed ($\epsilon < 10^{-2}$) (even for atomic oxygen) in the product-film regime. However the evaporation of boric oxide, being less complex than the product compounds considered here, led to simpler and thermodynamically predictable E behavior. In either case the low values of ϵ observed in this regime are indicative of low adsorption (sticking) probabilities on product-film surfaces, *i.e.*, most incident atoms or molecules are simply returned to the gas phase chemically unmodified and hence do not participate in the bond formation-rupture processes leading to surface recession.

Bare Surface Regime. The previous considerations suggest that (for any reactant pressure) "bare surface" behavior should be achieved at sufficiently high tem-

peratures. References to Figures 2 and 5 indeed reveals a high temperature transition to qualitatively different, plateau like behavior of ϵ on the Arrhenius plane (above $\approx 1900^\circ\text{K}$ for most cases investigated here). With the exception of our $\text{N}_2(\text{g})$ results, reaction probabilities in this "active" regime are quite high ($\epsilon > 10^{-1}$), weakly temperature dependent, and nearly independent of reactant pressure (*i.e.*, $n \approx 1$); presumably revealing the low-coverage, high temperature kinetic behavior of SiC-crystal planes exposed to incident atom or molecule fluxes.⁴⁰ Despite the fact that the SiC lattice should tend to lose its silicon atoms at these temperatures (*cf.* the equilibrium silicon vapor pressures over SiC, Table II)^{13,29} and is known to form carbon-rich surface layers when heated in argon or *in vacuo*, all high temperature reaction probabilities reported here far exceed those previously reported for

Table II: Equilibrium Silicon Vapor Pressures over Crystalline Silicon Carbide^a

p_{Si} , Torr	Temp., °K
10^{-4}	1794
10^{-3}	1924
10^{-2}	2075
10^{-1}	2252
10^0	2461

^a Based on the least-squares correlation equation of Grievson and Alcock²⁹ (1960) for $\text{SiC}(\beta)$; temperatures corresponding to the stated silicon pressure over $\text{SiC}(\alpha)$ are within 3°K of the values for $\text{SiC}(\beta)$ tabulated here.

(36) This model is intended to be only illustrative of the product film continuous weight loss regime; however, it is interesting to combine the present "passive" regime data with available data on k_p (extrapolated) to infer absolute film thicknesses and induction times. For example, if one uses the data of J. T. Law (see *J. Phys. Chem.*, **61**, 1200 (1957), giving $n_p \approx 1.6$, $E_p = 36$ kcal/mol) for SiO_2 growth on Si (s), and assumes $k_p(\text{O}_2/\text{SiC}) \approx (1/2)k_p(\text{O}_2/\text{Si})$ one finds $\delta_{ss} = 42 \text{ \AA}$ and $\tau = 0.55$ sec for $T = 1800^\circ\text{K}$, $p_{\text{O}_2} = 3 \times 10^{-2}$ Torr. While the inferred values of δ_{ss} and τ depend sensitively on the particular k_p data being extrapolated, it is clear that over most of the range explored here the inferred oxide films would be sub-microscopic and achieve their quasi-steady thicknesses in a time small compared to our observation times ($\Delta t > 1$ min). Clearly, the assumptions underlying the parabolic film growth law break down for sufficiently thin product films³¹—a fact which must be taken into account when extrapolating eq 4, and in analyzing the environmental conditions under which the surface passes from a "passive" (film-covered) state to an "active" (relatively film-free) state (see below).

(37) Fundamental evaporation kinetic studies for these compounds are evidently not available (even in the absence of simultaneous oxygen or nitrogen impingement).

(38) See, for example, G. A. Somorjai and J. E. Lester, "Progress in Solid State Chemistry," H. Reiss, Ed., Pergamon Press, Oxford, 1967, p 1.

(39) However, the present "passive" regime reaction probabilities are about an order of magnitude higher than would be expected for the sublimation of pure, continuous $\text{SiO}_2(\text{c})$ films under the imposed O_2 pressure. This probably indicates the simultaneous importance of $\text{SiO}_2(\text{c})$ reduction reactions at the $\text{SiO}_2(\text{c})/\text{SiC}(\text{s})$ interface.

(40) J. A. Dillon (in "Silicon Carbide—A High Temperature Semiconductor," J. T. O'Connor and J. Smiltens, Ed., Pergamon Press, Oxford, 1960, p 235) has reported an initial (zero-coverage) sticking probability of 10^{-2} for O_2 on the (0001) face of α -SiC at 300°K .

the attack of graphite by O(g),^{7,8} O₂(g),^{7,8} and N(g).⁴¹ This suggests that the surface carbon atoms are left in more "vulnerable" positions by the instability of the SiC surface layer at these temperatures, and/or silicon itself contributes to carbon atom removal through the formation-desorption of Si-C-O or Si-C-N ternary compounds. It is interesting to note that, if only CO(g) and SiO(g) were produced, the inferred atomic oxygen reaction probabilities above $\approx 2200^\circ\text{K}$ would exceed the corresponding "theoretical maximum" (1/2), again suggesting the existence of ternary products, or that it may be sufficient for the oxygen atoms to remove surface C atoms, thereby facilitating Si atom removal *via* sublimation. Similar remarks apply to the high temperature N-atom/SiC reaction, which would appear to be the most efficient N-atom/solid reaction yet studied. Also noteworthy is the drastic difference in the effect of reactant dissociation for oxygen and nitrogen at high surface temperatures (*cf.* Figures 2 and 5). In the former case ϵ is large even for O₂(g) (indicating a high sticking probability, $s \gtrsim 0.2$, for O₂ on nearly bare SiC).⁴² In contrast, Figure 5 suggests a very large difference in sticking probability between N and N₂ due, presumably, to the difficulty of dissociating N₂ (*cf.* Table I) and the low resulting binding energies for N atoms. By analogy with other gas-solid reactions at surface temperatures high enough to desorb atoms before they have had a chance to further react with the adsorbent,^{6,31} the ϵ maximum and regime of $d\epsilon/dT < 0$ ($E < 0$) for the SiC(s) + N(g) and SiC(s) + N₂(g) reactions is attributed here to appreciable N-atom desorption above $\approx 2200^\circ\text{K}$ (or, equivalently, insufficient N-atom residence times on the SiC surface).

p_i-T Locus at the Active-Passive Transition in Chemically Controlled Dissociated Gas Systems. It is tempting to try to "explain" the observed transition behavior using thermochemical data for the important vapor phase molecules and macroscopic condensed phases present. Wagner³² has outlined how this may be done for the oxidation of silicon in (the limiting) case O₂(g) transport to the surface is diffusion controlled. When the steady-state concentration of SiO(g) established at the reacting interface exceeds that corresponding to the equilibrium $\frac{1}{2}\text{SiO}_2(\text{c}) + \frac{1}{2}\text{Si}(\text{c}) \rightleftharpoons \text{SiO}(\text{g})$ condensed silica layers are considered feasible. This leads to a relation of the form

$$p_{\text{O}_2, \infty}^* \approx \frac{1}{2}(D_{\text{SiO}}/D_{\text{O}_2})^{1/2} K_p(T^*) \quad (6)$$

where $p_{\text{O}_2, \infty}$ is the oxygen pressure far from the specimen, K_p is the equilibrium constant for the reaction written above, D_{SiO} and D_{O_2} are, respectively, the Fick coefficients for molecular diffusion of SiO(g) and O₂(g) through the prevailing gas mixture and the asterisks denote the threshold condition of condensed film feasibility. Gulbransen, Andrew, and Brassart¹⁴ modified this approach to apply to SiC, by calculating

the ambient oxygen pressure at which p_{SiO} at the gas-solid interface corresponds to the equilibrium reaction $\text{SiC}(\text{s}) + 2\text{SiO}_2(\text{s}) \rightleftharpoons 3\text{SiO}(\text{g}) + \text{CO}(\text{g})$. However, while apparently successful for the diffusion-limited oxidation of silicon-containing materials it is clear that this procedure would be inappropriate for reactions which are kinetically controlled, and for which, *a fortiori*, diffusion coefficient ratios should have no bearing on the threshold condition.

A possible variant of this thermodynamic approach, based instead on our *observed* oxidation probabilities in the bare surface regime, would be the following. If it is assumed that SiO(g) and CO(g) are the dominant reaction products, then it would follow that $\dot{Z}''_{(\text{Si,C})} \approx \dot{Z}''_{\text{SiO}} \approx \dot{Z}''_{\text{CO}}$. But since these "observed fluxes" correspond to "effective" SiO and CO pressures at the gas-solid interface [in accord with the Hertz-Knudsen law (eq 1)], the condition that $p_{\text{CO,eff}} p_{\text{SiO,eff}}^3 = K_p(T)$ for the reaction $\text{SiC}(\text{s}) + 2\text{SiO}_2(\text{c}) \rightleftharpoons 3\text{SiO}(\text{g}) + \text{CO}(\text{g})$ can be written

$$p_i^* = \frac{1}{\epsilon_i^*} \left[\left(\frac{m_i}{m_{\text{SiO}}} \right)^{3/2} \left(\frac{m_i}{m_{\text{CO}}} \right)^{1/2} \right]^{1/4} [K_p(T^*)]^{1/4} \quad (7)$$

where $i = \text{O}$ or O₂. Since the bare surface (plateau) values of ϵ are weakly temperature dependent and not very dissimilar (*cf.* Figure 2), this approach leads to the expectation that $\log p_i^*$ would be (a) nearly linear in $1/T$, with a slope corresponding to about $(1/4)\Delta H^\circ \approx 83$ kcal/mol (where ΔH° is the standard enthalpy change across the above-mentioned reaction) for both the O(g) and O₂(g) oxidations; (b) of the same order of magnitude for both O(g) and O₂(g) over a wide temperature range, with p_{O}^* and $p_{\text{O}_2}^*$ standing in the approximate ratio $\approx (m_{\text{O}}/m_{\text{O}_2})^{1/2} (\epsilon_{\text{O}_2}^*/\epsilon_{\text{O}}^*) \approx (1/2)^{1/2} (0.2/0.3) \approx 0.5$. Estimates of our *observed* $p_i^*-T^*$ locus, obtained directly from Figures 3 and 4 are shown in Figure 8, where it should be recognized that the transition is not really abrupt, especially for the O₂ reaction.⁴³ One notices that, contrary to the prediction of eq 7, at all temperatures below $\approx 2100^\circ\text{K}$ passive behavior sets in at a much lower reactant pressure for O(g) than O₂(g), with the difference exceeding two orders of magnitude at the lowest temperatures investigated here. While the slope of the O₂ locus happens to correspond approximately to the above-mentioned 83 kcal/mol, the O-atom locus is much steeper (by ≈ 2.5 -fold). Moreover, the actual threshold O₂ pressure (*e.g.*, at 2000°K) is lower than that predicted by eq 7 by about

(41) H. W. Goldstein, *J. Phys. Chem.*, **68**, 39 (1964).

(42) Compare the similar high temperature reaction probabilities observed here for O and O₂ on SiC (see Figure 2) with the large enhancement produced by dissociation for the boron-oxygen,⁴ silicon-oxygen, and germanium-oxygen reactions (*cf.* R. J. Madix, G. Melin, and A. Susu, Second International Symposium on Molecular Beams, in press) below their respective melting points.

(43) It should be remarked that the reported $p_{\text{O}_2}^*$ is not very different from the oxygen pressure giving maximum absolute reaction rate ($\dot{Z}''_{(\text{Si,C})}$) at the temperature T^* (*cf.* Figure 4).

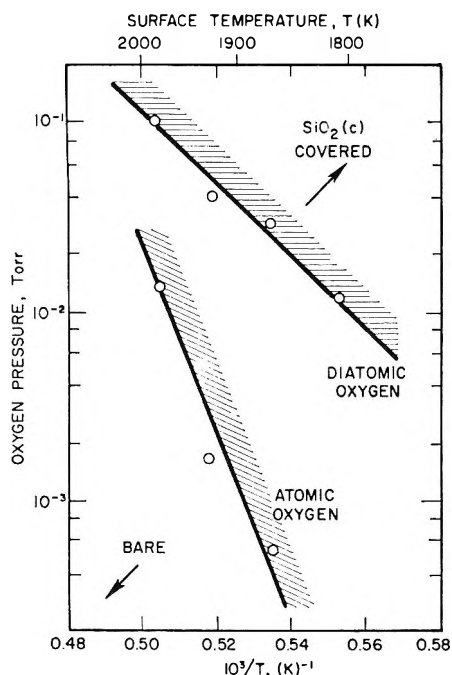


Figure 8. Approximate reactant pressure-temperature locus for the kinetic transition from bare ("active") surface behavior to semi-protective ("passive") condensed product surface behavior; oxidation of pyrolytic silicon carbide.

four orders of magnitude! We conclude that this quasi-thermodynamic approach fails to account for the observed p_i - T location of the active-passive transition in this chemically controlled system ($i = \text{O}, \text{O}_2$).⁴⁴

An alternative approach to the rationalization of p_i^* - T^* at the passive-active transition is suggested by generalizing our earlier discussion of the film-forming regime in the presence of evaporation. It seems reasonable to assume that transition behavior will set in when the steady-state film thickness, δ_{ss} , approaches some threshold value, δ^* , of molecular dimensions (see Figure 9). Since $(d\delta/dt)_{\text{form}}$ at $\delta = \delta^*$ is simply related to the reported bare surface reaction probability, ϵ_i^* , it then follows that, if ϵ_i^* is insensitive to reactant pressure and temperature, then the condition $\delta_{ss} \rightarrow \delta^*$ implies that p_i^* will have a slope corresponding approximately to $E/(1-n)$ kcal/mol in Figure 8. Since E is comparable for both O and O_2 attack in the passive range, we see that the difference in slopes in Figure 8 is essentially a consequence of the difference in reaction orders for the passive range. Summarizing, we may say that an understanding of the active-passive transition hinges on our knowledge of oxygen sticking probabilities in the active regime and the kinetics of product evaporation in the passive regime.⁴⁵ Since dissociation can influence the kinetics in both regimes it follows that dissociation can strongly influence the effective p_i^* - T^* location of the active-passive transition. In the present case (oxygen-silicon carbide) it appears that the dominant effect accounting for the observed loci is the marked difference in SiO_2 sublima-

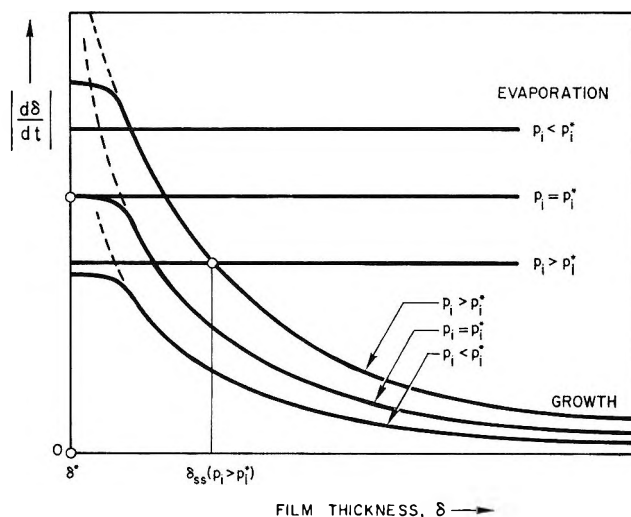


Figure 9. Competition between scale formation kinetics and scale evaporation kinetics in determining steady-state oxide scale thickness. Implications of the incipient condition $\delta_{ss} \rightarrow \delta^*$.

tion kinetics in dissociated and undissociated oxygen. Thus, dissociation significantly enlarges the p_i - T domain of product film behavior (cf. Figure 8) for $\text{SiO}(\text{s})$, and, very likely, for other silicon-containing refractory materials of interest in aerospace applications.⁴⁶

The corresponding situation for the nitridation of $\text{SiC}(\text{s})$ is less clear and will require experiments over a wider range of p_i - T conditions to define. However, our N-atom data (Figure 5) do suggest more gradual transition behavior than in the corresponding O-atom case.

Behavior of $\text{SiC}(\text{s})$ in $\text{N} + \text{O}$ Mixtures. While a discussion of the kinetic effects of reactant gas mixtures is beyond the scope of the present paper, it is relevant to mention here that the reactivity of $\text{SiC}(\text{s})$ in $\text{N} + \text{O}$ mixtures is rather unusual in that the reaction rate in nearly equimolar $\text{N} + \text{O}$ mixtures is less than would be expected from the individual N and O "contributions" (based on the data of Figures 2, 3, 5, and 6) by more than one order of magnitude, provided the temperature level is sufficiently low (e.g., $T < 2000^\circ\text{K}$ for $p_{\text{N}} = p_{\text{O}} = 0.5 \times 10^{-2}$ Torr). This poten-

(44) Surprisingly enough, C. Gelain, A. Cassuto, and P. LeGoff (in "Kinetics and Mechanism of Low Pressure and High Temperature Oxidation of Silicon," "Oxidation of Metals," Plenum Press, New York, N. Y., in press) report that a procedure equivalent to this is successful for the $\text{O}_2(\text{g})/\text{Si}(\text{s})$ reaction.

(45) J. L. Falconer and R. J. Madix (private communication, Sept 1969), who have independently come to a similar conclusion, attempt to predict the $p_{\text{O}_2^*}$ - T^* locus for silicon and germanium based on transition state theory applied to the sublimation process. As presently formulated, however, it appears that their method does not anticipate the strong oxygen impingement effects on product sublimation kinetics observed here.

(46) This phenomenon may be important in the design of silicide-coating systems for refractory metals¹⁶ exposed to dissociated air. Possible new effects due to the simultaneous presence of atomic nitrogen are indicated below.

tially important "coupling" phenomenon is discussed in ref 47, and attributed to the *in situ* formation of condensed *silicon oxynitride* surface films, with growth, stability, and evaporation behavior differing markedly from either $\text{SiO}_2(\text{c})$ or $\text{Si}_3\text{N}_4(\text{c})$.

5. Conclusions

Based on the experimental data reported herein and the discussion above, the following conclusions have been drawn. (1) The present experimental technique, employing a microwave discharge, a fast-flow subatmospheric system, and resistance-heated specimens in filament form, lends itself to the kinetic study of high temperature reactions of pyrolytic silicon carbide in well-defined streams of atomic oxygen and atomic nitrogen, as well as their diatomic counterparts. Chemically controlled kinetic data have been obtained in the regime of continuous specimen weight loss (hence filament diameter reduction) due to reaction product volatilization at constant (time-independent) rates. (2) $\text{O}(\text{g})$, $\text{O}_2(\text{g})$, and $\text{N}(\text{g})$ can chemically attack silicon carbide surfaces with extremely high reaction probabilities ($\epsilon > 10^{-1}$) provided the surface temperature is high enough and/or reactant arrival rate low enough to preclude the occurrence of semi-protective $\text{SiO}_2(\text{c})$ or $\text{Si}_3\text{N}_4(\text{c})$ product films. In this regime the true reaction probability is nearly independent of surface temperature and reactant pressure. In contrast, N_2 reaction probabilities are low even on relatively bare SiC. (3) At sufficiently low surface temperatures and/or high reactant pressures all reaction probabilities remain time independent (after an initial transient) but become low ($\epsilon < 10^{-2}$) and sharply temperature dependent. In this regime it appears that the rate-limiting step becomes the dissociative evaporation of steady-state condensed product films, in the presence

of an imposed reactant flux. This leads to activation energies which exceed the equilibrium heats of dissociative sublimation and true overall reaction orders which can be negative. Kinetic evidence for the existence of such films even within the presently studied regime of continuous weight loss demonstrates that continuous weight loss (or diameter reduction) cannot be used as a criterion for a "bare" (or "active") surface. (4) Reactant dissociation (*e.g.*, replacing $\text{O}_2(\text{g})$ by $\text{O}(\text{g})$) considerably extends the reactant pressure/temperature domain characterized by the presence of semi-protective condensed product films. Thus, the so-called active-passive transition for SiC oxidation by $\text{O}(\text{g})$ is shown to occur at lower oxygen pressures (at all surface temperatures lower than about 2100°K), this effect amounting to a 100-fold oxygen pressure reduction at about 1800°K . A quasi-thermodynamic criterion of the type successful in describing the oxygen pressure/temperature location of the active-passive transition in diffusion-limited silicon-containing systems fails to account for the location of this transition in the present chemically controlled case. Alternatively, an approach involving kinetic parameters describing reactant chemisorption and the evaporation of condensed product films appears more promising.

Acknowledgments. We wish to thank A. D. Freda and A. Marsh for their assistance in carrying out these experiments, Dr. A. Fontijn for his advice on the generation and detection of atomic species, and Dr. J. Berkowitz-Mattuck, Dr. R. J. Madix, Dr. R. Heckingbottom, and Dr. S. C. Kurzius for their helpful correspondence and/or comments. Revision and publication of this manuscript was supported in part by AFOSR Contracts F44620-70-C-0026, AF 49 (638)-1654.

(47) D. E. Rosner and H. D. Allendorf, *AIAA J.*, **8**, 166 (1970).

A Comparative Study of the Cosolvent Effect in Ethyl Alcohol-Benzene and Isopropyl Alcohol-Benzene Solutions. The Solvolysis of *m*-Fluorobenzoyl Chloride, *m*-Trifluoromethylbenzoyl Chloride, and Anisoyl Chloride

by Thomas F. Fagley, Jonathan S. Bullock, and Dale W. Dycus

Richardson Chemistry Laboratories, Tulane University, New Orleans, Louisiana 70118 (Received October 21, 1969)

A comparative study of the kinetics of solvolysis of *m*-fluorobenzoyl chloride, *m*-trifluoromethylbenzoyl chloride, and anisoyl chloride has resolved the apparently intractable case of anisoyl chloride. The exceptional range of variation of activation parameters with solvent composition in the latter compound is a consequence of extensive solvation; the solvating alcohol species can be distinguished from the reacting species *via* the cosolvent corrections to the kinetic parameters: apparent molal thermodynamic functions account for solvation and partial molal properties for the species involved in the activation step.

Introduction

In this laboratory studies of the "cosolvent effect" in kinetics of reactions in binary solvents have demonstrated that variations in activation parameters with solvent composition can be quantitatively interpreted in terms of the partial molal properties of the reactive component of the solvent pair. The solvolysis of phthalic anhydride in methanol-chloroform,¹ of fluoro-substituted benzoyl chlorides in isopropyl alcohol-benzene,² of phthalic anhydride in water-dioxane,³ and the rearrangement of 2',4'-dinitro-2-aminodiphenyl ether in methanol-carbon tetrachloride⁴ have been satisfactorily so interpreted.

One system has remained intractable to such a treatment: the solvolysis of anisoyl chloride in ethanol-benzene.^{5,6} The partial molal properties of ethanol in benzene are much too small to account for the remarkable range of variation of activation parameters with composition. Kivinen⁶ has suggested that the mechanism may be intermediate between SN1 and SN2, possibly closer to SN1. He also observed that the slope of the log k_1 vs. log (ethanol concentration) plot appeared to approach high values with increasing alcohol concentration, reaching $n = 5$ in pure ethanol.

Comparative studies in two binary solvent systems, reported here, indicate that the much higher degree of solvation of anisoyl chloride in the initial state (as a consequence of favorable resonance) can account for the remarkable range of values for the enthalpy and entropy of activation. In addition, the studies show that thermodynamics can explain these differences in terms of the different cosolvent corrections needed for solvation and the activation steps: apparent molal for solvation and partial molal for the species involved in

the formation of the transition state. This analysis, it seems to us, nicely confirms Hudson's contention⁷ that variations in ΔH^* provide information on the complexities of solvent structure whereas variations in $k(\Delta G^*)$ are related to the structure of the transition state.

Experimental Section

Materials. The spectrograde alcohols, isopropyl and ethyl, and the benzene were purified in the manner previously described.² The benzoyl chlorides (K & K Laboratories) were triply distilled under vacuum as also previously described.² The anisoyl chloride (Eastman Chemical Co.) was recrystallized from the melt and distilled.⁵

Apparatus. The spectrophotometric measurements were conducted in a Beckman DU spectrophotometer with a thermostated cell holder described in a previous publication.³

The conductance measurements were made with a General Radio Model 1615-A capacitance bridge capable of measuring conductances from 10^{-6} to 100μ mhos with 0.1% accuracy and capacitances from 10^{-17} to 10^{-6} F with an accuracy of 0.01% (at 1000 Hz). Conductance as displayed on the bridge was converted into true conductance by an equation supplied by the

- (1) T. F. Fagley and C. R. Brent, *J. Phys. Chem.*, **67**, 2587 (1963).
- (2) T. F. Fagley, G. A. Von Bodungen, J. J. Rathmell, and J. D. Hutchison, *ibid.*, **71**, 1374 (1967).
- (3) T. F. Fagley and R. L. Oglukian, *ibid.*, **73**, 1438 (1969).
- (4) F. W. Balfour and T. F. Fagley, *ibid.*, **72**, 1300 (1968).
- (5) G. L. Bertrand, Dissertation, Tulane University, 1964.
- (6) A. Kivinen, *Ann. Acad. Sci. Fennicae, Ser. AII*, 108 (1961).
- (7) R. F. Hudson, *J. Chem. Soc., B*, 761 (1966).

manufacturer. The 1000-Hz supply was a Hewlett-Packard audiooscillator, Model 1581-A. Null detection was provided by a General Radio Model 1232-A null detector, sensitive to 1.0 μ V. The bridge was connected to the cells *via* a standard three-terminal connector maintained as close as possible to the cell to reduce stray capacitance and pickup of noise to a minimum. Temperature regulation for the conductance cells was provided by an oil bath: an 8 in. \times 8 in. Pyrex jar filled with mineral oil, covered with a wooden top and insulated with fiber padding. A multibladed stirrer fixed by a Teflon gland was connected to a Sargent cone-drive stirring motor *via* a rubber coupling. The motor was fixed on a platform above the bath, through which passed the coaxial cables to the bridge and from which the Beckmann thermometers were suspended. Access holes in the bath top were provided for a 40-W cylindrical incandescent lamp (the switched heating element), a 100-W glass-encased heater (the auxiliary element), a Sargent Model S-81535 mercurial thermoregulator, and the conductance cells. All grounds to the electronic components were made *via* a 6 ft \times 0.75 in. copper earth ground.

The thermoregulator was connected to a Scientific Kit Model 300 solid state relay, whose output was used to operate a secondary relay. This arrangement substantially lowered the noise introduced by the relay system. Heater power was a very low-ripple dc power supply. The regulation achieved with this system was $\pm 0.002^\circ$ at 35° and $\pm 0.003^\circ$ at 45° . There was a constant differential making the cell area temperature lower than the thermometer area temperature by 0.003° at 35° and by 0.020° at 45° . Compensation was made for this.

A variety of conductivity cells was used depending on solvent composition and concentration of substrate; details of construction are described in ref 5 and 8. Since ion-pair formation occurs, the "infinity" solutions at the completion of the kinetic runs at each mole fraction of the binary solvent were used to calibrate, by dilution, the conductivity readings for conversion into concentration units. It was found necessary to age the cells with reactant solution at each mole fraction in the manner suggested by Robertson.⁹ For 10^{-5} – 10^{-6} M acid chloride in ethanol-benzene solutions the conductivity-concentration plots were linear; at higher concentrations curvature was observed. Even with calibration the k 's calculated for anisoyl chloride solvolysis in isopropyl alcohol-benzene solutions were lower than those obtained spectrophotometrically until X_{IPA} reached 0.7. It is believed that in this solvent system a hysteresis effect in the adsorption and desorption of HCl on the walls of the cell, even though the cells were aged with solutions of the same composition, occurred, so that dilution experiments at the completion of a run did not give a true correction. Support of this interpretation was found in plots of log

Table I: Rate Constants for *m*-Fluorobenzoyl Chloride in Ethanol-Benzene

X_{EtOH}	$10^4 k_1$, sec ⁻¹	M^2_{EtOH}	$10^4 k_2$, l. ² mol ⁻² sec ⁻¹
35.00°			
0.1000	1.520 \pm 0.003	1.306	11.638 \pm 0.023
0.2000	3.250 \pm 0.002	5.617	5.786 \pm 0.004
0.3000	5.525 \pm 0.025	13.653	4.673 \pm 0.021
0.4000	8.102 \pm 0.031	26.235	3.088 \pm 0.012
0.5000	11.958 \pm 0.036	44.475	2.689 \pm 0.008
45.00°			
0.1000	2.5334 \pm 0.0008	1.274	19.890 \pm 0.006
0.2000	5.728 \pm 0.003	5.490	10.433 \pm 0.005
0.3000	9.862 \pm 0.009	13.337	7.394 \pm 0.007
0.4000	14.733 \pm 0.009	25.654	5.743 \pm 0.004
0.5000	22.070 \pm 0.031	43.507	5.073 \pm 0.007

($C - C'$) *vs.* log C , where C' is the concentration of HCl calculated from k_{cond} at time t and C is the concentration of HCl calculated from k_{spect} . The plot had the linearity expected for an adsorption process.

Data acquisition was begun about 15 min after the cell had reached thermal equilibrium; at least two and usually three half-lives were covered, with 20 points per half-life. The rate constants for anisoyl chloride in isopropyl alcohol-benzene are recorded in Table VII; those for anisoyl chloride and the fluoro-substituted benzoyl chlorides in ethyl alcohol-benzene are listed in Table XIII and Tables I and II, respectively.

The most striking result of these studies is the remarkable range of ΔH^* and ΔS^* for anisoyl chloride in both ethanol- and isopropyl alcohol-benzene solu-

Table II: Rate Constants for *m*-Trifluoromethylbenzoyl Chloride in Ethanol-Benzene

X_{EtOH}	$10^4 k_1$, sec ⁻¹	M^2_{EtOH}	$10^4 k_2$, l. ² mol ⁻² sec ⁻¹
35.00°			
0.0500	1.27 \pm 0.050	0.2916	43.55 \pm 1.71
0.1000	2.833 \pm 0.001	1.306	21.690 \pm 0.007
0.2000	5.980 \pm 0.002	5.617	10.646 \pm 0.004
0.3000	10.501 \pm 0.006	13.653	7.691 \pm 0.004
0.4000	15.924 \pm 0.035	26.235	6.070 \pm 0.001
0.5000	22.410 \pm 0.018	44.475	5.039 \pm 0.004
45.00°			
0.0500	1.85 \pm 0.047	0.2756	67.13 \pm 1.70
0.1000	4.596 \pm 0.012	1.274	36.075 \pm 0.094
0.2000	10.175 \pm 0.005	5.490	18.534 \pm 0.009
0.3000	18.274 \pm 0.024	13.337	13.702 \pm 0.018
0.4000	28.122 \pm 0.013	25.654	10.962 \pm 0.005
0.5000	39.863 \pm 0.022	43.507	9.156 \pm 0.005

(8) J. S. Bullock, Dissertation, Tulane University, 1969.

(9) R. E. Robertson, "Progress in Physical Organic Chemistry," Vol. 4, Interscience Publishers, New York, N. Y., 1967.

tions. These large changes (7 kcal in enthalpy of activation and some 20 eu in entropy of activation in isopropyl alcohol (IPA)-benzene) cannot be accounted for by the partial molal properties of the alcohol. The effects are even larger in ethanol-benzene.

Through a large range of alcohol (IPA) concentration a slope for the $\log k_1$ vs. $\log C$ plot is 2; the slope becomes smaller at low concentrations until between $X = 0.1$ and $X = 0.2$ the value is 1.43 at 45° and 1.12 at 35°. The ambiguity of the physical significance of such plots has been remarked by many investigators. By itself it remains ambiguous but, in conjunction with other data establishing complex formation or specific solvation of the substrate³ and the thermodynamics of mixing data, it becomes less obscure. For example, in the ethanol-benzene solvent system, at $X_E = 0.4$ and $X_E = 0.5$, the partial molal enthalpies and entropies of ethanol cancel each other in their contributions to $\Delta \ln k = (1/RT)(\Delta \bar{L}_E) - (1/R)\Delta \bar{S}_E$. It is in this region that estimation of the order of the alcohol in the rate expression is least ambiguous; in this region the order is 2; and in this region the calculated k_3 is relatively constant. The usual procedure of determining the order of reactant alcohol by initial rate studies in dilute solution (a procedure used by us and other investigators in the past), we submit, is the least reliable, at least for hydroxylic solvents, for it is in this region that the thermodynamic properties change most rapidly.

In the discussion which follows, therefore, we assume that the activation process is a second-order attack of the acid chloride by the alcohol. Whether the alcohol species be two monomers or a dimer is thermodynamically of no consequence. However, the observations of Van Ness and coworkers¹⁰ and of Wolf¹¹ and of Ibbitson and Moore¹² suggest that the monomeric species is the least likely one. From entropic considerations it is also unlikely. The dimer species, moreover, shows how the formation of the "solvent-separated ion pair" is easily accommodated in the reaction. Justification for solvation of the incipient chloride ion is found in the observations of Allerhand and Schleyer¹³ and, recently, of Green, Martin, McG. Cassie, and Hyne.¹⁴ The former found infrared spectral evidence for hydrogen bonding between methanol and chloride ions of quaternary ammonium salts; the latter investigators found similar nmr evidence for anionic solvation by a number of alcohols. Ashdown¹⁵ found second-order alcohol participation for 29 alcohols in their reaction with *p*-nitrobenzoyl chloride in ether.

The solvolyses of *m*-fluorobenzoyl chloride and *m*-trifluoromethylbenzoyl chloride in isopropyl alcohol-benzene solutions have previously been interpreted² in the above described manner. In ethanol-benzene the same mechanism, involving, presumably, the attack of a dimer at both the carbonyl carbon and at the chlorine (hydrogen bonding) satisfactorily explains the variations in the activation parameters (Tables I-V).

Table III: Corrected k_3 Activation Parameters, *m*-Fluorobenzoyl Chloride in Ethanol-Benzene

X_{EtOH}	ΔH^\ddagger , kcal	$2\bar{L}_{EtOH}$, kcal	ΔH^\ddagger_{cor}
0.1000	9.82 ± 0.09	1.97 ± 0.09	11.79 ± 0.18 ^a
0.2000	10.85 ± 0.04	0.96 ± 0.05	11.81 ± 0.09
0.3000	11.12 ± 0.21	0.53 ± 0.03	11.66 ± 0.24
0.4000	11.47 ± 0.18	0.29 ± 0.03	11.76 ± 0.21
0.5000	11.74 ± 0.17	0.17 ± 0.04	11.91 ± 0.21
		Mean	11.79 ± 0.06 ^b
	ΔS^\ddagger , eu	$\Delta \bar{S}_{EtOH}$	ΔS^\ddagger_{cor}
0.1000	44.74 ± 0.30	4.72 ± 0.50	40.02 ± 0.80 ^a
0.2000	42.77 ± 0.40	2.70 ± 0.30	40.08 ± 0.70
0.3000	42.62 ± 0.90	1.75 ± 0.20	40.86 ± 1.10
0.4000	42.02 ± 0.60	1.21 ± 0.24	40.81 ± 0.84
0.5000	41.41 ± 0.80	0.90 ± 0.18	40.51 ± 0.98
		Mean	40.45 ± 0.33 ^b

^a Maximum estimated error. ^b Deviation from mean.

Table IV: Corrected k_3 Activation Parameters, *m*-Trifluoromethylbenzoyl Chloride in Ethanol-Benzene

X_{EtOH}	ΔH^\ddagger , kcal	$2\bar{L}_{EtOH}$, kcal	ΔH^\ddagger_{cor}
0.0500	7.81 ± 0.25	3.35 ± 0.17	11.16 ± 0.42 ^a
0.1000	9.29 ± 0.11	1.974 ± 0.09	11.26 ± 0.20
0.2000	10.18 ± 0.03	0.960 ± 0.05	11.14 ± 0.08
0.3000	10.63 ± 0.07	0.536 ± 0.03	11.16 ± 0.10
0.4000	10.89 ± 0.02	0.290 ± 0.05	11.18 ± 0.05
0.5000	11.01 ± 0.05	0.170 ± 0.04	11.18 ± 0.09
		Mean	11.18 ± 0.03 ^b
	ΔS^\ddagger , eu	$\Delta \bar{S}_{EtOH}$, eu	ΔS^\ddagger_{cor}
0.0500	48.63 ± 2.0	7.64 ± 0.80	40.99 ± 2.8 ^a
0.1000	45.21 ± 0.90	4.72 ± 0.50	40.49 ± 1.4
0.2000	43.74 ± 0.40	2.70 ± 0.30	41.04 ± 0.7
0.3000	42.93 ± 0.90	1.75 ± 0.20	41.18 ± 1.1
0.4000	42.55 ± 0.40	1.21 ± 0.24	41.33 ± 0.64
0.5000	42.52 ± 0.60	0.90 ± 0.18	41.62 ± 0.78
		Mean	41.11 ± 0.27 ^b

^a Maximum estimated error. ^b Deviation from mean.

For anisoyl chloride the same mechanism—dimer attack in the activation step—attains, but the striking variations in the activation parameters will be demonstrated to be a consequence of extensive solvation induced by resonance. This solvation does not occur in

(10) (a) H. C. Van Ness, J. V. Van Winkle, H. H. Richtol, and H. B. Hollinger, *J. Phys. Chem.*, **71**, 1483 (1967); (b) R. W. Haskell, H. B. Hollinger, and H. C. Van Ness, *ibid.*, **72**, 4534 (1968).

(11) K. L. Wolf, *Trans. Faraday Soc.*, **33**, 179 (1937).

(12) D. A. Ibbitson and L. F. Moore, *Chem. Commun.*, **15**, 339 (1965).

(13) A. Allerhand and P. von R. Schleyer, *J. Amer. Chem. Soc.*, **85**, 1233 (1963).

(14) R. D. Green, J. S. Martin, W. B. McG. Cassie, and J. B. Hyne, *Can. J. Chem.*, **47**, 1639 (1969).

(15) A. A. Ashdown, *J. Amer. Chem. Soc.*, **52**, 268 (1930).

Table V: Correlation of Observed and Predicted Rate Constants at 45° for *m*-Fluorobenzoyl and *m*-Trifluoromethylbenzoyl Chloride in Ethanol-Benzene

ΔX_{EtOH}	$2(\Delta \bar{L}_E)/RT$	$\Delta(\Delta \bar{S}_E)/R$	$-\Delta \ln k_s$ (obsd)		Calcd
			<i>m</i> -Fluoro	<i>m</i> -Tri-fluoro	
0.1-0.5	3.148	1.926	1.316	1.372	1.222
0.1-0.4	2.927	1.766	1.242	1.192	1.160
0.1-0.3	2.450	1.496	0.989	0.969	0.954
0.1-0.2	1.724	1.021	0.645	0.667	0.703
0.1-0.05	-2.061	-1.470	...	-0.621	-0.546

the fluoro compounds, presumably because of the field effect of the fluorine. Evidence for this difference in solvation is found in the heats of solution of the esters, the products of the reaction¹⁶ (Table VI). While the

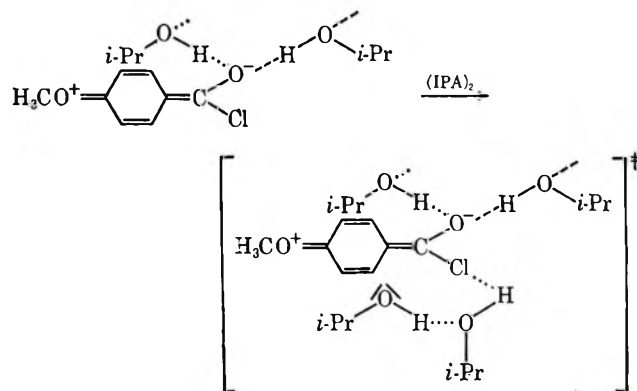
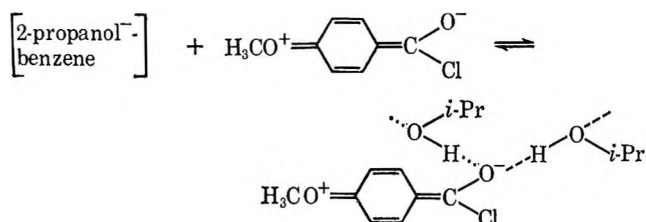
Table VI: Heats of Solution (\bar{L}) in kcal mol⁻¹ of Substrates in Ethanol-Benzene and Isopropyl Alcohol-Benzene Solutions at 25°

X_{ROH}	Substrates in ethanol-benzene			Substrates in IPA-benzene		
	(1) ^a	(2) ^b	(3) ^c	(1) ^a	(4) ^d	(5) ^e
0	0.39	0.06	0.02	0.36	0.82	0.23
0.05	0.19	-0.03	-0.03			
0.1	0.25	0.15	0.05	0.22	0.82	0.31
0.2	0.45	0.25	0.12	0.35	0.82	0.38
0.3	0.55	0.45	0.20	0.51	0.82	0.48
0.4	0.70	0.65	0.35	0.73	0.86	0.58
0.5	0.85	0.85	0.45	0.93	0.94	0.71
0.6	1.05	1.05	0.60	1.21	1.06	0.87
0.7	1.20	1.25	0.75	1.54	1.24	1.08
0.8	1.40	1.40	0.90	1.94	1.46	1.34
0.9	1.65	1.60	1.05	2.44	1.72	1.64
1.0	1.91	1.75	1.26	3.05	2.02	1.97

^a (1), *p*-methoxyacetophenone. ^b (2), ethyl anisate. ^c (3), ethyl benzoate. ^d (4), isopropyl-*m*-trifluoromethyl benzoate. ^e (5), isopropyl *m*-fluorobenzoate.

ethyl anisate product shows an exothermic minimum in ethanol solutions, the esters of the fluorobenzoyl acids, in isopropyl alcohol-benzene, show nearly constant endothermic heats of solution in the same mole fraction region.

The following is proposed as the reaction mechanism



Let C = complex between anisoyl chloride and alcohols at the oxygen. Then

$$\text{rate} = k_{\text{obsd}} \text{RCOCl}$$

$$\text{rate} = kC(\text{i-PrOH})^2$$

$$\text{rate} = k[K(\text{i-PrOH})^2\gamma^2|\text{RCOCl}(\text{i-PrOH})^2]$$

where it is understood that in the part of the expression describing the complex the second-order appearance of *i*-PrOH arises from the fact that two hydrogen bonds to alcoholic species have been formed. The exact nature of the species has not been described; indeed, there are no steric or other requirements on their nature imposed by their participation in the solvation process, except that they may not be cyclic. In contrast, the dimer (which is likely, or, alternatively, two monomers) attacking in the second step is asserted to be fully distinguished from other alcohols.

From absolute rate theory the rate constant for such a reaction may be written as

$$k_5 = \frac{k_B T}{h} e^{-\Delta G^\ddagger/RT}$$

where

$$k_5 = \frac{k_{\text{obsd}}}{(\text{i-PrOH})^4} = kK\gamma^2 \quad (1)$$

Since $\Delta G^\ddagger = \Delta H^\ddagger - T\Delta S^\ddagger$, the enthalpy of activation may be obtained by differentiation of

$$\ln \left(\frac{k_5}{T} \right) = \frac{-\Delta G^\ddagger}{RT} + \ln \frac{k_B}{h}$$

with respect to $(1/T)$, obtaining

$$\Delta H^\ddagger = -R \frac{d \ln (k_5/T)}{d(1/T)}$$

and

$$\Delta S^\ddagger = \frac{\Delta H^\ddagger - \Delta G^\ddagger}{T}$$

(16) J. D. Hutchison, Dissertation, Tulane University, 1966.

the equilibrium constant of which is K , followed by

The γ of eq 1 must be defined. Formally, the term γ must be included in order that when the operation

$$-R \frac{d \ln (k_5/T)}{d(1/T)}$$

is performed the nonideality of the polymer groups complexing to the carbonyl oxygen be described by an enthalpic term. It is asserted that $\gamma = \gamma_\phi$ is defined by

$$\phi G^e = \phi L - T\phi S^e = -RT \ln \gamma_\phi$$

where ϕ is the usual symbol to represent apparent molal properties and ϕS^e represents apparent excess entropy. Therefore

$$-R \frac{d \ln \gamma_\phi}{d(1/T)} = \phi L$$

A full differentiation of eq 1 yields, therefore

$$\Delta H^\ddagger_{ks} = \Delta H^\ddagger + \Delta H_c^c - 2\phi L_2$$

where ΔH_c^c is the standard enthalpy of formation of the complex and ϕL_2 is the relative apparent molal enthalpy of the 2-propanol. Since k is solvent dependent, its enthalpy of activation ΔH^\ddagger can be written as

$$\Delta H^\ddagger_{ks} = \bar{H}^\ddagger - \bar{H}_a - 2\bar{L}_2 + \Delta H_c^c - 2\phi L_2 \quad (2)$$

where \bar{H}^\ddagger and \bar{H}_a are the molar enthalpies of activated complex and acid chloride, respectively. Since the reference state is pure alcohol and $\bar{L}_2 = \bar{H}_2 - \bar{H}_2^*$, \bar{L}_2 has been used to represent the molar enthalpy of alcohol.

The $2\phi L_2$ term arises because of the undefined nature of the solvating species. The enthalpy change of the process of unmixing the solvating species is dependent on the size of the species and its degree of unmixing from the bulk solvent. Since \bar{L} is formally related to the unmixing of monomeric species, it is not the proper parameter to describe the solvation process.

The justification of the introduction of γ_ϕ and consequently ϕL_2^* may be more conveniently discussed by considering the reaction as the sum of several reactions. * [This is not the usual $\phi L_2 = \phi H_2 - \phi H_2^*$ but $\phi H_2 - \phi H_2^* = \phi H_2 - H_2^*$.] Let

$A_1 =$ monomer

$A_2 =$ dimer

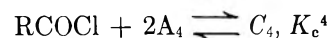
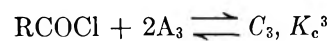
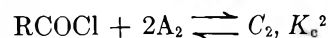
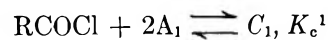
$A_3 =$ trimer

$A_4 =$ tetramer

$N = n$ -mer

The equilibrium constants for self-association of various alcohols have been given by Dannhauser and Bahe¹⁷: alcohol, $K(X^{-1})$; MeOH, 780; EtOH, 1000; *n*-PrOH, 320; *i*-PrOH, 150.

The formation of the complex C from the various polymers can now be written as



plus the cross terms such as



But K_c^n should be constant, so that the rate expression becomes

$$\text{rate} = k[K_c \text{RCOCl}(A_1 + A_2 + A_3 + A_4 + \dots)^2](i\text{-PrOH})^2$$

It remains to show that

$$(A_1 + A_2 + A_3 + A_4 + \dots)^2 = (i\text{-PrOH})^2 \gamma_\phi^2$$

If the reaction were to be analyzed as

$$k_1 = k_3(i\text{-PrOH})^2$$

but

$$k_3 = kK_c(A_1 + A_2 + A_3 + A_4 + \dots)^2$$

$$\frac{k_3}{T} = \frac{k}{T} K_c(A_1 + A_2 + A_3 + A_4 + \dots)^2$$

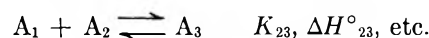
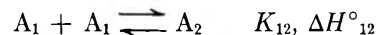
$$\ln(k_3/T) = \ln(k/T) + \ln K_c +$$

$$2 \ln(A_1 + A_2 + \dots)$$

But

$$\frac{d \ln(A_1 + A_2 + A_3 + \dots)}{dT} = \frac{1}{(A_1 + A_2 + A_3 + \dots)} \frac{d(A_1 + A_2 + A_3 + \dots)}{dT}$$

Gill and Farquhar¹⁸ consider the polymerization reactions



where all the K_{nm} and ΔH_{nm}° are assumed to be equal. They define

$$-m\phi L = K(A_1)^2 \Delta H^\circ + 2K^2(A_1)^3 \Delta H^\circ + \dots$$

where m is the molal concentration; the concentration can equally well be written in terms of M , the molar concentration, and this is the form considered here.

The distribution of polymers can now be rewritten as

$$(A_1 + K(A_1)^2 + K^2(A_1)^3 + \dots)$$

(17) W. Dannhauser and L. W. Bahe, *J. Chem. Phys.*, **40**, 3058 (1964).

(18) S. J. Gill and E. L. Farquhar, *J. Amer. Chem. Soc.*, **90**, 3039 (1968).

Table VII: Rate Constants for Anisoyl Chloride in Isopropyl Alcohol-Benzene

X_{IPA}	$k_1 \times 10^4, \text{sec}^{-1}$	C_{IPA}^a	C_{IPA}^b	$k_3 \times 10^4, \text{l.}^2 \text{mol}^{-2} \text{sec}^{-1}$
35°				
0.1	8.010 ± 0.008 (34.87°)	1.1175	1.249	6.413
0.3	35.09 ± 0.070 (34.90°)	3.4456	11.872	2.956
0.4	56.20 ± 0.068 (34.90°)	4.6618	21.732	2.587
0.5	85.68 ± 0.023 (34.90°)	5.9167	35.007	2.448
0.6	123.16 ± 0.072 (34.90°)	7.2121	52.014	2.368
0.7	175.90 ± 0.037 (35.00°)	8.551	73.120	2.406
0.8	245.61 ± 0.037 (35.00°)	9.937	98.744	2.487
0.9	333.51 ± 0.037 (35.00°)	11.369	129.254	2.580
1.0	419.07 ± 0.037 (35.00°)	12.850	165.123	2.538
45°				
0.1	14.75 ± 0.003	1.103	1.217	12.120
0.2	40.30 ± 0.001	2.234	4.991	8.075
0.3	79.49 ± 0.027	3.401	11.567	6.872
0.4	133.54 ± 0.003	4.602	21.178	6.306
0.5	210.94 ± 0.025	5.840	34.106	6.185
0.6	312.67 ± 0.182	7.121	50.709	6.166
0.7	446.25 ± 0.085	8.445	71.318	6.257
0.8	617.86	9.814	96.315	6.415
0.9	844.28	11.233	126.180	6.691
1.0	1103.71	12.702	161.341	6.841

^a The concentrations are those at the actual experimental temperature.

Table VIII: Activation Parameters Based on k_3 for Anisoyl Chloride in Isopropyl Alcohol-Benzene

X_{IPA}	$\Delta H^\ddagger,$ kcal	$\Delta G^\ddagger,$ kcal (45°)	$-\Delta S^\ddagger,$ eu (45°)
0.1	11.63 ± 0.24	25.824 ± 0.001	44.61 ± 0.74
0.2	15.78 ± 0.22	26.080 ± 0.0002	32.38 ± 0.69
0.3	15.65 ± 0.46	26.182 ± 0.002	33.12 ± 1.44
0.4	16.56 ± 0.24	26.237 ± 0.0001	30.42 ± 0.75
0.5	17.31 ± 0.08	26.249 ± 0.0006	28.08 ± 0.24
0.6	17.83 ± 0.13	26.251 ± 0.004	26.46 ± 0.41
0.7	18.00 ± 0.08	26.288 ± 0.001	26.06 ± 0.25
0.8	17.84 ± 0.10	26.226 ± 0.002	26.36 ± 0.31
0.9	17.94 ± 0.10	26.199 ± 0.002	25.95 ± 0.31
1.0	18.70 ± 0.10	26.185 ± 0.002	23.54 ± 0.31

or

$$(A_1 + A_2 + A_3 + \dots)$$

Therefore

$$\frac{d(A_1 + A_2 + A_3 + \dots)}{dT} = \frac{dA_1}{dT} + (A_1)^2 \frac{dK}{dT} + K \frac{d(A_1)^2}{dT} + \dots$$

But since

$$K = e^{-\Delta H^\circ/RT} e^{\Delta S^\circ/R}$$

then

$$\frac{dK}{dT} = \exp\left(\frac{-\Delta H^\circ}{RT}\right) \exp\left(\frac{\Delta S^\circ}{R}\right) \left(\frac{\Delta H^\circ}{RT^2}\right)$$

or

$$\frac{dK}{dT} = K \left(\frac{\Delta H^\circ}{RT^2}\right)$$

Now it can be written that

$$\frac{d(A_1 + A_2 + A_3 + \dots)}{dT} = \frac{dA_1}{dT} + K(A_1)^2 \left(\frac{\Delta H^\circ}{RT^2}\right) + 2(A_1)K \frac{d(A_1)}{dT} + \dots$$

But this yields

$$\frac{d(A_1 + A_2 + A_3 + \dots)}{dT} = \frac{d(A_1)}{dT} \left\{ 1 + 2(A_1)K + 3(A_1)^2 K^2 + \dots \right\} + \left[(A_1)^2 K \left(\frac{\Delta H^\circ}{RT^2}\right) + 2(A_1)^3 K^2 \left(\frac{\Delta H^\circ}{RT^2}\right) + \dots \right]$$

Both the first and second terms of the right side of the equation can be rewritten, the first as the partial of the polymer distribution with respect to T , at constant K , and the second by reference to the definition of Gill and Farquhar

$$\frac{d(A_1 + A_2 + A_3 + \dots)}{dT} = \frac{\partial}{\partial T} (A_1 + A_2 + A_3 + \dots)_{K_i} - \frac{M\phi L}{RT^2}$$

Since the whole expression must now be divided by $(A_1 + A_2 + A_3 + \dots)$, the following expression results

$$\frac{d \ln (A_1 + A_2 + A_3 + \dots)}{dT} = \frac{\left[\frac{\partial}{\partial T} (A_1 + A_2 + A_3 + \dots) \right]_{K_1}}{(A_1 + A_2 + A_3 + \dots)} - \frac{M\phi L}{(A_1 + A_2 + A_3 + \dots)RT^2}$$

At this point it must be noted that the term $(A_1 + A_2 + A_3 + \dots)$ contains $(A_1 + 2A_2 + 3A_3 + \dots)$ moles of alcohol as measured in terms of the *simple molecular formula*. Thus in terms of the simple molecular formula, that term is simply equal to M as it is operationally measured. Therefore the partial of the term with respect to T at constant K_1 simply reflects the density change with temperature and would be very nearly zero. Since in our analysis the k_1 is divided by the fourth power of ROH instead of the second, the term has actually been accounted for. And since $(A_1 + A_2 + A_3 + \dots) = M$, a cancellation can be performed in the final term, yielding

$$\frac{d \ln (A_1 + A_2 + A_3 + \dots)}{dT} = -\frac{\phi L}{RT^2}$$

Now full differentiation of $\ln (k_3/T)$ becomes

$$\frac{\Delta H_{k_3}^\ddagger}{RT^2} = \frac{\Delta H^*}{RT^2} + \frac{\Delta H^\circ}{RT^2} - 2\frac{\phi L}{RT^2}$$

and since RT^2 cancels out, ϕL has indeed been extracted from the original rate law, and the use of $(i\text{-PrOH})^2\gamma_\phi^2$ has been justified.

Similarly, the entropy should be described by

$$\Delta S_{k_3}^\ddagger = (\bar{S}^\ddagger - \bar{S}_a - 2\bar{S}_2) + \Delta S^\circ_c + 2\phi S_2^\circ \quad (3)$$

where \bar{S}_2 is actually $\bar{S}_2 - \bar{S}_2^\circ$. The $2\phi S_2^\circ$ arises, as does the $2\phi L_2$, from the nonideality of the solution as expressed by the γ_ϕ^2 term.

However, the $2S_2$ arises because of the unmixing of (1) the alcohol that forms the ester and (2) the alcohol that solvates the chlorine. It is suggested² that the entropy of the alcohol that is solvating the chlorine is the same as its entropy in the solution. This assumption was made by other workers² to explain the kinetics of four different acid chloride-alcohol reacting systems reference to which has already been made, and there is no reason to expect a change of that part of the mechanism in this case. On this basis eq 2 and 3 can be rewritten with rearrangement as

$$\Delta H_{k_3}^\ddagger = \Delta H_{\text{cor}}^\ddagger - 2\bar{L}_2 - 2\phi L_2 \quad (4)$$

and

$$\Delta S_{k_3}^\ddagger = \Delta S_{\text{cor}}^\ddagger - \bar{S}_2 - 2\phi S_2^\circ \quad (5)$$

Table IX: Activation Parameters Based on k_3^a for Anisoyl Chloride in Isopropyl Alcohol-Benzene

X_{IPA}	ΔH^\ddagger , kcal (40°)	ΔG^\ddagger , kcal (45°)	$-\Delta S^\ddagger$, eu (45°)
0.1	12.12	25.947	43.47
0.2	16.30	27.096	33.93
0.3	16.15	27.729	36.39
0.4	17.06	28.166	34.91
0.5	17.76	28.480	33.69
0.6	18.33	28.732	32.71
0.7	18.49	28.939	32.86
0.8	18.32	29.113	33.91
0.9	18.42	29.257	34.07
1.0	19.23	29.398	31.95

^a The errors are virtually identical with those in the table of k_3 activation parameters.

Table X: Correction to ΔS^\ddagger (45°) Derived from k_3 for Anisoyl Chloride in Isopropyl Alcohol-Benzene

X_{IPA}	$-\Delta S_{\text{obsd}}^\ddagger$	$\bar{S}_2 + 2\phi S_2^\circ$	$-\Delta S_{\text{cor}}^\ddagger$
0.1	43.47 ± 0.74	14.52 ± 0.43	28.96 ± 1.17
0.3	36.39 ± 1.44	6.23 ± 0.25	30.16 ± 1.69
0.4	34.91 ± 0.75	4.56 ± 0.20	30.35 ± 0.95
0.5	33.69 ± 0.24	3.34 ± 0.17	30.35 ± 0.41
0.6	32.71 ± 0.41	2.39 ± 0.12	30.32 ± 0.53
0.7	32.86 ± 0.25	1.62 ± 0.09	31.23 ± 0.34
0.8	33.91 ± 0.31	0.99 ± 0.06	32.93 ± 0.37
0.9	34.07 ± 0.31	0.45 ± 0.02	33.62 ± 0.33
1.0	31.95 ± 0.31	0.00	31.95 ± 0.31
			Av 31.09 ± 1.09 ^a

^a Average error in $-\Delta S_{\text{cor}}^\ddagger$ equals average deviation from mean.

Table XI: Correction to ΔH^\ddagger (40°) Derived from k_3 for Anisoyl Chloride in Isopropyl Alcohol-Benzene

X_{IPA}	$\Delta H_{\text{obsd}}^\ddagger$	$2\phi L_2 + 2\bar{L}_2$	$\Delta H_{\text{cor}}^\ddagger$
0.1	12.12 ± 0.24	7.664 ± 0.182	19.78 ± 0.42
0.3	16.15 ± 0.46	3.692 ± 0.123	19.84 ± 0.58
0.4	17.06 ± 0.24	2.770 ± 0.110	19.83 ± 0.35
0.5	17.76 ± 0.08	2.058 ± 0.089	19.82 ± 0.17
0.6	18.33 ± 0.13	1.474 ± 0.066	19.80 ± 0.20
0.7	18.49 ± 0.08	0.990 ± 0.042	19.48 ± 0.12
0.8	18.32 ± 0.10	0.592 ± 0.020	18.92 ± 0.12
0.9	18.42 ± 0.10	0.270 ± 0.010	18.69 ± 0.11
1.0	19.23 ± 0.10	0.000	19.23 ± 0.10
			Av 19.49 ± 0.36 ^a

^a Average error in $\Delta H_{\text{cor}}^\ddagger$ equals average deviation from mean.

with the only change in the treatment of this system from that of the other well-discussed systems being due to the solvation of the oxygen.

If the quantities $\Delta H_{\text{cor}}^\ddagger$ and $\Delta S_{\text{cor}}^\ddagger$ are constants, it should be possible to represent the change in $\Delta \ln k_3$

Table XII: Prediction of $\Delta \ln k_5$ at 45°; Anisoyl Chloride in Isopropyl Alcohol-Benzene (Reference is 1.0 X)

X_{IPA}	$(2\phi L_2 + 2\bar{L}_2)/RT$	$(\bar{S}_2 + 2\phi S_2)/R$	$\Delta \ln k_5$ (calcd)	$\Delta \ln k_5$ (obsd)
0.1	12.122	7.304	+4.818	+5.459
0.2	8.004	4.464	+3.540	+3.642
0.3	5.840	3.137	+2.703	+2.640
0.4	4.381	2.297	+2.084	+1.949
0.5	3.255	1.682	+1.573	+1.453
0.6	2.331	1.202	+1.129	+1.054
0.7	1.566	0.817	+0.749	+0.727
0.8	0.936	0.496	+0.440	+0.452
0.9	0.427	0.226	+0.201	+0.224
1.0	0	0	0	0

solely in terms of the thermodynamic corrections. Since pure alcohol is used as the reference state and the thermodynamic corrections are zero there, the expression

$$(\ln k_5)_{X_i} - (\ln k_5)_{X=1.0} = -\Delta \left(\frac{\Delta H^\ddagger}{RT} \right) + \Delta \left(\frac{\Delta S^\ddagger}{R} \right)$$

becomes

$$(\ln k_5)_{X_i} - (\ln k_5)_{X=1.0} = \frac{(2\bar{L}_2 + 2\phi L_2)}{RT} - \frac{(\bar{S}_2 + 2\phi S_2^\circ)}{R} \quad (6)$$

The success of the treatment given here will be indicated by the analysis in Tables VII-XVI. The

Table XIII: Rate Constants for Anisoyl Chloride in Ethanol-Benzene

X_E	$k_1 \times 10^4$, sec ⁻¹	M	$k_2 \times 10^6$, l. ² mol ⁻² sec ⁻¹
29.90°			
0.3	1.265 ± 0.028	3.712	9.159 ± 0.200 ^a
0.4	2.153 ± 0.003	5.149	8.118 ± 0.011 ^a
0.5	3.382 ± 0.025	6.706	7.515 ± 0.055 ^a
0.6	5.002 ± 0.020	8.401	7.082 ± 0.032 ^a
0.7	7.255 ± 0.018	10.250	6.907 ± 0.025 ^a
0.8	10.069 ± 0.015	12.275	6.680 ± 0.018 ^a
34.41°			
0.3	1.867 ± 0.008	3.691	1.370 ± 0.006 ^a
0.4	3.227 ± 0.012	5.122	1.229 ± 0.005 ^a
0.5	5.108 ± 0.015	6.671	1.148 ± 0.019 ^a
0.6	7.757 ± 0.020	8.356	1.110 ± 0.002 ^a
0.7	11.480 ± 0.015	10.195	1.104 ± 0.014 ^a
0.8	16.475 ± 0.017	12.210	1.105 ± 0.013 ^a
35.00°			
0.1	0.6506 ± 0.001	1.142	4.982 ± 0.005 ^b
0.2	1.315 ± 0.005	2.370	2.341 ± 0.009 ^b
45.00°			
0.1	1.159 ± 0.013	1.128	9.097 ± 0.098

^a Reference 5. ^b This work.

correction to ΔH^\ddagger is the average of the values at 35 and 45°. Corrections to ΔS^\ddagger and to $\Delta \ln k_5$ are taken from mixing parameters at 45°. The thermodynamics

Table XIV: Corrected k_3 Enthalpy of Activation for Anisoyl Chloride

	X_{EtOH}	ΔH^\ddagger	$4\Delta\phi H_{EtOH}$	$2\bar{L}_{EtOH}$	ΔH^\ddagger_{cor}	Total correction
35-45°	0.1	11.11 ± 0.4	7.64 ± 0.38	1.97 ± 0.09	20.72 ± 0.87	9.61
	0.3	15.95 ± 0.80	3.25 ± 0.06	0.52 ± 0.03	19.72 ± 0.99	3.77
	0.4	16.45 ± 0.21	2.38 ± 0.24	0.30 ± 0.03	19.13 ± 0.48	3.13
30-35°	0.5	16.82 ± 0.35	1.74 ± 0.17	0.16 ± 0.04	18.72 ± 0.55	1.90
	0.6	17.86 ± 0.24	1.24 ± 0.25	0.07 ± 0.01	19.17 ± 0.50	1.31
	0.7	18.67 ± 0.16	0.83 ± 0.25	0.02 ± 0.006	19.52 ± 0.42	0.85
	0.8	20.05 ± 0.09	0.49 ± 0.15	0.01 ± 0.003	20.55 ± 0.24	0.50
				Av	19.65 ± 0.59	

Table XV: Corrected k_3 Entropy of Activation for Anisoyl Chloride at 35° in Ethanol-Benzene

X_{EtOH}	$-\Delta S^\ddagger$	$-4R \ln M$	$4\bar{S}_{EtOH}$	$4\phi \bar{S}^\circ_{EtOH}$	$-\Delta S^\ddagger_{cor}$	Total correction
0.1	46.80 ± 1.0	1.05 ± 0.05	4.30 ± 0.43	6.84 ± 0.68	36.30 ± 2.06	10.50
0.3	28.42 ± 2.6	10.40 ± 0.52	1.66 ± 0.25	-0.40 ± 0.06	37.56 ± 3.34	-9.08
0.4	27.57 ± 0.7	12.99 ± 0.65	1.22 ± 0.18	-1.12 ± 0.17	40.46 ± 1.70	-12.89
0.5	26.60 ± 1.30	15.08 ± 0.75	0.91 ± 0.18	-1.36 ± 0.27	41.21 ± 2.50	-14.61
0.6	23.19 ± 0.80	16.88 ± 0.85	0.68 ± 0.14	-1.44 ± 0.29	40.84 ± 2.08	-17.65
0.7	20.57 ± 0.50	18.45 ± 0.93	0.51 ± 0.15	-1.24 ± 0.37	39.76 ± 1.95	-19.19
0.8	16.09 ± 0.30	19.89 ± 0.99	0.37 ± 0.12	-0.94 ± 0.28	36.56 ± 1.69	-20.47
					Av	38.95 ± 1.84

Table XVI: Calculated vs. Observed Changes in $\ln k_6$ for Anisoyl Chloride at 35.00° in Ethanol-Benzene

ΔX_{EtOH}	$4\Delta\phi H/RT$	$2\Delta\bar{L}/RT$	$4(\Delta\phi S_E^0)/R$	$\Delta(\Delta S_E)/R$	$\Delta \ln k_6$ (calcd)	$\Delta \ln k_6$ (obsd)
0.5-0.1	-8.96	-2.72	-4.12	-1.70	-5.86	-6.87
0.5-0.2	-4.460	-1.18	-1.40	-0.74	-3.50	-3.82
0.5-0.3	-2.48	-0.58	-0.47	-0.37	-2.22	-2.14
0.5-0.4	-1.04	-0.22	-0.12	-0.16	-0.98	-0.86
0.5-0.6	0.80	0.15	0.048	0.12	0.78	0.71
0.5-0.7	1.48	0.22	-0.048	0.20	1.548	1.31
0.5-0.8	2.04	0.24	-0.024	0.28	2.204	1.85

of mixing data are those of Mrazek and Van Ness¹⁹ and Brown, Fock, and Smith.²⁰

The treatment of the reaction of anisoyl chloride in ethanol-benzene requires that four ethanolic species solvate the carbonyl oxygen and, possibly, the chlorine. As its self-association constant indicates, ethanol is more acidic than isopropyl alcohol. The enthalpy of mixing data are those of Van Ness and coworkers.²¹

The free energies of mixing were those of Brown, Fock, and Smith; the entropies were calculated from these and the Van Ness enthalpy data.

(19) R. V. Mrazek and H. C. Van Ness, *A.I.Ch.E. J.*, **7**, 190 (1960).

(20) I. Brown, W. Fock, and F. Smith, *Aust. J. Chem.*, **9**, 364 (1956).

(21) C. S. Savini, D. R. Winterhalter, L. H. Kovach, and H. C. Van Ness, *J. Chem. Eng. Data*, **11**, 40 (1966), and personal communication of Professor Van Ness.

Nuclear Magnetic Resonance Study of the Reaction of Methoxide Ion with Methyl Formate in Methanol Solution

by Dallas L. Rabenstein¹

Chevron Research Company, Richmond, California 94802 (Received October 23, 1969)

Collapse of the long-range spin-spin coupling in the proton nmr spectrum of methyl formate in methanol-sodium methoxide solution has been investigated. At high sodium methoxide concentrations, the collapsed methyl resonance of methyl formate merges with the averaged methyl resonance of the solvent which establishes that the spin-spin coupling is collapsed by the symmetrical transesterification reaction $\text{HCOOCH}_3 + ^-\text{OC}^*\text{H}_3 \rightleftharpoons \text{HCOOC}^*\text{H}_3 + ^-\text{OCH}_3$. The rate constant for this reaction was determined to be $76 \pm 5 \text{ M}^{-1} \text{ sec}^{-1}$ at $31 \pm 1^\circ$ from the dependence of the collapse of the spin-spin coupling on the sodium methoxide concentration. Experimental methyl formate lifetimes were obtained by comparison of partially collapsed spectra with theoretical spectra calculated as a function of methyl formate lifetime.

Introduction

Long-range spin-spin coupling is observed in the high-resolution proton nuclear magnetic resonance (nmr) spectrum of methyl formate. Fraenkel attributed the long-range coupling to a 25% partial double-bond character in the carbonyl carbon-ether oxygen bond.² The coupling has been observed in the spectrum of neat methyl formate, in the spectrum of methyl formate dissolved in several polar and nonpolar solvents, and in the spectrum of methyl formate in strongly acidic solutions. The long-range coupling is also observed in the nmr spectrum of methyl formate dis-

solved in methanol; however, the coupling collapses upon the addition of sodium methoxide to the methanol solution, the amount of collapse depending on the sodium methoxide concentration. In the present paper, the reaction of methoxide ion with methyl formate which causes the collapse of the spin-spin coupling is established, and the kinetics of this reaction are determined from partially collapsed multiplet patterns.

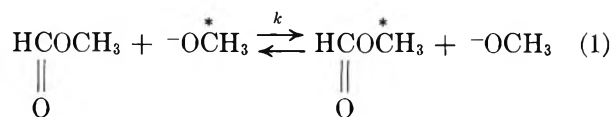
(1) Address inquiries to this author at Department of Chemistry, The University of Alberta, Edmonton, Alberta, Canada.

(2) G. Fraenkel, *J. Chem. Phys.*, **34**, 1466 (1961).

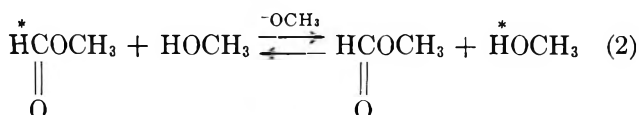
Results and Treatment of Data

The proton nmr spectrum of methyl formate in methanol solution consists of a doublet at 3.70 ppm due to the methyl protons and a quartet at 8.04 ppm due to the formyl proton. The coupling constant for the interaction between the methyl and formyl protons is 0.85 Hz. Addition of sodium methoxide to a methanol solution of methyl formate causes the multiplet patterns to collapse, the amount of collapse depending on the sodium methoxide concentration as shown in Figure 1. The methyl and formyl proton resonances are shown (not at the same instrument sensitivity) at each concentration of NaOCH₃ except 1.0 M. At NaOCH₃ concentrations greater than 0.8 M, the methyl resonance of methyl formate is merged with the methyl resonance of the methanol-sodium methoxide solvent.

It is well known that multiplet patterns due to spin-spin coupling begin to collapse when chemical exchange processes involving one of the partners in the coupling interaction are occurring at rates of the order of the spin-spin coupling constant (measured in cycles per second).³ There are two different exchange reactions involving methyl formate in methanol-sodium methoxide solution which would result in the collapse of the spin-spin coupling if their rates were fast enough, namely the symmetrical transesterification reaction (or methoxide exchange reaction) represented by eq 1,



and the methoxide-catalyzed exchange of the formyl proton of methyl formate with the hydroxyl proton of the solvent, represented by eq 2.



The reaction causing the collapse can be established from the spectra shown in Figure 1. In reaction 1, the formyl proton experiences only one magnetic environment because it remains bonded to the carbonyl carbon, while in reaction 2, it is exchanging between methyl formate and methanol. Thus, if reaction 1 is causing the collapse of the multiplet patterns, a single narrow resonance will be observed at 8.04 ppm for the formyl proton at high rates of exchange while reaction 2 will cause the formyl proton resonance to merge with the hydroxyl resonance of the solvent at high rates of exchange. For the same reason, if reaction 1 causes collapse of the multiplet patterns, the methyl resonance of methyl formate will merge with the methyl resonance of the solvent at high rates of exchange while reaction 2 will give a single narrow resonance at 3.70 ppm for the methyl protons of methyl formate at high rates of exchange. Experimentally, the formyl proton doublet collapses to a

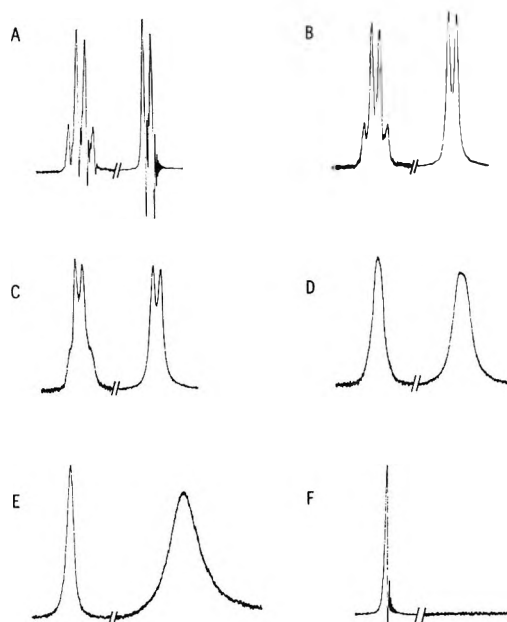


Figure 1. Nmr spectra of 2.0 M methyl formate in methanol-sodium methoxide solution at the following sodium methoxide concentrations: (A) 0.0 M, (B) 0.025 M, (C) 0.035 M, (D) 0.07 M, (E) 0.14 M, (F) 1.0 M. For 0.0 M NaOCH₃, the quartet is at 8.04 ppm and the doublet is at 3.70 ppm relative to TMS. The temperature is 31 ± 1°.

single narrow resonance at 8.04 ppm at high sodium methoxide concentrations while the methyl resonance of methyl formate merges with the solvent methyl resonance. Thus, the spin-spin coupling is collapsed by the methoxide exchange reaction.

The rate of decrease in the concentration of methyl formate, $-d[\text{HCOOCH}_3]/dt$, by reaction 1 is given by eq 3. Dividing eq 3 by the methyl formate concen-

$$-d[\text{HCOOCH}_3]/dt = k[\text{HCOOCH}_3][\text{}^-\text{OCH}_3] \quad (3)$$

tration gives eq 4, which relates the average lifetime of methyl formate between events which cause exchange of methoxide ion, τ_{HCOOCH_3} , to the methoxide ion con-

$$\frac{1}{\tau_{\text{HCOOCH}_3}} = k[\text{}^-\text{OCH}_3] \quad (4)$$

centration. τ_{HCOOCH_3} is the kinetic parameter experimentally measured from the nmr spectra, and exchange rate constant k was obtained from plots of $1/\tau_{\text{HCOOCH}_3}$ vs. $[\text{}^-\text{OCH}_3]$.

Dividing eq 3 by the methoxide ion concentration, $[\text{}^-\text{OCH}_3]$, gives an equation similar to eq 4 for the average lifetime of methoxide ion between events which cause it to exchange with methyl formate, τ_{OCH_3} . In methanol solution, rapid alcoholic proton exchange between methanol and methoxide ion results in one averaged resonance for the methyl protons of methanol

(3) J. W. Emsley, J. Feeney, and L. H. Sutcliffe, "High Resolution Nuclear Magnetic Resonance," Pergamon Press, Inc., New York, N. Y., 1965, p 488.

and methoxide ion. However, it was not possible to independently determine τ_{OCH_3} from the averaged methanol-methoxide methyl resonance because the concentration of methanol is much greater than the concentration of methyl formate and thus exchange of methoxide ion with methyl formate causes negligible broadening of the averaged methanol-methoxide methyl resonance.

τ_{HCOOCH_3} was determined from the shapes of the partially collapsed methyl formate resonances. For NaOCH_3 concentrations less than 0.07 M, the multiplet patterns are not collapsed completely; and, in this concentration region, τ_{HCOOCH_3} was determined by comparison of the experimental resonance line shapes with computer-calculated line shapes.

Partially collapsed quartet spectra were calculated for different τ_{HCOOCH_3} values using the equation presented by Grunwald, *et al.*⁴ The most convenient parameters to measure from the calculated and observed spectra were the valley-to-peak ratios. For the calculated quartet spectra, the ratio of the central valley to the central peaks and the ratio of the outermost valleys to the outermost peaks were measured for the different degrees of collapse. These ratios were plotted *vs.* τ_{HCOOCH_3} and experimental τ_{HCOOCH_3} 's were determined from the experimental valley-to-peak ratios using these plots.

Exchange-collapsed doublet spectra were calculated using the equation for two-site exchange originally derived by Gutowsky and Holm.⁵ Application of this equation to the calculation of partially collapsed doublet patterns has previously been discussed.⁶ Doublet spectra were calculated for a range of τ_{HCOOCH_3} 's, and the valley-to-peak ratios of the calculated spectra were plotted *vs.* τ_{HCOOCH_3} . Experimental τ_{HCOOCH_3} 's were determined from the experimental valley-to-peak ratios using this plot.

When the NaOCH_3 concentration is greater than 0.07 M, the width of the collapsed methyl resonance of methyl formate at resonance half-height increases as the NaOCH_3 concentration increases. This is because the OCH_3 group of methyl formate is exchanging between two environments of different chemical shift (methyl formate and exchange-averaged methoxide ion-methanol), and exchange broadening is observed when the exchange rate is on the order of the separation in cycles per second between the two environments. At NaOCH_3 concentrations greater than 0.8 M, the methyl resonance of methyl formate merges with the averaged methanol-methoxide ion methyl resonance to give one exchange-averaged methyl resonance. In the concentration range where a separate exchange-broadened methyl resonance is observed for methyl formate, τ_{HCOOCH_3} was calculated from the width of this resonance using eq 5, where $W'_{1/2}$ is the width at half-

$$\frac{1}{\tau_{\text{HCOOCH}_3}} = \pi(W'_{1/2} - W_{1/2}) \quad (5)$$

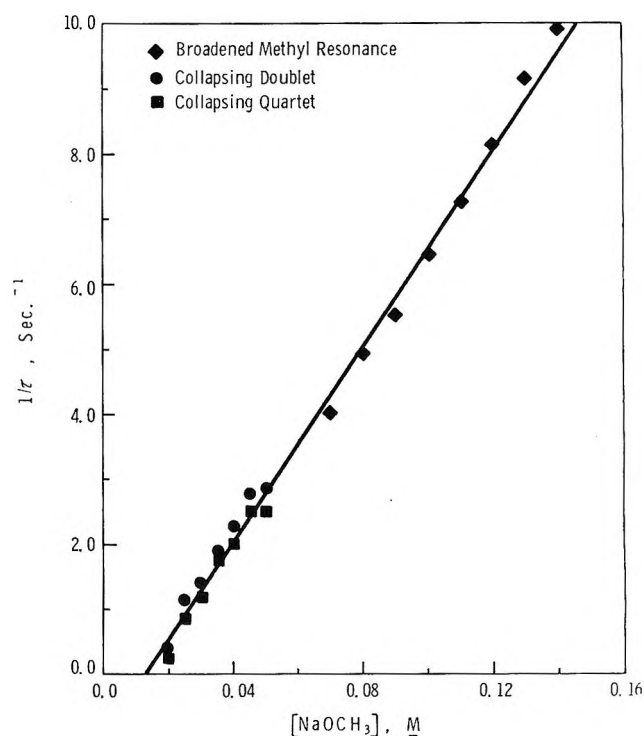


Figure 2. Experimental data for methoxide exchange with methyl formate. The temperature is $31 \pm 1^\circ$.

height of the exchange-broadened resonance and $W_{1/2}$ is the width at half-height in the absence of exchange.⁷ The $W_{1/2}$ values used in the calculation of τ_{HCOOCH_3} by eq 5 were measured from doublet spectra calculated using lifetimes predicted for the appropriate concentrations of methoxide ion from the lower concentration results. The uncertainty in $W_{1/2}$ limits the accuracy with which rate constant k can be determined to 7%.

After the quartet resonance collapses, it becomes more narrow as the NaOCH_3 concentration is increased until a limiting width at resonance half-height of 0.25 Hz is reached at 1.0 M NaOCH_3 . No broadening of this resonance occurs because the formyl proton is not exchanging between two environments of different chemical shift. Evidence for this is that the chemical shift of the center of the formyl proton resonance pattern is independent of the NaOCH_3 concentration.

Sample kinetic data are plotted according to eq 4 in Figure 2. The slope of the straight line gives a value of $76 \text{ M}^{-1} \text{ sec}^{-1}$ for the methoxide exchange rate constant at $31 \pm 1^\circ$. The nonzero concentration axis intercept

(4) E. Grunwald, A. Loewenstein, and S. Meiboom, *J. Chem. Phys.*, **27**, 630 (1957); Z. Luz, D. Gill, and S. Meiboom, *ibid.*, **30**, 1540 (1959). Equation A6 of the first reference is applicable to the exchange system studied in the present paper; however, several signs are in error in eq A6. The correct equation is given in footnote 10 of the second reference.

(5) H. S. Gutowsky and C. H. Holm, *ibid.*, **25**, 1228 (1956).

(6) Reference 3, p 489.

(7) J. A. Pople, W. G. Schneider, and H. J. Bernstein, "High Resolution Nuclear Magnetic Resonance," McGraw-Hill Publications, New York, N. Y., 1959, p 221.

in Figure 2 is due to the presence of a small amount of water in the methanol solvent used. The water reacts with methoxide ion forming methanol and hydroxide ion, thus decreasing the concentration of methoxide ion and shifting the concentration axis intercept. A plot having the same slope was obtained at a methyl formate concentration of 4.0 M .

Discussion

There are no previously reported studies of the symmetrical methyl formate transesterification reaction involving methoxide ion in methanol or in other solvents. This is probably because the reaction is inaccessible to most kinetic methods. The reaction is so rapid it is outside the kinetic range observable by conventional techniques. Also, the products are identical with the reactants unless radioisotope labeling or spin labeling, as in the nmr spectrum, is employed. Thus, no rate constants are available for direct comparison with the one reported in the present paper; however, a rate constant can be predicted from literature data for other reactions of esters of carboxylic acids.

The rate constant for the reaction of hydroxide ion with methyl formate in aqueous solution is $50.9 M^{-1} \text{sec}^{-1}$ at 29.97° .⁸ This reaction is formally similar to the reaction of methoxide ion with methyl formate, and experimental evidence has been presented indicating that the similarity can be extended to the reaction mechanisms.^{9,10} Assuming that this similarity does exist, a value of $82 M^{-1} \text{sec}^{-1}$ is calculated for the reaction of methoxide ion with methyl formate in aqueous solu-

tion from the hydroxide rate constant and the relative nucleophilicity of hydroxide and methoxide at carbonyl carbon.^{8,11} It has been reported that the rate of reaction of alkoxide ions with several carboxylic acid esters in alcohol-water solvents decreases as the alcohol content increases.¹⁰ Thus, the rate constant for the reaction of methoxide ion with methyl formate in methanol is predicted to be less than $82 M^{-1} \text{sec}^{-1}$ but greater than $50.9 M^{-1} \text{sec}^{-1}$, in good agreement with the rate constant determined in this investigation.

Experimental Section

Absolute reagent grade methanol (Baker) and sodium methoxide (Matheson Coleman and Bell) were used as received. The methyl formate (Baker) was dried by shaking with Drierite before using.

Nmr measurements were made on a standard Varian A-60 nmr spectrometer operated at an ambient probe temperature of $31 \pm 1^\circ$. Chemical shifts are reported relative to TMS. For the exchange rate measurements, spectra were recorded five times, and the average valley-to-peak ratios or the average widths at resonance half-height were used in the lifetime determinations.

(8) H. M. Humphreys and L. P. Hammett, *J. Amer. Chem. Soc.*, **78**, 521 (1956).

(9) R. W. Taft, Jr., M. S. Newman, and F. H. Verhoek, *ibid.*, **72**, 4511 (1950).

(10) M. C. Bender and W. A. Glasson, *ibid.*, **81**, 1590 (1959).

(11) J. March, "Advanced Organic Chemistry: Reactions, Mechanism and Structure," McGraw-Hill Publications, New York, N. Y., 1968, p 298.

The Reaction of (3P_1) Oxygen Atoms with Cyclopropane

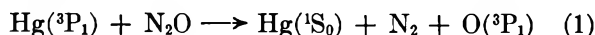
by Alfred A. Scala and Woo-Tien Wu

Department of Chemistry, Worcester Polytechnic Institute, Worcester, Massachusetts 01609 (Received July 7, 1969)

The reaction of a (3P_1) oxygen atom with cyclopropane in the gas phase has been investigated with regard for product analysis. Oxygen atoms were generated by the mercury-sensitized decomposition of nitrous oxide. Using nitrogen as an actinometer indicates that 40% of the oxygen in the system results in the production of water and 16% results in the production of carbon monoxide. The remainder of the oxygen is converted to formaldehyde which polymerizes. A mechanism for the reaction is proposed which involves electrophilic attack of the oxygen atom on the *bent* bond of cyclopropane forming a trimethylene oxide diradical. In the gas phase further decomposition of this product occurs and the initial products are formaldehyde and ethylene. Even at conversions of 0.2%, ethylene competes with cyclopropane for the oxygen atoms and a steady state is achieved. The data indicate that $k_{\Delta}/k_{C_3H_6} = 1.12 \times 10^{-4}$. Since the rate of production of nitrogen is a function of the hydrocarbon which is present, it is questionable whether nitrogen is a reliable actinometer in these systems.

Introduction

The reactions of oxygen atoms are of importance both in combustion processes and in photochemical smog formation. In the atmosphere, oxygen atoms produced by the photodecomposition of NO_2 and O_3 are present in greater concentration than any other reactive atomic or free radical species.¹ The simplest and most convenient method for the production of oxygen atoms in the laboratory is the mercury-sensitized decomposition of N_2O shown in reaction 1. The advantages of



this technique lie in the fact that the quantum yield for reaction 1 is 1.0² and that the yield of nitrogen provides a convenient actinometer.³ Other advantages of this technique which have been pointed out by Cvetanovic⁴ are the ability to study reactions of atomic oxygen in the absence of molecular oxygen and the accessibility to higher pressure ranges than are possible by microwave discharge techniques. Cvetanovic⁵ has also utilized reaction 1 in determining relative quenching cross sections of other molecules for $Hg(^3P_1)$. In this technique the yield of nitrogen serves as a measure of the extent of reaction 1.

This study was originally undertaken to determine the mechanism and the products of the reaction of electrophilic^{6,7} oxygen atoms with cyclopropane, a molecule of unusual structure⁸ which might be expected to be susceptible to electrophilic attack at the carbon-carbon σ bond. Recent theoretical⁹ and experimental¹⁰ studies have shown that there is a region of high electron density on the edge of the cyclopropane ring. The results of this study, while elucidating the mechanism for this reaction, also raise the serious question of whether or not nitrogen is a reliable actinometer in these systems.

Experimental Section

Materials. Cyclopropane and cyclopentene, both of which originally contained numerous impurities, were

purified by repeated injection of small quantities on a 10 ft long squalane column. They were trapped at the exit of the chromatograph and subsequently passed over Drierite and distilled at low temperature to remove any traces of water. The only impurities present in the cyclopropane were 0.0024% propylene and <0.001% propane. The cyclopentene did not contain any low hydrocarbon impurities and only 0.3% of another C_5 hydrocarbon, which was probably 1-pentene. Nitrous oxide was purified by low-temperature distillation and contained no hydrocarbon impurities. Ketene was prepared by the pyrolysis of acetic anhydride.¹¹ It was purified by low-temperature distillation.

Procedures. Mercury-sensitized photolyses were carried out in a cylindrical quartz cell, 4 cm in diameter and 10 cm long, containing a drop of mercury and fitted with a vacuum stopcock. The volume of the cell was 126 ml. The cell was flamed out after each experiment in order to remove the polymer which formed during the photolysis. The light source was a Hanovia 87A-45 low-pressure mercury vapor lamp. The absorbed intensity was approximately 3.0×10^{15} quanta/sec. Since the envelope of this lamp is Vycor, the radiation

(1) P. A. Leighton, "Photochemistry of Air Pollution," Academic Press, Inc., New York, N. Y., 1961, p 103.

(2) R. J. Cvetanovic, *J. Chem. Phys.*, **23**, 1203 (1955).

(3) R. J. Cvetanovic, *ibid.*, **23**, 1375 (1955).

(4) R. J. Cvetanovic, *Advan. Photochem.*, **1**, 115 (1963).

(5) R. J. Cvetanovic, *Progr. React. Kinet.*, **2**, 39 (1964).

(6) R. J. Cvetanovic, *J. Chem. Phys.*, **30**, 19 (1959).

(7) S. Sato and R. J. Cvetanovic, *J. Amer. Chem. Soc.*, **81**, 3223 (1959).

(8) W. Burnett, *J. Chem. Educ.*, **44**, 17 (1967).

(9) J. D. Petke and J. L. Whitten, *J. Amer. Chem. Soc.*, **90**, 3338 (1968).

(10) L. Joris, P. von R. Schleyer, and R. Gleiter, *ibid.*, **90**, 327 (1968).

(11) G. J. Fisher, A. F. MacLean, and A. W. Schnizer, *J. Org. Chem.*, **18**, 1055 (1953).

is pure 2537 Å and contains none of the 1849-Å mercury line. The conversion in a 20-min photolysis was about 0.2%. In all experiments conducted, the nitrous oxide pressure was 160 ± 2 Torr and the temperature was $25 \pm 3^\circ$.

Products noncondensable at 77°K were removed by a Toepler pump and measured in a gas buret. The composition of this fraction was subsequently determined using an A.E.I.-MS10 mass spectrometer. The condensable products were analyzed by gas chromatography using an F and M 810 gas chromatograph equipped with a flame ionization detector. The hydrocarbon products in this fraction were analyzed using a 30 ft long column packed with 20% squalane on 60–80 mesh Chromosorb P, operated at room temperature and a helium flow of 70 cm³/min. Because the ethylene peak is obscured by the large amounts of nitrous oxide, which has a similar retention time on the squalane column, ethylene was analyzed using a 6-ft alumina column, operated at 60° and a helium flow of 20 cm³/min. The oxygen-containing products were analyzed on a 10 ft long column packed with 20% bis(2-(2-methoxyethoxy))ethyl ether on 60–80 mesh Chromosorb P operated at room temperature and a helium flow of 60 cm³/min.

Formaldehyde which could not be analyzed by gas chromatography due to its tendency to polymerize in the gas phase was determined colorimetrically by the chromotropic acid method.¹² When this analysis was performed by simply pumping the contents of the cell through a trap, no formaldehyde was observed. However, when the cell was heated during the pumping, small amounts of formaldehyde were observed. Considerable difficulty was experienced in getting the polymer to pass through the stopcock of the cell. The amount of formaldehyde observed was only a small percentage (1%) of the yield of nitrogen. The infrared spectrum of polymer accumulated from a number of experiments contained an absorption band at 1150 cm⁻¹ which is indicative of the C–O stretching vibration. The analysis of water was performed by removing everything noncondensable at -78° from the cell. The residue was then passed over calcium carbide which converts water to acetylene. The acetylene was then determined by gas chromatography using the squalane column.

Results

Figure 1 presents the yield of nitrogen as a function of irradiation time for the cyclopropane–nitrous oxide and cyclopentene–nitrous oxide reaction mixtures.

It can be seen that the rate of nitrogen production in the cyclopropane–nitrous oxide system is approximately 56% higher than in the cyclopentene–nitrous oxide system. A calculation of the increase in the nitrogen yield in the cyclopropane–nitrous oxide system compared to the cyclopentene–nitrous oxide due to the lower

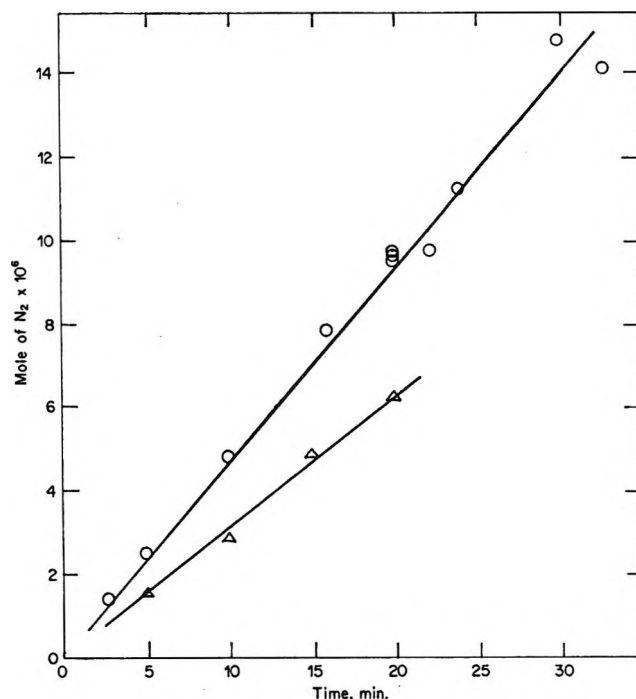


Figure 1. Production of nitrogen as a function of irradiation time: O, 2-6 Torr of cyclopropane, 160 Torr of nitrous oxide; Δ, 5 Torr of cyclopentene, 160 Torr of nitrous oxide.

quenching cross section of cyclopropane relative to cyclopentene for (³P₁) Hg atoms leads to an expected increase of only 8%.⁵ This observation, together with the data in Table I which show that approximately

Table I: Production of Water in the Mercury-Sensitized Decomposition of N₂O in the Presence of Cyclopropane

Exposure, min	c-C ₃ H ₆ , Torr	10 ⁶ N ₂ , mol	10 ⁶ H ₂ O, mol	H ₂ O/N ₂
0	6.5	0	0	...
20	7.4	9.4	3.5	0.38
24	9.4	10.7	5.0	0.47
30	8.0	14.8	5.8	0.39

40% of the oxygen in the cyclopropane–nitrous oxide system results in the production of water, by reactions which are shown not to involve the cyclopropyl or allyl radical, leads to the estimation that approximately 40% of the nitrogen produced in the cyclopropane reaction is the result of secondary reactions. Table II presents the noncondensable product yields for a series of experiments in which both the cyclopropane pressure and the irradiation time were varied. The yields of hydrogen, carbon monoxide, and methane are given relative to the estimated primary yield of nitrogen.

(12) J. M. Ramaradhyia and G. R. Freeman, *Can. J. Chem.*, **39**, 1836 (1961).

Table II: Noncondensable Products from the Mercury-Sensitized Decomposition of N_2O in the Presence of Cyclopropane

Exposure, min	$c\text{-C}_3\text{H}_6$, Torr	$10^6 N_2$, mol	$10^6 N_2^*$, ^a mol	H_2/N_2^*	CO/N_2^*	CH_4/N_2^*
20	7.1	9.7	5.8	0.44	0.42	0.05
22	3.7	9.8	5.8	0.32	0.25	0.05
20	1.7	9.7	5.8	0.30	0.24	0.05
20	6.0	9.3	5.6	0.45	0.32	0.07
20	4.3	9.3	5.6	0.35	0.32	0.06
20	5.1	9.5	5.7	0.35	0.29	0.06
10	3.4	4.9	3.0	0.20	0.25	0.04
5	2.8	2.5	1.5	0.27	0.27	0.05
16	3.4	7.9	4.7	0.24	0.22	0.05
3	2.2	1.4	0.8	0.29	0.27	0.04
33	4.0	14.1	8.5	0.22	0.22	0.05
				Av 0.31 ± 0.06	0.28 ± 0.04	0.05 ± 0.005

^a Primary yield of nitrogen based upon the estimate that 40% of the nitrogen arises from secondary reactions.

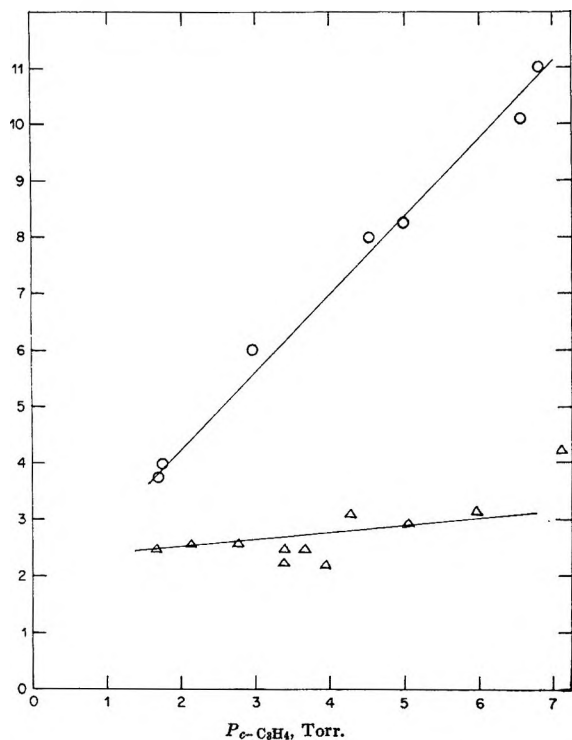


Figure 2. Yields of ethylene and carbon monoxide relative to the primary nitrogen yield as a function of cyclopropane pressure. Ordinate: \circ , $10^6 P_{C_2H_4}/P_{N_2^*}$; Δ , $10^6 P_{CO}/P_{N_2^*}$. Exposure time 20 min.

Although there is some scatter in the data given in Table II, the precision is fairly good. Table II presents the yields of the hydrocarbon and oxygen-containing products relative to the primary nitrogen.

Figure 2 presents the yields of ethylene and carbon monoxide relative to the primary nitrogen as a function of the cyclopropane pressure. The data given in Table III are too scattered to present in Figure 2. However, when the data are plotted there is no apparent dependence of any of these product yields upon the cyclopropane pressure just as the carbon monoxide yield is

independent of cyclopropane pressure. There is, however, a monotonic increase in the yield of ethylene as the cyclopropane pressure increases. Since the ethylene yields as a function of cyclopropane pressure given in Figure 2 will be used to determine the relative rate constants for the reactions of oxygen atoms with cyclopropane and with ethylene, these were determined in separate experiments. This reduced the error introduced by repeated sampling of the reaction mixture and thereby improved the precision of the data.

Since the data indicate that a large amount of secondary decomposition is occurring, an attempt was made to stabilize the initial addition product by performing the photolysis at 77°K in the solid phase. The data for these experiments are given in Table IV. Only in the first of these experiments was the conversion high enough to determine the nitrogen yield. It is significant, however, that in all four experiments reported in Table IV oxetane was the only oxygen-containing compound observed.

In addition to the data presented, it should be noted that propylene was never observed as a product, nor was any product which could be attributed to allyl radicals. When a mixture of 20 Torr of ketene and 20 Torr of nitrous oxide was photolyzed at 3000 Å, the ratio $CO:N_2$ observed was 4.2. During this experiment there was a noticeable formation of polymer in the cell.

Discussion

In this system the primary photochemical act is the absorption by mercury of its resonance radiation. Only the 3P_1 excited state of mercury is produced, since the envelope of the lamp is Vycor and does not transmit the 1849-Å mercury line required to produce the 1P_1 state. Although both nitrous oxide and cyclopropane are capable of quenching the $Hg(^3P_1)$, the extent of quenching by cyclopropane has been minimized by keeping the ratio $N_2O:c\text{-C}_3\text{H}_6$ greater than 30. Using the values of 1.3 and 15 Å² for the quenching cross sec-

Table III: Condensable Products from the Mercury-Sensitized Decomposition of N₂O in the Presence of Cyclopropane

Exposure, min	c-C ₃ H ₆ , Torr	Relative yield × 10 ⁴								
		C ₂ H ₄ /N ₂ ^a	C ₃ H ₂ /N ₂ ^a	C ₃ H ₆ /N ₂ ^a	c-C ₃ H ₄ /N ₂ ^a	CH ₃ CHO/N ₂ ^a	CH ₃ CH=CH ₂ /N ₂ ^a	CH ₃ CH ₂ CHO/N ₂ ^a	CH ₃ CH ₂ CH ₂ CHO/N ₂ ^a	CH ₃ CCH ₂ /N ₂ ^a
20	7.1	6.3	1.1	0.15	2.8	0.88	1.6	0.58	0.85	3.7
22	3.7	5.9	0.85	0.09	2.1	0.10	1.4	0.64	0.63	2.3
20	1.7	4.0	0.36	0.03	1.1	1.2	1.4	0.58	0.51	1.4
20	6.0	4.6	0.75	0.88	1.9	1.3	2.7	0.68	1.17	5.7
20	4.3	7.3	1.7	0.12	3.3	0.81	1.4	0.52	1.0	4.0
20	5.1	9.6	1.5	0.14	3.5	1.1	2.3	0.68	n.d.	4.9
10	3.4	7.9	1.5	0.15	3.2	0.52	n.d. ^b	0.49	n.d.	4.7
5	2.8	9.3	1.9	0.24	3.9	0.95	2.0	0.81	1.2	5.4
16	3.4	9.0	2.9	0.14	3.4	0.63	1.9	0.88	1.7	4.1
3	2.2	9.1	3.0	0.37	3.7	n.d.	2.3	0.85	1.5	5.8
33	4.0	8.3	1.0	0.07	2.9	n.d.	n.d.	0.59	1.4	4.1
		Av 7.4 ± 1.6	1.5 ± 0.61	0.22 ± 0.15	2.9 ± 0.52	0.83 ± 0.29	1.9 ± 0.4	0.66 ± 0.11	1.1 ± 0.2	4.2 ± 0.1

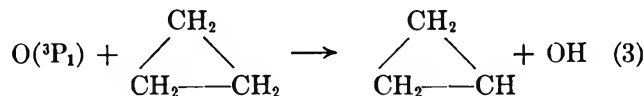
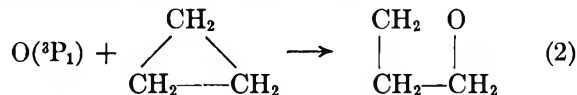
^a Primary nitrogen yield. ^b Not determined.Table IV: Solid-Phase Photolysis^a

Exposure, min	N ₂ , 10 ⁶ mol	Oxetane, 10 ⁶ mol
45	0.54	0.32
50	n.d. ^b	0.0086
70	n.d.	0.037
180	n.d.	0.069

^a Temp = 77°K. ^b Not determined.

tions of cyclopropane¹³ and nitrous oxide,⁵ respectively, we calculate that only one Hg(³P₁) atom in 350 will be quenched by cyclopropane.⁵ In the cyclopentene experiments shown in Figure 1, if we assume the quenching cross section for cyclopentene to be 40 Å²,^{14,15} then we can estimate that 8.3% of the Hg(³P₁) atoms will be quenched by cyclopentene. The fact that the increase in the rate of production of nitrogen in the cyclopropane reaction compared with the cyclopentene reaction is 56% indicates that nitrogen is produced by a reaction or reactions other than reaction 1, when cyclopropane is the reactant hydrocarbon. In Tables II and III the primary yield of nitrogen has been taken as 60% of the total nitrogen.

In considering the possible primary reactions of an oxygen atom with cyclopropane, two obvious alternatives are presented in reactions 2 and 3.



Reaction 2 is suggested by the fact that cyclopropane, a saturated molecule, does have π-character⁸ and undergoes reactions characteristic of π bonds^{16,17} and by the observation of Cvetanovic that (³P₁) oxygen atoms are electrophilic in nature.^{6,7} Reaction 3 is an example of the well known abstraction of a hydrogen from a hydrocarbon by a free radical or atom. Recently, Gunning, *et al.*,¹⁸ have investigated the mercury-sensitized reactions of cyclopropane. They observed that the major products, in addition to polymer, were propylene, bi-allyl, and 1-hexane which were the result of isomerization and the combination of allyl and propyl radicals.

(13) B. de B. Darwent and M. K. Phibbs, *J. Chem. Phys.*, **22**, 110 (1954).

(14) This estimate is based upon the reasonable assumption that the cross sections of cyclopentene and 1-pentene are similar.

(15) B. de B. Darwent, M. K. Phibbs, and F. G. Hurtubise, *J. Chem. Phys.*, **22**, 859 (1954).

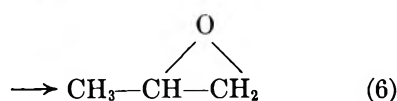
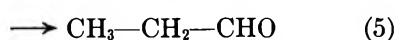
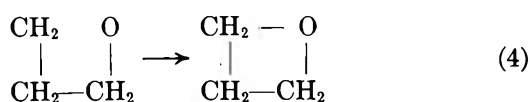
(16) N. C. Deno and D. N. Lincoln, *J. Amer. Chem. Soc.*, **88**, 5357 (1966).

(17) R. L. Baird and A. A. Aboderin, *ibid.*, **86**, 252 (1964).

(18) O. P. Strausz, P. J. Kozak, G. N. C. Woodall, A. G. Sherwood, and H. E. Gunning, *Can. J. Chem.*, **46**, 1317 (1968).

The fact that none of these products was observed in this study is an indication that, first, the sensitization of cyclopropane is unimportant, and second, that reaction 3 is unimportant since the cyclopropyl radical would isomerize to the allyl radical.¹⁸ Reaction 3 is endothermic by 1 kcal/mol. Although (¹D) oxygen atoms are known to abstract hydrogen,¹⁹ this is not a characteristic reaction of the lower energy (³P₁) oxygen atoms.

If the triplet trimethylene oxide diradical formed in reaction 2 is indeed the product of the reaction of an oxygen atom with cyclopropane, the question of the fate of this species needs to be considered. In view of the known reactions of diradicals produced when oxygen atoms react with olefins, the following reactions are probable after spin inversion.⁴

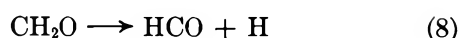


Oxetane, propionaldehyde, and propylene oxide are all products of the reaction of oxygen atoms with cyclopropane. However, it can be seen from Table III that the yields of these products per oxygen atom formed are only 0.0011, 0.0007, and 0.0019, respectively. These yields are quite small and represent only a small fraction of the oxygen atoms produced in this system. Even if we consider the yields of all the oxygen containing molecules in Table III, we can still only account for less than 1% of the oxygen atoms.

Examination of the noncondensable yields given in Table II indicates that 27% of the oxygen atoms produced in this system are incorporated into carbon monoxide. This observation is not entirely unexpected, since reaction 2 followed by reaction 4 would be exothermic by more than 80 kcal/mol.²⁰ In view of the photochemical decomposition of oxetane,^{20b} the most probable mode of decomposition of either the trimethylene oxide diradical or the oxetane is shown in reaction 7.



In view of the exothermicities of these reactions and the photochemical decomposition of formaldehyde,^{20b} it is likely that a sizable fraction of the formaldehyde will be vibrationally excited and will decompose further according to reaction 8. The formyl radical ultimately



results in the production of carbon monoxide. In view of the difficulty in analyzing formaldehyde and the presence of C-O bonds in the polymer, we must conclude

that the formaldehyde which does not react further polymerizes. The propensity of formaldehyde to polymerize in the gas phase is well known.²¹

The mechanism presented thus far has involved the secondary decomposition of either the trimethylene oxide diradical or of oxetane. The secondary decompositions of propionaldehyde and propylene oxide are of course possible. Since these molecules would be expected to produce ethyl and methyl radicals, respectively, and since these in turn would be consumed in fast reactions with oxygen atoms, it is difficult to estimate the importance of these reactions. Certainly the major primary process involves the formation of the trimethylene oxide diradical or a molecule of oxetane. This conclusion is further supported by the one high conversion solid-phase experiment in which oxetane was formed with a quantum yield of 0.6. Unfortunately, in subsequent attempts to duplicate this experiment, although oxetane was the only oxygen-containing compound observed in the gas chromatograph, it was not possible to obtain conversions high enough to analyze the noncondensable products and obtain a quantum yield. We cannot at present explain this difficulty, although it is no doubt related to the difficulty of doing mercury-sensitized reactions in the solid phase.

If reaction 4 is indeed the major reaction, followed by the secondary decomposition to formaldehyde and ethylene, then the ethylene produced should begin to compete with cyclopropane for the oxygen atoms, since the rate at which ethylene reacts with oxygen atoms is reported to be 1.1×10^3 times faster than the rate at which cyclopropane reacts with oxygen atoms.²² If we write the kinetic expression for the change of the ethylene concentration, assuming that every reaction of an oxygen atom produces a molecule of ethylene, we have

$$\frac{d(\text{C}_2\text{H}_4)}{dt} = k_{\Delta}(\text{O})(\Delta) - k_{\text{C}_2\text{H}_4}(\text{O})(\text{C}_2\text{H}_4)$$

Assuming a steady state for ethylene we obtain

$$(\text{C}_2\text{H}_4) = \frac{k_{\Delta}}{k_{\text{C}_2\text{H}_4}}(\Delta)$$

This indicates that the ethylene yield should be a linear function of the cyclopropane pressure with the slope having the value of $k_{\Delta}/k_{\text{C}_2\text{H}_4}$. Even at the low conversions used in this study a steady state is apparently

(19) H. Yamazaki and R. J. Cvetanovic, *J. Chem. Phys.*, **41**, 3703 (1964).

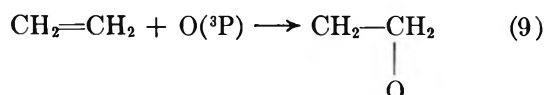
(20) This calculation is based upon an estimated heat of formation of -10 kcal/mol for oxetane. This estimate was made using the method of Benson (a). The other thermochemical data used are those given by Calvert and Pitts (b); (a) S. W. Benson, "Thermochemical Kinetics," John Wiley and Sons, New York, N. Y., 1968. (b) J. Calvert and J. N. Pitts, Jr., "Photochemistry," John Wiley and Sons, New York, N. Y., 1966.

(21) R. D. McQuigg and J. C. Calvert, *J. Amer. Chem. Soc.*, **91**, 1590 (1969).

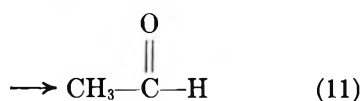
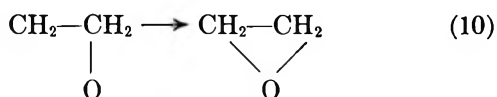
(22) D. Saunders and J. Hecklen, *J. Phys. Chem.*, **70**, 1950 (1966).

attained. This is indicated by the straight line relationship obtained when the ethylene yield is plotted against the cyclopropane pressure in Figure 2. The slope of this line gives a value of $k_{\Delta}/k_{C_2H_4}$ of 1.12×10^{-4} . This value is an order of magnitude lower than the value of 1.1×10^{-3} reported by Heicklen.²² This discrepancy is easily understood. Heicklen determined the value of $k_{\Delta}/k_{C_2H_4}$ by a technique involving the competition between perfluoropropylene and hydrocarbon. The rate constant for the hydrocarbon reaction relative to perfluoropropylene was then determined by measuring CF₂O and CF₃CFO, whose combined yield per oxygen atom reacting with perfluoropropylene is known to be 1.0,²² and the total nitrogen yield. The difference between these values was then ascribed to the oxygen atoms reacting with the hydrocarbon. Conversions in these studies were as high as 10%. Carbon monoxide and hydrogen were both products, indicating that some secondary decomposition did take place despite the higher pressures, and therefore ethylene was probably competing with both the hydrocarbon and the fluorocarbon for the oxygen atoms.

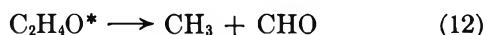
As demonstrated by Cvetanovic,^{3,4} the reaction of the product ethylene is shown in reaction 9. The



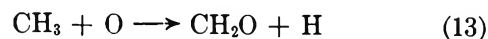
triplet dimethylene oxide diradical may either cyclize after spin inversion to form ethylene oxide or undergo hydrogen atom transfer to produce acetaldehyde as shown.



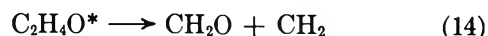
Reaction 9 followed by reaction 10 is exothermic by about 85 kcal/mol, while reaction 9 followed by reaction 11 is exothermic by 112 kcal/mol. Therefore it is not surprising that these molecules will be formed with excess vibrational energy and will undergo secondary decompositions. Recent work by Herron and Penzhorn²³ indicates that the major reaction of the vibrationally excited C₂H₄O* produced by the reaction of an oxygen atom with ethylene is decomposition to a methyl radical and a formyl radical. Since Niki, *et al.*,²⁴ have



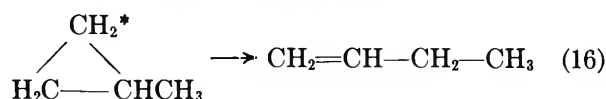
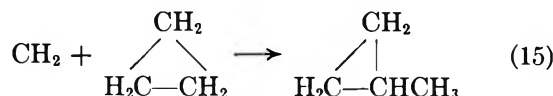
shown that the reaction of oxygen atoms with methyl radicals is at least forty times faster than their reaction with ethylene, it is not surprising that the methyl radical yield is low, since most of the methyl radicals produced in reaction 12 will be consumed in reaction 13.



The study by Herron and Penzhorn²³ also indicates that the direct decomposition of C₂H₄O* to formaldehyde and methylene is also possible. In reaction 12 followed by reaction 13 and in reaction 14 formaldehyde



is the ultimate product. That methylene is produced in our system is indicated by the observation that methylcyclopropane and butene are observed as products. These products most likely form by reactions 15 and 16, respectively.

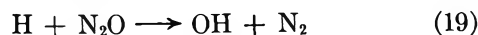
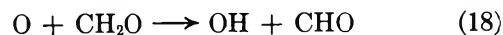


Another possible fate of the methylene produced in this system is shown in reaction 17. This reaction pro-



duces nitrogen without the production of an oxygen atom or an observable oxygen-containing molecule since the formaldehyde polymerizes. In order to determine if reaction 17 does indeed occur, ketene was photolyzed at 3000 Å in the presence of an equimolar amount of nitrous oxide. The observed ratio of 4.2 for carbon monoxide/nitrogen indicates that the reaction of methylene with nitrous oxide occurs at a rate which is approximately 2/3 the rate at which methylene reacts with ketene. The observation of polymer formation in this experiment is evidence for the formation of formaldehyde as predicted by reaction 17. These data indicate that reaction 17 probably consumes most of the methylene produced because of the high nitrous oxide:cyclopropane ratios used in this study. This reaction therefore results in the production of secondary nitrogen.

Two reactions which might account for the presence of large amounts of water as a reaction product are shown below.



The hydroxyl radicals produced in these reactions would ultimately result in the production of water. Reaction 18 has been proposed by both Niki, *et al.*,²⁴ and Herron and Penzhorn²³ as a secondary process in the reaction of oxygen atoms with ethylene. The importance of reaction 19 is difficult to estimate. Nitrous oxide has been

(23) J. T. Herron and R. D. Penzhorn, *J. Phys. Chem.*, **73**, 191 (1969).

(24) H. Niki, E. E. Daby, and B. Weinstock, *J. Chem. Phys.*, **48**, 5729 (1968).

thought to be inert with respect to reactions with free radicals.⁴ However, the large increase in the rate of production of nitrogen observed in the cyclopropane system compared to the cyclopentene system cannot be explained entirely on the basis of reaction 17 and so there must be some other source of secondary nitrogen. Castellion and Noyes,²⁵ who studied the reaction of oxygen atoms, produced by the direct photolysis of nitrous oxide with ethane, observed that there was a 40% increase in the yield of nitrogen when ethane was present and that the products of the reaction consumed oxygen atoms faster than ethane. Indeed, these authors concluded that ethylene actually reached a steady state in their system. These observations are similar to those reported here.

Because of the highly exothermic nature of the reactions of oxygen atoms with cyclopropane, the amount of secondary decomposition which occurs in this system is very high even at total pressures of slightly higher than 160 Torr. The extent to which the primary products undergo secondary decomposition will be dependent upon the number of active degrees of freedom into which the molecule may partition its excess energy. An examination of the data available for oxygen atom reactions reveals that even with larger molecules and at fairly high pressures there is still a fairly large amount of fragmentation which occurs.⁴ The results of this study indicate that N₂O is not as inert to free radical reactions as was previously thought, especially in the presence of relatively nonreactive hydrocarbons, and that kinetics based upon the rate of nitrogen production may not always be valid. In this connection the use of N₂O for the determination of relative quenching cross sections of molecules for Hg(³P₁), while convenient, is also subject to errors due to the production of nitrogen by reactions other than by N₂O quenching Hg(³P₁) atoms. In this case there are two possible sources of secondary fragments. The first is the decomposition of the hydrocarbon molecule which has quenched the mercury atom, while the second is the reaction of the oxygen atom, produced by the N₂O quenching reaction, with the hydrocarbon. Free radicals are apparently present in these systems which could react with N₂O to produce nitrogen. The recent work of Klein and Scheer²⁶⁻²⁸ using (³P₁) oxygen atoms and of DeMore²⁹ using (¹D) oxygen atoms indicates that fragmentation may be reduced although not completely eliminated by conducting reactions in the solid phase at low temperature.

Our data indicate that the cyclopropane ring is attacked by a (³P₁) oxygen atom at the *bent* carbon-carbon bond. This mode of attack is consistent with the electrophilic nature of (³P₁) oxygen atoms. It also appears to be consistent with the kinetic observations of Stuckey and Heicklen,³⁰ who observed that the reac-

tion of cyclopropane with an oxygen atom is slow compared to the other cycloalkanes because of an unfavorable entropy of activation. This unfavorable entropy could be the result of the requirement of attack at the edge of the ring. The recent suggestion of Klein and Scheer²⁸ that the transition state for the reaction of an oxygen atom with 2-butene involves attack in the plane of the atoms attached to the double bond would also be consistent with Heicklen's kinetic data. This suggested transition state is not, however, consistent with the electrophilic nature of (³P₁) oxygen atoms or the results of this study, since it requires attack in the nodal plane of the π bond where the π electron density is zero. It is the opinion of the present authors that the mode of attack suggested by Klein and Scheer does not provide an adequate explanation for their observation that *trans*-2,3-epoxybutane and 2-butanone originate from one precursor and *cis*-2,3-epoxybutane and isobutyraldehyde originate from another precursor. These observations could be explained if the ideas of both Cvetanovic and Klein and Scheer are combined. If the attack of the oxygen atom occurs perpendicular to the plane of the molecule as proposed by Cvetanovic and the intermediate diradical involves nonbonded interactions between the oxygen atom and the free radical on the carbon atom, such that the electron is essentially in an sp² hybrid orbital, then rotation about the C-C bond in such a way as to allow the hydrogen atom on the free radical carbon atom to interact with the oxygen atom and rearrangement from this conformation would produce the observed results. The interaction of the oxygen atom with both the carbon free radical and with the hydrogen atom are part of the Klein and Scheer mechanism. The interaction of the hydrogen with the oxygen may be either a hydrogen bonding type interaction or simply the most favorable interaction on steric grounds. Stereospecific free radical reactions at low temperature are not without precedent.³¹

Acknowledgment. We are happy to acknowledge partial support of this work by The Petroleum Research Fund of the American Chemical Society (PRF No. 1044-G1) and the U. S. Atomic Energy Commission [AT (30-1)-3945].

(25) G. A. Castellion and W. A. Noyes, *J. Amer. Chem. Soc.*, **79**, 290 (1956).

(26) A. H. Hughes, M. D. Scheer, and R. Klein, *J. Phys. Chem.*, **70**, 798 (1966).

(27) R. Klein and M. D. Scheer, *ibid.*, **72**, 616 (1968).

(28) R. Klein and M. D. Scheer, *ibid.*, **73**, 597 (1969).

(29) W. B. DeMore, *ibid.*, **73**, 391 (1969).

(30) W. K. Stuckey and J. Heicklen, *J. Chem. Phys.*, **46**, 4843 (1967).

(31) E. S. Gould, "Mechanism and Structure in Organic Chemistry," Holt, Rinehart & Winston, New York, N. Y., 1959, pp 735-737.

Isotope Effects in Recoil Tritium Reactions with Fluoroform and Deuteriofluoroform¹

by Thomas Smail and F. S. Rowland

Department of Chemistry, University of California, Irvine, California 92664 (Received November 25, 1969)

The primary replacement isotope effect for the energetic substitution reactions $T^* + CHF_3 \rightarrow CTF_3 + H$ and $T^* + CDF_3 \rightarrow CTF_3 + D$ is $k_H/k_D = 1.35 \pm 0.05$, with little variation between liquid and gas phases. The higher yield for the replacement of H vs. D is a mass effect reflecting the relative rapidity of response to changes in interatomic potentials during the interaction of tritium with fluoroform. The secondary hydrogen isotope effect for the substitution of T for F in CHF_3 vs. CDF_3 is $k_H/k_D = 1.45 \pm 0.05$. The large magnitude of this isotope effect is consistent with individual relaxation of the H and D atoms during interaction of T with fluoroform as a controlling factor in the T for F substitution. The isotope effect is inconsistent with inertial postulates treating the CHF_2 and CDF_2 radicals as rotating entities.

Introduction

The magnitude and sign of the various isotope effects in energetic tritium reactions have been the source of important information concerning the mechanisms and other characteristics of these reactions.²⁻⁷ Our recent measurement^{8,9} of a primary replacement isotope effect¹⁰ of 1.25 ± 0.05 for reaction 1 in isotopic isobutanes has encouraged us to seek confirmation of this effect and an additional measurement in a second system. We have again chosen to use a CHX_3 vs. CDX_3 system, in which no secondary isotope effect can contribute to (1), and have determined the yields of CTF_3 from CHF_3 and CDF_3 . In the earlier experiments with isobutane, the yields of substitution at the tertiary position were measured relative to those of the



substitution reaction in the primary position of the same molecule, *i.e.*, $X = CH_3$ or CD_3 in CHX_3 . Since no intramolecular standard reaction exists for fluoroform, our experiments have been performed in binary mixtures with CH_3Cl , using the yield of CH_2TCl as an intermolecular standard for comparison.¹¹

The substitution of T for F is also found for fluoroform,^{12,13} and the secondary isotope effect has been measured for reaction 2.



Experimental Section

Materials. Methyl chloride (Matheson) was stated to be 99.5% pure and was used without purification. Matheson also supplied CHF_3 (minimum purity 98%); CDF_3 came from Merck Sharp and Dohme (98% isotopically pure). For some runs the CHF_3 and CDF_3 were purified by vpc. All condensable gases were degassed at -196° before use.

Bromine (Baker reagent grade) was dried by distillation through a column of granulated P_2O_5 and stored in

a bulb fitted with a Viton stopcock. Hydrogen bromide was removed by several distillations on the vacuum line from a -80° bath, which retained most of the Br_2 . Oxygen was used directly from the tank. 3He was distilled away from O_2 impurity trapped on charcoal at -196° .

Sample Preparation. Samples were prepared by standard methods for gases and liquids.^{2,9,11} Fluoroform is readily soluble in liquid methyl chloride, permitting room temperature irradiations in both liquid and gas phases. Molecular bromine was added by condensation into the sample bulb of a known PV amount measured with a spiral gauge manometer. Sufficient Br_2 (2-5%) was used to ensure complete scavenging of all radicals.¹⁴ Reasonable agreement was found between ratios determined from filling pressures and by mass peak measurements after the irradiation. The

(1) This research was supported by Atomic Energy Commission Contract No. AT-(11-1)-34, Agreement No. 126. This work was presented in part at the 156th National Meeting of the American Chemical Society, Atlantic City, N. J., Sept 1968.

(2) E. K. C. Lee, J. W. Root, and F. S. Rowland, "Chemical Effects of Nuclear Transformations," International Atomic Energy Agency, Vienna, 1965, Vol. 1, p 55.

(3) R. Wolfgang, *Progr. React. Kinet.*, **3**, 97 (1965).

(4) H. C. Jurgeleit and R. Wolfgang, *J. Amer. Chem. Soc.*, **85**, 1057 (1963).

(5) E. K. C. Lee and F. S. Rowland, *ibid.*, **85**, 2907 (1963).

(6) E. K. C. Lee, G. Miller, and F. S. Rowland, *ibid.*, **87**, 190 (1965).

(7) J. Cross and R. Wolfgang, *J. Chem. Phys.*, **35**, 2002 (1961).

(8) T. Smail and F. S. Rowland, *J. Phys. Chem.*, **72**, 1845 (1968).

(9) T. Smail and F. S. Rowland, *ibid.*, **74**, 456 (1970).

(10) The term "primary replacement isotope effect" applies to comparisons such as $T^* + RH \rightarrow RT + H$ vs. $T^* + RD \rightarrow RT^* + D$. The term "primary substitution isotope effect" applies to comparisons such as $H^* + RD \rightarrow RH + D$ vs. $T^* + RD \rightarrow RT + D$.

(11) Y.-N. Tang, E. K. C. Lee, and F. S. Rowland, *J. Amer. Chem. Soc.*, **86**, 1280 (1964).

(12) R. Odum and R. Wolfgang, *ibid.*, **83**, 4668 (1961).

(13) R. Odum and R. Wolfgang, *ibid.*, **85**, 1050 (1963).

(14) D. Seewald and R. Wolfgang, *J. Chem. Phys.*, **47**, 143 (1967).

ratio $\text{CH}_3\text{Cl}:\text{CHF}_3$ was maintained at 3.5 ± 0.4 in all samples to ensure a substantial excess of CH_3Cl . A few samples were run with O_2 scavenger for comparison purposes.

Some of the excited CH_2TCl molecules from T for H reactions with CH_3Cl undergo secondary decomposition to form CH_2T radicals; these appear as CH_2TBr in the Br_2 -scavenged system.¹¹ The sum of the yields of ($\text{CH}_2\text{TCl} + \text{CH}_2\text{TBr}$) is an essentially phase-independent standard for comparison of CTF_3 yields.

Small, macroscopic amounts of CH_3Br and CF_3Br were detected in irradiated samples, but always represented $<0.5\%$ of ($\text{CHF}_3 + \text{CH}_3\text{Cl}$). Typical macroscopic gas chromatographic peaks are illustrated in the upper part of Figure 1. Irradiations were performed in the rotating specimen rack of the TRIGA reactor at Gulf General Atomic in San Diego.

Sample Analysis. Standard radio gas chromatography with a 50-ft dimethylsulfolane (DMS) column was used for product analysis, as shown in Figure 1.¹⁵ Mass peak areas (thermal conductivity detector) were determined by a Disk integrator and suitably converted for variations in response factors.¹⁶ Some samples were analyzed on other columns [50-ft propylene carbonate on alumina at 0° , and 50-ft tri-*o*-tolyl phosphate (TTP) on firebrick at 54°], confirming the purity of the peaks of CTF_3 and $\text{CHTF}_2(\text{D})$ observed with the DMS column. The TTP column was used to measure CTF_2Br and $\text{CHTFBr}(\text{D})$, which were well resolved from CH_3Cl and CH_3Br , as shown in Figure 2. An authentic sample of CHF_2Br was available for column calibration; CH_2FBr was identified both by boiling point and by its formation as a small macro-

scopic product during radiolysis of mixtures of $\text{CH}_3\text{F} + \text{Br}_2$. (No macroscopic peak of CH_2FBr was observed in the $\text{CHF}_3\text{-CH}_3\text{Cl-Br}_2$ recoil tritium samples.)

Calculations. All the data pertaining to the primary and secondary isotope effects were derived from samples analyzed on the DMS column. In this way, any systematic errors—for example, small changes in counting efficiency during the passage of a macroscopic amount of material through the proportional counter—will tend to cancel in the calculation of the isotopic ratios. For each sample the counts per minute appearing as CTF_3 , CHTF_2 (or CDTF_2), CH_2TCl , and CH_2TBr were measured, as was the $\text{CH}_3\text{Cl}:\text{fluoroform}$ ratio, M . The normalized yield of CTF_3 in a $\text{CHF}_3\text{-CH}_3\text{Cl}$ sample is given as (cpm as $\text{CTF}_3/\text{cpm as } (\text{CH}_2\text{TCl} + \text{CH}_2\text{TBr})) \times M$. The isotope effects are simply the ratios of the normalized yields from the CHF_3 and CDF_3 samples.

Results

The product analyses for typical $\text{CHF}_3\text{-CH}_3\text{Cl-Br}_2$ samples in both phases are shown in Table I.

Table I: Distribution of Radioactive Products from Recoil T* Reactions in $\text{CHF}_3\text{-CH}_3\text{Cl}$ Systems

Irradiated phase, compn of sample mixt	G_{aa} , ^a mol fractn	Liquid
CHF_3	0.193	0.227
CH_3Cl	0.746	0.730
Br_2	0.022	0.043
^3He	0.039	...

Product Yields Normalized to $(\text{CH}_2\text{TCl} + \text{CH}_2\text{TBr}) = 100^b$		
HT	141	133
CH_3T	39.7	46.3
CHTF_2	0.86	1.94
CTF_3	3.34	6.39
CH_2TCl	47.5	73.6
CH_2TBr	52.5	26.4
CTF_2Br^c	0.37	0.50
CHTFBr^c	<0.03	<0.05

^a Total pressure: 84 cm. ^b Variable yields of OC^{35}S were also observed. ^c These products were determined from separate samples having a composition very similar to that shown.

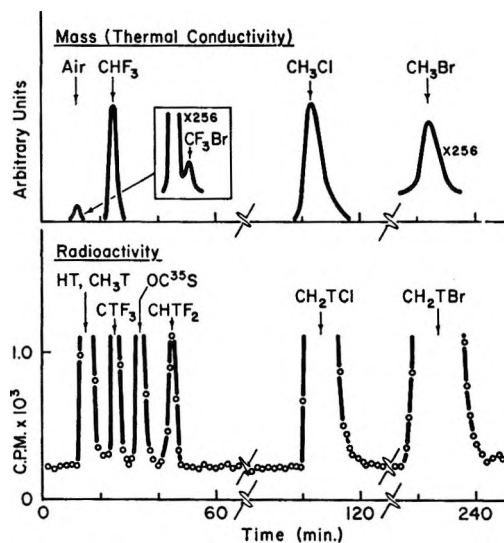


Figure 1. Gas chromatographic records for recoil tritium reactions in $\text{CHF}_3\text{-CH}_3\text{Cl}$ mixtures, as analyzed with the 50-ft DMS column. Upper trace: thermal conductivity response (uncorrected); inset: enlargement of "air" peak, showing CF_3Br ; lower trace: radioactivity measured by proportional counter.

The increased stabilization of CH_2TCl in the liquid phase with a complementary decrease in the CH_2TBr yield is apparent in the data.¹¹ The three products from T* reactions with CHF_3 (CTF_3 , CHTF_2 , and CTF_2Br) also show increases in the liquid phase. No $\text{CHTFBr}(\text{D})$ could be detected in samples containing purified fluoroform. Lesser amounts of ^{35}S are formed

(15) J. K. Lee, E. K. C. Lee, B. Musgrave, Y.-N. Tang, J. W. Root, and F. S. Rowland, *Anal. Chem.*, **34**, 741 (1962).

(16) The thermal response constants that were used were: CH_3Cl , 0.754; CHF_3 , 0.723; CDF_3 , 0.720; ($n\text{-C}_4\text{H}_{10} = 1.000$).

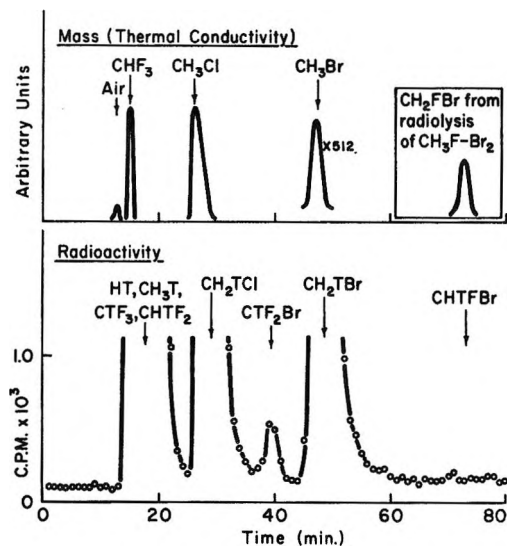


Figure 2. Gas chromatographic records for recoil tritium reactions in CHF_3 - CH_2Cl mixtures, as analyzed with the 50-ft TTP column. Upper trace: thermal conductivity response (uncorrected); inset: location of macroscopic peak formed by radiolysis of CH_3F - Br_2 mixtures; lower trace: radioactivity measured by proportional counter.

by the ^{36}Cl (n,p) ^{36}S reaction¹⁷ and ^{36}S atoms are known to be scavenged very efficiently by CO to form OC^{36}S . The yields of OC^{36}S were widely variable, and no other ^{36}S compounds were observed in these experiments.

Four gas-phase samples were handled in such a way that the absolute yields of each product could be directly compared. When corrections were applied for the amounts of ^3He in each sample (determined by thermal conductivity), the recoil loss and the variations in counting efficiency as discussed earlier,⁶ the data shown in Table II were obtained. The differences in the yields of CTF_3 and $\text{CHTF}_2(\text{D})$ from CHF_3 and CDF_3 are immediately apparent.

After correction for the 4% variation in the mole fraction of fluoroform in the mixtures, the calculated primary and secondary isotope effects are

$$\frac{(T \text{ for H}) \text{ CHF}_3}{(T \text{ for D}) \text{ CDF}_3} = 1.31 \pm 0.04$$

$$\frac{(T \text{ for F}) \text{ CHF}_3}{(T \text{ for F}) \text{ CDF}_3} = 1.51 \pm 0.05$$

These calculations are on an *absolute* comparison basis in contrast to the relative measurements based upon the reaction of T for H in CH_3Cl . The agreement between these absolute yields and the relative yields discussed below implies that the energy spectra for tritium atom collisions are quite similar in the two mixtures; since CH_2Cl is the chief component in each case, this similarity is expected.

The typical reproducibility of the measurements of CTF_3 and $\text{CHTF}_2(\text{D})$ relative to $(\text{CH}_2\text{TCl} + \text{CH}_2\text{TBr})$ is shown in Table III. Three or four separate samples

Table II: Normalized Yield Measurements for Recoil Tritium Reactions in the Fluoroform-Methyl Chloride System

Component	Pressure, cm			
	Sample composition			
CH_2Cl	63.7	64.0	62.0	61.0
CHF_3	15.9	15.9
CDF_3	16.0	16.0
^3He	2.5	2.2	3.0	2.1
O_2	5.6	...	6.8	...
Br_2	...	1.87	...	1.83
Relative yields (normalized to constant conditions)				
HT	7130	7080	6750	6560
DT	0	0	300	310
CTF_3	141	147	112	116
$\text{CH}(\text{D})\text{TF}_2$	40.2	37.8	25.7 ^a	27.2
CH_2TCl	2300	2290	2270	2250
CH_2TBr	0	2510	0	2500

^a Corrected for acetylene-*t* from traces of ethylene impurity in the CDF_3 .

of CHF_3 : CH_2Cl and CDF_3 : CH_2Cl were analyzed in both phases. Tables IV and V give the mean values for the yields of fluoroform-*t* and difluoromethane-*t* measured in this way and the isotope effects calculated from the ratios of these yields. The primary replacement isotope effect is quite similar in both the gas and liquid phases, the difference being just outside the quoted error limits.

Table III: Measurement of CTF_3 Yields Normalized to $(\text{CH}_2\text{TCl} + \text{CH}_2\text{TBr})$ for Recoil Tritium Reactions in CH_2Cl - CHF_3 Liquid Mixtures^a

Obsd activity as CTF_3	Obsd activity as $(\text{CH}_2\text{TBr} + \text{CH}_2\text{TCl})$	$M = \frac{(\text{CH}_2\text{Cl})}{(\text{CHF}_3)}$	CTF_3 yield ^b per C-H bond
8270 ± 110	$139,450 \pm 500$	3.37	60.0 ± 0.9
5640 ± 90	$94,650 \pm 340$	3.31	59.4 ± 1.0
6730 ± 150	$106,100 \pm 600^c$	3.24	61.8 ± 1.4
6230 ± 100	$94,830 \pm 340$	3.17	62.4 ± 1.2
			60.9 ± 1.1

^a All samples contained 4-5% Br_2 . The values of M were measured by a Disk integrator. ^b Yield of CTF_3 , per C-H bond = $\frac{1}{2} \times [(100 \times A_{\text{CTF}_3}) / (A_{\text{CH}_2\text{TCl}} + A_{\text{CH}_2\text{TBr}})]$. ^c CH_2TBr estimated from $\text{CH}_2\text{TBr}:\text{CH}_2\text{TCl} = 0.369$ (mean of 7 detn).

The secondary isotope effect on the T for F reaction is also independent of phase within the stated error limits. However, absolute yields of both CTF_3 and CHTF_2 (or CDTF_2) are roughly twice as large in the liquid phase as in the gas phase, indicating considerable decomposition of excited species in the gas phase.

(17) E. K. C. Lee, Y. N. Tang, and F. S. Rowland, *J. Phys. Chem.*, **68**, 318 (1964).

Table IV: Primary Replacement Isotope Effect for Recoil Tritium Reactions with CHF₃ and CDF₃

Compd	Irradiated phase			
	Gas		Liquid	
	Yield CTF ₃ ^a	[H]/[D]	Yield CTF ₃	[H]/[D]
CF ₃ -H	34.8 ± 0.6 (4) ^b	1.32 ± 0.05	60.9 ± 1.1 (4)	1.43 ± 0.08
CF ₃ -D	26.4 ± 0.9 (4)		42.6 ± 2.4 (3)	

^a Yield CTF₃ = 300 × (A_{CTF₃})/(A_{CH₂TCI} + A_{CH₂TBr}). ^b Number of separate determinations in parentheses.

Table V: Secondary Isotope Effect in T for F Reactions of Recoil Tritium with CHF₃ and CDF₃

Compd	Irradiated phase			
	Gas		Liquid	
	Yield, ^a CHTF ₂ (CDTF ₂)	[H]/[D]	Yield, CHTF ₂ (CDTF ₂)	[H]/[D]
CF ₂ H-F	3.01 ± 0.08 (4) ^b	1.40 ± 0.06	7.1 ± 0.3 (4)	1.48 ± 0.09
CF ₂ D-F	2.14 ± 0.06 (4)		4.8 ± 0.2 (3)	

^a Yield CHTF₂ (or CDTF₂) per C-F bond = 100 × (A_{CHTF₂})/(A_{CH₂TCI} + A_{CH₂TBr}). ^b Number of separate determinations in parentheses.

Small but measurable yields of CTF₂Br were found under all conditions, as shown in Table VI. The CTF₂Br yields are not corrected for number of bonds, since CTF₂ radicals could be formed, at least in principle, by decomposition of either CTF₃* or CHTF₂*. These data have relatively large error limits because of the small yield of CTF₂Br. No CHTFBr(D) was detected (<1% of CTF₃). The CTF₂Br yield was greater in the liquid phase, so that the CTF₂Br:CTF₃ ratio is approximately phase independent.

Table VI: Relative Yields of CTF₂Br from Recoil Tritium Reactions with Mixtures of Fluoroform and Methyl Chloride

System Phase	—CHF ₃ -CH ₃ Cl—		—CDF ₃ -CH ₃ Cl—	
	Gas	Liq.	Gas	Liq.
Relative yields ^a CTF ₂ Br	3.3 ± 0.3	4.8 ± 0.6	2.2 ± 0.2	3.3 ± 0.3
CTF ₂ Br × 100/CTF ₃ ^b	3.6 ± 0.3		3.9 ± 1.2	
	10.3 ± 1.0	7.9 ± 0.8	8.5 ± 0.8	8.5 ± 0.9

^a Yield CTF₂Br = 100 × (A_{CTF₂Br})/(A_{CH₂TCI} + A_{CH₂TBr}).

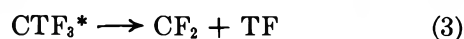
^b CTF₃ yields from Table IV.

Discussion

Energy Deposition in Hot Reactions; Effects of Secondary Reactions. Experimental measurements of the pressure and phase dependence of the product yields from recoil tritium reactions with hydrocarbons¹⁸ and halocarbons^{11,19,20} have demonstrated that considerable excitation energy is deposited in the products from substitution of T for H and T for F. Consequently, some consideration must be given to the possible perturbation of product distributions by sec-

ondary decompositions in order to compare the real primary yields of the hot reactions.

The data of Tables I and IV both permit comparison of gas and liquid phase yields and indicate clearly that almost twice as much CTF₃ is found in the condensed phase, as expected if secondary decomposition is depleting the CTF₃ yield in the lower collision density gas-phase experiments. In similar experiments with CH₂F₂, the CHTF₂ formed by substitution of T for H is also found to undergo extensive decomposition in the gas phase, and as much as 20% decomposition in the liquid phase.¹⁹ In those experiments, the excited fluoromethane decomposed through the loss of HF to give the reactive species CTF, which was readily captured by addition to olefins with the formation of stereospecific fluorocyclopropanes. Excited fluoromethane molecules similarly decompose by the loss of HF, as shown both in pyrolysis experiments²¹ and by the decomposition of CHF₂¹⁸F formed by ¹⁸F substitution reactions with CH₂F₂ and CHF₃.²² In the latter system, the product carbene, CF¹⁸F, has also been detected through the formation of difluorocyclopropanes by reaction with olefinic molecules. However, in the present system the decomposition of excited CTF₃ by (3) will always lead to the loss of the radioactive tracer as TF, with no measurable product left from which to estimate the fractional decomposition.²³ A reasonable estimate of the



(18) E. K. C. Lee and F. S. Rowland, *J. Amer. Chem. Soc.*, **85**, 897 (1963).

(19) Y.-N. Tang and F. S. Rowland, *ibid.*, **89**, 6420 (1967).

(20) Y.-N. Tang and F. S. Rowland, *ibid.*, **90**, 574 (1968).

(21) E. Tschuikow-Roux, *J. Chem. Phys.*, **42**, 3639 (1965).

(22) Y.-N. Tang, T. Smail, and F. S. Rowland, *J. Amer. Chem. Soc.*, **91**, 2130 (1969).

decomposition of excited CTF_3^* in the liquid phase is about 20%, in analogy with CH_2F_2 ,¹⁸ cyclobutane,¹⁹ and methyl chloride¹¹ (see Table I), all of which have decompositions in the 18–25% range in the liquid phase. The assumption of 20% decomposition in the liquid phase implies about 55% decomposition of CTF_3^* in the gas phase at about 1 atm.

Secondary decomposition of excited primary products is less significant in measurement of the primary replacement isotope effect than it is in direct assessment of primary yields, for the isotope effect is measured by comparison of two substitution reactions, each of which may be expected to have secondary decomposition corrections of similar magnitude. Furthermore, in the CHX_3 vs. CDX_3 systems, the hydrogen substitution product is the same molecule, CTF_3 , and only variations in the average energy deposition for T for H and T for D would lead to differing secondary decomposition correction factors. The data in Table IV show that the liquid–gas yield ratios for CTF_3 are 1.75 ± 0.05 and 1.61 ± 0.10 for CHF_3 and CDF_3 , respectively. The similarity in these ratios suggests approximately equivalent deposition of energy in the T for H and T for D reactions with fluoroform—with perhaps an indication of slightly more energy deposition for the former. Recent work with $c\text{-C}_4\text{H}_8$ and $c\text{-C}_4\text{D}_8$ has also suggested that T for H and T for D reactions deposit very similar amounts of excitation energy in isotopic molecules.²⁴

The close similarity in energy deposition following replacement of H or D furnishes an indirect confirmation of the inapplicability of simple atom–atom collision calculations (the “billiard-ball” model) to recoil tritium reactions.⁷ If energy transfer to the initially contacted H or D atom could be accurately estimated by assuming that the struck hydrogen atom were nonbonded and isolated, one would expect from the mass ratios that more kinetic energy should transfer to a D atom than to an H atom, with substantially lesser energy remaining with the molecule formed by T for D than by T for H reactions. While the overall dynamics of these substitutions must also include possible systematic variations in the initial tritium energies for T for H and T for D reactions, the present results furnish no support for a simplified atom–atom approximation to the problem of energy transfer to the struck molecule.

In spite of the increased stabilization in the liquid phase, the primary replacement isotope effect is quite similar in each phase (Table IV). The relative insensitivity of this isotope effect to this change of phase suggests that stabilization of all of the CTF_3 formed in the system, if it were possible, would not significantly alter the semiquantitative conclusion that replacement of H in CHF_3 proceeds with a yield 30–40% greater than that of D in CDF_3 under equivalent conditions. All of the data are consistent with a primary replace-

ment isotope effect of 1.35 ± 0.05 favoring substitution for H in CHF_3 over D in CDF_3 .

A similar argument can be applied to the secondary isotope effect in which the influence of H vs. D substituents is evaluated during the replacement of F by the energetic T atom. In this case, the ratios of liquid–gas yields for the T for F products are 2.36 ± 0.12 (CHTF_2) and 2.24 ± 0.11 (CDTF_2), indicating even more extensive gas-phase decomposition than for the replacement of a hydrogen atom with the formation of CTF_3 . The decomposition characteristics of the two isotopic molecules appear to be very similar,²⁵ and as shown in Table V, the secondary isotope effect is not significantly phase dependent. Again, these facts suggest that it is quite unlikely that correction for the decomposition in the liquid phase of CHTF_2^* and CDTF_2^* would alter the conclusion that there is a secondary isotope effect of 40–50% favoring the replacement of F in CHF_3 vs. F in CDF_3 . All of the present data are consistent with a secondary isotope effect of 1.45 ± 0.05 favoring the replacement of F in CHF_3 vs. CDF_3 .

Primary Replacement Isotope Effect. The primary replacement isotope effect has been measured with the intention of obtaining information about the factors which are important in controlling the T for H substitution reaction. The results obtained in these studies of CHX_3 vs. CDX_3 with $\text{X} = \text{F}$ are in essential agreement with the earlier studies with $\text{X} = \text{CH}_3$ and $\text{X} = \text{CD}_3$,^{8,9} indicating a marked preference for the replacement of H vs. D. Within the limitations of the measurements and of our quantitative understanding, we feel that the 1.35 ± 0.05 measured here for fluoroform and 1.25 ± 0.05 given for the isotopic isobutanes can be considered as equivalent isotope effects.

The time scale for the H-abstraction reaction by recoil tritium atoms has been estimated as $\sim 10^{-14}$ in accounting for deviations from the smooth correlation of HT yields with the bond dissociation energies of the C–H bonds from which abstraction takes place.^{26–28}

(23) The yield of TF is usually not determined in experiments such as these; even if it were, no method exists by which such yields can be unambiguously assigned to reaction 3 vs. such reactions as hot abstraction of F by T. Under most circumstances, yields of TF will be further grouped with all other tritium yields involving exchangeable hydrogen, including TBr or HTO formed by reactions of thermalized tritium atoms.

(24) A. Hosaka and F. S. Rowland, presented at the Fourth Informal International Conference on Hot Atom Chemistry, Kyoto, Japan, Oct 1967.

(25) With equal excitation energies, the rate of decomposition of CHTF_3^* should be approximately 1.3 times faster than CDTF_3^* because of the isotopic H/D difference. However, this effect is suppressed in measured isotopic ratios because of the broad spectrum of excitation energies involved in each case, and this source of isotopic difference has been neglected in our calculations. Such a correction, of course, would tend to increase slightly the measured isotope effect in the primary yields.

(26) E. Tachikawa and F. S. Rowland, *J. Amer. Chem. Soc.*, **90**, 4767 (1968).

(27) E. Tachikawa and F. S. Rowland, *ibid.*, **91**, 559 (1969).

(28) E. Tachikawa, Y.-N. Tang, and F. S. Rowland, *ibid.*, **90**, 3584 (1968).

Estimates of the time scale for the substitution reactions depend rather strongly on the assumptions made concerning the energy of the replaced atom or group—while the time of approach of the energetic tritium atom is readily calculated for a given kinetic energy, the exit velocity of the displaced group may be quite low if very little kinetic energy is removed with it. If a kinetic energy of 0.1 eV is assumed for the exiting group, the time required for traversal of 1 Å—a crude measure for the maximum range of important interactions between the displaced group and the product molecule—is about 2, 3, and 10×10^{-14} sec for H, D, and F atoms, respectively. The corresponding transit time for an approaching 5-eV tritium atom is, on the other hand, about 0.5×10^{-14} sec. The rapidity, on these time scales, with which an atom or a group can respond to a change in interatomic potential must be a major factor in determining the course of the chemical reaction. Some recent trajectory calculations with a model potential surface for the reaction of energetic T atoms with CH_4 and CD_4 have clearly indicated that, for a given set of initial conditions, the H atom responds more rapidly to the perturbations in potential than does a D atom, as expected from the lighter mass of the former.²⁹ While these trajectory calculations are not wholly successful in simulating the energetic reactions of T with CH_4 (in particular, the substitution reaction is only very infrequently observed), the qualitative explanation seems likely that those trajectories in which the struck atom moves away and the incoming tritium atom begins a bonding interaction are those which will more often lead to a successful substitution reaction of tritium for the replaced atom. As the molecular potentials are perturbed by the close approach of energetic T to the target molecule, the readier response of the H atom to the changing potentials will make successful replacement more likely than in an equivalent trajectory involving the replacement of the slower-moving D atom by T.

Additional factors certainly are involved in the replacement reactions, since, for example, the H in CHF_3 is replaced 0.56 ± 0.03 as readily as the H in CH_4 , per C-H bond.³⁰ Comparison of the yields of the T for H reaction with several hydrocarbons and halocarbons shows an excellent correlation with the electron density of the C-H bond in the reacting molecule, as indicated by proton nmr shifts. At this point, it is difficult to assess what additional influences on yields of the T for H substitution reaction arise from the possible mass-dependent relaxation of other substituents during the potential energy changes accompanying the atomic replacement process. Experiments with 2.8-eV tritium atoms have shown that significant T for H reaction occurs with the CH_4 below this initial energy, whereas CHF_3 is quite unreactive toward substitution processes.³¹ Since the methyl group has a much smaller moment of inertia than a trifluoromethyl group,³² a

redistribution of bonding orbitals to “catch” the tritium atom may be more feasible with residual CH_3 than with CF_3 . However, since most substitution reactions in recoil tritium systems occur at energies well in excess of 2.8 eV, substitution processes of this type observed with photochemically “hot” tritium atoms may represent only a rather minor contribution to the entire spectrum of reactions initiated by nuclear recoil.

Secondary Isotope Effect during Substitution of T for F; Inadequacy of the Rotational Inertia Hypothesis. Secondary isotope effects have previously been observed in the substitution of T for F in CH_3F vs. CD_3F ,^{5,6} as well as in the replacement of alkyl groups;⁹ no measurements have yet been possible for such effects during a T for H reaction. The isotope effect in methyl fluoride favors attachment to CH_3 over CD_3 by a factor of 1.4 with the spectrum of tritium atoms available from nuclear recoil;⁶ recent photochemical experiments show a corresponding value of 1.7 for 2.8-eV tritium atoms.³¹ These experiments suggest that relaxation of the attached atoms is increasingly important as the tritium energy is decreased.

The time scale and energetics for the replacement of heavy groups by energetic tritium atoms is likely somewhat different than for replacement of H or D atoms. Comparative measurements of the energy deposition for replacement of H in cyclobutane¹⁸ and CH_3 in 1,3-dimethylcyclobutane³³ indicate substantially larger energy deposition (6–8 eV, average) in the latter case than the 5 eV found for the former. While this greater energy deposition could arise from a higher average energy for the incoming tritium atom during heavy group replacement, the time of appreciable interaction may very well be substantially longer because of the relatively slow velocity of the leaving fluorine atom or methyl group. Indeed, the deposition of substantial excitation energy may be facilitated by the greater time interval for energy transfer to more distant atoms during the 10^{-13} sec required for the escape of a low energy heavier group. As a corollary to a longer time scale, the relaxation of other heavier substituents might begin to contribute to secondary effects on T for F or T for R substitution reactions.

The present experiments demonstrate a rather large 40–50% secondary isotope effect for a single H/D alteration between CHF_3 and CDF_3 during the replacement of F by energetic T. The variations in yields with sub-

(29) D. L. Bunker and M. Pattengill, *Chem. Phys. Lett.*, **4**, 315 (1969).

(30) F. S. Rowland, E. K. C. Lee, and Y.-N. Tang, *J. Phys. Chem.*, **73**, 4024 (1969).

(31) C. C. Chou and F. S. Rowland, unpublished data.

(32) Crude calculations indicate that the moment of inertia for rotation of a methyl group around the carbon atom and one C-H bond is 3×10^{-40} g cm². The corresponding moment of inertia for a CF_3 group is much larger, $\sim 84 \times 10^{-40}$ g cm². Differences of the same order of magnitude are found for other possible group motions.

(33) C. T. Ting and F. S. Rowland, *J. Phys. Chem.* **74**, 445 (1970).

stituents for the processes occurring in halomethanes were the most important experimental evidence in support of the "rotational inertia" hypothesis. However, as originally proposed,^{3,13} an almost negligible secondary isotope effect would be expected for the comparative rates of rotation of CHF_2 and CDF_2 radicals. Assuming bond lengths of C-F 1.33 Å and C-H (D) 1.09 Å, the moments of inertia about the carbon atom and an axis at right angle to the C-H (C-D) bond are 30 and 32×10^{-40} g cm², respectively, for CHF_2 and CDF_2 . Motion about other axes shows even less isotopic difference, and these variations seem totally inadequate to account for an isotope effect of 40–50%. The experiments suggest instead that the relaxation process involved is not really a relaxation of the radicals as a whole, but rather of individual atoms, and in fact almost entirely through relaxation of the H or D atom. This motion of the H or D atom, in response to perturbations of the interatomic potentials during the close approach of the tritium atom to fluoroform, is necessary for orbital electron redistribution making available electron density in the vicinity of the incoming tritium atom; the more rapid response of the H atoms results in a higher fraction of successful substitutions than with D as the secondary substituent. Since the time scale for the whole substitution process is long enough to permit substantial motion by the fluorine atom being replaced, sufficient time must also exist for some motion by the remaining two fluorine atom substituents, and some adjustment in their positions is certainly possible. Nevertheless, the chief deviations by a secondary substituent

from the original tetrahedral angles of the fluoroform molecule must be those made by the H or D atoms in order to account for the large secondary isotope effect.

Formation of CTF₂. The small but real yields of CTF_2 (observed as CTF_2Br) from both CHF_3 and CDF_3 correspond formally to the "replacement" of hydrogen fluoride in the parent molecule—the "double displacement" of HF (or DF) by T. As in other recoil tritium systems, it is not clear whether "double displacement" occurs in two steps (*e.g.*, the loss of F from CTF_3^* or H from CHTF_2^*) or in a single-step loss of HF in the primary collision.^{3,34} The single-bond breaking steps required for $\text{CTF}_3^* \rightarrow \text{CTF}_2 + \text{F}$ or $\text{CHTF}_2^* \rightarrow \text{CTF}_2 + \text{H}$ have not been observed for thermal decompositions of such molecules, but seem plausible as minor pathways for the much more highly excited molecules formed in recoil tritium substitution reactions. Decomposition from such highly excited molecules by these paths might even occur prior to complete equilibration of the excitation energy through all of the degrees of freedom of the molecules. Alternatively, the circumstances for a true single-step double displacement reaction are more favorable than for some other possible cases because of the great bond strength and possible influence of an incipient HF bond in promoting such reaction. In any event, the CTF_2 radicals appear to be themselves vibrationally "hot," since their yield is higher in the liquid than in the gas phase.

(34) Y.-N. Tang and F. S. Rowland, *J. Phys. Chem.*, **72**, 707 (1968)

The Insertion Reactions of Mono- and Difluorocarbene with Hydrogen Halides¹

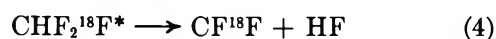
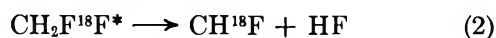
by Thomas Smail and F. S. Rowland

Department of Chemistry, University of California, Irvine, California 92664 (Received November 11, 1969)

Both monofluorocarbene (CH^{18}F) and difluorocarbene (CF^{18}F) react in direct insertion reactions with hydrogen halides to form $\text{CH}_2^{18}\text{FX}$ and CHF^{18}FX , respectively. The fluorocarbenes are produced by secondary decomposition reactions of excited ^{18}F -labeled molecules formed by hot ^{18}F atom reactions with various precursor molecules, including CF_4 , CHF_3 , CH_2F_2 , and C_2F_4 . Competitive studies show rapidly decreasing reactivity of HX toward CF^{18}F in the order $\text{HI} > \text{HBr} > \text{HCl}$. The reaction of CH^{18}F with HI forms $\text{CH}_2^{18}\text{FI}^*$ with sufficient excess energy to decompose these molecules to CH_2^{18}F and I in gas-phase experiments. The scavenging of CH^{18}F by two successive reactions with HI thus results in the formation of CH_3^{18}F . The exothermicity of the other reactions forming $\text{CH}_2^{18}\text{FX}$ and CHF^{18}FX is insufficient for appreciable secondary decomposition.

Introduction

The study of the chemical reactions of the fluorocarbenes, CHF and CF_2 , furnishes fruitful comparisons and contrasts with the known reactions of CH_2 , and has received increasing attention as convenient sources of these interesting species have become available. Difluorocarbene has been readily generated by several synthetic routes, including the pyrolysis of $(\text{CF}_3)_3\text{PF}_2$,² the decomposition of C_2F_4 by flash photolysis³ or Hg-sensitized photolysis,⁴ and by the pyrolysis or photolysis of difluorodiazirine,⁵ and its reaction products in various systems have therefore been available in macroscopic amounts. Monofluorocarbene, on the other hand, has been prepared only at radioactive tracer levels by a hot-atom technique involving the decomposition of a vibrationally excited precursor formed by an energetic substitution reaction. This technique has been used to form both CHF and CH^{18}F , initiated by energetic T and ^{18}F atoms, respectively, as well as CF^{18}F .⁶⁻⁸ The reactions leading to the formation of CH^{18}F and CF^{18}F from ^{18}F reactions with CH_2F_2 are illustrated in eq 1-4.⁹ The stereospecific nature of the fluorocarbene



addition to olefins has led to the suggestion that both CF_2 ⁵ and CHF ⁷ have a singlet electronic ground state.

The stoichiometric equivalent of insertion of CF_2 into HCl , as in (5), or HBr has been previously reported.^{2,10} We have utilized hot-atom generated CH^{18}F and CF^{18}F for a further study of reactions of this kind with HCl , HBr , and HI , and have measured the competitive rates of such reaction with those for scavenging by olefins. The energetic ^{18}F atoms have been formed by the $^{19}\text{F}(n, 2n) ^{18}\text{F}$ nuclear reaction in CH_2F_2 , CHF_3 , CF_4 , or C_2F_4 , and have reacted by (1) and

(2) to form CH^{18}F and by (3) and (4) to form CF^{18}F (or by similar reactions with the other molecules).



The experimental approach through hot atom reactions is relatively free from complications: the formation of F atoms and HF molecules at tracer levels from a relatively inert parent, such as CH_2F_2 , permits simple gas-handling techniques—Pyrex glass—without physical deterioration. Since the carbenes are formed by hot reactions, the yields are not altered significantly by the inclusion in the samples of small amounts of potential reactants such as ethylene or a hydrogen halide. This relative independence of carbene formation to detailed chemical composition enables the absolute yield of CH^{18}F and CF^{18}F from a given precursor to be easily established, leading directly to measurements of the relative efficiencies of various "scavenger" molecules for the carbenes.

Experimental Section

Sample Preparation and Irradiation. The Matheson Co. supplied, with the purities listed: CF_4 (99.7%), CHF_3 (98%), HCl (99%), HBr (99.8%) and HI (96%). CH_2F_2 and C_2F_4 were supplied by Peninsular Chemresearch and were shown to be free of significant impurities (< 0.1%) by vpc. All compounds were de-

(1) This research was supported by A.E.C. Contract No. AT-(11-1)-34, Agreement No. 126.

(2) W. Mahler, *Inorg. Chem.*, **2**, 230 (1963).

(3) W. J. R. Tyerman, *Trans. Faraday Soc.*, **65**, 1188 (1969).

(4) J. Heicklen and V. Knight, *J. Phys. Chem.*, **70**, 3901 (1966).

(5) R. A. Mitsch, *J. Amer. Chem. Soc.*, **87**, 758 (1965).

(6) Y.-N. Tang and F. S. Rowland, *ibid.*, **88**, 626 (1966).

(7) Y.-N. Tang and F. S. Rowland, *ibid.*, **89**, 6420 (1967).

(8) Y.-N. Tang, T. Smail, and F. S. Rowland, *ibid.*, **91**, 2130 (1969).

(9) Both reactions 2 and 4 can also give the isotopically alternate reaction in which the ^{18}F appears as H^{18}F with no radioactive label for CHF or CF_2 .

(10) J. W. Edwards and P. A. Small, *Nature*, **202**, 1329 (1964).

Table I: Yields of ^{18}F -Labeled Products from ^{18}F Reactions in CH_2F_2 Mixtures with HI, HCl, O_2 , and/or C_2H_4

Reactants	Pressure, Torr						
	4000	4160	3860	3800	3800	3800	3840
CH_2F_2	4000	4160	3860	3800	3800	3800	3840
HI	83	84	16	101
HCl	380	380
O_2	382	...	190	...	46
C_2H_4	190	190	190
^{18}F -labeled product	Absolute yields, %						
CH_3^{18}F	1.48 ± 0.09	2.90 ± 0.19	1.64 ± 0.05	Nd	1.91 ± 0.05	Nd	Nd
$\text{CHF}_2^{18}\text{F}$	0.79 ± 0.03	0.74 ± 0.08	0.71 ± 0.02	0.72 ± 0.07	0.76 ± 0.07	Nd	Nd
$\text{CHF}^{18}\text{FCI}$	2.57 ± 0.10	2.78 ± 0.20	Nd	Nd
$\text{CHF}^{18}\text{FCI}$	1.30 ± 0.03	Nd
$\text{CH}_2^{18}\text{FI}$	Nd	0.11 ± 0.07	Nd	Nd
$\text{CH}_2^{18}\text{FCI}$	1.83 ± 0.13	2.02 ± 0.07
CH_3^{18}F	0.26 ± 0.04	3.3 ± 0.13	...	0.3 ± 0.07	...	1.68 ± 0.03	3.24 ± 0.05
<i>c</i> - $\text{C}_2\text{H}_5^{18}\text{F}$	2.09 ± 0.08	1.72 ± 0.05	0.75 ± 0.04

gassed at -196° prior to use. Slow warming from -196° removed traces of I_2 from HI. After degassing at -196° , C_2F_4 was stored in a -80° bath and was removed as required, leaving behind the traces of polymerization inhibitor added by the manufacturer.

Samples were prepared in the routine manner described elsewhere.¹¹ The hydrogen halides were measured in a calibrated, grease-free, mercury-free vacuum line, using a spiral gauge and mirror arrangement for pressure monitoring.

Fast-neutron irradiations were performed with a Kaman A 711 neutron generator and samples were analyzed by radio chromatography.^{11,12} In a typical irradiation such as the left-hand column of Table I (4000 Torr of CH_2F_2 in a 10.7 ml bulb, irradiated for 10 min), 1900 ± 110 counts of ^{18}F were observed in a 25-ml external flow counter during the passage of the CH_2F_2 peak (flow rate 0.5 ml/sec). The absolute product yields, *i.e.* per cent of the total ^{18}F formed which appears in a particular chemical product, were determined using a calibrated Teflon-sleeve monitor, and are accurate to $\pm 10\%$.¹¹ The observed volatile ^{18}F radioactivity among the listed products never accounted for more than 10% of the total ^{18}F formed in any of these systems. Large amounts of ^{18}F appear as inorganic compounds, presumably almost entirely H^{18}F , or as $\text{CH}_2=\text{CH}^{18}\text{F}$ in C_2H_4 -scavenged systems. Since our interest in these experiments has been focused upon the reactions of CF^{18}F and CH^{18}F and not upon the primary hot reactions of ^{18}F , we have not been concerned with the assay of these other ^{18}F products and have not listed the yields, when measured, in the data tables. Our experimental procedures have taken these other products into account only insofar as necessary to avoid interference by them in the assay of the ^{18}F products involving fluorocarbene- ^{18}F precursors.

The temperature of the samples during irradiation was 10 – 15° —the temperature maintained by the cooling system of the neutron generator. This temper-

ature is neither precisely known, nor easily varied outside this range. Irradiations in the fast neutron beam of this neutron generator produce very little radiation damage in the system, usually unobservable with our standard measurement of macroscopic composition by thermal conductivity.¹¹

Radio Gas Chromatography. Several different chromatographic columns were used, often in combination in a column-switching technique¹¹ for rapid one-*aliquot* analysis of both low- and high-boiling components. Dimethylsulfolane columns of varying lengths were used for the analysis of 1,1-difluoro-2, 2-dimethylcyclopropane, as well as for CH_2FCI and CHF_2Cl . With a 25-ft column at room temperature and a helium flow rate of 0.5 ml sec^{-1} , the retention times in minutes were (boiling points in parentheses): air, 9; CF_3I (-22.5°), 18; CHF_2I (21.6°), 55; CH_3I (42.5°), 87; CH_2FI (53.4°), 114. CHF_2Br and CH_2FBr were separated by a 50-ft tri-*m*-tolyl phosphate column operated at 55° . Low-boiling fluorocarbons were separated by either a 50-ft column of 10% propylene carbonate on alumina (order of elution: CF_4 , CH_3F , CH_2F_2 , CHF_3), or a 100-ft column of 30% di-*n*-butylphthalate on Chromosorb P (order of elution: CF_4 , CHF_3 , CH_3F , $\text{C}_2\text{H}_3\text{F}$, CH_2F_2). Whenever possible, the columns were calibrated with authentic samples.¹³ 1,1-Difluoro-2,2-dimethylcyclopropane was identified by comparison of peak sizes and locations in mixtures containing CF^{18}F sources and either isobutene, *trans*-2-butene, or *cis*-2-butene. The CF^{18}F -olefin adduct shifts to progressively greater retention times in that order, as expected on the basis of earlier work.^{5,7} Additional confirmation was provided by the observa-

(11) T. Smail, G. E. Miller, and F. S. Rowland, *J. Phys. Chem.*, submitted.

(12) J. K. Lee, E. K. C. Lee, B. Musgrave, Y.-N. Tang, J. W. Root, and F. S. Rowland, *Anal. Chem.*, **30**, 903 (1962).

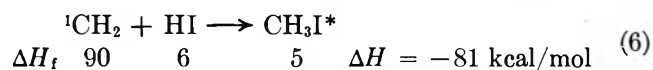
(13) Authentic samples of CH_2FCI and CH_2FBr were supplied by Dr. H. L. Jackson of DuPont Laboratories.

tion that the 1,1-F¹⁸-2, 2-Me₂-c-C₃H₂ was only found in ¹⁸F hot atom systems in which CF¹⁸F can be generated (e.g., CH₂F₂, CHF₃, and CF₄), but was not present among the ¹⁸F-labeled products found in an irradiated mixture containing SF₆, isobutene, and O₂.

The calibrations of CHF₂I and CH₂FI rest on the following points. (a) Macroscopic amounts of the compounds, detectable by thermal conductivity response, were formed by I₂ scavenging of radiolysis products in CH₃F (only CH₂FI observed), CH₂F₂ (both CHF₂I and CH₂FI found), and CHF₃ (only CHF₂I found). (b) The retention times were approximately those expected on the basis of the boiling points of the compounds (see above). (c) The yield of CF¹⁸F from several precursors determined as CHF¹⁸FI was in good agreement with the yield of 1,1-F¹⁸F-2,2-Me₂-c-C₃H₂ in isobutene scavenged systems (Table I). (d) As with the CF¹⁸F-olefin adducts, CHF¹⁸FI was only found in those samples in which CF¹⁸F is generated and was not observed in an irradiated sample containing only SF₆ and HI. While all of this evidence is indirect, taken together it strongly suggests that the identification of CHF₂I and CH₂FI has been correctly made.

Results and Discussion

Thermochemistry of Carbene Reactions with Hydrogen Halides. The exothermicity of the addition of ¹CH₂ to HI can be directly estimated from the heats of formation to be at least 91 kcal/mol (plus any vibrational excitation energy of ¹CH₂),¹⁴ as indicated in eq 6. Since



this excitation energy is ≥ 35 kcal/mol greater than the 56 kcal/mol bond dissociation energy of the C-I bond, almost complete dissociation of CH₃I into CH₃ and I would be anticipated for gas-phase experiments.¹⁵ The exothermicity for ¹CH₂ addition to other hydrogen halides is also approximately 90 kcal/mol, while the energies required for decomposition are progressively larger for CH₃Br, CH₃Cl, and CH₃F. Clearly, similar estimates of the stability toward decomposition of the corresponding reaction products of CHF or CF₂ with HX are pertinent to the understanding of gas-phase experiments with the fluorocarbenes. Unfortunately, the heats of formation of the corresponding fluorinated species—both fluorocarbenes and fluorohalomethanes—are much less accurately known than for methylene and the halomethanes.

We have estimated the following heats of formation in kcal/mol (the uncertainty in each is about ± 5 kcal/mol) CHF₂I, -90; CH₂FI, -43; CHF₂Br, -100; CHF₂Cl, -113; CH₂FCl, -66.¹⁶ From the heat of formation of CF₂ (-39 ± 3 kcal/mol)¹⁷ and the assumption that CF₂ has no vibrational excitation energy, the internal energies for CF₂ insertion into HX are (kcal/mol): CHF₂I, ~ 57 ; CHF₂Br, ~ 53 ; and CHF₂Cl,

~ 52 . Comparison of these excitation energies with assumed bond dissociation energies for these molecules would indicate that CHF₂Cl and CHF₂Br would never be sufficiently excited to decompose¹⁸ at any pressure. The calculation for CHF₂I is somewhat uncertain since the error margin on the excitation energy is quite large—some decomposition might be observed at low pressures, or the molecule might be completely stable against decomposition at pressures of 0.1 atm or greater. Thus, one can conclude from thermochemical estimates that the *insertion* reactions of CF₂ with the hydrogen halides would lead to stable, observable yields of CHF₂Cl, CHF₂Br, and CHF₂I, respectively.

No thermochemical estimate of the heat of formation of CHF appears to be available, so we have made estimates of excitation energies by assuming that the heat of formation of CHF is the arithmetic mean¹⁹ of the heats of formation of CH₂ and CF₂: 25 kcal/mol. The internal excitation energies so obtained for CHF reaction with HX are: CH₂FI, ~ 74 kcal/mol; CH₂FCl, ~ 69 kcal/mol. Comparison of these excitation energies with the assumed C-I and C-Cl bond energies indicates that CH₂FCl should also be completely stable against C-Cl bond break. However, the estimated 74 kcal/mol excitation energy of CH₂FI is about 19 kcal/mol in excess of the activation energy required for C-I bond dissociation, more than sufficient to cause extensive secondary decomposition for 5-atom molecules at these pressures.¹⁵ Consequently, the thermochemical estimates suggest that the observable product expected from the insertion reaction of CH¹⁸F + HCl is the stabilized CH₂¹⁸FCl, while the reaction of CH¹⁸F with HI should lead to CH₂¹⁸FI*, and then to CH₂¹⁸F plus I. In the absence of other

(14) The heat of formation of methylene in the singlet electronic state is not accurately known, and may be several kcal/mol higher than the 90 used in this calculation. Singlet methylene also is known frequently to react rapidly enough that excess vibrational energy (when formed by uv photolysis) is still present at the time of chemical reaction.

(15) J. C. Hassler and D. W. Setser, *J. Amer. Chem. Soc.*, **87**, 3793 (1965). The rate constant for C-I bond break in CH₃I with 25 kcal/mol excitation energy is $k \geq 5 \times 10^{11}$ sec⁻¹.

(16) The heats of formation of CH₃F and CH₂F₂ are quoted as -55.9 ± 0.8 kcal/mol and -108.2 ± 0.2 kcal/mol, respectively. [J. A. Lacher and H. A. Skinner, *J. Chem. Soc., A*, 1034 (1968)]. Assuming C-H bond dissociation energies of 101 ± 4 kcal/mol for each [J. A. Kerr, *Chem. Rev.*, **66**, 465 (1966)], the heats of formation of CH₂F and CHF₂ are estimated as -13 ± 4 and -60 ± 4 kcal/mol, respectively. The heats of formation of the chloro, bromo, and iodo combinations with these radicals are then obtained by assuming C-Cl, C-Br, and C-I bond dissociation energies of 82, 67, and 55 kcal/mol, respectively.

(17) H. F. Zmbov, O. M. Uy, and J. L. Margrave, *J. Amer. Chem. Soc.*, **90**, 5090 (1968).

(18) Alternate decomposition paths for excited CHF₂Cl* would include the intramolecular elimination of HF forming CFCl or the back reaction to CF₂ + HCl. There is, of course, just sufficient energy for the back reaction to occur, implying a rate constant sufficiently long that collisional stabilization would intervene before it could occur; the energetics and conclusion are presumably very similar for the alternate path to HF + CFCl.

(19) This assumption is frequently valid—see Skinner and Lacher, quoted in ref 16.

competing processes, these CH_2^{18}F radicals should abstract H from another molecule of HI, with CH_3^{18}F the final observable product from the initial reaction of $\text{CH}^{18}\text{F} + \text{HI}$.

Difluorocarbene Reactions. The inclusion of isobutene as a scavenger in systems containing CF^{18}F results in the formation of easily measurable yields of 1, 1- F^{18}F -2,2-dimethylcyclopropane.⁸ When HI is substituted for isobutene in the same systems, substantial yields of CHF^{18}FI are isolated in amounts essentially comparable to that scavenged by isobutene, as shown in Table II for ^{18}F reactions with CF_4 , CHF_3 , and C_2F_4 .

Table II: Formation and Trapping of CF^{18}F from Different Target Compounds Following $^{18}\text{F}(n, 2n)^{18}\text{F}$ Reaction

Target ^a molecule	CF^{18}F precursor	Yield, ratio, CF^{18}F adduct/ stabilized precursor	
		With isobutene: 1,1- F^{18}F -2,2- Mez-c-C ₃ H ₆	With HI: CHF^{18}FI
CF_4	CF_3^{18}F	0.53 ± 0.06	0.60 ± 0.06
CHF_3	$\text{CHF}_2^{18}\text{F}$ and CF_3^{18}F	2.4 ± 0.3	2.0 ± 0.2
C_2F_4	$\text{C}_2\text{F}_3^{18}\text{F}$	7.0 ± 0.7	8.5 ± 0.6

^a Total pressure: 3–4 atm.

It is clear, too, from Table II that precursor molecules vary greatly in their stability toward secondary decomposition: $\text{CF}_2=\text{CF}^{18}\text{F}$, for which the split into $\text{CF}_2 + \text{CF}^{18}\text{F}$ is 76 kcal/mol endothermic, is stabilized only in about 15% of the substitutions; CF_3^{18}F , for which the decomposition to $\text{CF}^{18}\text{F} + \text{F}_2$ is 184 kcal/mol endothermic (and the more probable $\text{CF}^{18}\text{F} + 2\text{F}$ is 224 kcal/mol endothermic) is stabilized for about 50% of the primary products.



Two questions can then be raised about the formation of CHF^{18}FI . What is the efficiency of scavenging of HI for CF^{18}F ? Is the mechanism of the reaction simply the one-step addition, or insertion, of CF^{18}F into the HI bond shown in eq 7? A series of experiments with CF_4 as the source of CF^{18}F showed that HI is an efficient trap, and that no additional CF^{18}F is recovered when the concentration of HI is raised above the lowest concentration used, as in Table III. The reduction in yield of $\text{CHF}_2^{18}\text{F}$ with increasing $\text{C}_2\text{H}_4:\text{HI}$ ratio found in Table III is a real effect, reflecting competition between HI and C_2H_4 in scavenging CF_2^{18}F . Although the reaction of CF_2^{18}F with HI has a low activation energy,²⁰ so also has the addition of CF_2^{18}F to ethylene²¹ and the direct competition is quite reasonable, as in (8) and (9). The reaction of CF_2 with C_2H_4 is known to be extremely slow (*i.e.* unobservable) under these



conditions,³ so that the introduction of C_2H_4 into a CF_4 -HI system should not be expected to influence the formation of CHF^{18}FI , in agreement with the observations of Table III.

An alternative mechanism to reaction 7 for the formation of CHF^{18}FI could involve a two-step reaction with two molecules of HI, in one of which the reaction proceeded by I-abstraction. Since there is a considerable body of evidence that monoradicals react with HI almost exclusively by H abstraction,²² the possible two-step sequence is that shown in (10) and (11). Reaction 10 is somewhat analogous to the known reaction of singlet methylene with methyl halides *via* ab-



straction of halogen atoms.^{23,24} However, if reaction 10 occurred, the following monoradical reaction 11 should be sensitive to the inclusion of O_2 in the system; Table I shows that the formation of CHF^{18}FI and $\text{CHF}^{18}\text{FCl}$ is essentially unaffected by the presence of O_2 in the system. At the same time, the yields of $\text{CH}_2\text{F}^{18}\text{F}$ and CH_3^{18}F in the same systems *are* depressed by the inclusion of O_2 , indicating monoradical precursors to some of the reaction yields of these molecules in HI scavenged systems. Consequently, we conclude that the major mechanism for the formation of CHF^{18}FI in these systems is the direct insertion reaction 7.

Two of the ^{18}F -labeled products in Table I are formed by direct substitution reactions of energetic ^{18}F atoms with CH_2F_2 : $\text{CH}_2\text{F}^{18}\text{F}$ and $\text{CHF}_2^{18}\text{F}$ by replacement of F or H, respectively. The yield of $\text{CHF}_2^{18}\text{F}$ is independent of any other additives, suggesting that the direct reaction is its sole mechanistic source. The yield of $\text{CH}_2\text{F}^{18}\text{F}$, on the other hand, is much higher in the presence of HI and absence of O_2 , implying that some CHF^{18}F monoradicals will abstract H from HI if not first removed by reaction with O_2 . The possible sources of CHF^{18}F radicals are discussed below.

Two of the products in Table I, CHF^{18}FI and $\text{CHF}^{18}\text{FCl}$, are formed by direct insertion reactions of CF^{18}F with HI and HCl. The lower yield of $\text{CHF}^{18}\text{FCl}$ implies inefficient scavenging of CF^{18}F by HCl. The last four products in Table I are all assigned to mechanisms involving CH^{18}F as a reactant, and are discussed later.

(20) $\log A = 11.9$ ($M^{-1} \text{sec}^{-1}$), $E_a = 0.68 \pm 0.45$ kcal/mol. N. L. Arthur and P. Gray, *Trans. Faraday Soc.*, **65**, 434 (1969).

(21) $\log A = 11.39$ ($M^{-1} \text{sec}^{-1}$), $E_a = 2.4$ kcal/mol, J. M. Sangster and J. C. J. Thynne, *J. Phys. Chem.*, **73**, 2746 (1969).

(22) D. M. Golden and S. W. Benson, *Chem. Rev.*, **69**, 125 (1969).

(23) R. L. Johnson and D. W. Setser, *J. Phys. Chem.*, **71**, 4366 (1967).

(24) P. S.-T. Lee and R. S. Rowland, presented at the Fifth International Conference on Photochemistry, Yorktown Heights, N. Y., Sept 1969.

Table III: Variation in Yields of ^{18}F -Labeled Products following $^{18}\text{F} + \text{CF}_4$ with Variations in Concentration of Ethylene and HI Scavengers

Reactants	Pressure, Torr			
	2470	2470	2500	2470
CF_4	2470	2470	2500	2470
C_2H_4	232	232	232	232
HI	14	52	131	260
	Absolute Yields, %			
CF_3^{18}F	1.95 ± 0.20	Nd ^a	1.97 ± 0.20	1.91 ± 0.19
$\text{CHF}_2^{18}\text{F}$	0.34 ± 0.03	1.09 ± 0.06	1.23 ± 0.04	1.19 ± 0.05
CHF^{18}FI	1.35 ± 0.08	1.11 ± 0.05	1.26 ± 0.07	1.10 ± 0.05

^a Nd means not determined.

Table IV: Yields from the Scavenging Reactions of Hydrogen Halides for CF^{18}F

Reactant	Pressure, Torr				
	2480	3500	2840	3800	3800
CHF_3	2480	3500	2840	3800	3800
HI	95	16
HBr	...	84	...	29	159
HCl	57	196	...
C_2H_4	228
^{18}F -Product	Absolute Yield, %				
CF_3^{18}F	0.91 ± 0.07	0.98 ± 0.02	0.91 ± 0.02	0.96 ± 0.02	Nd ^a
$\text{CHF}_2^{18}\text{F}$	1.24 ± 0.07	1.40 ± 0.03	0.92 ± 0.05	1.25 ± 0.02	Nd
CHF^{18}FI	3.63 ± 0.11	3.49 ± 0.08
$\text{CHF}^{18}\text{FBr}$...	3.84 ± 0.06	...	3.79 ± 0.08	0.49 ± 0.11
$\text{CHF}^{18}\text{FCl}$	0.52 ± 0.04	0.48 ± 0.07	...

^a Nd means not determined.

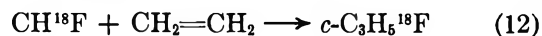
Relative Efficiencies of CF_2 Scavengers. Earlier competitive studies of CF_2 plus hydrogen halides had qualitatively shown that CHF_2Br was formed in preference to CHF_2Cl .¹⁰ Quantitative data for CF^{18}F reactions with HI, HBr, and HCl (using CHF_3 as the reactant for energetic ^{18}F atoms) are shown in Table IV. The yields of CHF^{18}FX are in the range 3.6–4.3% for samples containing HI or HBr, while HCl again fails to trap all of the CF^{18}F . The results of direct competition between HI–HBr and HBr–HCl (Table IV) show that HI is about 70 times as efficient as HBr, which in turn is about 50 times as efficient as HCl in scavenging CF^{18}F .

The order of increasing reactivity $\text{HCl} < \text{HBr} < \text{HI}$ can be understood in terms of the reaction mechanism proposed by Simons,²⁵ in which the initial interaction between CF_2 and HCl was represented by donation of electrons from a nonbonding 3p orbital on the Cl atom into the vacant $2b_1$ orbital of CF_2 . This process should become more favorable in the sequence HCl, HBr, HI. In other experiments, the scavenging of CF^{18}F by HI has been shown to be so much more efficient than by $\text{CF}_2=\text{CF}_2$ that no $c\text{-C}_3\text{F}_5^{18}\text{F}$ is observed in HI– $\text{CF}_2=\text{CF}_2$ scavenged systems.¹¹

The ultimate fate of the "missing" CF^{18}F when HCl is the only scavenger present is uncertain. Dimeriza-

tion of CF_2 , which is frequently observed in macroscopic studies of CF_2 reactions is not a major process in these experiments, since the total number of CF^{18}F fragments produced is $\sim 10^6/\text{cm}^3$ and the instantaneous concentrations must be $\leq 10^3/\text{cm}^3$.²⁶ Perhaps a slow wall reaction to give an oxygenated species such as CF^{18}FO is involved; if such a product were present, we would expect it not to emerge in a measurable molecular form from our particular chromatographic analysis systems.

Monofluorocarbene Reactions. Monofluorocarbene has been prepared by hot atom techniques previously^{6–8} and the addition to olefins has been extensively studied for CTF.⁶ The present experiments have used CH^{18}F



prepared by reactions 1 and 2, and have shown that CH^{18}F reacts efficiently with both HI and HCl. The olefin addition reaction 12 is known to occur readily for

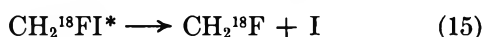
(25) J. P. Simons, *J. Chem. Soc.*, 5406 (1965).

(26) The total ^{18}F activity produced in the sample indicates that the number of ^{18}F -containing molecules is $\sim 10^8$ in a 10-ml bulb after a typical irradiation of 15 min. Assuming a 4% yield for CF^{18}F and a lifetime no longer than 10 sec for diffusion to the walls, the instantaneous concentration of CF^{18}F is not more than $\sim 10^{-3} \times$ the total CF^{18}F production.

monofluorocarbene,⁶ and the yield of $c\text{-C}_3\text{H}_5^{18}\text{F}$ (*i.e.*, the yield of CH^{18}F) has been measured as $2.09 \pm 0.08\%$ (Table I) in an $\text{O}_2\text{-C}_2\text{H}_4$ scavenged sample. Replacement of C_2H_4 by HCl results in the formation of an equivalent amount of $\text{CH}_2^{18}\text{FCl}$, suggesting that HCl is much more efficient in trapping CH^{18}F than it is for CF^{18}F . The independence of yield of $\text{CH}_2^{18}\text{FCl}$ upon the presence of O_2 indicates that reaction 13 also takes place *via* a direct insertion mechanism.



In $\text{HI-C}_2\text{H}_4$ scavenged systems, the yield of $c\text{-C}_3\text{H}_5^{18}\text{F}$ is reduced below that found in the presence of $\text{O}_2\text{-C}_2\text{H}_4$, consistent with the competitive removal of CH^{18}F by reaction 14 with HI . The ratio of rate constants, k_{14}/k_{12} , can be roughly estimated as about 3 at $\sim 10^\circ$. However, direct measurement with HI as the only scavenger shows only $0.11 \pm 0.07\%$ yield of $\text{CH}_2^{18}\text{FI}$. As indicated above by the thermochemical calculations, $\text{CH}_2^{18}\text{FI}$ is formed with vibrational energy about 19 kcal/mol in excess of the C-I bond dissociation energy, and the decomposition-scavenging process of (15) and (16) should result in the observation chiefly of CH_3^{18}F instead of $\text{CH}_2^{18}\text{FI}$ in gaseous systems. The data of Table I show several per cent yields of CH_3^{18}F under these conditions—more than adequate to account for the diverted 2% yield of CH^{18}F , while simultaneously indicating the necessity for a second mechanism for the production of CH_2^{18}F radicals.



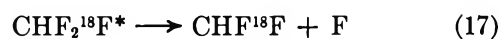
Comparison of the total yield of CH^{18}F when scavenged by HCl or C_2H_4 with the stabilized yield of $\text{CH}_2^{18}\text{FI}$, when scavenged by HI , indicates that approximately $5 \pm 3\%$ of the HI adduct is stabilized at these pressures. Since the collision frequency for stabilizing collisions is about $3 \times 10^{10} \text{ sec}^{-1}$ at 4000 Torr, the average rate constant for decomposition must be about $5 \times 10^{11} \text{ sec}^{-1}$. A crude estimate of the relationship between decomposition rate and excitation energy for CH_2FI can be obtained by comparison with the calculations for CH_3I .¹⁵ For the latter molecule, a rate constant of

$5 \times 10^{11} \text{ sec}^{-1}$ corresponds to 15–25 kcal/mol excitation energy above the bond dissociation energy, the higher value corresponding to the more rigid of two models used for the transition complex. This range of numbers is in satisfactory agreement with the 19 kcal/mol estimated from the thermochemical arguments and presumably provides the not surprising confirmation that our assumption that the heat of formation of CHF can be approximated by the arithmetic mean of those of CF_2 and CH_2 is within 5–10 kcal/mole of the correct value.

Other Sources of ^{18}F -Monoradicals. Quantitative interpretation of the CH_3^{18}F yields in this system is complicated by the fact that hot reactions with both CH_2F_2 and $\text{CH}_2=\text{CH}_2$ can form CH_2^{18}F radicals which will be indistinguishable from those produced *via* reaction 15.²⁷

The diminution of $\text{CH}_2\text{F}^{18}\text{F}$ yield by addition of O_2 to a $\text{CH}_2\text{F}_2\text{-HI}$ system indicates the presence of CHF^{18}F monoradicals. Although the abstraction of H from HI (or other molecule) by CF^{18}F could hypothetically be the source of CHF^{18}F radicals, related experiments with $\text{C}_2\text{F}_4\text{-HI}$ mixtures demonstrate that abstraction of H from HI by CF^{18}F is very unlikely. The distribution of ^{18}F products in such a system includes the following, in absolute percent yields: $\text{CF}_2=\text{CF}^{18}\text{F}$, 1.5%; CHF^{18}FI , 12.8%; $\text{CH}_2\text{F}^{18}\text{F}$, 0.25%. Thus, more than 98% of the CF^{18}F from the decomposition of vibrationally excited $\text{CF}_2=\text{CF}^{18}\text{F}$ appears as CHF^{18}FI , with less than 2% as $\text{CH}_2\text{F}^{18}\text{F}$. Even this small amount of $\text{CH}_2\text{F}^{18}\text{F}$ may be formed *via* a small partial decomposition of CHF^{18}FI (see thermochemical estimates) and subsequent scavenging of the CHF^{18}F radical.

The most likely sources of the excess CHF^{18}F radicals are by the secondary decompositions of excited molecules formed by direct substitution reactions, as in (17) and (18).



(27) $^{18}\text{F} + \text{CH}_2=\text{CH}_2 \rightarrow \text{C}_2\text{H}_4^{18}\text{F}^* \rightarrow \text{CH}_2 + \text{CH}_2^{18}\text{F}$, $^{18}\text{F} + \text{CH}_2\text{F}_2 \rightarrow \text{CH}_2\text{F}^{18}\text{F}^* + \text{F}$; $\text{CH}_2\text{F}^{18}\text{F}^* \rightarrow \text{CH}_2^{18}\text{F} + \text{F}$. In each case, the pathway shown is not the major decomposition pathway for this excited species, but does occur.

Photochemical Formation of Free Radicals from Acetonitrile as Studied by Electron Spin Resonance¹

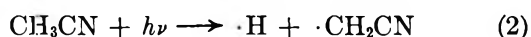
by P. Svejda and D. H. Volman

Department of Chemistry, University of California, Davis, California 95616 (Received November 11, 1969)

Electron spin resonance studies of $\text{CH}_3\text{C}^{14}\text{N}$, $\text{CH}_3\text{C}^{15}\text{N}$, and $\text{CD}_3\text{C}^{14}\text{N}$ irradiated at 185 nm in the frozen state at 77°K have been made. Evidence for two primary processes was obtained: (1) cleavage of the carbon-carbon bond; (2) cleavage of a carbon-hydrogen bond. Frozen solutions of acetonitrile-aqueous hydrogen iodide irradiated at 254 nm were also studied. Evidence for addition of a hydrogen atom to acetonitrile to form ethylenimino radical was found. INDO calculations of coupling constants for ethylenimino and cyanomethyl radicals were in general agreement with the observed spectra.

Introduction

There is, surprisingly, only a single literature report on the photolysis of an alkyl nitrile,² acetonitrile at 185 nm in the gas phase. The primary processes postulated were



Electron spin resonance studies of γ -irradiated acetonitrile in the frozen state at 77°K have shown that the cyanomethyl radical is formed³ and that methyl radical is formed on post- γ -irradiation by exposure to red or infrared light through a trapped-electron mechanism.^{4,5} The primary object of our work was to elucidate the photochemical primary process.

Experimental Section

Preparation of samples for irradiation, spectrometer system, temperature control, and observations were essentially as described previously.⁶ Acetonitrile was Eastman Spectroscopic grade. Perdeuterioacetonitrile, 98 atom % D, and ¹⁵N acetonitrile, 99.5 atom % ¹⁵N were obtained from Bio-Rad Laboratories. Two light sources were used: a low-pressure mercury resonance arc housed in quartz, allowing 185-nm light to be transmitted; a similar arc housed in Vycor, opaque to 185-nm light but which allowed 254-nm light to be transmitted.

Spectra and Interpretation

Acetonitrile irradiated at 77°K and 254 nm did not give an esr spectrum. As acetonitrile is transparent at 254 nm, this result indicates the absence of impurities which would yield a free radical spectrum either directly or by energy transfer to acetonitrile in this spectral region.

Acetonitrile irradiated at 77°K and 185 nm give the spectrum shown in Figure 1. Except for the end lines, h and i, this spectrum shows all the features of

spectra previously obtained in the γ irradiation of acetonitrile.^{3,4} It is particularly analogous to the spectrum observed by Ayscough, Collins, and Kemp⁴ for γ irradiation followed by exposure of the sample to infrared or red light which they identified as a mixture of cyanomethyl and methyl radicals.

Methyl radical is identified in Figure 1 by peaks b, d, f, and h, which have an average peak-to-peak separation of 25 G, the expected value for methyl radical. Cyanomethyl radical is identified in Figure 1 by peaks c, e, and g. Upon warming the sample from 77 to 118°K after uv irradiation, methyl radical was considerably diminished while the intensity of the cyanomethyl spectrum remained unchanged. To compare our result with the cyanomethyl spectrum as reported by Dunbar, *et al.*,³ from γ irradiation, the spectrum obtained on warming, Figure 2, was recorded at lower modulation and slower magnetic field scan rate than was used for Figure 1. The comparison, except for the outer lines in our spectrum, is good, and the evidence that the same radical is formed by uv and γ radiation is strong. Dunbar, *et al.*,³ have simulated their experimental spectrum with a computer fit using $a_{\text{H}} \cong 23$ G and $a_{\text{N}} \cong 5$ G. The average peak-to-peak separation for our spectrum, peaks c, e, and g, measured from Figure 1 is 24 G, in good agreement with the reported proton coupling constant. The nitrogen coupling constant is confirmed by experiments with $\text{CH}_3\text{C}^{15}\text{N}$ discussed below.

(1) This investigation was supported by a grant from the National Science Foundation.

(2) D. E. McElcheran, M. H. J. Wijnen, and E. W. R. Steacie, *Can. J. Chem.*, **36**, 321 (1958).

(3) D. Dunbar, D. Hale, L. Harrah, R. Rondeau, and S. Zakanycz, *Develop. Appl. Spectrosc.*, **3**, 361 (1964).

(4) P. B. Ayscough, R. G. Collins, and T. J. Kemp, *J. Phys. Chem.*, **70**, 2220 (1966).

(5) M. A. Bonin, K. Tsuji, and F. Williams, *Nature*, **218**, 946 (1968).

(6) S. G. Hadley and D. H. Volman, *J. Amer. Chem. Soc.*, **89**, 1053 (1967).

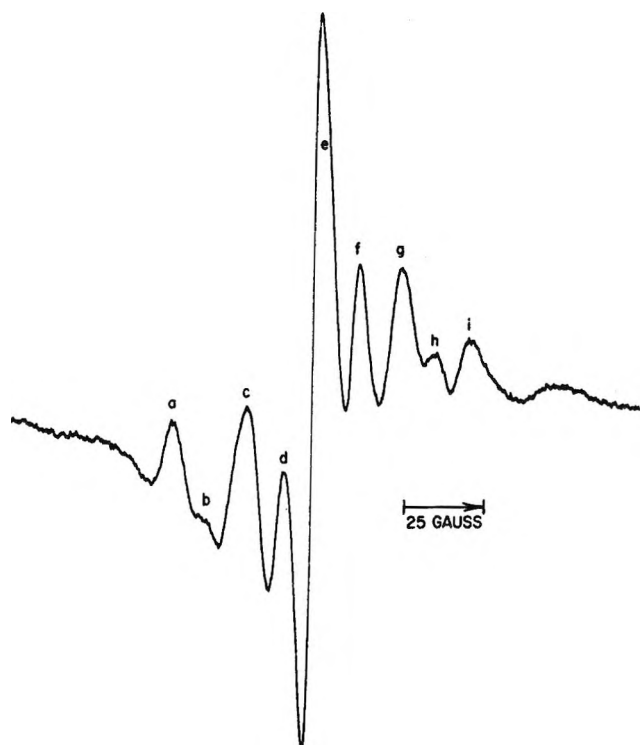


Figure 1. Esr spectrum of acetonitrile irradiated at 185 nm and 77°K.

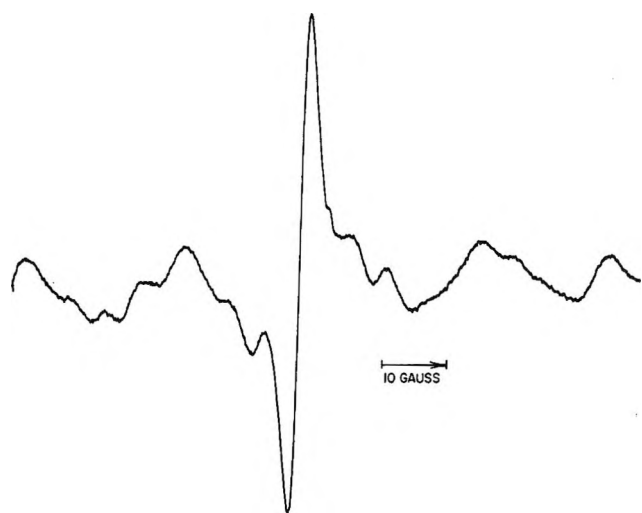


Figure 2. Esr spectrum of acetonitrile irradiated at 185 nm and 77°K. Spectrum recorded at 118°K.

Irradiation of $\text{CH}_3\text{C}^{15}\text{N}$ gave the spectrum shown in Figure 3. The methyl radical spectrum is clearly evident; the average peak-to-peak separation is 25 G and the intensities conform closely to the theoretical values, 1:3:3:1. The outer peaks of the cyanomethyl triplet indicate incomplete resolution into doublets. The center of the spectrum, however, is a well resolved doublet as would be expected from the 1.4 times greater ^{15}N nuclear g factor and elimination of the larger anisotropy accompanying the $M_1 = \pm 1$ components of the ^{14}N spectrum. The ^{15}N coupling constant calculated

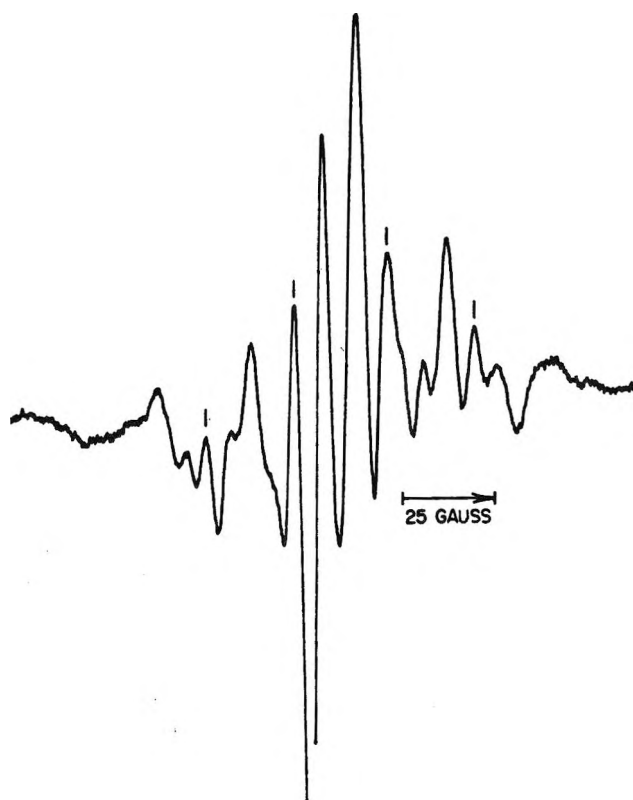


Figure 3. Esr spectrum of ^{15}N acetonitrile irradiated at 185 nm and 77°K. Methyl peaks marked.

from this splitting is 8.3 G. This corresponds to an ^{14}N coupling constant of 5.9 G.

Irradiation of CD_3CN at 77°K with subsequent warming to 113°K gave the spectrum shown in Figure 4. Ayscough, *et al.*,⁴ have interpreted spectra from γ irradiation and γ irradiation followed by exposure to red light as arising from a $\cdot\text{CD}_3$ septet and a $\cdot\text{CD}_2\text{CN}$ pentet analogous to the results with the protonated compound. However, they did not publish the spectra. Our spectrum observed at 77°K could be interpreted similarly but not with complete confidence as the many lines and narrow spacing give considerable overlap. At 113°K the methyl spectrum has disappeared and the resulting spectrum is the expected pentet (inner 5 lines) with an average peak-to-peak separation of 3.8 G. On the basis of the 24 G coupling for ^1H in cyanomethyl radical, the expected ^2H coupling constant is 3.6 G. The outer two lines clearly do not belong to the same spectrum.

Additional experiments were carried out with mixtures of hydrogen iodide and acetonitrile. The anhydrous compounds reacted rapidly in the dark and consequently an aqueous solution, the 57% HI-H₂O azeotrope, was used. Irradiation was carried out at 254 nm where acetonitrile is transparent. For a 3:1 mixture of aqueous HI and CH_3CN the spectrum shown in Figure 5 was obtained. Use of a 1:10 mixture did not affect the general character of the spectrum. Al-

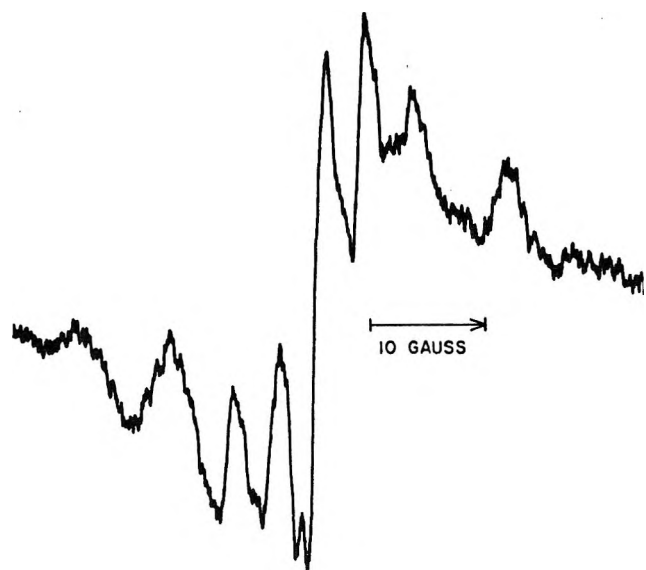


Figure 4. ESR spectrum of perdeuterioacetonitrile irradiated at 185 nm and 77°K. Spectrum recorded at 113°K.

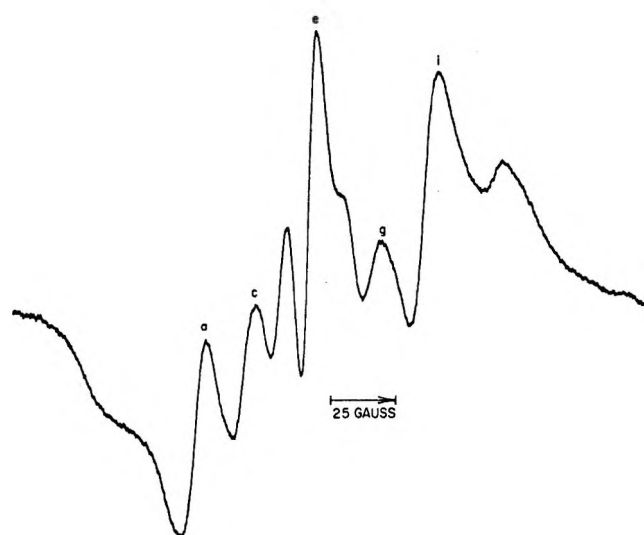


Figure 5. ESR spectrum of aqueous hydrogen iodide-acetonitrile irradiated at 254 nm and 77°K.

though the peak between lines c and e is at about the methyl position, it does not appear to come from free methyl. The other lines are missing and upon warming the sample to 133°K the peak did not disappear. The peaks at a and i and the cyanomethyl spectrum at c, e, and g, however, correspond to those obtained in the direct photolysis.

For the methylenimino radical, $\text{H}_2\text{C}=\text{N}\cdot$, formed by addition of H atoms to HCN, Cochran, Adrian, and Bowers⁷ give $a_{\text{H}} = 87$ G. Addition of H atoms to acetonitrile would yield the ethylenimino radical, $(\text{CH}_3)\text{HC}=\text{N}\cdot$, and the β proton coupling constant would be expected to be similar to that found for methylenimino radical. The spectra we have obtained indicate that this is indeed the case. The a-i separation

in Figures 1 and 5 is the same, 92 G. The end lines in Figure 4, which on this model are the outside lines of a triplet due to D substituted for H, are separated by 28 G, exactly equal to theory for the ratio of H:D coupling. Irradiation of a mixture of HI and CD_3CN also gave this proton doublet at 92 G, in this case well outside the field of other radicals.

For methylenimino radical, an anisotropic coupling due to N was noted.⁷ In Figure 5 two lines external to peaks a and i are observed, incipient on the low-field side and clear on the high-field side. Although a triplet would be expected, the interior lines would almost exactly overlap the outer lines of the cyanomethyl spectrum. The peak-to-peak separation in the postulated ethylenimino radical is 23 G while for methylenimino, as measured by us from the published spectrum, it is about 26 G. The spectrum of irradiated $\text{CH}_3\text{C}^{15}\text{N}$ may also be interpreted on this basis. External to both sides of the methyl radical spectrum are two peaks which can arise from predominantly isotropic coupling with ^{15}N . If the assumption is made that the external peak separation represents $a_{\text{H}} (92 \text{ G}) + a_{\text{N}}$, the value of $a_{^{15}\text{N}}$ obtained is 16 G. For methylenimino radical, the isotropic ^{14}N coupling has been reported as 32 Mcps, equivalent to 16 G for ^{15}N .

Calculated Isotropic Coupling Constants

Theoretical isotropic coupling constants were calculated for cyanomethyl and ethylenimino free radicals by the INDO (intermediate neglect of differential overlap) method⁸ using the computer program prepared by Dobash.⁹ The molecular geometries proposed by Pople and Gordon¹⁰ were used.

Cyanomethyl Radical. For cyanomethyl the geometry used was as follows: $\angle \text{CCN}$, 180°; $\angle \text{HCH}$, 120°; $\angle \text{HCC}$, 120°; R_{HC} , 1.08 Å; R_{CC} , 1.38 Å; R_{CN} , 1.24 Å. As the electron is delocalized the CC and CN bond lengths used were the average based on the canonical forms, $\text{H}_2\dot{\text{C}}-\text{C}\equiv\text{N}$ $\text{H}_2\text{C}=\text{C}=\text{N}\cdot$, with the convention that the electron contributes unity to the "connectivity" of the atom.¹⁰ From the calculated s orbital spin densities and expectation free atom coupling constants,⁸ the isotropic coupling constants found were $a_{\text{H}} = 20.1$, $a_{^{14}\text{N}} = 6.0$, and $a_{^{15}\text{N}} = 8.5$ G. These values are in good agreement with our experimental values of peak separation, 24 G for H and 8.3 G for ^{15}N .

Ethylenimino Radical. For ethylenimino the geometry used was as follows: $\angle \text{H}(1)[\text{H}(2),\text{H}(3)]\text{CC}$, 109.47° (tetrahedral); $\angle \text{CCN}$, 120°; $\angle \text{H}(4)\text{CC}$, 120°;

(7) E. L. Cochran, F. J. Adrian, and V. A. Bowers, *J. Chem. Phys.*, **36**, 1938 (1962).

(8) J. A. Pople, D. L. Beveridge, and P. A. Dobash, *J. Amer. Chem. Soc.*, **90**, 4201 (1968).

(9) P. A. Dobash, Program 142, Quantum Chemistry Program Exchange, Indiana University, 1969.

(10) J. A. Pople and M. Gordon, *J. Amer. Chem. Soc.*, **89**, 4253 (1967).

$\angle \text{H(4)CN}$, 120° ; $R_{\text{H(1)[H(2),H(3)]C}}$, 1.08 \AA ; R_{CC} , 1.52 \AA ; R_{CN} , 1.32 \AA ; H(1), H(2), and H(3) represent the methyl hydrogen atoms. H(4) represents the hydrogen atom bonded to the central carbon atom. H(1) and H(4) were taken as *cis* to each other. Also as for the cyanomethyl radical, the contribution of the free electron, here localized on the nitrogen atom, to the "connectivity" has been assumed unity. The isotropic coupling constants calculated were $a_{\text{H(1)}} = 0.5$, $a_{\text{H(2)}} = a_{\text{H(3)}} = 9.9$, $a_{\text{H(4)}} = 60.0$, $a_{^{15}\text{N}} = 9.2$, and $a_{^{14}\text{N}} = 13.0 \text{ G}$. The calculated coupling constants for the methyl protons are a function of the fixed configuration chosen for the methyl group. For a rotating methyl group the coupling constants would be the same for the three protons and could average out at a low value and therefore not resolvable in our experiments. It may be observed that, in general, couplings for hydrogen atoms in γ position relative to a localized electron are not resolvable. The value of 60 G for H(4) shows that this is an unusually large proton coupling interaction in accord with our experimental value of 92 G. The discrepancy between calculated and observed coupling constant is well within the range of differences found by Pople, *et al.*,⁸ for large proton coupling constants. For example, formyl yields 74.9 G calculated and 139.0 G experimental. The calculated isotropic coupling constant for ^{15}N , 13.0 G, is in reasonable agreement with our value of 16 G. Our peak separation of 23 G for ^{14}N represents anisotropic as well as isotropic contributions and therefore cannot be directly compared with the calculated value of 9.2 G. However, it may be observed that Cochran, *et al.*, have deduced that the isotropic coupling constant for ^{14}N in the homologous methylenimino radical is 11.4 G.⁷

Photochemical Mechanism

Since methyl radicals are not produced directly by γ irradiation but are instead formed by subsequent irradiation with red or infrared light through a trapped electron mechanism, it is pertinent to explore whether such a mechanism can explain the photochemical results. At 185 nm the available energy is some 5.3 eV below the ionization potential of gaseous acetonitrile. A concerted process yielding a trapped electron and solvated cation would reduce the energy requirement, but as the considerations below show, it is not likely to provide the 5.3 eV stabilization energy required. The stabilization energy for the electron trapped in γ irradiation is probably about 2.0 eV since the reaction forming methyl radical occurs in red light. A rough calculation of the stabilization energy for the cation, CH_3CN^+ , is possibly by use of Born's equation

$$-\Delta G = \left(1 - \frac{1}{\epsilon}\right) \frac{e^2}{2r}$$

for the Gibbs energy of a sphere of charge e and radius r immersed in a medium of dielectric constant ϵ .¹¹ Also

$$\Delta S = -\left(\frac{\partial \Delta G}{\partial T}\right)_p = \frac{e^2}{2r\epsilon^2} \left(\frac{\partial \epsilon}{\partial T}\right)_p$$

$$-\Delta E \cong -\Delta H = \left(1 - \frac{1}{\epsilon}\right) \frac{e^2}{2r} - \frac{Te^2}{2r\epsilon^2} \left(\frac{\partial \epsilon}{\partial T}\right)_p$$

The lowest temperature at which the dielectric constant has been reported¹² is 115°K where ϵ is 2.73 and $(\partial\epsilon/\partial T)_p$ is $2.7 \times 10^{-3} \text{ deg}^{-1}$. From the density of liquid acetonitrile at the melting point, 0.85, assuming about 5 vol % decrease on solidification and spherical molecules, $2r \cong 0.5 \text{ nm}$. From these values the calculated stabilization energy for the cation is 1.8 eV. The combined stabilization energy for the trapped electron and cation is then about 4 eV and below the 5.3 eV required. Thus, the mechanism proposed for methyl radical formation with γ irradiation appears to be untenable for the results obtained with uv irradiation.

The presence of methyl and cyanomethyl radicals in uv-irradiated acetonitrile is in accord with primary processes 1 and 2. Either primary process could account for both radicals by the postulated secondary processes² in the gas phase at 332°K .



However, the H atom cannot be formed by a secondary process. Our results yield evidence that ethylenimino radical is formed and therefore that H atoms are formed in accord with process 2. Also, the results with hydrogen iodide-acetonitrile mixtures indicate that reaction 4 does not occur. McElcheran, *et al.*, suggest that reaction 4 proceeds *via* an addition of H atom to form ethylenimino radical which dissociates to HCN and CH_3 .² It is reasonable that the intermediate radical would be stable at 77°K but not at 332°K . Further, in the γ radiolysis at 77°K there is excellent evidence that H atoms are formed and that neither methyl nor hydrogen cyanide are formed.⁴ If hydrogen atoms cannot give rise to methyl radicals at 77°K , then primary processes 1 must also occur. Therefore, it may be concluded that both primary processes, 1 and 2, occur on irradiation at 185 nm.

Although cyanomethyl radical is produced by reaction 2, another source could be by hydrogen atom abstraction by either methyl radical or hydrogen atom. The experiments with hydrogen iodide-acetonitrile mixtures provide evidence that abstraction by H atoms does indeed occur.

Acknowledgments. The authors wish to thank Professor J. S. Vincent for useful discussions and Professor G. E. Maciel for assistance with the INDO calculations.

(11) R. A. Robinson and R. H. Stokes, "Electrolyte Solutions," 2nd revised ed, Butterworth and Co. Ltd., London, 1959, p 69.

(12) R. Phillipe and A. M. Piette, *Bull. Soc. Chim. Belg.*, **64**, 600 (1955).

Influence of pH upon the Photolysis of the Uranyl Oxalate Actinometer System^{1,2}

by Lawrence J. Heidt, George W. Tregay,³ and Frederick A. Middleton, Jr.

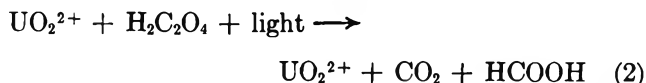
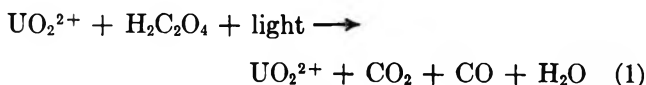
Department of Chemistry, Massachusetts Institute of Technology, Cambridge, Massachusetts 02139, Emmanuel College, Boston, Massachusetts 02115, and Institute of Chemistry, Islamabad University, Pakistan (Received February 24, 1969)

A study has been made at 25° of the influence of pH upon the relative quantum yields for the consumption of oxalate and the production of carbon dioxide, carbon monoxide, and uranous ion by light of 254 nm absorbed by the uranyl oxalate actinometer system. The uranyl ion was at 0.01 *F*, the oxalate at 0.06 *F*, and initial pH was at 0–6. About 12% of the oxalate was decomposed. The quantum yields for the consumption of oxalate were found to be independent of the pH between 1 and 5 but to decrease outside this range. The reaction at all values of pH was found to consume acid. The moles of carbon dioxide produced in all forms (CO₂, H₂CO₃, HCO₃⁻, CO₃²⁻ and the uranyl carbonate complexes) per mole of oxalate consumed very nearly equalled unity at pH 0 to 5. The moles of carbon monoxide produced per mole of oxalate consumed were always less than unity; they decreased with increase in pH abruptly between pH 1 and 2, and became negligible above pH 3. The mole ratio of uranous ion produced to oxalate consumed increased slowly from about 0.03 between pH 1.5 and 4 to about 0.08 at pH 6. The mechanisms of the reactions are discussed.

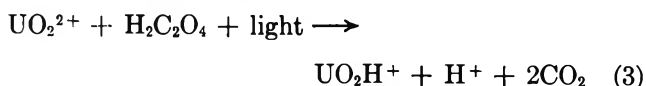
Introduction

The uranyl oxalate actinometer has been employed to measure within 3% the number of light quanta of 208 to 436 nm incident on a system when the mole ratio of oxalate to uranyl ions is 2 or greater and the concentration of uranyl ion is 0.001 *F* or greater. In these solutions most of the light is absorbed by the uranyl oxalate complexes which are decomposed into water, carbon dioxide, carbon monoxide, and formic acid. The uranyl ion is largely unchanged. The extent of the photochemical reaction is measured usually in terms of ϕ , the moles of oxalate consumed per mole of light quanta (Einstein) absorbed by the system.^{4–6} The quantum yield ϕ is about 0.6 at 208 to 436 nm independent of the light intensity in adequately stirred solutions.

The main photochemical overall reactions appear to be



A minor overall reaction appears to be



Earlier work has shown that the reaction producing carbon monoxide is independent of wavelength, light intensity, and temperature, but is favored by the addition of acid.^{7,8} Presented here is a study of the influence

of pH upon the photochemical reactions at 25°. The light employed was of 254-nm wavelength.

Experimental Section

Photolyses were carried out at 25 ± 0.1° with apparatus (Figure 1) designed to produce largely monochromatic light of 254 nm of uniform intensity incident upon the reaction vessel (Figure 2).⁹

Care was taken to mix (stir) the solutions adequately during and after photolysis especially next to the cell walls where most of the actinic light was absorbed. The stirring, however, was not so vigorous as to produce a significant vortex. Since the actinic light was of nearly uniform intensity around the reaction vessel, the fraction of the actinic light intercepted by the stirrer was independent of the rate of stirring.

A syringe was employed to sample the gas above the solution. The hollow needle through which the gas sample was taken into the syringe was long enough to reach through the no-air stopper and into the main body of the gas space.

(1) Presented in part to the Division of Physical Chemistry at the 155th National Meeting of the American Chemical Society, San Francisco, Calif., 1968.

(2) G. W. T. and F. A. M. were NSF Summer Undergraduate Research Participants.

(3) The present address of G. W. T. is Department of Chemistry, Boston College, Chestnut Hill, Mass. 02167.

(4) W. G. Leighton and G. S. Forbes, *J. Amer. Chem. Soc.*, **52**, 3139 (1930).

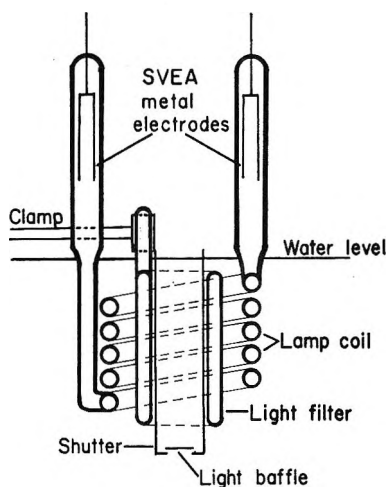
(5) F. P. Brackett and G. S. Forbes, *ibid.*, **55**, 4459 (1933).

(6) G. S. Forbes and L. J. Heidt, *ibid.*, **56**, 2363 (1934).

(7) D. H. Volman and J. R. Seed, *ibid.*, **86**, 5095 (1964).

(8) K. Porter and D. H. Volman, *ibid.*, **84**, 2001 (1962).

(9) L. J. Heidt and H. B. Boyles, *ibid.*, **73**, 5728 (1951).



PHOTOLYSIS ASSEMBLY

Figure 1. Photolysis system with light of 254 nm.

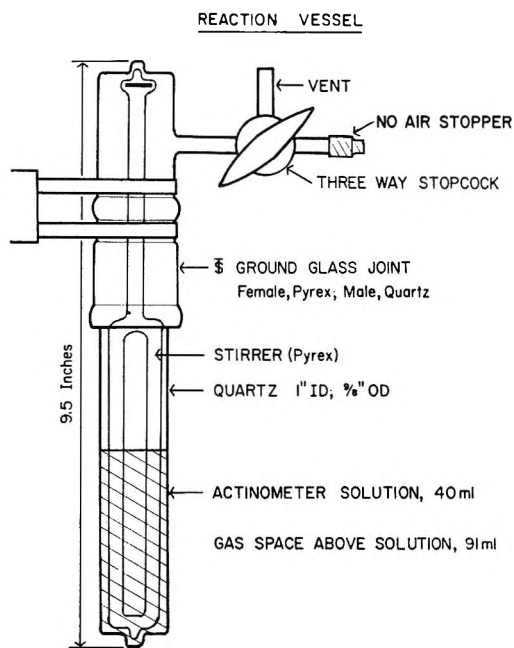


Figure 2. Reaction vessel ensemble.

Spectrometry was carried out with a Cary recording spectrophotometer, Model 11, Serial No. 69, calibrated as described elsewhere.¹⁰

pH measurements were made on 2-ml samples at 25° with a Model 4 pH meter manufactured by Radiometer Inc. of Copenhagen, Denmark. Calibration of the instrument was carried out with standard buffered solutions at pH 1.68, 4.01, 4.63, 6.86, 9.19, 10.00, and 12.45. Linear corrections were made for drift in the recorded pH values with time by employing 0.05 *F* potassium acid phthalate as the standard at pH 4.01.

The pH values of the actinometer solutions employed by other workers were estimated by us. The values between 2 and 3 assume that hydrogen ion was

freed by displacement from the oxalic acid when the oxalate formed $\text{UO}_2(\text{C}_2\text{O}_4)_2^{2-}$ and that H^+ was freed when the remaining oxalic acid dissociated into H^+ and HC_2O_4^- . Thus the $[\text{H}^+]$ of the solution containing 0.001 *F* uranyl oxalate and 0.010 *F* oxalic acid was estimated to be

$$[\text{H}^+] = 2[\text{UO}_2\text{C}_2\text{O}_4]_f + ([\text{H}_2\text{C}_2\text{O}_4]_f - [\text{UO}_2\text{C}_2\text{O}_4]_f) = 0.011 M$$

and the pH value is about 2. The pH values between 1 and 2 were estimated by adding the contribution of the excess acid to the $[\text{H}^+]$ of our solution of the nearest composition. Thus for a solution 0.01 *F* uranyl oxalate, 0.05 *F* oxalic acid, and 0.01 *F* sulfuric acid, the pH value was estimated to be 1.32 from the $[\text{H}^+]$ of 0.36 *M* measured for our solution 0.01 *F* uranyl oxalate and 0.05 *F* oxalic acid plus a contribution of 0.012 *F* to the $[\text{H}^+]$ from the sulfuric acid.

Materials. The uranyl oxalate was made by mixing filtered solutions of Merck Reagent grade uranyl nitrate and Fisher Certified Reagent oxalic acid. The precipitated uranyl oxalate was washed repeatedly until free from acid after which it was allowed to dry in the dark in air at room temperature. The product was assumed to be $\text{UO}_2\text{C}_2\text{O}_4 \cdot 3\text{H}_2\text{O}$. A solution made up to a calculated concentration of 0.0201 *F* was found by analysis to have an oxalate concentration of 0.0204 *F*.

Other materials were of reagent grade: uranyl sulfate from Amend Drug and Chemical Co., Primary Standard sodium oxalate from Mallinckrodt, ceric bisulfate and Ferrion indicator (1, 10-*o*-phenanthroline ferrous sulfate) from G. Frederick Smith Chemical Co., purified sodium perchlorate from Fisher Scientific, Reagent perchloric acid from Baker, and Reagent sulfuric acid from DuPont.

Analysis. The concentration of oxalate was determined in a way that avoided interference from formate or formic acid. Aliquots of the solution were made 3 *F* in sulfuric acid followed by the addition of a measured amount of about 0.06 *F* ceric sulfate solution in excess. The ceric sulfate solution was also 3 *F* in sulfuric acid. The mixtures of oxalate and ceric were heated rapidly to about 100° for about 2 min to ensure complete oxidation of the oxalate. The heating was carried out cautiously to avoid spatter. The heated mixtures were allowed to cool to about room temperature whereupon the excess ceric was titrated with ferrous sulfate to the orthophenanthroline end point. Two milliliters of 0.0012 *M* Ferrioin indicator was added just before completing the titration. Separate experiments showed that this procedure was unaffected by the initial presence of formate.

The CO_2 and CO produced by the photolyses were determined by gas chromatography employing ac-

(10) L. J. Heidt and D. E. Bosely, *J. Opt. Soc. Amer.*, **43**, 760 (1953).

Table I: Composition of Solutions (Concentrations Are in Gram Formula Weights per Liter.)

Soln	UO ₂ C ₂ O ₄	UO ₂ SO ₄	H ₂ C ₂ O ₄	Na ₂ C ₂ O ₄	HClO ₄	NaClO ₄	Approx pH
A		0.01	0.05				1.4
B	0.01		0.05		1.19		(-0.1)
C	0.01		0.05		0.2		0.8
D	0.01		0.05		0.1	0.1	1.0
E	0.01		0.05			0.17	1.5
F	0.01		0.025	0.025		0.11	2.3
G	0.01		0.01	0.04		0.074	3.9
H	0.01			0.05		0.05	6.0

cepted methods. The accuracy was better than 0.2 μ mol or 0.5 mol % of the 1-ml samples taken at about NTP. In most cases the solubility of the CO₂ and CO in the actinometer solutions was included directly in the calibration. The calibration procedure employed was as follows. 1. A known amount of gas was injected into the reaction vessel containing the usual 40 ml of actinometer solution. 2. The gas was equilibrated with both the gaseous and liquid phases. 3. A 1-ml sample of the gas mixture in the reaction vessel was withdrawn and injected into the gas chromatograph.

The calibration curve was constructed by plotting the moles of gas injected (which represents the total amount of gas in the equilibrated system) against the response of the gas chromatograph for the 1 ml sample. The amount of CO soluble in the actinometer solutions at pH 0-6 amounted to 0.02 ml of CO at NTP per milliliter of solution when the partial pressure of CO above the solution was one atmosphere and Henry's law was assumed.

The amount of CO₂ soluble in the actinometer solution at pH 0-4 was found to amount to 0.79 ml of CO₂ at NTP per milliliter of solution. In the case of actinometer solutions above pH 4, the CO₂ was determined by first acidifying the solution with H₂SO₄ to a pH of about 1 and then employing the above procedure to determine the amount of CO₂.

The analysis for uranous ion was carried out spectrophotometrically only when the solutions were kept under an atmosphere of nitrogen to prevent atmospheric oxidation of the U(IV) to U(VI). The extinction coefficients of the U(IV) per gram-atom of U(IV) per liter per centimeter of the solution were measured directly in three of our actinometer solutions, namely solutions E, G, and H. We found that for solution E at pH 1.39, $\lambda_{\max} = 664$, and $\epsilon_{\max} = 36.3$; solution G at pH 3.82, $\lambda_{\max} = 667$, and $\epsilon_{\max} = 44.9$ and for solution H at pH 5.82, $\lambda_{\max} = 667$ nm and $\epsilon_{\max} = 41.8$. We used the average ϵ value of $41.0 M^{-1} \text{ cm}$ in our calculations. This is reasonable because most of U(IV) in these solutions is presumably tied up in oxalate complexes.

Composition and approximate pH values of the solutions photolyzed are given in Table I. The pH was found to be about 1.4 for the usual actinometer solu-

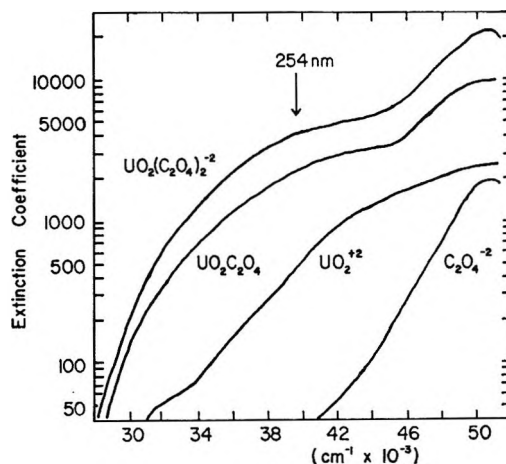


Figure 3. Ultraviolet absorption spectra of actinometer system and components. Extinction coefficients ϵ for the uranyl solutions are per gram-atom of uranium per liter per centimeter depth of solution at 25°. The UO₂(C₂O₄)₂²⁻ curve is for a solution at pH 5.86 containing 0.01 *F* UO₂C₂O₄ with 0.04 *F* Na₂C₂O₄; UO₂C₂O₄ is for 0.02 *F* UO₂C₂O₄ at pH 3.56; UO₂²⁺ is for 0.1 *F* UO₂(ClO₄)₂ with 5 *F* HClO₄; C₂O₄²⁻ is for 0.08 *F* Na₂C₂O₄. The values of ϵ at 254 nm are 4000, 2200, and 420 l. (mol of U(VI))⁻¹ cm⁻¹ in the three different uranyl solutions; ϵ for the oxalate in the sodium oxalate solution is comparatively negligible.

tion containing uranyl oxalate or uranyl sulfate at 0.01 *F* and oxalic acid at 0.05 *F*. Tenfold dilution of the solutions with distilled water increased the pH from 1.4 to 2.4. The replacement of oxalic acid by sodium oxalate changed the pH from 1.4 to 6.

Results

The absorption spectra of several pertinent solutions are presented in Figures 3 and 4. The fact that addition of oxalate to uranyl ions increases the absorption is well known but not that the charge-transfer portion of the absorption attributable to the bonds between the uranyl and oxalate ions has the same value, namely, 1800 at 254 nm per uranyl oxalate bond for both the mono and dioxalate uranyl complexes. The appropriate calculations can be made from the extinction coefficients at 254 nm given in Figure 3. Assuming solution 2 is predominantly the monoxalate complex then

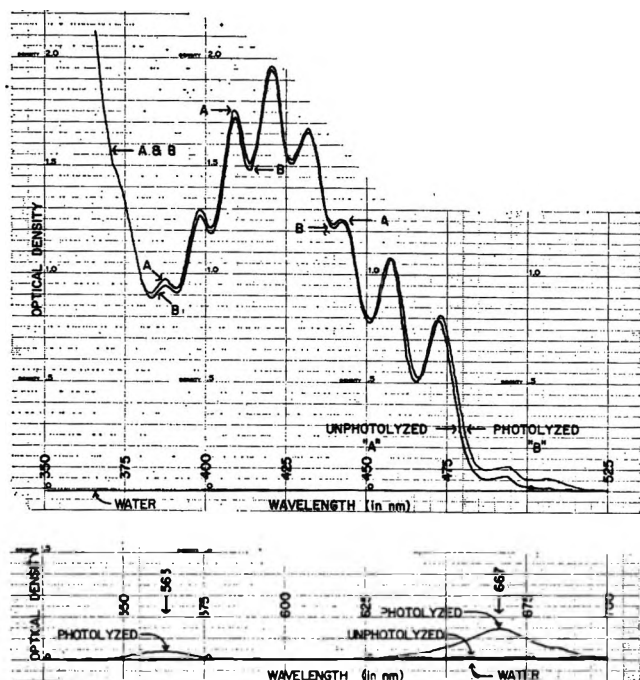


Figure 4. Visible absorption spectra of the actinometer system. The measurements are for the system at 25° under nitrogen before and after photolysis with light of 254 nm. Most of the light of wavelengths less than 525 nm is absorbed by the complex $C_2O_4^{2-} \cdot UO_2^{2+} + C_2O_4^{2-}$. The absorbance at 550 to 700 nm is mainly by the U(IV) species produced by photolysis; these species are rapidly oxidized to U(VI) species when oxygen is present. There was no evidence for any U(V) species of lifetimes greater than a few minutes. The optical density values are for a 10-cm depth of the solution: 0.01 *F* $UO_2C_2O_4$, with 0.01 *F* $H_2C_2O_4$, 0.04 *F* $Na_2C_2O_4$. Its pH was 3.85 before photolysis and 4.25 after photolysis of 12% of the oxalate.

1800 \approx 2200 - 420 in l. (mol of U(VI))⁻¹ cm⁻¹. Solution 1 corresponds to the dioxalate complex and the appropriate calculation is 1800 \approx (4000 - 420)/2. This situation, moreover, appears to exist throughout the spectrum between 200 and 500 nm except, of course, that the pertinent extinction coefficients are different.

The amount of oxalate decomposed in the various solutions at constant light intensity is presented in Table II. If the average of the standard solution of 0.01 *F* uranyl sulfate and 0.05 *F* oxalic acid is used to define the light intensity then the relative quantum yields of the solutions are as shown in Figure 5.

Table II: Decomposition of Oxalate at Constant Light Intensity

Soln	Oxalate decompd 10 ⁴ mol	Soln	Oxalate decompd 10 ⁴ mol
A	3.35	E	3.26
A	3.42	E	3.40
B	2.79 ^a	F	3.38
C	3.29	G	3.41
D	3.33	H	3.14

^a Corrected for a small change in light intensity.

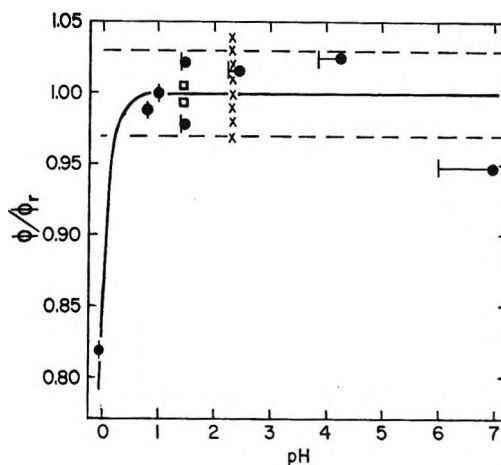


Figure 5. Quantum yields ϕ equal to moles of oxalate destroyed per einstein of light of 254 nm absorbed by the system as a function of pH. ϕ_r is defined as the average value of ϕ for the standard actinometer solution containing 0.01 *F* uranyl sulfate and 0.05 *F* oxalic acid at 25°. The relative values of ϕ for the standard solution are represented by \square . Values of the ratio ϕ/ϕ_r for the other solutions are represented by \bullet at the pH of the solution after photolysis. The vertical bars are at the initial pH values. The data of Forbes and Heidt⁶ are represented by \times .

The quantum yield for our uranyl oxalate solutions is found to be constant within the experimental error of $\pm 3\%$ over the pH range 1-5. The 20% drop in ϕ for the photolysis of solution B at pH 0 can be attributed to the decrease in the fraction of uranyl ions tied up as uranyl oxalate complexes of all kinds. An indication that a significant fraction of the uranyl ions are not in oxalate complexes in solution B comes from a comparison of the extinction coefficients for the solutions at the peak near 420 nm. Here the values of ϵ per gram atom of uranium per centimeter were found to be 20 for $UO_2(C_2O_4)_2^{2-}$, 15 for $UO_2C_2O_4$, and 8 for $UO_2^{2+}(aq)$. The value of ϵ for solution B is 11 which lies between 8 and 15 and implies that a significant fraction of the uranyl ion is present as UO_2^{2+} .

The consumption of acid by the photochemical reaction becomes evident when the photolysis is carried out at pH values above pH 2 where there is a noticeable shift in pH toward higher values as the photolysis progresses.

Table III presents a summary of all the experimentally measured quantities except for the values presented in Table II. The implication of these measurements is discussed below. The numbers are an average of at least three individual measurements except in the case of the determination of U(IV).

Figure 6 presents the fraction of oxalate photochemically decomposed to carbon monoxide vs. pH of the photolyzed solution. The decrease in the yield of carbon monoxide with increase in pH is seen to be greatest in the pH range 1-3. Both our data and the data of Volman and coworkers are in substantial agreement

Table III: Experimental Results^a

Soln	pH before photolysis	pH after photolysis	Oxalate destroyed, 10 ⁴ mol	CO ₂ above soln, 10 ⁴ mol	Total CO ₂ , 10 ⁴ mol	Total CO, 10 ⁴ mol	Total U(IV), 10 ⁴ mol	Remarks
B	(-0.08)	(-0.08)	2.92 ± 0.10	2.35 ± 0.25	3.17 ± 0.30	2.79 ± 0.15	...	
C	0.81	0.81	3.67	2.50	3.67	2.85	...	
D	0.99	1.00	4.18	3.02	4.07	2.92	...	
E	1.46	1.51	3.85	2.69	3.63	1.75	0.098 ± 0.01	b
E	1.46	1.50	3.94	2.67	3.60	1.79	0.098	b
E	1.45	1.50	4.02	2.89	3.89	2.13	...	
E	1.43	1.50	3.88	3.00	4.04	2.09	...	
E	1.39	(1.44)	6.47	...	7.46	c
E	1.39	(1.44)	6.83	...	7.08	c
F	2.25	2.45	3.44	2.77	3.73	0.74	...	
G	3.85	4.24	3.53	2.70	3.64	0.47	...	
G	3.85	4.28	3.42	2.79	3.77	0.51	0.117	b
G	3.82	(4.23)	7.03	...	7.91	c
G	3.82	(4.23)	7.45	...	8.00	c
E	5.85	(6.87)	6.72	1.26	6.39	c
E	5.85	(6.87)	6.93	1.31	6.10	c
E	6.02	(6.65)	(1.86)	0.56	...	0.0	...	b, d
		(7.04)	3.35	0.83	...	0.0	0.274	b
E	5.86	(6.20)	(1.12)	0.51	...	0.0	...	d
		(6.54)	(2.24)	0.79	...	0.0	...	d
		(5.88)	3.36	1.04	...	0.0	...	
E	5.95	(5.29)	(1.03)	0.58	...	0.0	...	d
		(5.63)	(2.05)	0.91	...	0.0	...	d
		6.97	3.08	1.13	...	0.0	...	e

^a Numbers enclosed in parenthesis are estimated. ^b Photolysis in a nitrogen atmosphere. ^c Total amount of carbon dioxide determined after acidification of actinometer solution. ^d Sample taken after partial photolysis but after ample equilibration time. ^e pH after photolysis measured without nitrogen bubbling through actinometer solution.

based on our estimates of the pH values of their solutions. The one instance in which their data differ substantially from ours is for the solution containing the 1 *F* acid. The difference we believe is due to the use of sulfuric acid in their solution compared to the use of perchloric acid in ours.

Figure 7 presents the ratio of the moles of gaseous CO₂ above the solution to the moles oxalate consumed. These results are unique to the situation of 40 ml of actinometer solution and 91 ml of gas space but they show that the solubility of CO₂ in actinometer solutions follows reasonably close to what would be predicted assuming reaction 3 to be minor and employing the literature values for the solubility of CO₂ in salt solutions.

The fact that all the data between pH 6 and 7 fall below the line can be explained by the formation of uranyl carbonate complexes. The great stability of uranyl carbonate complexes in water above pH 6 is well known in connection with the geological transport of uranium.¹¹

Figure 8 presents the ratio of the total moles of CO₂ produced to the moles of oxalate consumed. The yield of CO₂ is equal to

$$\begin{aligned}(\text{CO}_2) &= (1 - a)\Delta(\text{C}_2\text{O}_4^{-2}) + a2\Delta(\text{C}_2\text{O}_4^{-2}) \\ &= (1 + a)\Delta(\text{C}_2\text{O}_4^{-2})\end{aligned}$$

where *a* is the fraction reaction 3 contributes to the overall photochemical reaction. The value of *a* is equal to the ratio of the U(IV) produced to the oxalate decomposed. The data fall within or very close to the limits of error of this calculated yield.

Figure 9 presents the ratio of the production of U(IV) to the ratio of oxalate decomposed. The reaction producing U(IV) is minor below pH 5 and is only a small contribution to the overall photochemical reaction at pH 6. Our yields of U(IV) are higher than those of McBrady and Livingston¹² but the difference is not significant.

Discussion

Insight into the mechanism of the uranyl oxalate actinometer system has been obscured by several problems. The first is the nature of the photosensitive complex. Almost all possible forms of the complex have been proposed, namely, UO₂C₂O₄, UO₂HC₂O₄⁺, UO₂(HC₂O₄)₂, UO₂H₂C₂O₄²⁺, and UO₂(C₂O₄)₂²⁻.¹³⁻¹⁶

(11) R. M. Garrels and C. L. Christ, "Solutions, Minerals, and Equilibria," Harper and Row, New York, N. Y., 1965, pp 253-256.

(12) J. J. McBrady and R. Livingston, *J. Phys. Chem.*, **50**, 176 (1946).

(13) G. K. Rollefson, *Chem. Rev.*, **17**, 425 (1935).

(14) L. J. Heidt, *J. Phys. Chem.*, **46**, 624 (1942).

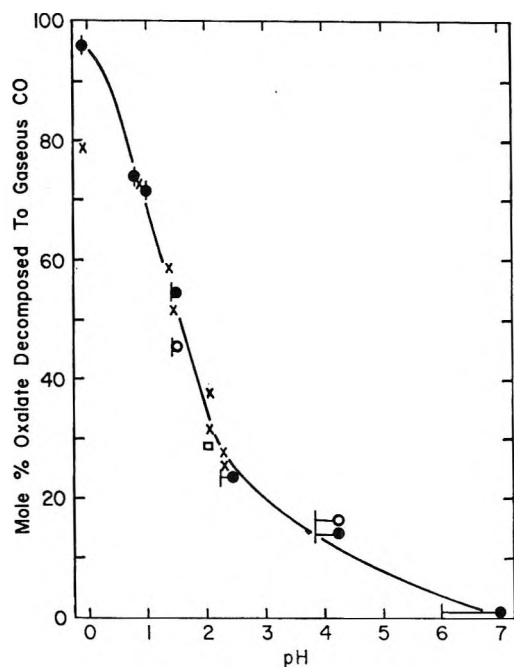


Figure 6. Fraction of oxalate decomposed to carbon monoxide vs. pH. The ● and ○ represent our data for photolyses carried out in an atmosphere of air and nitrogen, respectively, vs. pH of the solution after photolysis. The vertical bars are at the initial pH values of the solutions. The data of Volman and Seed⁷ and Porter and Volman⁸ for solutions with similar concentrations are represented by × and □, respectively. The data of Volman and coworkers are plotted at pH values estimate by us.

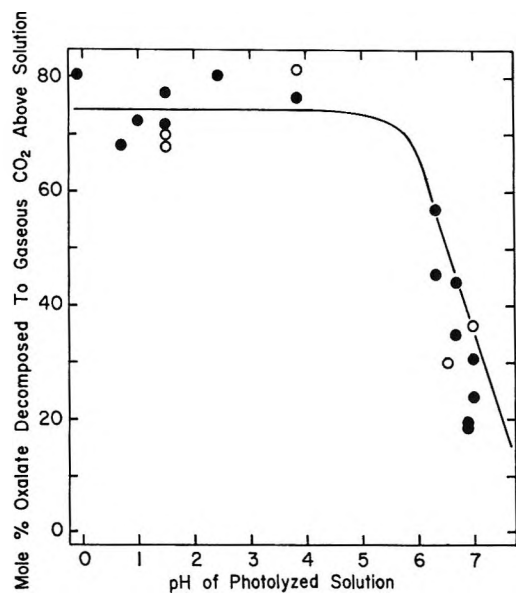


Figure 7. Fraction of oxalate decomposed to gaseous CO₂ above solution. The ● and ○ represent data for photolyses carried out in an atmosphere of air and nitrogen, respectively, vs. the pH of the solution after photolysis. These values will pertain only to a reaction vessel containing 40 ml of actinometer solution and 91 ml of gas space. The line was calculated assuming one oxalate ion was decomposed into one carbon dioxide molecule and using Henry's law and literature values for the solubility of carbon dioxide.

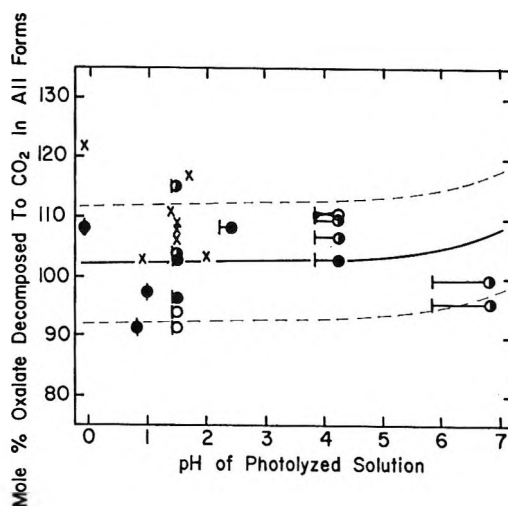


Figure 8. Fraction of oxalate decomposed to CO₂ in all forms. The ● and ○ represent our data for photolyses carried out in an atmosphere of air and nitrogen, respectively, vs. the pH of the solution after photolysis. In these experiments the CO₂ was determined at the pH of the solution after photolysis. The ● represent our data for photolyses carried out in a nitrogen atmosphere in which the CO₂ was determined after the photolyzed solution was acidified to about pH 1.5. The line was calculated from the moles of oxalate decomposed and the moles of U(IV) produced. The data of Volman and Seed⁷ for actinometer solutions at similar concentrations are represented by × and are plotted at the pH value estimated by us for their solutions.

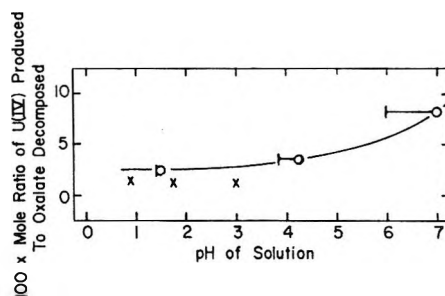


Figure 9. Fraction of oxalate decomposed which was accompanied by production of U(IV). The ○ represent our data for photolyses carried out in an atmosphere of nitrogen vs. the pH of the photolyzed solution. The data of McBrady and Livingston¹² are represented by × and plotted at pH values estimated by us.

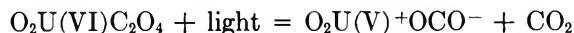
The protonated species have been assumed in the analysis of experimental results but have not been shown to offer a unique solution. Conductance measurements of uranyl oxalate solutions,¹⁵ pH measurements of solutions containing uranyl ion with excess oxalic acid¹⁵ and our spectroscopic measurements indicate strongly the predominant uranyl species in our solutions at pH 1 to 7 are UO₂C₂O₄ and UO₂(C₂O₄)₂²⁻.

(15) E. C. Pitzer, N. E. Gordon, and D. A. Wilson, *J. Amer. Chem. Soc.*, **58**, 67 (1936).

(16) N. C. Li, W. M. Westfall, A. Lindenbaum, J. M. White, and J. Schubert, *ibid.*, **79**, 5864 (1957).

The second problem is the nature of the excited uranyl oxalate complex which is produced by the absorption of a quanta of light at wave lengths of 436 nm and less. The absorption of light by the complexes could result in an energy transfer to the oxalate or in a charge transfer from the oxalate to the uranium. The products do not differentiate the process which is occurring but some analogy can be made to similar processes. The photolysis of uranyl ion with an *excess* of formic acetic acid produces mainly U(IV).¹⁷ The photolysis of cobalt, iron, and manganese oxalate complexes also results in a reduction of the metal ion even at wavelengths where the incident light is absorbed in a transition which is localized on the metal atom.¹⁸ Thus, it seems likely that the absorption of light by uranyl oxalate even as long as 436 nm results in a charge transfer from the oxalate to the uranyl ion. This is substantiated by the flash photolysis study of Parker and Hatchard¹⁹ in which a long-lived but reversible change in the absorption of uranyl oxalate was observed. This observation is consistent with a reaction scheme in which the U(VI) is reduced to U(V) in the initial step and then later oxidized back to U(VI).

Our data combined with that of other workers is sufficient to suggest a reaction sequence for the photolysis of uranyl oxalate. The primary reaction in accord with these observations is an electron transfer from the oxalate ligand to the U(VI) with the liberation of CO₂ and the production of the U(V) radical.

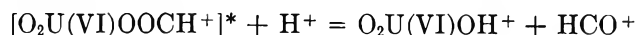


The formation of CO₂ in such a primary reaction is consistent with the production of CO₂ by the photolysis of all aqueous acid solutions when the actinic light is absorbed by uranyl ions complexed with the carboxyl group and with the consistency of the CO₂ yield over a reasonable range of pH not complicated by reactions removing the CO₂. The OCO⁻ species has been observed spectroscopically in an irradiated system of formate and oxalate ions.²⁰

The main secondary reaction we infer from the influence of pH upon the yields of carbon monoxide appears to be a concerted electron transfer from the U(V) to the OCO⁻ radical involving a proton from water. The product would be an energy rich uranyl formate complex containing the energy released in going from two unstable species to two stable ones. The proton

$\text{O}_2\text{U(V)+OCO}^- + \text{H}_2\text{O} = [\text{O}_2\text{U(VI)OOCH}^+]* + \text{OH}^-$
must come largely from water since the carbon-hydrogen bond of formate is produced readily even at high pH and is much less acidic than the OH bond of water.

Carbon monoxide would be produced at low pH if hydrogen ions are effective in breaking one of the carbon-oxygen bonds of the energy rich complex *via* the reaction



The HCO⁺ would rapidly decompose to carbon monoxide and hydrogen ions. In the absence of sufficient hydrogen ions the uranyl formate species would lose its excess thermal energy and formate ions would be the product of the photochemical reaction as observed. The formation of CO must require an energy rich complex because uranyl formate has not been observed to thermally produce CO in water at 1 *F* or smaller acid concentrations at 25°.

The production of small amounts of U(IV) can be accounted for by the reaction of the O₂U(V)+OCO⁻ species with U(VI) to produce two U(V) species and carbon dioxide from the OCO⁻. The lifetime of U(V) in water is known to increase with pH²¹ and would increase the production of U(IV) as observed. The disproportionation of U(V) to U(IV) has been studied in detail.²²

Summary

The experimental results can be summarized as follows. 1. The quantum yield for the destruction of oxalate is constant between pH 1 and 5. 2. The mole ratio of CO produced to oxalate decomposed is approximately 1 at pH 0 but falls off rapidly between pH 1 and 3 and becomes 0 at pH 6. 3. The mole ratio of total CO₂ produced to oxalate decomposed is slightly greater than 1 in the pH range 0-7. The yield of gaseous CO₂ decreased rapidly above pH 6. 4. The extinction coefficient of U(IV) was measured in our actinometer solutions and had an average value of 41 l. (mol of U(IV))⁻¹ cm⁻¹ between pH 1 and 6. The mole ratio of U(IV) produced to oxalate decomposed increased with pH but was never greater than 10%. 5. A reaction mechanism is proposed which is in accord with the experimental measurements.

(17) E. Rabinowitch and R. L. Belford, Ed., "Spectroscopy and Photochemistry of Uranyl Compounds," Vol. 1, Monographs on Nuclear Energy, Chemical Division, Macmillan Co., New York, N. Y., 1964.

(18) A. W. Adamson, W. L. Waltz, E. Zinato, D. W. Watts, P. D. Fleischauer, and R. D. Lindholm, *Chem. Rev.*, **68**, 541 (1968).

(19) C. A. Parker and C. G. Hatchard, *J. Phys. Chem.*, **63**, 22 (1959).

(20) P. W. Atkins, N. Keen, and M. C. R. Symons, *J. Chem. Soc.*, 119, 2873 (1962).

(21) L. J. Heidt and K. A. Moon, *J. Amer. Chem. Soc.*, **75**, 5803 (1953).

(22) J. J. Katz and G. T. Seaborg, "The Chemistry of the Actinide Elements," Methuen and Co. Ltd., London, 1957, p 176.

Chemical Effects in Thin Films of 1-Hexene at 77°K Due to Low-Energy Electron Impact

by Linda M. Hunter, Toshiaki Matsushige,¹ and William H. Hamill

Department of Chemistry and the Radiation Laboratory,² University of Notre Dame, Notre Dame, Indiana 46556
(Received December 9, 1969)

Thin films ($\sim 500 \text{ cm}^2 \times 700 \text{ \AA}$) of 1-hexene at 77°K have been bombarded by low-energy electrons and the products subsequently analyzed. At $\sim 50 \text{ eV}$ the yields of dimeric products per unit absorbed energy approximate those of conventional samples at the same temperature following ^{60}Co irradiation. Both C_{12} and fragmented hydrocarbons begin to form at $\sim 3 \text{ eV}$, reach pronounced maxima at $\sim 4 \text{ eV}$, then fall nearly to zero at $\sim 8 \text{ eV}$, and nearly attain plateaus by $\sim 20 \text{ eV}$. The peaks at low energy are attributed to triplet excitation of π electrons for dimerization and to triplet excitation of σ electrons for C-C scission.

Introduction

The chemical effects of high-energy radiation are complicated by the lack of selectivity in the interactions of high-energy photons and particles with molecules in the system. Further complications arise from high local concentrations of ionized and excited species in the tracks of energetic electrons. In contrast, the electron impact phenomena susceptible to measurement in the mass spectrometer can often be described with considerable precision and detail. To supplement the powerful technique of pulse radiolysis for detecting and observing transient species, it is desirable to develop other methods which can correlate yields of chemical products in condensed media with a spectrum of electron energies. An example of this for low-pressure gaseous systems is the ionization efficiency curve of mass spectrometry, with the included ionization and appearance potentials, both at and above onset.

For a practical device it is necessary to use a thermionic emitter, and to prevent pyrolysis the target must have a negligible vapor pressure. In order to achieve even 1-eV precision in measuring the appearance potential of a product species, the target must conduct incident electrons to the underlying anode. These requirements can be met by depositing the sample as an ultrathin film at 77°K. For subsequent gas chromatographic analysis of the irradiated film one chooses $\sim 10^{-3} \text{ g}$ of sample and compromises with a 1-l. spherical vessel to give a film $\sim 700\text{-\AA}$ thick.

The test substance chosen was 1-hexene since it (and other terminal monoolefins) have been thoroughly studied. Wagner, *et al.*,³ have shown that γ irradiation of 1-hexene at $\sim 20^\circ$ yields dimers as the principal products (together with appreciable yields of trimers and tetramers), which are mostly monoolefins. The structures were not those obtained by free-radical induced reactions, which yield nonterminal dimeric olefins containing two double bonds, and an ion-molecule mech-

anism was postulated. A related recent study of 1-pentene at 30° , -78° , and -196° provides similar but more detailed information.⁴ The major peak in the decenes ("dimer A") was enhanced, and the others diminished, by adding electron scavengers. The yield of dimer A decreased somewhat at reduced temperatures; the yields of the other dimers were markedly reduced. Free-radical scavengers had little effect on dimer A, but the yields of other dimers were strongly suppressed. This and other evidence supports the proposal of an ionic precursor for dimer A, the "ionic dimer." It would be expected, therefore, that an onset or appearance potential for such a product could be observed at the ionization potential of 1-hexene, which should be somewhat less than 9.5 eV observed for the low-pressure gas, and this feature provided a nominal objective. The larger purpose was simply to explore the technique.

Experimental Section

Material. For thin film experiments 1-hexene in a nitrogen-purged ampoule (Chemical Sample Co.) was opened under vacuum and used without treatment. For ^{60}Co radiolysis the 1-hexene from the same supplier was passed through a 3-ft freshly activated alumina column, then outgassed and sealed under vacuum.

Radiolysis. About 0.4 ml of 1-hexene in an evacuated, sealed Pyrex tube was irradiated at 77°K, at a dose rate $1.64 \times 10^{18} \text{ eV/g min}$, to a maximum total dose of $3.44 \times 10^{20} \text{ eV/g}$.

(1) This work is based on a dissertation submitted in partial fulfillment of the requirements of the Ph.D. degree at the University of Notre Dame.

(2) The Radiation Laboratory of the University of Notre Dame is operated under contract with the U. S. Atomic Energy Commission. This is AEC document No. COO-38-700.

(3) P. Chang, N. C. Yang, and C. D. Wagner, *J. Amer. Chem. Soc.*, **81**, 2060 (1959).

(4) C. D. Wagner, *Trans. Faraday Soc.*, **64**, 163 (1968).

Low-Energy Electron Impact. A schematic diagram of the apparatus appears as Figure 1. This apparatus bears a general resemblance to the one described by Gill⁵ for low-energy electron bombardment of thin films of ethene and ethane at 63°K. The inner surface of the 1-l. Pyrex flask was coated with platinum using Liquid Platinum Alloy, No. 130-A, Hanovia Liquid Gold Div. Mounted tungsten filaments were removed from GE 1458 1.5-V flashlight bulbs, providing nearly point sources, and centered in the flask. Prior to electron bombardment the filament was maintained at operating temperature for ~ 2 min before drawing an electron current to the film. The diode characteristic emission current-voltage curve was determined (with no film) with the flask at 77°K.

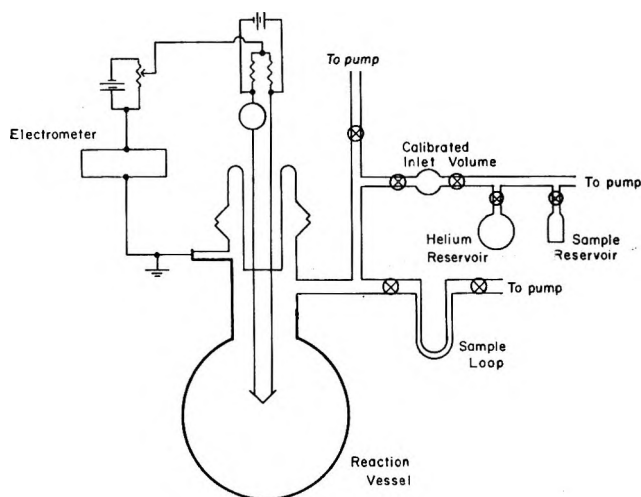


Figure 1. Apparatus for low-energy electron bombardment of thin films deposited at 77°K on a Pt anode in a spherical Pyrex vessel. Samples were collected in the loop at 77°K and transferred *via* Swagelok fittings to a chromatograph.

Sample ampoules were broken under vacuum, outgassed, measured in a calibrated volume (45.7 ml) at 14 Torr (unless specified), and expanded into the reaction flask precooled to 77°K. To improve uniformity of film deposition *ca.* 1 Torr of He was admitted before the 1-hexene for some experiments. This extended the time for subsequent evacuation prior to electron bombardment so greatly that this step was abandoned with no evident change in the results. Allowing for thermal contraction, films were nominally ~ 750 Å thick. During electron bombardment the applied potential was adjusted to maintain a constant anode current. The effective potential was taken from the diode characteristic curve at the measured anode current.

The irradiated sample was recovered in a loop of $1/8$ in. i.d. stainless steel at 77°K while pumping for 1 hr, the rest of the system being heated. Swagelok connections and metal valves were used for sample inlet and recovery, and the system was maintained under bakeout except during an experiment.

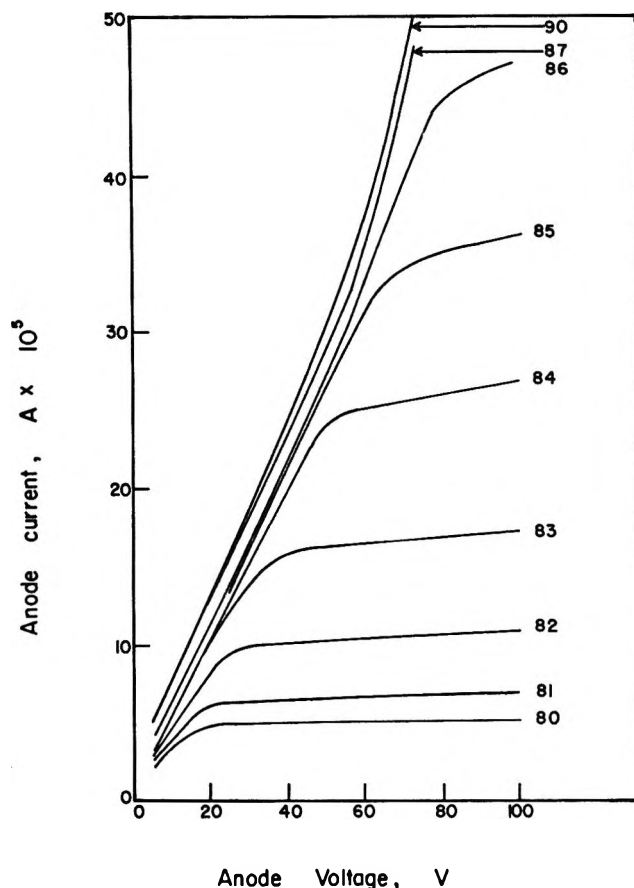


Figure 2. Anode current *vs.* applied voltage of the diode reactor at several filament currents for a nominally clean anode.

Analysis. Both ⁶⁰Co irradiated and electron bombarded samples were analyzed using a Beckman GC-5 gas chromatograph with the flame-ionization detector and a column of 3% silicone gum rubber (SE-30) on a 12-ft Chromosorb-P column. The inlet port of the chromatograph was modified with a Carl microvalve to accept the sample loop. The loop was wrapped with heating tape and brought to $\sim 200^\circ$ before the valve was opened. Dimer products were assumed to give the same response as 1-dodecene, and they were identified by their vapor pressures at column temperature and their retention times.

Results

The electron energy resolution is low because there is no slit to limit emission to a short length of the filament and the energy spread arises from *IR* drop across the center-tapped filament as well as the Boltzmann distribution. The distribution is somewhat skewed for runs at energies below the *I-V* plateau of the characteristic curve because of space charge limited emission. Current to the bare anode decreased $\sim 50\%$ at -0.8 V and dropped to $\sim 1\%$ at -2 V.

(5) P. S. Gill, Ph.D. dissertation, Kansas State University, 1967; *Diss. Abstr. B*, 28, 1879 (1967).

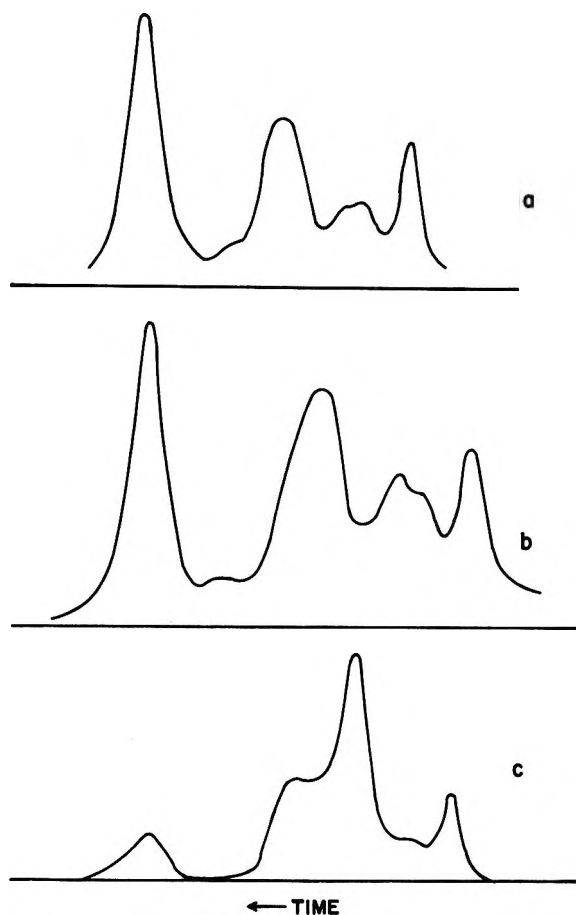


Figure 3. Chromatograms of C_{12} products from 1-hexene at 77°K (a) using ^{60}Co γ irradiation, (b) 100 eV electrons, and (c) 8.7 eV electrons.

For a given filament temperature the current I_{af} transmitted through a film to the anode was somewhat smaller than the current I_a to the nominally bare anode under bakeout. For an accelerating voltage 50 to 100 V, I_{af} remained nearly constant; at 20–30 V there was a small, slow decrease; at 10–15 V, I_{af} decreased 50% during the first 15 sec and more slowly during the next 1 or 2 min. This behavior suggested electron trapping which persists until the traps are filled, or until the increasing space charge within the film empties the traps at a critical local field. This would be consistent with the observation that I_{af} was constant at higher accelerating voltages which lay on the plateau of the diode characteristic curve. Based on this interpretation, the procedure to use is to maintain that value of I_{af} which corresponds to the desired electron energy available to molecules in the film by reference to the diode characteristic curve for the bare anode. From the diode characteristics of Figure 2 it can be seen that in the region of low electron energy, which is of greatest interest, $\Delta I/I \cong \Delta V/V$, and precise measurement is readily obtained. For a given small anode voltage, most of the decay in I_{af} occurs within a few seconds and this will introduce no significant uncertainty for the absorbed

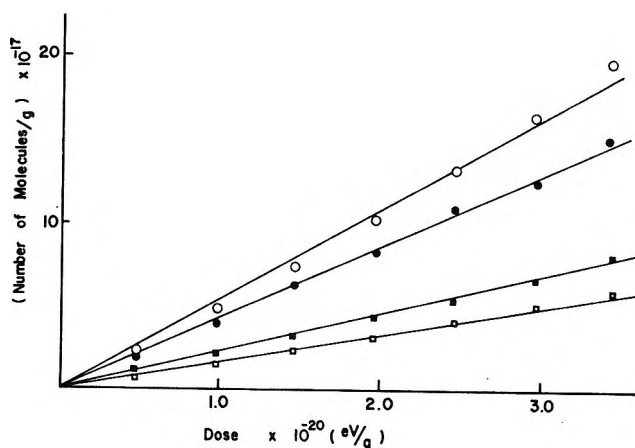


Figure 4. Yield vs. dose of dimer A ("ionic dimer") from 1-hexene, γ irradiated at 77°K , lower curves; other dimers not identified, O.

energy. It should be noted that yields in customary units G , the number of molecules consumed (produced) per 100 eV of absorbed energy, can be obtained directly without resorting to dosimetry provided the energy incident on the film is completely absorbed by it. This is considered to be very probable since the incident electrons must enter the anode. This applies even to electrons which may be elastically backscattered on initial impact. The number m of molecules reacting per n electron impacts is obtained by inspection as $m/n = GV/100$.

The chromatograms of C_{12} products from ^{60}Co γ irradiation are compared in Figure 3 with results for 100- and 8.7-V electron bombardment. There appear to be 6 products in the C_{12} group, of which only the one of longest retention time (dimer A) is fully resolved. There is no significant difference, either qualitatively or quantitatively, for γ irradiation and 100-eV electron impact, with $G(\text{dimer A}) \cong 0.18$ molecules/100eV and $G(\text{total } C_{12}) \cong 0.37$, both for 77°K . The distribution of products at 8.7-eV electron energy differs considerably from that at higher energy.

The comparatively small yield of ionic dimer made it necessary to use fairly large doses. Although mere measurement of G 's under various conditions was not a principal objective of this work, some information of yield-dose dependence is desirable for a new technique. The results in Figure 4 for C_{12} products from γ irradiation and in Figure 5 from low-energy electron irradiation, both at 77°K , provide this information as well as an indication of reproducibility and also give limited evidence of the effect of film thickness.

A summary of results for dimeric products appears in Figure 6. The yield of dimer A, the "ionic dimer," varied monotonically with incident electron energy as it was decreased to ~ 8 eV, which is somewhat less than the ionization potential of 1-hexene in the gas phase. The possibility of chemical changes at still lower electron energy was investigated because other low-energy

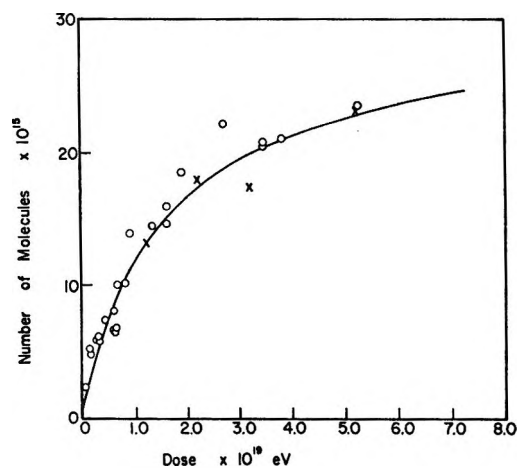


Figure 5. Yield vs. dose absorbed by the film for dimer A from 50-V electron impact on a thin film of 1-hexene at 77°K; nominal thickness of film: O, 10^8 Å and X, 820 Å.

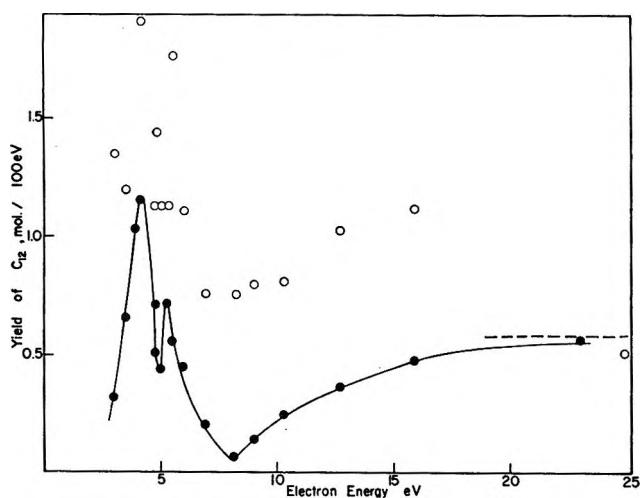


Figure 6. Yield of dimer A (solid circles) and other dimers combined (open circles) vs. electron energy for a thin film of 1-hexene at 77°K. The broken line represents the ^{60}Co yield.

electron impact experiments on aliphatic hydrocarbons provided evidence of energy loss events in the 3 to 5-eV region.⁶ The remarkable results in the region below 8 eV of Figure 6 show that dimer A can be generated by a nonionic precursor.

In addition to the C_{12} products there is a group of 4 distinguishable low molecular weight hydrocarbons ($< \text{C}_6$) present in very small yields and originally of no interest. Their yields could not be established from the chromatograms used for C_{12} analysis, the column being quite unsuitable and the peaks crowded together, but their relative yields can be estimated by using the peak heights. The precision is necessarily poor. Their identities are not critical for the present purpose, but tests with propene, propane, propadiene, propyne (calculated), 1-butene, *n*-butane, *n*-pentane, and 1-pentene, in the order of retention times, plausibly identify the fragments as propane, propyne, 1-butene,

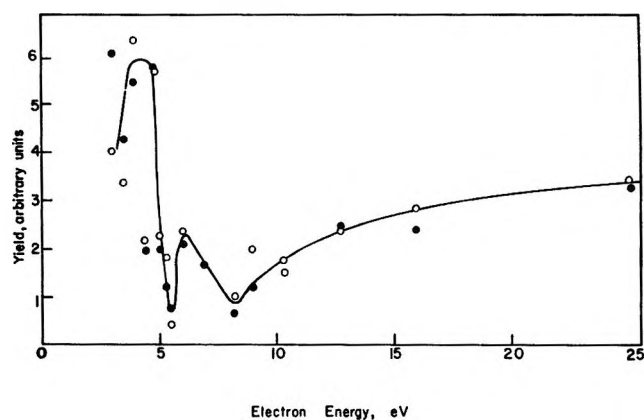


Figure 7. Relative yields of fragment products from low energy electron impact on 1-hexene at 77°K: ●, propane; ○ 1-butene.

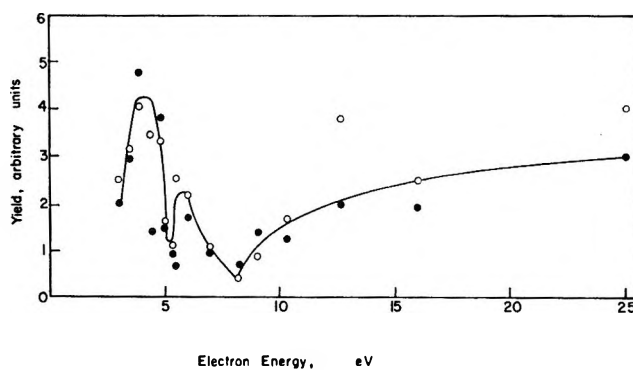


Figure 8. Relative yields of ●, propyne and ○, 1-pentene; the scale is the same as Figure 7.

and 1-pentene. Smaller fragments would not have been recovered efficiently. These results appear as Figures 7 and 8 in which quite tentative profiles of the energy dependence have been sketched in.

When experiments were conducted with the film held several volts below filament potential the yields of dimeric and fragment products did not exceed 2% of those at 25 V from Figures 6–8.

Discussion

The dependence of the yield of dimer A on the energy of electrons above ~ 8 eV is consistent with the ionic precursor proposed by Wagner. However, the resonance processes which generate the same product at much lower energy indicate precursor excited neutrals, and it is quite possible that only the lower of these is the immediate precursor of dimer A. The more energetic neutral may decay to the lower, *e.g.*, triplet \rightarrow triplet, and the ion may generate either or both of these states by neutralization. The effects of electron scavengers, *e.g.* CCl_4 , can then be accounted for in terms of the recombination of $\text{C}_6\text{H}_{12}^+$ with Cl^- , since 4–5 eV is still

(6) L. M. Hunter, D. Lewis, and W. H. Hamill, *J. Chem. Phys.*, **52**, 1733 (1970).

available for excitation, while more energetic fragmentation processes from ion-electron recombination would be suppressed, as observed.⁴

Not more than 3 mechanisms of energy transfer can be imagined below ~ 6 eV. The electron impact may transfer its energy to (a) a vibrationally excited electronic ground state, (b) a transient negative ion, or (c) a triplet state. There is no evidence for mechanism (a) for any molecule, which is also theoretically improbable. The trapped electron technique provides evidence for inelastic collisions at 2 eV with ethylene and propylene which may be due to temporary negative ion formation.⁷ The energy is too small to implicate this mechanism in chemical changes. The third possibility is inherently plausible by spin exchange and is consistent with a variety of evidence. It is generally accepted that Hg (6^3P_1) quenching by olefins produces an excited molecule,⁸ and isomerization of olefins is sensitized by triplet benzene. The acetone photosensitized dimerization of cyclopentene to tricyclodecane at $h\nu > 2700$ Å presumably proceeds *via* a triplet state since the singlet state of olefins lies at ~ 5.5 eV.⁹

If we attribute the 4.3-eV peak in Figure 6 to an olefin triplet precursor, then each of the four hydrocarbon fragments (which show similar energy profiles) must be similarly explained. This interpretation of fragmentation is fully supported by the observation of Lossing, *et al.*,¹⁰ that Hg (6^3P_1) sensitized decomposition of 1-butene at low pressure forms methyl and allyl radicals as the principal primary products, with methallyl radical also present. It is to be expected that 1-hexene will produce not only allyl and propyl radicals but also 1-pentenyl and 1-butenyl by analogy with the Hg (6^3P_1) sensitized decomposition of 1-pentene.¹¹ Excepting the product identified as propyne, the C_3 , C_4 - and C_5 products observed in the present work are thus consistent with the cracking of triplet 1-hexene. The CH_4 and C_2H_6 also expected would have been lost by pumping on the refrigerated loop. Because the glc column was not suited for low-boiling products their retention times were not precisely measurable and an incorrect assignment cannot be ruled out. The order of retention times excludes the possibility that propyne has been mistaken for propene, which would preserve a simple pattern. Of the possible alkanes, only C_3H_8 is to be expected since C_4H_{10} would require formation of vinyl radicals which is not expected.¹¹ To produce propyne from allyl would require disproportionation and intramolecular rearrangement.

If triplet alkene decomposes at a σ bond, the spin state of the radical pair must be considered. In the present work one observed C-C cracking at electron energies which approximate D_{C-C} and the alkenyl radical therefore cannot be in a quartet state. It appears to be necessary to assume a triplet pair of doublets R' , R'' which forms by opening a C-C triplet σ bond, since spin conservation rules cannot be ignored without justi-

fication. The experimental methods described in this work have also been applied to *n*-hexane, with C-C bond dissociation beginning at ~ 3.5 eV.¹² This result can also be attributed to a low-lying Σ triplet state and is supported by electron reflection spectra for *n*-hexane which shows energy loss maxima at ~ 3.9 and ~ 4.6 eV.⁸ The onsets occur at appreciably lower energies.

Triplet Σ states of tricyclodecane from triplet cyclopentene⁹ and of isopentane from triplet ethylene and propane¹³ are also to be inferred. Induced optical absorption in alkanes and alkenes arising from O_2 and I_2 perturbation at energies far below the first allowed transitions are also consistent with low-lying triplet states.¹⁴ Recent mass spectrometric measurements of ionization efficiency curves for rearrangement processes provide excitation potentials of neutral fragments. For fragments C_2H_6 and *n*- C_6H_{14} (from *n*- C_8H_{18} and *n*- $C_{12}H_{26}$) evidence for excited-state onsets at 2.4 and 2.7 eV support the proposal for low-lying triplet σ excitation of alkanes.¹⁵

The similarity of fragment yield dependence on energy, both among themselves and also with dimer A, can be accounted for most easily by a common precursor. In the low-energy region, < 5 eV, this is presumably a triplet state, or manifold of triplet states. For the interval 5 to 8 eV, singlet excitation must occur but the continuity in the product distribution indicates intersystem crossing. Above the minimum at ~ 8 eV, which appears to correspond to ionization, one might invoke an ionic mechanism for dimerization, but this would require a new mechanism for fragmentation. It appears to be preferable to postulate that charge recombination yields triplets and excited singlets which react about the same as those produced directly. The photolysis of propylene at 1470 Å and 1236 Å, above and below the ionization potential, also yields a distribution of products which is independent of energy.¹⁶

The distribution of C_{12} products other than dimer A follows a somewhat different pattern. Since the indi-

(7) C. R. Bowman and W. D. Miller, *J. Chem. Phys.*, **42**, 681 (1965).

(8) J. G. Calvert and J. N. Pitts, "Photochemistry," John Wiley and Sons, New York, N. Y., 1966.

(9) H. D. Scharf and F. Korte, *Ber. Deut. Chem. Ges.*, **97**, 2425 (1964).

(10) F. P. Lossing, D. G. H. Marsden, and J. B. Farmer, *Can. J. Chem.*, **34**, 701 (1956).

(11) J. R. Majer, B. Mile, and J. C. Robb, *Trans. Faraday Soc.*, **57**, 1336 (1961).

(12) T. Matsushige, work in progress.

(13) J. R. Majer, B. Mile, and J. C. Robb, *Trans. Faraday Soc.*, **57**, 1692 (1961).

(14) D. F. Evans, *J. Chem. Phys.*, **23**, 1424 (1955); A. U. Munk and J. F. Scott, *Nature*, **177**, 587 (1956); M. Itoh and R. S. Mulliken, *J. Phys. Chem.*, **73**, 4332 (1969).

(15) D. Lewis and W. H. Hamill, *J. Chem. Phys.*, submitted for publication.

(16) D. A. Becker, H. Okabe, and J. R. McNesby, *J. Phys. Chem.*, **69**, 538 (1965).

vidual components have not been resolved, and since the profile of the chromatogram changes with electron energy, we cannot account for these results. By analogy

with Wagner's results for 1-pentene,⁴ they can be considered to have free-radical precursors and therefore to arise from C-H scission.

Further Studies on the Properties of Electrons Trapped in Glassy Hydrocarbons¹

by A. Ekstrom, R. Suenram, and J. E. Willard

Department of Chemistry, University of Wisconsin, Madison, Wisconsin 53706 (Received November 3, 1969)

The observation that the concentration of trapped electrons observable by infrared absorption and esr in γ -irradiated hydrocarbon glasses at 77°K increases with increasing dose, passes through a maximum, and then falls to zero at *ca.* 2×10^{20} eV g⁻¹ has been further confirmed. It is shown that this phenomenon is not due to the reaction $H + e^- \rightarrow H^-$, previously suggested, but probably results from reaction of mobile electrons with trapped positive charge and radicals, and reaction of mobile positive charge with trapped electrons. Thermal annealing of γ -irradiated 3-methylpentane (3MP) at 90°K, which removes free radicals and electrons, regenerates the capacity of the matrix to trap electrons at 77°K. γ Irradiation of 3MP at 77°K produces at least three species which absorb in the near-uv region. The evidence suggests that these are olefins, alkyl radicals, and anions of alkyl radicals. The carbanion spectrum can be enhanced by photobleaching the infrared band of the trapped electrons, and the latter can be partially regenerated by photobleaching the absorption band of the carbanions. γ Irradiation of a matrix containing both 3MP and *n*-C₃H₇OH produces two trapped electron spectra, one with λ_{max} at 1600 nm characteristic of trapping in the hydrocarbon environment and one with λ_{max} at 540 nm characteristic of the alcohol. Thermal annealing at 90°K transfers electrons from the hydrocarbon to the alcohol environment. Photobleaching with 540-nm radiation removes both electron populations while 1600-nm radiation removes only those in the hydrocarbon environment. In contrast to the hydride ion hypothesis, the results of this paper do not require the conclusion that the matrices contain only a limited number of electron trapping sites.

Introduction

The concentration of physically trapped electrons produced by γ irradiation of hydrocarbon glasses^{2,3} or aqueous sodium hydroxide glasses⁴ at 77°K, and measured by infrared or esr absorption, increases to a maximum and then decreases to zero, with increasing dose. This has been interpreted to indicate that the matrix has only a limited number of trapping sites and that these are destroyed, or preempted, by reaction of a second radiolysis product with the trapped electrons. For the aqueous glasses there is evidence that dielectron formation may occur.⁴ Reaction of electrons, radicals, or cations with the trapped electrons in hydrocarbon matrices has appeared to be improbable,² and it has been suggested² that the preempting reaction might be $H + e^- \rightarrow H^-$. We have now tested and eliminated this hydride ion hypothesis and have obtained further information on the phenomena of electron trapping by bleaching experiments, by use of matrices with two components and by observations of uv spectra.⁵ The new evidence indicates that electron scavenging by positive charge and by radicals is responsible for the manner in which the electron concentration varies with dose.

Experimental Section

3-Methylpentane (3MP) (Phillips Pure Grade), methylcyclohexane (MCHx) (Aldrich), and 3-ethylpentane (3EP) (Aldrich) were purified by passage through freshly activated silica gel and were stored under vacuum over a sodium mirror. 1-Propanol (Fisher Certified Reagent) was used as received. The degassed samples were irradiated and observed in Suprasil cells with optical paths of either 1 cm or *ca.* 1 mm. γ -Irradiation was carried out under liquid nitrogen at a dose rate of 3×10^{18} eV g⁻¹ min⁻¹ from a ⁶⁰Co source.

(1) This work has been supported in part by the U. S. Atomic Energy Commission under Contract AT(11-1)-1715 and by the W. F. Vilas Trust of the University of Wisconsin.

(2) M. Shirom and J. E. Willard, *J. Amer. Chem. Soc.*, **90**, 2184 (1968).

(3) A. Ekstrom and J. E. Willard, *J. Phys. Chem.*, **72**, 4599 (1968).

(4) J. Zimbrick and L. Kevan, *J. Amer. Chem. Soc.*, **89**, 2483 (1967).

(5) For reviews of related investigations and further references see: (a) V. A. Roginski and B. B. Kotov, *Khimiya Vysokikh Energii*, **1**, 291 (1967), UDC 541.15; (b) W. H. Hamill, "Ionic Processes in γ -Irradiated Organic Solids at -196°C," a chapter in "Radical Ions," E. T. Kaiser and L. Kevan, Ed., John Wiley and Sons, New York, N. Y., 1968; (c) J. E. Willard, "Radiation Chemistry of Organic Solids," a chapter in "Fundamentals of Radiation Chemistry," P. Ausloos, Ed., John Wiley and Sons, New York, N. Y., 1968.

Most photobleaching experiments were done with the aid of a Bausch and Lomb high-intensity monochromator using a uv-visible or infrared grating. For the uv experiments (monochromator setting 375 nm) a Corning 7-37 filter (cut-offs above 400 nm and below 300 nm) was used to further ensure spectral isolation. A Corning 2-64 filter which cuts off wavelengths below 680 nm was used in the ir bleaching experiments where the monochromator was set at 1400 nm. As indicated in the text, some bleaching experiments were done with the full light of a tungsten lamp.

Optical absorption measurements were made with a Cary 14-R spectrophotometer.

Results

Test of Hydride Ion Hypothesis. According to the hydride ion hypothesis,² all H atoms produced by radiolysis of a glassy hydrocarbon matrix diffuse and react with other H atoms or radicals during the initial stages of irradiation, but as the e_{tr}^- concentration builds up, some react with the trapped electrons to form hydride ions. This would account for the disappearance of the esr and ir absorptions of the electrons and for the removal of the available trapping sites if the total number of such sites is limited. To test this hypothesis a glassy hydrocarbon (95 mol % MCHx + 5 mol % 3MP) sample was irradiated to a dose of 2.4×10^{20} eV g⁻¹ at 77°K while under continuous illumination from a 100-W tungsten lamp at a distance of a few inches. This dose is sufficient to reduce the electron concentration and yield to nearly zero in irradiations made in the dark. The light photobleached the trapped electrons as fast as they were formed, thus preventing the buildup in concentration necessary for significant H⁻ formation. According to the hydride ion hypothesis, the matrix should have retained nearly all of its trapping sites despite the irradiation, and subsequent γ irradiation without illumination should have led to the same initial growth in concentration of e_{tr}^- as observed in an unirradiated sample. No growth occurred, indicating that the reaction $H + e_{tr}^- \rightarrow H^-$ is not responsible for the decrease in trapped electron concentration with dose. The hydride ion hypothesis is likewise invalidated by recent evidence that H atoms are not produced by the γ radiolysis of alkane glasses other than CH₄.⁶

Does Photo or Thermal Bleaching Regenerate Trapping Capacity? Figure 1 shows plots of the optical density due to trapped electrons, as a function of dose, for a sample of 3-ethylpentane (3EP) which was γ irradiated to a dose of 3.5×10^{20} eV g⁻¹ without photobleaching and for an identical sample in which the accumulated electrons were photobleached at three different points during the irradiation. The fact that the curves for the second experiment lie in the envelope of that for the first indicates that removal of the trapped

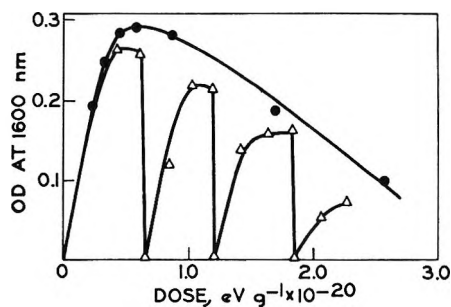


Figure 1. Effect of photobleaching of γ -irradiated 3EP glass at 77°K on production of trapped electrons during subsequent γ irradiation. ●, Total dose given without photobleaching. Δ, Photobleaching with tungsten lamp after doses of 0.6×10^{20} , 1.2×10^{20} , and 1.8×10^{20} eV g⁻¹; 1-mm cell.

electrons by photobleaching does not regenerate the original ability of the matrix to trap electrons.

To determine whether thermal bleaching of a γ -irradiated hydrocarbon glass regenerates the electron trapping capability, a sample of 3EP was irradiated at 77°K (where the decay rate of e_{tr}^- is very slow) to a dose of 6×10^{19} eV g⁻¹, to produce an electron concentration near the maximum of the concentration vs. dose curve. The sample was then transferred to a bath of liquid oxygen (90°K) for 45 min, during which time the trapped electrons all disappeared. Figure 2 (sample A) shows that the infrared absorption attributable to e_{tr}^- rose to only half its original height when the sample was again irradiated at 77°K. An identical sample (sample B) which was immersed in liquid argon (87°K) instead of liquid oxygen showed only ca. 30% decay of the electrons in 45 min. (The rate of decay of electrons in 3EP changes rapidly in the temperature range of 87–90°K, as it does in the temperature range of 75–80°K in 3MP.) Further exposure of this sample to γ irradiation at 77°K led to a much lower yield of trapped electrons than the irradiation prior to photobleaching. Both the experiment at 90°K and that at 87°K indicate that thermal removal of the electrons does not regenerate the original trapping capacity of the matrix.

Since trapped free radicals may be expected to be quite stable in 3EP at 90°K, this result is not inconsistent with the hypothesis that free radicals are responsible for the decrease in the physical trapping of electron with increase in dose.

In order to determine whether electron trapping ability is regenerated when a γ -irradiated matrix is warmed to a temperature where the trapped free radical concentration as well as the electron concentration is reduced, a sample of 3MP, in which radicals decay relatively rapidly at 90°K, was subjected to a γ dose of 3.2×10^{20} eV g⁻¹ at 77°K in a 2-mm cell, following which it was held at 90°K for 10 min, re-

(6) D. Timm and J. E. Willard, *J. Phys. Chem.*, **73**, 2403 (1969).

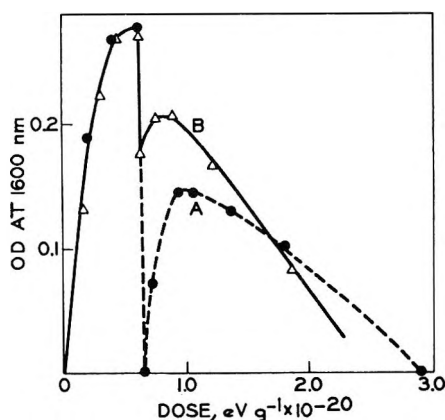


Figure 2. Effect of thermal annealing of γ -irradiated 3EP glass on production of trapped electrons during subsequent γ irradiation. Separate samples irradiated to 6×10^{19} eV g^{-1} at $77^\circ K$. Sample A was then held 45 min at $90^\circ K$ and sample B 45 min at $87^\circ K$, following which irradiation was continued at $77^\circ K$; 1-mm cell.

turned to $77^\circ K$, and exposed to a further γ dose of 0.9×10^{20} eV g^{-1} . The optical density at 1600 nm at $77^\circ K$ following the first irradiation was 0.2 and following the second 0.7, indicating that the annealing had at least partially regenerated the electron trapping capacity (0.9×10^{20} eV g^{-1} would produce an OD of ca. 1.2 in an unirradiated sample in the 2-mm cell).

Selective Electron Trapping and Transfer in an Alcohol-Hydrocarbon Glass. When a solution of $n\text{-C}_3\text{H}_7\text{OH}$ in 3MP glass at $77^\circ K$ is γ irradiated, two separate absorption peaks attributable to trapped electrons are observed,³ one at 540 nm characteristic of electrons trapped in the alcohol, and one at 1600 nm characteristic of electrons trapped in the 3MP. These results have been interpreted to mean that the alcohol is aggregated in the nonpolar solvent,³ perhaps in the form of hydrogen-bonded clusters containing several alcohol molecules each. In the present work glassy solutions of 18 mol % (12 electron %) of $n\text{-C}_3\text{H}_7\text{OH}$ in MCHx have been used to investigate the properties of the two populations of trapped electrons. Figure 3 shows that the qualitative dependence on dose of the e_{tr}^- concentration in the hydrocarbon environment is identical with that in the pure hydrocarbon. It passes through a maximum and falls to zero at a dose of about 2×10^{20} eV g^{-1} . However, the rate of increase of electron concentration in the alcohol environment reaches a gently sloping plateau at a dose of ca. 2×10^{20} eV g^{-1} , whereas in pure $\text{C}_2\text{H}_5\text{OH}$ the concentration increases nearly linearly^{3,7} up to ca. 7×10^{20} eV g^{-1} , at which concentration $G(e_{tr}^-)$ begins to drop. Most of the electrons produced in the sample of Figure 3 are produced from the MCHx, which constitutes 88 electron % of the matrix. At low doses these are largely transferred to the alcoholic part. At doses above ca. 2×10^{20} eV g^{-1} , however, such transfer essentially ceases.

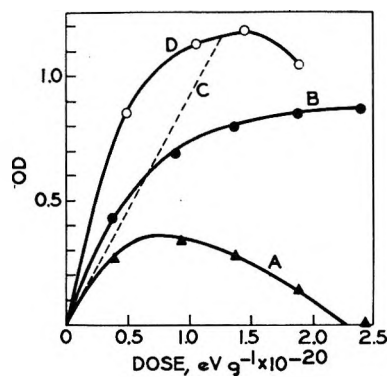


Figure 3. Effect of γ dose on trapped electron concentrations in 82 mol % MCHx-18 mol % $n\text{-C}_3\text{H}_7\text{OH}$ glass at $77^\circ K$; 1-mm cell. Line A: OD of electrons trapped in MCHx (1600 nm). Line B: OD of electrons trapped in alcohol environment (540 nm). Line C: Extrapolation of initial rate of trapped electron production in hydrocarbon environment. Line D: OD at 540 nm for samples irradiated to the total doses indicated by the points and then thermally bleached at $90^\circ K$.

When a sample of γ -irradiated $n\text{-C}_3\text{H}_7\text{OH}$ in MCHx such as that of Figure 3 is warmed momentarily from 77 to $90^\circ K$ and returned to $77^\circ K$, the 1600-nm absorption disappears and that at 540 nm increases (Figure 3) showing that electrons originally trapped in the hydrocarbon environment are transferred to the alcohol environment by the warming.

Exposure of γ -irradiated $n\text{-C}_3\text{H}_7\text{OH}$ -MCHx mixtures to 1400-nm radiation bleaches the electrons which are trapped in the hydrocarbon environment (1600-nm peak) without changing the concentration of electrons trapped in the alcohol environment (540-nm peak), whereas exposure to 540-nm radiation bleaches the alcohol band and also the hydrocarbon band. The fact that photobleaching, in contrast to thermal bleaching, does not increase the concentration of e_{tr}^- in the alcohol environment is consistent with earlier evidence that photobleached electrons react chemically with the alcohol.⁸

Reversible Anionic Uv Absorption. When pure 3MP in a 1-cm quartz cell is γ irradiated to a dose of 6.8×10^{19} eV g^{-1} at $77^\circ K$ the trapped electron peak is far off scale (estimated OD at 1600 nm ca. 10) and there is a broad absorption gradually rising from about 500 nm toward lower wavelengths. When the infrared peak is completely bleached with 1400-nm radiation an increase in absorption occurs in the visible-uv range (spectrum C of Figure 4). Exposure to 375-nm radiation regenerates the 1600-nm peak to about 10% of its initial intensity while the uv band is blue shifted and reduced in intensity relative to its value immediately after

(7) S. Fujii and J. E. Willard, unpublished results.

(8) For an extensive review of the trapping and reactions of electrons in alcohols see L. Kevan, "Radiolysis of Frozen Polar Systems," in *Action Chimiques et Biologiques des Radiations*, M. Haissinsky, Ed., Masson et C.,¹⁶ Paris, France, 1969.

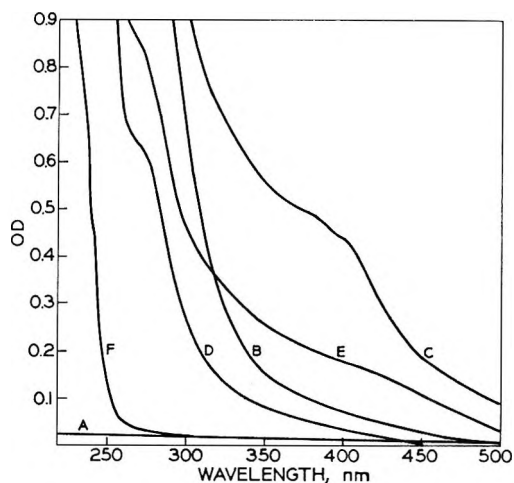
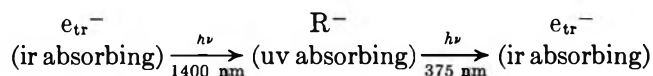


Figure 4. Visible-uv absorption spectra of γ -irradiated 3MP glass at 77°K before and after various bleaching processes; 1-cm cell; dose, 6.8×10^{19} eV g^{-1} . A, before irradiation; B, immediately after irradiation; C, after complete bleaching of 1600-nm band with 1400-nm radiation; D, after irradiation to constant intensity with 375-nm radiation following C; E, after subsequent 1400-nm irradiation; F, after subsequent warming to room temperature and returning to 77°K. The base line for the optical density scale has been chosen equal to the minimum value of the spectrum between the broad e_{tr}^- peak of the visible ir region and the broad visible uv absorption. The absolute values of the optical densities may be as much as 0.1-0.2 higher than shown on the scale.

γ irradiation (spectrum D). When the sample is bleached again with 1400-nm radiation the visible-uv absorption is partially regenerated (spectrum E). Subsequent exposure to 375-nm radiation regenerates *ca.* 50% of the previous intensity of the infrared peak. After melting and recooling to 77°K, the sample of Figure 4 gave spectrum F. The absorption between 250 and 200 nm is due to an unidentified stable product. Olefin solutes in 3MP glass tested in our laboratory (*cis*-2-pentene and 2-methylbutene-2) do not absorb significantly above 200 nm.

The data of Figure 4 indicate reactions of the type



The results are consistent with the conclusion that electrons detrapped by the 1400-nm radiation are in part neutralized by positive charges and in part captured by free radicals to form carbanions which account for the uv absorption. Retrapping also occurs but complete bleaching is achieved by continued exposure to the detrapping radiation. Some of the electrons removed from the anions by 375-nm radiation are neutralized and some are trapped in the matrix, regenerating the ir absorption. Curves A and B of Figure 5 show the growth of the 1600-nm absorption as a function of time of irradiation at 375 nm after 1400-nm bleaching for two samples which received γ doses differing by tenfold.

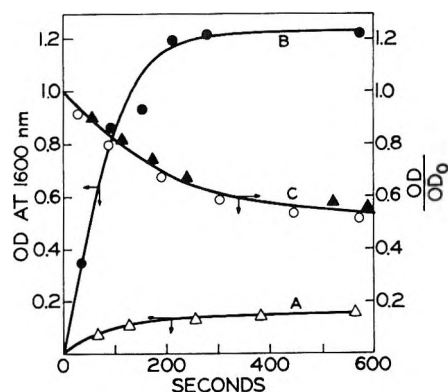


Figure 5. Effect of 375-nm irradiation on trapped electron concentration in γ -irradiated 3MP glass at 77°K, measured by 1600-nm absorption. Curves A and B show the growth of absorption at 1600 nm as a function of time of irradiation at 375 nm when the 1600-nm band is bleached with 1400-nm radiation prior to exposure of the γ -irradiated sample to 375 nm. Sample A received a γ dose of 6.8×10^{18} eV g^{-1} and B a dose of 6.8×10^{19} eV g^{-1} , both in 1-mm cells. Curve C, fractional decrease in 1600-nm OD with 375 nm irradiation of unbleached samples which had received 3.4×10^{19} (\blacktriangle) and 6.8×10^{19} (O) eV g^{-1} of γ irradiation; 1-mm cell.

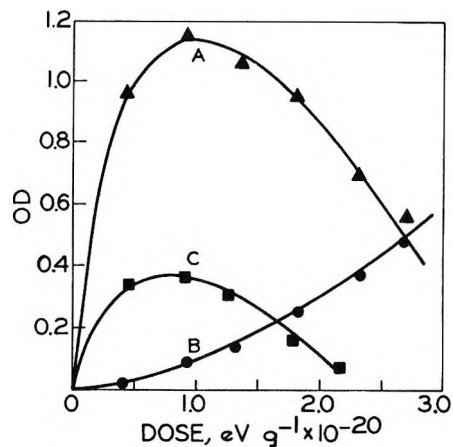


Figure 6. Optical density as a function of γ dose at 77°K. Curves A and C show the OD at 1600 nm of 3MP and 3EP respectively. Curve B shows the OD of 3MP at 350 nm.

Curve B of Figure 6 indicates that the OD at 350 nm of γ -irradiated 3MP glass increases with increasing dose with a dependency greater than first power, while the OD at 1600 nm rises to its maximum and then decreases (curve A). This is the result to be expected from a linear increase^{2,3} in the concentration of trapped free radicals capable of capturing electrons while the concentration of positive holes approaches a steady state and the trapping capability of the matrix remains constant. The data with respect to the curvature of B of Figure 6 must be regarded as tentative because of uncertainties in base line corrections (see caption of Figure 4) in this region of the spectrum. Curve C of Figure 6 shows the 1600-nm OD of a 3EP sample as a function of dose for comparison with curve A for 3MP,

to illustrate the differences in ir intensity produced by equal γ doses to different hydrocarbons.

3-Ethylpentane glass showed a spectrum qualitatively similar to B of Figure 4 after a dose of 3×10^{20} eV g⁻¹ at 77°K. This shifted to a spectrum similar to D of Figure 4 after irradiation at 375 nm.

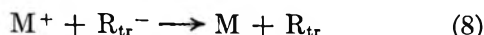
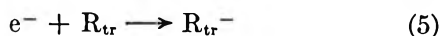
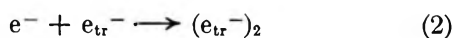
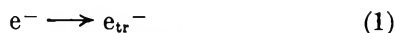
Initial Bleaching at 375 nm. From the discussion above it, would be predicted that exposure of γ -irradiated 3MP glass to 375-nm radiation without initial ir bleaching would release electrons from R⁻ and cause an increase in OD at 1600-nm similar to the increase after ir bleaching illustrated in Figure 4. However, such exposure caused a decrease in the 1600-nm band (curve C of Figure 5), indicating that overlapping spectra (see caption of Figure 4) and overlapping photochemical effects complicate the observations.

The effect of 375-nm radiation on absorption in the 1600-nm band was also tested on a freshly irradiated sample which had received 3×10^{20} eV g⁻¹, enough to reduce the concentration of electrons to zero (Figure 6). Illumination for 5 min with the low-pressure mercury lamp with a 7-37 filter under conditions which would have caused the shift from spectrum C to spectrum D of Figure 4 gave no increase in absorption at 1600 nm. The visible-uv spectrum of this sample had optical densities of 0.4 and 0.8 at 350 and 300 nm, respectively, before bleaching. After the 375-nm, irradiation these optical densities had decreased to 0.15 and 0.25.

Discussion

Cause of Decrease in Electron Trapping with Increasing Dose. The results presented above indicate that the decrease in the concentration of trapped electrons in glassy hydrocarbons as the γ dose is increased above $\sim 1 \times 10^{20}$ eV g⁻¹ (e.g. curves A and C of Figure 6) is not due to the reaction $H + e_{tr}^- \rightarrow H^-$. What then is the mechanism responsible?

Equations 1-8 show the competitive reactions in which mobile electrons and mobile positive charge (e⁻ and M⁺), trapped electrons and positive charge (e_{tr}⁻ and M_{tr}⁺), and trapped radicals (R_{tr}) may be involved



Dielectron formation (reaction 2) appears improbable in a nonpolar matrix, on the basis of coulombic repulsion

considerations. Increasing probability of reaction of the newly born electrons with cations (reaction 4), as the cation concentration increases with dose, could account for approach to a steady-state concentration of e_{tr}⁻, but cannot alone account for the decrease in [e_{tr}⁻] after reaching the maximum. Reaction with cations could account for the decrease if: (1) the matrix has only a limited number of trapping sites for electrons; (2) the trapping sites are nearly 100% populated at the maximum of the electron concentration curve; (3) the trapping sites are destroyed when the trapped electrons are neutralized by freshly formed positive holes migrating through the matrix, or by "radiation catalyzed" or thermal reaction with neighboring trapped positive holes.

Although this hypothesis involving loss of electrons only to positive holes is attractive in some respects, the requirement that the available traps are fully populated is inconsistent with the data of Figure 3. For a given γ dose the total yield of electrons which escape geminate recombination and are potentially able to be trapped in the MCHx of the matrix is proportional to the area under line C of Figure 3 (i.e., the line tangent to curve A at very small doses) whereas the number of electrons actually trapped in the MCHx is proportional to the area under curve A. If the electrons represented by the difference of these two areas (C - A) fail to be trapped in the MCHx simply because the original trapping sites have been destroyed, these electrons would be expected to increase the concentration of the species responsible for the 540-nm band in the alcohol (curve B), since electrons generated in the MCHx (82 mol %) are readily transmitted to and trapped in the n-C₃H₇OH environment. Since thermal bleaching of the 1600-nm band (species A) after various doses produces curve D, rather than curve B, for the 540-nm band, it follows that the alcohol environment in an irradiated sample such as illustrated by Figure 3 retains unused trapping capacity.

The conclusion that the transfer of electrons from the MCHx environment to the n-C₃H₇OH environment during radiolysis decreases with increasing dose requires that one or more electron scavenging species, which grow in concentration with increasing dose, must capture electrons in the hydrocarbon matrix and prevent them from entering the alcohol environment. Presumably the same scavengers are responsible for the decrease in the trapped electron concentrations in pure hydrocarbons with increasing dose above 1×10^{20} eV g⁻¹. The data of Figure 4 demonstrate the presence of a radiation product which is able to capture electrons to produce an anion. This anion shows an accelerating increase in yield with increasing dose (Figure 6, curve B) in the same dose region that the trapped electron concentration shows an accelerating decrease (Figure 6, curve A). The most probable anionic species to account for these observations is C₆H₁₃⁻ formed by

electron capture by the 3-methylpentyl radical. We have already noted that when 3MP which has received a γ dose of 3.2×10^{20} eV g⁻¹ is annealed at 90°K, where radical decay as well as electron decay occurs, electron trapping capacity is regenerated.

In previous work² the possibility that the decrease in electron trapping with increasing γ dose results from reaction of electrons with free radicals was ruled out because the evidence indicated that the free radical concentration grows linearly to doses higher than those at which the electron concentration falls to zero. It was reasoned that the initial G value of trapped radicals which is *ca.* 1.6⁹ would have to be reduced by an amount equal to the initial G value of trapped electrons which is *ca.* 0.7^{10a,11} to account for the reduction of $G(e_{tr}^-)$ to zero. It now seems probable, however, that the decrease of $G(e_{tr}^-)$ with increasing dose is due primarily to increasing probability of reaction of electrons with trapped positive ions, *i.e.*, the rate of reaction 4 approaches the rate of reaction 3 as the increasing concentration of M_{tr}^+ allows reaction 4 to compete more effectively with reaction 1. In this case the decrease in total radical yield required to account for the fall in $[e_{tr}^-]$ between 1×10^{20} eV g⁻¹ and 3×10^{20} eV g⁻¹ (Figure 6) is equal to the number of trapped electrons present at their maximum concentration and amounts to less than 8% of the radical yield. This is within the experimental error of the determination of this yield. The decrease in $[e_{tr}^-]$ may result from occasional reaction of a mobile electron with a trapped radical (reaction 5) and occasional encounter of a mobile M^+ with an e_{tr}^- (reaction 6). Then at constant dose rate $d[e_{tr}^-]/dt = I - k_4 [e^-][M_{tr}^+] - k_5 [e^-][R_{tr}^-] - k_6 [M^+][e_{tr}^-]$, where I is the rate per unit volume of production of electrons which escape geminate recombination, $[e^-]$ is the steady-state concentration of mobile electrons, and k_4 is significantly larger than k_5 or k_6 .

The concentration of cations and radicals (Table I) is too low at 2×10^{20} eV g⁻¹ to account for the decrease in $[e_{tr}^-]$ by reaction with radicals or cations formed by chance in the solvent wall surrounding the e_{tr}^- . Since the radicals formed in MCHx and 3EP cannot migrate sufficiently rapidly at 77°K to account for the decrease, the e_{tr}^- must be removed by mobile positive charge, unless: (1) the mechanisms of energy transfer and utilization in the glass favor radical formation in proximity to a trapped electron rather than with a random distribution, thus favoring reaction 7, or (2) energy deposited in the matrix causes $e_{tr}^- - M_{tr}^+$ pairs to undergo self-neutralization, or (3) electrons are detrapped under the influence of continuing irradiation of the matrix and travel far enough without retrapping to be scavenged. None of these mechanisms can be ruled out at the present state of knowledge.

Related Observations. The model proposed above, involving M_{tr}^+ and R_{tr}^- as radiation-produced electron

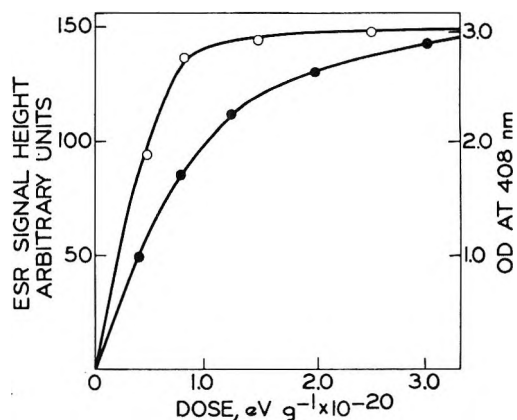


Figure 7. Effect of dose on yields of products of reaction of electrons with added electron scavengers in the radiolysis of 3MP glass at 77°K: O, optical density at 408 nm due to biphenyl anion from 0.058 mol % biphenyl in 3MP in 1-mm cell; ●, ethyl radical yield from $C_2H_5I + e^- \rightarrow C_2H_5 + I^-$ process, measured by esr, in sample containing 1 mol % C_2H_5I in 3MP.

scavengers, may account for the fact that the G values of products from *added* electron scavengers decrease sharply at doses above about 1×10^{20} eV g⁻¹. Examples of such a decrease, involving the $C_2H_5I + e^- \rightarrow C_2H_5 + I^-$ reaction and the $C_{12}H_{10} + e^- \rightarrow C_{12}H_{10}^-$ reaction, are given in Figure 7. If the decrease in product yield with dose is due to competition for electrons by radiation-produced cations and radicals, one or both of these must have a higher cross section than the additives have for capture of electrons. Assuming trapped cations or radicals for which $G = 1$ the concentration at a dose of 1×10^{20} eV g⁻¹ is 0.016 mol %, whereas the biphenyl and ethyl iodide were present at 0.058 and 1.0 mol %, respectively.

Further evidence for the reaction of electrons with radicals has been obtained by Kieffer and coworkers¹² who have observed that γ -irradiated solutions of durene or styrene in MCHx glass show luminescence on warm-up which is attributable to neutralization of the anion or cation formed from the radical of the aromatic solute, in addition to fluorescence from the matrix cation and phosphorescence from the solute cation. This luminescence is observed at progressively lower temperatures the higher the γ dose. The techniques and related results have been discussed in a review article.¹³

It is of interest to note that the phenomenon of trapped electron saturation and removal illustrated by curves A and C of Figure 6 has likewise been suggested by the

(9) M. Shirom and J. E. Willard, *J. Phys. Chem.*, **72**, 1702 (1968).

(10) (a) D. W. Skelly and W. H. Hamill, *J. Chem. Phys.*, **44**, 2891 (1966); (b) P. J. Dyne and A. O. Miller, *Can. J. Chem.*, **43**, 2696 (1965).

(11) J. Lin, K. Tsuji, and F. Williams, *J. Amer. Chem. Soc.*, **90**, 2766 (1968).

(12) F. Kieffer, private communication.

(13) F. Kieffer and M. Magat, in press.

Table I: Concentrations and Spatial Distributions of Radicals and Cations Produced with $G = 1$

Dose, eV g ⁻¹	Mole fraction ^a	Dist between nearest neighbors, ^b molec diams	Probability of formation in solvent wall of e ⁻ trap	Average dist of trapped e ⁻ from radical or cation, molec diams, Å	Coulombic attrac- tion of cation at average dist, ^c eV
1 × 10 ¹⁹	1.6 × 10 ⁻⁵	39.7	1.6 × 10 ⁻⁴	15 (75)	0.096
1 × 10 ²⁰	1.6 × 10 ⁻⁴	18.4	1.6 × 10 ⁻³	6 (30)	0.24
2 × 10 ²⁰	3.2 × 10 ⁻⁴	14.8	3.2 × 10 ⁻³	5 (25)	0.29
1 × 10 ²¹	1.6 × 10 ⁻³	8.5	1.6 × 10 ⁻²	3 (15)	0.48

^a If 1 g = 6 × 10²¹ molecules. ^b Assuming equal regular spacing. ^c Assuming no influence from fields of other ions.

results of quite a different technique than those used here, that of recombination luminescence.¹⁴

Radical and Cation Concentrations. Some population statistics for free radicals and cations, assuming nominal G values of unity for each, are given in Table I for the dose range of the experiments discussed here. At a dose of 2×10^{20} eV g⁻¹ the mole fraction of each species would be 3×10^{-4} . The average distance between nearest neighbors for equal spacing would be 15 molecular diameters (ca. 75 Å in 3MP). The statistical probability of a radical or cation being in a shell of 10 molecules surrounding a trapped electron is ca. 1 in 300 and the average distance from a trapped electron to a trapped radical or a trapped cation is ca. 5 molecular diameters (15 Å), assuming random distribution. At this distance the coulombic attraction between an electron and a positive ion in a medium with a static dielectric constant of 2 would be 0.5 eV if there were no influence from the fields of other ions.

Yields of Interconversion of the Ir and Uv Species. The fact that conversion of the trapped electrons absorbing at 1600 nm to the uv absorbing anions and of the anions back to e_{tr}⁻ by alternate irradiation at 1600 nm and 375 nm is not quantitative indicates that some electrons are lost to neutralization of cations or form anions which do not absorb in the uv. The observation that the fraction of the e_{tr}⁻ transferred to the uv species is much smaller in the first ir bleaching than the second suggests that neutralization of positive ions in the process of the first bleaching may have significantly reduced the ratio of positive ions to radicals.

Uv Absorption by Free Radicals. The uv absorption represented by the difference between spectra D and F of Figure 4 is presumably due principally to *sec*-3-methylpentyl radicals which are known¹⁵ to be the predominant type of radical formed by γ radiolysis of 3MP. Experiments at lower dose in 3EP have produced a similar, better resolved absorption in the region of 210–290 nm, which corresponds approximately in both wavelength and absorption coefficient to the *n*-hexyl radical spectrum observed in the pulse radiolysis of liquid *n*-hexane by Sauer and Mani.¹⁶

Number of Trapping Sites Available for Electrons. The nature of the dependence of trapped electron concentration on dose in solid hydrocarbons has previously been interpreted^{2,3} to indicate that such matrices contain only a limited number of sites at which electrons can be trapped. If the reactions with positive holes and cations proposed in the present paper are responsible for the dose dependence, the data do not give evidence either for or against the concept that trapping can occur only in a limited number of preformed trapping sites. The rate of growth of [e_{tr}⁻] with dose must decrease with increasing [M_{tr}⁺], even if the number of trapping sites is unlimited, because of increasing competition of reaction 4 with reaction 1. At higher doses [e_{tr}⁻] must decrease due to attrition by the combined effects of reactions 5, 3, 6, and 7.

(14) V. G. Nikolski, V. A. Tochinn, and N. Ya. Buben, *Fiz. Tverd. Tela.*, **5**, 2248 (1963); *Sov. Phys. Solid State*, **5**, 1636 (1964).

(15) D. J. Henderson and J. E. Willard, *J. Amer. Chem. Soc.*, **91**, 3014 (1969).

(16) M. Sauer and J. Mani, *J. Phys. Chem.*, **72**, 3857 (1968).

Excitation Transfer in the Pulse Radiolysis of Naphthalene and Benzophenone Solutions¹

by R. A. Holroyd,²

Atomics International, Canoga Park, California, and Chemistry Department, Brookhaven National Laboratory, Upton, New York 11973

L. M. Theard, and F. C. Peterson

Gulf General Atomic Inc., San Diego, California (Received August 4, 1969)

The nanosecond pulse radiolysis of solutions of 1,2-benzanthracene in liquid naphthalene at 100° and of anthracene in benzophenone at 30° was investigated. In both solutions solute molecules are not excited at the end of the pulse. After the pulse, excited solute molecules in singlet and triplet states are formed by excitation transfer from the solvent. Ions are not involved in the transfer. The transfer of triplet state energy from benzophenone solvent to anthracene solute was detected by observing that the rate of decay of the excited benzophenone triplet is equal to the rate of formation of anthracene triplets. The rate constant of triplet-triplet transfer in molten benzophenone at 30° is $(1.6 \pm 0.1) \times 10^9 M^{-1} \text{sec}^{-1}$ and in molten naphthalene at 100° is $1.1 \times 10^{10} M^{-1} \text{sec}^{-1}$. In both solvents the rate of triplet transfer is diffusion controlled. Singlet-singlet transfer was also time resolved for a solution of benzanthracene in naphthalene by observing the fluorescence intensity which rose to a maximum 16 nsec after a 5-nsec pulse. Singlet energy transfer is an order of magnitude faster than triplet-triplet transfer in this solvent.

Introduction

In the radiolysis of organic solutions there are several possible processes including excitation transfer, ionization transfer, charge neutralization, and direct excitation by low-energy electrons by which solutes may become electronically excited. In aromatic solutions excitation transfer from solvent to solute is believed to be important for many systems. This excitation transfer can be of two types in general: singlet-singlet transfer and triplet-triplet transfer. By employing a pulse radiolysis apparatus with a system response time that is short compared to the excitation transfer lifetime it can be expected that excitation transfer can be observed, since in certain cases singlet excitation is detectable by fluorescence,^{3,4} and singlet^{5,6} and triplet excitation are detectable by light absorption.

In principle, singlet-singlet excitation transfer may be observable by detection of time-resolved decay of solvent fluorescence, buildup of solute fluorescence, decay of light absorption by solvent singlet states, and buildup of absorption by solute singlet states. Triplet-triplet excitation transfer may be observable by time-resolved decay of light absorption by solvent triplet states and buildup of light absorption by solute triplet states. In practice, however, a careful choice of solvents, solutes, and concentration is required to detect excitation transfer.

In the present work, both singlet-singlet and triplet-triplet excitation transfer were detected by nanosecond pulse radiolysis of solutions of 1,2-benzanthracene in molten naphthalene at 100°. Further, triplet-triplet

excitation transfer was observed in liquid solutions of anthracene in benzophenone at 30°.

In previous pulse-radiolysis studies^{6,7} in which the solvent was benzene it was observed that solute triplets were present within a few nsec after the pulse and there was no subsequent grow-in to demonstrate the occurrence of triplet-triplet energy transfer. In a steady-state study of the radiolysis of liquid naphthalene containing stilbene,⁸ kinetic evidence was obtained which suggested that isomerization of the stilbene occurs as a result of triplet-triplet transfer.

Experimental Section

The naphthalene and benzophenone were purified by zone refining prior to use. Anthracene and 1,2-benzanthracene (Eastman White Label) were used as received. The solutions were thoroughly degassed prior to sealing in high-purity quartz absorption cells. The

(1) This research was supported in part by the Research Division of the U. S. Atomic Energy Commission.

(2) Present affiliation, Department of Chemistry, Brookhaven National Laboratory, Upton, New York 11973; previous work at Atomics International, Canoga Park, Calif.

(3) M. A. Dillon and M. Burton, "Pulse Radiolysis," Academic Press, Inc., Ltd., London, 1965, p 259 ff.

(4) S. Lipsky, "Physical Processes in Radiation Biology," Academic Press, Inc., New York, N. Y., p 215 ff.

(5) L. M. Theard, F. C. Peterson, and R. A. Holroyd, *J. Chem. Phys.*, **51**, 4126 (1969).

(6) R. Cooper and J. K. Thomas, *ibid.*, **48**, 5097 (1968).

(7) J. W. Hunt and J. K. Thomas, *ibid.*, **46**, 2954 (1967).

(8) O. G. Malan, H. Gusten, and D. Schulte-Frohlinde, *J. Phys. Chem.*, **72**, 1457 (1968).

benzophenone, either pure or containing anthracene, could readily be kept liquid at 30° for long periods of time. Details of the pulse-radiolysis apparatus have been published elsewhere.⁵ For dosimetry the yield of electrons from air-saturated water was measured and $G(e_{aq}^-)$ was assumed to be 2.65 at 10^{-8} sec and ϵ_{578} was taken to be $1.06 \times 10^4 M^{-1} \text{ cm}^{-1}$.⁹

Results

Solutions of Anthracene in Benzophenone. In the pulse radiolysis of pure benzophenone a transient absorbing in the visible ($\lambda_{\text{max}} 540$) is observed. There is no fluorescence to interfere with absorption measurements. The observed absorption spectrum is very similar to that reported for the benzophenone triplet state¹⁰ which has an absorption maximum at 532 $m\mu$. The decay of the triplet determined from plots of $\log(OD - OD_{\infty})$ vs. time is first order and the half-life at 30° is 0.46 μsec . There is a 10% residual absorption at 540 $m\mu$ remaining after decay of the triplet which is attributed to ions. The yield of triplets based on 90% of the initial absorption at 540 $m\mu$ and a value of $\epsilon = 10,300^{10} M^{-1} \text{ cm}^{-1}$ is $G(^3BP^*) = 2.2 \pm 0.1$.

With anthracene present as the solute, triplet-state anthracene molecules are formed after the pulse. In solutions containing 20 mM or less anthracene, triplet benzophenone is present at the end of the pulse (Figure 1) as in pure benzophenone. However, this transient decays more rapidly than in the absence of anthracene (Figure 2a) and concurrently a new transient builds in (Figure 2b) which absorbs with a peak at 435 $m\mu$. The new transient was identified as the triplet state of anthracene on the basis of its absorption spectrum

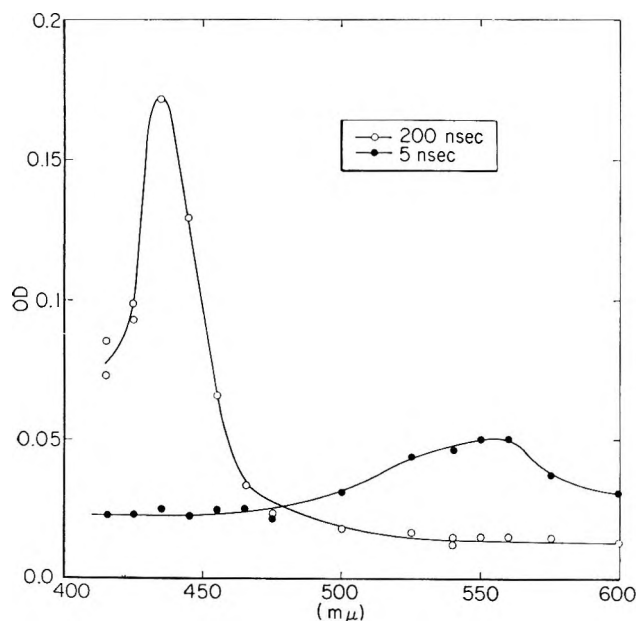


Figure 1. Absorption spectra of intermediates in pulse radiolysis of a solution of $10^{-2} M$ anthracene in benzophenone: ●, 5 nsec after the pulse, O, 200 nsec after a 5-nsec pulse.

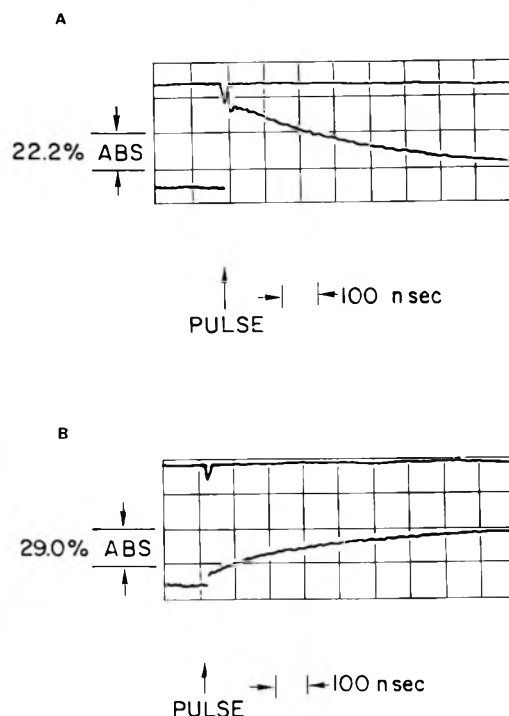


Figure 2. Oscilloscope traces showing time-resolved changes in absorption for 1.1 mM anthracene in benzophenone: A, decay of absorption at 540 $m\mu$; B, grow-in of absorption at 435 $m\mu$.

(Figure 1) which compares well with the published absorption spectrum for anthracene.¹⁰

The time dependence of triplet-triplet transfer from benzophenone to anthracene was investigated as a function of the concentration of anthracene. Plots of $\log(OD - OD_{\infty})$ vs. time for the data at 540 and 435 $m\mu$ were found to be linear (Figure 3). At each concentration the half-life of the benzophenone triplet (determined from data at 540 $m\mu$) is approximately the same as the half-life of the buildup of the anthracene triplet (determined from the grow-in of absorption at 435 $m\mu$). The half-life of these processes decreases

Table I: Results for Solutions of Anthracene in Benzophenone (30°) Irradiated with 5-nsec Pulses

Anthracene concn, mM	Half-life in nsec of		$G(^3BP^*)$ at 10 nsec	$G(^1A^*)^a$	$10^{-9}k_t$, $M^{-1} \text{ sec}^{-1}$
	Decay at 540 $m\mu$	Growth at 435 $m\mu$			
0	460	...	2.2
1.1	233	184	2.2	0.95	1.7
10	44	39	1.9	1.7	1.5
20	21	19	...	1.3	1.65
50	12 ^b	10 ^b	...	1.45	1.2 ^b

^a Plateau value measured at 0.1 to 1.0 μsec . ^b Only approximate since response time is 5 nsec.

(9) L. M. Dorfman and M. S. Matheson, *Progr. React. Kinet.*, **3**, 237 (1965).

(10) E. J. Land, *Proc. Roy. Soc.*, **A305**, 457 (1968).

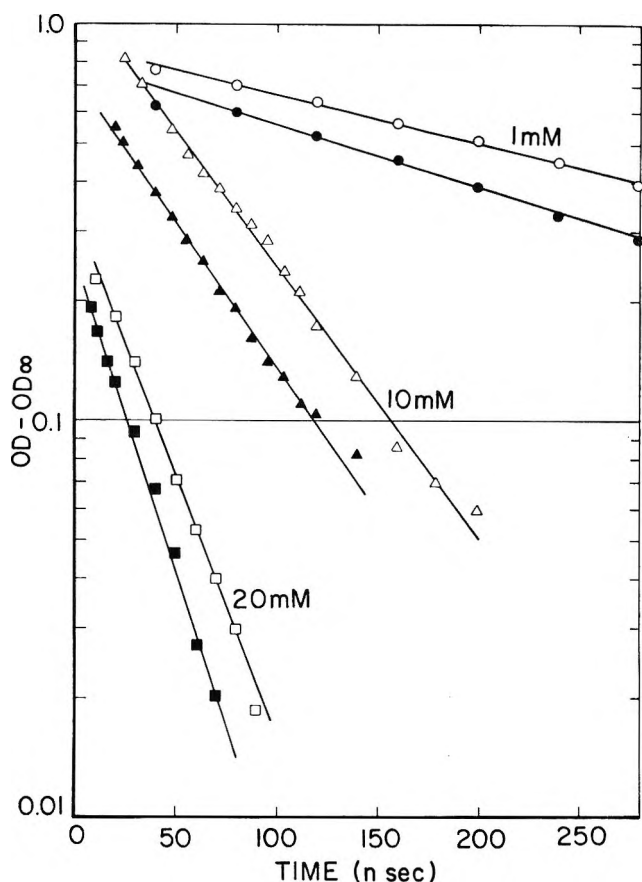


Figure 3. First-order plots of decay at $540 \text{ m}\mu$ (open points) and grow-in at $435 \text{ m}\mu$ (solid points) for solutions of anthracene in benzophenone; (circles) for 1 mM ; (triangles) 10 mM ; and (squares) 20 mM .

from 208 nsec at 1.1 mM anthracene to 20 nsec at 20 mM anthracene (Table I). The yield of anthracene triplets (measured 150 nsec after the pulse) increases with the concentration of anthracene and plateaus above 10 mM . The yield is $G(^3A^*) = 1.5 \pm 0.2$ if the extinction coefficient at the maximum is taken as $57,200$.¹⁰

Solutions of Benzantracene in Naphthalene. In the pulse radiolysis of solutions of 1,2-benzanthracene in naphthalene, time-resolved changes in both the fluorescence and the absorption spectra were observed. The sechanges indicate, respectively, singlet and triplet energy transfer to the benzantracene.

The time dependence of fluorescence of a solution of benzantracene in naphthalene does not follow a simple exponential decay as observed for pure naphthalene.⁵ Instead, at wavelengths about $475 \text{ m}\mu$, where benzantracene fluoresces much more strongly than naphthalene, the fluorescence intensity for a 1 mM solution of benzantracene increases immediately after a 4-nsec pulse, rises to a maximum at 16 nsec and then decays exponentially with a half-life of 26 nsec (Figures 4 and 5a). The following facts indicate that the first excited singlet state of benzantracene is populated in

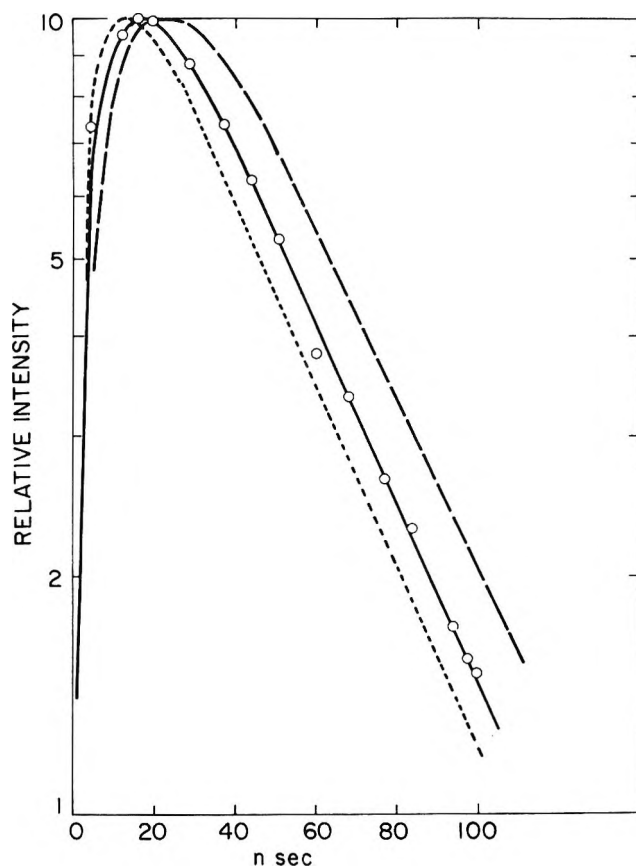


Figure 4. Fluorescence response at $460 \pm 5 \text{ m}\mu$ for a solution of 1 mM benzantracene in naphthalene at 100° as a function of time after a 4-nsec pulse. Circles are experimental points; lines are for various values of k_5 (see text); —, $k_5 = 9 \times 10^{10}$; ····, $k_5 = 15 \times 10^{11}$; ----, $k_5 = 5 \times 10^{10}$; $k_7 = 2 \times 10^7$ and $k_6 = 2.65 \times 10^7$.

tens of nanoseconds after the pulse. The fluorescence is more intense than for pure naphthalene by a factor of 4.2 at $475 \text{ m}\mu$. The fluorescence spectrum 100 nsec after the pulse is similar to the known fluorescence spectrum for 1,2-benzanthracene.¹¹ The half-life of benzantracene fluorescence in solution at room temperature is reported to be 31 nsec,¹² which compares well with 26 nsec.

The absorption spectrum changes with time after the pulse (Figure 5). The absorption spectrum observed 300 nsec after the pulse shows peaks at 435, 475, and $495 \text{ m}\mu$ of relative intensities: 0.66, 0.83, and 1.0. This compares well with the reported triplet-triplet absorption spectrum¹³ of 1,2-benzanthracene which has bands at 434, 461, and $485 \text{ m}\mu$ of relative intensities: 0.53, 0.84, and 1.0. There is a small red shift because the solvent is molten naphthalene.

The rate of formation of the benzantracene triplet

(11) J. B. Birks and L. G. Christophorou, *Proc. Roy. Soc.*, **A274**, 552 (1963).

(12) J. B. Birks, D. J. Dyson, and J. A. King, *ibid.*, **A277**, 270 (1964).

(13) G. Porter and M. Windsor, *ibid.*, **A245**, 238 (1958).

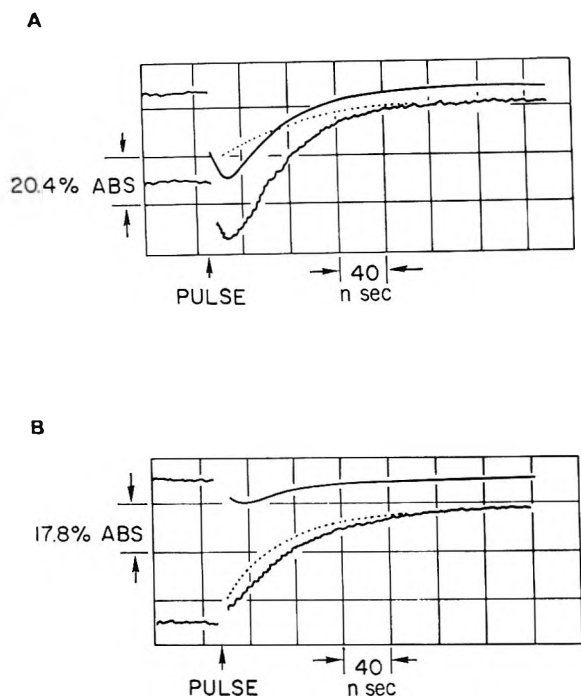


Figure 5. Oscilloscope traces for 1 *mM* benzantracene in naphthalene. Smooth curves are fluorescence; lower curves are combined fluorescence plus absorption; dashed curves are true absorbance corrected for fluorescence; A, 465 *mμ*; B, 495 *mμ*.

is concentration dependent. From the absorption data at 495 *mμ*, plots of $\log(\text{OD}_{300 \text{ nsec}} - \text{OD})$ vs. time were made (Figure 6) and found to be linear. The half-lives determined from such plots are given in Table II. The

Table II: Results for Solutions of Benzantracene in Naphthalene 100°

(Benz-anthracene) concn, <i>mM</i>	Half-life of triplet grow-in at 495 <i>mμ</i> , <i>nsec</i>	$10^{-9}k_2^a$, <i>M</i> ⁻¹ <i>sec</i> ⁻¹	$10^{-9}k_1^b$, <i>M</i> ⁻¹ <i>sec</i> ⁻¹
1	50 ± 2	14.0	8.1
3.4	23 ± 2	8.8	8.8
10	8 ± 5	~8.6	~11.5

^a Ignoring contribution of intersystem crossing from benzantracene singlet. ^b Contribution of ISC from benzantracene singlets taken into account (see Discussion).

rate of formation of solute triplets increases with increasing concentration of benzantracene. A corresponding decay of naphthalene triplets presumably occurs concurrent to the buildup of naphthalene triplets. Measurements were not made at the wavelengths where the naphthalene triplets absorb because of the strong fluorescence of 1,2-benzanthracene.

The yield of benzantracene triplets was determined for the maximum absorption at 495 *mμ*. At 300 *nsec* $G \times \epsilon_{495}$ was 94,000 for a 1 *mM* solution. This value

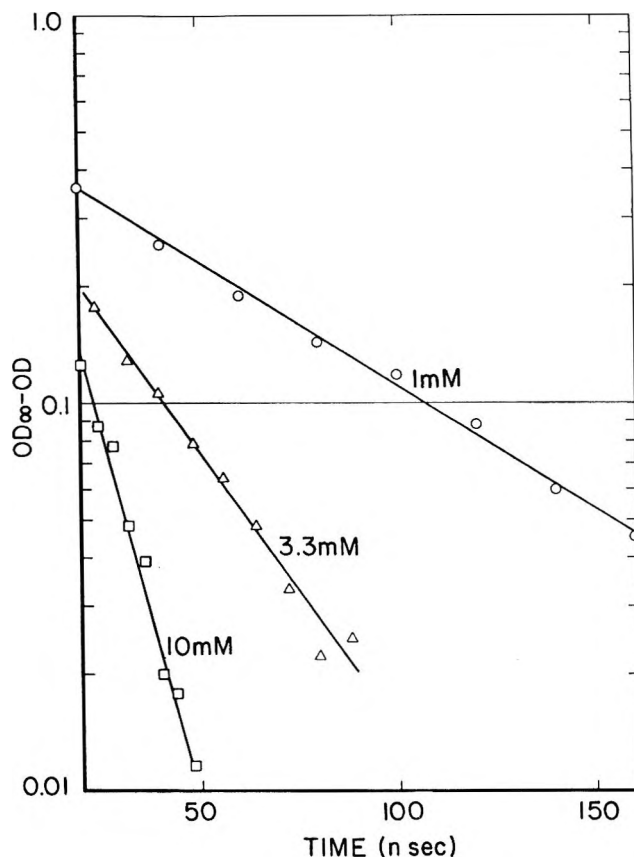


Figure 6. First-order plots of grow-in at 495 *mμ* for solutions of benzantracene in naphthalene at 100°: \circ , 1 *mM*; Δ , 3.4 *mM*; \square , 10 *mM*.

corresponds to $G(^3\text{BA}^*) = 3.7$ if ϵ is 25,100 *M*⁻¹ *cm*⁻¹.¹¹ Absorption by ions at this wavelength can be neglected. The benzantracene negative ion has a strong absorption band at 422 *mμ*,¹⁴ but absorbs weakly throughout the visible and there is a band at 502 which could interfere but $\epsilon_{495} \sim 1800$ *M*⁻¹ *cm*⁻¹ for the anion.¹⁵ The yield of benzantracene triplets present at the end of the pulse is estimated to be small. For a 1 *mM* solution, the observed optical density 10 *nsec* after the pulse is 22% of the final value. About one-third of this initial absorption is observed for pure naphthalene (and thus can be attributed to naphthalene transients) and some is probably due to energy transfer to benzantracene occurring during the pulse (see Discussion); thus the initial yield of solute triplets is small.

Discussion

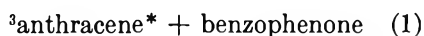
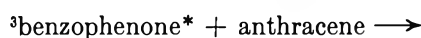
The results show that for the aromatic solutions studied, excitation of the solute to the triplet state occurs after the pulse. The rate of grow-in of the solute triplet is dependent on solute concentration.

(14) A. G. Evans and B. T. Tabner, *J. Chem. Soc.*, 5560 (1963).

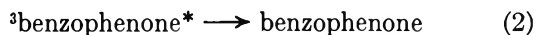
(15) The extinction coefficients for the anion BA^- were determined by partially reacting a 0.9 *mM* solution of 1,2-benzanthracene in THF with sodium. The concentration of BA^- was determined by esr. Values for the extinction coefficients of $\epsilon_{495} = 1800$ and $\epsilon_{422} = 6000$ *M*⁻¹ *cm*⁻¹ were measured.

Further, for solutions of anthracene in benzophenone, the triplet state of benzophenone is formed initially and the rate of its decay is identical with the rate of grow-in of the anthracene triplet at each concentration. For solutions of benzanthracene in naphthalene the fluorescence peaks 16 nsec after the pulse. This fluorescence is associated mainly with the excited benzanthracene singlet. These facts indicate that solute molecules are not excited initially in these solvents but become excited subsequently as a result of energy transfer. Other mechanisms of triplet excitation can be shown not to occur or to be unimportant. The recombination of ions is expected to lead to triplet excitation but the lifetimes of most of the ions in aromatic solvents is much shorter^{5,6} than the lifetimes of triplet grow-in observed in this work. Triplets can also be formed by intersystem crossing from the excited singlet state of the solute. This mechanism is unimportant for anthracene in benzophenone because the excited singlets are short-lived (lifetime < 5 nsec)¹⁶ and no initial yield of anthracene triplet was observed. For the solutions of benzanthracene in naphthalene, intersystem crossing may occur since benzanthracene singlets are formed, as shown by the fluorescence results. However, triplet-triplet transfer is shown to be a principal mode of solute excitation in this case also.

Triplet-Triplet Transfer. The data for solutions of anthracene in benzophenone can be interpreted entirely in terms of a mechanism in which excitation of the anthracene occurs by triplet-triplet transfer, reaction 1. Benzophenone triplets are also removed by the first-order process, reaction 2, which includes



self-quenching and phosphorescence. Thus the life-



time τ of the benzophenone triplet is given by eq I.

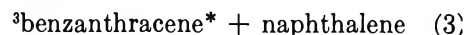
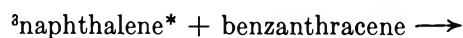
$$\tau = (k_2 + k_1[\text{anthracene}])^{-1} \quad (I)$$

The value of k_2 is determined from the triplet lifetime in the absence of solute (Table I) and is $1.5 \times 10^6 M^{-1} \text{sec}^{-1}$. Values of k_1 , the rate constant for energy transfer, were calculated from the lifetime of triplet-triplet transfer at each concentration and the value is $k_1 = (1.6 \pm 0.1) \times 10^9 M^{-1} \text{sec}^{-1}$. The rate of diffusional encounters in molten benzophenone at 30° can be estimated from the relationship $k_D = 8RT/3000\eta$.¹⁷ Since the viscosity is 0.136 poise, at 25°,¹⁸ k_D is $\sim 0.6 \times 10^9$. Thus the experimental rate constant is comparable to the diffusion-controlled rate, considering the uncertainty in the estimated value of k_D .

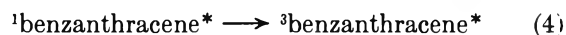
The observed yield of anthracene triplets at high anthracene concentrations is less than the yield of

benzophenone triplets observed for pure benzophenone. The explanation for this discrepancy may be that the absorption spectra of the benzophenone and anthracene triplets are broadened to different extents,¹⁹ and the extinction coefficients used may not apply in this solvent. The actual yield of triplets is probably greater than either of the yields reported.

In the solutions containing benzanthracene in naphthalene the half-life of formation of benzanthracene triplets also decreases with increasing concentration of benzanthracene. This fact requires that the solute triplets are formed, as in benzophenone, by triplet-triplet transfer, reaction 3. Values of k_3 cal-



culated from the observed half-lives are shown in Table II (column 3) and k_3 is $1.0 \times 10^{10} M^{-1} \text{sec}^{-1}$ if a contribution by intersystem crossing is neglected. However, a contribution by intersystem crossing should be considered since excited benzanthracene singlets are formed. A fraction equal to 0.55²⁰ of the singlets is expected to intersystem cross to the excited triplet state, reaction 4. The occurrence of two first-order processes can often be detected in plots of log



OD vs. time, but when the two processes have comparable half-lives, as is the case here, their sum yields a plot which is linear within experimental error. Thus intersystem crossing, which is assumed²¹ to have a half-life of 26 nsec, probably contributes to the formation of triplet benzanthracene, although direct evidence for this process was not obtained. Thus the observed half-lives may be averages of the half-lives of intersystem crossing and energy transfer. If intersystem crossing is taken into account then slightly different decay times corresponding to energy transfer are obtained. However, the average value of k_3 obtained in this way (see Table II) is the same as the value obtained neglecting intersystem crossing in benzanthracene.

The observed rate of triplet-triplet transfer in molten naphthalene is close to the rate of diffusional encounters in naphthalene which is $1.1 \times 10^{10} M^{-1} \text{sec}^{-1}$, estimated from viscosity data.¹⁸ If triplet excitons²² or excimers were present to any significant

(16) I. B. Berlman, "Handbook of Fluorescence Spectra of Aromatic Molecules," Academic Press, Inc., New York, N. Y., 1965.

(17) P. J. Debye, *Trans. Electrochem. Soc.*, **82**, 265 (1942).

(18) "International Critical Tables," McGraw-Hill Book Co., New York, N. Y., 1926, Vol. VII, p 220.

(19) The half-width for anthracene is $\sim 250 \text{ \AA}$ in Figure 1 and in cyclohexane the half-width is reported to be $\sim 100 \text{ \AA}$ (see ref 9).

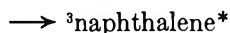
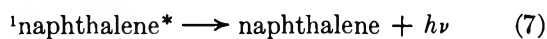
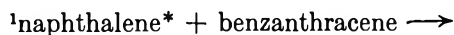
(20) H. Labhart, *Helv. Chim. Acta*, **47**, 2279 (1964).

(21) It is assumed here that intersystem crossing has the same lifetime as fluorescence.

(22) H. Baessler, *J. Chem. Phys.*, **49**, 5198 (1968).

extent, a larger rate constant might have been observed. The observed rate constant is explicable entirely in terms of a diffusion-controlled reaction of excited naphthalene triplets with benzantracene molecules.

Singlet-Singlet Transfer. The observed changes in fluorescence intensity with time (Figure 4) can best be accounted for in terms of singlet-singlet transfer, reaction 5, followed by fluorescence of the benzantracene, reaction 6. The first-order processes of fluorescence and intersystem crossing, reaction 7, compete



with energy transfer. The time dependence of the fluorescence has been analyzed in terms of the assumed mechanism. The intensity of naphthalene fluorescence at $465 \text{ m}\mu$ is much less than that of benzantracene and is neglected. The intensity of benzantracene fluorescence is proportional to the concentration of excited benzantracene [${}^1\text{B}^*$] which is given as a function of time after the pulse by eq II where [${}^1\text{N}^*$] $_0$ is the initial concentration of excited naphthalene

$$[{}^1\text{B}^*] = \frac{k_5[\text{B}][{}^1\text{N}^*]_0}{k_6 - k_7 - k_5[\text{B}]} \{e^{-(k_7+k_5[\text{B}])t} - e^{-k_6 t}\} \quad (\text{II})$$

singlets, and [B] is the concentration of benzantracene. All the rate constants in eq II are known except k_5 , the rate constant for singlet energy transfer. The fluorescence half-life of benzantracene is 26 nsec thus k_6 is 2.6×10^7 ; k_7 is $2 \times 10^7 \text{ M}^{-1} \text{ sec}^{-1}$.⁵ Various

values of k_5 were tried and the best fit to the data was obtained for a value of $k_5 = 9 \times 10^{10}$ (see Figure 4). This value is an order of magnitude greater than the rate of triplet-triplet transfer in this liquid and the latter process is diffusion controlled.

Rates of excitation transfer greater than the diffusion-limited rate have been observed for other solutions where solvent molecules are initially excited. For example, for quenching of excited benzene by oxygen in benzene the apparent quenching rate constant is $9 \times 10^{10} \text{ M}^{-1} \text{ sec}^{-1}$.⁴ There are several mechanisms²³ which may account for energy migration at a rate faster than molecular diffusion. Since excimers are present in naphthalene,⁵ rapid migration *via* repeated sequences of excimer formation and dissociation may be significant in this case.

Conclusion

The results show that radiation-induced excitation of solutes, when present at low concentrations in aromatic solvents, occurs largely by excitation transfer from the solvent. The transfer of triplet-state energy is diffusion controlled while singlet-state energy transfer is much faster than the diffusion-limited rate. Ion recombination does not result in solute excitation, since most of the ions recombine in times shorter than a few nanoseconds⁶ and solute triplets are not present a few nanoseconds after the pulse. This further indicates that solute ions are not formed in these solvents as they are in cyclohexane.^{24,25} Apparently charge and electron transfer to the solutes is a minor process in aromatic solvents.

(23) J. B. Birks in "Energetics and Mechanisms in Radiation Biology," Academic Press, Inc., Ltd., London, 1968, p 203 ff.

(24) J. K. Thomas, K. Johnson, T. Klippert, and R. Lowers, *J. Chem. Phys.*, **48**, 1608 (1968).

(25) R. R. Hentz and R. J. Knight, *J. Phys. Chem.*, **72**, 1783 (1968).

Electron Spin Resonance Studies on γ -Irradiated Frozen Aqueous Solutions of Sodium Formate

by R. A. Nazhat, N. B. Nazhat, P. N. Moorthy, and J. J. Weiss

Laboratory of Radiation Chemistry, School of Chemistry, University of Newcastle upon Tyne, The University, Newcastle upon Tyne NE1 7RU, England (Received August 12, 1969)

γ -Irradiated frozen aqueous solutions of formate have been investigated by esr. OH radicals from the ice and HCO, HCOO, and CO₂⁻ from the formate have been identified from a study of g factors and hfs of the esr spectra. (Experiments were also carried out with deuterioformate and in D₂O matrices.) From the dependence of the spectra on solute concentration and the effects of different scavengers, possible mechanisms for the formation of these radicals have been discussed. Some trapped electrons are also formed by the radiation, as indicated by the blue color of the irradiated matrices; these can be bleached by visible light. The strong signal from the CO₂⁻ radical ion did not allow direct observation of the esr spectrum of the trapped electron.

Introduction

The formation and stabilization of hydrogen atoms, hydroxyl radicals, electrons, and holes in irradiated frozen aqueous solutions has been extensively investigated. Esr studies on irradiated frozen systems have revealed that the primarily formed electrons and holes can react with suitable acceptor solutes to form paramagnetic species. The electrons can react with acidic solutes such as HSO₄⁻ to form hydrogen atoms,^{1,2} with cations Mg²⁺, Zn²⁺, Cd²⁺ and Hg²⁺ to form the corresponding univalent ions,³ and with acetone to give the acetone negative ions.² The hole can react with HSO₄⁻, H₂PO₄⁻ to give SO₄⁻, HPO₄⁻ and with OH⁻ to form O⁻ radical ions.^{4,5} In addition to the electrons and holes, radiolysis of ice also leads to some direct formation of hydrogen atoms and hydroxyl radicals in smaller yields. Hydrogen atoms which have been identified⁶ in irradiated pure ice at 4°K can take part in chemical reactions between 4 and 77°K unless stabilized at suitable trapping sites. Hydroxyl radicals are stable up to ~110°K even in pure ice and can enter into chemical reactions above this temperature.

The work reported here deals with esr studies of the different paramagnetic species which result from reactions of the radiation-produced electrons and holes in γ -irradiated frozen aqueous solutions of formate.

Experimental Section

Analar reagents were used whenever possible without further purification and triply distilled water. Ice cylinders were prepared as previously described.² The D₂O used was of 99.8% isotopic purity (Norsk Hydroelektrisk). The deuterated formate (99.8%) was supplied by Merck Sharp and Dohme Ltd. and was used without further purification. The ice cylinders were irradiated at 77°K in Pyrex tubes to

doses of 2.0–2.5 Mrads with a ⁶⁰Co γ source at a dose rate of approximately 0.1 Mrad/hr. After irradiation, the ice cylinders were transferred directly to a quartz-tipped dewar containing liquid nitrogen. The dewar was placed into the esr cavity and the spectrum recorded. After annealing to 110°K, the esr spectra were measured at 77°K. Photobleaching was carried out with light from a 500-W tungsten lamp for 3–5 min.

A Microspin esr spectrometer operating at 9.4 kMcps, 100-kcps modulation, and a microwave power of approximately 5 mW was used for most of the measurements. The magnetic field was current regulated and calibrated with a proton resonance magnetometer.

Results and Discussion

The esr spectrum of γ -irradiated frozen 1.0 M aqueous HCOONa at 77°K is shown in Figure 1a. Comparison of this with the esr spectrum of γ -irradiated pure ice (Figure 1b) reveals the presence of OH radicals, in addition to other paramagnetic species, in the irradiated frozen formate solutions. Annealing the irradiated 1 M HCOONa ice to 110°K at which temperature the OH radicals disappear⁷ leaves the spectra given in Figure 2. This now shows a considerable increase in the resonance marked C and the appearance

(1) L. Kevan, P. N. Moorthy, and J. J. Weiss, *Nature*, **199**, 639 (1963).

(2) L. Kevan, P. N. Moorthy, and J. J. Weiss, *J. Amer. Chem. Soc.*, **86**, 771 (1964).

(3) P. N. Moorthy and J. J. Weiss, *Nature*, **201**, 1317 (1964).

(4) P. N. Moorthy and J. J. Weiss, *Phil. Mag.*, **10**, 659 (1964).

(5) P. N. Moorthy and J. J. Weiss, *Advances in Chemistry Series*, No. 50, American Chemical Society, Washington, D.C., 1965, p 180.

(6) S. Siegel, J. M. Flournoy, L. H. Baum, *J. Chem. Phys.*, **34**, 178 (1961).

(7) S. Siegel, L. H. Baum, S. Skolnik, and J. M. Flournoy, *ibid.*, **32**, 1249 (1960).

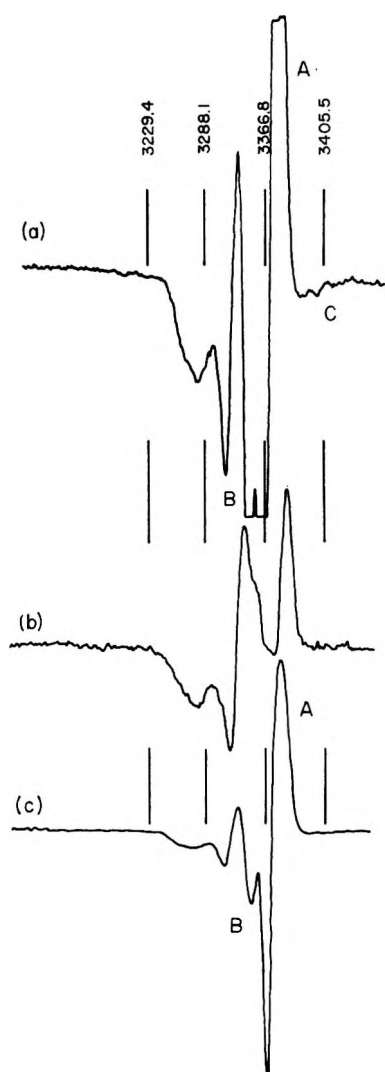


Figure 1. ESR spectra of γ -irradiated ice matrices at 77°K: (a) 1 M HCOONa (gain 10); (b) H₂O; (c) same as (a) (gain 1.0).

of another resonance (marked C'). Signal C' could have been present in the spectrum of Figure 1a but obscured by the resonance of the lower field line of the OH radical. The signals CC' can be attributed to the same paramagnetic species as is revealed by the similar changes in the intensities of these lines with solute concentration as shown in Figure 3b. Before annealing, the intensity of the CC' doublet does not vary markedly with concentration of formate, while that of line A increases to a plateau and that of line B is proportional to the solute concentration (Figure 3a). The irradiated specimens have a violet-blue color which is attributed to the formation of some trapped electrons. The ESR signal of the electron has not been observed because it is evidently masked by the intense line A which, as will be discussed below, is due to the CO₂⁻ radical ion. Photobleaching leads to disappearance of the color and of the lines B and CC', but results in some increase of line A. Annealing to about 110°K

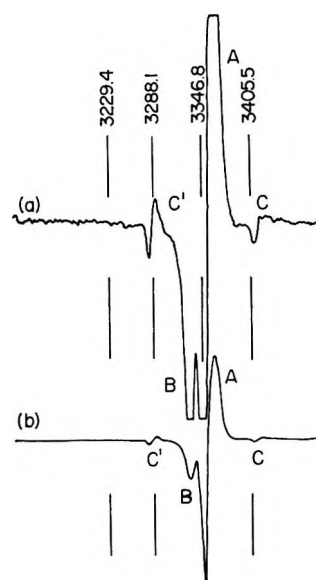


Figure 2. ESR spectra of γ -irradiated frozen 1 M HCOONa after annealing to 110°K: (a) at gain 10, (b) at gain 1.0.

causes an increase in the intensity of the CC' pair, whereas the intensities of the lines A and B are decreased due to the disappearance of the OH radical resonance which also contributes to the intensities of these two lines before annealing.

In what follows only the spectra obtained after annealing and photobleaching have been considered for the analysis of g factors, line shape, and line widths, because this eliminates interference from the OH radical resonance and from line B. On slow scan, the line shape of A (Figure 4) is seen to correspond to that of a radical with three principal g factors randomly oriented in a polycrystalline medium.⁸ The principal g factors of line A computed on the basis of this interpretation are given in Table I. This line has a similar shape and the same overall width in D₂O matrices, but the individual inflexions are better resolved than in the H₂O matrices. This would be the case if the protons (or deuterons) of the water molecules in the vicinity of the radical contribute to the line broadening.

The g factors for the radical in the D₂O and H₂O matrices are identical within the limits of experimental

Table I: g Factors for CO₂⁻ Formed by γ Irradiation of Sodium Formate

	Frozen aq soln, 77°K	Single crystal ^a
g_1	1.9971	1.9975
g_2	1.9988	2.0014
g_3	2.0034	2.0032

^a See ref 9.

(8) F. K. Kneubühl, *J. Chem. Phys.*, **33**, 1074 (1960).

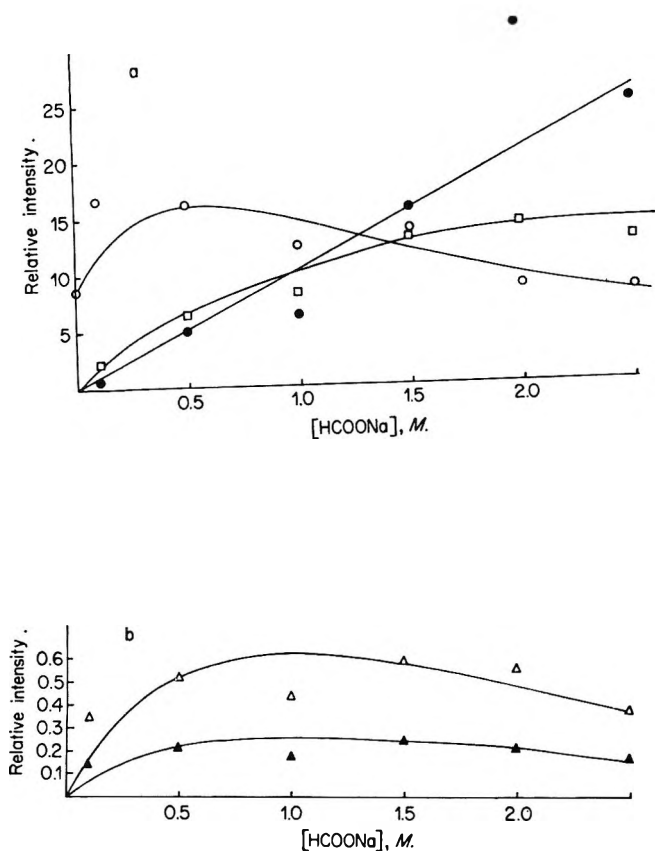


Figure 3. Relative esr line intensities as a function of HCOONa concentration. a: ●, HCOO; □, CO₂⁻; ○, OH. b: △, high CHO (after annealing); △, low CHO (before annealing).

error. Comparison of these *g* factors with those for the CO₂⁻ ion radical identified in the single crystal of γ -irradiated HCOONa⁹ (which are also given in Table I) strongly suggests the identity of the paramagnetic species in the formate single crystal and in the frozen aqueous formate systems. In the single crystal study, a hyperfine splitting of 168 G has been reported for CO₂⁻ radical ion due to C¹³(*I* = 1/2) present at a natural abundance of 1.1%. In a search for the C¹³O₂⁻ in the irradiated solutions a specimen was irradiated to a high dose and the spectrum scanned in the field positions where the doublet due to C¹³O₂⁻ is to be expected. Although these positions are close to the lines of the CC' pair, they were resolvable from the latter. Thus both the CC' lines and C¹³O₂⁻ doublet could be scanned after annealing. On subsequent exposure to light from a tungsten lamp, only the CC' lines disappear. The intensity ratio of the C¹³O₂⁻ doublet to that of the C¹²O₂⁻ singlet was the same as expected from their relative abundances. In the single crystal study, a small hyperfine splitting (8.2 G) of the unpaired electron in CO₂⁻ with the neighboring Na²³ nucleus (*I* = 3/2) has also been reported. This, however, was not observed in the frozen solutions presumably due to the fact that the

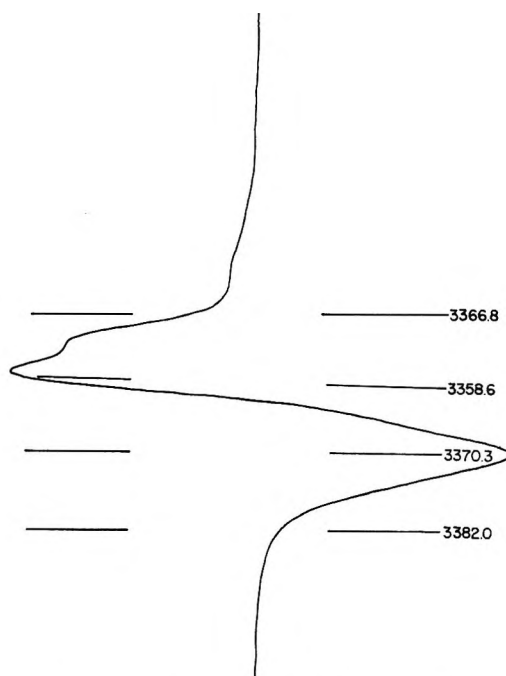
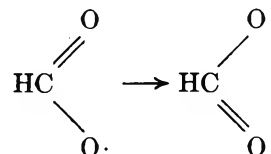


Figure 4. ESR of CO₂⁻ in 1.0 M HCOONa on slow scan in ice.

radicals in the present case are separated from Na⁺ cations by the intervening water molecules. The relatively large width (~12 G) of the CO₂⁻ line in the frozen aqueous systems can be considered to result from unresolved hyperfine interaction of the unpaired electron with the protons of neighboring water molecules. Such an unresolved hyperfine interaction with a number of magnetic nuclei has been shown previously to exist in the case of the trapped electron in γ -irradiated aqueous alkali hydroxides. This leads to an inhomogeneously broadened line which is the envelope of the individual hyperfine lines.^{4,5}

Line B is symmetrical and does not show inflexions attributable to an anisotropic *g* tensor; its *g* factor corresponding to the line center was found to be 2.0121. This large positive *g* shift from the free electron value (2.0023) suggests that the radical is an electron deficient center with large spin-orbit coupling. This line can reasonably be ascribed to the species HCO₂, which could be stabilized through resonance between the two structures



Addition of iodide ions which is an efficient hole scavenger leads to decrease in the intensity of line B which is a further indication that this radical is formed by an oxidative process.

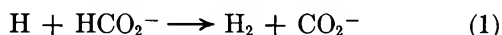
(9) D. W. Ovenall and D. H. Whiffen, *Mol. Phys.*, **4**, 135 (1961).

Since line B is a singlet, the unpaired electron would be localized on the oxygen atom.

The lines of the CC' pair show a similar behavior on annealing and after photobleaching and follow the same trend of intensity variation with the concentration of sodium formate. It can, therefore, be considered to be a doublet due to a single paramagnetic species. The only magnetic nuclei which can give rise to a doublet hyperfine splitting in the present systems are H^1 and C^{13} (both $I = 1/2$). If the doublet splitting is due to C^{13} , then at the center of the doublet there should be a very intense line due to the corresponding C^{12} as discussed above for the case of CO_2^- . The absence of such a line rules out the possibility that the CC' doublet is due to a species containing C^{13} . The doublet splitting therefore is most likely due to a proton. The value of this splitting (127 G) as well as the asymmetric shape of the high-field line are very similar to those recorded previously for the CHO radical.¹⁰⁻¹³

Mechanism of Formation of the Radicals. In irradiated single crystals of HCOONa there is evidence only for the formation of the CO_2^- radical ion; the other radicals found in the irradiated frozen aqueous solutions have not been observed in the crystal. The high yield of CO_2^- in the irradiated frozen solutions does reveal a large indirect effect compared to the reaction in the solid formate. From these observations one may conclude that in the frozen solutions practically all the radicals are formed by reactions of the primary products, from the radiolysis of ice, with the solute. The initial act of radiation on ice will result in formation of electrons and holes, in addition to hydrogen atoms and hydroxyl radicals. In what follows, it will be shown how the reactions of these species with the solute can account for the formation of the observed radicals.

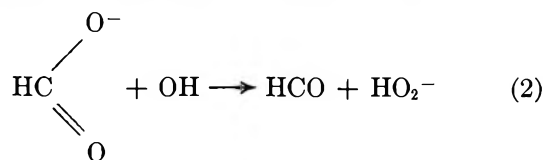
The CO_2^- radical ions can be considered to be formed by the reaction of hydrogen atoms with formate ions according to



This explains satisfactorily the shape of the yield of CO_2^- vs. the concentration of HCOONa as shown in Figure 3a; since the hydrogen atom yield remains constant, with increasing solute concentration, more and more hydrogen atoms are removed according to reaction 1 until at sufficiently high concentrations of HCOONa practically all the hydrogen atoms have been consumed so that there is no further increase in the CO_2^- yield. The reaction of hydrogen atoms with formate have been fully established in the radiolysis of aqueous formate solutions.¹⁴ The occurrence of reaction 1 was also shown by the following experiment. In irradiated frozen aqueous NaOH, (unlike pure ice) hydrogen atoms which are formed by the action of radiation on water are stable at 77°K and are identi-

able by their characteristic esr spectrum. However, in the presence of a small amount of HCOONa in the NaOH solutions the hydrogen atoms esr signals were not observed. This suggests that the hydrogen atoms must have disappeared by a reaction with the second solute, viz., HCOONa.

As seen from Figure 3a and 3b the disappearance of the OH radicals on annealing at 110°K is accompanied by an increase in the intensity of the CC' doublet which was assigned to the HCO radical. The shape of the yield curve for this radical after annealing resembles that of the OH radicals before annealing. The hf splitting of this radical was 127 G compared with 135 G obtained for the CHO radical obtained photochemically by the photolysis of HI in a CO matrix.^{11,12} This suggests that the radical which was observed here is the HCO radical. It is possible that during annealing it may be formed according to



The slight difference in hf splitting could be due to the fact that the angle of the HCO radical in the ice matrix is somewhat different to that in the CO matrix.

The failure to observe the hyperfine structure due to DCO in irradiated 1.0 M DCOO⁻ in a D₂O matrix could be due to the fact that this radical would have an expected splitting of (127/3.2 = 39 G) which could be masked by the strong signal from the CO_2^- radical ion. In Table II where the results on 1 M HCOO⁻ and

Table II: Yields of HCO Radicals in Different Ice Matrices

System	Yield, arbitrary units	System	Yield, arbitrary units
DCOO ⁻ -H ₂ O	2.3	HCOO ⁻ -H ₂ O	3.00
HCOO ⁻ -D ₂ O	0.7	DCOO ⁻ -D ₂ O	0

1 M DCOO⁻ in H₂O and D₂O matrices are given, the results suggest some exchange between deuterium on the carbon with the hydrogen from the H₂O matrix.

As mentioned earlier, the large positive *g* shift in the HCOO radical spectrum suggests this to be an electron deficient center with large spin-orbit coupling. Also in the presence of hole scavengers such as iodide ions

(10) P. J. Sullivan and W. S. Koski, *J. Amer. Chem. Soc.*, **84**, 1 (1962).

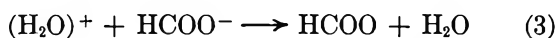
(11) E. L. Cochran and F. J. Adrian, The 5th International Symposium on Free Radicals, Uppsala, July 1961.

(12) E. L. Cochran, *Bull. Amer. Phys. Soc.*, **116**, 151 (1961).

(13) J. A. Bravati, N. Keen, and M. C. R. Symons, *J. Chem. Soc.*, 237 (1962).

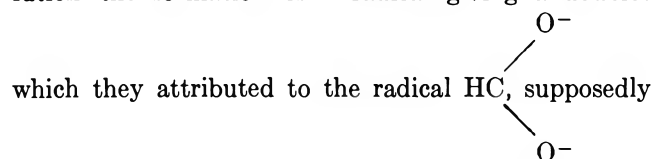
(14) G. Scholes and M. Simic, *J. Phys. Chem.*, **68**, 1738 (1964).

the radical decreases in intensity. This suggests that it is formed by an electron transfer reaction from the solute ion to the radiation-produced hole (H₂O)⁺ according to



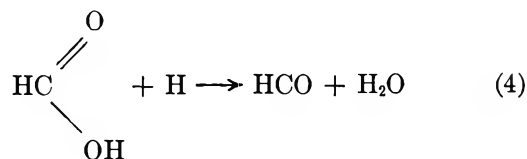
The disappearance of the HCOO and the HCO radical on photobleaching is believed to be due to reaction of the electron which is thereby released to react with these radicals to form HCOO⁻ and HCO⁻.

Recently Khodzhaev, Ershov, and Pikaev¹⁵ have suggested in the irradiation of frozen formate solution the formation of a radical giving a doublet

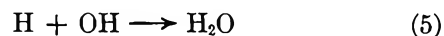


formed by the reaction of an electron with formate ions. We have found that such a signal is also observed in acid matrices, *e.g.*, containing sulfuric acid, where the electrons would react predominantly with HSO₄⁻ and hydrogen ions. This would confirm our identification that this is in fact the HCOO radical as discussed above.

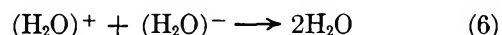
In the irradiation of these acid systems a second resonance was observed with a splitting of about 140 G. This could again be due to HCO radical, and the difference in the splitting could be due to slight distortion of the hydrogen bond angle. This radical could be formed according to the reaction



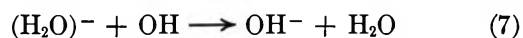
It is also seen from Figure 3a that with increasing solute concentration the OH radical yield passes through a maximum. As a result of reaction 1 a corresponding number of OH radicals escape the recombination reaction with hydrogen atoms



and therefore the OH radical yield should increase with solute concentration. At the same time the reaction of the holes with the solute according to eq 3 results in an equivalent number of electrons escaping the annihilation process with the holes



which otherwise could react with OH radicals according to



The extent to which these processes will proceed, *viz.*, one leading to an increase and the other to a decrease in the OH radical yield, depends on the relative reactivities as well as on the solute concentration so that, under certain conditions, the OH radical yield may go through a maximum.

Acknowledgments. We should like to thank Professor D. H. Whiffen, F. R. S., and Dr. G. Scholes for useful discussions. N. B. N. wishes to thank the Ministry of Education of Iraq for financial support.

(15) O. F. Khodzhaev, B. G. Ershov, and A. K. Pikaev, *Izv. Akad. Nauk SSSR Ser. Khim.*, **10**, 2253 (1967).

Ultraviolet and Infrared Studies of Free Radicals in Irradiated Polyethylene

by D. C. Waterman and M. Dole¹

Department of Chemistry and Materials Research Center, Northwestern University, Evanston, Illinois 60201
(Received September 19, 1969)

Electron spin resonance, infrared, and ultraviolet spectral measurements have been made on the alkyl, allyl, and dienyl free radicals in electron beam-irradiated high-density polyethylene. G values and extinction coefficients have been determined. Additional evidence for the assignment of the 215-nm band to the alkyl free radical, the 258-nm band to the allyl free radical, and the 943-cm⁻¹ band to stabilized allyl and dienyl free radicals is given. At 77°K the growth of the alkyl free radical is linear with dose up to at least 80 Mrads, but the allyl radicals, which are formed at room temperature subsequent to the irradiation at 77°K, approach a limiting concentration of about 0.02 M .

Introduction

Among the possible free radicals that might be produced by the high-energy irradiation of polyethylene the secondary alkyl, $-\text{CH}_2\dot{\text{C}}\text{HCH}_2-$, the allyl, $-\dot{\text{C}}\text{HCH}=\text{CH}-$, and the polyenyl free radicals, $-\dot{\text{C}}\text{H}(\text{CH}=\text{CH}-)_n$, have been detected by electron spin resonance studies.²⁻⁵ One of the problems of observing free radicals in polyethylene by esr techniques is that the spectra of the different radicals superimpose on each other, thus making the spectra difficult to analyze. Further, if a radical is only present as a small fraction of the total free radical concentration, it will not be detected, since the observed spectrum will be dominated by the main portion of the radicals. For example, the only free radical, relatively stable at room temperature, that can be detected in polyethylene after a low radiation dose is the allyl radical, although it is clear that dienyl and possibly higher polyenyl free radicals must be present.

Studies^{6,7} on the ultraviolet absorption spectra of irradiated polyethylene show that two types of uv absorption bands can be detected, those whose wavelength at the absorption maximum approach a limit as the number of conjugated double bonds increases, the polyenes, and those whose wavelengths at the maximum absorption increase linearly with the number of conjugated double bonds, the polyenyl free radicals. Table I^{8,9} gives the observed absorption bands and their assignments. The assignment of the 215-nm band to the alkyl free radical by Dole and Böhm⁹ was tentative. Additional evidence for this assignment is given below.

In the case of infrared studies, Koritskii, *et al.*,¹⁰ and Dole and Böhm⁹ have assigned the 943-cm⁻¹ absorption band to the allyl free radical, the assignment of Koritskii, *et al.*, being based on esr comparisons and Dole and Böhm's on comparison of the 943 ir band with the 258 uv band.

It can be seen that uv and to a lesser extent ir observations provide a means to observe changes in radical concentrations which would be difficult to observe by esr studies. Up to the present time, such observations have been limited to relative changes in concentration. One of the purposes of this work was to obtain extinction coefficients of the free radical absorption bands so that quantitative calculations of free radical

Table I: Ultraviolet Absorption Bands in Irradiated Polyethylene

Number	Polyenes $-(\text{CH}=\text{CH}-)_n$	λ_{max} , nm	Polyenyl free radicals $-\dot{\text{C}}\text{H}(\text{CH}=\text{CH}-)_n$	λ_{max} , nm
1	Vinylene	185 ^a	Allyl	258
2	Diene	229, 236, 245	Dienyl	285
3	Triene	264, 275, 288	Trienyl	323
4	Tetraene	310	Tetraenyl	359
5	Pentaene	340	Pentaenyl	396
0	Secondary alkyl free radical		$-\text{CH}_2\dot{\text{C}}\text{HCH}_2-$	215 ^a

^a See ref 9.

- (1) Address inquiries to the Department of Chemistry, Baylor University, Waco, Texas 76703.
- (2) R. J. Abraham and D. H. Whiffen, *Trans. Faraday Soc.*, **54**, 1291 (1958).
- (3) E. J. Lawton, J. S. Balwit, and R. S. Powell, *J. Chem. Phys.*, **30**, 345 (1960).
- (4) S. Ohnishi, Y. Ikeda, M. Kashiwagi, and I. Nitta, *Polymer*, **2**, 119 (1961).
- (5) A. Charlesby, D. Libby, and M. G. Ormerod, *Proc. Roy. Soc.*, **A262**, 207 (1961).
- (6) M. B. Fallgatter and M. Dole, *J. Phys. Chem.*, **68**, 1988 (1964).
- (7) D. M. Bodily and M. Dole, *J. Chem. Phys.*, **45**, 1433 (1966).
- (8) R. H. Partridge, *ibid.*, **45**, 1679 (1966).
- (9) M. Dole and G. G. A. Böhm, *Advances in Chemistry Series*, No. 82, American Chemical Society, Washington, D.C., 1968, p 525.
- (10) A. T. Koritskii, Y. N. Molin, V. N. Shamshev, N. Y. Bulen, and V. V. Voevodskii, *Vysokomol. Soedin.*, **1**, 1182 (1959).

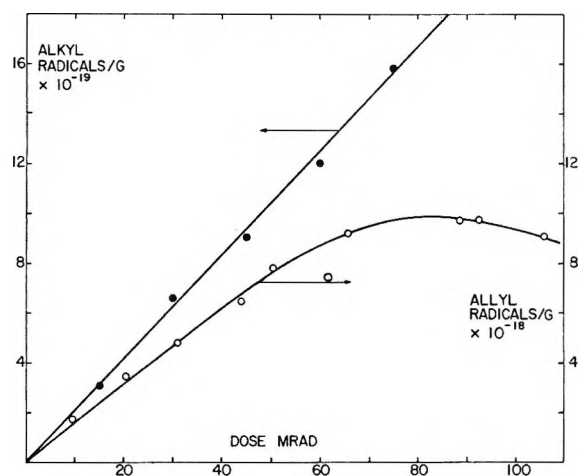


Figure 1. Growth of alkyl free radicals at 77°K, solid circles, and of allyl (total stabilized free radicals at 24°), open circles, as a function of dose at 77°K.

concentrations can be made. Additional evidence for the absorption band assignments is also given.

Experimental Section

General techniques used for the electron beam irradiations and dosimetry, esr measurements, and the materials studied have already been described.¹¹ All of the uv and ir spectra were taken at 77°K using a combined irradiation and spectroscopic cell which was a modified version of the one described by Dole and Böhm.⁹ The uv irradiations of the previously electron beam irradiated polyethylene were carried out at 77°K on the esr samples contained in quartz tubes using a quartz dewar with a narrow unsilvered tail section. The uv irradiations of the samples studied by uv or ir spectroscopy were made at 77°K through a quartz window of the irradiation-spectroscopic cell. All esr, uv, and ir measurements were made on samples of 10.4-mil Marlex 6002 polyethylene film.

Results and Discussion

Alkyl and Allyl Free Radical G Values. Figure 1 illustrates the increase in concentration of the alkyl and stabilized free radicals (allyl and polyenyl) as a function of dose as measured by esr. The alkyl free radicals were measured at 77°K after an irradiation at that temperature while the stabilized free radical concentrations were measured at room temperature after all of the alkyl free radicals had decayed. Note that the alkyl growth is accurately linear with dose, but that the allyl free radical concentration attains a maximum at a dose of about 90 to 100 Mrads. The allyl free radicals are produced from the alkyl radicals,¹¹ with the alkyl radicals reacting competitively to form cross-links. With increase of alkyl concentration the yield of cross-links, which must be formed by a process second order in the alkyl free radical concentration, should increase. This would leave relatively fewer alkyl free radicals at room

temperature to form allyl free radicals and the yield of the latter should decrease. These ideas can be put into a more quantitative form by the following kinetic analysis.

The rate of decrease of alkyl free radical concentration with time can be expressed by the equation

$$d[R\cdot] = -k_x[R\cdot]^2dt - k_a[R\cdot]dt \quad (1)$$

where $[R\cdot]$ is the alkyl free radical concentration, k_x is the second-order constant for the recombination of the free radicals to form cross-links, k_a the first-order constant for the reaction of the alkyl free radicals to form allyl radicals, and t the time. In writing down this equation it is assumed that the double bond concentration remains constant during the free radical decay. Integrating eq 1 we obtain

$$[R\cdot] = k_a / \{ \exp(k_a t) [(k_a/[R\cdot]_0) + k_x] - k_x \} \quad (2)$$

where $[R\cdot]_0$ is the alkyl radical concentration at time zero. Assuming that allyl formation follows the kinetic expression

$$d[A\cdot]/dt = k_a[R\cdot] \quad (3)$$

substituting (2) into (3) and integrating, we find

$$[A\cdot] = \frac{k_a}{k_x} \left[\ln \{ [1 + ([R\cdot]_0 k_x / k_a)] \exp(k_a t) - (k_x / k_a) [R\cdot]_0 \} - k_a t \right] \quad (4)$$

At infinite time when all the alkyl free radicals have decayed

$$[A\cdot]_\infty = (k_a/k_x) \ln \{ 1 + [R\cdot]_0 k_x / k_a \} \quad (5)$$

If this treatment is valid, a plot of $[A\cdot]_\infty$ as a function of the logarithmic factor of eq 5 should yield a straight line with slope equal to k_a/k_x . However, to calculate $[R\cdot]_0 k_x / k_a$ we need to know k_a/k_x . At high doses $[A\cdot]_\infty$ plotted as a function of $\ln [R\cdot]_0$ should also yield a straight line with slope equal to k_a/k_x . A provisional value of k_a/k_x was obtained by this procedure, inserted into eq 5, the logarithmic function calculated, and a plot of $[A\cdot]_\infty$ as a function of $\ln \{ 1 + [R\cdot]_0 k_x / k_a \}$ made. From the slope of this line a new value of k_a/k_x was determined and the calculation repeated until the best value of k_a/k_x was found. In Figure 2 a plot is illustrated of eq 5, but exact agreement of the data with eq 5 is not to be expected because eq 1 is based on isothermal conditions whereas the reactions of alkyl free radical recombination and of alkyl with double bond to yield the allyl free radicals actually occurred as the irradiated polyethylene was heated from 77°K to room temperature. One would hardly expect k_a and k_x to have the same temperature coefficient. Nevertheless the agreement of the data with eq 5 is surprisingly good, Figure 2, and yields a k_x/k_a ratio of $2.8 \times 10^{-19} \text{ g (spins)}^{-1}$.

(11) D. C. Waterman and M. Dole, *ibid.*, **74**, 1913 (1970).

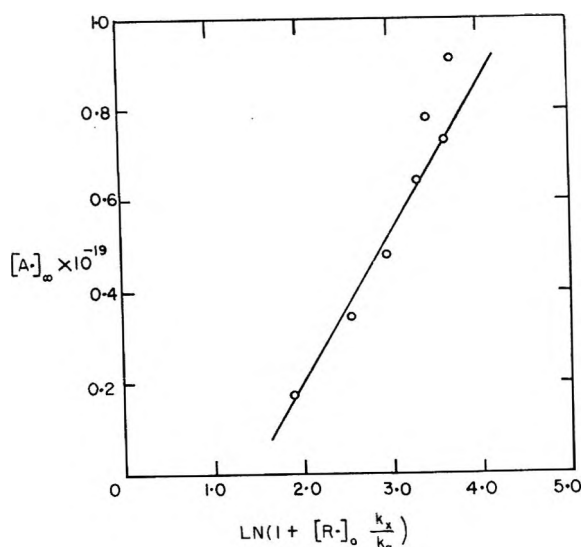


Figure 2. Test of eq 5. Units of $[\text{A}\cdot]_\infty$ are spins g^{-1} .

Equation 5 appears to be invalid at high doses; it is also incorrect in that it predicts that at very low doses when $k_x[\text{R}\cdot]_0$ becomes negligible with respect to k_a the allyl free radical concentration should be equal to the initial alkyl free radical concentration. If homogeneous kinetics governed the reactions of the free radicals in solid polyethylene, this might be true, but inasmuch as the free radicals are formed in spurs and react for the most part preferentially with nearest neighbors without migration, it is easily understandable why $[\text{R}\cdot]_0$ is about tenfold $[\text{A}\cdot]_\infty$ even at doses as low as 10 Mrads.

From the data of Figure 1 we obtain as average values over the first 50 Mrads of radiation: $G(\text{alkyl})$ at $77^\circ\text{K} = 3.3 \pm 0.5$, $G(\text{allyl and polyenyl free radicals})$ at $24^\circ = 0.25 \pm 0.04$. These G values compare favorably with other measured values; for example, Charlesby, *et al.*,⁵ obtained $G(\text{alkyl}) = 2.4\text{--}2.8$ and $G(\text{allyl}) = 0.2\text{--}0.3$; Lawton, *et al.*,³ found $G(\text{alkyl}) = 3.0$; Koritskii, *et al.*,¹⁰ $G(\text{alkyl}) = 3.1$; and Ohnishi¹² $G(\text{allyl}) = 0.31$. Ohnishi¹² also found $G(\text{alkyl})$ to be 6.1, but this result cannot be correct because on heating to room temperature practically all of these free radicals must form cross-links. A few form allyl free radicals¹¹ but practically none recombine to form the vinylene unsaturated group.¹³ Ohnishi's result would require $G(\text{X})$ to be 3.0 whereas the most recent results of Kang, Saito, and Dole¹⁴ give $G(\text{X})$ equal to 1.5 for irradiations at room temperature and dose of 27 Mrads. Ohnishi also found that $G(\text{alkyl})$ decreased with dose above a dose of about 20 Mrads while our data illustrated in Figure 1 show $G(\text{alkyl})$ to be constant up to 80 Mrads. We have no explanation for this difference in the two experimental observations.

The Ultraviolet Absorbance of the Alkyl Free Radical. Dole and Böhm suggested that the uv absorption band at 215 nm was to be attributed to the alkyl free radical.

Further evidence for this assignment is the following. A sample of polyethylene was irradiated at 77°K and its esr spectrum taken. The temperature was raised briefly to room temperature and the esr spectrum again taken at 77°K . By measuring the height of the wing absorbance of the alkyl radical spectrum it was estimated that 14% of the initial alkyl radicals survived this annealing treatment. Experiments carried out under similar conditions to observe the absorbance at 215 nm showed that 13% of the absorbance remained after the brief heating to room temperature.

Ohnishi, *et al.*,¹⁵ found that allyl radicals when irradiated with uv light at 77°K disappear and are converted, in part at least, to alkyl radicals. We repeated this experiment and observed that in addition to the complete disappearance of the allyl absorbance at 258 nm, the absorbance at 215 nm increased. Esr experiments confirmed that under these conditions the only detectable radicals were indeed alkyl radicals although the uv studies showed a small increase in dienyl and trienyl free radical concentrations. The increase in absorbance at 215 nm can be quantitatively correlated with the concentration of the allyl radicals as follows. The increase in absorbance at 215 nm on uv irradiation was 0.063. For the same radiation dose of 4.5 Mrads the absorbance at 215 nm due to alkyl radicals initially produced by the irradiation at 77°K was 0.70. If it is assumed that all allyl radicals were converted to alkyl radicals by the uv irradiation, then

$$G(\text{initial alkyl}) = [0.700/0.063]G(\text{final allyl}) \quad (6)$$

It will be shown later that $G(\text{allyl})$ is 0.24; hence $G(\text{initial alkyl})$ calculated from eq 6 is 2.7 ± 0.4 in fair agreement with the estimates of $G(\text{alkyl})$ given above. As the latter values were obtained from esr measurements and the value of 2.7 from absorbances at 215 nm, we have additional evidence that the 215-nm uv absorbance is to be assigned to the alkyl free radical.

Finally, the uv absorption peak at 215 nm decays with the same first-order rate constant as that calculated from the esr values of the decay of the alkyl free radical.¹¹

In Figure 3 the absorbance at 215 nm is plotted as a function of dose. Knowing $G(\text{alkyl})$, the extinction coefficient of the 215-nm absorption is easily calculated to be $1800 \pm 300 \text{ M}^{-1} \text{ cm}^{-1}$. From the data of Figure 3 we can conclude that the growth with dose of both the alkyl at 77°K and stabilized allyl free radicals at room temperature is accurately linear in the low dose range.

(12) S. Ohnishi, *Bull. Chem. Soc. Jap.*, **35**, 254 (1962).

(13) M. Dole, D. C. Milner, and F. Williams, *J. Amer. Chem. Soc.*, **80**, 1580 (1958).

(14) H. Y. Kang, O. Saito, and M. Dole, **89**, *ibid.*, 1980 (1967).

(15) S. Ohnishi, S. Sugimoto, and I. Nitta, *J. Chem. Phys.*, **39**, 2647 (1963).

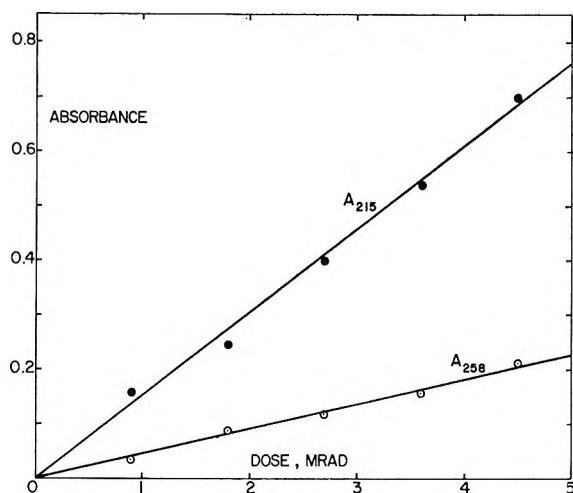


Figure 3. Growth of the absorbances at 215 nm at 77°K (solid circles) and at 258 nm at 24° (open circles) as a function of dose at 77°K. Uv measurements at 77°K.

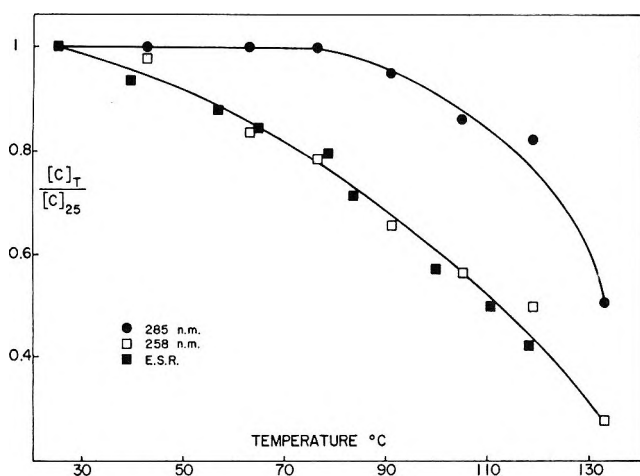


Figure 4. Decay of the allyl free radicals (open squares) and of the dienyl free radicals (solid circles) as a function of temperature. ESR estimates of the total polyenyl free radicals, solid squares.

The Ultraviolet Absorbance of the Allyl and Dienyl Free Radicals. Allyl radicals have been observed^{9,16} to have an absorption maximum in the uv at 258 nm. Further evidence that this assignment is correct was obtained by comparison of the thermal stability of the 258-nm absorbance and the allyl radical esr spectrum. A sample of polyethylene which contained stabilized allyl and dienyl free radicals, but no alkyl radicals, was heated in steps of about 15° upward from room temperature. After each temperature increment the sample was cooled to room temperature and the esr spectrum taken. This experiment was duplicated to observe changes in the 258 and 285-nm absorbances. Figure 4 gives the results. It can be seen that the 258-nm absorbance decayed in the same way as the allyl esr spectrum decayed. These experiments clearly support the assignment of the 258-nm absorption band to the

allyl radical. Further, it indicated that the dienyl radical concentration must be substantially smaller than the allyl radical concentration inasmuch as an appreciable dienyl contribution to the esr spectrum would shift the esr data curve of Figure 4 toward the curve of the 285-nm absorbance. In fact, the analysis given below shows the dienyl *G* value to be about one-tenth that of the allyl free radical.

Allyl and Dienyl Free Radical Absorbance in the Infrared. The absorption observed in irradiated polyethylene at 943 cm⁻¹ has been assigned by Koritskii, *et al.*,¹⁰ and Dole and Böhm⁹ to the allyl radical. Further evidence that this assignment is correct and that the 943-cm⁻¹ absorption band is a composite band due to single C—H groups of the type — $\dot{C}H-(CH=CH-)_n$ is as follows.

Polyethylene was irradiated at 77°K, heated to room temperature for about 10 min, and the ir spectrum taken at 77°K. The sample was annealed at room temperature in the presence of 40 cm pressure of hydrogen to accelerate the decay of alkyl radicals,¹¹ and the ir spectra again taken at 943 cm⁻¹. A similar cycle of experiments was performed and the uv absorbance at 258 nm studied. The data obtained are collected in Table II

Table II: Comparison of Infrared and Ultraviolet Absorbances of the Allyl Radical

Treatment after irradiation at 77°K	Dose, Mrads	
	50	5
	Absorbances at	
	943 cm ⁻¹	258 nm
None	0.00	0.00
After heating briefly to 24°	0.029	0.148
After annealing with H ₂ at 24°	0.050	0.250
% of final absorbance after second annealing that appeared when sample first heated to 24°	58	59

where the close correspondence between the growth in absorbances at 943 cm⁻¹ and 258 nm can be seen. Although the ir spectra were taken after a dose of 50 Mrads and the uv after a dose of 5 Mrads, Figure 1 demonstrates that the formation of the allyl radical is linear with dose up to 50 Mrads; hence the ratios given in the last line should be equal.

The fraction of the 943-cm⁻¹ absorbance which developed during the annealing at room temperature was produced by a first-order process with a rate constant which was the same as that for the allyl free radical growth as measured by the increase in the absorbance at 258 nm.¹¹

A sample of polyethylene, which contained only allyl and polyenyl free radicals, was irradiated with uv light

(16) D. M. Bodily and M. Dole, *J. Chem. Phys.*, **45**, 1478 (1966).

at 77°K, and it was observed that whereas the 258-nm absorbance completely disappeared in accordance with the known effect of the uv light on allyl radicals,^{15,16} and the 285-nm absorbance grew somewhat also in accord with the effect of uv light on the dienyl free radical concentration,¹⁰ the infrared absorbance at 943 cm⁻¹ only partially disappeared, see Table III. On heating

Table III: Effect of Ultraviolet Irradiations on the Infrared and Ultraviolet Absorbances of the Allyl and Dienyl Free Radicals

Polymer treatment after electron beam irradiation at 77°K	Irradiation dose, Mrads		
	50	5	5
	Absorbances ^a at		
	943 cm ⁻¹	258 nm	285 nm
Annealed at 24° with H ₂ until absorbances constant	0.033	0.252	0.05
First uv irradiation at 77°K	0.0065	0.00	0.09
Annealed at 24° with H ₂ until absorbances constant	0.020	0.110	0.180
Second uv irradiation at 77°K	0.012	0.00	0.210

^a All measured at 77°K.

the sample to room temperature the 943 cm⁻¹ grew back partially as did the 258-nm peak while the 285-nm peak increased further. A second uv irradiation again eliminated the allyl free radical, partially reduced the 943-cm⁻¹, and again increased the 285-nm peak. Note that the 943-cm⁻¹ peak did not decrease as much during the second uv irradiation as during the first. The portions of the 943-cm⁻¹ peaks which remained after the first and second uv irradiations before heating to room temperature are in approximately the same ratio as the absorbances of the 285-nm absorption band measured under the same conditions, *e.g.*

$$\frac{(A_{943})_2}{(A_{943})_1} = \frac{0.012}{0.0065} = 1.9 \pm 0.4$$

$$\frac{(A_{285})_2}{(A_{285})_1} = \frac{0.210}{0.09} = 2.3 \pm 0.3$$

A similar correlation between the portions of the 943 cm⁻¹ absorbances due to the allyl free radical and the 258 nm absorbances can be carried out by subtracting from the 943 cm⁻¹ absorbances the absorbances due to the dienyl free radical and then calculating the ratios as follows

$$\frac{(A_{943})_1, \text{ Allyl}}{(A_{943})_2, \text{ Allyl}} = \frac{0.033 - (0.0065)(5/9)}{0.020 - (0.012)(18/21)} = 3.0 \pm 0.5$$

$$\frac{(A_{258})_1}{(A_{258})_2} = \frac{0.252}{0.110} = 2.3 \pm 0.3$$

in which the ratios 5/9 and 18/21 come from the fourth column of Table III.

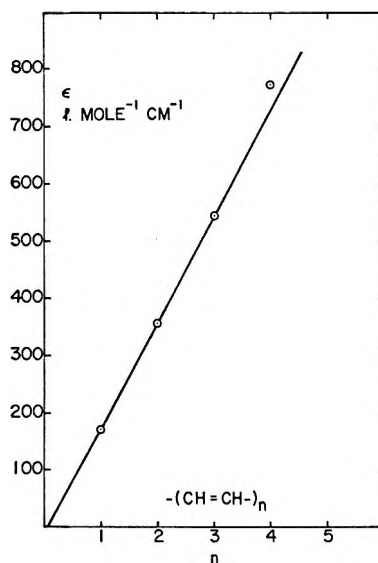


Figure 5. Extinction coefficients of the polyenes at 990 cm⁻¹ except for *n* equal to unity where the extinction coefficient is for the band at 968 cm⁻¹.

We conclude from the above that the portion of the 943 cm⁻¹ absorbance which can be bleached by uv irradiation is to be assigned to the allyl free radical and the residual unbleachable absorbance to the dienyl free radical.

G Values and Extinction Coefficients of the Allyl and Dienyl Free Radicals. Inasmuch as the esr spectra of the stabilized free radicals involve both the allyl and dienyl free radicals, it is incorrect to calculate *G*(allyl) solely from the esr data. To carry out such calculations making use of esr, uv, and ir spectra we have made the assumption that the extinction coefficients of the dienyl and allyl free radicals at 943 cm⁻¹ are in the ratio of the number of C—H bonds in the conjugated system or 5/3. If the extinction coefficients^{17,18} in the ir of the polyenes are plotted as a function of the number of —CH=CH— groups, a linear relationship is seen to exist, Figure 5. It seems reasonable to suppose that a similar relationship would also be valid for the polyenyl free radicals, especially since both the allyl and dienyl groups absorb in the ir at the same wavelength. Hence, estimates could be made of the contribution of the dienyl radical to the 943-cm⁻¹ absorbances given in Table III. The allyl and dienyl absorbances at 943 cm⁻¹ before any uv irradiation were then calculated to be 0.0294 and 0.0036, respectively, or 0.0098 and 0.00072 per hydrogen atom. In percentages the radicals giving rise to the 943-cm⁻¹ absorbance appear to consist of 93% allyl and 7% dienyl free radicals after a dose of 50 Mrads.

An uncertainty of the above calculation is that it uses

(17) R. J. de Kock and P. A. H. M. Hol, *Polym. Lett.*, **2B**, 339 (1964).

(18) N. H. E. Ahlers, R. A. Brett, and N. G. McTaggard, *J. Appl. Chem.*, **3**, 433 (1953).

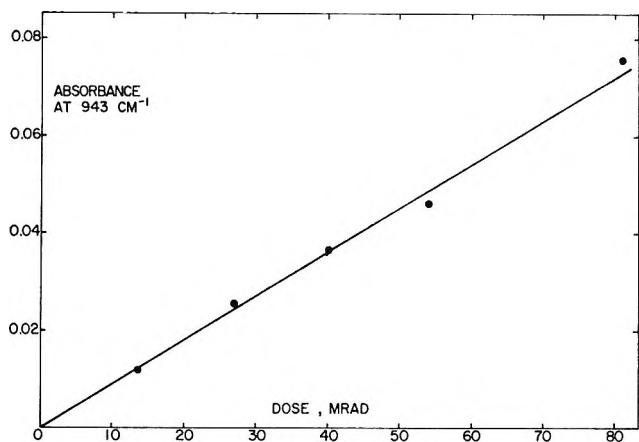


Figure 6. Absorbances at 943 cm^{-1} as a function of dose. Radiations at 77°K and samples annealed with H_2 at 24° .

uv data after a dose of 5 Mrads to calculate allyl and dienyl ratios after a dose of 50 Mrads. However, experiments were performed in which the 285-nm absorbance was measured after doses of 54 and 4.5 Mrads, ratio equal to 12, with the observed ratio of the absorbances $0.625/0.05$ equal to 12.5. Coupled with the data of Figure 6 which demonstrates that the total stabilized free radical production is linear with dose up to at least 50 Mrads, it would appear that our assumption of a constant ratio between the allyl and dienyl free radical G values as a function of dose is valid.

Another approach to the ratio of allyl and dienyl free radicals in irradiated polyethylene is the following: let x = mole fraction of allyl free radicals in the stabilized free radicals, y = the same for the dienyl free radicals, ϵ_A and ϵ_D = the extinction coefficients in the ir of the allyl and dienyl radicals, respectively, C_A' , C_A'' = concentration of allyl groups before and after the irradiation with uv light including the H_2 annealing at 24° , C_D' , C_D'' = the same for the dienyl free radicals, $x = C_A'/(C_A' + C_D')$, $y = C_D'/(C_A' + C_D')$, l = film thickness, then

$$\epsilon_A C_A'' l + \epsilon_D C_D'' l = 0.020$$

$$\epsilon_A C_A' l + \epsilon_D C_D' l = 0.033$$

Also (from the uv measurements)

$$C_A'' = \frac{0.110}{0.252} C_A' \text{ or } C_A'' = 0.437 C_A'$$

$$C_D'' = \frac{0.180}{0.050} C_D' \text{ or } C_D'' = 3.6 C_D'$$

With our assumption above that ϵ is proportional to the number of C—H bonds in the conjugated-free radical system, $\epsilon_D = (5/3)\epsilon_A = 1.666\epsilon_A$. Solving the above equations for x and y , we find $x = 0.967$ and $y = 0.033$.

A third method of estimating the separate G values of the allyl and dienyl free radicals which does not involve

assuming that $\epsilon_A = (3/5)\epsilon_D$ is the following. After the uv irradiation with annealing at room temperature and with consideration of the uv data of Table III which showed (1) that the allyl concentration had decreased to 0.44 of its initial value, (2) that the dienyl concentration had increased to $3.6y$, and (3) that the total radical concentration (as determined by esr after a dose of 45 Mrads) had decreased to 68% of its initial value we can write $0.44x + 3.6y = 0.68$. Solving for x and y we find $x = 0.92$ and $y = 0.08$. Taking the average of the three different results given above, namely 94% allyl and 6% dienyl, we obtain $G(\text{allyl})$ equal to 0.235 and $G(\text{dienyl})$ 0.015.

Knowing the G values the concentrations of the allyl and dienyl groups in terms of M are readily calculated from the product $(1.038 \times 10^{-3}) (\text{Mrad})(G)$. The thickness of the films was 2.616×10^{-2} cm; hence ϵ_{allyl} was calculated to be $7.34 \times 10^3 M^{-1} \text{ cm}^{-1}$ from the absorbance at 258 nm and $\epsilon_{\text{dienyl}} 2.90 \times 10^4 M^{-1} \text{ cm}^{-1}$ from the absorbance at 285 nm. These calculations were made using the absorbances after a dose of 4.5 Mrads.

Figure 6 illustrates the increase in absorbance in the infrared at 943 cm^{-1} with dose. In contrast to the esr measurements of the allyl and dienyl free radicals, the curve of Figure 6 is linear up to a dose of 80 Mrads. The cause of the difference to be seen between the results of Figures 1 and 6 is not known, but it may be due to the fact that the esr spectra are dominated by that of the allyl radical whereas in the ir, the dienyl free radical has about a twofold higher extinction coefficient than that of the allyl free radical. At high doses the dienyl free radical may contribute an ever increasing fraction of the absorbance if the ratio $G(\text{dienyl})/G(\text{allyl})$ increases. The absorbances of Figure 6 were also measured at a narrower slit width than the data of Table III, so that the latter data cannot be directly compared with the data of Figure 6.

The absorbance in the ir at 943 cm^{-1} after a dose of 54 Mrads was 0.0487. Knowing that 94% of the stabilized radicals were allyl and 6% dienyl radicals and assuming that the extinction coefficient of the dienyl was $5/3$ that of the allyl free radical, we estimated that the absorbance due to the allyl radical was 0.0440 and that of the dienyl 0.00468. With these absorbances and the above mentioned G values the extinction coefficients of the allyl and dienyl free radicals at 943 cm^{-1} were readily calculated to be 133 and $222 M^{-1} \text{ cm}^{-1}$, respectively.

It is possible to estimate these extinction coefficients without initially assuming that ϵ_{dienyl} equals $(5/3)\epsilon_{\text{allyl}}$. As mentioned above the total absorbance at 943 cm^{-1} after the dose of 54 Mrads was 0.0487. This absorbance has to be partitioned between that due to the allyl and dienyl free radicals. From the data of Table III this can be accomplished in two ways from the relations

Table IV: G Values and Extinction Coefficients

Radical	G value, radicals per 100 eV	Extinction coefficients, $M^{-1} \text{ cm}^{-1}$			
		215 nm	258 nm	285 nm	943 cm^{-1}
Alkyl at 77°K	3.3 ± 0.5	1800 ± 300			
Stabilized free radicals at 24°	0.25 ± 0.04				
Allyl at 24°	0.235 ± 0.04		$7.34 \times 10^3 \pm 1.5 \times 10^3$		133 ± 2
Dienyl at 24°	0.015 ± 0.005			$2.90 \times 10^4 \pm 0.6 \times 10^4$	222 ± 4

$$\left[\frac{A_{\text{dienyl}}^{943}}{A_{\text{total}}^{943}} \right]_{\text{dose A}} = \left[\frac{A_{\text{dienyl}}^{943}}{A_{\text{total}}^{943}} \right]_{\text{dose B}}$$

and

$$[A_{\text{dienyl}}^{943}]_{\text{After initial irrad, dose B}} = [A_{\text{dienyl}}^{943}]_{\text{After 2nd uv irrad, dose B}} \times \frac{[A_{\text{dienyl}}^{285}]_{\text{After initial irrad, dose B}}}{[A_{\text{dienyl}}^{285}]_{\text{After 2nd uv irrad, dose B}}}$$

for example

$$A_{\text{dienyl}} = 0.0487 \left(\frac{0.012}{0.033} \right) \left(\frac{0.05}{0.21} \right) = 0.00421$$

$$A_{\text{dienyl}} = 0.0487 \left(\frac{0.0065}{0.033} \right) \left(\frac{0.05}{0.09} \right) = 0.00533$$

Taking the average of these two numbers or 0.00477, the extinction coefficient of the dienyl free radical is cal-

culated to be 226. Similarly, the extinction coefficient of the allyl free radical at 943 cm^{-1} is estimated to be 133 $M^{-1} \text{ cm}^{-1}$. These numbers agree very well with those given above and their ratio is 1.699 instead of 1.666.

Thus, the assumption that the ir extinction coefficient of the dienyl free radicals is $5/3$ that of the allyl appears to be verified within the limits of accuracy of the data given here.

In Table IV are summarized the G values and extinction coefficients obtained in this work.

Acknowledgments. This research was supported by the U. S. Atomic Energy Commission, their document No. COO-1088-35, and by the Advanced Research Projects Agency of the Department of Defense through the Northwestern University Materials Research Center. We are indebted to J. A. Reid of the Phillips Petroleum Co. for the gift of the polyethylene samples used.

The Radiation Chemistry of Polyethylene. X. Kinetics of the Conversion of Alkyl to Allyl Free Radicals¹

by D. C. Waterman and Malcolm Dole²

Department of Chemistry and Materials Research Center, Northwestern University, Evanston, Illinois 60201
(Received September 19, 1969)

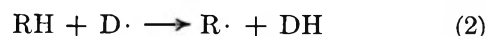
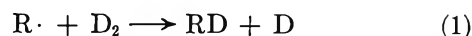
Evidence is given in this paper that alkyl free radicals which persist at room temperature after an electron beam irradiation at liquid nitrogen temperature quantitatively convert to allyl free radicals by reaction with *trans*-vinylene or vinyl double bonds. The decay of the alkyl radicals is accurately first order and is markedly catalyzed by molecular hydrogen. Whereas the catalyzed reaction rate constant has the order of magnitude expected on the basis of analogous gas-phase reactions, the rate constant for the uncatalyzed reaction is smaller than similar gas reactions by a factor of 10⁷, due partly to a higher activation energy and partly also very probably to a greatly reduced frequency factor in the solid state. A small number of alkyl radicals regenerated from the allyl by ultraviolet irradiation at 77°K and which persist to room temperature have no measurable decay at room temperature in the absence of molecular hydrogen. In the presence of hydrogen they decay by a second-order process, but do not re-form allyl radicals. At the present time no plausible explanation exists for this unexpected behavior.

Introduction

Free radicals in polyethylene produced by high-energy radiation have been identified chiefly by electron spin resonance (esr) methods.³⁻⁶ Thus, three general types of radicals can be detected, namely: the alkyl free radical, CH₂·CHCH₂; the allyl, ·CHCH=CH; and the polyenyl, ·CH(CH=CH—)_n. Alkyl radicals only are produced by irradiation at liquid nitrogen temperature. At this temperature they are quite stable and are observed in the esr spectrum as a sextet.⁴⁻⁷ When polyethylene containing alkyl radicals is heated to room temperature, there is a substantial decrease in radical concentration,^{4,6,8} and the esr spectrum is observed to be a mixture of a sextet and a septet. On standing at room temperature, the contribution from the sextet disappears, leaving only the septet with a doublet substructure. This septet has been assigned to allyl radicals.^{6,6} When polyethylene is irradiated to doses of several thousand megarads, the observed esr spectrum becomes a singlet which has been assigned to polyenyl free radicals.^{4,9}

Voevodskii, *et al.*,¹⁰ suggested that alkyl radicals in the presence of double bonds changed into allyl radicals. A similar suggestion was made for the production of allyl radicals in 17-pentatriacontene by Charlesby, *et al.*⁶ Previously the suggestion had been made¹¹ that alkyl radicals could migrate in polyethylene by a random walk process, and Voevodskii¹⁰ had adopted this concept to explain how the alkyl radicals reached the double bonds. Support for the hydrogen migration process was obtained by Dole and Cracco,¹² who studied the exchange of deuterium gas with polyethylene subsequent to its irradiation. They sug-

gested that free radical migration occurred by the chain process



where R· represents the alkyl free radical. Dole and Cracco observed indirectly that the decay rate of the alkyl free radical increased with deuterium gas pressure. This will be discussed in another section.

Work by Ormerod¹³ on the decay of alkyl radicals at room temperature indicated that the decay was a composite effect caused by reactions of the type

(1) Paper IX of this series: H. Y. Kang, O. Saito, and M. Dole, *J. Amer. Chem. Soc.*, **89**, 1980 (1967).

(2) Address inquiries to Department of Chemistry, Baylor University, Waco, Texas 76703.

(3) R. J. Abraham and D. H. Whiffen, *Trans. Faraday Soc.*, **54**, 1291 (1958).

(4) E. J. Lawton, J. S. Balwit, and R. S. Powell, *J. Chem. Phys.*, **33**, 395 (1960).

(5) S. Ohnishi, Y. Ikeda, M. Kashiwagi, and I. Nitta, *Polymer*, **2**, 119 (1961).

(6) A. Charlesby, D. Libby, and M. G. Ormerod, *Proc. Roy. Soc. A262*, 207 (1961).

(7) A. G. Kiselev, M. A. Mokulskii, and Yu. S. Lazurkin, *Vysokomol. Soedin.*, **2**, 1678 (1960).

(8) F. Cracco, A. J. Arvia, and M. Dole, *J. Chem. Phys.*, **37**, 2449 (1962).

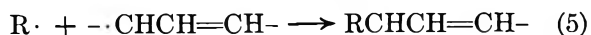
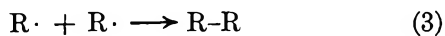
(9) S. I. Ohnishi, Y. Ikeda, S. I. Sugimoto, and I. Nitta, *J. Polym. Sci.*, **47**, 503 (1960).

(10) A. T. Koritskii, Yu. N. Molin, V. N. Shamshev, N. Y. Bulen, and V. V. Voevodskii, *Vysokomol. Soedin.*, **1**, 1182 (1959).

(11) M. Dole, C. D. Keeling, and D. G. Rose, *J. Amer. Chem. Soc.*, **76**, 4304 (1954).

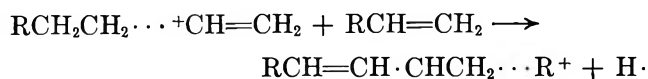
(12) M. Dole and F. Cracco, *J. Phys. Chem.*, **66**, 193 (1962).

(13) M. G. Ormerod, *Polymer*, **4**, 451 (1963).



He also found that the decay was catalyzed by hydrogen, and explained this effect by migration steps of the type shown by reactions 1 and 2 prior to reactions 3, 4, and 5.

Other mechanisms for the formation of the allyl free radical have been suggested. Thus Auerbach^{14,15} proposed that allyl radicals result directly from vinyl decay by a process which involves the initial formation of alkyl positive ions $RCH_2CH\cdots CH=CH_2 \rightsquigarrow RC^+H_2CH_2\cdots CH=CH_2 + \epsilon^-$ followed by migration of the positive charge to the vinyl group $RC^+H_2CH_2\cdots CH=CH_2 \rightarrow RCH_2CH_2\cdots CH=CH_2^+$. The vinyl ions thus formed react with other vinyl groups to form ion radicals, which are then converted to allyl radicals by the process



Similar reaction schemes were suggested whereby allyl radicals could be generated from *trans*-vinylene groups or from a *trans*-vinylene group and a vinyl group. However, all mechanisms involving positive ions are undoubtedly incorrect because, as demonstrated below, all allyl free radical formation, in the case of irradiations at 77°K at least, occurs subsequent to the irradiation when positive ions will have largely disappeared, especially after heating to room temperature.

In this paper evidence will be presented to show that at least 40% of the allyl radicals, which are formed at room temperature after an irradiation at 77°K, result from the combination of an alkyl radical with a vinyl or *trans*-vinylene double bond. Dienyl and trienyl radicals are formed by a similar process involving an alkyl radical and diene and triene, respectively. There is no reason to suggest that the formation of the remaining 60% of allyl radicals, which could not be studied kinetically, is not by a similar process. Especial attention will be paid to the mechanisms of the uncatalyzed and hydrogen catalyzed alkyl to allyl conversion processes.

Experimental Section

Marlex 6002 polyethylene film, 10.4 mils thick, was used throughout. Density was 0.962 g cm⁻³ at 15°, crystallinity was 75–80%, and weight and number average molecular weights, as supplied by the manufacturer, were 230,000 and 20,000, respectively. Initial vinyl group concentration was 7.75×10^{-5} mol g⁻¹.

Irradiations were performed with 1-MeV electrons from a General Electric resonant transformer electron beam generator. Dosimetry was carried out using the vinyl decay data of Kang, *et al.*¹

The accuracy of the dosimetry was not considered to be better than $\pm 5\%$, but relative doses, as used for comparison of esr and spectrophotometric experiments are probably accurate within $\pm 2\%$.

For the esr experiments samples were evacuated in quartz tubes for at least 12 hr before sealing off. All irradiations were performed at 77°K by floating the quartz tubes on liquid nitrogen using a Styrofoam float. Radiation-induced paramagnetic centers in the quartz were removed by heating one end of the tube with the sample at the other end of the tube immersed in liquid nitrogen. After the annealing the whole tube was cooled to 77°K, the sample shaken to the annealed end, and esr measurements made on the annealed end. All measurements were made on a Varian E-3 spectrometer, with the exception of one power saturation study on allyl radicals which was carried out using an E-4 spectrometer in the Varian Associates laboratory. Absolute radical concentrations were measured by comparison of the polymer samples with standard solutions of diphenyl picryl hydrazyl in benzene, with double integration of all spectra. At 77°K frozen solutions of DPPH in benzene were the standards. Care was taken to observe radicals under conditions where no power saturation of the signal occurred, namely in regions where a plot of integrated intensity of the signal against the square root of the microwave power was a straight line. In the case of allyl radicals this was not possible on the E-3 spectrometer, and corrections to the integrated intensities were made by extrapolation to zero microwave power. The validity of this extrapolation was confirmed by the experiment performed on the Varian E-4 spectrometer mentioned above. Data for the allyl radical saturation characteristics, as measured on both the E-3 and E-4 spectrometers, are shown in Figure 1. Changes in alkyl radical concentration were followed by observing the height of the wing peak of the sextet spectrum, which can be measured free from interference from the allyl radical septet as illustrated in Figure 2.

A suitable refluxing liquid served as a constant-temperature bath for experiments done above room temperature; at 0° an ice-water bath was used. In both cases esr measurements were made at 77°K so as to freeze the reaction. Radiation-produced hydrogen could be removed from the esr tube or hydrogen or deuterium gas added subsequent to the irradiation by connecting the quartz tube to a vacuum line by means of a break-seal. Linde H₂, Matheson D₂, and in a few experiments Matheson research grade hydrogen, which contained 4 ppm of helium and no other detectable impurities, were used.

As a valuable complement to the esr data ultraviolet and infrared absorption spectra were taken at 77°K on

(14) I. Auerbach, *Polymer*, **7**, 283 (1966); **8**, 63 (1967).

(15) I. Auerbach, *ibid.*, **9**, 1 (1968).

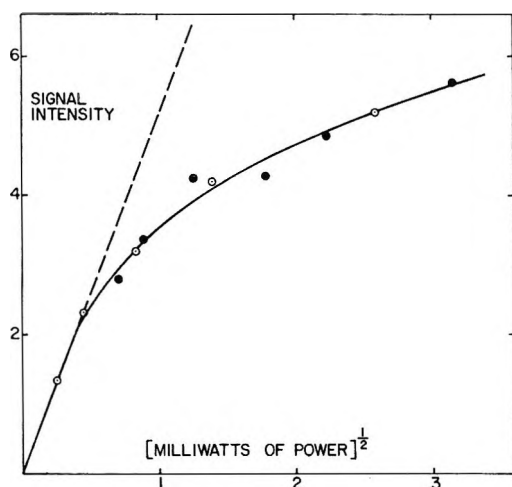


Figure 1. Relative intensity of esr signal plotted as a function of the square root of the microwave power. Open circles, measurements on the E-4 spectrometer, closed circles on the E-3 Spectrometer. E-3 and E-4 signals adjusted to be equal at 1 MW of power.

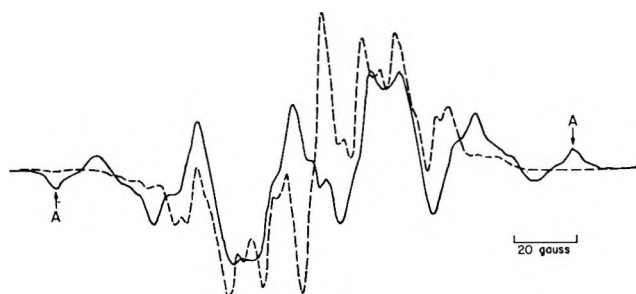


Figure 2. ESR spectra of allyl free radicals (dotted curve) and of mixed alkyl and allyl free radicals after heating to room temperature (solid curve). Decay of alkyl free radicals was calculated from height of peaks marked A.

samples irradiated at 77°K in the special combined irradiation and spectroscopic cell previously described.¹⁶ Cary 14 and Beckman IR-9 spectrophotometers were used in these measurements. By observing the uv and ir absorption bands at 77°K they were considerably sharpened and more accurate measurements were possible. Alkyl radicals were observed at 215 nm, allyl at 258 nm and 943 cm^{-1} , dienyl at 285 nm, trienyl at 322 nm, vinyl end groups and *trans*-vinylene groups at 910 and 966 cm^{-1} , respectively. Concentrations were calculated using extinction coefficients for vinyl and *trans*-vinylene groups of 153¹⁷ and 169¹⁸ $M^{-1} \text{cm}^{-1}$, respectively.

Results

Alkyl radicals at room temperature, in the absence of hydrogen, decay quite slowly (half-life *circa* 900 min), and measurement of the total radical concentration immediately after heating from 77 to 297°K gave G -(total radicals) at 24° equal to 0.252. The height of the wing peak of the esr spectrum (peak marked A in Figure 2) showed that at this stage 3.6% of the initial

alkyl radicals remained; in other words, 96.4% of the alkyl radicals decayed on heating from 77°K to room temperature. Hence G -(residual alkyl) at room temperature is 3.6% of 3.3 or 0.119. Thus, the residual alkyl radicals represented 47.2% of the total radicals present immediately after warming to room temperature.

Another calculation of G -(residual alkyl at 24°) is the following. If the alkyl free radicals remaining on heating to room temperature after the irradiation at 77°K converted quantitatively to allyl and dienyl free radicals, then the total amount of the latter two radicals that formed after heating to room temperature must equal the initial residual amount of the alkyl free radicals, or G -(residual alkyl at 24) = 0.41 G -(total allyl) + 0.50 G -(total dienyl) = 0.105. In the accompanying paper G -(allyl) was shown to be 0.235 and G -(dienyl), 0.015. Thus the G -(residual alkyl) value agrees with the one given above within the experimental uncertainties and demonstrates a 1:1 stoichiometric relation between alkyl free radical decay and allyl and dienyl free radical formation. The factors of 0.41 for allyl and 0.50 for the dienyl free radicals come from Table I where the uv absorbances at 258 (allyl) and 285 (dienyl) nm after the initial irradiation, after the first heating to 24° and after complete decay of the alkyl free radical, are given.

Table I: Absorbances of the Allyl and Dienyl Radicals after an Irradiation Dose of 4.5 Mrads at 77°K

Treatment of sample	Absorbances	
	258 nm	285 nm
Immediately after irradiation	0	0.01
After heating to 24°	0.148	0.025
After annealing at 25° with H ₂ until no further change	0.250	0.050

The 1:1 stoichiometric relation between the moles of alkyl free radical which decayed at room temperature and the moles of allyl radical that formed was also demonstrated by direct esr measurements. Thus after a dose of 54 Mrads at 77°K the radical concentrations were (in units of 10¹⁸ spins g⁻¹) 8.7 for residual alkyl at 24° and 8.5 for allyl radicals formed. Two other experiments at 18 and 36-Mrad doses gave 2.8 and 5.2 for the residual alkyl radical at 24° and 2.9 and 4.8 for the allyl radicals formed also at 24°. These experiments at room temperature were done in the presence of 40 cm H₂ pressure to accelerate the alkyl to allyl radical con-

(16) M. Dole and G. G. A. Böhm, *Advances in Chemistry Series*, No. 82, American Chemical Society, Washington, D. C., 1968, p 525.

(17) M. Dole, D. C. Milner, and F. Williams, *J. Amer. Chem. Soc.*, **80**, 1580 (1958).

(18) R. J. de Kock, P. A. H. M. Hol, and H. Bos, *Z. Anal. Chem.*, **205**, 371 (1964).

version process. Another experiment demonstrated that the presence of hydrogen did not affect the ultimate yield of allyl radicals. Two samples were irradiated to 60 Mrads, heated to room temperature, the hydrogen evacuated from one sample, and 60 cm of H₂ pressure added to the other. The samples were then held at 78° until all alkyl radicals had decayed. In relative units the esr signal was 2.59 in the first case and 2.68 in the second.

Table II gives the decreases in concentration of the vinyl $\Delta[\text{Vi}]$ and *trans*-vinylene $\Delta[\text{t-VI}]$ groups on

Table II: Decrease in Unsaturation Compared with Increase of Allyl Free Radical Concentration

Dose, Mrads	$-\Delta[\text{Vi}]$	$-\Delta[\text{t-VI}]$ 10 ⁶ mol g ⁻¹	$-\Delta[\text{Uns}]^a$	$\Delta[\text{allyl}]$ 10 ⁶ mol g ⁻¹
27	2.0	0.78	2.78	2.66
54	3.95	1.13	5.08	4.88
81	2.23	3.22	5.45	5.70
108	2.53	3.58	6.11	6.15

$$^a \Delta[\text{Uns}] = \Delta[\text{Vi}] + \Delta[\text{t-VI}].$$

standing at room temperature during the period when alkyl radicals decayed and allyl were formed. Included in Table II are the concentrations of allyl radicals formed during this period. These were calculated by multiplying the final allyl radical concentration (as measured by esr) by the fraction formed at room temperature as observed by means of the 258-nm absorbance. The agreement between the concentration of allyl radicals formed and the decrease in the concentration of vinyl and *trans*-vinylene unsaturation is excellent. Thus, it is apparent that the allyl radicals, which are formed at room temperature, do so by direct reaction of one alkyl radical with one double bond as illustrated by reaction 4.

Infrared measurements of the *G* values of *trans*-vinylene, *cis*-vinylene, and conjugated diene groups resulted in the following average values over a dose of 55 Mrads: *G*(*trans*-vinylene), 1.5; *G*(*cis*-vinylene), 0.15; and *G*(diene), 0.09. Inasmuch as the latter two are small with respect to the first, changes in *cis*-vinylene and conjugated diene concentrations were ignored in compiling the data of Table II.

The kinetics of conversion of alkyl to allyl free radicals was studied in detail. It was possible to follow the alkyl decay by esr and uv spectroscopic measurements, vinyl decay by ir, the formation of allyl, dienyl and trienyl radicals by uv, and combined allyl and polyenyl radicals by ir. The most accurate and extensive of the measurements were those made by esr.

Figure 3 illustrates first-order plots for alkyl decay at 24° as followed by the height of the wing peak in the esr spectra. Doses of 15 and 60 Mrads were given, and the reaction was followed after removing the hydrogen pro-

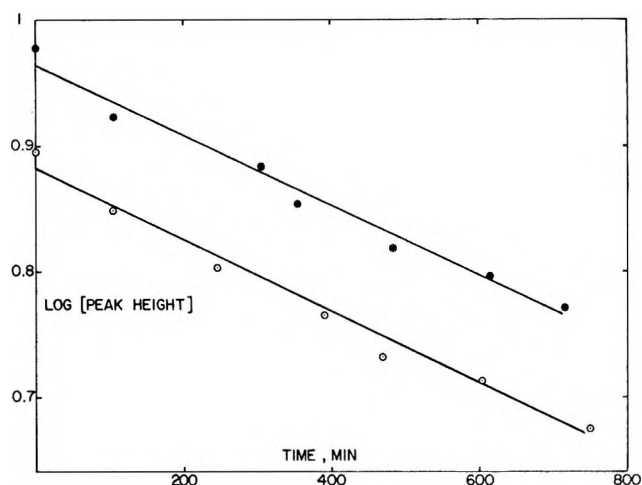


Figure 3. First-order decay of alkyl free radicals *in vacuo* at 24° as observed by esr. Open circles, 15-Mrad dose; solid circles, 60-Mrad dose.

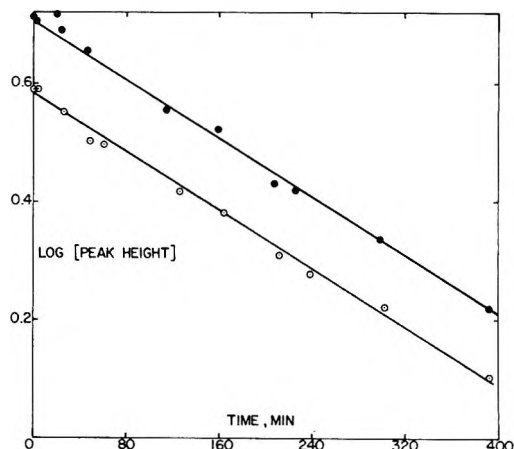


Figure 4. Same as Figure 3, but in presence of 10 cm of H₂ pressure.

duced by the irradiation. It can be seen that the plots are linear and parallel, despite the initial alkyl radical concentration difference of a factor of 3.3. The decay was observed to be catalyzed by the presence of H₂ or D₂ over the polyethylene in agreement with earlier observations.^{12,13,19,20} Figure 4 shows the first-order plots for the alkyl radical decay in the presence of 20 cm of hydrogen pressure for doses of 15 and 60 Mrads, and once again the graphs are linear and parallel. Thus both the uncatalyzed and the hydrogen catalyzed decay of alkyl radicals are first order in the alkyl radical concentration. Figure 5 illustrates the first-order rate constants for alkyl decay plotted as a function of hydrogen and deuterium gas pressures. The plots are accurately linear and demonstrate that the transition state for the process must involve one alkyl radical and one hydrogen molecule.

(19) M. Dole and F. Cracco, *J. Amer. Chem. Soc.*, **83**, 2584 (1961).

(20) W. V. Smith and B. E. Jacobs, *J. Chem. Phys.*, **37**, 141 (1962).

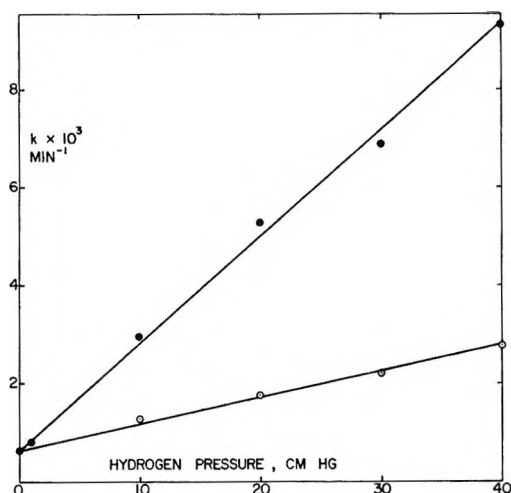


Figure 5. Variation with hydrogen and deuterium pressures of the first-order alkyl decay constant at 24°. H₂, solid circles; D₂, open circles.

It has been suggested that the catalytic effect of hydrogen on radical processes in polyethylene is caused by oxygen impurities in the hydrogen.²¹

In the present work this was definitely not the case, because no difference was observed when the reaction was carried out in the presence of hydrogen containing about 40 ppm of oxygen and hydrogen containing less than 1 ppm of oxygen. Further, it was necessary to add in excess 1 Torr pressure of oxygen before any change in the reaction rate was observed.

As illustrated in Figure 5, the catalytic effect of deuterium was also significant, but definitely less than that of hydrogen. In the work of Dole and Cracco¹² the first-order alkyl radical decay constants were estimated indirectly from an analysis of the hydrogen-deuterium exchange rates as a function of time. Dole and Cracco found that increasing the deuterium gas pressure from 8 to 14 cm increased the alkyl decay constant from 9.25×10^{-4} to $12.3 \times 10^{-4} \text{ min}^{-1}$, a rate of increase of the decay constant with deuterium pressure of $5.1 \times 10^{-5} \text{ min}^{-1} \text{ cm}^{-1}$. The slope of the deuterium curve of Figure 5 is $5.45 \times 10^{-5} \text{ min}^{-1} \text{ cm}^{-1}$. This excellent agreement between the indirectly calculated and directly observed values strengthens Dole and Cracco's conclusion that the H-D exchange was the result of free radical reactions and did not involve excited states or ions.

Table III gives the first-order rate constants for the reactions as indicated. The allyl growth constant was obtained from the slope of the plot of $\ln \{[\text{Allyl}]_{\infty} - [\text{Allyl}]\}$ as a function of the time where $[\text{Allyl}]_{\infty}$ is the allyl concentration when all the alkyl free radicals have decayed; and the dienyl and trienyl constants from similar plots. It is considered that all of the rate constants at each pressure of hydrogen are equal to each other within the experimental errors. The agreement of the different rate constants of Table III is strong evidence

Table III: First-Order Decay and Growth Constants at 24°

Reaction	Method of obsn	Dose, Mrads	Hydrogen pressure, cm		
			0	20	40
Alkyl decay	Esr	60	0.62	5.27	9.32
Alkyl decay	Uv	5		5.43	
Vinyl decay	Ir	55			11.3
Allyl growth	Uv	5		5.8	10.0
Allyl growth	Ir	55			12.2
Dienyl growth	Uv	5		5.57	9.6 ^a
Trienyl growth	Uv	55			10.5

^a Average for doses of 5 and 55 Mrads.

that alkyl free radicals reacted only with unsaturated groups to form allyl, dienyl, and trienyl free radicals, respectively. Coupled with the 1:1 stoichiometric evidence given above for this conversion it would appear that the alkyl free radicals, which survived the initial heating to 24°, did not recombine to form cross-links or react by disproportionation to form vinylene groups.

The rate of alkyl decay *in vacuo* was measured at temperatures of 0, 24, 38.5, and 55° and the first-order rate constants are plotted according to the Arrhenius function in Figure 6. From the accurately linear curve obtained the activation energy of the uncatalyzed reaction was calculated to be 17 kcal mol⁻¹.

The H₂ and D₂-catalyzed radical decay reaction was studied only at two temperatures, 0 and 24°, inasmuch as the solubility of hydrogen²² in Marlex polyethylene was available only for these temperatures. In Table IV the data obtained in these experiments are given.

Table IV: Rate Constants of the Hydrogen- and Deuterium-Catalyzed Reaction

	Temp. °C	
	0	24
Soly const of H ₂ × 10 ⁻⁴ , M atm ⁻¹		
Soly const of D ₂ × 10 ⁻⁴ , M atm ⁻¹	20.2 (13.0)	8.6
k_{H_2} , min ⁻¹ M ⁻¹	3.14	21.7
k_{D_2} , min ⁻¹ M ⁻¹	0.545 (0.847)	4.79

From the normalized rate constants of Table IV the activation energy of the hydrogen-catalyzed reaction was calculated to be 13.0 kcal mol⁻¹ for H₂ catalysis and 17.7 kcal mol⁻¹ for the D₂ catalysis. However, the difference between these two activation energies is greater than the difference in the zero point energies²³

(21) S. E. Bresler and E. N. Kazbekov, *Fortschr. Hochpolym. Forsch.*, **3**, 688 (1964).

(22) M. Dole and M. B. Fallgatter, unpublished.

(23) I. Kirschenbaum, "Physical Properties and Analysis of Heavy Water," McGraw-Hill Publications, New York, N. Y., 1951, p 44.

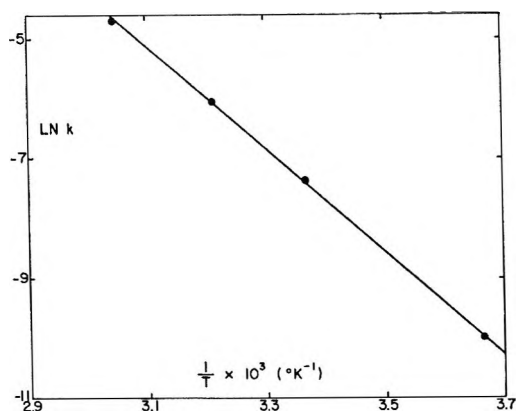


Figure 6. Arrhenius plot of first-order alkyl free radical decay constants for the uncatalyzed reaction.

of H_2 and D_2 which is $1.80 \text{ kcal mol}^{-1}$. Only one solubility measurement of deuterium in polyethylene was made at 0° , and we believe that this solubility value given in Table IV may be in error. If we increase the solubility of D_2 on cooling from 24 to 0° in the same ratio that the H_2 solubility is increased, we obtain the data given in parentheses in Table IV. From the latter, the activation energy is calculated to be $14.6 \text{ kcal mol}^{-1}$ and the difference between this value and that for the H_2 -catalyzed reaction is $1.6 \text{ kcal mol}^{-1}$, very close to the difference in zero point energies. Note that the difference in activation energies of reactions 3 and 4 of Table V is $1.5 \text{ kcal mol}^{-1}$, close to the difference estimated here despite the fact that reactions 3 and 4 of Table V involve perfluoro radicals. We believe that the activation energy for the D_2 -catalyzed reaction equal to $14.6 \text{ kcal mol}^{-1}$ is much nearer the true value than is 17.7 .

It is interesting to note that the activation energy 13.0 given above for the H_2 -catalyzed reaction is very close to that, $12.5 \text{ kcal mol}^{-1}$, for the gas-phase reaction $H_2 + CH_3\cdot CHCH_3 \rightarrow CH_3CH_2CH_3 + H\cdot$ found by Hoey and LeRoy.²⁴

Allyl radicals were converted to alkyl radicals by uv irradiation²⁶ at 77°K . When the polyethylene sample was heated briefly to room temperature, about 65% of the uv-regenerated alkyl radicals decayed as shown by the decrease in height of the wing peak of the esr spectrum. The uv spectrum showed that under similar conditions 44% of the initial allyl radicals and 3.6-fold of the initial dienyl radicals had been produced. On standing at room temperature, in contrast to the previously described behavior of the allyl radicals, the allyl and dienyl radical concentrations did not increase although the residual (35%) alkyl radicals decayed. Also in contrast to the behavior of the alkyl radicals produced initially by the electron beam irradiation, the residual alkyl radical decay followed a second-order rate law better than the first-order law, see Figure 7. This decay was observed to be catalyzed by hydrogen and deuterium as shown in Figure 8. It can be seen that

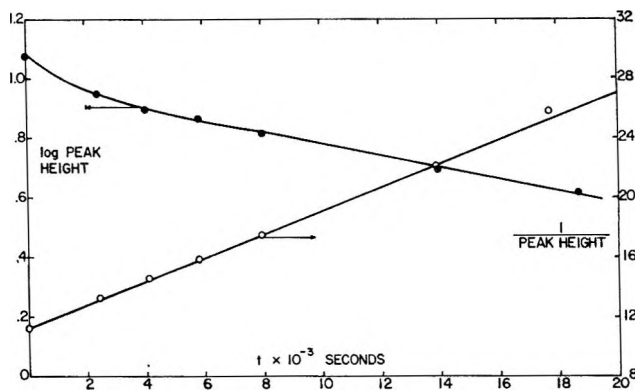


Figure 7. Room temperature decay of uv-regenerated alkyl free radicals according to both first- and second-order kinetics.

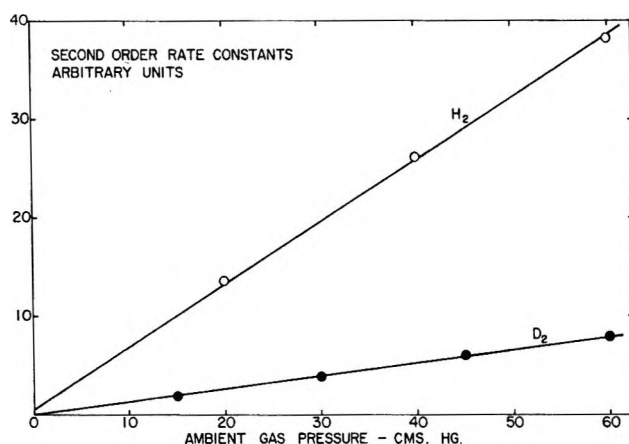


Figure 8. Effect of hydrogen and deuterium gas pressure on the second-order alkyl free radical decay constant.

the reaction is first order in hydrogen pressure, but in contrast to the data illustrated in Figure 5, and within the limits of experimental error these seems to be no uncatalyzed decay at room temperature of these uv-regenerated alkyl free radicals. The ratio of the slopes of the straight lines of Figure 8 is 4.97 while the ratio of those of Figure 5 is 4.03.

Discussion

The allyl radicals which were formed when polyethylene containing alkyl radicals was warmed from 77 to 297°K were probably formed in the amorphous regions of the polymer. The remaining 41% on which all kinetic measurements were made were probably produced in the crystalline regions. The reason suggesting this is twofold. Firstly, oxygen diffusion experiments,²⁶ which were performed on Marlex 6002 irradiated under conditions identical with the present work, could be interpreted assuming that about 50% of the allyl radicals were present in the amorphous regions and 50% in the

(24) G. R. Hoey and D. J. LeRoy, *Can. J. Chem.*, **33**, 580 (1955).

(25) S. Ohnishi, S. I. Sugimoto, and I. Nitta, *J. Chem. Phys.*, **39**, 2647 (1963).

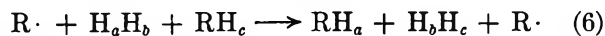
(26) G. G. A. Böhm, *J. Polym. Sci.*, **5**, 639 (1967).

crystalline. Secondly, Charlesby, *et al.*,⁶ have observed that radical processes in low-density polyethylene occur with rate constants about 100 times greater than those in high-density polyethylene. Auerbach¹⁴ has also emphasized the greater rate of radical decay in amorphous polyethylene. Since more than 90% of all allyl radicals are formed at temperatures above -30° , it would seem reasonable to suggest that the allyl and polyenyl radicals that are formed on heating to room temperature are formed by a similar mechanism to that of those which are formed on standing at room temperature. The difference in the rates of formation at room temperature and below can be explained, therefore, on the suggestion that below room temperature allyl formation occurs rapidly in the amorphous regions, leaving trapped alkyl radicals only in the crystalline regions, and these radicals then convert slowly to allyl free radicals.

The fact that plots of first-order rate constants for the decay of alkyl radicals at room temperature are a linear function of the hydrogen pressure with a positive intercept as illustrated in Figure 5 indicates that there are two distinct processes whereby alkyl radicals reach the vinyl or *trans*-vinylene groups.

The intercept represents the portion of the reaction which is not catalyzed by hydrogen and is probably caused by interchain migration of alkyl radicals to double bonds, *i.e.*, migration across polymer chains rather than along the same chain. However, at the present time we have no definite experimental evidence that favors either inter- or intrachain migration although calculations given below indicate the high improbability of intrachain migration.

The hydrogen catalysis is almost certainly to be accounted for by exchange processes of the type represented by reactions 1 and 2. Probably the hydrogen atoms are never free atoms and the overall process occurs by a concerted mechanism which can be represented by the reaction as has been suggested by Orme-



rod.¹³ Evidence is in favor of the postulate that hydrogen atoms never become free. (1) Free hydrogen atoms would be expected to combine with $R\cdot$ to form RH or with other free hydrogen atoms to form H_2 . If the former occurred, there would be a net loss of both free radicals and hydrogen, and if the latter, a net loss of molecular hydrogen, neither of which was observed. However, it must be remembered that the concentration of free radicals or hydrogen atoms is much less than that of $-CH_2-$ groups, ratio of perhaps one to 700 or more; hence, not much reaction of H atoms with $R\cdot$ or other H atoms would be expected. (2) If free hydrogen atoms existed, one would expect hydrogen atoms to react partly with olefin groups as well as to abstract hydrogen atoms to form the allyl free radical. Back²⁷ has estimated that the fraction of hydrogen

atoms that add to propylene rather than abstract other hydrogen atoms is about 0.95. If many hydrogen atoms added to the vinylene double bond to form an alkyl free radical then the growth of the allyl free radical would not be stoichiometrically equal to the decay of the unsaturation. (3) As shown below, the calculated average distance of migration of one free radical per exchange step is only slightly larger than that calculated for the closest distance between hydrogen nuclei on neighboring chains. If the hydrogen atom became free for any significant length of time, one would expect it to diffuse rapidly and to migrate at least farther than the nearest chain before abstracting another hydrogen to form molecular hydrogen.

Using the deuterium exchange data of Dole and Cracco¹² and the average G value from the present work for alkyl free radicals present at room temperature immediately after heating from $77^{\circ}K$, it is possible to calculate the average number of exchanges per single alkyl radical decay. We estimate that each alkyl radical undergoes on the average about 14.6 migration steps before it is trapped by the vinyl, *trans*-vinylene, or polyene group. The probability weighted average distance of the trapped free radical from an olefinic group can be estimated to be about 12 \AA at the concentrations encountered in this research. Assuming that a random walk calculation is valid, *i.e.*, that

$$r^2 = l^2n \quad (7)$$

where r is the net distance travelled after n steps each of length l , then l is easily calculated to be 3.1 \AA . The distance of hydrogen atom centers between neighboring chains is about 5.2 \AA along the a axis, 2.7 along the b axis and about 2.6 \AA along an axis bisecting the unit cell. The closest intrachain distance is 1.93 \AA along the c axis. Thus the calculated distance per jump favors the interchain migration mechanism rather than the intrachain.

Further insight into the mechanism of the room temperature alkyl decay rates can be gained by a consideration of activation energies of the relevant processes. For convenience, these are collected together in Table V. It will be noticed that the activation energy of the hydrogen catalyzed decay, 13 kcal mol^{-1} , is very close to that of reaction 5 of Table V, $12.5 \text{ kcal mol}^{-1}$. However, there are two significant differences between reaction 5 of the table and reaction 6 above. The data of Table V are for gas-phase reactions whereas in irradiated polyethylene we are dealing with reactions in the solid phase. Secondly, reaction 6 above in all likelihood is a concerted reaction which would not occur in the gas phase with any degree of probability. In light of these two differences the agreement in activation energies is all the more remarkable. Perhaps one factor tends to cancel the other; *i.e.*, the lowering of the

(27) R. A. Back, *Can. J. Chem.*, **37**, 1834 (1959).

Table V: Activation Energies of Free Radical Reactions

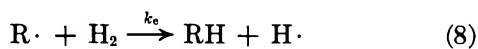
Reaction	Activn energy, kcal mol ⁻¹	Ref
Gas Phase		
1. C ₂ H ₅ + H ₂ → C ₂ H ₆ + H·	11.5	a
2. C ₂ H ₅ · + D ₂ → C ₂ H ₅ D + D·	13.3	a
3. C ₃ F ₇ · + H ₂ → C ₃ F ₇ H + H·	12.3	b
4. C ₃ F ₇ · + D ₂ → C ₃ F ₇ D + D·	13.8	b
5. CH ₃ ĊHCH ₃ + H ₂ → C ₃ H ₈ + H·	12.5	24
6. C ₂ H ₆ + H· → C ₂ H ₅ · + H ₂	7	a
7. C ₂ H ₅ · + <i>n</i> -heptane → C ₂ H ₆ + C ₇ H ₁₅ ·	11.6	c
8. C ₂ H ₅ · + 1-heptene → C ₂ H ₆ + R·CHCH=CH ₂	9.3	c
In Solid Polyethylene		
1. Uncatalyzed alkyl decay	17	
2. H ₂ -catalyzed alkyl decay	13	
3. D ₂ -catalyzed alkyl decay	14.6 (estd)	

^a M. H. J. Wijnen and E. W. R. Steacie, *J. Chem. Phys.*, **20**, 205 (1952). ^b G. H. Miller and E. W. R. Steacie, *J. Amer. Chem. Soc.*, **80**, 6486 (1958). ^c D. G. L. James and E. W. R. Steacie, *Proc. Roy. Soc.*, **A244**, 289 (1958).

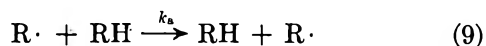
activation energy because the reaction is a concerted one tends to counterbalance the possibly greater activation energy due to the solid phase.

The effect of the solid phase in raising the activation energy is seen in comparing the activation energy of the uncatalyzed reaction, 17 kcal mol⁻¹, with that of reaction 7 of Table V, 11.6 kcal mol⁻¹. For neighboring chains to move together by a chain vibration or oscillation so that free radical transfer could occur evidently more activation energy is needed than in the gas-phase reaction 7 of Table V. The low activation energy of the reaction forming the allyl free radical by chain transfer, reaction 8 of Table V, only 9.3 kcal mol⁻¹, suggests that in neither the hydrogen-catalyzed nor the uncatalyzed reaction is the allyl radical formation reaction rate determining.

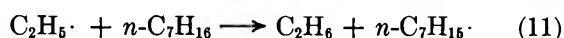
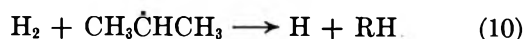
We conclude that the rate-determining steps are the following: catalyzed reaction



uncatalyzed reaction



It is interesting to compare the rate constants of reactions 8 and 9, k_8 and k_9 , as observed in solid polyethylene at 24° with the analogous gas-phase reaction. For reaction 10, Hoey and LeRoy²⁴ found 12.5 kcal



mol⁻¹ for its activation energy, but the A factor was not determined by them. We have selected 10¹²

mol⁻¹ cm³ sec⁻¹ as a reasonable value for the latter. In the case of reaction 11, we use James and Steacie's value of 11.6 kcal mol⁻¹ for the activation energy and 9 × 10¹¹ for the A factor. The latter was estimated from their table of A values. At 24° we find

$$k_{10} \text{ (calcd)} = 1.05 \times 10^2 \text{ mol}^{-1} \text{ cm}^3 \text{ sec}^{-1}$$

$$k_{11} \text{ (calcd)} = 2.6 \times 10^3 \text{ mol}^{-1} \text{ cm}^3 \text{ sec}^{-1}$$

The experimental values of reactions 10 and 11, or rather of the analogous reactions 8 and 9, are k_8 (obsd from Table IV) = 3.6 × 10³ mol⁻¹ cm³ sec⁻¹, k_9 (calcd from data of Table III) = 0.75 × 10⁻⁴ cm³ mol⁻¹ sec⁻¹. In calculating the experimental value of k_9 , the concentration of the RH groups was assumed to be the stoichiometric value; *i.e.*, 2 (960)/14 in M . The density of the polyethylene was taken as 0.96.

One immediately observes that whereas the rate constant of reaction 8 is somewhat greater than that of the analogous gas-phase reaction, the uncatalyzed reaction rate constant is 10⁷-fold smaller than expected from the rates of similar gaseous reactions.

Geymer and Wagner²⁸ estimated the rate constant in the abstraction of secondary hydrogen atoms by secondary radicals to be 2.4 × 10² mol⁻¹ cm³ sec⁻¹ which is tenfold lower than our estimate of 2.6 × 10³ for reaction 11. Their estimate of the rate constant of reaction 10, calculated for D₂ instead of H₂ was 7.8 instead of our value of 1.02 × 10² mol⁻¹ cm³ sec⁻¹. They thought that the experimental abstraction reaction was 10⁶-fold faster than the exchange reaction. This estimate, however, was based on data of free radical decay obtained by Charlesby, Libby, and Ormerod⁶ under conditions where the free radicals were decaying probably to produce cross-links because the decay was second order and not first order as observed in this work. Also the rates of decay were so fast that probably the free radical concentration range was not in the range where the random walk process was rate determining.

That the abstraction reaction in some cases can be immeasurably slow is seen in the data of Figure 8 where the linear extrapolation to zero hydrogen pressure indicates no measurable alkyl radical decay at room temperature greater than the limits of experimental uncertainty. Dole, Böhm, and Waterman²⁹ estimated that the free valency center and the nucleus of the hydrogen atom must be closer than 0.9 Å for a jump to occur whereas in the case of the linear zig-zag polyethylene chain the nearest hydrogen nuclei on the same chain are 1.93 Å apart. This means that hydrogen atoms cannot jump along a chain in the uncatalyzed case, but must migrate across chains when neighboring chains oscillate toward each other until the free valency center on one chain and the hydrogen atom on the neighboring chain

(28) D. O. Geymer and C. D. Wagner, *Nature*, **208**, 72 (1965).

(29) M. Dole, G. G. A. Böhm, and D. C. Waterman, "European Polymer Supplement," 1969, pp 93-104.

are about 0.6 Å apart. This distance was estimated from the potential energy *vs.* nuclei separation of the CH molecule curve, calculated by means of a Morse function²⁹ such that the activation energy would be 17 kcal mol⁻¹.

In the case of crystalline polyethylene when an abstraction occurs, the reverse reaction could also occur restoring the free radical to its original site, unless the chain rotates or oscillates into a position where the abstraction reaction would more readily take place involving a -CH group different from the group on its original site. In the case of the hydrogen-catalyzed reaction the situation is different, because hydrogen molecules are mobile in the crystalline polyethylene and because the hydrogen-catalyzed reaction does not require the chains to oscillate toward each other until a certain minimum distance between chains is attained. Furthermore, in the hydrogen-catalyzed case the probability of an immediate back reaction restoring the free radical to its original site would be slight if the hydrogen molecule involved in the reaction has diffused to another location. Of course, the free radical could be restored to its original site by reaction with another hydrogen molecule, but with several possible spatial arrangements involving the free radical, the bridging hydrogen molecule and a neighboring chain, the probability of such restoration would be less than in the uncatalyzed case.

Inasmuch as the experimental activation energy of the uncatalyzed reaction was found to be 17 kcal mol⁻¹, Table V, while that of reaction 11 is only 11.6 kcal mol⁻¹, one would expect the rate constant of reaction 9 in polyethylene to be $\exp\{(17,000 - 11,600)/RT\}$ or nearly 10⁴ smaller than its analogous gas phase reaction merely on the basis of the activation energy considerations. Hence on the basis of both the activation energy differences and the differences in the mechanism of the random walk process, the much slower rate constant of the uncatalyzed reaction can be understood.

If polyethylene containing only polyenyl free radicals is irradiated with uv light at liquid nitrogen temperature, allyl free radicals disappear, the concentration of the dienyl free radical increases, and alkyl free radicals are regenerated. On heating to room temperature the allyl free radical is reformed, but after room temperature is attained no further formation of allyl radical occurs. About 35% of the alkyl radicals regenerated at 77°K persist to room temperature. At room temperature these residual free radicals then decay by a second-order process without further increase in the allyl free radical concentration. The final allyl concentration is about 44% of its initial concentration, whereas the dienyl concentration has increased about 3.6-fold to a value equal to 60% of that of the final allyl concentration.

Some of this behavior is difficult to understand. It is reasonable to expect the allyl free radicals to be readily reformed because in the uv regeneration of the alkyl

free radicals the latter are probably produced in locations very close to their former allylic site. However, at the moment there seems to be no plausible explanation of the fact that no further allyl formation takes place once room temperature has been attained. It is interesting to note that the room temperature second-order decay occurs only to a measurable extent when catalyzed by hydrogen, Figure 8; hence the rate-determining step is again that of free radical migration along or across chains (in the presence of hydrogen). Inasmuch as in the absence of hydrogen the alkyl decay rate at room temperature is practically zero, it must mean that of those alkyl radicals that persist to room temperature few are in a position to make interchain jumps. As discussed above, uncatalyzed free radical migration along a linear chain is highly improbable.

Shimada, Kashiwabara, and Sohma³⁰ have recently found that photolysis of previously γ -irradiated polyethylene by light of wavelength greater than 3900 Å produced main chain scission leading to the radical -CH₂·CHCH₃. The γ irradiation was carried out at room temperature. In our work some of the free radicals formed by the uv photolysis may have been of this type in which case their decay kinetics would probably be different from that of the alkyl radical CH₂·CHCH₂.

The first-order formation of the allyl free radical at room temperature following the electron beam irradiation requires that the concentration of double bonds in the polyethylene remains constant with time. The first-order rate constant, on the other hand, should increase with the double bond concentration. For the first 70 Mrads the latter remains approximately constant, but at high doses the total unsaturation increases. Table VI contains data for *k*, [*t*-Vi], and [Vi]

Table VI: Alkyl Decay Constants^a and Unsaturation as a Function of Dose

Dose, Mrads	<i>k</i> , 10 ³ min ⁻¹	[<i>t</i> -Vinylene], 10 ² M	[Vi], 10 ² M	Sum of [<i>t</i> -Vi] and [Vi]	<i>k</i> /sum mol ⁻¹ min ⁻¹ 10 ³
20	9.81	2.15	5.0	7.15	13.7
45	9.64	4.64	3.5	8.14	11.8
90	10.3	9.27	3.25	12.5	8.2
135	10.9	13.8	3.25	17.0	6.4
180	12.0	18.4	3.37	21.8	5.5
225	15.3	23.1	3.62	26.7	5.7

^a Measured at 26° and 30 cm H₂ pressure.

as a function of dose. It can be seen that *k* does increase with the unsaturation, but not linearly. With increase of unsaturation, the average distance required for migration of the alkyl free radical to the allylic

(30) Paper presented by H. Kashiwabara at the 2nd U. S.-Japan Conference on Radiation Chemistry, Hakone, Japan, Nov 13, 1969.

position would be reduced, and the alkyl decay reaction rate should increase. However, there are many complicating factors such as increased cross-linking with dose, a possibly increased uncatalyzed rate, and increased formation of *cis*-vinylene, diene, and triene groups, all of which have not been considered here, which prevent any simple relationship from being valid. Calculations show that inclusion of *cis*-vinylene and diene group concentrations in [total unsaturation] would not change significantly the ratio of k /[total unsaturation]. Despite these uncertainties, the general trend of the effect of unsaturation on the alkyl free radical decay rate is clearly evident.

To conclude, we have shown that alkyl free radicals, which persist to room temperature following electron beam irradiation, decay by first-order kinetics to form allyl free radicals quantitatively. This room temperature reaction is about 10^7 -fold slower than analogous gas-

phase reactions, but is markedly catalyzed by molecular hydrogen acting through an easily understood mechanism. Alkyl radicals which are regenerated from allyl free radicals by uv irradiation at 77°K and which persist to room temperature have a negligible decay rate in the absence of molecular hydrogen, but in the presence of the latter decay by second-order kinetics without reforming the allyl free radical.

Acknowledgment. This research was supported by the U. S. Atomic Energy Commission, their document No. COO-1088-36, and by the Advanced Research Projects Agency of the Department of Defense through the Northwestern University Materials Research Center. We are indebted to J. A. Reid of the Phillips Petroleum Co. for the gift of polyethylene samples used and to James S. Hyde of Varian Associates for the measurements on the allyl free radical carried out with an E-4 spectrometer.

Line-Width Parameters for the ($1 \leq J \leq 8, K = 1$) Lines of the Inversion Spectrum of Ammonia

by James A. Roberts

Department of Physics, North Texas State University, Denton, Texas (Received August 19, 1969)

A study was made of the line-width parameters of the ammonia inversion spectra for the transitions ($1 \leq J \leq 8, K = 1$). These lines have fine structure due to the removal of the K degeneracy of the rotational energy levels. This degeneracy removal produces spectral lines for ($J, K = 1$) which have small relative frequency spacings. Line-width parameters were determined experimentally for the spectral lines with quantum numbers ($1 \leq J \leq 8, K = 1$) and are reported. These experimental line-width parameters were corrected using a mathematical model of superposition of Lorentzian shape spectral line.

Introduction

There is a relationship between the frequency spacing at half-power points for spectral lines and the processes by which the spectral line is generated. The line width, as this frequency spacing is called, is related to the mean time between events which generate the spectral line. If the spectral line is generated by radiation interruption due to collisions of the radiating molecules with other molecules, the line width is related to the interaction mechanism between the molecules. A study of the line width is a key to the reaction processes between the radiator and its environment. Accurate line widths must be obtained if useful information concerning the interaction between the emitting molecule and its surroundings is to be obtained. Spectral line widths may be studied over broad ranges of frequencies. The line-width information presented here was obtained at microwave frequencies.

The microwave spectra of ammonia for the case $K = 1$ has complex structure due to the interaction of the hydrogen nuclear spins with the molecular rotation.^{1,2}

Line-width parameters for many microwave spectral lines which were assumed to have Lorentzian shape have been determined and reported.³⁻⁵ Doppler and wall-broadening of spectral lines at low pressures are known to distort spectral line shapes from a Lorentzian profile.⁶ The presence of spectral lines near an observed line produces similar distortion of the line shape.

Frequency spacings have been determined for seven of the inversion lines of NH_3 for $K = 1$, and these results, with the calculated relative intensities, used to construct correction curves, Figure 1, to account for distortion of the spectral lines due to the presence of other near spectral lines.⁷ The true line width, $2\Delta\nu$, and the observed line width, corrected for finite modulation and Doppler distortion, $2\delta\nu$, are related by these curves. An equation of a family of closely spaced spectral lines may be written as⁸

$$f(x) \equiv \sum_{j=1}^n I_j [(x + a_j)^2 + (\Delta\nu)^2]^{-1} \quad (1)$$

where $x = (\nu - \nu_0)$ is introduced for ease of handling the equation, a_j is the separation of the center frequencies of the spectral lines, $I_j =$ the intensity of the lines, and $\Delta\nu$ is the half width of the spectral lines.

The microwave spectrometer employed uses the double modulation technique as described by Rinehart, *et al.*,⁹ and therefore measures separation of points of steepest slope for the line. The expected points of steepest slope were obtained for the spectral lines by introducing arbitrary values of $\Delta\nu$ into the equation for $f'(x)$ and obtaining values of x at half-width frequency. The correction curves are employed after all observed line widths have been corrected for finite modulation, Doppler broadening,¹⁰ and wall collision effects.

The experimental line-width parameters for the ($1 \leq J \leq 8, K = 1$) inversion transitions of ammonia are compared with values obtained from pressure broadening theories.¹¹⁻¹⁴

(1) G. R. Gunther-Mohr, R. L. White, A. L. Schawlow, W. E. Good, and D. K. Coles, *Phys. Rev.*, **94**, 1184 (1954).

(2) G. R. Gunther-Mohr, C. H. Townes, and J. H. Van Vleck, *ibid.*, **94**, 1191 (1954).

(3) C. O. Britt and J. E. Boggs, *J. Chem. Phys.*, **45**, 3877 (1966).

(4) O. R. Gilliam, H. D. Edwards, and W. Gordy, *Phys. Rev.*, **75**, 1014 (1949).

(5) R. L. Legan, J. A. Roberts, E. A. Rinehart, and C. C. Lin, *J. Chem. Phys.*, **43**, 4337 (1965).

(6) J. A. Roberts, "Studies of Linewidth of Microwave Spectra of Symmetric Top Molecules," Dissertation Abstracts, 1649-B, 1967.

(7) J. A. Roberts, *J. Mol. Spectrosc.*, **30**, 351 (1969).

(8) J. H. Van Vleck and V. Weisskopf, *Rev. Mod. Phys.*, **17**, 225 (1945).

(9) E. A. Rinehart, R. L. Legan, and C. C. Lin, *Rev. Sci. Instrum.*, **36**, 511 (1965).

(10) R. W. Parsons and J. A. Roberts, *J. Mol. Spectrosc.*, **18**, 412 (1965).

(11) P. W. Anderson, *Phys. Rev.*, **76**, 647 (1949).

(12) C. J. Tsao and B. Curnutte, *J. Quant. Spectrosc. Radiat. Transfer*, **2**, 41 (1961).

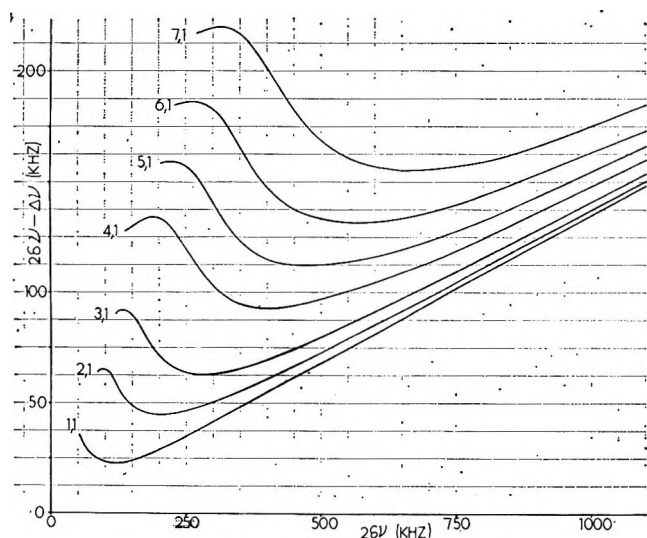


Figure 1. Correction curves for deducing true line widths from observed line widths for the ($1 \leq J \leq 7$, $K = 1$) inversion lines of NH_3 .

stabilized with a 100-kHz driving standard. The 1-MHz markers which came from the mixer were detected by an interpolation receiver, Hammarlund Model HQ-180A, and fed to one pen of the G-22 Varian recorder. The resultant display of markers and line-shape derivative is shown in Figure 3.

All pressure measurements were made using a standardized McLeod gauge. All line-width and pressure measurements were made at a temperature of $26 \pm 1^\circ$. Apparatus effects are assumed to be minimized; errors due to apparatus effects are assumed to be less than 1%.

All line-width measurements were determined from chart recorder outputs similar to Figure 3. Ten or more sweeps through the spectral line were recorded for each pressure of the gas in the waveguide after a stabilization period of 30 min was allowed to elapse. The observations of separation between points of steepest slope, $2\delta\nu$, were corrected for finite modulation in accordance with the formula given in ref 9.

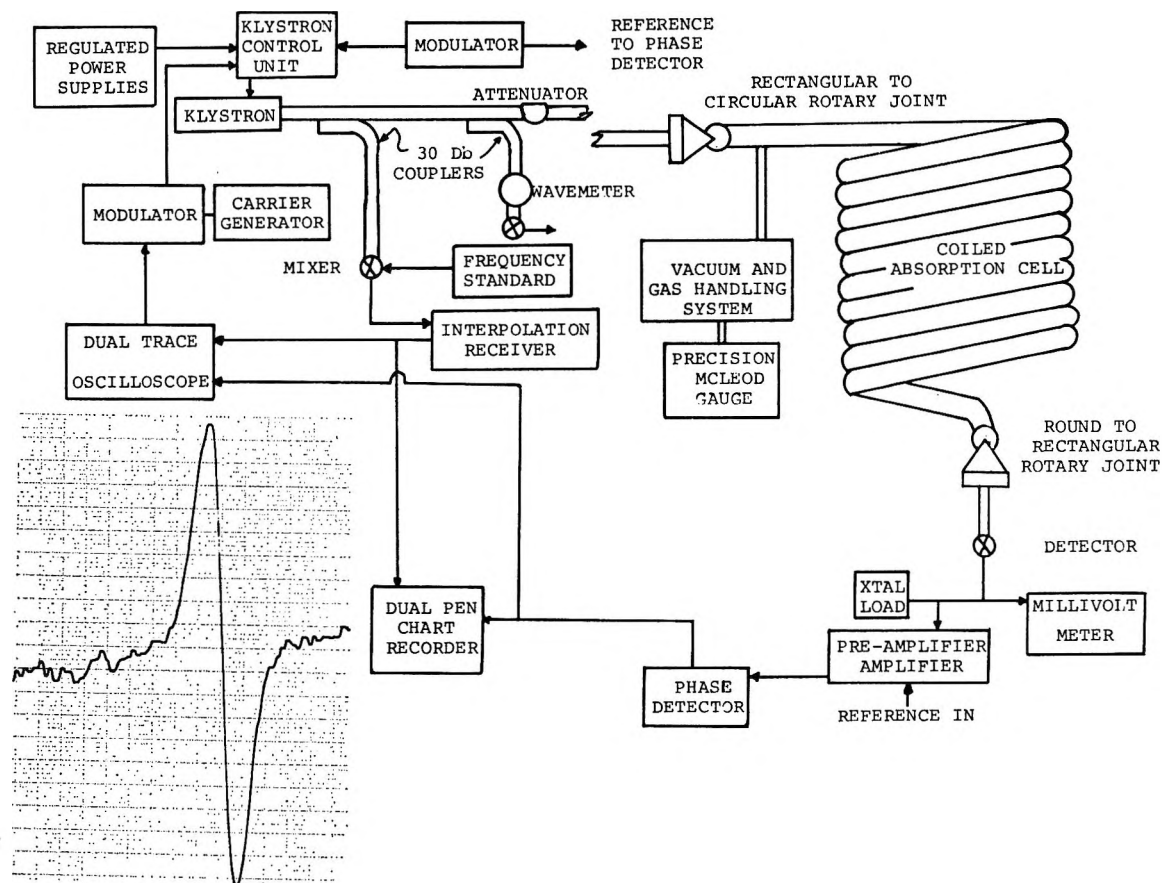


Figure 2. Block diagram of the microwave spectrograph for making line-width measurements.

Experimental Section

A block diagram of the apparatus used¹⁶ is shown in Figure 2. All recommended precautions for measuring line widths as described in ref 8 were followed.

The sources for frequency markers were the General Radio Models 1112A and 1112B generators, properly

Results

The observed values of $\delta\nu$, with modulation and

(13) B. Bleaney and R. P. Penrose, *Proc. Phys. Soc. London*, **60**, 540 (1948).

(14) J. S. Murphy and J. E. Boggs, *J. Chem. Phys.*, **50**, 3320 (1969).

(15) J. A. Roberts, *Rev. Sci. Instrum.*, **40**, 935 (1969).

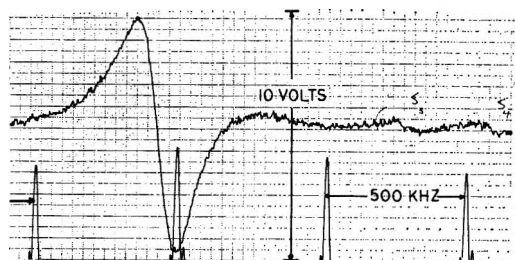


Figure 3. Typical chart recorder output containing line-shape derivative and frequency markers for determining line widths of spectral lines.

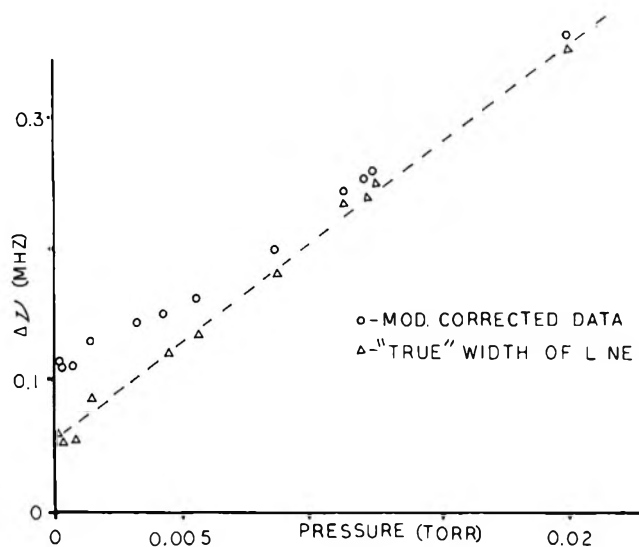


Figure 4. Line-width parameter curve for the (5,1) inversion line of NH_3 .

doppler broadening corrections applied, were used to obtain true values of $\Delta\nu$ by employing the correction curves given in Figure 1. These values, with appropriate pressures, were plotted to obtain the line-width parameters. A typical plot of the line width *vs.* pressure is given in Figure 4. The plot of $\delta\nu$, corrected for finite modulation only, is given for comparison with the result when the line widths have been corrected due to distortion by near spectral lines.

Figure 5 shows the derivative profile of the (5,1) inversion line of NH_3 as the pressure in the absorption cell is increased. The derivative envelope obviously departs from that expected for a Lorentzian shape line as overlapping of the lines occurs.

The correction curves of Figure 1 were derived using only the resolved central components of each transition since frequency spacings and relative intensity values are not available for the unresolved spectral components.

The accumulated errors in the line-width parameter due to uncertainty in intensity, frequency spacings of the spectral components, and instrumentation effects is no more than 5%. Systematic errors due to unresolved overlapping spectral components may increase the error

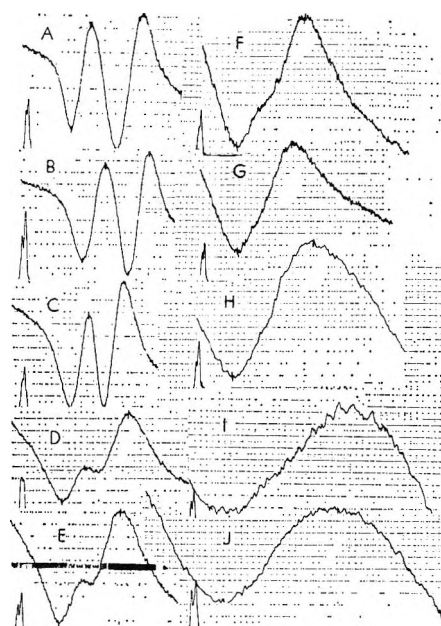


Figure 5. Line-shape distortion of the (5,1) inversion line of NH_3 as the pressure is increased from 0.1 mTorr to 40 mTorr pressure.

Table I: Line-Width Parameters (MHz per Torr) of the ($1 \leq J \leq 8, K = 1$) Spectral Lines of the Inversion Spectrum of NH_3

Spectral lines	$\Delta\nu_p^a$	$\Delta\nu_p^b$	$\Delta\nu_p^c$	$\Delta\nu_p^d$	$\Delta\nu_p^e$	$\Delta\nu_p^f$
(1,1)	16.3	19.6	21.2	15.0		
(2,1)	15.1	17.7	12.2	11.5	14.4	14.8
(3,1)	13.8	11.7	8.7	10.6	14.4	12.8
(4,1)	10.7	(10.6)	6.7	10.6		
(5,1)	8.8	9.5	5.5	10.0	10.8	
(6,1)	6.0	8.1	4.6	9.0		
(7,1)	3.8	6.6	4.0	7.9		
(8,1)	2.7	5.2	3.5	6.4		

^a Observed line-width parameter of this work. ^b Calculated using Anderson's theory and normalizing to the (4,4) inversion line. ^c Calculated using the formula of Bleaney and Penrose. ^d Two-channel system (normalized) of Boggs and Murphy.¹⁴ ^e B. Bleaney and R. P. Penrose, *Proc. Roy. Soc.*, **A189**, 358 (1947). ^f C. A. Porter, A. V. Bushkovitch, and A. G. Rouse, *Phys. Rev.*, **83**, 987 (1951).

in line-width measurements, for high values of J , at pressures less than 10 mTorr, to as much as 20%. It is not possible to assess the error precisely without knowing the relative intensity and frequency spacings for the unresolved components.

Discussion

Although the Anderson collision theory, employing a suitable normalization scheme, gives good results when applied to the $J = K$ inversion lines of NH_3 , there is a systematic departure of the calculated line-width parameters from the experimentally obtained data for the

lines ($J, K \neq J$). The difference between theoretical and experimental values of line-width parameters becomes greater as $(J - K)$ increases. Comparison of the calculations based on Anderson's theory and experimental values for the ($J, K = 1$) inversion lines of NH_3 shows a systematic difference in these values. The calculated line-width parameters in Table I have been normalized to the line-width parameter of the (4,4) inversion line of NH_3 in order to obtain the relative trend of the theoretical line-width parameter.

Calculations based on the predictions of ref 13 yield reasonable results for lines with $J = K$, excluding $J = K = 1$. As J increases, $K = 1$, to high values the results of ref 13 and experiment are in better agreement. Clearly this semiempirical formula does not predict the proper trend of the quantum number dependence of the line-width parameters for all lines with ($J, K = 1$).

It is surprising that as $(J - K)$ becomes large the experimental line-width parameters agree better with the prediction of Bleaney and Penrose and the statistical theory of Margeneau¹⁶ than they do with those obtained from other theories. The collision diameter cal-

culated from the experimental value of $\Delta\nu_p$ for the (8,1) transition has a value comparable to the value obtained from kinetic theory. This trend could not be pursued for higher J -valued lines using the present equipment.

The two-level system proposed by Boggs, ref 14, yields line-width parameter values which are too large for the cases ($J > 4, K = 1$). Extension of the theory to take into consideration high energy transition does not improve the absolute line width although the same relative trend is observed in the Boggs formulation and the experimental data for line-width parameters with ($J > 3, K = 1$).

It is clear that further theoretical work must be done in order to understand fully the nature of the interaction forces existing between confined molecules. The problem appears to be one of better understanding the role played by rotational resonance terms in the modified Anderson formulation.

(16) H. Margeneau, *Phys. Rev.*, **76**, 121, 585A (1949).

Solvation of Extracted Complex Metal Acids. VI. The Transfer of HFeCl_4 to Bis(2-chloroethyl) Ether-Benzene Mixtures¹

by R. L. McDonald and T. H. Hufen

Department of Chemistry, University of Hawaii, Honolulu, Hawaii 96822 (Received November 6, 1969)

The effects of HCl, ether, and iron concentrations on the transfer of HFeCl_4 from aqueous HCl to benzene solutions of bis(2-chloroethyl) ether have been studied. Ion-pair dissociation constants were also determined from the extraction data. Log-log plots of the distribution and ion-pair dissociation constants vs. ether concentration yield straight lines; the slopes are interpreted as solvation parameters. An average of 13 molecules of the ether solvate the free ions; 7.5 of these are lost when the ions associate to form an ion pair. The ion-pair dissociation constant of HFeCl_4 is ca. 10^{-7} in wet HCl-saturated benzene; extrapolation yields a value of 2×10^{-2} in the ether. Although a Born approach will also explain the data, it fails to account for the differences between the ether system and the nitrobenzene system studied earlier.

Introduction

Several papers from this laboratory²⁻⁶ have dealt with the changes in free energy that accompany the transfer of HMX_4 species from fairly concentrated HX aqueous phases to mixed organic phases of varying composition. ($X = \text{Cl}$ or Br ; $M = \text{Fe}$, In , or Au). In fact, we measure the distribution coefficient which can be quantitatively related to ion-ion and ion-solvent interactions in the organic phase. We have chosen not to interpret our

results in terms of the Born charging equation or one of its variations^{7,8} but rather in terms of the law of mass

(1) Research sponsored by the Air Force Office of Scientific Research, Office of Aerospace Research, U. S. Air Force under Grant No. AFOSR-68-1387.

(2) R. L. Erickson and R. L. McDonald, *J. Amer. Chem. Soc.*, **88**, 2099 (1966).

(3) C. V. Kopp and R. L. McDonald, "Solvent Extraction Chemistry," D. Dyrssen, *et al.*, Ed., North-Holland Publishing Co., Amsterdam, 1967, pp 447-453.

action (corrected for nonideality). This leads to solvation numbers larger than can be readily accounted for by any simple model. Rather than abandon this approach, we have continued these studies with the aims of resolving this difficulty and gaining insight into the behavior of ions in solution.

In this work, the distribution of Fe(III) between aqueous HCl and solutions of bis(2-chloroethyl) ether in benzene was studied. From these data, it has been possible to obtain values of the ion-pair dissociation constant of $\text{H}^+\text{FeCl}_4^-$ in the organic phases as well as solvation information for both the free ions and the ion pairs.

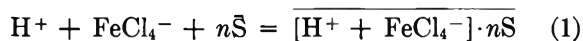
Experimental Section

Eastman White Label bis(2-chloroethyl) ether was purified by distillation under a reduced pressure of N_2 in a Podbielniak still. The middle fraction was collected and diluted with reagent grade benzene to the desired concentrations. These solutions were stored in the dark and used for distribution measurements within six weeks. Reagent grade HCl was diluted with deionized water. Reagent grade $\text{FeCl}_3 \cdot 6\text{H}_2\text{O}$ was dissolved in HCl solutions and the iron concentration determined by the Zimmerman-Reinhard method. Each series of solutions of desired iron concentrations was prepared from these stock solutions by diluting with HCl of the same concentration as the stock solution. High specific-activity iron-59 in aqueous HCl was purchased from International Chemical and Nuclear Corp. and diluted with 6 M HCl.

All distribution experiments were done in triplicate as described elsewhere.⁵ The reproducibility between triplicates was almost always better than 10%.

Theoretical Section

We have argued elsewhere²⁻⁶ that extraction systems of this type can be treated by simple thermodynamics; *i.e.*, for a constant aqueous phase



The bar represents the organic phase and the right-hand side is written to indicate that the free ions are solvated by n molecules of the polar solvent, S (in this case the ether), but we have been unable to assign a number to each ion. It is assumed, and all of our data substantiate this assumption, that the ions are preferentially solvated by the polar solvent. The proton, of course, is hydrated, probably with four water molecules,^{2,9} and solvation occurs outside this hydration shell. We do not mean to imply that this solvation necessarily results in the formation of discrete species analogous to the aquo complexes of some of the transition metals in aqueous solutions. Rather, we picture the ions surrounded by n polar solvent molecules which are oriented as a result of principally electrostatic interactions.

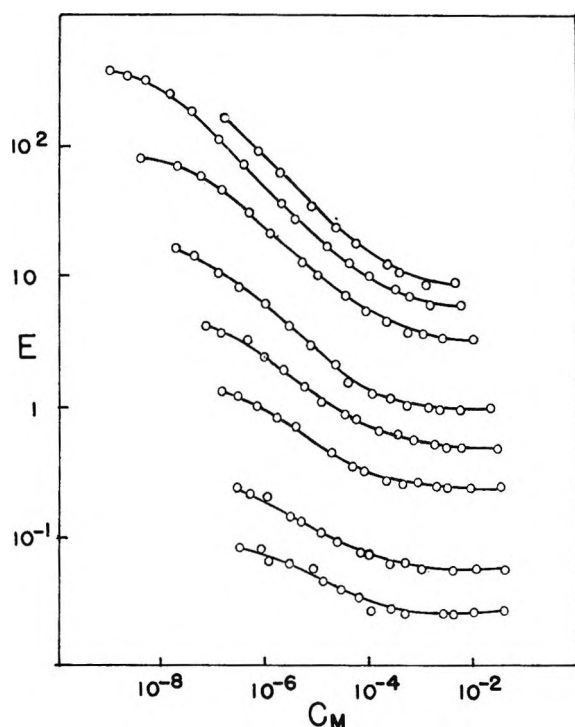
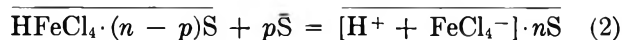


Figure 1. Log-log plots of the distribution coefficient vs. the equilibrium aqueous phase iron concentration (moles per liter) for extraction from 9.16 M HCl into (from the top) 5.94, 5.50, 5.09, 4.24, 3.82, 3.39, 2.54, and 2.12 M bis(2-chloroethyl) ether in benzene.

The degree of orientation around a pair of free ions is greater than around an ion pair; therefore we write



with the equilibrium constant

$$\bar{K}_M' = \bar{g}_{\pm}^2(\text{H}^+)(\text{FeCl}_4^-) / \overline{(\text{HFeCl}_4)[\bar{\text{S}}]^p} = \bar{K}_M[\bar{\text{S}}]^{-p} \quad (3)$$

\bar{g}_{\pm} is the mean ionic activity coefficient in the organic phase; parentheses represent concentration; brackets represent activity; the ions and the ion pair are written without their molecules of solvation for brevity, and the activity coefficient of the ion pair is assumed constant at the concentrations of interest here ($<10^{-2}$ M). \bar{K}_M' is a true constant in that it is independent of solvent concentration. An expression analogous to eq 3 can also be written for the ion-pair dissociation constant,

(4) D. A. Meyers and R. L. McDonald, *J. Amer. Chem. Soc.*, **89**, 486 (1967).

(5) S. L. Law and R. L. McDonald, *J. Phys. Chem.*, **72**, 1617 (1968).

(6) T. H. Hufen and R. L. McDonald, "Solvent Extraction Chemistry" (tentative title), A. S. Kertes and Y. Marcus, Ed., Wiley, Interscience Publishers, New York, in press.

(7) G. R. Haugen and E. L. Friedman, *J. Phys. Chem.*, **72**, 4549 (1968).

(8) W. A. Millan and D. W. Watts, *J. Amer. Chem. Soc.*, **89**, 6051 (1967).

(9) J. Axelrod and E. H. Swift, *ibid.*, **62**, 33 (1940)

Table I: Apparent Distribution and Ion-Pair Dissociation Constants for HFeCl_4 Extracted from HCl by Bis(2-chloroethyl) Ether in Benzene

$(\beta\beta), M$	[HCl], M							
	9.16		8.06		6.72		6.04	
	J	\bar{K}_M	J	\bar{K}_M	J	\bar{K}_M	J	\bar{K}_M
0.00	(2.27×10^{-11})	(ca. 10^{-7})
2.12	7.90×10^{-9}	3.52×10^{-7}
2.54	3.96×10^{-8}	7.52×10^{-7}	7.90×10^{-10}	3.16×10^{-7}
3.39	9.93×10^{-7}	4.47×10^{-6}	5.78×10^{-7}	10.3×10^{-6}	7.26×10^{-8}	7.57×10^{-6}	1.72×10^{-8}	7.15×10^{-6}
3.82	6.15×10^{-6}	1.28×10^{-5}	1.82×10^{-6}	1.44×10^{-5}	8.12×10^{-8}	1.23×10^{-5}
4.24	3.25×10^{-5}	3.82×10^{-5}	1.06×10^{-5}	3.93×10^{-5}	4.25×10^{-7}	4.25×10^{-5}
5.09	5.65×10^{-4}	1.99×10^{-4}	1.82×10^{-4}	1.98×10^{-4}	2.84×10^{-5}	1.89×10^{-4}	4.33×10^{-6}	1.33×10^{-4}
5.50	2.21×10^{-3}	4.21×10^{-4}	5.42×10^{-4}	3.62×10^{-4}
5.94	5.16×10^{-3}	5.87×10^{-4}	1.54×10^{-3}	6.02×10^{-4}	6.91×10^{-5}	4.94×10^{-4}

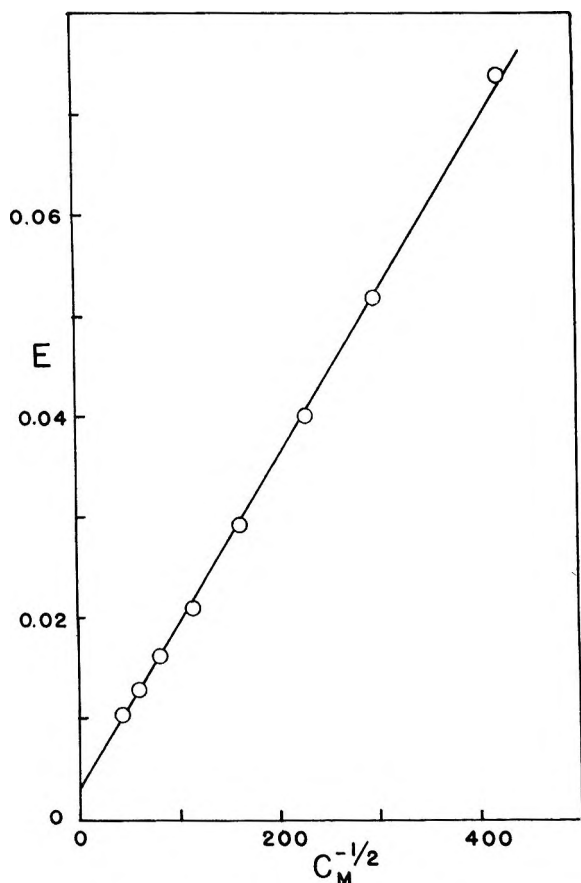


Figure 2. Plot of the distribution coefficient vs. the inverse square root of the equilibrium aqueous phase iron concentration (moles per liter) for extraction from 6.04 M HCl into 3.39 M bis(2-chloroethyl) ether in benzene.

$\bar{K}_{\text{HX}'}$, of extracted HCl which gains m molecules of S upon dissociation.⁵ With these modifications, the expression for the distribution coefficient, E , derived earlier² becomes

$$E = (K/\bar{K}_M')[\bar{S}]^{n-p} + K[\bar{S}]^n / g_{\pm} \{ KC_M[\bar{S}]^n + \bar{K}_{\text{HX}'}\bar{C}_{\text{HX}}[\bar{S}]^m \}^{1/2} \quad (4)$$

where K , the distribution constant (defined elsewhere²) is a function of the aqueous phase and temperature

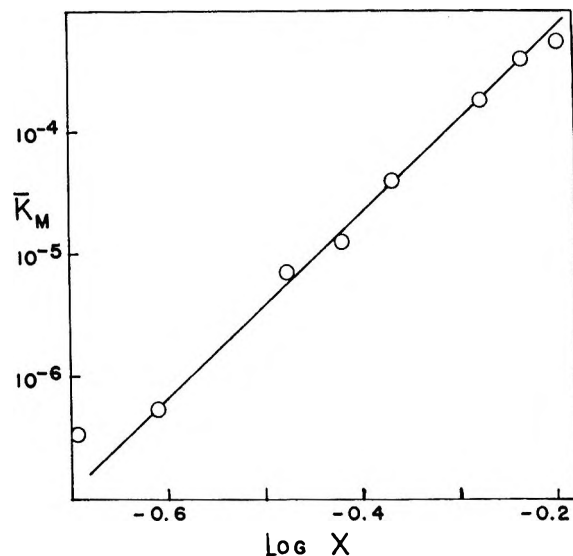


Figure 3. Log-log plot of the apparent ion-pair dissociation constant of HFeCl_4 vs. the mole fraction of bis(2-chloroethyl) ether in benzene.

only, and C_M and \bar{C}_{HX} are the equilibrium aqueous phase metal and organic phase HX concentrations, respectively.

Results

Figure 1 shows typical log-log plots of the distribution coefficient, E , vs. C_M . The curves have the general shape predicted by eq 4. However, the slopes of the middle portions of the curves are all greater than -0.5 , the value expected when ion-pair dissociation is complete.² In order to assure ourselves that this behavior was not due to the presence of iron impurity in the reagent grade HCl ,² we repeated the experiments at 4.24 M ether using HCl that had been preextracted twice with either the ether or with nitrobenzene. (This reduced the iron concentration in the HCl by a factor of at least 10^4 .)⁹ The extraction results were unchanged by these purification treatments. It is highly unlikely that changes in the activity coefficient, g_{\pm} are causing this behavior; Debye-Hückel theory predicts g_{\pm} to be

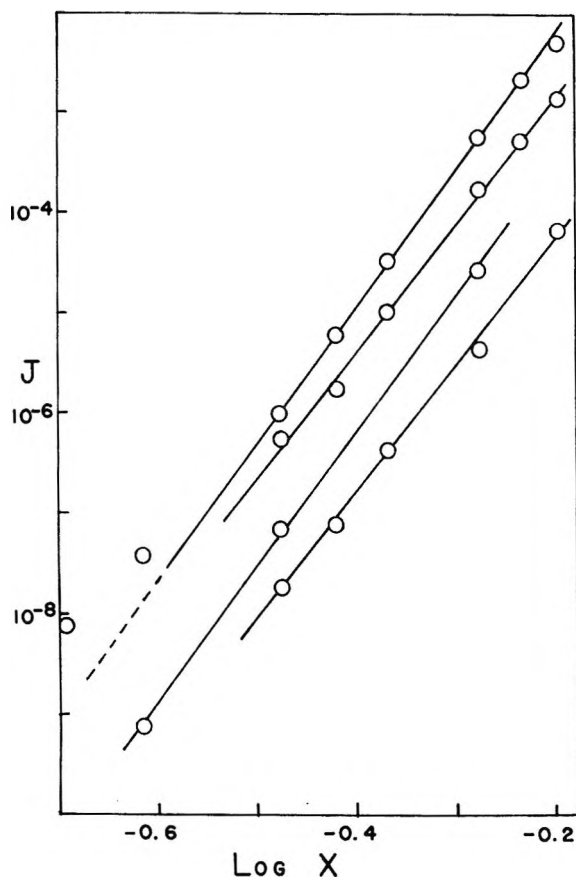


Figure 4. Log-log plot of the apparent distribution constant vs. the mole fraction of bis(2-chloroethyl) ether for extraction from (from the top) 9.16, 8.06, 6.72, and 6.04, *M* HCl.

essentially unity except perhaps at the highest metal concentrations. Thus it appears that in the ether system, as opposed to nitrobenzene,^{2,5} HFeCl_4 is not completely dissociated; *i.e.* the first term in eq 4 is not negligible compared to the second term.

Equation 4 predicts that so long as the term $\bar{K}_{\text{HX}}' - \bar{C}_{\text{HX}} [\text{S}]^n$ is negligible ($C_M > \text{ca. } 10^{-6} \text{ M}$), a plot of E vs. $C_M^{-1/2}$ should yield a straight line for a given ether concentration. Figure 2 shows such a plot. The values of $J = K[\text{S}]^n$ and \bar{K}_M obtained from the slopes and intercepts of these plots are shown in Table I. The agreement among the values of \bar{K}_M obtained at a given $[\text{S}]$ but at different aqueous HCl concentrations (and, therefore, at different organic phase HFeCl_4 , HCl, and H_2O concentrations) is indeed satisfying. This supports our assumptions that variations in the activity of H_2O in the organic phase do not affect ionic behavior and that g_{\pm} can be ignored at the ionic strengths of interest here.

Solutions of bis(2-chloroethyl) ether in benzene deviate only slightly from Raoult's law behavior over the range in ether mole fraction, $X = 0-0.6$; for our purposes they may be considered ideal.⁶ Figure 3 shows a plot of $\log \bar{K}_M$ (average values) vs. $\log X$. Except for the value at $X = 0.202$, the points fall nicely on a

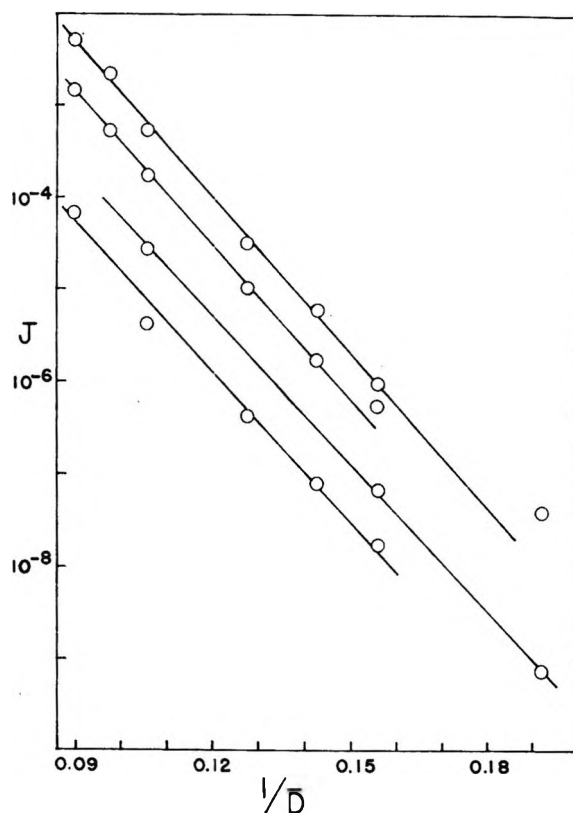


Figure 5. Semilog plot of the apparent distribution constant vs. the inverse dielectric constant of the organic phase for extraction from (from the top) 9.16, 8.06, 6.72, and 6.04 *M* HCl.

straight line of slope 7.5; *i.e.* $p = 7.5$. At very low ether concentrations, eq 2 is not sufficient to describe completely the ionization behavior of HFeCl_4 . A small amount of dissociation occurs in the wet benzene without solvation by the ether as can be seen from the data for 0.0 *M* ether in Table I. It is this decrease in p at low ether concentrations which explains the point at mole fraction 0.202 ($\log X = -0.695$) in Figure 3. Finally, the intercept in Figure 3 yields $\bar{K}_M' = 2 \times 10^{-2}$.

Plots of $\log J$ vs. $\log X$ are shown in Figure 4. Values of n obtained from the slopes of the lines are 13.7, 12.7, 13.3, 12.5 for (HCl) = 9.16 *M*, 8.06 *M*, 6.72 *M*, and 6.04 *M*, respectively. This gives an average value for the solvation number of the free ions of $\langle n \rangle = 13$. As with p , it is encouraging that the n values do not appear to be dependent on the metal, HCl, or H_2O concentrations in the organic phase. The decrease in slope at low ether concentrations (9.16 *M* HCl) is not easy to explain. As can be seen from the data in Table I for pure benzene, it is not due to extraction by benzene. The data here are insufficient to tell whether the decrease occurs at acid strengths other than 9.16 *M*, but it has been observed at lower acid strengths in other systems.^{2,5} It may be due to a decrease in n at low ether concentrations.

Discussion

In recent years there has been considerable interest in the fundamental theories of ion transfer and ion association;^{2-8,10-12} some authors lean toward the Born approach while others prefer thermodynamic approaches similar to the one discussed above (and hereafter referred to law of mass action, L.M.A., approaches). It should be noted that the Born charging equation will also serve to explain our data. Assuming that a modified Born equation, such as that used by Friedman⁷ to treat the nitromethane system, applies to mixed solvents as well, a plot of $\log J$ vs. $1/\bar{D}$ (\bar{D} = dielectric constant of the organic phase estimated from data for the dry solvent mixtures)¹³ should yield a straight line whose slope = $-[e^2/4.606 kT] [1/(r_+ + \Delta_+) + 1/(r_- + \Delta_-)]$; r indicates the crystal radius, and Δ is an empirical parameter. Figure 5 shows these plots for our data. The lines are essentially parallel and yield $[1/(r_+ + \Delta_+ + 1/r_- + \Delta_-)] = 4.5 \times 10^7 \text{ cm}^{-1}$. A similar plot can be made for \bar{K}_M with an equally good fit. Taking the slope of this line¹² to be $-e^2/2.303akT$, a = distance of closest approach = $8.2 \times 10^{-8} \text{ cm}$. No doubt both of these distance terms can be called reasonable.

It is instructive to use the Born approach to compare the iron extraction data reported here with those obtained for nitrobenzene-benzene mixtures.² Figure 6 shows plots of $\log J$ vs. $1/\bar{D}$ for two different HCl concentrations. Although the lines are nearly parallel, indicating similar apparent radii for the ions in both solvent mixtures, the data for a given HCl concentration do not fall on a single line as predicted by the Born equation.

Feakins¹¹ has discussed this phenomenon and his ideas appear to be applicable here also. He envisions the principal contribution to the free energy of transfer as coming from the "interaction between the charge on the ion and the totality of charges on the solvent molecules." These interactions lead to orientation of the solvent molecules in the first solvation shell and probably orientation of the solvent molecules in the second shell as well. Only out beyond this shell will the field strength be low enough for any additional contribution to the free energy of transfer to be accurately represented by the Born equation. Mullen and Watts⁸ suggested that this be handled by correcting the Born equation for dielectric saturation near the surface of ions. Alternatively; although the L.M.A. approach is essentially phenomenological in nature, it not only treats these systems adequately, it can also be readily interpreted in terms of molecular interactions.

Let us first look at the cation. Those solvent molecules in contact with this ion are oriented with their oxygen atoms toward the ion. The ether is more basic than nitrobenzene, and this presence of a higher charge density on the ether oxygen enhances hydrogen bond formation. Thus the result of primary solvation is to

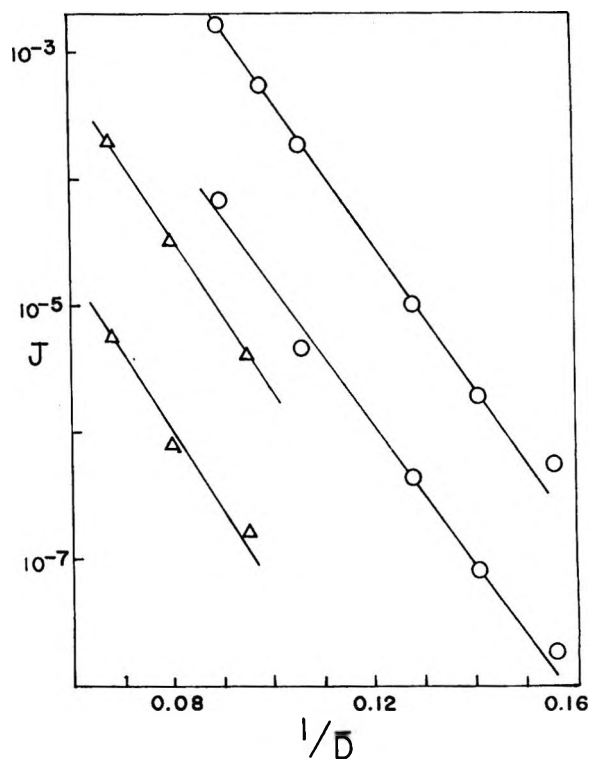


Figure 6. Semilog plot of the apparent distribution constant vs. the inverse dielectric constant of the organic phase for extraction from 8 M (upper) and 6 M HCl into nitrobenzene, Δ ; or bis(2-chloroethyl) ether, \circ . The J values for nitrobenzene were obtained from ref 2 and the \bar{D} values from ref 13, p 623.

lower the standard free energy of an H_3O_4^+ ion solvated by the ether relative to one solvated by nitrobenzene. Outside the primary-solvation sphere, the ions "see" the solvent molecules only as structureless dipoles.¹¹ Since nitrobenzene ($\mu = 4.0$) is more polar than bis(2-chloroethyl) ether ($\mu = 2.6$), secondary solvation has a reverse effect: *i.e.*, it tends to lower the standard free energy of the cation solvated by nitrobenzene relative to the ether solvated species.

It is more difficult to compare anion solvation in the two-solvent systems. The positive end of the solvent dipole is sterically hindered in both molecules. For this reason it seems likely that the anions see only structureless dipoles, even for those solvent molecules in contact with them; this leads to a lower anion standard free energy in nitrobenzene.

In Table II, we have compared values of the distri-

(10) A. S. Quist and W. L. Marshall, *J. Phys. Chem.*, **72**, 1536 (1968).

(11) D. Feakins, "Physico-Chemical Processes in Mixed Aqueous Solvents," F. Franks, Ed., American Elsevier Publishing Co., Inc., New York, N. Y., 1967, pp 71-89.

(12) M. Szwarc, "Carbanions, Living Polymers and Electron Transfer Processes," Interscience Publishers, New York, N. Y., 1968, pp 212-296.

(13) J. Timmermans, "The Physico-chemical Constants of Binary Systems in Concentrated Solutions," Interscience Publishers, New York, N. Y., 1959, Vol. 1, p 449.

Table II: Distribution Constants for Iron Extraction from HCl

[HCl], <i>M</i>	Log <i>K</i>		[HCl], <i>M</i>	Log <i>K</i>	
	Bis(2-chloro-ethyl) ether	Nitrobenzene		Bis(2-chloro-ethyl) ether	Nitrobenzene
6.04	-1.8	-1.2	8.06	-0.32	-0.49
6.72	-0.88	...	9.16	0.51	...

bution constants, *K*, obtained by extrapolation of plots such as Figure 4, for the transfer of HFeCl_4 from a given aqueous phase to either nitrobenzene or the ether at unit activity (*i.e.*, the pure solvents). The standard free energies of transfer are almost the same for the two solvents; this is understandable from (but not a requirement of) the preceding discussion. Figure 6 can now be explained also. There we have compared the *apparent* distribution constants, *J*, for benzene solutions of the two solvents as functions of the dielectric constant. At any given value of *D*, the concentration of nitrobenzene is appreciably less than that of

bis(2-chloroethyl) ether; this results in a smaller value of the apparent constant $J = K[\bar{S}]^n$ for the nitrobenzene solutions.

The discussion above emphasizes the necessity of using the L.M.A. approach to ion transfer, even in solvents of low coordinating ability; *i.e.*, ones in which physical rather than chemical solvation predominates. In these systems the Born approach in various forms is generally considered adequate, and little mention has been made of specific solvation involving definite numbers of solvent molecules. Nevertheless, we are in agreement with Quist and Marshall¹⁰ and Glover,¹⁴ who have pointed out the importance of including the solvent as a variable in equilibrium constants. As we have shown repeatedly,²⁻⁶ this leads naturally to the concept of ion solvation and to constant and reproducible solvation numbers. However, in view of the large solvation numbers obtained here, a test of the L.M.A. approach by an independent determination of these solvation numbers, *e.g.*, by Hittorf transference techniques, would be a valuable experiment.

(14) D. J. Glover, *J. Amer. Chem. Soc.*, **87**, 5279 (1965).

Activity Coefficients for the Systems Sodium Benzenesulfonate-Xylose-Water and Sodium Benzenesulfonate-Urea-Water at 25° from Isopiestic Measurements

by Hatsuho Uedaira and Hisashi Uedaira

Research Institute for Polymers and Textiles, 4, Sawatari, Kanagawa-ku, Yokohama, Japan (Received October 22, 1969)

Osmotic and activity coefficients for the two ternary systems sodium benzenesulfonate-xylose-water and sodium benzenesulfonate-urea-water were measured by the isopiestic vapor pressure method at 25°. A method for predicting the concentrations of the solutions in vapor pressure equilibrium was devised. The activity coefficients of sodium benzenesulfonate were increased by xylose and decreased by urea. The activity coefficients of xylose were increased by sodium benzenesulfonate, and those of urea were decreased by the salt. The results show that disruption of water structure by structure-breaking ions leads to stronger solvation of xylose. For the system containing urea, the stronger the structure-breaking effect of the ion, the greater is the decrease in activity coefficient of urea caused by addition of the ion.

Introduction

The transport properties of the aromatic sulfonates are affected by the interaction between solvent water and the ionized groups and also by the ordered structure of water around the nonpolar groups.^{1,2}

In a previous paper,³ the change of activation energy of the exchange of water molecules in the immediate

vicinity of the organic ion, ΔE_i , was calculated by Samoilov's theory.⁴ The ions for which $\Delta E_i > 0$ are

- (1) H. Uedaira and H. Uedaira, *Bull. Chem. Soc. Jap.*, **37**, 1885 (1964).
- (2) H. Uedaira and H. Uedaira, *ibid.*, **38**, 2194 (1965).
- (3) H. Uedaira and H. Uedaira, *Zh. Fiz. Khim.*, **42**, 3024 (1968).
- (4) O. Ya. Samoilov, "Struktura Bodn'kh Rastvorov Elektrolitov i Gidrataziya Ionov," Nauka, Moscow, 1957, Chapter 5.

structure makers and the ions for which $\Delta E_i < 0$ are structure breakers. For homologous ions, the values of ΔE_i were found to increase with an increase in size of the nonpolar group. The water molecules in the immediate vicinity of the nonpolar group become less mobile than in pure water. That is, the water structure in the immediate vicinity of the nonpolar group is more stable than that of the pure water. It was shown that for the benzenesulfonate ion, the structure-breaking effect of the sulfonic group outweighs the structure-making effect of the benzene ring.

The interaction between the ion and the water molecule is important for the equilibrium properties as well as for the transport properties of the electrolyte solutions. Bonner and Rogers⁵ obtained the osmotic and activity coefficients for the salts of benzenesulfonic, *p*-ethylbenzenesulfonic, 2,5-dimethylbenzenesulfonic, and mesitylenesulfonic acids at 25°. They found that these coefficients decrease with an increase in the organic content of the molecule and that the values are smaller than those of the common uni-univalent-type electrolytes.

In this paper, the investigation on the behavior of the organic electrolyte in ternary solution was undertaken to throw light on the nature of the interaction of the organic electrolyte with the solvent water. Osmotic and activity coefficients for the two systems sodium benzenesulfonate (NaBS)-urea-water, and NaBS-xylose-water were measured by the isopiestic vapor pressure method at 25°.

Experimental Section

Materials. The purification procedure for NaBS has been adequately described elsewhere.¹ Xylose was recrystallized three times from water and ethanol. Potassium chloride was analytical grade (Merck & Co.) and was used without further purification. NaBS and xylose were dried *in vacuo* over phosphorus pentoxide at 100°. The urea was analytical grade and was recrystallized twice from water, without heating above 60°, and dried *in vacuo* over phosphorus pentoxide at room temperature. Solutions were prepared with conductance water which was freed of air by boiling.

Osmotic and Activity Coefficient Measurements. Osmotic and activity coefficients were determined with the apparatus described previously.⁶ Potassium chloride was used as the reference solute. In the activity measurements, it is desirable that the initial concentrations in the prepared solutions be reasonably close to the equilibrium concentrations. A method for predicting the concentrations of the solutions in equilibrium was devised and will be described later.

All the measurements were performed at 25.00 ± 0.01°. The time required for equilibrium to be attained depended on the concentration of the solution; it

was usually 3 or 4 days. Concentration was measured by weighings corrected to vacuum.

Notation

γ_1, γ_2 are the molal activity coefficients of solutes 1 and 2 in a ternary solution containing solutes 1 and 2 with molalities m_1 and m_2 , respectively. ϕ_1, γ_1^0 are the molal osmotic and activity coefficients, respectively, of a binary solution containing only solute 1 at molality m_1 ; ϕ_2, γ_2^0 are the molal osmotic and activity coefficients, respectively, of a binary solution containing only solute 2 at molality m_2 . m_R, ϕ_R are the molality and molal osmotic coefficient, respectively, of the reference solution in vapor pressure equilibrium with a ternary solution containing the solutes 1 and 2 at molalities m_1 and m_2 . M_1, M_2 are the molalities of the binary solution containing either solute 1 or solute 2, respectively, which is in vapor pressure equilibrium with a ternary solution containing the solutes 1 and 2 at molalities m_1 and m_2 . a_w is the activity of the solvent. M_w is the molecular weight of the solvent. Suffix 1 is NaBS; suffix 2 is the nonelectrolyte (urea or xylose).

Calculation of the Activity Coefficient of the Three-Component System

An experimental quantity Δ was defined by

$$\Delta = \frac{1000}{M_w} [\ln a_w(m_1) + \ln a_w(m_2) - \ln a_w(m_1, m_2)] \quad (1)$$

Considering that solute 1 is a 1-1 electrolyte and that solute 2 is a nonelectrolyte, we have the following equation from the definition of the osmotic coefficient

$$\Delta = 2m_R\phi_R - 2m_1\phi_1 - m_2\phi_2 \quad (2)$$

The value of Δ can be calculated from the data of the ternary solutions provided that the osmotic coefficients of the binary solutions are known. The values of osmotic coefficients for reference potassium chloride were obtained from the values tabulated by Robinson and Stokes.⁷ The values of osmotic coefficients for NaBS were taken from the data of Bonner and Rogers.⁵ The values for xylose were calculated by use of the equation⁶

$$\phi_2 = 1 + 0.01407m_2 + 0.002288m_2^2 - 0.000482m_2^3 \quad (m_2 \leq 3.46) \quad (3)$$

and the values for urea were calculated from⁸

$$\phi_2 = 1 - 0.043702m_2 + 0.006348m_2^2 - 0.000695m_2^3 + 0.000034m_2^4 \quad (m_2 \leq 7.0) \quad (4)$$

(5) O. D. Bonner and O. C. Rogers, *J. Phys. Chem.*, **64**, 1499 (1960).

(6) H. Uedaira and H. Uedaira, *Bull. Chem. Soc. Jap.*, **42**, 2137 (1969).

(7) R. A. Robinson and R. H. Stokes, "Electrolyte Solutions," 2nd ed, Butterworth, London, 1959.

(8) H. D. Ellerton and P. J. Dunlop, *J. Phys. Chem.*, **70**, 1831 (1966).

Table I: Ternary Isopiestic Data at 25° for the System Sodium Benzenesulfonate-Xylose-Water

m_R	m_1	m_2	Δ/m_1m_2		Diff. %
			Exptl	Calcd	
1.1442	0.47565	1.1232	0.05305	0.04863	-0.22
	0.47580	1.1229	0.05312	0.04863	-0.22
	0.85638	0.43927	0.03268	0.04322	+0.51
1.3311	0.69633	1.0331	0.06582	0.04557	-0.85
	0.86457	0.75075	0.03064	0.04285	+0.51
	0.96864	0.55479	0.04387	0.04155	-0.10
1.3829	0.86397	0.84559	0.05261	0.04291	-0.39
1.5132	1.1862	0.49118	0.02470	0.03845	+0.50
	1.1868	0.48869	0.02717	0.03845	+0.41
1.5334	0.94291	0.96596	0.02668	0.04185	+0.55
	0.95645	0.93985	0.02854	0.04161	+0.47
1.7005	1.0495	1.0499	0.04405	0.04020	-0.13
	1.0576	1.0396	0.04003	0.04005	-0.00
1.7525	0.80847	1.5687	0.04786	0.04619	-0.05
	0.80988	1.5660	0.04790	0.04615	-0.06
1.7651	1.0839	1.0849	0.04930	0.03964	-0.30
	1.1026	1.0624	0.03915	0.03928	+0.00
2.2783	1.0309	2.0744	0.05170	0.04534	-0.15
	1.0455	2.0512	0.05029	0.04483	-0.13
	1.7509	0.86879	0.02096	0.02596	+0.12
2.8948	1.7655	0.84308	0.02130	0.02570	+0.11
	1.2703	2.7614	0.03693	0.04605	+0.12
	1.7076	2.0484	0.02783	0.02781	-0.00
	1.7380	2.0006	0.02661	0.02671	+0.00
	1.9724	1.6231	0.02078	0.01889	-0.04
3.2029	2.3339	1.0427	0.01267	0.00920	-0.06
	1.1979	3.4173	0.04501	0.05720	+0.20
	1.7874	2.4741	0.02741	0.02782	+0.01
	2.1693	1.8217	0.03386	0.01280	-0.35

The value of Δ/m_1m_2 is expressed by the following equation

$$\frac{\Delta}{m_1m_2} = A + Bm_1 + Cm_2 + Dm_1^2 + Em_1m_2 + Fm_2^2 \quad (5)$$

By a method similar to that described by Ellerton and Dunlop,⁸ the activity coefficient for the 1-1 electrolyte in the ternary solution is given by

$$\ln \gamma_1 = \ln \gamma_1^\circ + \frac{A}{2}m_2 + \frac{B}{2}m_1m_2 + \frac{C}{4}m_2^2 + \frac{D}{2}m_1^2m_2 + \frac{E}{3}m_1m_2^2 + \frac{F}{6}m_2^3 \quad (6)$$

and that of the nonelectrolyte is given by

$$\ln \gamma_2 = \ln \gamma_2^\circ + Am_1 + \frac{B}{2}m_1^2 + Cm_1m_2 + \frac{D}{3}m_1^3 + \frac{2E}{3}m_1^2m_2 + Fm_1m_2^2 \quad (7)$$

The values of $\ln \gamma_1^\circ$ for NaBS⁵ and $\ln \gamma_2^\circ$ for xylose⁶ and urea⁸ are obtained from data in the indicated references.

Results and Discussion

The isopiestic data for the system NaBS-xylose-water are given in Table I. The first column gives the molality of the reference potassium chloride solution, and the second and third columns give the values of the molalities of NaBS and xylose in the ternary solutions in equilibrium with the reference solution. The values of the experimental quantities Δ/m_1m_2 derived from eq 2 are shown in the fourth column. The fifth column gives the values of Δ/m_1m_2 calculated from a least-squares treatment of eq 5 and Table III. The last column gives the per cent error in the molality of the reference solution which would account for the difference between the experimental and the computed values. This per cent error is defined by⁸

$$\text{diff. } \% = 100 \times \frac{m_R(\text{calcd}) - m_R}{m_R} \quad (8)$$

where

$$m_R(\text{calcd}) = \frac{2m_1\phi_1 + m_2\phi_2 + \Delta(\text{calcd})}{2\phi_R}$$

and $\Delta(\text{calcd})$ is calculated from eq 5 and Table III.

Isopiestic data for the system NaBS-urea-water are shown in Table II with an arrangement similar to that of Table I.

Table II: Ternary Isopiestic Data at 25° for the System Sodium Benzenesulfonate-Urea-Water

m_R	m_1	m_2	Δ/m_1m_2		Diff. %
			Exptl	Calcd	
1.0771	0.62137	0.88802	-0.14499	-0.13576	+0.48
	0.74093	0.63948	-0.15216	-0.13627	+0.82
1.1442	0.52304	1.2243	-0.13341	-0.13422	-0.04
	0.52562	1.2192	-0.13345	-0.13423	-0.04
1.3311	0.62852	1.4046	-0.12169	-0.13116	-0.40
	0.80961	1.0223	-0.11991	-0.13223	-0.51
1.3829	0.66764	1.4559	-0.13672	-0.13007	+0.27
	0.66918	1.4568	-0.14036	-0.13003	+0.42
1.4389	0.93831	1.0004	-0.13182	-0.13057	+0.01
	1.0541	0.74873	-0.13500	-0.13129	+0.14
1.5132	0.79391	1.4758	-0.12729	-0.12786	-0.02
	0.79627	1.4750	-0.13010	-0.12783	+0.08
1.5334	1.0343	1.0153	-0.13689	-0.12891	+0.29
1.7005	1.1339	1.1865	-0.13171	-0.12527	+0.21
	1.1595	1.1196	-0.12616	-0.12559	+0.02
1.7525	1.4457	0.59180	-0.12733	-0.12650	+0.03
1.7651	0.89345	1.8521	-0.12263	-0.12148	+0.04
	0.90442	1.8049	-0.11125	-0.12189	-0.33
	1.2304	1.0759	-0.10145	-0.12481	-0.73
2.2783	1.5889	1.5633	-0.10696	-0.11017	-0.08
	1.5914	1.5606	-0.10784	-0.11015	-0.06
2.3783	0.48261	4.1176	-0.08885	-0.09361	-0.11
	0.95033	3.1805	-0.09286	-0.09870	-0.13
	1.2455	2.5608	-0.09670	-0.10206	-0.12
	1.5305	1.9331	-0.09899	-0.10551	-0.15
	1.9630	0.96927	-0.11084	-0.11024	+0.01
2.6086	1.5445	2.5272	-0.09873	-0.09410	+0.10
	2.0932	1.2843	-0.10485	-0.10143	+0.07
2.6578	1.3537	2.9699	-0.07697	=0.09099	-0.25
	1.7477	2.1800	-0.09412	-0.09480	-0.01
	1.9786	1.6603	-0.09687	-0.09787	-0.02
	2.2007	1.1571	-0.10101	-0.10064	-0.01
3.2029	1.7580	3.6176	-0.07836	-0.06200	+0.27
	2.1255	2.7969	-0.07906	-0.06845	+0.18
	2.4437	2.0762	-0.07975	-0.07378	+0.10

Table III: Coefficients in Eq 5 for Ternary Solutions Sodium Benzenesulfonate-Xylose-Water (I) and Sodium Benzenesulfonate-Urea-Water (II) at 25°

Coefficients	I	II
$A \times 10$	0.49258	-1.4279
$B \times 10^4$	-7.58	-0.86
$C \times 10^4$	-5.11	3.26
$D \times 10^3$	-5.390	5.020
$E \times 10^3$	-4.922	5.841
$F \times 10^3$	3.295	2.070

To reduce the time required for equilibrium to be attained, the concentrations of the ternary and the reference solutions should be prepared so as to be initially fairly close to equilibrium values. Figure 1 gives the plots of m_1 vs. m_2 from the data in Table I. Lines are drawn passing through the points which correspond to the solutions in vapor pressure equilibrium. The points on the ordinate and the abscissa represent the concentrations of binary solutions of NaBS (M_1) and

xylose (M_2), respectively. The concentrations M_1 and M_2 can be calculated from the osmotic coefficient data in the binary solutions. The compositions of solutions in vapor pressure equilibrium, including M_1 and M_2 , lie nearly on a straight line, as was shown by Stokes and Robinson⁹ in the case of no interaction between solutes. That is, the relation $m_1 = am_2 + b$ holds approximately, where a is a constant depending on the system, and b is a constant depending on the sets of isopiestic solutions. Figure 2 shows the relation for the system NaBS-urea-water. The lines are almost parallel in this system too, though they show a slight curvature. Similar parallel lines or slightly curved lines can be drawn for many ternary solutions: sodium chloride-mannitol-water,¹⁰ sodium chloride-urea-water,¹¹ mannitol-sucrose-water,¹² and sucrose-urea-water.⁸

(9) R. H. Stokes and R. A. Robinson, *J. Phys. Chem.*, **70**, 2126 (1966).(10) F. J. Kelly, R. A. Robinson, and R. H. Stokes, *ibid.*, **65**, 1958 (1961).(11) V. E. Bower and R. A. Robinson, *ibid.*, **67**, 1524 (1963).(12) R. A. Robinson and R. H. Stokes, *ibid.*, **65**, 1954 (1961).

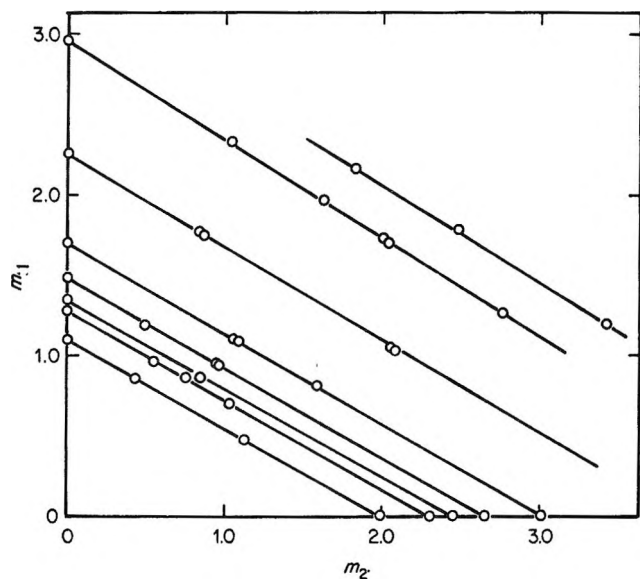


Figure 1. Sodium benzenesulfonate-xylose-water system.

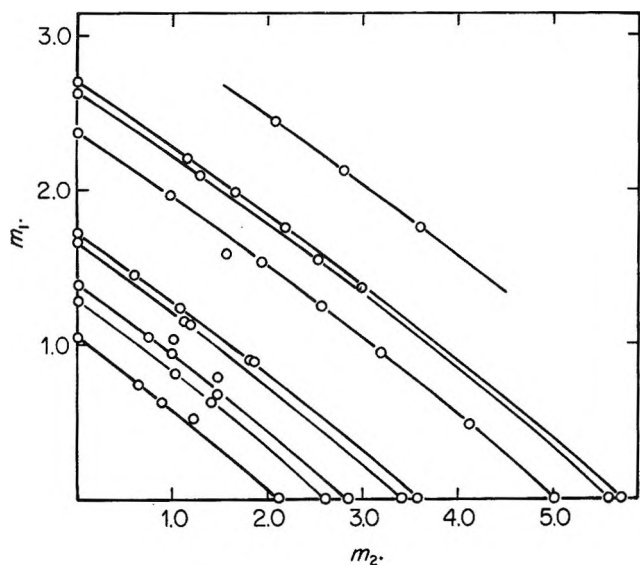


Figure 2. Sodium benzenesulfonate-urea-water system.

Thus the prediction of the composition of the solutions which are in vapor pressure equilibrium is made as follows. The concentration of xylose (M_2), which is in vapor pressure equilibrium with a certain concentration of NaBS (M_1), can be calculated from the osmotic data in binary solutions^{5,6} and the relation $2M_1\phi_1 = M_2\phi_2$. The values of M_1 and M_2 are plotted on both axes, and a straight line is drawn through M_1 and M_2 . The solutions, the compositions of which are represented by the arbitrary points on this line, are approximately in vapor pressure equilibrium with each other. At higher concentrations where the value of ϕ_1 or ϕ_2 at M_1 or M_2 is not available, the line corresponding to the solutions in vapor pressure equilibrium is obtained by parallel displacement of the line at lower concentration.

The coefficients of eq 5, which are calculated from the

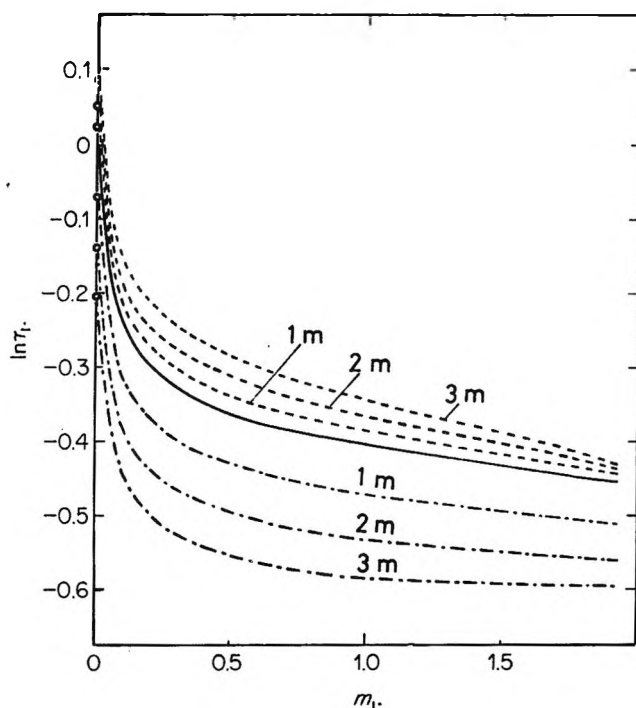


Figure 3. Activity coefficients of sodium benzenesulfonate in xylose and urea solutions: —, in water; ---, in xylose solution; - · - ·, in urea solution, at several concentrations of xylose or urea.

experimental values of Δ/m_1m_2 by the method of least squares, are given in Table III for both systems NaBS-xylose-water and NaBS-urea-water. An IBM 7090 computer was used for the calculations. Substituting the numerical values into eq 6 and 7, we have

$$\ln \gamma_1 = \ln \gamma_1^\circ + 0.02463m_2 - 0.00038m_1m_2 - 0.000128m_2^2 - 0.002695m_1^2m_2 - 0.001641m_1m_2^2 + 0.000549m_2^3 \quad (9)$$

$$\ln \gamma_2 = \ln \gamma_2^\circ + 0.04926m_1 - 0.000379m_1^2 - 0.000511m_1m_2 - 0.001797m_1^3 - 0.003281m_1^2m_2 + 0.003295m_1m_2^2 \quad (10)$$

for the system NaBS-xylose-water, and

$$\ln \gamma_1 = \ln \gamma_1^\circ - 0.07139m_2 - 0.000043m_1m_2 + 0.000081m_2^2 + 0.002510m_1^2m_2 + 0.001947m_1m_2^2 + 0.000345m_2^3 \quad (11)$$

$$\ln \gamma_2 = \ln \gamma_2^\circ - 0.14279m_1 - 0.000043m_1^2 + 0.000326m_1m_2 + 0.001673m_1^3 + 0.003895m_1^2m_2 + 0.002070m_1m_2^2 \quad (12)$$

for the system NaBS-urea-water.

Figure 3 shows the activity coefficients of NaBS in binary solution, and in ternary solutions containing several concentrations of urea or xylose. Xylose in-

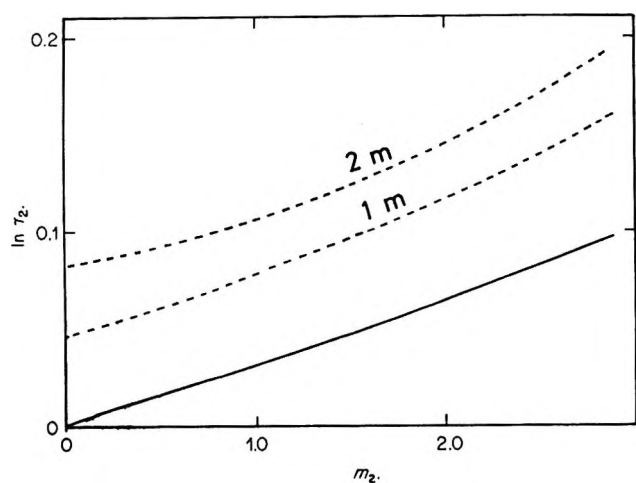


Figure 4. Activity coefficients of xylose in sodium benzenesulfonate solution: —, in water; - - -, in sodium benzenesulfonate solution at several concentrations of the salt.

creases the value of the activity coefficient of NaBS, and urea decreases it.

The activity coefficient of xylose is plotted against the concentration of xylose in Figure 4. Added NaBS increases the activity coefficient of xylose.

The activity coefficient of xylose in aqueous binary solution increases with concentration and is greater than unity.⁶ The hydration number of xylose can be calculated from eq 3 by the method of Robinson and Stokes,¹² and the value is 1.3. Water molecules around xylose are bound, and xylose can be regarded as a structure maker.

In addition, it was shown that BS^- ion is a strong structure breaker from the temperature dependence of ionic mobility³ and the spectral data.¹³ As Na^+ ion is a weak structure maker,^{4,14} NaBS must behave as structure-breaking solute. Thus, NaBS breaks the hydrogen bond between water molecules and increases the concentration of "free water." According to Samoilov's salting-out theory,¹⁵ the breakup of water structure by structure-breaking ions leads to stronger hydration of the structure-making solute. Thus, a molecule of xylose binds water molecules much more in NaBS solution than in aqueous solution, and the activity coefficient of xylose in NaBS increases with increasing concentration of NaBS.

The activity coefficients of urea are shown in Figure 5. The effect of sodium chloride¹¹ and NaBS on the values of activity coefficients of urea is shown also. As the cation of sodium chloride and NaBS is common, the difference in the effect on the activity coefficient of urea is caused by the difference in the action of the anions. The formation of a complex of urea and BS^- ion would decrease the activity coefficient of urea in

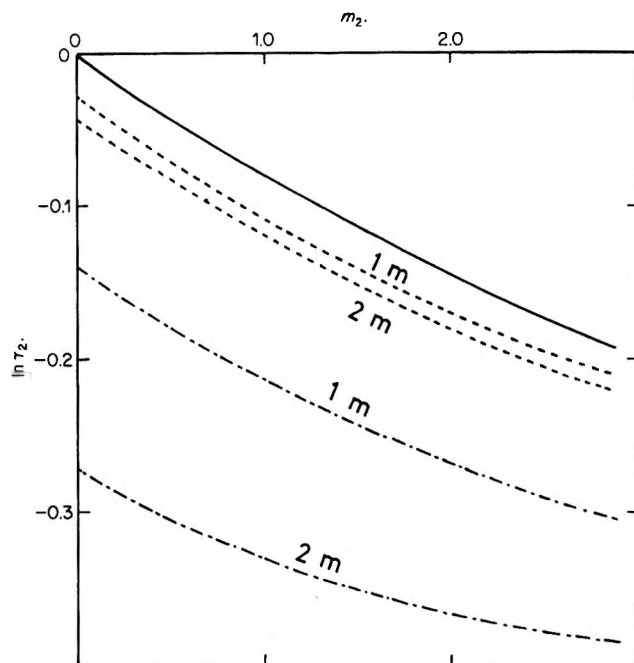


Figure 5. Activity coefficients of urea in sodium benzenesulfonate and sodium chloride solutions: —, in water; - - -, in sodium benzenesulfonate solution; - · -, in sodium chloride solution, at several concentrations of the salts.

ternary solution; however, such a complex may not be formed.

The change in water structure by solute must be considered also in the ternary solution NaBS-urea-water. BS^- ion behaves as a stronger structure breaker than Cl^- ion. The triangular shape of urea prevents it from entering into the four-coordinated clusters, with their tetrahedral bonding, and breaks the structure of water.¹⁶ Both BS^- ion and the urea increase the concentration of "free water." In this case, the activity coefficient of urea in NaBS decreases with increasing concentration of NaBS, and likewise, that of NaBS decreases on adding urea, as suggested by Samoilov¹⁶ and Frank.¹⁷ It is shown from Figure 5 that their theory can be extended to a system containing nonelectrolytes. In addition, the figure shows that the stronger the structure-breaking effect of the ion, the greater the decrease in activity coefficient of urea caused by addition of the ion.

(13) O. D. Bonner, *J. Phys. Chem.*, **72**, 2512 (1968).

(14) H. S. Frank and M. W. Evans, *J. Chem. Phys.*, **13**, 507 (1945).

(15) O. Ya. Samoilov, V. I. Tikhomirov, V. P. Ionov, and A. A. Kuznetsova, *Radiokhimiya*, **1**, 14 (1961); O. Ya. Samoilov, *Zh. Strukt. Khim.*, **7**, 15, 175 (1966); O. Ya. Samoilov, "Sostoyanie i Rol' Vodui v Biologicheskiv Obiektov," Nauka, Moscow, 1967.

(16) H. S. Frank, *Fed. Proc.*, **S24**, 1 (1965).

(17) H. S. Frank, *J. Phys. Chem.*, **67**, 1554 (1963).

Acidity Measurements at Elevated Temperatures. IV. Apparent

Dissociation Product of Water in 1 *m* Potassium Chloride up to 292°¹

by R. E. Mesmer, C. F. Baes, Jr., and F. H. Sweeton

Reactor Chemistry Division, Oak Ridge National Laboratory, Oak Ridge, Tennessee 37830 (Received October 27, 1969)

An apparatus for measurement of acidities at elevated temperatures is described which employs a hydrogen-hydrogen ion concentration cell in a Teflon-lined vessel. Nernst behavior to high precision was demonstrated at 150°. The apparatus was used to measure the apparent dissociation quotient of water (Q_w') assuming complete dissociation of KOH and HCl in 1 *m* KCl from 50 to 292°. The results at 50° agree with the best published data to 0.01 log unit and the values range from -13.01 at 50° to -10.04 at 292°. The data are represented within experimental error by the equation $\log Q_w' = -(5909.13/T) + 0.007279T - 27.3973 \log T + 71.6761$. Differences between these values and values of $\log K_w$ reported by Noyes and coworkers from early conductance measurements are discussed in terms of activity coefficients, possible association of KOH and HCl, and the uncertainty in conductance measurements.

Introduction

In previous studies of this series, the hydrolysis behavior of metal ions in aqueous solutions up to 95° was reported.² The extension of such studies to much higher temperatures is of interest from a fundamental as well as practical view. There are presently no techniques available, however, for measurements with the precision needed for identification of hydrolytic species in solution from potentiometric data at temperatures above 100°.

The utility of glass electrodes is limited to temperatures below about 150° because of the rate of attack of acids and particularly bases.^{2a} Hydrogen electrodes, in spite of the chemical reactivity of hydrogen, might provide the best means for accurate measurements of acidity since many of the metal ions are stable in hydrogen, and hydrogen electrodes have already been shown to function at high temperatures and pressures. Hainsworth, *et al.*,^{3a} have employed hydrogen electrodes up to 1000 atm at 25° and Lietzke and his coworkers^{3b-3f} have employed hydrogen electrodes in combination with silver halide electrodes to determine the thermodynamic properties of HX-MX_n mixtures up to 275°. In cells of the type Pt, H₂|HCl(*m*)|AgCl, Ag, where low pressures of H₂ were used, Lietzke, *et al.*, observed a small amount of the reaction



which gave rise to drifts that had to be corrected for in solutions of HCl from 0.01 *m* to 1.0 *m* and at temperatures greater than about 150°.

We have developed a hydrogen electrode concentration cell which is intended for precise measurements of acidity to 300°. An initial application of this apparatus has been a determination of the apparent concentration product for the dissociation of water (Q_w') in 1 *m*

KCl within the temperature range 60–300°. The word apparent is used (and Q_w' is primed) to indicate that the evaluation of this product is made with the assumption that KOH and HCl are completely dissociated electrolytes under the conditions of the measurements. The relationship between Q_w' and K_w is

$$K_w = Q_w' \frac{\gamma_{\text{H}}\gamma_{\text{OH}}}{a_w} \quad (2)$$

where a_w is the activity of water and γ_{H} and γ_{OH} are the stoichiometric activity coefficients.

At the present time the dissociation constant for water as well as the apparent dissociation product in salt media are well defined by results of Harned and his coworkers⁴ up to 60°. The only high-temperature studies carried out between 100 and 300° at the saturation pressures were the early conductance work of Noyes, *et al.*,⁵ and the recent similar work by Fisher.⁶ Both measured the hydrolysis of ammonium acetate. The uncertainty of this method has not been assessed but is expected to be relatively high judging from the poor reproducibility in the two studies, particularly below 200°.

(1) Research sponsored by the U. S. Atomic Energy Commission under contract with Union Carbide Corp.

(2) (a) C. F. Baes, Jr. and N. J. Meyer, *Inorg. Chem.*, **1**, 780 (1962); (b) C. F. Baes, Jr., N. J. Meyer, and C. E. Roberts, *ibid.*, **4**, 518 (1965); (c) R. E. Mesmer and C. F. Baes, Jr., *ibid.*, **6**, 1951 (1967).

(3) (a) W. R. Hainsworth, H. J. Rowley, and D. A. MacInnes, *J. Amer. Chem. Soc.*, **46**, 1437 (1924); (b) M. H. Lietzke, *et al.*, *J. Phys. Chem.*, **64**, 652 (1960); (c) *ibid.*, **64**, 1445 (1960); (d) *ibid.*, **64**, 1861 (1960); (e) *ibid.*, **68**, 3043 (1964); (f) *ibid.*, **69**, 2395 (1965); (g) *ibid.*, **70**, 756 (1966); (h) *ibid.*, **71**, 662 (1967).

(4) H. S. Harned and B. B. Owen, "The Physical Chemistry of Electrolytic Solutions," Van Nostrand-Reinhold Co., Princeton, N. J., 1958, pp 633–696.

(5) A. A. Noyes, Y. Kato, and R. B. Sosman, *J. Amer. Chem. Soc.*, **32**, 159 (1910).

(6) J. R. Fisher, Thesis, "The Ion-Product Constant of Water to 350°C," Pennsylvania State University, June, 1969.

Recently, Marshall and Quist of this laboratory have estimated the ionization constant of water up to 800° and 4000 bars from conductance data on ammonium bromide solutions.⁷ The data do not extend below about 300° but they are in approximate agreement with those of Noyes, *et al.*

Experimental Section

Materials. A stock solution of 3.3 *M* KCl prepared from J. T. Baker analyzed reagent was acidified to pH 3.5 and purged with N₂ to remove CO₂. The fluoride content of the neutralized stock was 7×10^{-6} *m* as determined by the lanthanum fluoride electrode. The protolytic impurities in a 1 *m* solution made from the stock were $<10^{-6}$ *m* as determined by titration near the end point.

Ultrahigh purity hydrogen (99.999%) from the above manufacturer was used. Reagent KOH was analyzed for CO₂ and then CO₂ was removed by precipitation with a slight excess of Ba(OH)₂. Certified Fisher reagent HCl was used and all acid and base solutions were stored under N₂ in polyethylene-lined vessels.

Apparatus. The potentiometric cell employed in this study is illustrated in Figure 1. It consists of a heavy walled pressure vessel containing two Teflon compartments, joined by a liquid junction and each containing a hydrogen electrode. Hastelloy B was chosen as the material of construction because of its general resistance to corrosion—particularly stress corrosion cracking—and its resistance to hydrogen embrittlement. The concentric Teflon compartments were machined with 1–2 mm wall thickness to minimize temperature equilibration times. The inner compartment is suspended from a threaded Teflon cap and it contains a 2.5-mm diameter plug of porous Teflon pressed into a hole at the bottom which provides the liquid junction between the solutions. Because the plug must be compressed to provide a suitably slow leak rate (*ca.* 0.002 ml/cm head of water/hr) and because the Teflon is not wetted, the flow must be initiated by applying a small pressure before assembling the apparatus. Considerable difficulty was experienced with interruption of flow at high temperatures whenever the Teflon was compressed excessively.

Agitation in both compartments was provided by means of magnetic stirring bars driven by a large Alnico permanent magnet located below the oil bath. The temperature of the bath was controlled usually to $\pm 0.1^\circ$ with mercury regulators and was monitored with mercury thermometers calibrated against a platinum resistance thermometer to $\pm 0.1^\circ$.

Chromel–alumel thermocouples encased in 0.020-in. platinum tubing insulated with MgO were placed in both compartments. The platinum tips were platinized lightly (by electrodeposition for 10 sec at 10 mA) to double as the electrodes. This reduced the number of

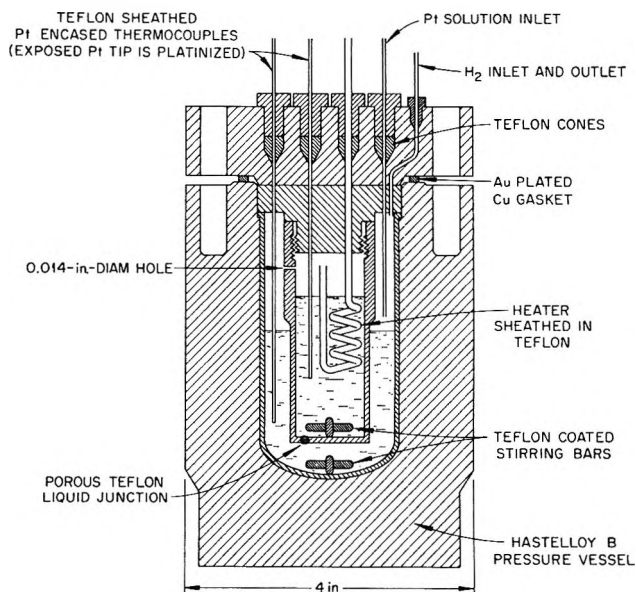


Figure 1. Emf apparatus for high-temperature acidity measurements.

openings through the top of the pressure vessel. The difference of the emf of the thermocouples was fed to a Leeds and Northrup control unit set to maintain zero emf during the heat-up operation. Heat could be applied to the internal compartment through a nichrome heating element (26 Ω) encased in 0.045-in. monel tubing insulated with MgO and sheathed with shrinkable Teflon to provide electrical insulation as well as chemical inertness. The thermocouples and heater were supplied by American Standard. With this setup the temperature difference could be held to 0.4° even with rapid heating rates. Distillation was negligible in these experiments since the temperature differences were minimal during the heat-up and the gas phases were connected only through a 0.014-in. hole. Also a 500 psi overpressure of hydrogen were used to minimize such transfer. In experiments up to 250° the loss of weight of both compartments was less than 0.6%. Only at 292° was the rate of transfer of HCl observed to be significant. This was observed as a drift in the potential which was extrapolated to zero time at this temperature, and also the change in composition of the solutions was verified by titration after the apparatus was cooled.

We could find no evidence for significant contamination of the solutions due to the Teflon. After an extended series of measurements at temperatures up to 292°, analysis of the fluoride content of the compartment by means of the lanthanum fluoride electrode⁸ showed

(7) A. S. Quist and W. L. Marshall, Reactor Chemical Division Annual Report, 1968, ORNL-4400. Clearinghouse for Federal Scientific and Technical Information, National Bureau of Standards, Springfield, Va.

(8) R. E. Mesmer, *Anal. Chem.*, **40**, 443 (1968).

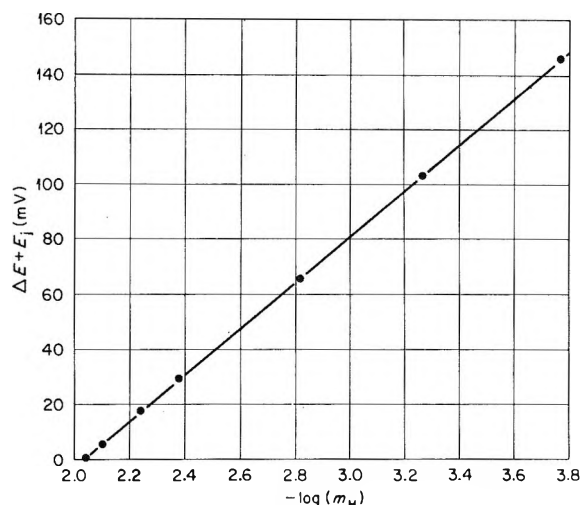


Figure 2. Nernst behavior of hydrogen electrodes at 150° in 1 *m* KCl. Slope = 83.94 mV.

only 4×10^{-5} *M* fluoride in the base compartment and only 4×10^{-6} *M* fluoride in the acid compartment.

In the titration experiment shown in Figure 2 the titrant base was stored in a titanium vessel and was displaced by Hg driven by a calibrated pressure generator from High Pressure Equipment Co. The titrant was transmitted through titanium tubing and valves and a segment of platinum tubing which passed through the oil bath for preheating before addition.

A Cary vibrating reed electrometer Model 31 was used to measure the difference in emf of the cell and that output from a K-3 potentiometer. The voltage was recorded until a constant value was obtained and was measured to about 0.05 mV.

The hydrogen pressure, although the information is not needed in the calculations for cell III below, was measured by means of a Heise gauge.

The cell was checked for any thermal emf due to possible slight differences in the composition of the electrode leads or other bias at temperature by carrying out experiments with 0.01 *m* HCl in 1 *m* KCl in both compartments. The maximum difference attained was 0.19 mV up to 250°. No correction was made for this effect since in no case was it equivalent to a change of more than 0.5% in the acid concentration.

Procedures. The electrodes were replatinized just before each run and the air in the cell was removed after assembling the apparatus by successively pressurizing with hydrogen to 500 psi and venting three times.

For the measurement of Q_w' about 50 g of 0.008245 *m* KOH in 1.00 *m* KCl was placed in the larger outer compartment and 21 g of 0.00917 *m* HCl in 1.00 *m* KCl was placed in the inner compartment. The direction of flow under these conditions was from the inner compartment to the outer compartment.

For the first equilibration 2 hr was required to reach a constant potential and for the subsequent equili-

brations about 1–1.5 hr was required including the time used in raising the temperatures. Measurements were made for successively increasing temperatures in several experiments over different temperature intervals. In one case after measurements were made at 200° the temperature was lowered to 100° to repeat the measurements. The emf values obtained in both directions agreed within 0.5 mV. However, data were generally not taken after lowering the temperature because often the liquid junction flow is interrupted during cooling, and the Teflon seals begin to leak after cooling 50–100°. Also, the apparatus was not designed to maintain the same temperature in the two compartments during cooling. The data are summarized in Table I.

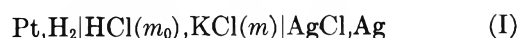
Table I: Voltage of Cell III and Apparent Ion Product of Water in 1 *m* KCl

Temp, °K	ΔE , V	$\log Q_w'^a$	P_{total} , psi
322.89	0.56902	-13.010	505
372.80	0.57608	-11.915	588
423.12	0.59114	-11.168	708
472.69	0.61295	-10.662	896
524.01	0.64110	-10.292	1214
565.18	0.66350	-10.043	1600
372.69	0.57577	-11.913	577
473.96	0.61320	-10.648	886
372.60	0.57510	-11.906	535
322.99	0.56915	-13.009	498
323.07	0.56948	-13.012	504
373.00	0.57610	-11.911	587
424.07	0.59140	-11.155	705
472.91	0.61280	-10.657	886
524.31	0.64060	-10.284	1196

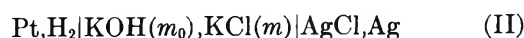
^a From eq 8.

Results and Discussion

The ion product of water in KCl solutions was carefully measured over the temperature interval 0–60° by Harned and Hamer⁹ using the following cells without liquid junction



and



Values of the dissociation constant of water (K_w) were derived from the potential of cell II, (E_{II}), and the standard potential of cell I

$$\ln K_w + \ln \left[\frac{\gamma_{\text{Cl}} a_{\text{H}_2\text{O}}}{\gamma_{\text{OH}}} \right] = (E_{\text{I}}^0 - E_{\text{II}}) \frac{F}{RT} - \ln \left(\frac{m_{\text{Cl}}}{m_{\text{OH}}} \right) \quad (3)$$

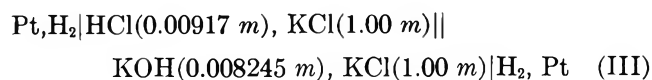
(9) H. S. Harned and W. J. Hamer, *J. Amer. Chem. Soc.*, **55**, 2194 (1933).

K_w was also derived from the difference between the potentials of cells I and II when the cells contained 0.01 m HCl and KOH and equal concentrations of KCl where

$$\ln K_w - \ln (\gamma_{H(I)}\gamma_{OH(II)}/a_{H_2O}) = \ln Q_w' = (E_I - E_{II})\frac{F}{RT} + \ln [m_{H(I)}m_{OH(II)}] \quad (4)$$

These determinations were made by appropriate extrapolations *vs.* ionic strength to infinite dilution. With K_w determined, values of the quantity $(\gamma_H\gamma_{OH}/a_{H_2O})$ then could be obtained from eq 4 as a function of the electrolyte composition.

The cell we chose



eliminates the difficulty encountered with such cells due to the reduction of AgCl by H₂ at elevated temperatures.

Liquid junction potentials in cells of this kind can be estimated^{2a-c} using the Henderson equation in the form pertaining to solutions of nearly constant composition, *i.e.*

$$E_j = \sum D_i([i]_1 - [i]_2) \quad (5)$$

where $[i]_1$ and $[i]_2$ denote, respectively, the actual (molal) concentrations of species i on the left and right sides of cell III, and where¹⁰

$$D_i = RT|Z_i|\lambda_i / (Z_i F \sum (|Z_i|[i]\lambda_i)) \quad (6)$$

and λ_i is the equivalent conductance of the i th ion. Values of λ_i have been reported for K⁺, Cl⁻, H⁺, and OH⁻ by Quist and Marshall¹¹ up to 400° at the saturation vapor pressure. The variation of conductance with density, known from their work, was neglected at the low pressures involved in this study.

The potential of cell III then is given by

$$\Delta E = \frac{RT}{F} \ln \left[\frac{[H^+]_1}{[H^+]_2} \right] - \sum D_i([i]_1 - [i]_2) \quad (7)$$

Assuming complete dissociation of KCl, KOH, and HCl, introducing stoichiometric concentrations and introducing $Q_w' = m_H m_{OH}$

$$\Delta E = \frac{RT}{F} \ln \left[\frac{m_{H,1} m_{OH,2}}{Q_w'} \right] - \sum D_i(m_{i,1} - m_{i,2}) \quad (8)$$

The low concentrations of acid and base were chosen to minimize the contribution of the liquid junction potential. The magnitude of these potentials calculated from eq 5 at 50, 100, 150, 200, 250, and 300° are 0.48, 0.46, 0.45, 0.46, 0.47, and 0.50 mV, respectively. These values are equivalent to 0.008 and 0.004 unit in $\log Q_w'$, respectively, at 50 and 300°.

The performance of the cell in accordance with the theoretical behavior predicted by eq 7 was evaluated

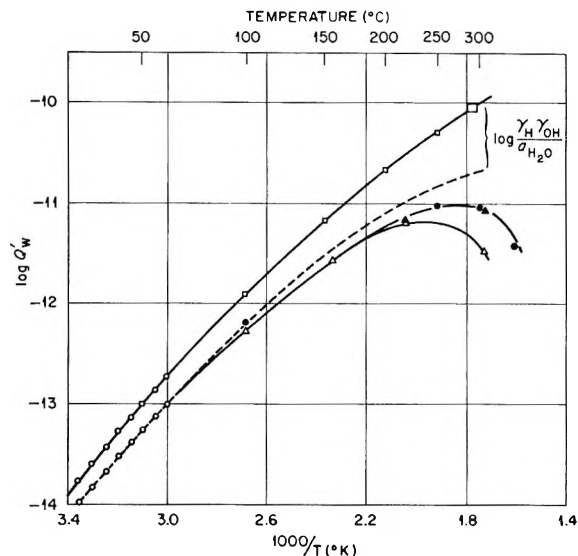


Figure 3. Experimental data on apparent dissociation product of water in 1 m KCl (molal units): \square , present data; \circ , data of Harned and Hamer in 1 m KCl and at infinite dilution; Δ , conductance data of Noyes, *et al.*; \bullet , Conductance data of Fisher; \blacktriangle , data of Noyes, *et al.*, recalculated by Fisher; ---, curve representing K_w based on our results and extrapolated values of $\gamma_H\gamma_{OH}/a_{H_2O}$ from eq 9.

at 149.9° by an experiment in which the acid concentration in one compartment was varied by adding base while the other was kept constant at 0.00917 m in 1 m KCl. The results are summarized in Figure 2 where the slope drawn is the theoretical Nernst slope 83.94 mV. In this experiment the total pressure was 500 psi. In this titration the maximum difference between the calculated (eq 7) and the stoichiometric acidities was $3 \times 10^{-5} m$, which represents an error of less than 0.5% in the original acidity (0.00917 m).

The assumption of complete dissociation of electrolytes was also made in the work of Harned and Hamer⁹ which enables us to make a comparison with our data on $\log Q_w'$ at 1.0 m KCl at 50° where the two studies overlap. The value obtained by Harned and Hamer is -13.007 at 50°. We have obtained values of -13.010 at 49.7°, -13.009 at 49.8°, and -13.012 at $49.9 \pm 0.1^\circ$. The work of Owen and Brinkley¹² shows that the ionization constant increases slightly with pressure and the relative increase is greater the lower the temperature. The calculated effect at 50° of the 500 psi overpressure in our cell is 0.009 log unit. The agreement of our data with those of Harned and Hamer is about 0.01 log unit, which appears to be about the experimental error in either study.

(10) In the previous papers (ref 1) in which this expression was used, the $|Z_i|$ terms were erroneously omitted. This error generally was of little consequence since the calculated values of D_i for monovalent ions were unaffected and the values of D_i actually were determined by experiment wherever possible.

(11) A. S. Quist and W. L. Marshall, *J. Phys. Chem.*, **69**, 2984 (1965).

(12) B. B. Owen and S. R. Brinkley, Jr., *Chem. Rev.*, **29**, 461 (1941).

The values for $\log Q_w'$ calculated from eq 8 are given in Table I. These are compared in Figure 3 with the original values of Noyes, *et al.*, for $\log K_w$, with values of Fisher, with values of Noyes, *et al.*, recalculated by Fisher, and finally with values of Harned and Hamer for $\log K_w$ and $\log Q_w'$ to 60°. The activity coefficient term ($\gamma_H\gamma_{OH}/a_w$) needed to relate Q_w' to K_w' has been given by Harned and Cook¹³ in terms of the following relationship

$$\log \frac{\gamma_H\gamma_{OH}}{a_{H_2O}} = -\frac{2S\sqrt{I}}{1+A\sqrt{I}} + BI + CI^{3/2} \quad (9)$$

where $S = 1.814 \times 10^6/(DT)^{3/2}$ and $A = 50.30a/(DT)^{1/2}$. Here a is a temperature-independent parameter taken as 3.6 for KCl and B and C are assumed to have linear dependences on temperature (t°). The following values for B and C reproduce experimental data to 1/2 to 1% up to 3 *m* KCl and 60°.

$$B = 0.266 + 5.2 \times 10^{-4}t$$

$$C = -0.0350 - 4.88 \times 10^{-4}t$$

The dashed curve in Figure 3 represents the calculated values of $\log K_w$ derived from the present Q_w' values and the extrapolated values of the quotient ($\gamma_H\gamma_{OH}/a_{H_2O}$) obtained from eq 9. The uncertainty in this estimate of K_w obviously increases rapidly with increasing temperature because of the lengthening extrapolation of eq 9—an expression which, moreover, may become an unsuitable representation of the behavior of γ_H and γ_{OH} if there is appreciable association of KOH and HCl with increasing temperature. The discrepancy between the present (dashed) curve for K_w and the results of Noyes, *et al.*, and Fisher therefore is not necessarily significant.

Association of KOH and HCl. It is important to emphasize that the definition of Q_w' is based on the assumption of complete ionization of the KOH, HCl, and KCl. There is evidence that KOH is slightly associated even at room temperature.¹⁴ If one considers the order of the arrangement of $\log \gamma_{\pm}$ vs. \sqrt{I} curves for the alkali metal halides as the normal order, then the reverse order which is found for the alkali hydroxides could be attributed to ion association. This was interpreted in terms of "localized hydrolysis" to form ion pairs by Harned and Robinson.¹⁴ If indeed there is ion association of KOH at any temperature then corrections can be made for this effect on $\log Q_w'$ whenever such information becomes available (*cf.* eq 10 below).

Likewise, the HCl may become significantly associated at some elevated temperature. The vapor pressure data on HCl solutions have been interpreted by Robinson¹⁶ in terms of the amount of association of HCl and this is extremely small below 50° (the association constant was 10^{-5}). Pearson, *et al.*,¹⁶ have

estimated $\log K$ values of about 3 in the vicinity of the critical point. Also, E. U. Franck¹⁷ has derived association constants for HCl and KOH from conductance data at 400–700° and at high pressures. The isothermal equivalent conductances of both HCl and KOH solutions when measured as a function of density reach a maximum in the vicinity of 300°. There are, however, no reliable estimates of the dissociation of KOH and HCl up to 300°.

The effect of association of either HCl or KOH on $\log Q_w'$ can be approximated by

$$\log Q_w = \log Q_w' -$$

$$\log(1 + Q_{KOH}m_{K^+}) - \log(1 + Q_{HCl}m_{Cl^-}) \quad (10)$$

where Q_{KOH} and Q_{HCl} are the association quotients for KOH and HCl, respectively.

An evaluation of these effects may result from experiments currently in progress in which the dissociation product of water will be measured as a function of concentration in a high-temperature flowing cell designed to operate at low concentrations.

Apparent Ion Product of Water. The data in Table I and ref 9 were fit with the three expressions in Table II derived on the basis of three different assumptions for the ΔC_p , for the reaction: (I) that ΔC_p is constant, (II) that ΔC_p is proportional to temperature, and (III) that ΔC_p is linearly related to the temperature. The equations and the coefficients derived by least-squares analysis along with their agreement factors¹⁸ are given in Table II.

In our experiments we estimate the errors to be equivalent to about 0.01 log unit in $\log Q_w'$ at 250° and below, and about 0.04 log unit at 292°. The errors assigned to the data of ref 9 were 0.005 log unit for the above calculations.

In view of the better fits of cases I and III we have calculated the thermodynamic parameters based on these two assumptions for ΔC_p and the results are shown in Table III. It is noteworthy that the values obtained for ΔH and ΔS are not greatly affected by the assumption regarding ΔC_p . It should be emphasized,

(13) H. S. Harned and M. A. Cook, *J. Amer. Chem. Soc.*, **59**, 2304 (1937).

(14) R. A. Robinson and H. S. Harned, *Chem. Rev.*, **28**, 419 (1941).

(15) R. A. Robinson, *Trans. Faraday Soc.*, **32**, 743 (1936).

(16) D. Pearson, C. S. Copeland, and S. W. Benson, *J. Amer. Chem. Soc.*, **85**, 1047 (1963).

(17) E. U. Franck, *Z. Phys. Chem.* (Frankfurt am Main), **88**, 192 (1956).

(18) The agreement factor is computed by the relationship

$$\sigma(\log Q_w') = \left| \frac{\sum W(\log Q_{w,o}' - \log Q_{w,v}')^2}{N_o - N_v} \right|^{1/2} \quad (11)$$

where the numerator is the sum of the weighted squares of the differences in the observed and calculated values for $\log Q_w'$ and N_o and N_v are the number of observations and the number of variables, respectively. This quantity is the ratio of the calculated standard error to the estimated error.

Table II: Equations Expressing Temperature ($^{\circ}\text{K}$) Dependence of $\log Q_w'$ Based on Three Assumptions for ΔC_p

I. $\Delta C_p = B$; $\sigma(\log Q_w') = 0.81$
$\log Q_w' = \frac{-4883.26}{T} - 14.6585 \log T + 38.8840$
II. $\Delta C_p = -CT$; $\sigma(\log Q_w') = 1.56$
$\log Q_w' = \frac{-3694.36}{T} - 0.008316T + 1.1011$
III. $\Delta C_p = -B - CT$; $\sigma(\log Q_w') = 0.39$
$\log Q_w' = -\frac{5909.13}{T} + 71.6761 + 0.007279T - 27.3973 \log T$

however, that these values which are based on the assumption of complete dissociation of all the electrolytes, may be considerably altered when the effects of such association are included.

Table III: Tabulation of Thermodynamic Parameters Derived for the Apparent Ionization of Water

Temp, $^{\circ}\text{C}$	ΔH , kcal, mol $^{-1}$	ΔS , cal mol $^{-1}$ deg $^{-1}$	ΔC_p , cal mol $^{-1}$ deg $^{-1}$
$\Delta C_p = B$			
50	12.93 ± 0.02	-19.52 ± 0.07	-29.1 ± 0.36
100	11.47 ± 0.01	-23.72 ± 0.03	-29.1 ± 0.36
150	10.02 ± 0.02	-27.38 ± 0.05	-29.1 ± 0.36
200	8.56 ± 0.04	-30.63 ± 0.09	-29.1 ± 0.36
250	7.11 ± 0.06	-33.56 ± 0.12	-29.1 ± 0.36
300	5.56 ± 0.07	-36.22 ± 0.15	-29.1 ± 0.36
$\Delta C_p = -B - CT$			
50	12.92 ± 0.01	-19.53 ± 0.03	-32.9 ± 0.5
100	11.36 ± 0.01	-24.03 ± 0.04	-29.6 ± 0.2
150	9.96 ± 0.01	-27.55 ± 0.03	-26.3 ± 0.4
200	8.73 ± 0.03	-30.30 ± 0.06	-22.9 ± 0.7
250	7.67 ± 0.07	-32.43 ± 0.14	-19.6 ± 1.1
300	6.78 ± 0.13	-34.07 ± 0.25	-16.3 ± 1.4

Behavior of Electrolytes in Propylene Carbonate. II. Further Studies of Conductance and Viscosity Properties. Evaluation of Ion Conductances^{1a}

by L. M. Mukherjee,^{1b}

Chemistry Department, Illinois State University, Normal, Illinois 61761

David P. Boden, and Richard Lindauer

Chemistry Department, Polytechnic Institute of Brooklyn, Brooklyn, New York 11201 (Received January 5, 1970)

Conductance and viscosity characteristics of solutions of (*i*-Am)₄N(*i*-Am)₄B, (*i*-Am)₄NI, KI, and KClO₄ in propylene carbonate have been investigated at 25°. The value of Λ° of (*i*-Am)₄N(*i*-Am)₄B and those of transference number of ClO₄⁻ and Li⁺ as determined using concentration cells have been utilized in obtaining the conductance of Li⁺, K⁺, Et₄N⁺, *n*-Bu₄N⁺, and (*i*-Am)₄N⁺ as well as Cl⁻, Br⁻, I⁻, ClO₄⁻, and (*i*-Am)₄B⁻.

Introduction

In a previous article,² results of conductance and viscosity measurements of certain lithium and quaternary ammonium salts in propylene carbonate (PC) were reported. Although the conductances of the anions do not appear to differ appreciably, comparison of the limiting conductances of the perchlorates, for instance, suggests that the mobility of Li⁺ is noticeably lower than that of *n*-Bu₄N⁺ and Et₄N⁺. Moreover, the viscosity F coefficients of the same series of salts were found to follow the order: LiClO₄ > *n*-Bu₄NClO₄ > Et₄NClO₄. Thus, in all probability the relative

sizes of these three cations are: Li⁺ > *n*-Bu₄N⁺ > Et₄N⁺, indicating that the lithium ions in PC are substantially solvated. It is of further interest to note in this connection that unlike the quaternary ammonium salts the agreement between the sums of crystallographic radii and the a^0 parameters for the lithium salts² is generally good.

(1) (a) Based on a Ph.D. thesis to be submitted by D. P. Boden to the Graduate School of the Polytechnic Institute of Brooklyn, Brooklyn, N. Y.; (b) to whom all correspondence should be addressed.

(2) L. M. Mukherjee and D. P. Boden, *J. Phys. Chem.*, **73**, 3965 (1969).

On this basis, it was surmised that for the lithium salts bare ions rather than their solvated cospheres would be involved in the event of ion-ion contacts.

In the light of the above considerations, subsequent studies in PC of the conductance and viscosity characteristics of electrolytes containing very large cations seem especially interesting. In the present work the quaternary ammonium salts $(i\text{-Am})_4\text{N}(i\text{-Am})_4\text{B}$ and $(i\text{-Am})_4\text{NI}$ have been considered suitable for such studies. An additional advantage in using $(i\text{-Am})_4\text{N}(i\text{-Am})_4\text{B}$ is that in this case the cation and the anion are practically of the same size so that their mobilities can be assumed equal. The results of conductance measurements on $(i\text{-Am})_4\text{N}(i\text{-Am})_4\text{B}$ can be combined with those of $(i\text{-Am})_4\text{NI}$ for obtaining the conductance of the iodide ion. With a view to relate these systems to the ones studied previously² two additional electrolytes, *viz.*, KI and KClO_4 , have also been investigated in the present work. Furthermore, as a verification of the ion conductances derived in this manner, the determination of transference number of perchlorate ion using cell I: $\text{Li}(\text{Hg}), 2 \text{ mole } \%, \text{LiClO}_4(\text{C}_1) | \text{LiClO}_4(\text{C}_2) / \text{Li}(\text{Hg}), 2 \text{ mole } \%$, has also been resorted to in this investigation.

Theory

The plots of the equivalent conductance *vs.* the square root of molar concentration for $(i\text{-Am})_4\text{N}(i\text{-Am})_4\text{B}$, $(i\text{-Am})_4\text{NI}$, KI, and KClO_4 lie above the corresponding limiting tangents. Using this as a criterion for the absence of association,² the data for these systems were treated according to the procedure of Fuoss and Accascina,³ using the equation

$$\Lambda = \Lambda^\circ - SC^{1/2} + EC \log C + JC - F\Lambda^\circ C \quad (1)$$

where Λ , Λ° , C , S , E , J , and F have their usual significance.

In analyzing the viscosity data, the Jones and Dole equation was used in the form

$$(\eta/\eta_0 - 1)/C^{1/2} = A + FC^{1/2} \quad (2)$$

Assuming that the ions of the electrolyte $(i\text{-Am})_4\text{N}(i\text{-Am})_4\text{B}$ are of equal size, the limiting equivalent conductance of the cation and anion in this case can be considered to be the same. Thus, if the additivity of conductance is valid, one obtains

$$\lambda_{(i\text{-Am})_4\text{N}^+}^\circ = \lambda_{(i\text{-Am})_4\text{B}^-}^\circ = 1/2\Lambda_{(i\text{-Am})_4\text{N}(i\text{-Am})_4\text{B}}^\circ \quad (3)$$

where $\Lambda_{(i\text{-Am})_4\text{N}(i\text{-Am})_4\text{B}}^\circ$ is the observed limiting conductance of $(i\text{-Am})_4\text{N}(i\text{-Am})_4\text{B}$.

In general, the constant A of the Jones and Dole equation can be related to the ion conductances and Λ° of an electrolyte in the following manner.

$$A = \frac{81.97\Lambda^\circ}{320\eta_0(DT)^{1/2}\lambda_+^\circ + \lambda_-^\circ} \left[1 - 0.6863 \left(\frac{\lambda_+^\circ - \lambda_-^\circ}{\Lambda^\circ} \right)^2 \right] \quad (4)$$

Accordingly, as a consequence of eq 3, eq 4 would transform into

$$A = \frac{327.88}{320\eta_0(DT)^{1/2}\Lambda_{(i\text{-Am})_4\text{N}(i\text{-Am})_4\text{B}}^\circ} \quad (4a)$$

in the case of $(i\text{-Am})_4\text{N}(i\text{-Am})_4\text{B}$. A satisfactory agreement between the value of A as obtained from actual viscosity measurements and the one calculated using eq 4a would indicate the validity of our assumption that the conductances of the ions of the electrolyte $(i\text{-Am})_4\text{N}(i\text{-Am})_4\text{B}$ are equal. The latter, in turn, would indicate the reliability of the ion conductances calculated on the basis of the conductance of either $(i\text{-Am})_4\text{N}^+$ or $(i\text{-Am})_4\text{B}^-$.

The emf, E , of cell I used for the determination of the transference number of perchlorate ion can be expressed as

$$E = 2t_{\text{ClO}_4^-} \frac{RT}{F} \ln \frac{a_2}{a_1} \quad (5)$$

where $t_{\text{ClO}_4^-}$ denotes the transference number of ClO_4^- and the a 's represent the mean activities of the LiClO_4 solutions.

From our previous studies LiClO_4 was found to be unassociated. Therefore, eq 5 can be rewritten as

$$E = 2t_{\text{ClO}_4^-} \frac{RT}{F} \ln \frac{C_2 f_2}{C_1 f_1} \quad (6)$$

where C_1 and C_2 are the stoichiometric concentrations of LiClO_4 solutions used, and f_1 and f_2 are the mean activity coefficients of the two solutions. Assuming that the ionic activity coefficients are equal, the mean activity coefficients can be estimated from the extended form of the Debye-Hückel equation which assumes the form

$$-\log f_{\pm} = \frac{0.6851\mu^{1/2}}{1 + 0.3629 \times 10^8 a^0 \mu^{1/2}}$$

in PC at 25°, using $a^0 = 2.75 \text{ \AA}^2$.

In the present measurements, the ratio $C_2:C_1$ was kept between 1.5 and 2.0. The transference number of ClO_4^- calculated from each measurement using equation 6 was then plotted against the "mean" concentration defined as $(C_1 + C_2)/2$, and finally extrapolated to zero mean concentration. The product of this extrapolated value of $t_{\text{ClO}_4^-}$ and the $\Lambda_{\text{LiClO}_4}^\circ$ was taken to give the value of $\lambda_{\text{ClO}_4^-}^\circ$. Conductances of all other ions were then calculated using this value of $\lambda_{\text{ClO}_4^-}^\circ$.

Experimental Section

Chemicals. Propylene carbonate was purified according to the procedure described previously. Fisher certified reagent grade potassium iodide and potassium

(3) R. M. Fuoss and F. Accascina, "Electrolytic Conductance," Interscience Publishers, New York, N. Y., 1959, pp 191-205, 207-247.

perchlorate were used without further treatment. The purification of lithium perchlorate has been given before.²

Tetraisoamylammonium iodide was prepared by refluxing tri-*iso*-amylamine (5.68 g) and 1-iodo-3-methylbutane (5.93 g) in 25 ml ethyl acetate for 18 hr, cooling to -10° , filtering the crystals, and repeating the cycle for two more times with the filtrates. The combined crystals thus obtained were recrystallized from methyl acetate-*n*-hexane mixture to yield octagonal platelets (mp $147-149^\circ$).

Tetraisoamylammonium tetraisoamylboride was prepared essentially according to the method of Coetzee and Cunningham.⁴ A solution of isoamyl lithium was obtained by the reaction of isoamyl bromide and lithium in diethyl ether while the solution of triisoamylboron in tetrahydrofuran was prepared by the reaction of diborane with 3-methylbutene-1. The two solutions were then combined under dry, oxygen-free conditions to afford a solution of lithium tetraisoamylboride. This was stored overnight and treated the following day with a solution of tetraisoamylammonium iodide in acetonitrile. The product, after the prescribed work-up, yielded the desired product, *viz.*, tetraisoamylammonium tetraisoamylboride as short needles with mp $250-251^\circ$, after two recrystallizations from methyl acetate-*n*-hexane mixture. *Anal.* Calcd for C, 80.88; H, 14.94; N, 2.36. Found: C, 80.73; H, 15.26; N, 2.69.

Conductance and Viscosity Measurements. The techniques have been described previously.²

Potentiometric Measurements. A three-compartment cell similar to the one described by Durst and Hume⁵ was used with some modifications. Each of the two outer compartments contained a pool of lithium amalgam and the lithium perchlorate solution of appropriate concentration. The middle chamber which was separated at both sides by fritted disks was filled with the more dilute of the two LiClO_4 solutions. The cell was set up in a glove box which was purged with pure argon gas and maintained at a temperature of $25 \pm 0.1^\circ$. All emf measurements were made under identical conditions, using a type K, L and N potentiometer. For each run an initial period of 30 min was allowed for the attainment of equilibrium. Saturated lithium amalgam (~ 2 mol %) prepared by shaking lithium ribbon with triple-distilled mercury has been used in all cells.

Results and Discussions

The results of conductance and viscosity measurements for the systems $(i\text{-Am})_4\text{N}(i\text{-Am})_4\text{B}$, $(i\text{-Am})_4\text{NI}$, KI, and KClO_4 are summarized in Tables I and II. The values of Λ° , a^0 , and F obtained for the different cases are presented in Table III. Both KI and KClO_4 yield Λ° of 30.75, which indicates that the iodide and perchlorate ion have equal mobilities in PC. The large

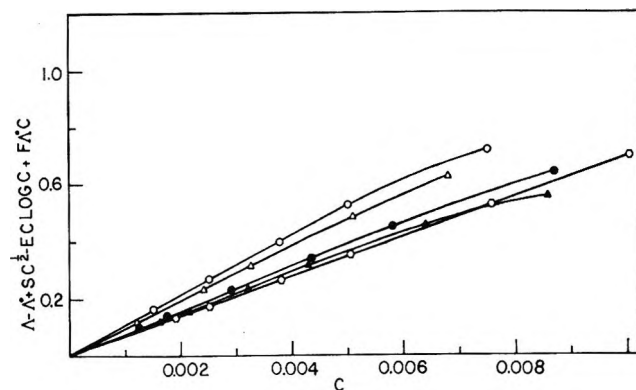


Figure 1. Plot of $\Lambda - \Lambda^\circ + SC^{1/2} - EC \log C + F\Lambda^\circ C$ vs. C . \circ , $n\text{-Bu}_4\text{NClO}_4$; Δ , Et_4NClO_4 ; \bullet , $(i\text{-Am})_4\text{N}((i\text{-Am})_4\text{B})$; \circ , $(i\text{-Am})_4\text{NI}$; \blacktriangle , $n\text{-Bu}_4\text{NBr}$.

difference between the limiting conductances of $(i\text{-Am})_4\text{N}(i\text{-Am})_4\text{B}$ and $(i\text{-Am})_4\text{NI}$, on the other hand, suggests that the mobility of $(i\text{-Am})_4\text{B}^-$ is considerably less than that of I^- . The viscosity F coefficients of KClO_4 , KI, and $(i\text{-Am})_4\text{NI}$ are noteworthy in this connection. The value of F for KClO_4 is about two-thirds of that obtained for LiClO_4 ,² indicating that K^+ is significantly smaller in size than Li^+ in PC; similar comparison between KI and $(i\text{-Am})_4\text{NI}$ suggests that $(i\text{-Am})_4\text{N}^+$ is slightly bigger than K^+ .

The a^0 values of the two potassium salts are reasonable and are comparable to the sums of their crystallographic radii. For the tetraisoamylammonium salts, however, the derived a^0 values are almost half of the values expected on the basis of the crystallographic radii of the ions. Among the quaternary ammonium salts studied previously,² Et_4NClO_4 , $n\text{-Bu}_4\text{NBr}$, and $n\text{-Bu}_4\text{NClO}_4$ also indicated similar relationship. One of the possible explanations for this deviation may lie in the somewhat arbitrary assumption of a total absence of ion association as implied in the treatment of the data (*cf.* eq 1). In fact, plots of $\Lambda - \Lambda^\circ + SC^{1/2} - EC \log C + F\Lambda^\circ C$ vs. C for these five quaternary ammonium salts do tend to diverge from linearity (Figure 1) at concentrations greater than $\sim 0.005 M$, possibly indicating a small but significant degree of association in each case. It is to be remarked in this connection, however, that the data for $(i\text{-Am})_4\text{NI}$ show the least departure from linearity although the relative difference between the experimental value of a^0 and the sum of the crystallographic radii is greatest for this salt.

The low values of the a^0 parameters in the case of the tetraalkylammonium salts may also be due to the omission of the $-J_2C^{3/2}$ term in the present treatment from the more comprehensive Fuoss-Onsager equation.

(4) J. F. Coetzee and G. P. Cunningham, *J. Amer. Chem. Soc.*, **86**, 3403 (1964).

(5) R. A. Durst and D. N. Hume, *J. Electroanal. Chem.*, **7**, 248 (1964).

Table I: Summary of Results of Conductance Measurements at 25°

$(i\text{-Am})_4\text{N}^-$ $(i\text{-Am})_4\text{B}^-$		$(i\text{-Am})_4\text{NI}$		KI		KClO ₄	
10 ³ C, M	Λ	10 ³ C, M	Λ	10 ³ C, M	Λ	10 ³ C, M	Λ
0.9660	15.5083	1.682	25.6070	1.246	29.5915	1.919	29.2757
1.243	15.3998	1.892	25.5407	1.662	29.4103	2.239	29.1559
1.740	15.2316	2.523	25.3397	2.493	29.1313	2.878	28.9437
2.900	14.9389	3.785	24.9741	3.324	28.9100	4.030	28.6079
4.351	14.6428	5.05	24.7039	4.99	28.4903	6.72	28.0080
5.80	14.4041	7.57	24.2108	6.65	28.1573	10.075	27.3796
8.70	14.0077	10.09	23.8172	9.97	27.6133	13.43	26.8816
		15.14	23.1384	13.29	27.1847	20.15	26.0055
				20.00	26.4455		

Table II: Summary of Results of Viscosity Measurements at 25°

$(i\text{-Am})_4\text{N}^-$ $(i\text{-Am})_4\text{B}^-$		$(i\text{-Am})_4\text{NI}$		KI		KClO ₄	
10 ³ C, M	η, cP ^a	10 ³ C, M	η, cP ^a	10 ³ C, M	η, cP ^a	10 ³ C, M	η, cP ^a
1.740	2.485	1.514	2.483	3.989	2.492	4.030	2.491
3.808	2.492	4.542	2.490	7.98	2.501	8.06	2.500
5.01	2.497	7.57	2.4965	12.00	2.510	12.09	2.508
7.11	2.504	11.35	2.5075	15.955	2.520	14.05	2.513
8.70	2.510	15.14	2.516	19.94	2.530	16.12	2.518
						20.15	2.528

^a η_{solvent} = 2.480 cP.

Table III: Physical Constants Determined from Analysis of Conductance and Viscosity Data

Electrolyte ^a	Λ°	a°, Å	F
$(i\text{-Am})_4\text{N}(i\text{-Am})_4\text{B}$	16.37	5.22	1.27 ± 0.018
$(i\text{-Am})_4\text{NI}$	26.95	3.30	0.96 ± 0.054
KI	30.75	3.70	0.904 ± 0.037
KClO ₄	30.75	3.175	0.874 ± 0.038

^a J values: $(i\text{-Am})_4\text{N}(i\text{-Am})_4\text{B}$ (78); $(i\text{-Am})_4\text{NI}$ (70); KI (85); KClO₄ (72.5).

No detailed consideration of this point has been undertaken in this paper.

Assuming that the ions of the electrolyte $(i\text{-Am})_4\text{N}^-$ $(i\text{-Am})_4\text{B}^-$ are idealized spheres (of equal size) in a continuum, the hydrodynamic radius (R) of its ions can be calculated using the Einstein relation: $F = (N\pi/300)(R_+^3 + R_-^3)$. The radius so obtained for $(i\text{-Am})_4\text{N}^+$ (or $(i\text{-Am})_4\text{B}^-$) from the observed value of the viscosity F coefficient (Table III) is 4.69 Å yielding a total center-to-center distance of 9.38 Å for $(i\text{-Am})_4\text{N}(i\text{-Am})_4\text{B}$. This value of 9.38 Å is only slightly lower than the value of 10.8 Å⁶ estimated from molecular models, but it is evidently much greater than the conductometric estimate of the a^0 parameter (5.22 Å) possibly due to reasons discussed above.

Substituting the value of 16.37 obtained for the limiting conductance of $(i\text{-Am})_4\text{N}(i\text{-Am})_4\text{B}$ (Table III) into

eq 4a the constant A of the Jones and Dole equation is calculated to be 0.018 in close agreement with the experimental value of 0.0174, suggesting that the inherent assumption of equality of ion conductances in this case (cf. eq 3) is apparently valid. The value of 8.185 calculated on this basis for the limiting conductance of $(i\text{-Am})_4\text{N}^+$, has been used in the subsequent calculation of the conductances of other ions.

The results of transference number measurements using cell I are given in Table IV.

Table IV: Determination of Transference Number of Perchlorate Ion Using Cell I

C ₁ , M	C ₂ , M	E, V	t _{ClO₄-}
0.020	0.040	0.0245	0.757
0.025	0.050	0.0245	0.765
0.050	0.100	0.0243	0.789
0.100	0.150	0.0144	0.816
0.120	0.200	0.0181	0.820

The transference number of ClO₄⁻ extrapolated to zero mean concentration, is found to be 0.72. On this basis, the transference number of Li⁺ is calculated to be 0.28. Thus, using the value of 26.08 for the Λ° of LiClO₄,² the

(6) J. F. Coetzee and G. P. Cunningham, *J. Amer. Chem. Soc.*, **87**, 2529 (1965).

limiting conductances of Li^+ and ClO_4^- are found to be 7.30 and 18.78, respectively.

In Table V a summary of the conductances for the various ions is presented. These results are based on the conductance of $(i\text{-Am})_4\text{N}^+(\lambda^\circ = 8.185)$ and those of Li^+ ($\lambda^\circ = 7.30$) and ClO_4^- ($\lambda^\circ = 18.78$) as determined above, and the Λ° values obtained for the different electrolytes. The excellent agreement between the calculated values of the mobility of iodide ion based on these two different approaches is indeed remarkable. This is considered particularly important insofar as the present evaluation of the mobilities of other ions is concerned.

The fact that the mobility of lithium ion is the lowest of all cations including the tetraisoamylammonium ion supports our previous² notion that the lithium ions are extensively solvated in PC and the effective size of a Li^+ is fairly large. The slight differences in the conductances of ClO_4^- , I^- , Br^- , and Cl^- seem to indicate that the effective sizes of these anions in PC are practically the same. This behavior would signify that very little solvation, if any, is involved in these cases. The lowest mobility of the tetraisoamylboride ion is to be attributed to its much larger size.

At the footnote to Table V are given the calculated values (*cf.* eq 4) of the constant A of the Jones and Dole

Table V: Ion Conductances in Propylene Carbonate at 25^oa

Salt	Λ°	λ_+°	λ_-°
LiClO_4	26.08	7.30	18.78
LiCl	27.50	7.30	20.20
KClO_4	30.75	11.97	18.78
KI	30.75	11.97	18.78
Et_4NClO_4	32.06 ^b	13.28	18.78
$n\text{-Bu}_4\text{NClO}_4$	28.17	9.39	18.78
$n\text{-Bu}_4\text{NBr}$	28.65	9.39	19.26
$(i\text{-Am})_4\text{N}(i\text{-Am})_4\text{B}$	16.37	8.185	8.185
$(i\text{-Am})_4\text{NI}$	26.95	8.185	18.765

^a A° values are given in the format: calcd, exptl (salt): 0.016, 0.0095 (LiClO_4); 0.010, 0.0075 (KClO_4); 0.010, 0.0065 (KI); 0.010, 0.008 (Et_4NClO_4); 0.012, 0.0075 ($n\text{-Bu}_4\text{NClO}_4$); 0.013, 0.006 ($n\text{-Bu}_4\text{NBr}$); 0.018, 0.0174 ($(i\text{-Am})_4\text{N}(i\text{-Am})_4\text{B}$); 0.014, 0.005 ($(i\text{-Am})_4\text{NI}$). ^b Result of rerun ($J = 92$). The cell constant used in previous work (ref 2) with this salt was found in slight error; the present value of Λ° is considered more reliable.

equation for different systems. As is evident, the agreement between the calculated and the experimental values is generally as close as can be expected.

Acknowledgment. D. P. Boden acknowledges the cooperation of ESB, Inc., Research Center, Yardley, Pa.

Heats of Transport of Gases. II. Thermoosmosis of

Binary Gaseous Mixtures without Chemical Reaction

by R. P. Rastogi and H. P. Singh

Chemistry Department, Gorakhpur University, Gorakhpur (U.P.), India (Received August 25, 1969)

Thermoosmotic pressure of mixtures of carbon dioxide and oxygen across porous unglazed porcelain has been measured. Experimental data are found to be consistent with the thermodynamic theory of thermoosmosis of mixtures. The concentration dependence of heats of transport Q^* for the mixtures has been estimated from the data. Q^* is found to vary with concentration in a linear manner showing that the transport of carbon dioxide and oxygen takes place almost independently.

1. Introduction

Thermoosmosis of gases through membranes has been studied by a number of workers.¹⁻⁵ Thermoosmosis is influenced by the nature of the membrane and pore radii. Denbigh and Raumann¹ found that it depended on the solubility of the permeant in the membrane. Hanley and coworkers^{3,4} measured thermoosmosis of He, Ne, and Ar through stainless

steel tubes under nonisothermal conditions. Thermoosmosis was found to depend on the ratio of tube

(1) K. G. Denbigh and G. Raumann, *Proc. Roy. Soc.*, **A210**, 518 (1951).

(2) R. J. Bearman, *J. Phys. Chem.*, **61**, 708 (1957).

(3) H. J. M. Hanley and W. A. Steele, *Trans. Faraday Soc.*, **61**, 2661 (1965).

(4) H. J. M. Hanley, *ibid.*, **62**, 2395 (1966).

radius to the mean free path of the permeating species. Recently, Rastogi and coworkers⁵ have studied the dependence of thermoosmotic pressure on temperature, pressure, and mean free path.

All the above studies involved investigation of a single gas. Thermoosmosis of mixtures has considerable interest since it may give some insight into the interaction between gases. It has some additional interest in view of its likely use for separation of gaseous components.

The present investigation was undertaken since the thermoosmosis of mixtures had not been investigated earlier. In the present paper thermoosmosis of mixtures of carbon dioxide and oxygen across porous unglazed porcelain has been studied in order to examine the thermodynamic theory of thermoosmosis of mixtures. Heat of transport has been estimated and its dependence on the composition of the mixture has been examined.

2. Theoretical Section

We consider an n -component system having two chambers separated by a barrier having pore size comparable to mean free path. The two chambers are maintained at different temperatures T_1 and T_2 , on account of which mass flux and heat flux take place. The linear phenomenological relations may be expressed as⁶

$$J_i = \sum_{k=1}^n L_{ik} X_k + L_{iq} X_q \quad (1)$$

$$J_q = \sum_{k=1}^n L_{qk} X_k + L_{qq} X_q \quad (2)$$

J_i denotes the mass flux of the component i and J_q denotes the heat flux. L is called a phenomenological coefficient. Further, the corresponding forces are given by⁶

$$X_k = -\Delta\left(\frac{\mu_k}{T}\right) + h\Delta\left(\frac{1}{T}\right) \quad (3)$$

$$X_q = \Delta\left(\frac{1}{T}\right) = -\frac{\Delta T}{T_1 T_2} \quad (4)$$

where μ_k is the chemical potential of component k . Δ represents the difference of the particular quantity in the two compartments. h denotes enthalpy. When ΔT is small, $X_q = -\Delta T/T_m^2$ where T_m is the arithmetic mean of the temperature on the two sides of the membrane.

Heats of transport Q^* may be defined as amount of heat flowing per unit mass flux of the mixture with the same ΔP and $\Delta T = 0$ so that

$$Q^* = \left(\frac{J_q}{\sum_i J_i}\right)_{\Delta T=0} \quad (5)$$

For a binary mixture

$$Q^* = \left(\frac{J_q}{J_1 + J_2}\right)_{\Delta T=0} \quad (6)$$

Further, J_q can be expressed as⁶

$$J_q = Q_1^* J_1 + Q_2^* J_2 \quad (7)$$

where Q_1^* and Q_2^* are the heats of transport of components 1 and 2 in the mixture. Since

$$Q_i^* = \left(\frac{J_q}{J_i}\right)_{\Delta T=0, J_j=0} \quad (i \neq j = 1, 2) \quad (8)$$

It can be shown that

$$Q_1^* = \frac{L_{2q} L_{21} - L_{1q} L_{22}}{L_{12} L_{21} - L_{11} L_{22}} \quad (9)$$

$$Q_2^* = \frac{L_{q2} L_{11} - L_{12} L_{q1}}{L_{11} L_{22} - L_{21} L_{12}}$$

using eq 1 and 2.

If $L_{11} L_{22} \gg L_{12} L_{21}$ and $L_{1q} L_{22} \gg L_{2q} L_{21}$ then $Q_1^* \approx L_{1q}/L_{11} = [Q_1^*]$ where $[Q_i^*]$ denotes the heat of transport for the pure component i . Similarly, if $L_{12} L_{q1} \ll L_{q2} L_{11}$ and $L_{21} L_{12} \ll L_{11} L_{22}$, we could have $Q_2^* \approx L_{q2}/L_{22} = [Q_2^*]$.

If we substitute the value of J_q from eq 7 in eq 6 then we get

$$Q^* = \frac{Q_1^* J_1 + Q_2^* J_2}{J_1 + J_2} \quad (10)$$

when we put $J_1 = c_1 J$ and $J_2 = c_2 J$, eq 10 reduces to

$$Q^* = c_1 Q_1^* + c_2 Q_2^* \quad (11)$$

where J denotes the mass flux of the mixture; C_1 and C_2 are the mass fractions of the components 1 and 2, respectively. It is assumed that no chemical reaction takes place in the system.

In the steady state for a two-component system, $J_1 = 0$; $J_2 = 0$ so that on solving eq 1 we get⁶ for small ΔT

$$\frac{\Delta P}{\Delta T} = -\frac{Q^*}{v T_m} \quad (12)$$

$$\frac{\Delta c_1}{\Delta T} = c_2 \{v_1 Q_2^* - v_2 Q_1^*\} / \left(\frac{\partial \mu_1}{\partial c_1}\right) v T_m \quad (13)$$

$$\Delta \mu_k = v_k \Delta P + \sum_{i=1}^{n-1} (\partial \mu_k / \partial c_i) \Delta c_i - s_k \Delta T \quad (14)$$

where s_k is the partial specific entropy of component k , $v = c_1 v_1 + c_2 v_2$ is the mean specific volume of the mixture, and v_k is the partial specific volume of component k . Equations analogous to eq 12 will yield

(5) R. P. Rastogi, K. Singh, and H. P. Singh, *J. Phys. Chem.*, **73**, 2798 (1969).

(6) S. R. de Groot, "Thermodynamics of Irreversible Processes," North-Holland Publishing Co., Amsterdam, 1952, Chapter V.

$[Q_i^*]$ for the pure components. When ΔT is large, eq 12 would be transformed as follows

$$\frac{\Delta P}{\Delta T} = -\frac{Q^* T_m}{v T_1 T_2} \quad (15)$$

Since v is a linear function of T_m , on plotting ΔP against $\Delta T/T_1 T_2$ a straight line should be obtained.

Experimental Section

Carbon dioxide was prepared in the laboratory and was purified by passing through concentrated sul-

Table I: Thermoosmotic Pressures of Mixture of CO₂ and O₂ ($P = 5.2$ cm)

$T_1, ^\circ\text{C}$	$T_2, ^\circ\text{C}$	$\Delta P,$ cm	Least-square value of $Q^*,$ cal/mol
Mass fraction of CO ₂ = 0			
74.0	29.0	0.074	
94.0	29.0	0.104	
114.0	29.0	0.127	-67 ± 1
139.0	29.0	0.156	
159.0	29.0	0.172	
Mass fraction of CO ₂ = 0.31			
77.0	32.0	0.068	
97.0	32.0	0.094	
117.0	32.0	0.114	-63 ± 1
142.0	32.0	0.143	
162.0	32.0	0.159	
Mass fraction of CO ₂ = 0.42			
77.0	32.0	0.067	
97.0	32.0	0.093	
117.0	32.0	0.118	-61 ± 1
142.0	32.0	0.141	
162.0	32.0	0.155	
Mass fraction of CO ₂ = 0.58			
77.0	32.0	0.064	
97.0	32.0	0.089	
117.0	32.0	0.111	-59 ± 1
142.0	32.0	0.135	
162.0	32.0	0.150	
Mass fraction of CO ₂ = 0.80			
77.0	32.0	0.061	
97.0	32.0	0.086	
117.0	32.0	0.106	-56 ± 1
142.0	32.0	0.125	
162.0	32.0	0.145	
Mass fraction of CO ₂ = 0.90			
77.0	32.0	0.059	
97.0	32.0	0.083	
117.0	32.0	0.105	-55 ± 1
142.0	32.0	0.127	
162.0	32.0	0.137	
Mass fraction of CO ₂ = 1			
77.0	32.0	0.057	
97.0	32.0	0.079	
117.0	32.0	0.100	-53 ± 1
142.0	32.0	0.120	
162.0	32.0	0.134	

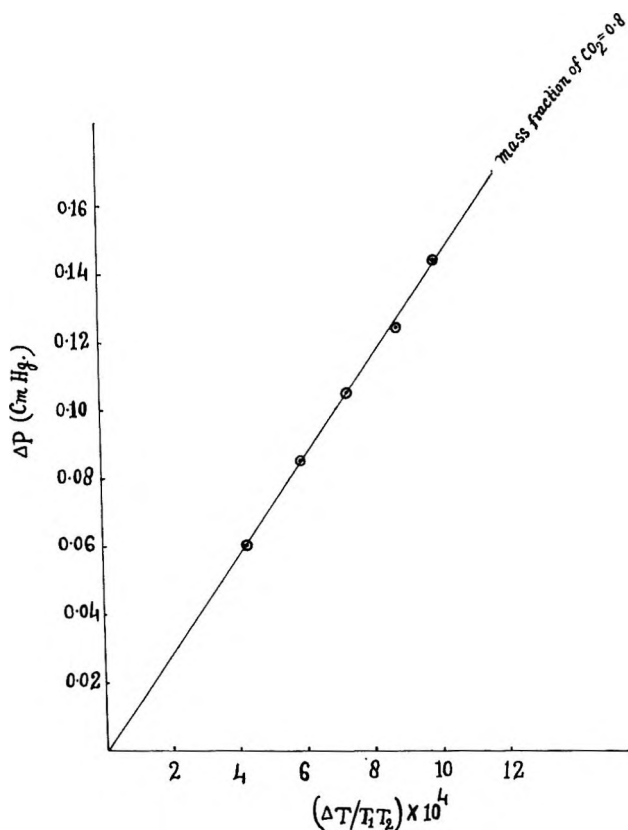


Figure 1. Dependence of thermoosmotic pressure ΔP on $\Delta T/T_1 T_2$.

furic acid. Commercially available oxygen (obtained from Indian Oxygen Ltd., Kanpur) was purified by passing through soda lime and subsequently dried with concentrated sulfuric acid. Porous unglazed porcelain (porous plate used in organic preparation) was used as the membrane throughout the investigations. The membrane was 0.5 cm thick and its area was 1.76 cm².

Measurement of Thermoosmotic Pressure Difference. The apparatus and technique for the measurement of thermoosmotic pressure described earlier⁵ was used. The cell was filled with a gaseous mixture of a known composition in the following manner. The cell was evacuated and subsequently filled with one of the gaseous components. The pressure of the gas was noted when the cell attained the steady temperature. Now the second component was introduced into the cell and the pressure of the mixture recorded. Partial pressure of the second component could thus be known. From a knowledge of the partial pressures of the constituents their respective mass fractions in the mixtures could be computed. In all cases the volume of the gas was kept practically constant. The two chambers were maintained at different temperatures and the thermoosmotic pressure of mixtures of carbon dioxide and oxygen was measured. Measurements were made at different mean temperatures and for different magnitudes of temperature gradient.

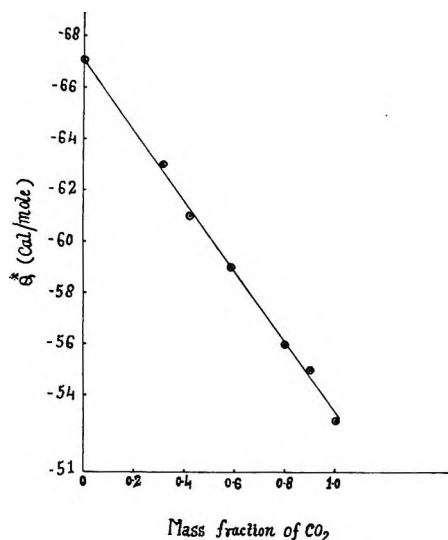


Figure 2. Concentration dependence of heat of transport Q^* .

Results

The thermoosmotic pressures of mixtures corresponding to different values of T_1 and T_2 are given in Table I.

Discussion

Data on thermoosmotic pressure ΔP given in Table I were plotted against $\Delta T/T_1T_2$ for all mixtures. Straight lines were obtained for all cases showing thereby that eq 15 satisfies the data. A typical plot is given in Figure 1. It also follows that Q^* is independent of the mean temperature. The values of Q^*

were estimated by the method of least squares. These are recorded in Table I. The values of $[Q_1^*]$ and $[Q_2^*]$ obtained in a similar manner are also recorded in Table I.

It would be interesting to examine the concentration dependence of heat of transport Q^* . This is done in Figure 2. The results satisfy the relation

$$Q^* = c_1\{[Q_1^*] - [Q_2^*]\} + [Q_2^*]$$

which means that for the case under consideration

$$Q_1^* \rightarrow [Q_1^*] \text{ and } Q_2^* \rightarrow [Q_2^*]$$

This would essentially happen when there is no interaction between the flows of either components. Phenomenologically it means that $L_{12}L_{q1} \ll L_{q2}L_{11}$ and $L_{12}L_{21} \ll L_{11}L_{22}$.

Knowing that $Q_1^* \approx [Q_1^*]$ and $Q_2^* \approx [Q_2^*]$ for $\text{CO}_2 + \text{O}_2$ systems, we can calculate the separation ΔC_1 using eq 13. In a typical case, when $P_1 = 3.9$ cm, $P_2 = 1.3$ cm, $c_1 = 0.80$, $c_2 = 0.20$, $Q_1^* = -53$ cal/mol, $Q_2^* = -67$ cal/mol, and $T = 370^\circ\text{K}$; $\Delta c_1 = 1.86 \times 10^{-3} \text{ deg}^{-1}$. In fact Δc_1 would depend on the magnitude of $v_1Q_2^* - v_2Q_1^*$. Greater the magnitude of $v_1Q_2^* - v_2Q_1^*$, greater would be Δc_1 . Considerable separation would be obtained when Q_2^* and Q_1^* have different signs. This would be achieved when the permeating gas interacts with the membrane.

Acknowledgment. This work is part of a project sponsored by CSIR. H. P. S. is thankful for the award of a Junior Research Fellowship. Thanks are due to Dr. Kehar Singh for many useful discussions.

Interactions between Surface Hydroxyl Groups and Adsorbed Molecules.

II. Infrared Spectroscopic Study of Benzene Adsorption

by J. A. Cusumano and M. J. D. Low

Department of Chemistry, New York University, New York, New York 10453 (Received October 17, 1969)

Infrared spectra were recorded of benzene adsorbed on porous glass which had been dehydroxylated to various extents, as well as on deuterated and fluoridated porous glass, and on silica. There is a specific adsorbate-adsorbent interaction, the π systems of the adsorbed benzene molecules interacting with the surface hydroxyls. At low degrees of coverage, the B-OH $\cdots\pi$ interaction predominates, the Si-OH $\cdots\pi$ interaction becoming important only at higher coverage.

We have studied the adsorption of benzene and of other substances on porous glass to gain information about the nature of the interactions between aromatic molecules and surface hydroxyl groups. The thermodynamic aspects of the benzene-porous glass system, deduced from gravimetric measurements, were described in detail elsewhere;¹ complementary data obtained by infrared spectroscopic methods are the subject of the present paper. Additional gravimetric and infrared data concerning the adsorption of other compounds, as well as the nature of the π -OH interaction, will be considered in a subsequent paper.

Experimental Section

Materials, their purification, and the general adsorption technique have been described in detail in part I.¹ Porous glass specimens (Corning Code 7930) used for infrared studies were approximately 1 \times 2 cm, cut from a 1 mm thick sheet. Specimens were brought to a reproducible stage of dehydroxylation by a procedure described earlier.¹ Also, some porous glass specimens were deuterated² or fluoridated.^{2,3} Some samples of the pure silica, Cab-O-Sil,⁴ were also used.

Spectra were recorded with a Perkin-Elmer Model 621 spectrophotometer fitted with a Reeder thermocouple, using a compensation cell in the reference beam. The theoretical slit widths were 3.9 and 2.9 cm^{-1} at 3500 and 2500 cm^{-1} , respectively. Band positions were measured to $\pm 1 \text{ cm}^{-1}$ and, when abscissa expansion was used, to $\pm 0.5 \text{ cm}^{-1}$. Note that, as a direct consequence of the type of adsorption isotherm exhibited by benzene on porous glass (*i.e.*, Henry's law behavior), the apparent fractional coverage, θ , is a direct function of the relative pressure from low values of θ to $\theta \approx 1.2$, as shown by Figure 2 of part I.¹ The spectroscopic parameters of the various figures thus show the same functional relationship to P/P_0 and to θ .

Results and Discussion

Figure 1 shows the "background" spectra in the OH region of porous glass specimens which had been pre-

treated by the standard procedure¹ and subjected to a final degassing for 12 hr. The spectral features have been described earlier.^{2,3,5} When such samples were exposed to benzene vapor at room temperature, significant changes occurred in the spectra, particularly in the 3800-2900- cm^{-1} region. Some typical spectra are shown in Figure 2.

The effects observed with increasing benzene coverage on porous glass can be summarized as follows. (a) Three new bands attributed to adsorbed benzene appeared in the aromatic C-H stretching region. Their intensities increased and their positions shifted slightly to lower frequencies with increasing coverage. The band positions and assignments⁶ are summarized in Table I. Weak combination bands appeared at benzene pressures near 60 Torr; their positions and assignments⁶ are summarized in Table II. Also, at pressures above 20 Torr, a weak doublet appeared near 3930 ± 2 and $3955 \pm 2 \text{ cm}^{-1}$, *e.g.*, spectra E-G, Figure 2. (b) The 3747- cm^{-1} Si-OH and 3703- cm^{-1} B-OH bands² declined in intensity, as shown by Figure 2 and the plots of Figure 3. The band frequencies, however, did not shift by more than 1 cm^{-1} . (c) The decline of the "free" hydroxyl bands was accompanied by the growth of a broad but well defined band, termed the perturbed hydroxyl band, initially detected near 3632 cm^{-1} , *e.g.*, spectrum B, Figure 2. With increasing coverage, the intensity of the perturbed hydroxyl band increased substantially (Figures 2 and 4), and the band

(1) Part I of this series: J. A. Cusumano and M. J. D. Low, *J. Phys. Chem.*, **74**, 792 (1970).

(2) M. J. D. Low and N. Ramasubramanian, *ibid.*, **70**, 2740 (1966); Preprints, Division of Petroleum Chemistry, 152nd National Meeting of the American Chemical Society, New York, N. Y., Sept 1966, p 133.

(3) M. J. D. Low, N. Ramasubramanian, and P. Ramamurthy, *J. Amer. Ceram. Soc.*, **52**, 124 (1969).

(4) G. Cabot Co., Boston, Mass.

(5) M. J. D. Low and N. Ramasubramanian, *J. Phys. Chem.*, **71**, 3077 (1967).

(6) G. Herzberg, "Infrared and Raman Spectra of Polyatomic Molecules," Van Nostrand, Princeton, N. J., 1945.

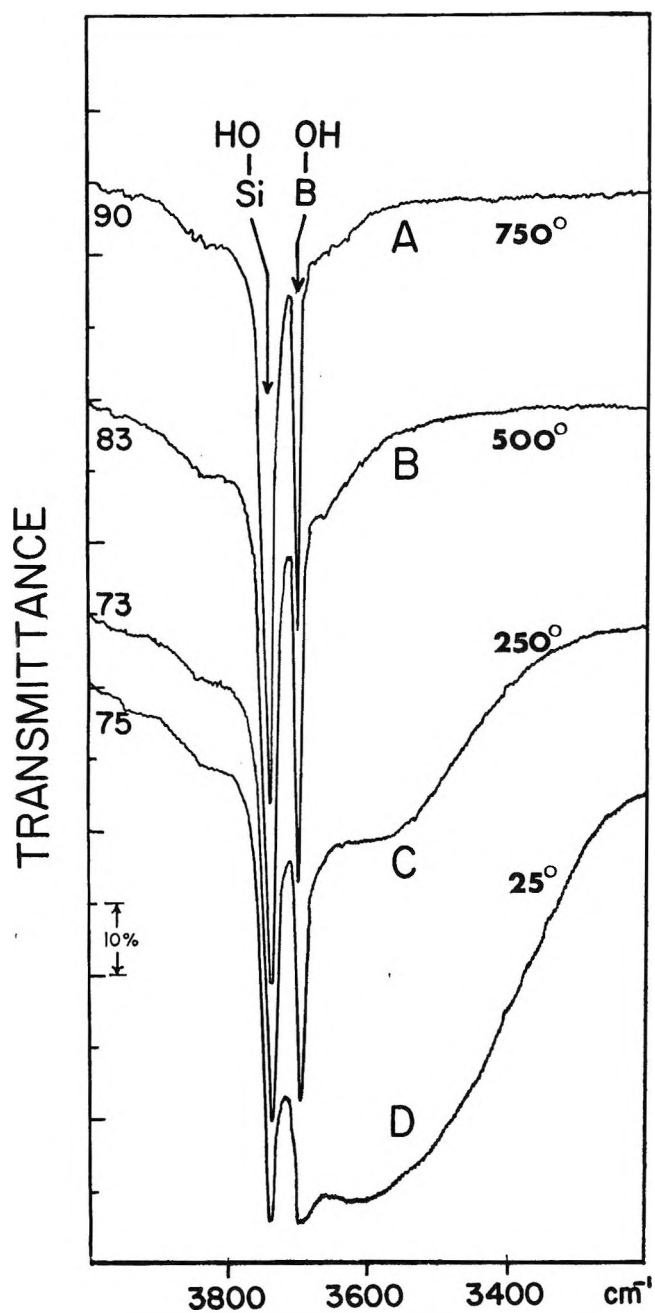


Figure 1. Infrared spectra of the O-H region of porous glass. The samples were subjected to a standard degassing and water treatment (see text) and then were degassed for 12 hr at the temperatures shown. The ordinates are displaced. The numbers next to each trace near the ordinate give the per cent transmittance at 4000 cm^{-1} .

center moved to lower wave numbers. It is convenient, useful, and in keeping with other workers to characterize the frequency of the perturbed hydroxyl band in terms of the difference, $\Delta\nu_{\text{OH}}$, of the frequencies of the free silanol and perturbed hydroxyl bands (Figure 5). This "shift" of the hydroxyl band could also be characterized in terms of the difference of the frequencies of the free B-OH band and the perturbed hydroxyl band. As shown by Figure 6, there is a constant relation between the shift from the Si-OH or B-OH band posi-

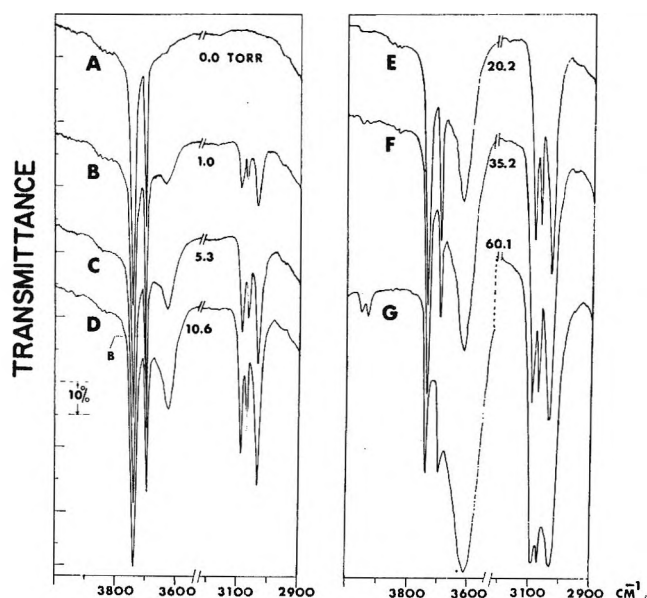


Figure 2. Benzene adsorption on porous glass. A 750° -degassed sample was exposed to benzene at room temperature at the benzene equilibrium pressures in Torr shown next to each trace. The ordinates are displaced. Each sample showed 90% transmittance at 4000 cm^{-1} .

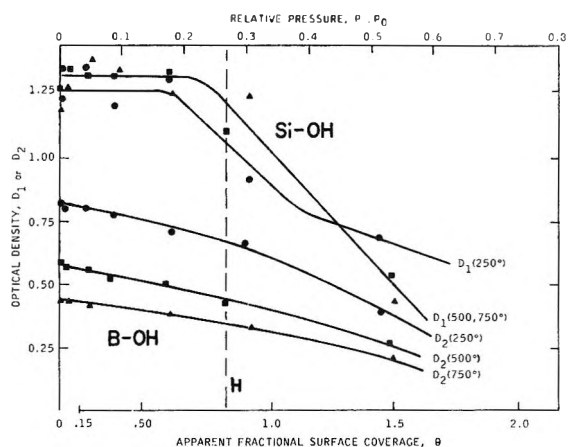


Figure 3. Effect of benzene adsorption on free hydroxyl bands. Samples degassed at the temperatures indicated were exposed to various equilibrium pressures of benzene at room temperature. The optical density of the free silanol band, D_1 , and that of the free B-OH band, D_2 , were calculated from the sequence of spectra. The same spectra were used to obtain the data shown in Figures 4-6. The region H marks the onset of adsorption hysteresis.

tions, so that either band presents a convenient zero of reference for measuring $\Delta\nu_{\text{OH}}$. In the present work the Si-OH band was used as this reference point. The half-width of the perturbed hydroxyl band increased with increasing coverage, but some uncertainty in establishing its true base line made it difficult to define the increase precisely. Also, with samples degassed at 25° , the changes of the perturbed hydroxyl band were observed by overlapping with the broad and unsymmetrical absorption caused by hydrogen-bonded mate-

Table I: Absorption Frequencies of Benzene in the Liquid, Gaseous, and Adsorbed States^a

Gas	Liquid	Degassing temp., °C	Adsorbed on porous glass			Adsorbed on Cab-O-Sil $\theta = 1.0$	Assignment
			$\theta = 0.5$	$\theta = 1.0$	$\theta > 1.0$		
3099	3089	750	3096 \pm 1	3095 \pm 1	3095 \pm 1	3093 \pm 1	str $\nu_{12}^{\text{CH}} \text{E}_{1\text{u}}$
		500	3096	3095			
		250	3095	3095	3092		
3073	3070	25	3095	3094	3089		str $\nu_2^{\text{CH}} \text{A}_{1\text{g}}$ + str $\nu_{16}^{\text{CH}} \text{E}_{2\text{g}}$ + def $\nu_{18}^{\text{C}} \parallel \text{E}_{2\text{g}}$
		750	3075	3074	3070	3071	
		500	3074	3074			
		250	3073	3073	3072		
3045	3035	25	3074	3074	3070		str $\nu_{13}^{\text{CH}} \text{E}_{1\text{u}}$ + str $\nu_{16}^{\text{CH}} \text{E}_{2\text{g}}$
		750	3041	3041	3030	3041	
		500	3041	3041			
		250	3040	3040	3030		
		25	3040	3040	3030		

^a All band positions in reciprocal centimeters; notation and vibrational assignments were obtained from ref 6; str = stretching and def = deformation. The symbol \parallel corresponds to vibration in the molecular plane, and the upper-case letters give the symmetry element designation for the given vibration.

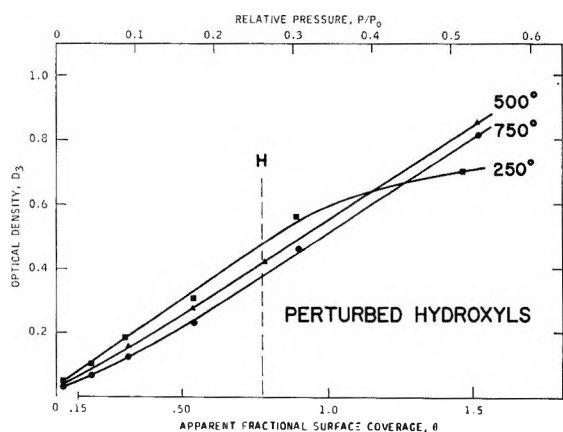


Figure 4. Effect of benzene adsorption on perturbed hydroxyls. D_3 is the optical density of the perturbed hydroxyl band. See legend of Figure 3.

rial in the 3700–3200-cm⁻¹ region, *e.g.*, spectrum D, Figure 1, so that only data obtained with samples degassed at 250° or higher will be considered. (d) The intensities and shifts of the perturbed hydroxyl band decreased when the degree of dehydroxylation was increased (except for the 250° sample at high coverage). The effect is particularly noticeable with the 250° sample, which contains a relatively large concentration of B-OH groups (Figure 1).

Spectra of benzene adsorbed on Cab-O-Sil were also measured in order to afford comparison of porous and nonporous adsorbents. The effects observed (Figure 7) were qualitatively similar to those found with porous glass except, of course, that the B-OH band was missing. The half-width of the perturbed hydroxyl band remained constant, and the change in $\Delta\nu_{\text{OH}}$ with coverage was less marked than that found with porous glass. This is indicative of the stronger interactions involved in the benzene-porous glass system.

Table II: Weak Absorption Bands Observed at High Coverages for Benzene Adsorbed on Porous Glass

Liquid ^e	Band positions, cm ⁻¹		Assignment ^d
	Adsorbed ^c 750° ^a	250° ^b	
2883	2888	2882	(?)
2648	2653	2648	def $\nu_{19}^{\text{H}} \perp \text{E}_{2\text{u}}$ + str $\nu_9^{\text{CH}} \text{B}_{2\text{u}}$
2324	2320	...	str $\nu_{15}^{\text{CH}} \text{E}_{2\text{g}}$ + str $\nu_9^{\text{CH}} \text{B}_{2\text{u}}$
2208	2210	2208	def $\nu_{18}^{\text{C}} \parallel \text{E}_{2\text{g}}$ + str $\nu_9^{\text{CH}} \text{B}_{2\text{u}}$

^a Benzene pressure = 60.2 Torr. ^b Benzene pressure = 59.5 Torr. ^c The samples were degassed for 12 hr at the temperatures shown. ^d Same nomenclature as in Table I. ^e These band positions were taken from ref 6.

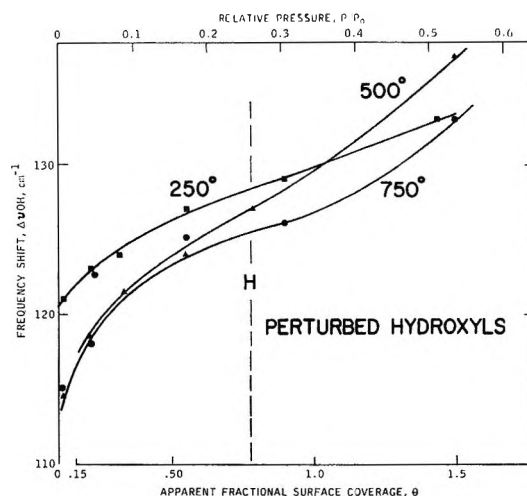


Figure 5. Shift of the perturbed hydroxyl band. $\Delta\nu_{\text{OH}}$ is the difference of the frequencies of the free Si-OH and perturbed hydroxyl bands. See legend of Figure 3.

Similar effects were found when benzene was adsorbed on deuterated porous glass. The changes in the 2760-cm⁻¹ Si-OD and the 2733-cm⁻¹ B-OD bands² with

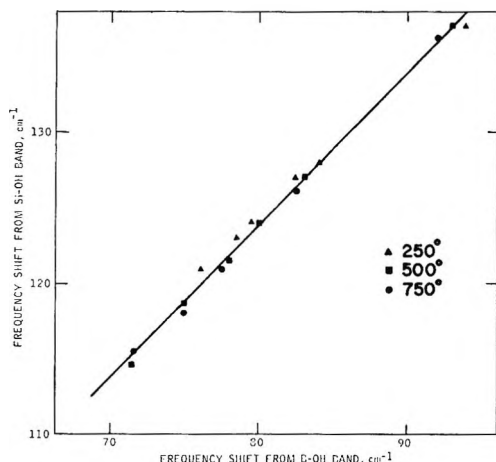


Figure 6. Shift of the perturbed hydroxyl band. The shifts (differences in frequencies of the perturbed and free hydroxyl bands) relative to the free Si-OH band (ordinate) and to the free B-OH band (abscissa) are shown for a variety of experiments carried out with samples degassed at the temperatures indicated.

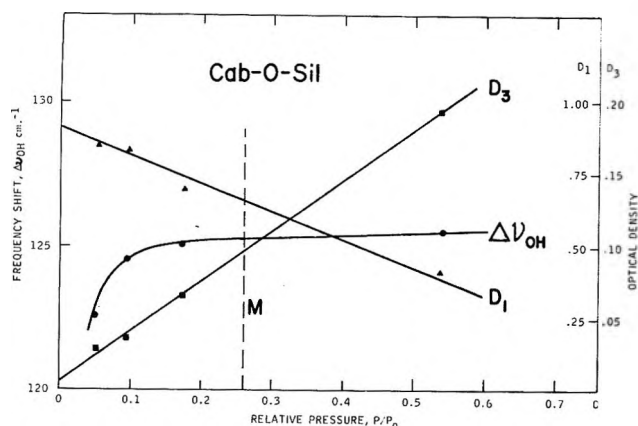


Figure 7. Benzene adsorption on Cab-O-Sil. A Cab-O-Sil sample was degassed at 750° for 12 hr and then exposed to benzene vapor at room temperature. D_1 is the optical density of the free Si-OH band, D_3 that of the perturbed hydroxyl band, and $\Delta\nu_{OH}$ the shift of the perturbed hydroxyl band from the free Si-OH band position. M indicates the surface coverage at which the theoretical monolayer coverage is complete.

changing coverage were like those of the Si-OH and B-OH bands. A band analogous to the perturbed hydroxyl band appeared near 2688 cm^{-1} ($\nu_H/\nu_D = 1.349$) at low coverage, and increased in intensity and shifted to lower frequencies with increasing adsorption. There was no evidence for an isotopic exchange between surface deuterioxylys and the hydrogen of the adsorbed benzene.

When a fully fluoridated (all hydroxyls removed^{2,3}) porous glass sample was exposed to benzene, the spectra showed that no adsorption occurred at benzene pressures up to 20 Torr. However, weak C-H bands (but no perturbed hydroxyl band) were found under the same conditions with a specimen which had been com-

pletely dehydroxylated only by degassing at high temperatures ($800\text{--}850^\circ$), indicating that a very small amount of benzene was weakly held to the surface, probably by dispersion forces. The absence of such a weak adsorption on the fully fluoridated surface suggests that surface fluoride groups inhibited the weak, nonspecific adsorption, perhaps by coulombic repulsion of the aromatic π -electron bond.

The spectra showed that the adsorption of benzene on all of the adsorbents studied was fully reversible in all cases.

The overall behavior outlined above is typical of that observed for a weak, specific adsorbate-adsorbent interaction.⁷ In view of the results obtained with the various adsorbents, such as the decrease in adsorption with increasing degree of dehydroxylation, the perturbation of the hydroxyls with increasing adsorption, and the like, there is little doubt that surface hydroxyls were involved in the adsorption. In agreement with others,⁸ the broad absorption which was earlier termed the perturbed hydroxyl band, shown to be caused by a hydrogenous species, is attributed to surface hydroxyls perturbed by the benzene adsorption. The shift $\Delta\nu_{OH}$ is indicative of a change in the O-H bond of the free surface hydroxyl group. The progressive weakening of the O-H bond is reflected in the decline of the O-H force constant with increasing coverage (Figure 8). Here k_{OH} was calculated using the harmonic-oscillator approximation, and assuming the surface Si-O group to have infinite mass relative to the hydroxylic hydrogen atom. The nature of the perturbation will be considered in part III.

Unlike the thermodynamic data,¹ which lead to information of a general nature, the infrared spectra provide a more detailed picture of the adsorption process. The changes in the OH region, in terms of variations in the intensities of the free and perturbed hydroxyl bands and especially of the shift of the perturbed hydroxyl band, provide information about the perturbation of the surface during adsorption; to a lesser extent, changes in the C-H region provide some information about the perturbation of the adsorbed benzene.

The changes in the intensities of the free hydroxyl bands (Figure 3) indicate that both Si-OH and B-OH groups were affected by benzene adsorption, but to different extents. In Figure 3 the optical densities for the free Si-OH bands for the 500 and 750° degassed samples were averaged. This was done because of the experimental uncertainty in calculating the peak optical density for such an intense band.⁹ Thus, the data points at higher benzene coverages (*i.e.*, weaker Si-OH

(7) L. H. Little, "Infrared Spectra of Adsorbed Species," Academic Press, New York, N. Y., 1966.

(8) See the discussion in Little's book, as well as the references cited in part I.

(9) W. J. Potts, Jr., "Chemical Infrared Spectroscopy," Vol. I. John Wiley & Sons, Inc., New York, N. Y., 1963, p 170.

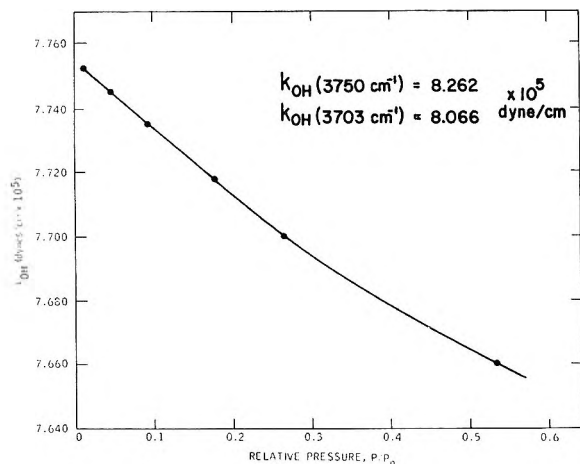


Figure 8. Weakening of the O-H bonds by benzene adsorption. Values of the force constant k_{OH} for the O-H bond of hydroxyls perturbed by benzene adsorption were estimated from the data of Figure 5.

band) are more reliable than those at lower coverages. Similarly, the B-OH optical density data could be estimated more precisely because the B-OH band intensity was weaker. The free B-OH band decreased almost linearly with increasing surface coverage over the entire range. The free Si-OH band, however, showed only small changes in the region below the onset of hysteresis but declined rapidly above it. The B-OH groups consequently were more "reactive" and participated in the specific interaction with benzene at low degrees of coverage to a greater extent than Si-OH groups. This order of reactivity is in accord with the charge-transfer model developed in part III of this series. Thus, because boron is more electronegative than silicon, B-OH groups will be more acidic than Si-OH groups and consequently will form surface complexes with electron-donating molecules much more readily than Si-OH groups. As the surface coverage increased, particularly past the onset of hysteresis, the participation of Si-OH groups became more important.

A similar greater reactivity of B-OH than Si-OH sites has been described for the adsorption of H_2O ,^{2,5} NH_3 ,¹⁰ or HCN ¹¹ on porous glass, and is likely to be responsible for some of the results presently observed. However, the data suggest that an additional effect was involved at the higher coverages.

In the present case, the changes in the intensity and shift of the perturbed hydroxyl band reflect the changes in the number of B-OH groups rather than the total number of hydroxyls present in the samples. The intensities of the free Si-OH bands were not greatly affected by degassing, but those of the free B-OH band were decreased substantially (Figures 1 and 3). The greatest shift was obtained with the 250° sample (Figure 5), which also contained the largest number of B-OH groups (spectrum C, Figure 1, as mentioned earlier; effects with the 25° degassed sample, D of Figure 1, are not considered).

Comparison of the Cab-O-Sil and porous glass data indicates that at least one aspect of the adsorptions on the two adsorbents was similar, in that the linear decline of the silanol band of Cab-O-Sil (Figure 7) caused by the Si-OH $\cdots\pi$ interaction was much like that of the B-OH band of porous glass (Figure 3). The OH $\cdots\pi$ interaction would occur preferentially with the more reactive hydroxyl, so that the continuous decline of the B-OH band over the entire θ range can be ascribed to a B-OH $\cdots\pi$ interaction much like the Si-OH $\cdots\pi$ interaction found with Cab-O-Sil. The OH $\cdots\pi$ interaction leads to the formation of the perturbed hydroxyl band and, in the case of porous glass, the Si-OH $\cdots\pi$ interaction makes a minor contribution to the shift and intensity of the perturbed hydroxyl band at low to medium coverages (Figure 3). Under these conditions one might expect the behavior of the frequency shift for the perturbed hydroxyl band to be similar to that observed for Cab-O-Sil or Aerosil.^{7,11} This is because in both cases the benzene interacts with only one type of surface hydroxyl group: B-OH groups on porous glass and Si-OH groups on the pure silica. Thus for porous glass as for Cab-O-Sil at low to medium coverages one should observe $\Delta\nu_{OH}$ to increase rapidly with coverage, changing only very slowly after monolayer coverage has been reached. However, the situation could and does change at higher coverages when the Si-OH $\cdots\pi$ interaction comes into play in addition to that of the B-OH $\cdots\pi$ type.

Two distinct perturbed hydroxyl bands corresponding to Si-OH $\cdots\pi$ and B-OH $\cdots\pi$ interactions on porous glass were not observed. However, the change in the nature of the adsorbed layer¹ implies that changes in the intensity (Figure 4) and position (Figure 5) of the single perturbed hydroxyl band were influenced by the increasing importance of the interaction of adsorbed benzene with free silanols as the coverage was increased. The greater part of the frequency shift (Figure 5) at low coverage can thus be attributed to the B-OH $\cdots\pi$ interaction, in line with earlier discussion. This is particularly noticeable with the 250° sample (Figure 5) containing the highest concentration of B-OH groups. However, the additional frequency shift of the perturbed hydroxyl band and the intensity decreases of the free silanol band observed past the hysteresis point appear to require an additional mechanism.

It seems unlikely that the formation of benzene multilayers *per se* would be responsible for the increased participation of silanols in the adsorption or the increased shift of the perturbed hydroxyl band, because we have found that benzene adsorption past monolayer coverage caused only small additional perturbations

(10) M. J. D. Low, N. Ramasubramanian, and V. V. Subba Rao, *J. Phys. Chem.*, **71**, 1726 (1967).

(11) M. J. D. Low, N. Ramasubramanian, P. Ramamurthy, and A. V. Deo, *ibid.*, **72**, 2371 (1968).

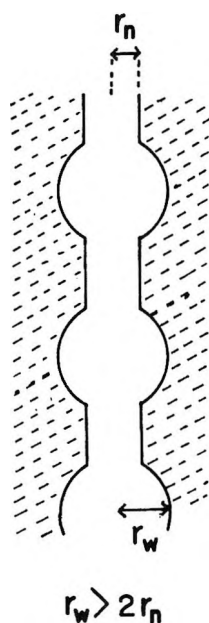


Figure 9. Schematic of pore system.

with nonporous Cab-O-Sil or Aerosil silicas (Figure 7). The nature of the porous glass adsorbent leads to the suggestion that these effects were caused by adsorbate-adsorbate interactions occurring within micropores. The effects became noticeable in a region of relative pressure where adsorption hysteresis began¹ and, with the two highly degassed samples, became more important as the apparent fractional surface coverage increased. It is suggested that the increased density of benzene molecules within micropores led to increased adsorbate-adsorbate interactions, which in turn led to enhanced π -OH interactions. Crudely, the first adsorbed layer might become more tightly pressed against the surface of a micropore and become somewhat more tightly packed, so that multiple interactions with hydroxyls would become possible. A reasonable model for such enhanced interactions follows from the pore structure of the glass. In part I¹ we suggested the pore structure to be similar to that illustrated in Figure 9. From pore-size distribution data for porous glass similar to that used in the present study, we have found r_w sharply distributed about the 20–30-Å range and $r_n \approx 10$ –15 Å. If the benzene molecule is assumed to be 3.7 Å thick,¹² one can then show that two superimposed adsorbed benzene molecules, each interacting with a surface hydroxyl on opposite pore walls, would fit only very tightly into the connecting channels. At low relative pressures this effect would not predominate. However, with increasing coverage, benzene molecules would begin to interact with surface hydroxyls in these channels, thus leading to “clogged” channels, and in many instances preventing further entry of molecules into parts of the spherical pore system.^{13,14} With increasing relative pressure ($\theta \approx 0.6$) these channels would then empty into the spherical pores, thus allow-

ing the benzene to interact with more highly active sites which were previously inaccessible at lower pressures. The interaction of benzene with these freshly exposed sites could contribute to the enthalpy and entropy maxima described in part I.¹ Of course, normal adsorbate-adsorbate interactions of the van der Waals type which occur in porous adsorbents at high coverages could also contribute to such maxima. However, the enhanced interactions which occur with surface hydroxyls are probably initiated by tight packing of benzene molecules in the pore channels. This effect would become especially noticeable as monolayer coverage is approached, because an increased number of narrow channels would be “filled.” Similar effects should occur in the spherical pores as θ increased beyond the monolayer point. The trends of $\Delta\nu_{OH}$ and D_3 with increasing severity of degassing (Figures 4 and 5) lend some support to this picture. The smallest effects were observed with the 750° sample, which contained the smallest concentrations of both Si-OH and B-OH groups. Somewhat larger effects were obtained with the 500° sample, the higher Si-OH concentration of the latter leading to an enhanced shift at higher coverages. The 250° sample had the highest B-OH concentration but, as indicated by the broad 3700–3400 cm^{-1} absorption of its spectrum (C, Figure 1), also contained hydrogen-bonded material which would tend to block the pore system of the adsorbent, especially if it were located in the narrower connecting channels. The 250° sample would consequently lead to the highest shift at low coverage (Figure 5); at the higher coverages the shift and intensity of the perturbed band would be smaller, because the hydrogen-bonded material made the hydroxyls of the smaller pores less accessible to benzene. This would also account for the low value of D_3 at the highest coverage for the 250° sample (Figure 4). This decreased participation of Si-OH groups at higher coverages for the 250° sample is also supported by the data of Figure 3, where one can note a decreased rate of change in the Si-OH peak optical density (D_1) for the 250° sample with increasing coverage beyond $\theta \approx 1.2$.

Small shifts were observed in the C-H region when benzene became adsorbed (Tables I and II). Unfortunately, the porous glass was opaque in the region where the C-C stretching (1483 cm^{-1}) and the out-of-plane C-H deformation (685 cm^{-1}) modes of adsorbed benzene would be expected,¹⁵ so that it was not feasible to derive information in the manner of Galkin, Kiselev, and Lygin¹⁵ about the disturbance of the π -electron

(12) L. H. Boulton, B. R. Clark, M. F. Coleman, and J. M. Thorp, *Trans. Faraday Soc.*, **62**, 2928 (1966).

(13) W. J. Jones and R. A. Ross, *J. Chem. Soc.*, **A**, 1787 (1968).

(14) D. A. Cadenhead and D. H. Everett, *J. Phys. Chem.*, **72**, 3201 (1968).

(15) G. A. Galkin, A. V. Kiselev, and V. I. Lygin, *Trans. Faraday Soc.*, **60**, 431 (1964).

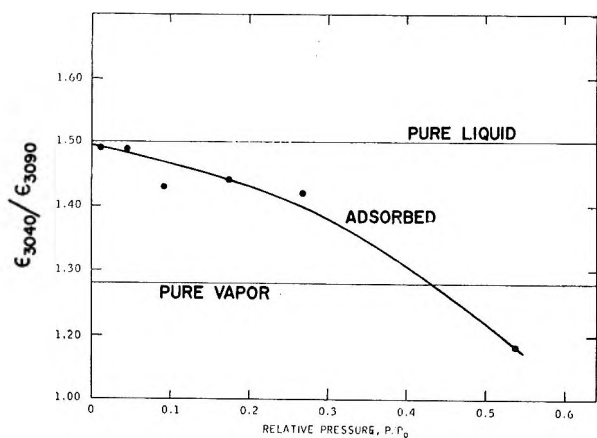


Figure 10. Perturbation of C-H bands. The ratio of the extinction coefficients ϵ of two benzene absorptions was obtained from spectra similar to those of Figure 2, for benzene adsorption on porous glass degassed at 500°.

system of the benzene ring upon adsorption. However, it was found possible to use the benzene bands in the C-H region. For the present system, the ratio of the extinction coefficients ϵ of two bands is also equal to the ratio of the optical densities of the two bands, and hence can be readily calculated from a single spectrum. The variation of $\epsilon_{3040}/\epsilon_{3090}$ with coverage is shown in Figure 10 and, like similar changes reported by Galkin, Kiselev, and Lygin, is indicative of a perturbation of the benzene molecule by the π -OH interaction. This follows from the fact that the value of the extinction coefficient for infrared absorption is a sensitive indicator of redistribution of electronic charge in

a π system, being proportional to the square of the change in dipole moment of the molecule when it vibrates along the pertinent normal coordinate.

The anomalous doublet at 3930 ± 2 and 3955 ± 2 cm^{-1} (e.g., spectra E-G, Figure 2) was not observed for benzene adsorbed on Cab-O-Sil, even at the highest pressures (60–70 Torr). No definite assignment can be made at this time for this absorption. However, it is interesting to note that its appearance seemed to parallel the disappearance of the 3747-cm^{-1} high-frequency shoulder with increased adsorption. Also, a weak band corresponding to $\nu_{20} + \nu_{10}$ for pure benzene has been previously reported at 3940 cm^{-1} .¹⁶

In summary, we have found the adsorption of benzene on porous glass to be qualitatively similar to that on pure nonporous silicas. However, a detailed study of these two systems has shown benzene adsorption on porous glass to be much more complex than that on a pure nonporous silica. These differences appear to be due primarily to the micropore structure and surface B-OH groups on the porous adsorbent. Also, changes in infrared parameters, such as band frequencies, optical densities, and extinction coefficients, appear to parallel analogous changes in the thermodynamic functions previously discussed.¹

Acknowledgments. Support by means of grants from the Communicable Disease Center and the National Center for Air Pollution Control is gratefully acknowledged, as are useful discussions with Dr. Lloyd Abrams and Dr. P. Ramamurthy.

(16) R. D. Mair and D. F. Hornig, *J. Chem. Phys.*, 17, 605 (1949).

Hydrogen Diffusion through (Palladium-Silver)-Tantalum-(Palladium-Silver) Composites

by Gerhard L. Holleck

Tyco Laboratories, Inc., Waltham, Massachusetts 02154 (Received November 4, 1969)

The diffusion coefficient of hydrogen in tantalum between 270 and 600° was determined from transient and steady-state measurements of hydrogen permeation through Pd_{0.75}Ag_{0.25}-Ta-Pd_{0.75}Ag_{0.25} clads. The results can be represented by $D = (7.5 \pm 2.2) \times 10^{-8} \exp[(-10,380 \pm 480)/RT]$.

Introduction

Like palladium and its alloys, tantalum forms a wide range of solid solutions with hydrogen which at lower temperatures are interrupted by miscibility gaps. Several more recent measurements on the thermodynamic properties of Ta-H solutions¹⁻³ are in good agreement with each other. There have also been attempts to measure the hydrogen diffusion in tantalum.⁴⁻⁶ Mostly, however, they were hampered by slow surface processes due mainly to oxide layers. To meet this problem, Makrides, *et al.*,⁶ activated their tantalum membranes by thin Pd coatings. In the following article, we will investigate hydrogen permeation through (Pd-Ag)-Ta-(Pd-Ag) composites. Besides the possibility of evaluating hydrogen diffusion data for Ta, the study of hydrogen permeation through composites is of great interest in itself.

Theory and Principle of Measurement

A general treatment of diffusion in multiple laminates has been given by Ash, Barrer, and Palmer.⁷ For the derivation of these equations, we assume that the diffusion coefficient is independent of concentration and time. Further, at a phase boundary, the distribution of diffusant between the two phases shall be governed by Henry's law. The special configuration of the slab and nomenclature used is shown in Figure 1.

Initially, the hydrogen concentration in the composite is zero. At time zero, a constant hydrogen concentration, $n_{1,0}$, is established and maintained by a constant hydrogen gas pressure, P_h . The concentration $n_{3,1}$ is kept effectively zero at all times (in practice, $P_1 \ll P_h$). The hydrogen flux, J , emerging from the low-pressure face of the membrane is continuously monitored.

It has been found that in general the hydrogen solution behavior in metals at low concentrations ($n \rightarrow 0$) can be described by Sieverts' relationship

$$P_{H_2}^{1/2} = Kn \quad (1)$$

Under these conditions, the time lag, L , represented by the intercept on the t axis of a plot of the total

amount of hydrogen that emerged from the low-pressure side of the slab *vs.* time, is given by

$$L = \frac{\frac{s_1^2}{D_1} \left(\frac{4s_1K_1}{3D_1} + \frac{s_2K_2}{D_2} \right) + \frac{s_2^2}{D_2} \left(\frac{s_1K_1}{D_1} + \frac{s_2K_2}{6D_2} \right) + \frac{s_2s_1^2K_1^2}{D_1^2K_2}}{\frac{2s_1K_1}{D_1} + \frac{s_2K_2}{D_2}} \quad (2)$$

where K_1 and K_2 are Sieverts' constants for layer 1 (Pd-Ag) and 2 (Ta).

By solving eq 2 for D_2 , one obtains

$$D_2 = \frac{-B - (B^2 - AC)^{1/2}}{2A} \quad (3)$$

where

$$A = \frac{4s_1^3K_1}{3D_1^2} + \frac{s_2s_1^2K_1^2}{D_1^2K_2} - \frac{2Ls_1K_1}{D_1}$$

$$B = \frac{s_1^2s_2K_2}{D_1} + \frac{s_2^2s_1K_1}{D_1} - Ls_2K_2$$

$$C = \frac{s_2^3K_2}{6}$$

The hydrogen diffusion coefficient can also be calculated from the steady-state flux density through the composite slab

(1) P. Kofstad, W. E. Wallace, and L. J. Hyvönen, *J. Amer. Chem. Soc.*, **81**, 5015 (1959).

(2) M. W. Mallett and B. G. Koehl, *J. Electrochem. Soc.*, **109**, 611 (1962).

(3) E. Veleckis and R. K. Edwards, *J. Phys. Chem.*, **73**, 683 (1969).

(4) E. A. Gulbransen and K. F. Andrew, *Trans. AIME*, **188**, 586 (1950).

(5) M. W. Mallett and B. G. Koehl, *J. Electrochem. Soc.*, **109**, 968 (1962).

(6) A. C. Makrides, M. Wright, and R. McNeill, Final Report on Contract DA49-186-AMC-136(D), Harry Diamond Laboratories, 1965.

(7) A. Ash, R. M. Barrer, and D. G. Palmer, *Brit. J. Appl. Phys.*, **16**, 873 (1965).

$$\bar{J} = D_1 \frac{n_{1,0} - n_{1,1}}{V_{Me_1} s_1} = D_2 \frac{n_{2,0} - n_{2,1}}{V_{Me_2} s_2} = D_1 \frac{n_{3,0} - n_{3,1}}{V_{Me_1} s_1} \quad (4)$$

where V_{Me_1} and V_{Me_2} are the volume of 1 g-atom of metals 1 and 2. With eq 1, one obtains for D_2

$$D_2 = \frac{JV_{Me_2}K_2s_2}{P_h^{1/2} - P_1^{1/2} - (2JK_1V_{Me_1}s_1/D_1)} \quad (5)$$

Evaluation of D_2 from both eq 3 and 5 requires the knowledge of D_1 , K_1 , and K_2 . Equation 5, however, contains, in addition to these unknowns, the membrane area (steady-state flux density), whereas the time lag is independent of it.

Experimental Section

A detailed description of the apparatus and experimental procedure has been given previously.⁸ The composite membrane was clamped into a stainless steel sample holder leaving a well defined area of 3.14 cm². The sample holder was connected to a vacuum apparatus designed to closely approach the condition for which the above equations are valid. The hydrogen flow emerging from the low-pressure side of the membrane was continuously monitored by a thermistor arrangement measuring the pressure difference across a calibrated capillary. These pressures (P_1) ranged from 0 to 300 μ depending on P_h sample thickness and temperature. In general, however, they were kept below 150 μ . The sample was surrounded by an aluminum ring and thick-walled copper tubing (to ensure an equal heat distribution) and heated by a temperature-controlled tube furnace. A suitably placed chromel-alumel thermocouple was used to measure the membrane temperature.

The Pd_{0.75}Ag_{0.25}-Ta-Pd_{0.75}Ag_{0.25} clad was obtained by explosive bonding of 0.090-in. tantalum sheet (extra high-purity annealed from Kawecki Chemical Co.) and 0.020-in. Pd_{0.75}Ag_{0.25} sheets (Engelhard Industries,

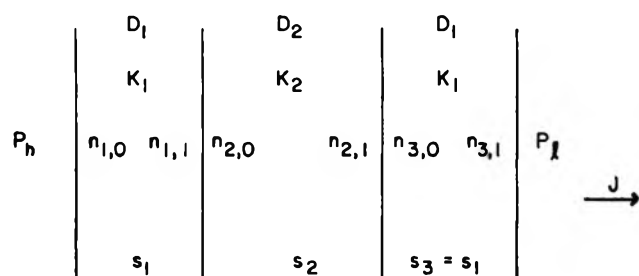


Figure 1. Schematic of composite slab showing nomenclature P_h , P_1 = high and low gas pressure, respectively (Torr); s_i = thickness of layer i (cm); $n_{i,0}$, $n_{i,1}$ = g-atom H/g-atom Me at the flux entrance and exit side of the i th layer, respectively; J = flux density (g-atom H/cm² sec); D_i , K_i = diffusion coefficient and Sieverts' constant for hydrogen in layer i , respectively.

Inc.). A microscopic examination suggested a good bond between the layers. During rolling of the composite, separation of the layers was observed in some instances. In the following, we will report on hydrogen diffusion measurements at two membranes of different thickness (I = 0.052 cm, II = 0.108 cm) which did not show any signs of separation upon microscopic investigation of microsections of the edges. The thickness of the individual layers was also determined by these microsections. For activation, the Pd-Ag surfaces were mechanically cleaned, shortly etched in concentrated nitric acid, and electrolytically coated with Pd black. The hydrogen used for the diffusion studies was purified by permeation through a Pd-Ag membrane.

Results and Discussion

The evaluation of D_2 from eq 3 and 5 requires that interface inhibitions are insignificant and that Sieverts' relationship is valid. We know from previous investigations⁸ that these conditions can be met with Pd-Ag alloys and activated surfaces. Possible deviations from the idealized behavior at the (Pd-Ag)-Ta interface will be discussed later.

Recently, we reported on hydrogen diffusion and solubility in Pd-Ag alloys. From these measurements, we interpolated the following relationships for Pd_{0.75}Ag_{0.25}: $D_1 = 2.24 \times 10^{-3} \exp(-5500/RT)$ and $K_1 = 1.11 \times 10^4 \exp(-1795/T)$.

The results of hydrogen solubility studies in tantalum mentioned above are in quite close agreement with each other. They suggest that the hydrogen solubility behavior at low concentrations and at higher temperatures can be described to a good approximation by Sieverts' equation. With decreasing temperature, systematic deviations from an ideal behavior have been observed. In our experiments, the average hydrogen concentration in tantalum ranged generally between $\bar{n} = 0.005$ and $\bar{n} = 0.1$ [only at 269.8°, $P_h = 101$ Torr, was \bar{n} considerably larger (0.37)]. We therefore used for our calculations $K_2 = 3.033 \times 10^4 \exp(-4170/T)$. This relationship was obtained from the data at $n = 0.053$ of Kofstad,¹ *et al.*, Mallett and Koehl,² and Veleckis and Edwards³ by a least-squares fit of $\log K$ vs. $1/T$. The effect of possible error introduced by the use of Sieverts' law will be discussed later.

The experimental results and the calculated diffusion coefficients for hydrogen in tantalum are summarized in Table I. The hydrogen flux emerging from the membrane increased after an initial induction period and finally reached a constant value (column 4, Table I). The total amount of hydrogen, Q , which emerged up to each time was obtained by graphical integration of the flux vs. time curve. The time lag, L , was evaluated from plots at Q vs. t as mentioned earlier.

(8) G. L. Holleck, *J. Phys. Chem.*, **74**, 503 (1970).

Table I: Diffusion Coefficients, D , for Hydrogen in Tantalum and Experimental Data from Which They Were Calculated

Temp, °C	P_h , Torr	$10^3 P_1$, Torr	$10^3 J$, g-atom H per cm ² sec	$10^6 D$, permeation, cm ² /sec	L , sec	$10^6 D$, time lag, cm ² /sec
Sample I Pd _{0.75} Ag _{0.25} -Ta-Pd _{0.75} Ag _{0.25}			0.0075-0.0370-0.0075 cm			
269.8	101.0	158.2	7.82	0.69	727.0	0.63
269.8	20.0	59.8	2.78	0.51	888.0	0.41
332.8	92.5	159.3	7.88	1.52	309.0	1.34
332.8	22.0	74.6	3.46	1.34	323.0	1.24
366.8	99.0	176.8	8.83	2.37	222.0	1.72
366.8	47.5	127.2	6.12	2.40	226.0	1.67
366.8	25.0	88.6	4.11	2.18	230.0	1.63
366.8	11.0	49.0	2.27	1.73	239.0	1.53
366.8	6.2	36.7	1.70	1.75	253.0	1.42
440.8	102.5	208.8	10.58	5.51	80.8	5.42
440.8	52.5	144.3	7.06	5.04	96.3	4.00
446.8	16.6	80.6	3.74	4.99	97.2	3.80
446.8	7.0	47.5	2.22	4.46	98.1	3.75
543.8	198.5	398.0	20.92	17.79	24.0	25.64
543.8	100.0	289.5	14.99	18.32	27.3	19.19
543.8	50.5	216.0	10.98	19.58	27.6	18.76
543.8	29.0	166.5	8.27	19.75	29.5	16.39
543.8	14.0	107.6	5.05	16.50	33.6	12.83
543.8	5.3	55.2	2.56	12.79	30.9	14.98
Sample II Pd _{0.75} Ag _{0.25} -Ta-Pd _{0.75} Ag _{0.25}			0.0112-0.0857-0.0112 cm			
323.0	25.0	31.2	1.45	0.98	1174.0	1.85
328.0	52.0	55.9	2.59	1.27	1248.0	1.67
380.0	99.8	91.4	4.24	2.61	603.6	3.56
380.0	46.0	59.6	2.77	2.50	673.9	2.97
380.0	21.5	34.0	1.58	2.02	670.2	3.00
380.0	8.2	16.5	0.77	1.53	820.7	3.21
460.0	99.5	100.8	4.68	5.72	297.5	6.60
460.0	51.2	68.7	3.19	5.40	310.3	6.19
460.0	21.8	40.7	1.89	4.85	318.9	5.94
460.0	8.6	20.6	0.96	3.79	374.2	4.70
600.0	56.5	76.0	3.53	13.72	104.8	18.08
600.0	11.0	31.4	1.46	12.96	102.7	18.65
616.8	81.5	85.6	3.97	13.80	96.6	19.34

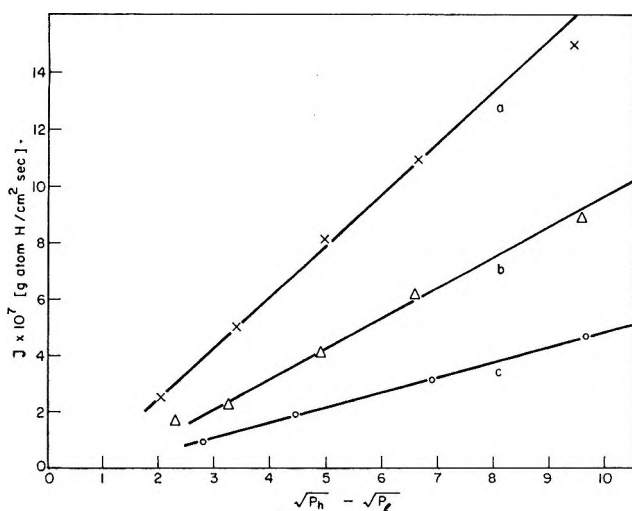


Figure 2. Hydrogen flux through Pd_{0.75}Ag_{0.25}-Ta-Pd_{0.75}Ag_{0.25} composites at different temperatures against the square root of pressure. (a) Sample 1, 543.8°; (b) sample 1, 366.8°; (c) sample 2, 460°.

The experimental data in Table I are sequentially ordered with respect to temperature and hydrogen pressure to show certain trends which will be discussed later. It should be noted, however, that the measurements at each temperature were not taken in the shown repetitive sequence. The temperature was changed stepwise, but after the highest temperature a control measurement at lower temperature was taken to detect any irreversible changes.

The steady-state hydrogen flux through the composite can be described quite well by straight lines in a plot of J vs. $(P_h)^{1/2} - (P_e)^{1/2}$ (Figure 2). These lines do, however, intersect the abscissa between 0.3 and 1.5 instead of passing through the origin. The same behavior has also been observed by A. C. Makrides, *et al.*⁸ Kofstad, *et al.*,¹ found in their solubility measurements unexpected deviations from Sieverts' equation at very low hydrogen concentrations towards a decreased hydrogen solubility. This would appear as a decreased slope in a plot of J vs. \sqrt{P} at low pres-

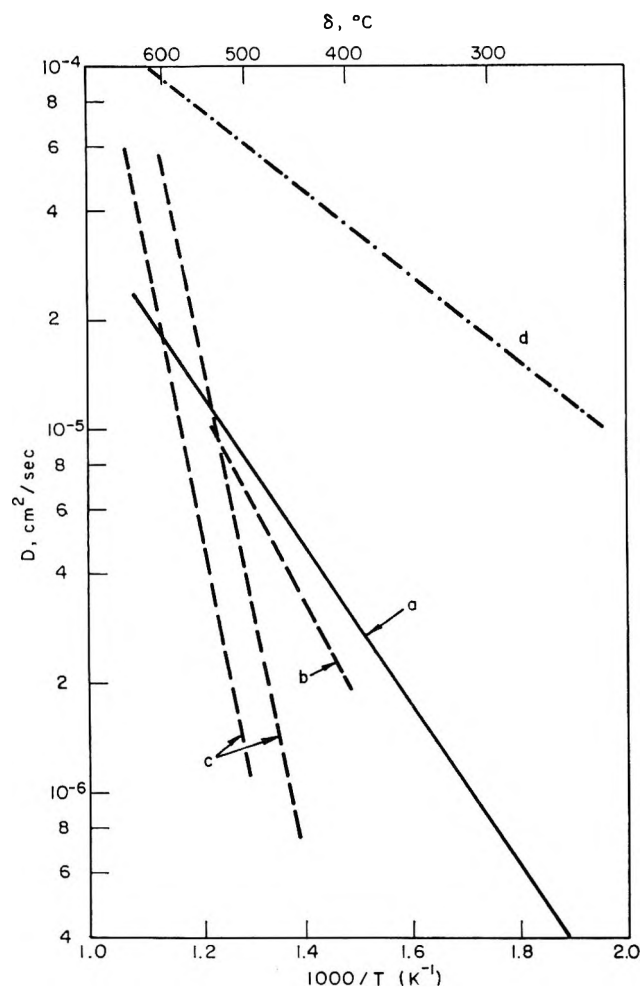


Figure 3. Arrhenius plot of hydrogen diffusion coefficients in Ta. (a) This investigation; (b) see ref 6; (c) see ref 5 (for comparison: d = hydrogen diffusion coefficient in $\text{Pd}_{0.75}\text{Ag}_{0.25}$).

tures. Thus the results shown in Figure 2 seem to reflect the irregularities in the hydrogen solubility behavior observed in earlier investigations.

The diffusion coefficients for hydrogen in Ta calculated from the steady-state flux (eq 5) and from the transient behavior (eq 3) are shown in columns 5 and 7 of Table I. The results can be empirically represented by $D = D_0 \exp(-E/RT)$. A least-squares fit of $\log D$ vs. $1/T$ led to

$$D = (7.16 \pm 2.1) \times 10^{-3} \exp\left(-\frac{10,340 \pm 480}{RT}\right)$$

for the values obtained from the steady-state flux and to

$$D = (7.8 \pm 2.2) \times 10^{-3} \exp\left(-\frac{10,420 \pm 460}{RT}\right)$$

for the results of the time lag measurements.

The agreement between these results is extremely good and of considerable importance. As mentioned earlier, inhibitions at the interfaces have to be negligible in order to obtain meaningful results for the diffusion of hydrogen. A closer analysis of this point seems

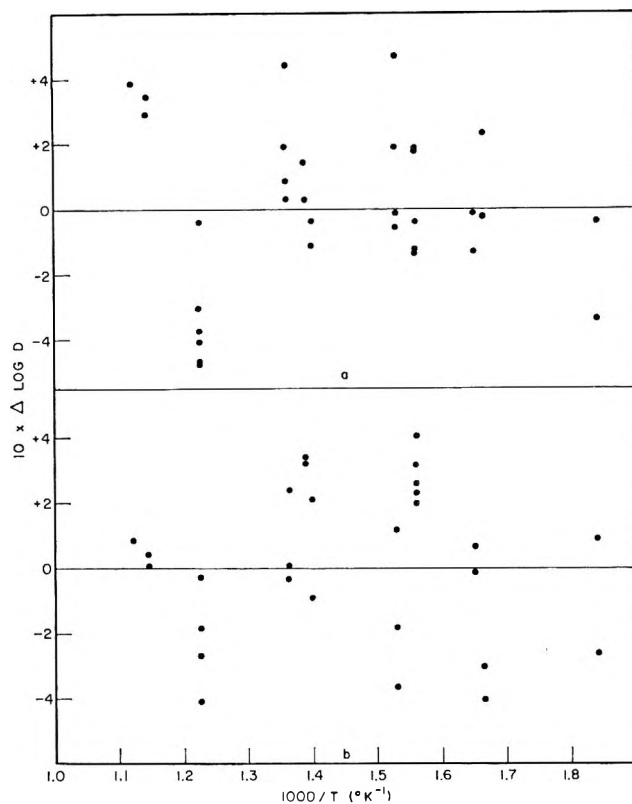


Figure 4. Deviation of experimental values for D from calculated least-squares line. (a) From hydrogen permeation; (b) from transient behavior.

therefore in order. The following findings suggest that there are no significant interface inhibitions: (1) the hydrogen diffusion coefficients were found to be independent of sample thickness, and (2) the evaluation of the transient behavior and the steady-state flux result in the same values for the diffusion coefficients. Contrary to the transient behavior which is independent of the sample area and depends on the ratio of the hydrogen solubilities in the composite layers, the evaluation of D from the steady-state flux requires the knowledge of solubility and membrane area. An example of this can be seen in the case of the thicker sample at the highest temperature where, obviously, a part of the sample area became inactive. This led to a steady-state flux lower than expected without changing the result of the transient behavior.

A closer look at the individual data shows that the values for D tend to increase with an increase in P_h . It can be expected that the hydrogen diffusion coefficient will not be independent of concentration over a wider range of n . In our case, however, the observed trend will be mainly a result of the deviation of hydrogen solubility from the ideal behavior as discussed earlier. In the evaluation of the time lag measurements, a small trend arrives also from deviations of the boundary condition $c_{3,1} = 0$ for $t > 0$ in the actual experiments. This effect will be relatively larger for low values of P_h and will tend to lead to values of D

which are too small. Thus, even though one could expect that the (Pd-Ag)-Ta interface would have some effect on the hydrogen diffusion behavior through such composites, it seems to be too small to influence the reported results.

It is possible to arrive at an estimate for the entropy of activation for the hydrogen diffusion process in Ta from the preexponential factor, D_0 , by applying the theory for interstitial diffusion of Wert and Zener^{9,10}

$$D_0 = \frac{1}{6} \kappa Z_p \lambda^2 \nu_0 \frac{2kT}{h\nu_0} \sinh\left(\frac{h\nu_0}{2kT}\right) \exp\left(\frac{\Delta S^\circ}{R}\right)$$

where κ = transmissions factor (~ 1), Z_p = number of exits from interstitial site, λ = jump distance, ν_0 = vibrational frequency of H atom in interstice, h = Planck's constant, k = Boltzmann constant, and ΔS° = entropy of activation.

The evaluation of ΔS° requires, however, some assumptions with respect to the remaining parameters. It has been concluded¹ that at the condition of the present investigation the hydrogen atoms should be statistically distributed and occupy the tetrahedral interstices. An approximate value for the vibrational frequency of the H atom can be obtained by $\nu_0 = (E/2m\lambda^2)$, where E = activation energy for H diffusion, m = mass of H, and λ = distance between two tetrahedral sites. With $\lambda = a\sqrt{2}/4$ (a = lattice constant = 3.29 Å), then $\nu_0 = 4.01 \times 10^{13}$ (sec⁻¹). The transition with the lowest activation energy from one tetrahedral site to another will most likely be through one of the tetrahedron faces (that means $Z_p = 4$). The distance between the tetrahedral sites is $\lambda = a(\sqrt{2}/4)$; the progress in direction of the overall flux will, however, be only $a/4$ per jump. With these assumptions and $D_0 = 7.8 \times 10^{-3}$, one obtains a reasonable value of $\Delta S^\circ \approx 2.3$ cal/g-atom deg. (The less likely jump through the edges of the tetrahedron would yield $Z_p = 6$, $\lambda = a/2$, and $\Delta S^\circ = -1.3$ cal/g-atom deg.)

Figure 3 shows an Arrhenius plot of the hydrogen diffusion coefficients in tantalum. The deviations of the experimental values from the calculated line are shown in Figure 4. This figure demonstrates clearly the statistical distribution of the data points. Figure 3 also contains the literature data for hydrogen diffusion. Mallett and Koehl⁵ measured the kinetics of hydrogen absorption by tantalum rods. They give the diffusion coefficients from measurements leading to two concentrations as

$$D_{n \rightarrow 0.053} = 1560 \exp[(-32,230 \pm 3140)/RT] \quad (500-700^\circ)$$

$$D_{n \rightarrow 0.111} = 13960 \exp[(-33,620 \pm 1370)/RT] \quad (450-600^\circ)$$

These activation energies seem to be too high and are probably due to surface inhibitions which had been observed during their investigations. Makrides, Wright, and McNeill⁶ measured the hydrogen permeation through tantalum samples coated with a thin Pd layer (~ 1000 Å) and calculated the hydrogen diffusion coefficient in Ta to be

$$D_{n \rightarrow 0.07} = 7.5 \times 10^{-2} \exp(-14,400/RT) \quad (400-525^\circ)$$

The quite close agreement of this result with the present findings becomes even more apparent when comparing the actual data points, since the variance in activation energy is quite large due to the relatively narrow temperature range of Makrides' investigation.

Acknowledgment. The author wishes to thank Dr. A. C. Makrides for supporting this research. The author is also grateful to Explosive Fabricators Division of Tyco for the preparation of the (Pd-Ag)-Ta-(Pd-Ag) clad.

(9) C. Wert and C. Zener, *Phys. Rev.*, **76**, 1169 (1949).

(10) C. Zener, *J. Appl. Phys.*, **22**, 272 (1951).

Reflection of a Voltage Step from a Section of Transmission

Line Filled with a Polar Dielectric

by H. Fellner-Feldegg and E. F. Barnett

Hewlett-Packard Laboratories, Palo Alto, California 94304 (Received November 4, 1969)

A simple method of determining relaxation times for Debye dielectrics from time domain reflectivity measurements is given. The method also makes it possible to check for ideal dielectric behavior. It is a correction of the method given in an earlier paper.¹

Introduction

One of us¹ reported on the measurement of dielectrics in the time domain by measuring the reflection of a voltage step from the air-dielectric interface. The shape of the reflected signal gives information about the high-frequency and low-frequency dielectric constant, κ_∞ and κ_0 , respectively, and the relaxation time τ (see Figure 1) with

$$\kappa_\infty = \left(\frac{1 - \rho_\infty}{1 + \rho_\infty} \right)^2$$

$$\kappa_0 = \left(\frac{1 - \rho_0}{1 + \rho_0} \right)^2$$

where

$$\rho_\infty = \frac{V_1 - V_0}{V_0}; \quad \rho_0 = \frac{V_2 - V_0}{V_0}$$

are the reflection coefficients. V_0 is the amplitude of the incident step pulse, $V_1 - V_0$ the amplitude of the reflected pulse at the time $t = 0$, and $V_2 - V_0$ the reflected pulse height when the relaxation of the dielectric is complete.

For the determination of the relaxation time it was assumed that this voltage step is applied to the dielectric at the interface as well. It has been pointed out by Whittingham² and Omura,³ however, that this is not true in the case of dielectric dispersion. Here the reflected pulse is a complicated function of time, as shown in Figure 3 of ref 1. The voltage actually applied to the dielectric at any instant is the sum of the incident voltage step and the voltage of the reflected waveform at that instant. Using the Laplace transform method, we have derived expressions for the reflected voltage as a function of time in the form of infinite series for Debye dielectrics. With the aid of a computer, these series have been used to compute this function for a wide range of cases of practical interest. These results are presented in graphical form in such a way as to facilitate determining the true relaxation time from observed reflected

waveforms. Furthermore, several independent determinations of the relaxation time can be made from different features of the reflected waveform. The consistency of the several values obtained for a given dielectric serves as a powerful check of the correctness of the assumptions underlying the method. The most important of these assumptions is that the dielectric is of the Debye type, having a single relaxation time.

Mathematical Derivations

A polar dielectric having a single relaxation time τ has a complex dielectric constant which depends on frequency according to the equation

$$\kappa(p) = \kappa_\infty + \frac{\kappa_0 - \kappa_\infty}{1 + p\tau} = \frac{\kappa_0 + \kappa_\infty p\tau}{1 + p\tau} \quad (1)$$

where $p = j\omega$, κ_0 is the low-frequency permittivity, and κ_∞ is the high-frequency permittivity.

Let a transmission line be filled with such a dielectric on one side of a transverse plane, the line on the other side being empty. For a sinusoidal signal of angular frequency ω incident on the interface from the empty side, the voltage reflection coefficient is

$$\rho(p) = \frac{1 - \sqrt{\kappa(p)}}{1 + \sqrt{\kappa(p)}} = \frac{\sqrt{1 + p\tau} - \sqrt{\kappa_0 + \kappa_\infty p\tau}}{\sqrt{1 + p\tau} + \sqrt{\kappa_0 + \kappa_\infty p\tau}} \quad (2)$$

Let a voltage step of amplitude V_0 be incident on the interface from the empty side. The reflected voltage as a function of time is $V_0 P(t)$, where $P(t)$ is given by

$$P(t) = \mathcal{L}^{-1} \left[\frac{1}{p} \rho(p) \right] \quad (3)$$

Here \mathcal{L}^{-1} represents the inverse Laplace transform.

(1) H. Fellner-Feldegg, *J. Phys. Chem.*, **73**, 616 (1969).

(2) T. A. Whittingham, *ibid.*, **74**, 1824 (1970).

(3) M. Omura, Ames Research Center, private communication.

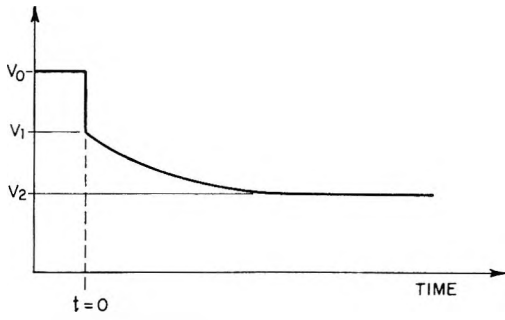


Figure 1. Typical reflection of a step pulse V_0 from an air-dielectric interface.

We denote the time-dependent reflection coefficient by $P(t)$ to emphasize that it has been derived from $\rho(\omega)$ by transformation. It is identical with $\rho(t)$ in ref 1. Apparently, $P(t)$ cannot be expressed in closed form in terms of well-known or tabulated functions. In the following analysis two series expansions for $P(t)$ will be derived, one of which converges rapidly for $t \gg \tau$, and the other for $t \ll (\kappa_\infty/\kappa_0)\tau$. Both series converge (although in some cases slowly) for all values of t , κ_0 , and κ_∞ , provided $0 < \kappa_\infty < \kappa_0$, a condition which is always satisfied for polar dielectrics.

Series Suitable for $t \gg \tau$. Equation 1 may be transformed into

$$\kappa(p) = \kappa_0(1 - u) \tag{4}$$

where

$$u = \frac{\left(1 - \frac{\kappa_\infty}{\kappa_0}\right)p\tau}{1 + p\tau}$$

$\rho(p)$ (eq 4) now becomes

$$\rho(p) = g(u) = \frac{1 - \sqrt{\kappa_0(1 - u)}}{1 + \sqrt{\kappa_0(1 - u)}} \tag{5}$$

The inverse Laplace transform can be expressed as an integral where the range of integration is the imaginary axis in the p plane. It is easy to see that for pure imaginary p , $|u| < 1$ provided that $0 < \kappa_\infty < \kappa_0$. This last condition, as previously noted, always holds for actual dielectrics. The condition $|u| < 1$ is sufficient for the convergence of the Taylor expansion of $g(u)$ about $u = 0$. This Taylor expansion can be written

$$g(u) = \sum_{n=0}^{\infty} \frac{1}{n!} g_n u^n \tag{6}$$

$$g_n = \sum_{m=0}^n \binom{n}{m} a_m b_{n-m} \tag{7}$$

$$\left. \begin{aligned} a_0 &= -\kappa_0 - 1 + 2\sqrt{\kappa_0} \\ a_1 &= \kappa_0 - \sqrt{\kappa_0} \quad a_2 = -1/2\sqrt{\kappa_0} \\ a_{m+1} &= \frac{2m-1}{2} a_m, \quad m \geq 2 \end{aligned} \right\} \tag{8}$$

$$\left. \begin{aligned} b_0 &= \frac{1}{\kappa_0 - 1} \\ b_{m+1} &= \frac{(m+1)\kappa_0}{\kappa_0 - 1} b_m, \quad m \geq 0 \end{aligned} \right\} \tag{9}$$

The step-function response is now given by

$$P(t) = \rho_0 u(t) + \sum_{n=1}^{\infty} \frac{g_n}{n!} \mathcal{L}^{-1} \left[\frac{1}{p} u^n(p) \right] \tag{10}$$

where $u(t)$ is a unit step function, and $\rho_0 = g_0$ is the low-frequency limit of the reflection coefficient.

$$\begin{aligned} \mathcal{L}^{-1} \left[\frac{1}{p} u^n(p) \right] &= \left(1 - \frac{\kappa_\infty}{\kappa_0} \right)^n \mathcal{L}^{-1} \left[\frac{p^{n-1}}{(p + \mu)^n} \right] = \\ &= \left(1 - \frac{\kappa_\infty}{\kappa_0} \right)^n e^{-\mu t} \sum_{m=0}^{n-1} \frac{(-1)^m}{m!} \binom{n-1}{m} (\mu t)^m \end{aligned} \tag{11}$$

where $\mu = 1/\tau$.

Series Suitable for $t \ll (\kappa_\infty/\kappa_0)\tau$. Equation 1 may be transformed into

$$\kappa(p) = \frac{\kappa_\infty}{1 - v} \tag{12}$$

where

$$v = \frac{\frac{\kappa_0}{\kappa_\infty} - 1}{p\tau + \frac{\kappa_0}{\kappa_\infty}}$$

$\rho(p)$ (eq 2) now becomes

$$\rho(p) = h(v) = \frac{\sqrt{1-v} - \sqrt{\kappa_\infty}}{\sqrt{1-v} + \sqrt{\kappa_\infty}} \tag{13}$$

Here again we have $|v| < 1$ for pure imaginary p and $0 < \kappa_\infty < \kappa_0$. Hence we can make a Taylor expansion about $v = 0$, followed by a term-by-term inverse Laplace transformation.

$$h(v) = \sum_{n=0}^{\infty} \frac{1}{n!} h_n v^n \tag{14}$$

$$h_n = \sum_{m=0}^n \binom{n}{m} c_m d_{n-m} \tag{15}$$

$$\left. \begin{aligned} c_0 &= -\kappa_\infty - 1 + 2\sqrt{\kappa_\infty} \\ c_1 &= 1 - \sqrt{\kappa_\infty} \quad c_2 = -1/2\sqrt{\kappa_\infty} \end{aligned} \right\} \tag{16}$$

$$c_{m+1} = \frac{2m-1}{2} c_m, \quad m \geq 2$$

$$\left. \begin{aligned} d_0 &= \frac{1}{\kappa_\infty - 1} \\ d_{m+1} &= -\frac{m+1}{\kappa_\infty - 1} d_m, \quad m \geq 0 \end{aligned} \right\} \tag{17}$$

The step-function response is given by eq 18.

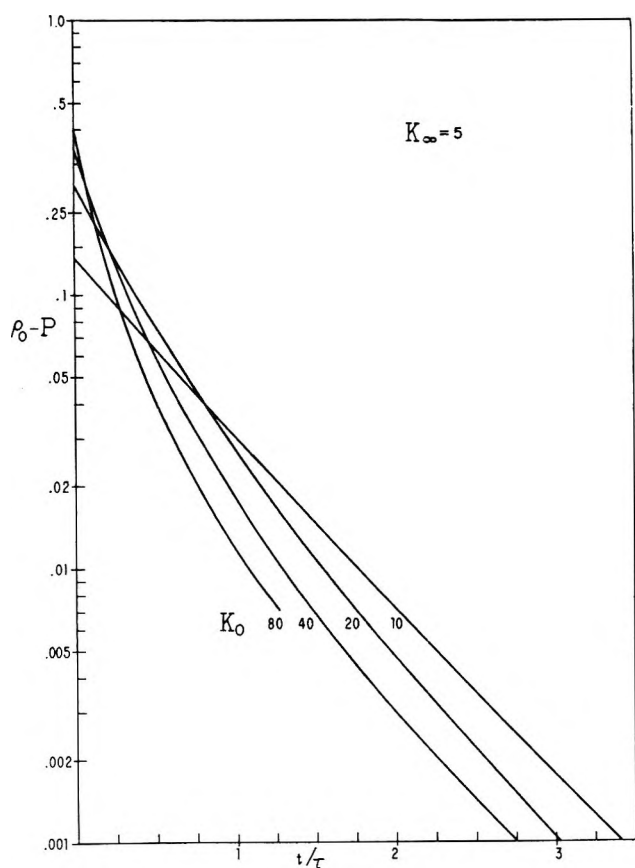


Figure 2. Normalized time dependence of the reflection coefficient $P(t)$ for Debye dielectrics with $\kappa_\infty = 5$.

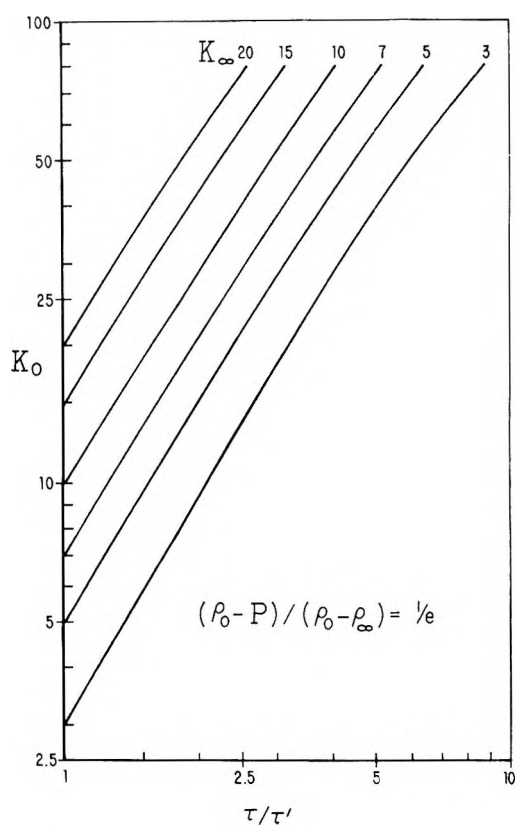


Figure 4. Ratio of the true relaxation time τ to the measured time τ' at the $1/e$ point of the reflected coefficient.

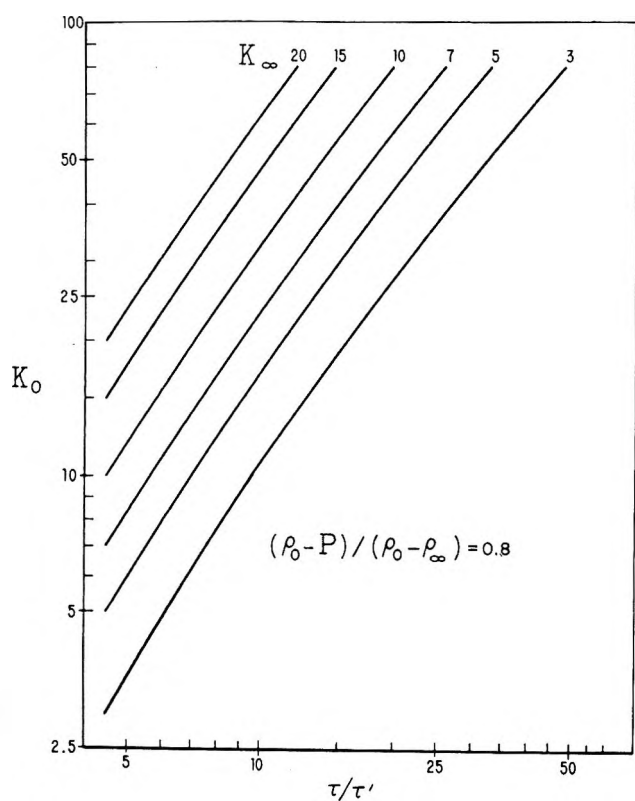


Figure 3. Ratio of the true relaxation time τ to the measured time τ' at the 80% point of the reflection coefficient.

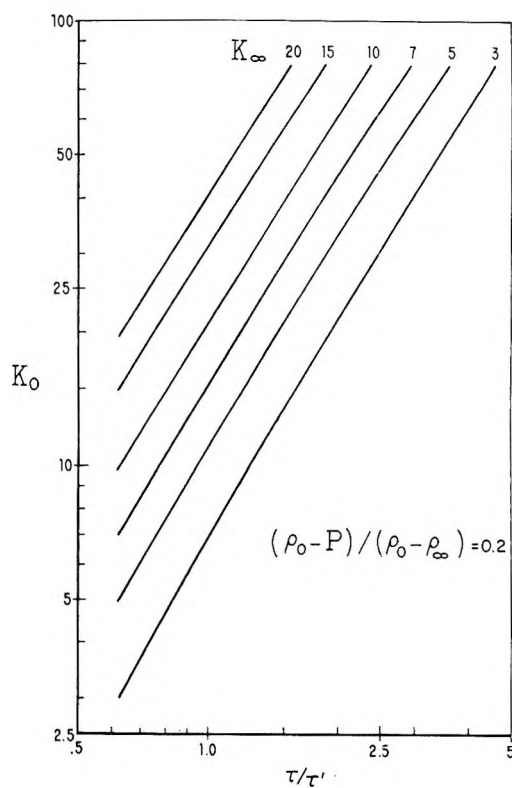


Figure 5. Ratio of the true relaxation time τ to the measured time τ' at the 20% point of the reflection coefficient.

$$P(t) = \rho_{\infty}u(t) + \sum_{n=1}^{\infty} \frac{h_n}{n!} \mathcal{L}^{-1}\left[\frac{1}{p} v^n(p)\right] \quad (18)$$

where $\rho_{\infty} = h_0$ is the high-frequency limit of the reflection coefficient.

$$\mathcal{L}^{-1}\left[\frac{1}{p} v^n(p)\right] = \left(\frac{\kappa_0}{\kappa_{\infty}} - 1\right)^n \frac{1}{\tau^n} \mathcal{L}^{-1}\left[\frac{1}{p(p + \nu)^n}\right] = \left(1 - \frac{\kappa_{\infty}}{\kappa_0}\right)^n \left[1 - e^{-\nu t} \sum_{m=0}^{n-1} \frac{(\nu t)^m}{m!}\right] \quad (19)$$

where $\nu = (\kappa_0/\kappa_{\infty})/\tau$.

Numerical Results and Discussion

Figure 2 shows some typical step-function response curves obtained by computer using the series 10 and 18. The ordinate is $\rho_0 - P$, and the abscissa is t/τ . The cases plotted are $\kappa_{\infty} = 5, \kappa_0 = 10, 20, 40, 80$. The plot is semilogarithmic, so that a straight line with constant negative slope corresponds to simple exponential decay. The response functions plotted have negative slopes which vary with time and with

κ_0 . The magnitude of the slope decreases with increasing time and with decreasing κ_0 . It can be shown that this function approaches a simple exponential decay with time constant τ as $\kappa_0/\kappa_{\infty} \rightarrow 1$.

The relaxation time τ can conveniently be determined from the measured time τ' for $\rho_0 - P$ to decrease to some specified fraction of its initial value $\rho_0 - \rho_{\infty}$, provided κ_0 and κ_{∞} are determined as described in ref 1. Figures 3-5 show τ/τ' as abscissa with κ_0 as ordinate for a range of values of κ_{∞} of practical interest. τ' is the time necessary for $(\rho_0 - P)/(\rho_0 - \rho_{\infty})$ to reach the values 0.8, $1/e$, and 0.2, respectively, in the three figures. Both coordinates are plotted logarithmically. The resulting curves have relatively little curvature and are nearly parallel to each other over the range plotted.

The derivation of $P(t)$ for lossy dielectrics (eq 12), given in ref 1, is correct since it was derived in closed form by Laplace transform from the frequency domain. We are extending these calculations for dielectrics with relaxation spectra and will report these at a later date.

Electron Spin Resonance Studies of Ion Association between Alkali Metal Ions and Hydrocarbon Radical Ions¹

by Ira B. Goldberg and James R. Bolton

Department of Chemistry, University of Minnesota, Minneapolis, Minnesota 55455 (Received November 7, 1969)

The alkali metal hyperfine splittings in the esr spectra of ion pairs with aromatic hydrocarbon radical anions have been examined for the naphthalene, anthracene, and biphenylene systems. A molecular orbital theory incorporating the methods of Hückel, McClelland, and Atherton and Weissman has been developed which provides an estimate of the unpaired-electron density on the alkali metal ion as a function of the position of the ion relative to the molecular plane. Unpaired-electron density maps have been prepared for each of the systems. From these it has been possible to interpret the experimental alkali metal hyperfine splittings in terms of the most likely positions for the alkali metal ion. Alkyl-substituted compounds have been used to provide further evidence. The calculations have also aided in the interpretation of alkali metal spin density variations in the series Na, K, Rb, Cs for the three aromatic systems. Negative alkali metal hyperfine splittings are predicted in some cases and a model is presented to account for this possibility.

Introduction

Alkali metal hyperfine splittings (hfs) arising from ion pairs of alkali metal ions with hydrocarbon radical ions^{2a} have been used to measure kinetics and equilibria between structurally different ion pairs.^{2b} In many of these cases, the observed alkali metal splitting was assumed to be a time average of the splittings from two of these ion-paired species. The source of the dif-

ferences of the alkali metal hfs among various ion pairs has been partially attributed to solvation, but no detailed qualitative explanation of these differences is available. In addition, little attempt has been made to elucidate the structure of these ion pairs, that is, the

(1) Supported in part by grants from the National Science Foundation (GP-8416) and the Graduate School, University of Minnesota.

most favorable positions of the alkali metal ion relative to the π -electron system.

Recently there has been some interest in the detailed structure of these ion pairs. A calculation which involves a perturbation to Hückel molecular orbital theory has been suggested by McClelland.³ This model, which considers only point-charge electrostatic forces acting on the π -electron system, has been used to compute potential energy surfaces of ion-paired systems.^{4,5} Among the drawbacks of using this calculation alone to derive the probable structure of the ion pair is that repulsion between the electrons in the π -system and those of the cation is not considered.

On the other hand, models which have been proposed to account for alkali metal hfs have not been used to elucidate the structures of ion pairs. Atherton and Weissman^{2a} suggested that the alkali metal ion is coordinated to the π -electron system, and therefore the unpaired electron may be delocalized onto the "empty" alkali metal s orbital. This model has been used by Atherton in the study of pyrazine⁶ and the naphthalene and bipyridyl negative ions.⁷ de Boer⁸ reported that this mechanism does not explain negative alkali metal hfs which are observed in pyracene and the biphenyl⁹ systems. To account for this, he proposed that electron correlation effects may cause polarization of the inner electrons of the alkali metal ion.

We have considered alkali metal ion pairs with naphthalene, biphenylene, and anthracene under a variety of conditions of solvent composition and temperature. The results are analyzed in terms of the models which have been proposed. In addition, we have used alkyl-substituted compounds to aid in the assignment of specific structures to these ion pairs.

Experimental Section

Samples were prepared in a manner similar to that described in the literature.¹⁰ Additional details of these procedures are available.¹¹ Solvents were refluxed over sodium or potassium, several times over lithium aluminum hydride, and were then vacuum distilled and stored in solvent vessels containing the disodium salt of tetracene. The hydrocarbons were sublimed immediately before use. All hydrocarbons were commercially available except 2,3,6,7-tetraethylbiphenylene which was a gift of McOmie.¹² All spectra reported here were taken on a modified Varian V-4502 esr spectrometer with a dual cavity and 12-in. magnet. A sample of either Wursters Blue¹³ in ethanol or the perylene negative ion in 1,2-dimethoxyethane¹⁴ was used as a secondary standard to calibrate the magnetic field. Temperature control was achieved by boiling nitrogen through a cylindrical quartz dewar inserted in the sample cavity. The temperature was monitored by a copper-constantan thermocouple.

Theory

When an alkali metal ion approaches an aromatic

hydrocarbon anion, two effects may be anticipated. First there will be an effect on the π -molecular orbitals due to the electrostatic perturbation $-e^2/r_{tm}$ where r_{tm} is the distance between the alkali metal nucleus and the electron t of the π system. The second effect arises when overlap of the empty alkali metal ion s orbital with the π system is considered. This leads to a charge transfer to the alkali metal ion resulting in an alkali metal hyperfine splitting.

The electrostatic effect of the alkali metal ion acting on a π -electron system has been treated by McClelland.³ When Hückel molecular orbital (HMO) theory is used to describe the π -electron system, the effect of the positive point charge may be represented by changing the coulomb integral of each atom in the π -electron system to

$$\alpha_t = \alpha_t^0 + \frac{5.69\beta_{cc}^0}{r_{tM}} \quad (1)$$

where α_t is the coulomb integral of atom t in the π -electron system, α_t^0 is the coulomb integral in the absence of the electric field, β_{cc}^0 is the resonance integral of of carbon-carbon π bond (considered to be -2.50 eV), and r_{tM} is the distance between atom t and the center of positive charge M, in Å. The factor 5.69 converts α_t to units of β_{cc}^0 . More generally, one may solve the determinant

$$\left| H_{st}^0 + \sum \frac{5.69\beta_{cc}^0 S_{st}}{1/2(r_s + r_t)} - ES_{st} \right| = 0 \quad (2)$$

where H_{st}^0 is the Hückel matrix element between atoms s and t, and S_{st} is the overlap integral between s and t.

- (2) (a) N. M. Atherton and S. I. Weissman, *J. Amer. Chem. Soc.*, **83**, 1330 (1961); (b) N. Hirota, *J. Phys. Chem.*, **71**, 127 (1967); N. Hirota and R. Kreilick, *J. Amer. Chem. Soc.*, **88**, 614 (1966); A. Crowley, N. Hirota, and R. Kreilick, *J. Chem. Phys.*, **46**, 4815 (1967); N. Hirota, *J. Amer. Chem. Soc.*, **90**, 3603 (1968); N. Hirota, W. Carraway, and W. Schook, *ibid.*, **90**, 3611 (1968).
- (3) B. J. McClelland, *Trans. Faraday Soc.*, **57**, 1458 (1961); *Chem. Rev.*, **64**, 301 (1964).
- (4) (a) M. Iwaizumi, M. Suzuki, T. Isobe, and H. Azumi, *Bull. Chem. Soc. Jap.*, **41**, 732 (1968); (b) *ibid.*, **40**, 1325 (1967).
- (5) C. A. McDowell and K. F. G. Paulus, *Can. J. Chem.*, **43**, 224 (1965); N. M. Atherton and A. E. Goggins, *Trans. Faraday Soc.*, **62**, 1702 (1966).
- (6) N. M. Atherton, *ibid.*, **62**, 1707 (1966).
- (7) S. Aono and K. Oohashi, *Progr. Theor. Phys.*, **30**, 162 (1963).
- (8) E. de Boer, *Rec. Trav. Chim. Pays-Bas.*, **84**, 609 (1965).
- (9) G. W. Canters, E. de Boer, B. M. P. Hendriks, and H. van Willigen, *Chem. Phys. Lett.*, **1**, 627 (1968); G. W. Canters, E. de Boer, B. M. P. Hendriks, and A. A. K. Klassen, to be published in *Proc. Colloq. Ampere*, **15** (1968).
- (10) See, for example, P. R. Hindle, J. dos Santos-Veiga, and J. R. Bolton, *J. Chem. Phys.*, **48**, 4703 (1968).
- (11) I. B. Goldberg, thesis, University of Minnesota, 1969.
- (12) D. V. Gardiner and J. F. W. McOmie, *J. Chem. Soc., C*, 2420 (1968).
- (13) J. R. Bolton and W. R. Knolle, unpublished results: $a_N = 7.051 \pm 0.006$ G; $a_{CH_3} = 6.773 \pm 0.004$ G; $a_H = 1.989 \pm 0.009$ G.
- (14) J. R. Bolton, *J. Phys. Chem.*, **71**, 3702 (1967); hfs are 0.450, 3.043, and 3.493 G, respectively, for each set of four equivalent protons.

In this case $S_{st} = \delta_{st}$. This method enables both the energy of the ion pair and the molecular orbitals to be calculated. To consider the energy of ion association where the alkali metal is in a fixed position, the energy of the filled orbitals of the free ion, E_i^0 , must be subtracted from the energy of those of the ion pair, E_i^{IP} . Thus

$$E_A = \nu_i \sum_i (E_i^{IP} - E_i^0) - 5.69 \sum_t \frac{q^2}{r_{tM}} \quad (3)$$

where E_A is the energy of association of the ion pair and ν_i is the number of electrons in molecular orbital i . In eq 3, the repulsion between the nuclear cores of the conjugated system and the positive charge of the alkali metal ion must be subtracted.^{4b} This repulsion arises since the atoms in the conjugated system each contribute one electron to the π -electron system.

Atherton and Weissman^{2a} report that Robertson has used their method to calculate the unpaired electron density on alkali metal ions in ion pairs; however, to our knowledge, the results have not been published as yet. Aono and Oohashi⁷ have also used the Atherton-Weissman model to estimate the sodium hfs in sodium naphthalenide systems and have had moderate success.

We have developed a modified form of the Atherton-Weissman model. The unpaired electron density on the alkali metal nucleus is estimated subject to the following assumptions. 1. There will be negligible contributions to the alkali metal hfs from the σ system of the aromatic hydrocarbon. 2. The alkali metal ion will be located at some position above (or below) the nuclear plane of the hydrocarbon. 3. Covalency between the alkali metal ion and the aromatic system is small and may be treated by perturbation theory. 4. HMO theory incorporating the McClelland model may be used to provide a representation of the molecular orbitals of the aromatic hydrocarbon in the presence of the cation. These molecular orbitals form the zero order basis set for the perturbation calculation.

The term in the Hamiltonian which gives rise to the mixing in of the alkali metal s orbital with the π molecular orbitals is $-e^2/r_{tM}$. The application of this perturbation modifies each molecular orbital i to

$$\psi_i \rightarrow \psi_i^0 + \lambda_i \phi_M \quad (4)$$

where ψ_i^0 is a member of the zero order basis set, ϕ_M is the lowest empty alkali metal s orbital and λ_i is the admixture coefficient. λ_i is obtained from first-order perturbation theory as

$$\lambda_i = \sum_t \frac{c_{it} \left\langle t \left| \frac{e^2}{r_{tM}} \right| M \right\rangle}{E_i - E_M} \quad (5)$$

Here c_{it} is a coefficient in an expansion of ψ_i^0 in terms of ϕ_i in the zero order basis set. The matrix element in eq 5 is equivalent to the "resonance" integral,

H_{tM} , for purposes of this calculation. It may be estimated from a modified Wolfsberg-Helmholtz approximation,¹⁵ *i.e.*

$$H_{tM} = \frac{k}{2} (H_{tt} + H_{MM}) S_{tM} \quad (6)$$

Here H_{tt} and H_{MM} are the coulomb integrals of atoms t and M , respectively; S_{tM} is the overlap integral between t and M and k is a scaling factor usually taken to be about 2.^{15b} H_{tt} for a carbon atom in a conjugated system was taken to be 7.07 eV. This value is reported by Streitwieser from ionization potential measurements¹⁶ and agrees with 6.93 eV calculated from spectroscopic information.¹⁷ H_{MM} was assumed to be equal to the measured alkali metal ionization potentials.¹⁸ Regardless of the precise values of these parameters, the important feature is that λ_i is related to the overlap integrals S_{tM} .

Overlap integrals between a carbon 2p orbital and the alkali metal s orbitals were calculated by the method of Mulliken, *et al.*,¹⁹ using Slater atomic orbitals.²⁰ Since the cation may not be directly over any particular carbon atom, S_{tM} was estimated by

$$S_{tM} = S_{tM}(\sigma) \cos \theta \quad (7)$$

where $S_{tM}(\sigma)$ is the σ -type overlap integral between an s and a p orbital, and θ is angle between the axis of symmetry of the p orbital and the internuclear axis between t and M . The difference between the ionization potentials of the radical ion and alkali metal may be used, but these values would only apply to a vapor system. A better approximation would be to use the difference between reduction potentials of the hydrocarbon and the cation as a measure of the energy. Hoijtink^{16b,21} determined the relationship between reduction potentials in aqueous dioxane and the Hückel energy.

$$\epsilon = (2.368 \pm 0.099)E_j - 0.924 \pm 0.109 \quad (8)$$

where ϵ is the reduction potential of the hydrocarbon *vs.* a saturated calomel electrode (+0.244 V *vs.* nhe), and E_j is the Hückel energy in units of β_{oc}^0 . Before eq 8 was used, the electrostatic attraction between the alkali metal ion and the radical was subtracted from

(15) (a) M. Wolfsberg and L. Helmholtz, *J. Chem. Phys.*, **20**, 837 (1952); (b) C. J. Ballhausen and H. B. Gray, "Molecular Orbital Theory," W. A. Benjamin Inc., New York, N. Y., 1964, p 118.

(16) (a) A. Streitwieser, Jr., *J. Amer. Chem. Soc.*, **82**, 4123 (1960); (b) "Molecular Orbital Theory for Organic Chemists," John Wiley and Sons, New York, N. Y., 1961, p 192.

(17) I. J. Goldfarb and H. H. Jaffee, *J. Chem. Phys.*, **30**, 1622 (1959).

(18) C. E. Moore, "Atomic Energy Levels," Vol. 1-3, U. S. National Bureau of Standards, 1949-1952.

(19) R. S. Mulliken, C. A. Rieke, D. Orloff, and H. Orloff, *J. Chem. Phys.*, **17**, 1248 (1949); overlap integrals which included 4s or 6s orbitals required a numerical integration, see L. Leifer, F. A. Cotton, and J. R. Leto, *ibid.*, **28**, 364 (1958).

(20) J. C. Slater, *Phys. Rev.* **36**, 57 (1930).

(21) G. J. Hoijtink, *Rec. Trav. Chim.*, **74**, 1525 (1955); ref 16b, p 176.

the eigenvalues obtained from the solution of eq 2. This is equal to $5.69 \Sigma_i c_{ji}^2 / r_{iM}$. Oxidation potentials of alkali metals in aqueous solution have been calculated by Latimer.²²

The preceding method of calculating $E_i - E_M$ may tend to overcompensate for solvation. However, these values tend to be more indicative of the chemical behavior of the system than the use of a set of fixed values, although similar results are obtained in either case.

Once the contribution of the alkali metal atomic orbital to the molecular orbital, λ_i , is computed, the unpaired electron density on the alkali metal wave function may be interpreted to be λ_i^2 .

Finally, the estimation of alkali metal hfs, a_M , requires a relation between a_M and the unpaired electron density on the metal ion, ρ_M . For this we have assumed that the relation

$$a_M = Q_M \rho_M \quad (9)$$

holds. The proportionality factor Q_M has been approximated as the atomic hfs of the gaseous alkali metals as measured by Kusch and Taub.²³ It is recognized that Q_M may in fact be somewhat larger due to the contraction of the orbitals on removal of one electron from the alkali metal. Nevertheless, relative values of Q_M among the alkali metals should be well represented. Thus the single empirical value of k in eq 6 should compensate for these effects. Also we shall be interested primarily in relative changes in ρ_M rather than absolute values.

Results and Discussion

In the analysis that follows we shall consider alkali metal hfs in the ion pairs of naphthalene, anthracene, and biphenylene. We shall use the McClelland model to provide an energy contour map for each ion pair. This map plus a consideration of electron repulsion will be used to ascertain the most favorable positions for the alkali metal ion in the ion pair. Then the modified Atherton-Weissman model will be utilized to provide an alkali metal unpaired-electron density map. Finally the predictions of this map will be used to interpret the experimental alkali metal hfs.

The validity of the McClelland model for calculating the energy of ion associations must now be considered. First, the energy of the solvation of the system is not considered and therefore changes of solvation with respect to the motion of the cation around the radical ion are neglected in calculating the potential energy surface. More important, however, is the fact that the cations have a finite size, and repulsion between the electrons of either ion as well as mutual polarization between the anion and cation may become significant at the close interionic distances characteristic of ion pairs.

Although it is difficult to estimate the effect of electron-electron repulsion between the alkali metal ion

and the radical, some qualitative predictions may be derived. The McClelland calculation predicts that as the center of positive charge approaches the nuclear plane, the electrostatic attraction between the two ions increases. At very close interionic distances the repulsion between electrons becomes important, and thus the cation center would tend to rest over regions in which there is minimum electron density. In aromatic systems, this may be over the center of an aromatic ring. Some experimental evidence is available to support this conclusion. At low temperatures esr spectra of the potassium salt of heptafulvalene in 2-methyltetrahydrofuran exhibit an alternating line width which has been attributed to motion of the potassium ion between the seven-numbered rings.²⁴ In the biphenyl system the same effect is not observed.^{9,11} This may be because the larger ring of the heptafulvalene anion provides a deeper potential well than in the biphenyl anion, and therefore the rate of motion between the larger rings is slower.

In the calculations which follow, we have taken the effective "height" of the π system to be ~ 0.19 nm. This value is derived from the interplanar distance in graphite (~ 0.34 nm) with some allowance for the expansion of the orbitals. We used Pauling's values for the cation radii although these values may be too small.²⁵

Sodium Naphthalenide and Substituted Naphthalenides. A contour map of the energy of ion association of a point charge 0.3 nm above the molecular plane of naphthalene is shown in Figure 1. (All of the calculations, such as that depicted in Figure 1, were carried out at a constant height above the nuclear plane. If the variation between the potential energy minima and the central maximum were as much as 4 kcal mol⁻¹ then the maximum variation in cation height would be 0.015 nm. Clearly, this variation is small and justifies the assumption of a constant height in the calculations.) The shallow double-minimum potential well in Figure 1 becomes more plausible when electron repulsion is considered. As indicated earlier, electron repulsion will be a minimum when the cation is over the center of either of the rings. Nevertheless, it appears that the cation is not fixed in one of these potential wells, since large changes in the spin distribution in the molecule would be expected if it were. Only small changes are observed; thus one must assume that the alkali metal ion possibly jumps back and forth from one side

(22) W. N. Latimer, "The Oxidation States of the Elements and Their Potentials in Aqueous Solutions," 2nd ed, Prentice Hall, New York, N. Y., 1952, p 328.

(23) Atomic hfs are ⁷Li, 143.3 G; ²³Na, 316.06 G; ³⁹K, 82.7 G; ⁸⁵Rb, 361.05 G; ⁸⁷Rb, 1219.1 G; ¹³³Cs, 820.1 G; calculated from P. Kusch and H. Taub, *Phys. Rev.*, **75**, 1477 (1949).

(24) M. D. Sevilla, S. H. Flajser, G. Vincow, and H. J. Dauben, Jr., *J. Amer. Chem. Soc.*, **91**, 4139 (1969).

(25) D. F. C. Morris, "Ionic Radii and Enthalpies of Hydration of Ions," in "Structure and Bonding," Vol. 4, 1969, p 63.

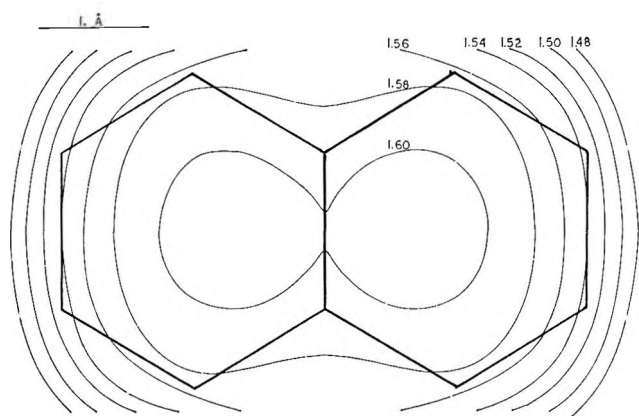


Figure 1. Electrostatic attraction between a positive point charge and the naphthalene anion where the positive charge is 3 Å above the nuclear plane of naphthalene. Energy in units of β°_{cc} .

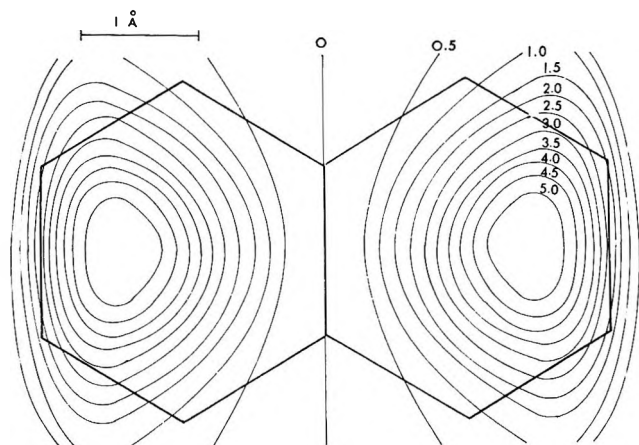


Figure 2. Calculated unpaired electron density on a sodium ion in ion pairs with the naphthalene anion. Sodium is 3 Å above the nuclear plane.

to the other so that the observed alkali metal hfs is a weighted time average of a large number of possible values.

The contour map of the unpaired electron density on a sodium ion 0.3 nm above the nuclear plane is shown in Figure 2. It should be noted that the region of maximum unpaired electron density occurs when the sodium ion is near the center of each of the benzene rings (not at the center as predicted by Aono and Oohashi.⁷ On the other hand, a position near the center of the radical would result in a very small sodium hfs. Typical sodium hfs in this system are in the range of 1–2 G which corresponds to $\rho_M \sim (3-6) \times 10^{-3}$. Thus it is reasonable to assume that the sodium ion spends most of its time near a position over each ring with a rapid hopping from one side to the other.

The choice of 0.3 nm as the height of the sodium ion above the nuclear plane is somewhat arbitrary; however, errors here may be compensated for in the choice of the value of k in eq 6. It is interesting to examine

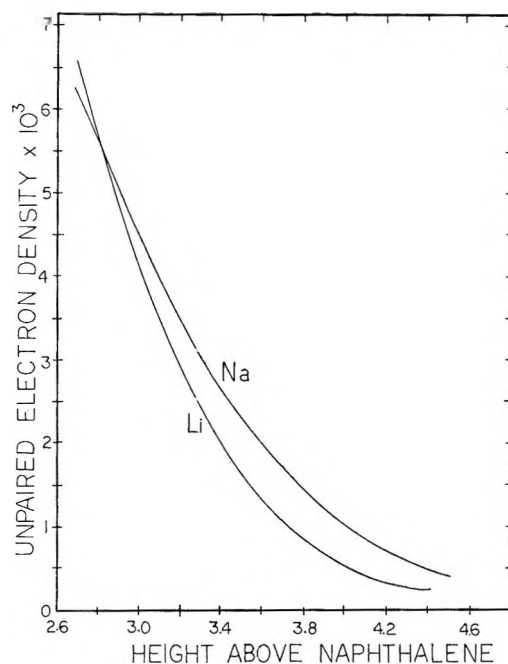


Figure 3. Calculated unpaired-electron density on sodium and lithium ions centered over a six-membered ring of naphthalene vs. height above the nuclear plane.

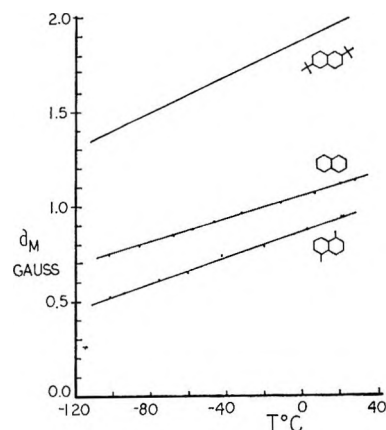


Figure 4. Temperature dependence of sodium hyperfine splittings in ion pairs with alkyl naphthalenides in MTHF. Data for the 2,6-di-*t*-butyl naphthalenide system are taken from ref 2b.

the variation of the sodium hfs with the height of the ion above the plane. The results of a sample calculation are shown in Figure 3. As expected, the sodium hfs decreases as the height increases. This result will have a bearing when solvent effects are considered (*vide infra*).

Further insight into the structure of this ion pair is provided by a consideration of the sodium ion pairs of alkyl-substituted naphthalenides. Usually one does not observe large changes in the unpaired electron distribution (as determined from the proton hfs) in the naphthalene system on alkyl substitution, especially when substitution is equivalent on each ring.²⁶

Thus it is reasonable to assume that the contour maps of the substituted naphthalenides will be nearly the same as that of the unsubstituted naphthalenide. Nevertheless, large changes in the sodium hfs are observed in different substituted naphthalenes under the same conditions as shown in Figure 4.

We interpret these marked changes in terms of a "steric" effect of the alkyl groups which forces the sodium ion away from the regions near the alkyl groups. First consider the 1,5-dimethyl naphthalene. The observed sodium hfs is ~ 0.1 G less than in the unsubstituted naphthalene. The methyl groups will force the sodium ion away from the 1 and 5 positions and thus closer to the 4 and 6 positions. (Redistribution of spin in the radical because of the alkyl groups is not considered important in this result because, although the spin density on the carbon atoms at the 4 and 8 positions is decreased, that of the 3, 7, 9, and 10 positions is increased. Since the overlap integral changes slowly with distance, the redistribution of the unpaired electron in the substituted naphthalene should not have a large effect.) From Figure 2 one would thus anticipate a reduction in ρ_M in agreement with observation.

By way of contrast, consider the 2,6-di-*t*-butyl naphthalene system. Here the sodium hfs is ~ 0.4 G larger than in naphthalene. The large *t*-butyl groups will cause a "hardening" of the potential well on the out-sides of the well. Oscillations of the sodium ion will thus be confined more to the regions above each of the benzene rings and hence in a region of higher unpaired electron density as seen in Figure 2.

Sodium Anthracenides. The sodium hfs, under the same conditions, is generally observed to be larger in sodium anthracenide than in sodium naphthalenide²⁶ (e.g., see Table I). Anthracene ion pairs are found to

Table I: Sodium Hyperfine Splittings (G) at Room Temperature

Solvent	MTHF	DEE
Biphenylene	0.204	0.15
Naphthalene	1.115	2.09 ^a
Anthracene	1.54 ^a	2.68 ^a

^a From ref 2.

be more loosely bound than naphthalene ion pairs,^{26,27} presumably due to the fact that the net negative-charge distribution is more diffuse in the former case. Thus the observed behavior of the sodium hfs is at first somewhat surprising.

The McClelland calculations show a marked qualitative difference in the potential energy surfaces for naphthalene and anthracene. A cross section of this surface along the long axis of each molecule is shown in Figure 5. The lower energy portion of the well is

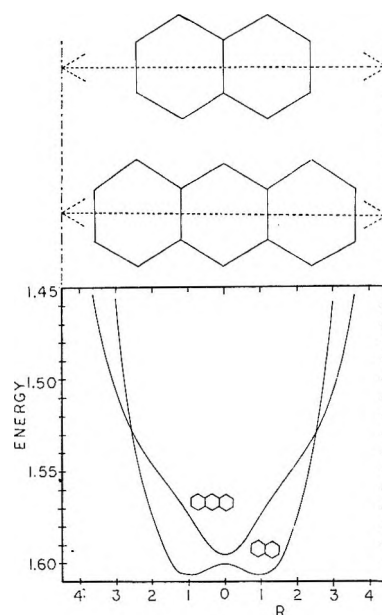


Figure 5. Electrostatic energy of a positive point charge associated with an anthracene or naphthalene anion 3 Å above the nuclear plane vs. the position of the positive charge. Anthracene and naphthalene drawn to scale; dotted line shows coordinates of the point charge.

much steeper in the anthracene case and confines the alkali metal ion largely to positions over the central ring. A consideration of electron repulsion would not change this conclusion as this region is also one of low electron density.

The contour map for the unpaired electron density on the sodium ion is shown in Figure 6. The conditions are the same as in the naphthalene calculation (see Figure 2). The unpaired-electron density on the sodium ion for the region of minimum energy is $\sim 11 \times 10^{-3}$ for anthracene as compared with $\sim 5 \times 10^{-3}$ for naphthalene. Thus it is reasonable to expect that the sodium hfs will be larger in the sodium anthracenide ion pair as compared with the sodium naphthalenide ion pair.

Sodium Biphenylenide. The sodium hfs in ion pairs with the biphenylene anion is considerably smaller than in ion pairs with either anthracene or naphthalene, Table I. At low temperatures, the sodium hfs decreases and appears to become negative at temperatures lower than -37° .

The contour maps for the energy and the unpaired-electron density on a sodium ion in an ion pair with the biphenylene anion are shown in Figures 7 and 8, respectively. Several properties are different in this system as opposed to anthracene and naphthalene. First, the maximum unpaired electron density is much less than in either of the other systems, and the maxi-

(26) C. deWaard and J. C. M. Henning, *Phys. Lett.*, **4**, 31 (1963); J. R. Bolton, Thesis, University of Cambridge, 1962.

(27) K. K. Brandes and R. J. Gerdes, *J. Phys. Chem.*, **71**, 508 (1967).

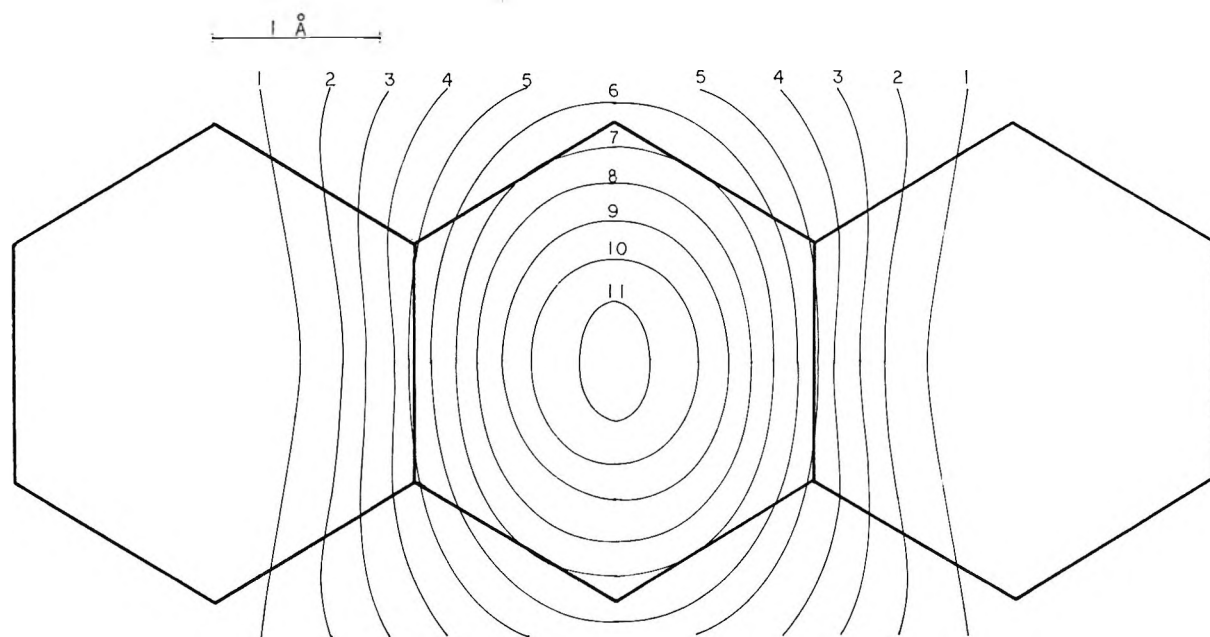


Figure 6. Calculated unpaired-electron density on a sodium ion in an ion pair with the anthracene anion. Sodium is 3 Å above the nuclear plane. Unpaired electron density in units of 10^{-3} .

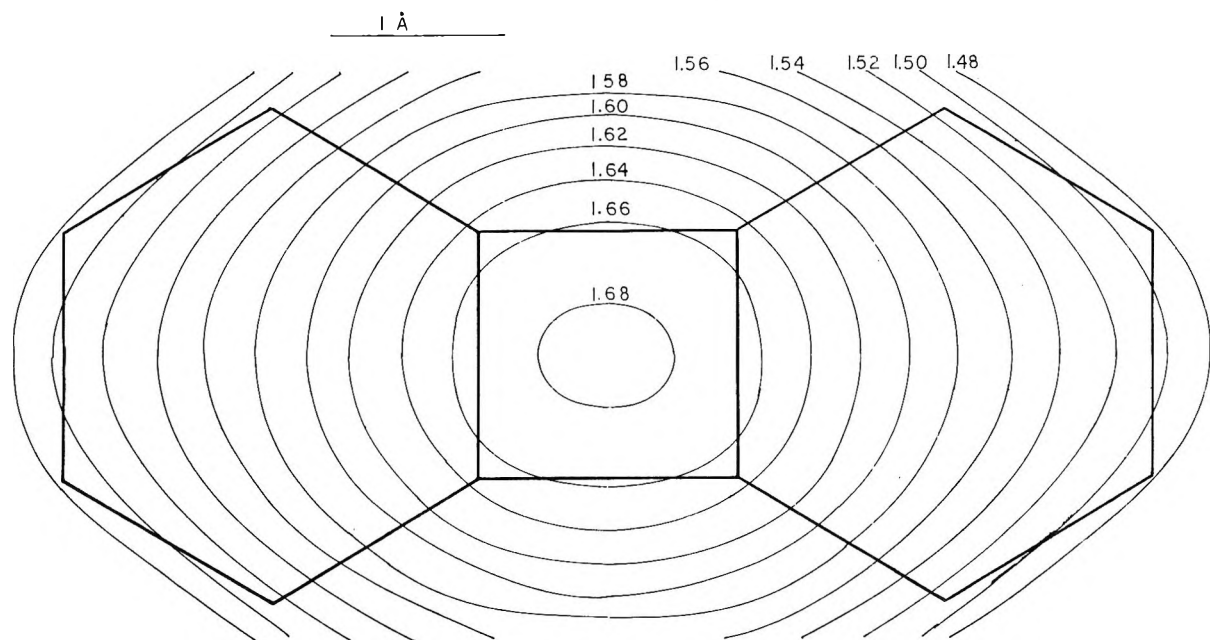


Figure 7. Electrostatic attraction between a positive point charge and the biphenylene anion where the positive charge is 3 Å above the nuclear plane of biphenylene. Energy in units of β^2_{∞} .

imum occurs outside of the centers of charge in regions where the energy of ion association is relatively high; second, there is a nodal plane in the unpaired electron distribution along the long axis of biphenylene which is not present in the naphthalene or anthracene systems. (The nodes of the lowest antibonding molecular orbitals for these molecules are compared in Figure 9.) Thus in the biphenylene system, sodium ion positions near a plane passing through the long axis of the molecule and perpendicular to the plane of the molecule

will result in very small sodium hfs. A nodal plane for the unpaired electron density also exists in the naphthalene system through the 9 and 10 positions. However, these positions appear to be unfavorable for the cation.

The McClelland model predicts that the most stable position for the sodium ion should be over the four-membered ring (see Figure 7) since this has been shown to be a region of large electron density.²⁸ However, because this region has high electron density, significant

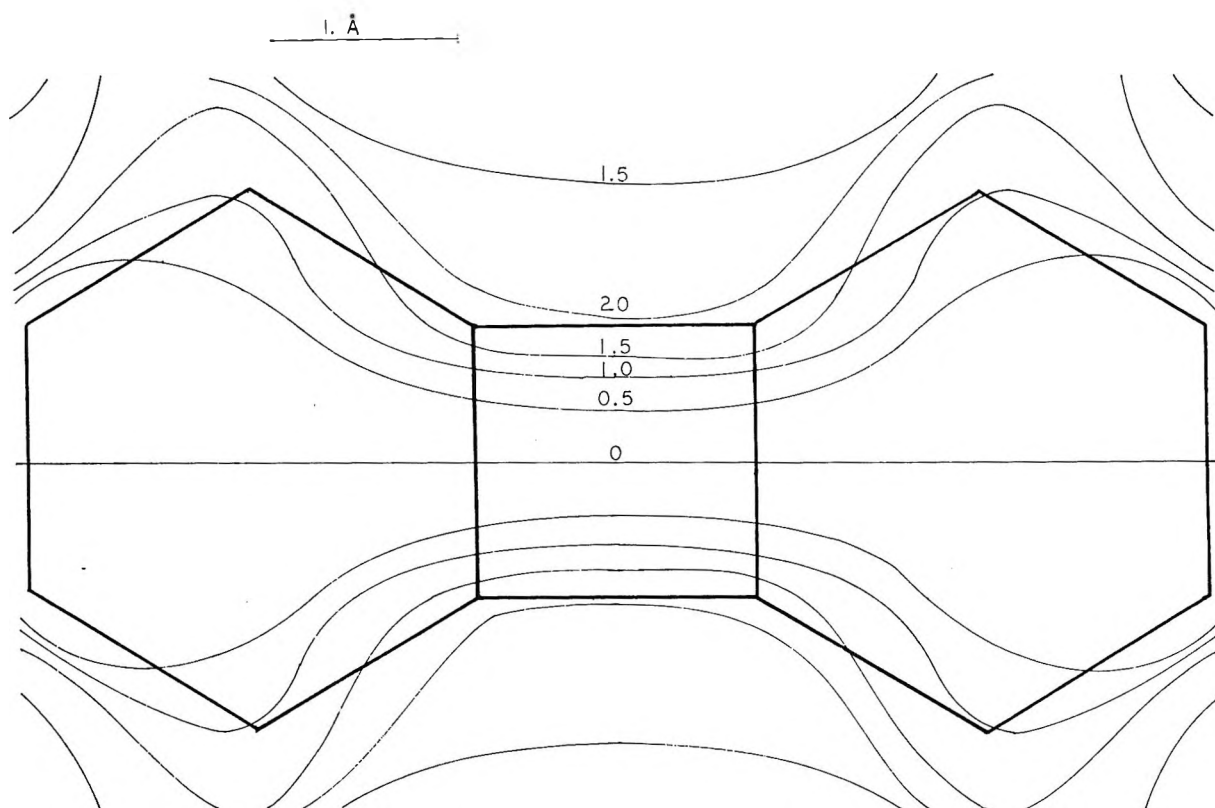


Figure 8. Calculated unpaired-electron density on a sodium ion in an ion pair with the biphenylene anion. Sodium is 3 Å above the nuclear plane. Unpaired-electron density in units of 10^{-3} .

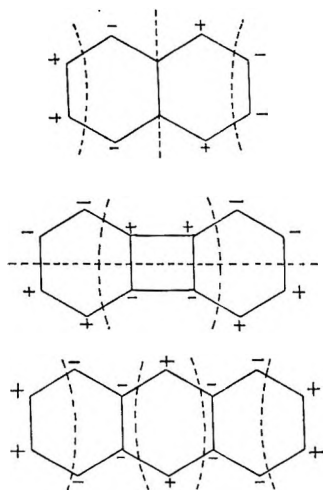


Figure 9. Symmetry and nodes of the molecular orbitals containing the unpaired electron in naphthalene, biphenylene, and anthracene anions.

contributions from electron repulsion may be expected. Thus we feel that positions over either of the benzene rings would be more favorable from the consideration of minimum electron repulsion. This may be illustrated by the following argument. If the electrostatic attraction is considered to be proportional to r^{-2} , and the net repulsion is considered to be proportional to r^{-n} where $n > 2$, and r is the internuclear distance between the cation and carbon nuclei, then the

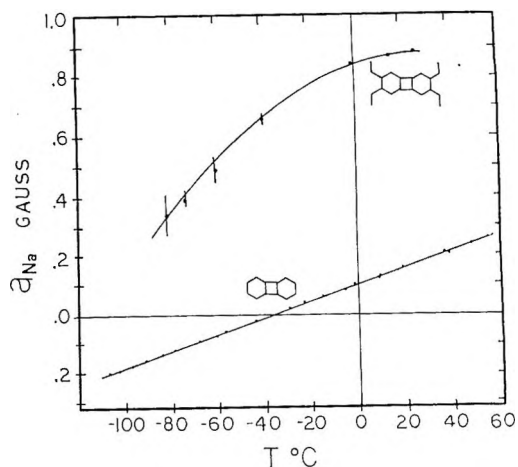


Figure 10. Sodium splittings in sodium 2,3,6,7-tetraethylbiphenylenide and sodium biphenylenide in MTHF.

π -electron system may be represented as a surface to which the cation has a minimum distance of approach. If the cation is over the four-membered ring, it may not approach the molecular plane as close as if it were over the six-membered ring, because of the reduced repulsion around the center of the six-membered ring. The net effect would be a greater attraction of the cation to

(28) A. Carrington and J. dos Santos-Veiga, *Mol. Phys.*, **5**, 285 (1962); P. R. Hindle, J. dos Santos-Veiga, and J. R. Bolton, *J. Chem. Phys.*, **48**, 4703 (1968).

regions near the six-membered ring although the electron density is less in this region.

A test of the proposed structure of the sodium biphenylenide ion pair is provided by the sodium hfs in the 2,3,6,7-tetraethyl biphenylenide system. It is clear from Figure 10 that the sodium hfs has increased by a factor of 4 to 5 in the substituted system. If the sodium ion were located over the four-membered ring, substitution in the 2, 3, 6, and 7 positions would not be expected to cause a significant change in the sodium hfs. However, if the sodium ion is located over one of the benzene rings in the unsubstituted ion, then the ethyl groups would force the sodium ion toward the central four-membered ring in the substituted ion. From Figure 8 it is clear that oscillation of the ion perpendicular to the long axis and parallel to the short axis will result in a much higher unpaired-electron density on the sodium if the ion is over the central ring than when it is over one of the benzene rings.

Negative Alkali Metal Hyperfine Splittings. de Boer^{8,9} has shown that under certain conditions alkali metal hyperfine splittings may be negative (*e.g.*, see Figure 10). He accounted for this phenomenon in terms of a spin polarization of inner-core s electrons on the alkali metal ion by the unpaired electron. Since the probability density of an *ns* orbital is greater than an (*n* + 1)s orbital, a negative alkali metal hfs would result. We feel that de Boer's mechanism is not likely the origin of the *negative* hfs since the energies of the excited states which would have to mix with the ground state of the alkali metal are in excess of 30 eV for the sodium ion and 13 eV for the cesium ion.

Instead we propose the following mechanism for *negative* alkali metal hfs. One may define the *spin* density in the lowest empty s orbital on the alkali metal ion as

$$\rho_M = P_M(\alpha) - P_M(\beta) \quad (10)$$

where $P_M(\alpha)$ is the total probability density of electrons with α spin (*i.e.*, with $M_S = 1/2$) which are transferred from the aromatic anion radical to the alkali metal ion and $P_M(\beta)$ is the corresponding probability density for β electrons. The model of different orbitals for different spins²⁹ describing the spin distribution in an aromatic anion radical in terms of two sets of molecular orbitals, one for electrons with α spin and one for electrons with β spin, may then be used to compute $P_M(\alpha)$ and $P_M(\beta)$ as

$$P_M(\alpha) = \sum_j \left\{ \frac{\sum_t c_{jt} \left\langle \phi_M(s) \left| \frac{e}{r_{tM}} \right| \phi_t(2p) \right\rangle}{E_j - E_M} \right\}^2 \quad (11)$$

where the summation over *j* includes only molecular orbitals containing electrons with α spin. A similar expression will apply for $P_M(\beta)$ with the summation taken over molecular orbitals containing electrons with

β spin. One should note that the term inside the curly brackets in eq 11 is analogous to λ_j in eq 5.

Now suppose that the alkali metal ion is at a position which corresponds to a node in the molecular orbital of the unpaired electron. Obviously, the *unpaired-electron density* on the alkali metal ion will be zero. However, this position will certainly not be a node for some of the lower "filled" molecular orbitals. "Polarization" of these molecular orbitals by the unpaired electron will cause the contributions to $P_M(\alpha)$ and $P_M(\beta)$ from these molecular orbitals to be unequal. The result will be a nonzero value of ρ_M . By analogy with similar situations in the spin distribution in aromatic radical ions, it is not unreasonable to expect that ρ_M will be *negative*, and hence a_M negative, when λ_j^2 from the singly occupied π molecular orbital is zero or very small.

The mechanism which we propose above is more reasonable from an energetic standpoint as the excitation energies required for a configuration interaction calculation are about 7 eV or less. Some preliminary calculations show that our model does indeed predict ρ_M to be negative under the conditions outlined above.

Effect of Changing the Alkali Metal Ion. In Figure 11 we have collected the data available on the alkali metal ion pairs of naphthalene, anthracene, and biphenylene, all in 2-methyltetrahydrofuran (MTHF). These diagrams have been drawn with the data expressed in ρ_M , the alkali metal spin density, as defined in eq 9.

Dodson and Reddoch³⁰ observed that in the naphthalene system, ρ_M decreases as the atomic number of the alkali metal ion increases (see Figure 11a). They suggested that ρ_M for cesium and rubidium may be *negative*. A similar progression is found in the anthracene system^{2b} (see Figure 11b). The biphenylene system provides a striking contrast as the trend is exactly opposite (see Figure 11c).

An explanation of these trends must start with a consideration of the potential energy surface for these ion pairs. According to the McClelland calculations, as the "point charge" cation moves higher above the nuclear plane of the radical anion, the potential well becomes more shallow. Thus, any irregularities in the surface, such as the double minimum for the naphthalene system, will tend to disappear.^{4a} At the greater distances characteristic of the larger cations, the minimum energy positions will tend toward positions over the center of the radical plane. Even when electron repulsion is considered, the same conclusion is reached since the larger cations are too large to "fit" into the small potential well over the center of a benzene ring. Hence these positions will no longer be favorable.

(29) L. Salem, "The Molecular Orbital Theory of Conjugated Systems," W. A. Benjamin, New York, N. Y., 1966, pp 81-96 and 264-275.

(30) C. L. Dodson and A. H. Reddoch, *J. Chem. Phys.*, **48**, 3226 (1968).

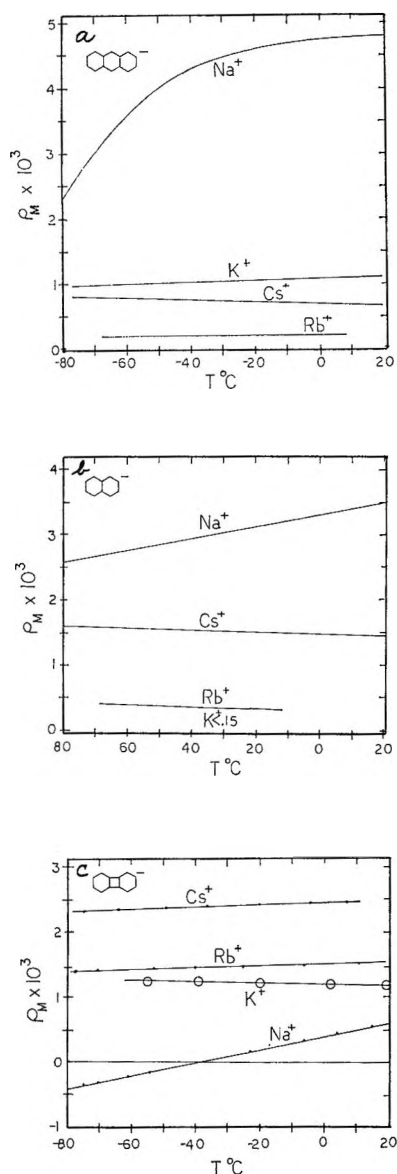


Figure 11. Spin density (ρ_M) on alkali metal ions in ion pairs with anthracene, naphthalene, and biphenylene ions in MTHF (except rubidium⁺ naphthalene⁻ is in THF). Data for anthracene and naphthalene ion pairs are taken from ref 2b.

The effect of changing the cation from sodium to rubidium ions is demonstrated by comparing Figure 2 with Figure 12a. The maxima in the alkali metal unpaired-electron distribution are shifted further away from the central regions. Since the rubidium ion is expected to be confined more to the central regions, a much lower unpaired-electron density is expected on the rubidium ion. Calculations show that the lowest molecular orbital of naphthalene will transfer an electron density of ~ 0.020 to rubidium when it is over the central region of the ion. Thus it seems reasonable that electron correlation could alter the electron distributions of these orbitals so as to give a *negative* value of ρ_M . Similar arguments would apply even more so in the cesium naphthalenide system. A further possi-

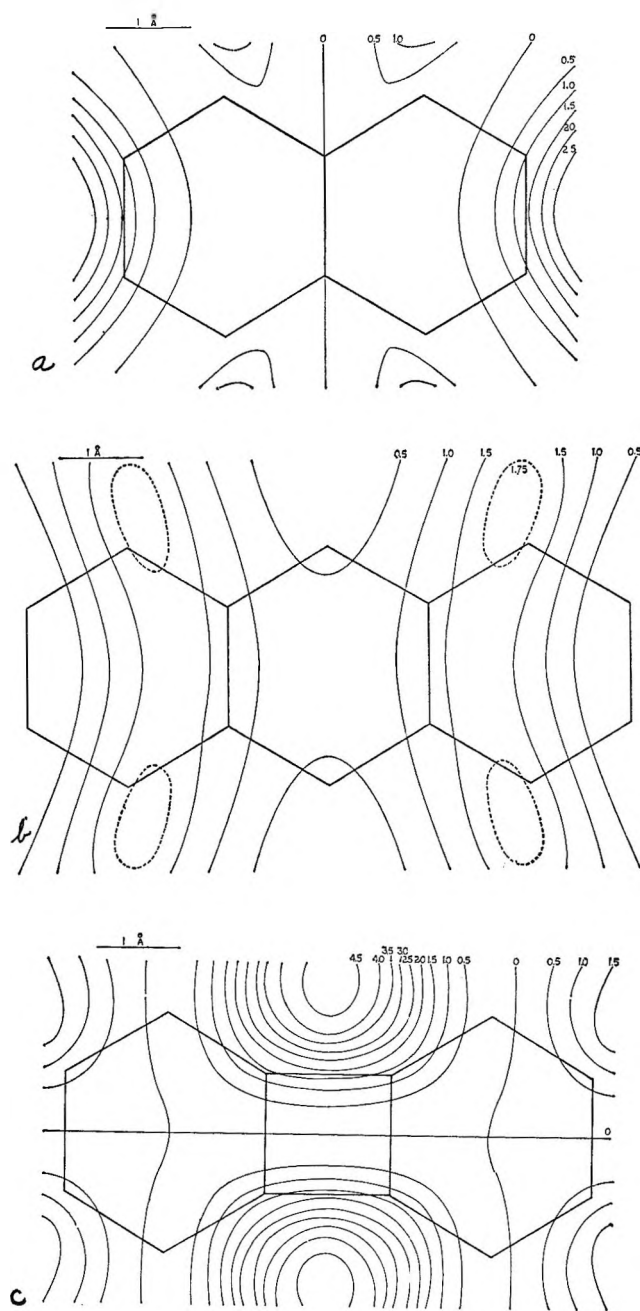


Figure 12. Calculated unpaired-electron density on a rubidium ion in ion pairs with (a) naphthalene, (b) anthracene, and (c) biphenylene ions. Rubidium is 3.5 Å above the nuclear plane. Unpaired-electron density is in units of 10^{-3} .

ble indication that a_M may be negative in the rubidium and cesium naphthalenide systems is provided by the fact that the sign of the temperature coefficient seems to be reversed in the Rb and Cs cases as compared to the Na case. This effect may not be significant since it may be due to solvation changes.

The anthracene results in Figure 11b may be explained in a manner very similar to the naphthalene cases. Figure 12b shows an interesting contrast to Figure 6 in that the maxima of the unpaired-electron distribution are now well away from the central regions

of the molecule. It appears that in this system negative and positive contributions to ρ_M nearly cancel for Rb and that a_M is probably *negative* for the cesium anthracenide ion pair.

The biphenylene system is the most interesting of the three. A comparison of Figures 7 and 12c shows that there is no major qualitative change in the alkali metal unpaired electron density distribution in going from Na to Rb. However, as indicated earlier, one would expect the minimum-energy positions to move closer to the central region of the molecule as the size of the ion increases. Here small oscillations of the ion perpendicular to the long axis and parallel to the short axis will result in a larger net value of ρ_M . This would explain the experimental results if ρ_M is positive in these cases. This must, however, be confirmed by experiment.

Solvent Effects. In general, the greatest solvent- and temperature dependence of alkali metal hfs are observed in systems containing the sodium or lithium ion.^{2b,31} This has been attributed to the fact that the larger ions are less easily solvated.^{2b} The effect of solvation in relation to the model proposed to account for alkali metal hfs must be considered.

Figure 3 shows the variation of the calculated unpaired electron densities on the sodium ion in an ion pair with the naphthalene ion when the sodium ion is moving perpendicular to the nuclear plane of the radical and over the center of one of the benzene rings. To increase the spin density by a factor of 2, such as observed in the change of solvents from MTHF to DEE, in the sodium naphthalenide system the sodium ion must move closer to the molecular plane by ~ 0.05 nm. This appears to be considerably too much to expect in view of the strong electrostatic forces. Rather, if the ion is permitted to move only slightly closer to the molecular plane, one would tend to favor the minimum energy positions of the radical ion to a greater extent, thus increasing the time average spin density on the alkali metal ion. Thus, in the systems of sodium naphthalenide and anthracenide, the sodium hfs increases significantly at higher temperatures or as the degree of solvation decreases. On the other hand, in the biphenylene system, the sodium hfs is lower in DEE than MTHF. This can be explained by the fact that the minimum energy positions of the alkali metal would be in a region where no spin would be predicted to be transferred to the sodium.

It is interesting to compare the behavior of sodium biphenylenide in MTHF to that in THF. At low temperature, negative hfs are observed in MTHF, but no negative hfs are observed in THF. In the sodium naphthalenide THF system conversion between different ion pairs is observed.^{2b} We therefore conclude that in THF the sodium ion is permitted to move farther from the radical. This will decrease the positive

spin density on the radical and also decrease the effect of electron correlation.

Lithium Ion Pairs. We have said little about the ion pairs containing a lithium ion. The reason is that this system appears to be somewhat anomalous. Table II compares the data on the lithium ion pairs with

Table II: Sodium and Lithium Hyperfine Splittings (G) in Aromatic Systems

	MTHF		DEE	
	a_M	$10^3\rho_M$	a_M	$10^3\rho_M$
Naphthalene				
Na	1.115	3.52	2.09 ^a	6.62
Li	0.48 ^b	3.95	0.52 ^a	3.55
Anthracene				
Na	2.68 ^a	8.5
Li	1.75 ^a	12.2
Biphenylene				
Na	0.204	0.65		
Li	0.104	0.72	Not reduced	

^a Reference 2. ^b Reference 31.

data on other alkali metal ion pairs.³¹ It is clear that the trends noted for the other alkali metal ion pairs do not extend to lithium. There are several possible reasons for this. It is well known that lithium ions are usually strongly solvated. This solvation would tend to increase the height of the lithium ion over the plane of the molecule. Figure 3 compares the magnitudes of the unpaired electron density on sodium and lithium ions centered over one of the benzene rings in naphthalene. At closer distances the unpaired electron density on the lithium ion is nearly the same as for the sodium ion; however, at greater distances, the values for lithium drop off more rapidly than for sodium. Thus a greater height due to increased solvation might explain the data for naphthalene and biphenylene but not for anthracene. Another effect which should be considered is the change in Q_M with the charge on the cation. This may be considerably greater for lithium than sodium and would result in an overestimation of ρ_M in the lithium case. At this point we do not wish to speculate further on the lithium ion pairs until more data are available.

Conclusion

The model utilized in this paper appears to give some insight into the behavior of the alkali metal hfs in various systems. By no means is this intended to predict accurately the value of the hyperfine splitting although

(31) P. B. Ayscough and F. P. Sargent, *J. Chem. Soc. (B)*, 900 (1966).

relative magnitudes are well represented. Among the problems which must still be solved are determining the potential surface of ion-paired systems; accurately predicting the effect of the electrostatic field of the cation upon the radical, and finally a model which gives

a more accurate spin distribution of the radical ion, taking electron correlation into account, must be used. In addition, the signs of the hfs of many of these systems are surmised, and although they are believed to be correct, they still must be verified by experiment.

A Semicontinuum Model for the Hydrated Electron

by Kenji Fueki,

Department of Synthetic Chemistry, Faculty of Engineering, Nagoya University, Nagoya, Japan

Da-Fei Feng,

Department of Chemistry, University of Kansas, Lawrence, Kansas 66044

and Larry Kevan

Department of Chemistry, Wayne State University, Detroit, Michigan 48202 (Received December 5, 1969)

A semicontinuum model is developed for the hydrated electron. Long-range interactions are represented by a polarization potential and short-range attractive interactions are represented by a point dipole approximation. Energy levels as a function of cavity radius are calculated within a self-consistent field approximation. The optical transition energy is rather insensitive to different configurations of the water molecules in the first solvation shell around the electron. The observed optical absorption of the hydrated electron in both water with $D_s = 80$ and in ice at 77°K with $D_s = 3$ can be satisfactorily explained with this model for cavity radii near 1 Å. The calculated heat of solution and charge distribution of the hydrated electron with this cavity radius are also in good agreement with the experimental values.

I. Introduction

The hydrated electron is the simplest reducing species known. Its reactivity has been extensively studied and reactivity correlations have been developed which have considerable predictive utility.¹ In contrast to its reactivity, the structure of the hydrated electron is much less well understood. Two types of theoretical models have been used to treat the structure. The dielectric continuum model^{2,3} includes only long-range interactions as represented by a polarization potential. This model does not explicitly treat the structure of the hydrated electron, but it does assume that the dipoles of the solvent molecules are oriented toward the electron. The tetrahedral structure model^{4,5} includes only short-range interactions represented by the potential from four water molecules with one OH bond of each molecule tetrahedrally oriented around the electron. In both of these models a distance in the potential function can be varied to obtain agreement between the calculated and experimental optical transition energies. A similar structural model was used in the calculation of the proton hyperfine interaction of the hydrated electron in ice.⁶

In actuality, the electron interacts with the solvent through both long- and short-range interactions. Here we present energy level calculations on a semicontinuum model which includes both ranges of interaction. We also explore the effect on the energy levels of three different types of configurations of the water molecules in the first solvent layer.

A low yield of electrons are trapped in pure γ -irradiated ice at 77°K.⁷ These trapped electrons have similar optical characteristics to solvated electrons in water although the static dielectric constant of ice at 77°K is much lower than the value of 80 for water.⁸

(1) E. J. Hart, *Accounts Chem. Res.*, **2**, 161 (1969).

(2) J. Jortner, *Radiat. Res., Suppl.*, **4**, 24 (1964).

(3) J. Jortner in "Radiation Chemistry of Aqueous Systems," G. Stein, Ed., Wiley-Interscience, New York, N. Y., 1968, p 91.

(4) M. Natori and T. Watanabe, *J. Phys. Soc. Jap.*, **21**, 1573 (1966).

(5) M. Natori, *ibid.*, **24**, 913 (1968).

(6) K. Fueki, *J. Chem. Phys.*, **45**, 183 (1966).

(7) K. Eiben and I. A. Taub, *Nature*, **216**, 782 (1967).

(8) There are no available data on D_s for ice at 77°K, but a value of 3 for ice at 88°K has been reported. See N. E. Dorsey, "Properties of Ordinary Water Substances in All Its Phases," Van Nostrand-Reinhold Co., Inc., Princeton, N. J., 1940, pp 485, 500. We assume $D_s = 3$ for ice at 77°K.

The continuum model is not satisfactory for explaining the observed optical absorption of electrons in both water at 300°K and ice at 77°K. However, we show that the semicontinuum model developed here does satisfactorily account for the optical absorption in water and ice.

II. The Model

We assume that the solvated electron interacts with the dipoles of specifically oriented water molecules in the first solvation shell by a short-range attractive potential. The solvent molecules beyond the first solvation shell are treated as a continuous dielectric medium with which the electron interacts by a long-range polarization potential. This model may be called a semicontinuum model for the solvated electron.

We shall consider three types of configuration for the water molecules in the first solvation shell. In all models, the geometry of the individual water molecules is taken to be the same as in the gas phase. Model I is a tetrahedral configuration in which the electron is located in a tetrahedron formed by the oxygens of four water molecules. One of the O-H bonds of each water molecule points toward the center of the tetrahedron. This configuration is the same as used by Natori⁴ and is similar to the structure of ice with two of the water dipoles rotated.

Model II is also a tetrahedral configuration but the dipoles of the four tetrahedrally fixed water molecules are allowed to reach thermal equilibrium. The resulting orientation of the water dipoles is determined both by the local electric field at the dipoles from the electron and by the random disorientation due to thermal fluctuations. The equilibrium orientation of the dipoles deviates several degrees from the line joining the corner and the center of the tetrahedron. The deviation is greater in water than in ice. The configuration of Model II is similar to models used for anion hydration.

Model III is an octahedral configuration similar to Model I. The electron is located in an octahedron formed by the oxygens of six water molecules. One of the O-H bonds of each water molecule points toward the center of the octahedron. This configuration was studied because of the epr results of Bennett, Mile, and Thomas⁹ which indicate that the trapped electron in ice of unknown structure¹⁰ interacts equivalently with six protons.

In the following treatment, we use a point dipole approximation for the water molecules in the first solvation shell and employ an average, spherically symmetric potential arising from charge-dipole (permanent and induced) interactions to calculate the short-range interactions associated with Models I-III. A similar treatment for short-range interactions was previously used by O'Reilly¹¹ for the solvated electron

in liquid ammonia. Short-range repulsive interactions are not included in the present calculation.

III. Outline of Calculation

A. Ground State. The total ground-state energy, E_t , for the solvated electron in a dielectric medium is given by the sum of the electronic energy, E_{1s} , and the medium rearrangement energy, E_m ¹²

$$E_t = E_{1s} + E_m \quad (1)$$

The reference state of E_{1s} is that of the polarized medium. The electronic energy in the present model consists of three components: (1) the kinetic energy of the electron, (2) the short-range attractive interaction energy, and (3) the long-range polarization interaction energy. The medium rearrangement energy arises from the following contributions: (1) the long-range polarization energy, π , of the medium; (2) the dipole-dipole repulsion energy, E_{dd} , between the oriented dipoles in the first solvent layer; (3) the energy, E_v , required to form a void in the medium which is approximately taken to be the surface tension energy; (4) the pressure-volume work which is unimportant at normal pressures; and (5) the energy required for rearranging hydrogen bonds. Since we have no knowledge about how much hydrogen bond rearrangement occurs on solvation, we neglect contribution (5) to the medium rearrangement energy.

Thus, we can express the total ground-state energy as

$$E_t = E_{1s} + \pi + E_{dd} + E_v \quad (2)$$

Since E_{dd} and E_v do not involve the coordinates of the solvated electron, we can apply a variational procedure to $E_{1s}^0 = E_{1s} + \pi$ to find the best energy value and wave function. We choose a hydrogen-like 1s wave function for the ground state

$$\psi_{1s} = \left(\frac{\lambda^3}{\pi}\right)^{1/2} \exp(-\lambda r) \quad (3)$$

where λ is a variational parameter. The potential energy function is taken as

$$V = V_0 + \frac{e}{2} \left(1 - \frac{1}{D_s}\right) f_{1s}(R) \quad r < R$$

$$V = \frac{e}{2} \left(1 - \frac{1}{D_s}\right) f_{1s}(r) \quad r > R \quad (4)$$

(9) J. E. Bennett, B. Mile, and A. Thomas, *J. Chem. Soc., A*, 1393 (1967).

(10) The ice is formed by condensation of water vapor at 77°K and is probably amorphous. However, the hyperfine structure is only seen after warming to 140°K at which temperature amorphous ice crystallizes to a cubic structure.

(11) D. E. O'Reilly, *J. Chem. Phys.*, **41**, 3736 (1964); R. H. Land and D. E. O'Reilly, *ibid.*, **46**, 4496 (1967).

(12) A general discussion on the energetics of solvated electrons has been given by Jortner and Kestner at the Conference on the Nature of Metalammonia Solutions, Ithaca, N. Y., 1969. The authors thank Professors J. Jortner and N. R. Kestner for sending them a preprint of their paper.

where R is the distance between the center of the cavity (*i.e.*, the tetrahedron or octahedron) and the point dipole. D_s is the static dielectric constant of the medium and it is taken to be 80 for water at 300°K and 3 for ice at 77°K.⁸

The long-range polarization potential, f_{1s} , is obtained by solving Poisson's equation.²

$$\nabla^2 f_{1s} = 4\pi e |\psi_{1s}|^2 \quad (5)$$

This guarantees self-consistency between the potential and the wave function. The short-range charge-dipole interaction potential is taken as that at the center of the cavity and to be constant for $r < R$. Thus, the short-range potential energy function is given by

$$\begin{aligned} V_o &= V_p + V_i \\ V_p &= -\frac{ne\mu}{D_{op}R^2} \langle \cos \delta \rangle_{av} \\ V_i &= -\frac{ne^2\alpha}{2D_{op}^2R^4} \end{aligned} \quad (6)$$

where μ and α are the magnitudes of the dipole moment ($\mu = 1.85$ D) and of the isotropic polarizability ($\alpha = 1.51 \text{ \AA}^3$) for the water molecule, respectively, and D_{op} is the optical dielectric constant ($D_{op} = 1.78$). n is the number of water molecules in the first solvation shell and it is 4 for Models I and II and 6 for Model III. δ is the angle between the dipole moment vector and the line joining the center of the cavity to the point dipole. $\langle \cos \delta \rangle_{av}$ is taken to be $\cos 52.25^\circ$ for Models I and III, and it is given by $1 - (kT/\mu E_{loc})$ for Model II, where $E_{loc} \simeq e/D_{op}R^2$, k is Boltzmann's constant and T is the absolute temperature. The introduction of D_{op} arising from the polarization of the atoms in the water molecule in eq 6 was previously made in the calculation of ion hydration and led to the successful results.¹³

Thus, the energy, E_{1s}^0 , is expressed by eq 7. The

$$\begin{aligned} E_{1s}^0 &= \int \psi_1 \left(-\frac{\hbar^2}{8\pi^2m} \nabla^2 \right) \psi_{1s} d\tau + \\ &\left[V_o + \frac{e}{2} \left(1 - \frac{1}{D_s} \right) f_{1s}(R) \right] \int_{r < R} \psi_{1s}^2 d\tau + \\ &\frac{e}{2} \left(1 - \frac{1}{D_s} \right) \int_{r > R} f_{1s}(r) \psi_{1s}^2 d\tau \end{aligned} \quad (7)$$

energy, E_{1s}^0 , is minimized with respect to λ to find the best energy value and wave function.¹⁴ Using the wave function and the potential, f_{1s} , obtained, the long-range polarization energy of the medium is given by

$$\pi = -\frac{e}{2} \left(1 - \frac{1}{D_s} \right) \int_{r > R} f_{1s}(r) \psi_{1s}^2 d\tau \quad (8)$$

The energy level, E_{1s} , of the ground state is obtained as the difference in energy between E_{1s}^0 and π .

The dipole-dipole interaction energy between the oriented dipoles in the first solvent layer is expressed as

$$E_{dd} = \sum_j E_{dd}^{(j)} \quad (9)$$

$$E_{dd}^{(j)} = \frac{n_j \mu^2}{D_{op} l_{12}^3} (2 \cos \theta_1 \cos \theta_2 + \sin \theta_1 \sin \theta_2 \cos \psi)$$

where l_{12} is the distance between any two dipoles 1 and 2; θ_1 and θ_2 are the angles between dipole 1 and line l_{12} and between dipole 2 and line l_{12} , respectively. ψ is the angle between the planes formed by dipole 1 and line l_{12} and by dipole 2 and line l_{12} . n_j is the number of the j th type of equivalent dipole pairs. The summation is taken over all types of dipole pairs in the first solvent shell. In our case, there are six dipole pairs for Models I and II, all of which are of the same type. There are two types of dipole pairs for Model III, twelve of one type and three of the second type. Equation 9 included D_{op} so that it may be consistent with eq 6. In the calculation of E_{dd} for Model II, we have used an approximation that the dipoles in the first layer are completely aligned toward the center of the cavity, since it is found that $\langle \cos \delta \rangle_{av}$ is close to unity. Since the permanent dipole term dominates, we have considered, to a first approximation, only permanent dipole-dipole interactions.

The surface tension energy is approximately given by

$$E_v = 4\pi(R^2 - r_s^2)\gamma \quad (10)$$

where γ is the plane surface tension of water ($\gamma = 72$ ergs cm^{-2}) and r_s is the radius of the water molecule, which is taken as 1.45 \AA for water and 1.38 \AA for ice.¹⁵ We have assumed roughly the same value for E_v in ice as that in water for the same R . The heat of solution, ΔH , of the electron is given by

$$\Delta H = -E_{1s} - E_m \quad (11)$$

The mean radius of the charge distribution in the ground state is

$$\bar{r}_{1s} = \int r \psi_{1s}^2 d\tau = \frac{3}{2\lambda} \quad (12)$$

B. Excited State. We assume the lowest optically allowed excited state to be the 2p state. This excited state is not an equilibrium state because of Franck-Condon restrictions. We choose a hydrogen-like 2p wave function for the excited state²

$$\psi_{2p} = \left(\frac{\mu^5}{\pi} \right)^{1/2} r \exp(-\mu r) \cos \theta \quad (13)$$

where μ is a variational parameter.

(13) G. Sposito and K. C. Babcock, *J. Chem. Phys.*, **47**, 153 (1967).

(14) The required computations were carried out on the GE 635 computer at the University of Kansas.

(15) G. Némethy and H. A. Scheraga, *J. Chem. Phys.*, **36**, 3382 (1962).

The excited-state energy is expressed as

$$\begin{aligned}
 E_{2p^0}(1s) = & \int \psi_{2p} \left(-\frac{\hbar^2}{8\pi^2m} \nabla^2 \right) \psi_{2p} d\tau + \\
 & \left[V_i + \frac{e}{2} \left(1 - \frac{1}{D_{op}} \right) f_{2p}(R) \right] x \int_{r < R} \psi_{2p}^2 d\tau + \\
 & \frac{e}{2} \left(1 - \frac{1}{D_{op}} \right) \int_{r > R} f_{2p}(r) \psi_{2p}^2 d\tau + \\
 & \left[V_p + e \left(\frac{1}{D_{op}} - \frac{1}{D_s} \right) f_{1s}(R) \right] \int_{r < R} \psi_{2p}^2 d\tau + \\
 & e \left(\frac{1}{D_{op}} - \frac{1}{D_s} \right) \int_{r > R} f_{1s}(r) \psi_{2p}^2 d\tau - \\
 & \frac{e}{2} \left(\frac{1}{D_{op}} - \frac{1}{D_s} \right) f_{1s}(R) \int_{r < R} \psi_{1s}^2 d\tau - \\
 & \frac{e}{2} \left(\frac{1}{D_{op}} - \frac{1}{D_s} \right) \int_{r > R} f_{1s}(r) \psi_{1s}^2 d\tau \quad (14)
 \end{aligned}$$

Here $f_{2p}(r)$ is obtained by averaging $f_{2p}(r, \theta)$ over the polar angle θ . This is an approximation necessary for the potential to have continuity at $r = R$. The long-range polarization potential, $f_{2p}(r, \theta)$, is the solution of Poisson's equation

$$\nabla^2 f_{2p}(r, \theta) = 4\pi e |\psi_{2p}|^2 \quad (15)$$

We have assumed that the short-range attractive potential for the excited state is the same as that for the ground state.

The energy, $E_{2p^0}(1s)$, is minimized with respect to μ to get the best energy value and wave function. The energy level, $E_{2p}(1s)$, of the excited state is obtained by subtracting the polarization energy, π of the medium from $E_{2p^0}(1s)$. The mean radius of the charge distribution in the excited state is

$$\bar{r}_{2p}(1s) = \int r \psi_{2p}^2 d\tau = \frac{5}{2\mu} \quad (16)$$

The $1s \rightarrow 2p$ transition energy is given by

$$h\nu = E_{2p}(1s) - E_{1s} \quad (17)$$

In the calculation of the oscillator strength, f , for the $1s \rightarrow 2p$ transition, we use the dipole velocity form which involves the matrix element of the momentum operator

$$f = \frac{\hbar^2}{2\pi^2m[E_{2p}(1s) - E_{1s}]} \left| \int \psi_{2p} \frac{\partial}{\partial z} \psi_{1s} d\tau \right|^2 \quad (18)$$

It has been shown previously¹⁶ that the dipole velocity form gives better results for the oscillator strength of the solvated electron in liquid ammonia than does the more commonly used dipole length form. It appears that the dipole velocity form is the more reliable for evaluation of oscillator strengths from

Table I: Semicontinuum Model Calculations for the Solvated Electron in Water ($D_s = 80$)

Model I					
$R, \text{\AA}$	1.85	2.12	2.25	2.38	2.65
E_{1s}, eV	-3.704	-3.161	-2.955	-2.776	-2.476
$E_{2p(1s)}, \text{eV}$	-1.329	-1.285	-1.260	-1.233	-1.173
$h\nu, \text{eV}$	2.375	1.876	1.695	1.543	1.303
$\bar{r}_{1s}, \text{\AA}$	2.05	2.32	2.45	2.57	2.80
$\bar{r}_{2p(1s)}, \text{\AA}$	3.65	3.93	4.06	4.18	4.43
Model II					
$R, \text{\AA}$	2.12	2.38	2.49	2.65	2.91
E_{1s}, eV	-3.612	-3.124	-2.964	-2.759	-2.474
$E_{2p(1s)}, \text{eV}$	-1.328	-1.281	-1.257	-1.229	-1.176
$h\nu, \text{eV}$	2.284	1.843	1.707	1.530	1.298
$\bar{r}_{1s}, \text{\AA}$	2.13	2.37	2.47	2.61	2.84
$\bar{r}_{2p(1s)}, \text{\AA}$	3.44	3.74	3.85	4.00	4.27
Model III					
$R, \text{\AA}$	2.38	2.49	2.65	2.91	
E_{1s}, eV	-3.189	-3.023	-2.806	-2.511	
$E_{2p(1s)}, \text{eV}$	-1.292	-1.273	-1.239	-1.186	
$h\nu, \text{eV}$	1.897	1.750	1.567	1.325	
$\bar{r}_{1s}, \text{\AA}$	2.34	2.45	2.58	2.80	
$\bar{r}_{2p(1s)}, \text{\AA}$	3.65	3.78	3.94	4.20	

Table II: Semicontinuum Model Calculations for the Solvated Electron in Ice at 77°K ($D_s = 3$)

Model I					
$R, \text{\AA}$	1.59	1.75	1.85	2.12	2.38
E_{1s}, eV	-3.125	-2.681	-2.470	-2.087	-1.823
$E_{2p(1s)}, \text{eV}$	-0.816	-0.777	-0.764	0.734	-0.699
$h\nu, \text{eV}$	2.309	1.904	1.706	1.353	1.124
$\bar{r}_{1s}, \text{\AA}$	1.88	2.10	2.23	2.55	2.84
$\bar{r}_{2p(1s)}, \text{\AA}$	6.13	6.13	6.15	6.21	6.30
Model II					
$R, \text{\AA}$	1.59	1.85	2.06	2.12	2.38
E_{1s}, eV	-3.964	-3.081	-2.635	-2.543	-2.181
$E_{2p(1s)}, \text{eV}$	-0.672	-0.682	-0.680	-0.676	-0.665
$h\nu, \text{eV}$	3.292	2.399	1.955	1.867	1.516
$\bar{r}_{1s}, \text{\AA}$	1.67	1.97	2.21	2.25	2.52
$\bar{r}_{2p(1s)}, \text{\AA}$	5.25	5.13	5.11	5.13	5.21
Model III					
$R, \text{\AA}$	1.85	2.01	2.12	2.38	
E_{1s}, eV	-3.233	-2.825	-2.611	-2.209	
$E_{2p(1s)}, \text{eV}$	-0.669	-0.675	-0.674	-0.665	
$h\nu, \text{eV}$	2.564	2.150	1.937	1.544	
$\bar{r}_{1s}, \text{\AA}$	1.93	2.11	2.23	2.51	
$\bar{r}_{2p(1s)}, \text{\AA}$	4.81	4.88	4.96	5.13	

Table III: Fraction of the Solvated Electron Within the First Solvent Layer Denoted by Radius, R

Model	Water ($D_s = 80$)			Ice ($D_s = 3$)		
	$R, \text{\AA}$	P_{1s}	$P_{2p(1s)}$	$R, \text{\AA}$	P_{1s}	$P_{2p(1s)}$
I	2.25	0.520	0.148	1.75	0.455	0.015
II	2.49	0.583	0.225	2.06	0.533	0.055
III	2.49	0.589	0.236	2.12	0.542	0.066

(16) K. Fueki and S. Noda, presented at the Conference on the Nature of Metal-Ammonia Solutions, Ithaca, N. Y., June, 1969.

Table IV: Properties of the Solvated Electron in Water and Ice

Model	Water at 300°K ($D_s = 80$)				Ice at 77°K ($D_s = 3$)			
	I ^c	Calcn II ^d	III ^e	Expt ^a	I ^f	Calcn II ^g	III ^h	Expt ^b
R , Å	2.25	2.49	2.49		1.75	2.06	2.12	
$h\nu$, eV	1.70	1.71	1.75	1.72	1.90	1.96	1.94	1.94
f	0.85	0.88	0.88	0.65	0.43	0.58	0.61	
ΔH , eV	1.75	1.76	1.84	1.7	1.57	1.49	1.53	
\bar{r}_{1s} , Å	2.5	2.5	2.5	2.5-3.0	2.1	2.2	2.2	

^a J. Jortner in "Radiation Chemistry of Aqueous Systems," G. Stein, Ed., Wiley-Interscience, New York, N. Y., 1968, p 91. ^b K. Eiben and I. A. Taub, *Nature*, **216**, 782 (1967). ^c $\pi = 0.96$ eV, $E_{dd} = 0.07$ eV, $E_v = 0.17$ eV. ^d $\pi = 0.79$ eV, $E_{dd} = 0.18$ eV, $E_v = 0.23$ eV. ^e $\pi = 0.79$ eV, $E_{dd} = 0.17$ eV, $E_v = 0.23$ eV. ^f $\pi = 0.90$ eV, $E_{dd} = 0.15$ eV, $E_v = 0.06$ eV. ^g $\pi = 0.70$ eV, $E_{dd} = 0.31$ eV, $E_v = 0.13$ eV. ^h $\pi = 0.67$ eV, $E_{dd} = 0.27$ eV, $E_v = 0.14$ eV.

wave functions determined by the variational principle.¹⁷

IV. Results and Discussion

The results of the calculations are given in Tables I-IV. Table I shows the energy levels and charge distributions of the ground and excited states, and the optical transition energies calculated as a function of radius R for solvated electrons in water. The optical transition energy increases and the mean radius of the charge distribution decreases with decreasing R .

Table II presents the results of the calculations for the solvated electron in ice for $D_s = 3$. It is of interest to compare these results with those obtained for the solvated electron in water. Although general trends in the calculated quantities are similar to each other, the binding energy of the excited state of the solvated electron in ice is considerably less than that in water, and the mean radius of the charge distribution of the excited state of the solvated electron in ice is significantly greater than that in water. These differences arise from the different long-range interactions characterized by the different static dielectric constants for each system.

Table III shows the fraction of the solvated electron probability density within the first solvation shell. In the ground state, this fraction is about half of the total electron population for both water and ice although it is somewhat higher in water. The fraction is much less for the excited state and is only several per cent of the total electron population in the case of ice. In other words, the solvated electron in the excited state in ice is almost completely outside the first solvent shell.

The radius R defined in this paper is not necessarily equal to the actual radius of a cavity in which the solvated electron is located, since in the present model we have assumed point dipoles for the water molecules in the first solvent layer. The cavity radius may be estimated by subtracting the radius of the water molecule from R . Thus, we obtain a value of about 1 Å as the cavity radius in water.

Table IV summarizes the calculated optical transition energy, oscillator strength, heat of solution, and mean radius of the charge distribution of the ground state, for the solvated electron in water and ice together with the experimental values. These results were obtained for the values of R indicated in the table which were chosen to give the best fit with the observed optical transition energies. As can be seen, the calculated values are in excellent agreement with the experimental values for all the quantities listed. In the calculation of the heat of solution, any energy required to break hydrogen bonds was neglected since there is no information on the possible hydrogen bond rearrangement necessary to solvate the electron. If some of the hydrogen bonds in the water molecules in the first solvent layer are broken, then the calculated heat of solution would be less than the values cited in Table IV. For example, if one hydrogen bond is broken, on the average, per each molecule in the first solvent layer in water, the heats of solution are less than the values in Table IV by 0.28 eV for Models I and II and by 0.42 eV for Model III.¹⁶

It should be noted that the calculated oscillator strength for the solvated electron in ice is 30-50% less than that for the solvated electron in water. The calculated heat of solution for the solvated electron in ice is somewhat less than that for the solvated electron in water, and the mean radius of the charge distribution for the ground state is also less than that in water.

There are no great differences between the calculated values for Models I, II, and III. Thus, within the framework of the calculation, the orientation of the molecules in the first solvation shell around the electron is not too critical. This implies that even in a disordered glassy system, such as in 10 *M* NaOH,¹⁸ trapped or solvated electrons may be well characterized by narrow ground- and excited-state energy levels. It is striking that the values for Models II and III agree so closely. This is true even of the individual

(17) S. Chandrasekhar, *Astrophys. J.*, **102**, 223 (1945).

(18) L. Kevan, *J. Phys. Chem.*, **69**, 1081 (1965).

contributions to the overall energy (see footnotes to Table IV).

In Model II, the four dipoles are rotated with respect to the orientation in Model I so as to increase the dipole-dipole interaction. In Model III, the configuration of I is retained but the number of dipoles is increased from 4-6. It appears that the net short-range attractive interaction is increased by similar amounts in Models II and III compared to Model I.

It is pertinent to compare the semicontinuum model presented here with the dielectric continuum model^{2,3} and the tetrahedral structure model.^{4,5} As shown in Table IV, the semicontinuum model with the self-consistent field (SCF) approximation satisfactorily accounts for the optical absorption peak in both water and ice. It also predicts a corrected cavity radius of about 1 Å in both water and ice. The dielectric continuum model with the SCF approximation² predicts a somewhat low optical transition energy (1.35 eV) in water at the limit of zero cavity radius and predicts a transition energy far into the infrared for electrons in ice. If a more empirical adiabatic approximation is made to the continuum model,³ which approximation is less comparable with our semicontinuum model treatment, the observed transition energy in water can be calculated for a cavity radius of about 1.5 Å. However, this approximation to the continuum model also predicts that the transition energy in ice for radii around 1.5 Å is much lower than experiment shows.

The tetrahedral structural model can account for the transition energy in both water and ice. However, to do this requires rather extreme distortion of the bonds and angles of the water molecules in the first solvation shell.⁵

It is also of interest to compare the absolute energies calculated within the different models for the first excited states of solvated electrons in water. For

the continuum and semicontinuum models, the reference state with respect to which the energy is measured is the polarized medium. The excited-state energies given are for the calculation which gave the best calculated optical transition energy for each model. The first excited-state energies are -1.26 eV, -2.61 eV, and -2.19 eV for the semicontinuum, continuum,² and structural⁵ models, respectively. The semicontinuum model gives the least strongly bound excited state by far. It seems probable that the real excited state for solvated electrons in water is only slightly bound if at all. In fact, recent work has suggested that the first excited state for electrons trapped in alkaline ice matrices is probably not even bound.¹⁹

In summary, the semicontinuum model explains various properties of the solvated electron in water and in ice well and perhaps more satisfactorily than previous models. The model achieves this by inclusion of short-range attractive interactions. The model is still approximate, though. Since short-range repulsive interactions are not included, it does not give the ground-state configuration with minimum energy in the range of cavity radius studied. The semicontinuum model could be further developed by incorporating short-range repulsive interactions, by using multiparameter wave functions, and by using more exact treatments of short-range attractive interactions.

Acknowledgment. We thank Professor R. Christoffersen for his encouragement and interest in this work. The work was supported by the Air Force Rocket Propulsion Laboratory, the Atomic Energy Commission, and the University of Kansas Computing Center. This is AEC Document No. COO-1528-38.

(19) I. Eisele, R. Lapple, and L. Kevan, *J. Amer. Chem. Soc.*, **91**, 6504 (1969).

The Extent of Self-Association of Trifluoroacetic Acid in Different Nonpolar Solvents

by Wafaa S. Higazy and Ahmed A. Taha

Department of Chemistry, University College for Girls, Ain Shams University, Cairo, U. A. R. (Received September 15, 1969)

The vapor pressure of trifluoroacetic acid (TFA) at low concentrations has been determined for its solutions in two nonpolar, nonvolatile solvents, diphenylmethane and tetradecane. Self-association constants, at a wide range of temperature, and enthalpies of the association reactions of TFA in these two solvents have been determined. A discussion is given for the solvents effect on the extent of association, and a comparison is made between this effect and that of comparable volatile solvents.

Introduction

The self-association of TFA in diphenylmethane at 30 and 40° was reported before and interpreted as a monomer-dimer equilibrium.¹ In attempting to obtain a reliable value for the enthalpy of association, we extended the investigation to cover the temperature region 30 to 60°. In searching for the effect of the nature of the solvent on the extent of association, we carried the same type of investigation in the nonpolar, nonvolatile aliphatic solvent, tetradecane. Preliminary studies showed that the association of TFA in this solvent is very high, so we carried the investigation at very low concentrations of TFA and at a relatively high temperature region, to attain a reasonable equilibrium. The temperature region covered was from 40 to 60° for which it was found that the monomer-dimer equilibrium of TFA prevails over any other probable equilibria.

Experimental Section

The TFA used was purified by double distillation through a 30-plate column at a reflux ratio in excess of 10:1. The solvents were purified by distillation through a 15-plate column at reduced pressure. All reagents were stored in vacuum desiccators containing an appropriate drying agent.

The association of TFA at each temperature was determined as a function of the total vapor pressure, using a vapor pressure technique developed previously.^{2,3} One hundred milliliters of pure solvent was placed in the sample flask and evacuated until a constant pressure, P_s^0 , was attained. Increments of TFA varying from 0.01 to 0.15 ml were added successively to the evacuated system by means of a microburet. Total vapor pressures were measured to ± 0.05 mm with a cathetometer. The vapor pressure of dissolved air entering the system with TFA,² was subtracted from this total pressure to give the solution pressure, P . Since the solvents employed have very small vapor pressures at the experimental temperatures, it was

sufficient to subtract the measured vapor pressure of the pure solvent from the solution pressure to obtain the partial pressure of TFA according to the equation $P_{\text{TFA}} = P - X_s P_s^0$, where X_s is the mole fraction of solvent in solution.

Results and Discussion

Variation of partial pressures with formal concentrations of TFA in solutions in diphenylmethane and in tetradecane at the various temperatures investigated are shown in Figures 1 and 2, respectively. The lines are calculated and the points are experimental.

In fitting the data for both solvents, we assumed the presence of a mixture of monomers and not more than two polymeric species of TFA obeying Henry's law. The formal concentration of TFA in solution can be represented by

$$f_A = C_A + xk_x^s C_A^x + yK_y^s C_A^y \quad (1)$$

where C_A is the monomer acid concentration in solution, which is used to replace the respective activity since we are dealing with dilute solutions. K_x^s and K_y^s are association constants for the formation of the polymers $(\text{TFA})_x$ and $(\text{TFA})_y$ in solution. Since we are assuming that these species obey Henry's law, we can write $P_A = K^H C_A$ where P_A is the monomer vapor pressure and K^H is Henry's law constant. Substituting for the value of C_A in eq 1, we obtain

$$\begin{aligned} f_A &= P_A/K^H + xK_x^s(P_A/K^H)^x + yK_y^s(P_A/K^H)^y \\ &= \alpha P_A + \beta x P_A^x + \gamma y P_A^y \end{aligned} \quad (2)$$

Equation 2 was fitted with a computer program designed to calculate the values of the least-squares parameters and root-mean-square deviation (RMSD) in formal concentration of TFA obtained for various choices of

(1) A. A. Taha and S. D. Christian, *J. Phys. Chem.*, **73**, 3430 (1969).

(2) A. A. Taha, R. D. Grigsby, J. R. Johnson, S. D. Christian, and H. E. Afsprung, *J. Chem. Educ.*, **43**, 432 (1966).

(3) G. O. Wood, D. D. Mueller, S. D. Christian, and H. E. Afsprung, *J. Phys. Chem.*, **70**, 2691 (1966).

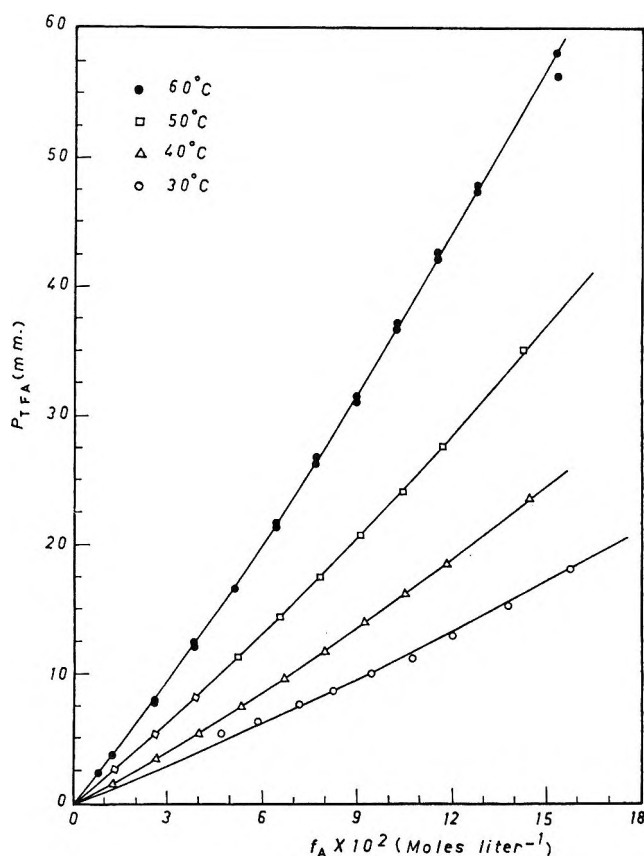


Figure 1. Variation of total pressure with formal concentration of trifluoroacetic acid in solution in diphenylmethane from 30 to 60°.

Table I: Dimerization Constants, Henry's Law Constants, and Enthalpies of Formation of TFA Dimers at Different Temperatures

Temp, °C	K_2^0 , M^{-1}	K^H , $mm M^{-1}$	RMSD M
Diphenylmethane Solvent			
30	4.42 ± 0.52	80.6 ± 6.5	0.004079
40	2.84 ± 0.13	114.4 ± 2.2	0.000871
50	1.99 ± 0.11	181.8 ± 3.1	0.000853
60	1.46 ± 0.09	285.9 ± 4.7	0.001301
$\Delta H = -7.447 \pm 0.139 \text{ kcal mol}^{-1}$			
Tetradecane Solvent			
40	377.0 ± 17.0	1968 ± 36	0.000063
45	212.0 ± 6.0	2008 ± 22	0.000046
50	149.0 ± 4.0	2176 ± 22	0.000049
55	68.5 ± 3.3	1951 ± 30	0.000113
60	63.4 ± 1.4	2337 ± 16	0.000042
$\Delta H = -18.097 \pm 0.174 \text{ kcal mol}^{-1}$			

x and y . In obtaining the least-squares results, we assumed that all the error lies in the measured values of the formal concentrations of TFA.

The data were best fitted by assuming the presence of only monomers and dimers of TFA in both solvents. The introduction of a third parameter either does not

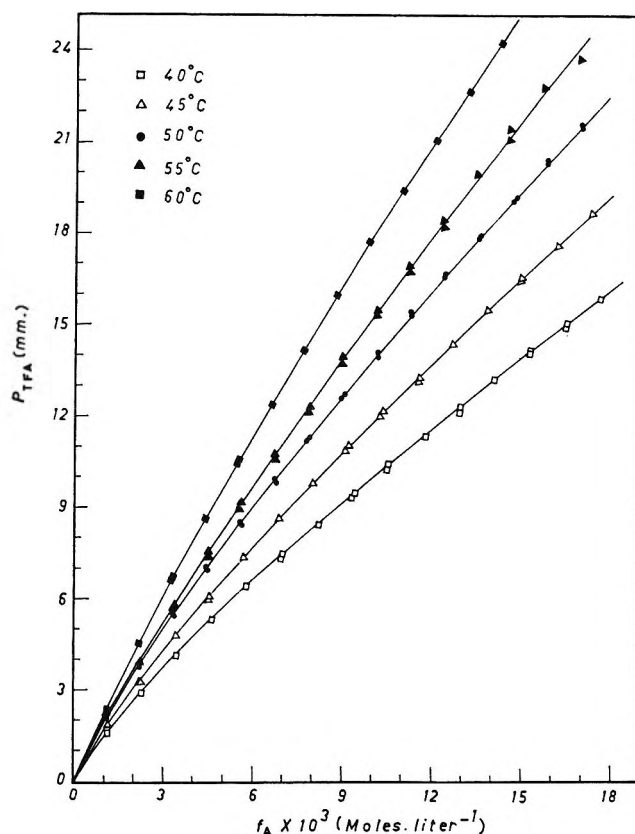


Figure 2. Variation of total pressure with formal concentration of trifluoroacetic acid in solution in tetradecane from 40 to 60°.

significantly improve the fit for any system or leads to negative values of association constants which have no physical meaning.

Enthalpies of dimerization were calculated from the temperature dependence of the dimerization constants, K_2^0 , according to the relationship

$$\partial \ln K_2^0 / (\partial 1/T) = -\Delta H/R \quad (3)$$

Equation 3 was fitted by least squaring each value of K_2^0 .

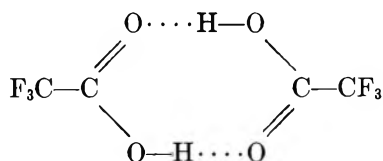
Table I summarizes the least-squares values of the dimerization constants and Henry's law constants for each temperature for the two solvents used. It also includes the least-squares values for the enthalpies of formation of $(TFA)_2$ from monomers in each solvent.

The conclusion that TFA polymerizes only to the extent of formation of dimers in diphenylmethane and in tetradecane supports a previous conclusion that in dilute solutions of carboxylic acids in nonpolar solvents the only equilibrium of importance is that which exists between monomer and dimer species.⁴ It also supports recent investigations done on TFA in different nonpolar solvents.⁵

(4) H. A. Pohl, M. E. Hobbs, and P. M. Gross, *J. Chem. Phys.*, **9**, 408 (1941).

(5) T. L. Stevens, Ph.D. Dissertation, The University of Oklahoma (1968).

The equivalence of the probable hydrogen bonding sites in both TFA molecules suggests that the structure of $(\text{TFA})_2$ is most likely the cyclic form



which is a generally accepted fact, that in dilute non-polar solutions the cyclic dimer is the only complex of primary importance, if not the only associated species.^{6,7}

Concerning the solvents effect on the association, we find that tetradecane has greater association thermodynamic values than diphenylmethane; *i.e.*, TFA associates to a much larger degree in tetradecane than in diphenylmethane, and also the hydrogen bond formed between the TFA molecules to form dimers is much stronger in tetradecane than in diphenylmethane. These results substantiate previous studies on solvent effects done by Allen, *et al.*,⁸ and by Christian, *et al.*,⁹ that association thermodynamic functions will decrease in the order of increasing solvent interaction capability (solvation power). In the present study we find that diphenylmethane will have a higher solvation power than tetradecane due to the presence

of the benzene rings in the former and the possible interaction between the π bonds of the phenyl groups and the TFA monomers.

This investigation gives also a means of comparing the extent of association of a volatile solute in nonvolatile, and in volatile, nonpolar solvents. We can conclude that the association of TFA in diphenylmethane is of a comparable magnitude to that in benzene,⁵ a volatile solvent of similar solvating properties. On the other hand, the association of TFA in tetradecane is of an approximate magnitude to that in the similar volatile solvents carbon tetrachloride and cyclohexane.⁵ It is also known that, in general, self-association constants of carboxylic acids in benzene are of the order of $1/10$ to $1/100$ of the values in carbon tetrachloride. It is interesting to note that the ratio of the association constants of TFA in diphenylmethane to those in tetradecane is similar to the ratio of the constants in benzene to those in carbon tetrachloride.

(6) G. C. Pimentel and A. L. McClellan, "The Hydrogen Bond," W. H. Freeman and Co., New York, N. Y., 1960.

(7) T. C. Chiang and R. M. Hammaker, *J. Phys. Chem.*, **69**, 2715 (1965).

(8) G. Allen, J. G. Watkinson, and K. H. Webb, *Spectrochim. Acta*, **807** (1966).

(9) S. D. Christian, J. R. Johnson, H. E. Afsprung, and P. J. Kilpatrick, *J. Phys. Chem.*, **70**, 3376 (1966).

The Role of Hindered Rotation in the Physical Adsorption of Hydrogen Weight and Spin Isomers

by P. L. Gant, K. Yang,

Central Research Division, Continental Oil Company, Ponca City, Oklahoma

M. S. Goldstein,

Organic Chemicals Division, American Cyanamid Company, Stamford, Connecticut

M. P. Freeman, and A. I. Weiss

Central Research Division, American Cyanamid Company, Stamford, Connecticut 06904 (Received September 12, 1969)

Gas adsorption chromatographic techniques are employed to study the limiting adsorptions of all six weight isomers of molecular hydrogen on Molecular Sieve 4A in the temperature range from 169 to 219°K. Further, the separation factors for *o*-H₂/*p*-H₂ are also determined in the range from 135 to 160°K. It is found that adsorption models based on the Kirkwood-Wigner partition function (developed for spherical molecules through terms in h^4) are inadequate to explain the observed relative adsorptions and of course they predict no separation of the spin isomers. On the other hand, an adsorption model based on a hybrid partition function which takes full account of molecular rotation and libration (developed for adsorption on a plane surface elsewhere) fits the differenced data of the symmetric weight isomers to within experimental precision with reasonable values of the parameters, but for two different energies. The fit of this model to the raw data gives essentially the same parameters with substantially greater residual error, probably reflecting the departure of molecular sieve geometry from a plane surface. No attempt was made to include the asymmetric weight isomers in this analysis because of clear-cut inconsistency with behavior predicted by the hybrid-partition-function model. Furthermore, the observed *o*-H₂/*p*-H₂ separation factors are accounted for to within the ambiguity of this hybrid-partition-function model, demonstrating that the effects of hindered rotation are of paramount importance in this temperature regime for the adsorption of molecular hydrogen.

Introduction

The physical interaction of gases, far above their normal boiling points, with solid surfaces is of considerable interest. Static *P*, *N*, *T* (pressure, amount, temperature) adsorption measurements, probably the most revealing in this regime,¹⁻³ are difficult because of the unwonted precision with which such measurements must be carried out. Gravimetric measurements,⁴ still in their infancy, show great potential, but thus far most of the work in this area has been done by gas adsorption chromatography (gsc). Kobayashi, *et al.*,⁵ have compiled a substantial list of workers who have used gsc techniques to infer thermodynamic information, or its equivalent, about high-temperature physical adsorption. The present work is such a study of the interaction of the variously isotopically substituted isomers, the weight isomers, of molecular hydrogen with a molecular sieve adsorbent.

DeMarcus, *et al.*,⁶ have long since shown that the different weight isomers of hydrogen should display different equilibrium adsorption properties because of the differences in the widely spaced negative discrete energy levels in their interactions with the surface. This theoretical development, based on the Kirkwood-Wigner expansion (through terms in h^2) of the quantum-

statistical partition function, has since been tested by Freeman⁷ and, using the lower temperature data of Constabaris, *et al.*,² by Yaris and Sams⁸ and found to be functionally correct with reasonable values of fitted parameters. (Note that these latter authors extended the theory, albeit incorrectly,⁹ to terms in h^4 .)

The purpose of the present work is twofold. On the one hand, by using gsc techniques to measure a subtle differential equilibrium effect, it serves as an excellent check on the validity of using these techniques for adsorption studies. On the other hand, by extending the measurements to tritium and tritium-containing

(1) For a summary of earlier work, see M. P. Freeman, *J. Phys. Chem.*, **62**, 723, 729 (1958).

(2) G. Constabaris, J. R. Sams, Jr., and G. D. Halsey, Jr., *ibid.*, **65**, 367 (1961).

(3) J. R. Sams, Jr., G. Constabaris, and G. D. Halsey, Jr., *J. Chem. Phys.*, **64**, 1689 (1960).

(4) Y. Y. Huang, J. E. Benson, and M. Boudart, in press.

(5) R. Kobayashi, R. S. Chappellear, and H. A. Deans, *Ind. Eng. Chem.*, **59**, 63 (1967).

(6) W. C. DeMarcus, E. H. Hopper, and H. M. Allen, AEC Bulletin K-1222, Carbide & Carbon Chemicals Company, Oak Ridge, Tenn., 1955.

(7) M. P. Freeman, *J. Phys. Chem.*, **64**, 32 (1960).

(8) R. Yaris and J. R. Sams, Jr., *J. Chem. Phys.*, **37**, 571 (1962).

(9) M. P. Freeman and M. J. Hagyard, *ibid.*, **49**, 4020 (1968).

isomers (a somewhat hazardous procedure not yet undertaken by static measurement techniques) a much more sensitive test of the theory can be made than has hitherto been possible. Theoretical considerations of Friedmann¹⁰ and of White and his coworkers^{11,12} have shown that the early DeMarcus treatment may have been oversimplified in that it treats the molecules as spherical systems. In fact the rotational energy levels of the molecules, greatly perturbed by the presence of the surface, should substantially modify the relative locations of the lowest negative discrete energy levels for the different isomers and consequently modify their relative equilibrium behavior. Where one would expect this effect to be of the greatest significance is in the experimentally observed separation of the nuclear spin isomers of the symmetric weight isomers¹³ for which the theory of DeMarcus provides no basis. Although no measurable spin isomer separations occur in the relatively high and restricted temperature interval in which the bulk of the experimental work reported here was done, a special lower temperature study was made to determine separation factors for the spin isomers of H₂; the results constitute an important part of the present study.

To interpret the data we have chosen to use the formalism of the virial equation of state¹ which has been shown by Barker and Everett¹⁴ to be completely equivalent to more conventional formalisms based on models related to the Gibbs boundary condition. Although the "Gibbsian" models have the advantage of greater familiarity (and indeed for some problems such as the lateral interaction of admolecules, greatly simplify numerical calculation,^{15,16}) the virial approach is more nearly tied to gsc and to the area to be examined. That is, the excess retention volume of gas chromatography may be directly identified with the prime measurable of the virial approach, the excess apparent volume,^{17,18} while the fitted parameters of this approach are a capacity factor (simply related to the area) and the cogent parameters of the adsorption potential energy expression. Hence the virial approach should be the most sensitive in indicating apparent changes in this potential due to quantum effects.

Experimental Method

Materials. Deuterium was obtained from Airco, Allentown, Pennsylvania. ³He was obtained from Monsanto Research Corp., Miamisburg, Ohio. Tritium obtained from Oak Ridge National Laboratories, Oak Ridge, Tenn., was purified by passing it through a short Molecular Sieve 3A column maintained at liquid methane temperature.¹⁹ Samples of H₂, HD, and D₂ were prepared by heating a mixture of hydrogen and deuterium to 500° in a nickel bomb. Mixtures containing all the hydrogen isotopes and ³He were prepared by transferring 2.2 Ci of T₂ gas and 500 ml ³He at 70 Torr into a 500-ml glass bulb. The bulb was then

pressurized to 700 Torr with H₂, HD, and D₂ mixture and allowed to stand for 2 weeks to allow HT and DT to form through β radiolysis from T₂.

Chromatographic Conditions. The Linde 4A 50-60-mesh Molecular Sieve obtained from Analabs Inc., Hamden, Connecticut, was treated to remove fines²⁰ and activated in the following manner. A 50-mm glass column, 60 cm long, with a coarse glass frit at the bottom was filled about two-thirds full with deionized water. About 100 g of sieve was slowly poured into the column and washed with a gentle stream of deionized water for about half an hour. This removed about 5 g of fine material. The washed 4A sieve was transferred as a slurry to a beaker, allowed to settle, and most of the water decanted. It was then placed in a glass column heating mantle, gently heated to remove the remaining water, and activated at 400° for 24 hr. The column used in this investigation was a 20-ft, 1/8-in. o.d. by 0.075-in. i.d. Type 303, stainless steel tubing obtained from Greenville Tube Co., Greenville, Pa. Since this tubing was cleaned and capped, no additional treatment was necessary. The column was packed with house vacuum and gentle tapping. The columns were then coiled on a 3.5-in. mandrel and heated to 400° for 24 hr with about 30 cm³/min helium flow. This long activation was found necessary for optimum resolution.

The low-temperature column compartment consisted of a double-walled foamed-polystyrene box cooled with liquid nitrogen. Pressurized liquid nitrogen from a Linde 110-l. vessel was fed to a flat refrigerator coil between the two polystyrene boxes and was controlled by a Teflon-seated solenoid valve. The nitrogen gas emerging from the coil provides even temperature without the added complexity of a blower. Temperature was controlled by a transistorized controller of our own design which used a low-temperature thermistor for sensing. These thermistors were mounted near the gas outlet holes from the refrigerator coil. Using this controller, column temperatures between 0 and -175° could be maintained to at least $\pm 1^\circ$ inside the inner box. Temperature was continuously recorded on a

(10) H. Friedmann, *Physica*, **30**, 921 (1964).

(11) D. White and E. N. Lasettre, *J. Chem. Phys.*, **32**, 72 (1960).

(12) A. Katorski and D. White, *ibid.*, **40**, 3183 (1964).

(13) For a review, see S. Akhtar and H. A. Smith, *Chem. Rev.*, **64**, 261 (1964).

(14) J. A. Barker and P. H. Everett, *Trans. Faraday Soc.*, **58**, 1608 (1962).

(15) J. R. Sams, Jr., G. Constabaris, and G. D. Halsey, Jr., *J. Chem. Phys.*, **36**, 1334 (1962).

(16) J. R. Sams, Jr., *ibid.*, **43**, 2243 (1965).

(17) J. F. Hanlan and M. P. Freeman, *Can. J. Chem.*, **37**, 1575 (1959).

(18) J. F. Hansen, H. A. Murphy, and T. C. McGee, *Trans. Faraday Soc.*, **60**, 597 (1964).

(19) K. Yang and P. L. Gant, *J. Phys. Chem.*, **66**, 1619 (1962).

(20) F. Farre-Rius and G. Guiochon, *J. Gas Chromatogr.*, **7**, 33 (1963).

Table I: Net Retention Volume (cm³/g) of H₂ at Different Sample Pressure and at Different Temperatures

P _s Torr	Temp (°K)							
	219	211	203	197	189	181	174	169
300	1.47	1.79	2.17	2.50	3.04	3.66	4.58	5.45
150	1.55	1.88	2.25	2.57	3.11	3.77	4.70	5.54
75	1.59	1.90	2.32	2.62	3.20	3.93	4.79	5.69
15	1.65	1.97	2.40	2.69	3.28	3.97	4.83	5.77
0 ^a	1.65	1.96	2.39	2.68	3.27	3.99	4.85	5.77
Standard dev	±0.01	±0.01	±0.02	±0.02	±0.03	±0.03	±0.09	±0.04

^a The retention volume, V_N° , at zero pressure is estimated by assuming a relation, $V_N = V_N^\circ + \text{const } P$.

Foxboro low-temperature recorder. Columns were mounted in the inner box with long, low-volume Swagelok bulkhead connectors.

A small volume gas injection system was constructed using 1/8-in. Whitey Swagelok type valves, 1/8-in. tubing, and a Wilkens Instrument and Research Corp. (Walnut Creek, California) gas injection valve. The sample size was 0.25 ml at 15–300 Torr. Fenwall Type 112 thermistors were used for detection of H₂, HD, and D₂. These were mounted in a low-volume stainless steel block and were screened in the manner described by Kieselbach.²¹ An independent supply of carrier (He) was fed to the reference thermistor at a rate of 5 cm³/min. The block temperature was maintained at 28° with a water bath. A 0.5-ml ion chamber of our own design was used for detection of HT, DT, and T₂ peaks. Potential for this chamber was supplied by a 6-V dry cell. This was connected to an Applied Physics Corp. Model 31 vibrating reed electrometer equipped with a turret switch containing a 10¹¹-ohm resistor, which allowed a response time of approximately 1 sec. Peaks from both detectors were registered on a Brown dual-pen potentiometric recorder.

Experimental Results

Table I summarizes a typical set of net retention volumes, V_N , at different sample pressures and at different temperatures. V_N is calculated from the relations²²

$$V_N = (t_R - t_{He})F_c/W_s \quad (1)$$

$$F_c = F_o(T_c/T_a)[1 - (P_w/P_a)] \frac{3 [(P_i/P_a)^2 - 1]}{2 [(P_i/P_a)^3 - 1]} \quad (2)$$

where t_R = retention time measured at peak maximum, t_{He} = retention time of ³He, W_s = weight of solid, F_o = flow rate measured at ambient condition with a soap bulb flowmeter, T_c = column temperature, T_a = ambient temperature, P_w = vapor pressure of water at ambient temperature, P_a = ambient pressure, and P_i = pressure at column inlet. As seen in Table I, V_N decreases with increasing sample pressure. By supposing a linear relation,¹ V_N is extrapolated to zero sample pressure. Resulting retention volumes, V_N° , at zero sample pressure are summarized in Table II.

Table II: Net Retention Volumes (cm³/g) at Zero Sample Pressure^a

Temp. °K	H ₂	HD	HT	D ₂	T ₂
219	1.65	1.75	1.91	1.87	2.05
211	1.96	2.10	2.28	2.26	2.49
203	2.39	2.57	2.77	2.83	3.07
197	2.68	2.84	3.12	3.13	3.49
189	3.27	3.56	3.80	3.91	4.43
181	3.99	4.37	4.67	4.87	5.38
174	4.85	5.36	5.75	6.07	6.76
169	5.77	6.40	7.23	7.30	8.21

^a For DT, $V_N^\circ = 6.30$ at 174° and 7.85 at 169°K.

At temperatures above 169°K, where data for the weight isomers are determined, there is no measurable separation of any of the spin isomers. The spin isomer effect in H₂ is investigated at lower temperatures from 160 to 135°K. Table III summarizes the results in terms of the separation factor S

$$S = (t_{ortho} - t_{He})/(t_{para} - t_{He}) \quad (3)$$

Table III: The Separation Factors, $S = (t_{ortho} - t_{He})/(t_{para} - t_{He})$, at Different Temperatures

S	Temp. °K				
	135	141	147	152	160
	1.108	1.088	1.073	1.058	1.042

Discussion

Kirkwood-Wigner Partition Function. The possibility exists that the spin isomer separations, though ubiquitous, may be due to some form of specific magnetic interaction with the surface and so the first attempt to interpret the adsorption results involved the weight isomer data only and used the formulation of DeMarcus, *et al.*,^{6,7} based on the Kirkwood-Wigner

(21) R. Kieselbach, *Anal. Chem.*, **32**, 1749 (1960).

(22) For example, see S. D. Nogare and R. S. Jevet, Jr., "Gas Liquid Chromatography," Interscience Publishers, New York, N. Y., 1962, pp 73-78.

partition function expanded through terms in h^2 . This is of the form

$$V_N/A s_0 = B(\psi(\sigma)/kT) + \frac{I_1}{m s_0^2} (\psi'(\sigma)/kT, \psi''(\sigma)/kT) \quad (4)$$

where A is the area, s_0 is that distance, s , ($\sigma = s/s_0$) of the molecule from a reference plane running through the surface where attractive and repulsive forces exactly cancel, and m is the molecular mass of the weight isomer is question. The integrals B (the classical contribution) and I_1 are functions of ψ , the potential energy function of interaction of the molecule with the surface (and its derivatives), while kT has its usual significance. This partition function has been applied successfully to account for the difference in adsorption between H_2 and D_2 on a fairly homogeneous carbon black over a much wider temperature range⁷ than that studied here.

Friedmann²³ has shown in connection with vapor pressure isotope effects, it is possible to use eq 4 to apply a necessary, but not sufficient, test of consistency to data that is independent of the actual values of the integrals and indeed of the potential energy expression. That is, given data for three isomers, *e.g.*, H_2 , D_2 , T_2 , one can write

$$\frac{V_N(D_2) - V_N(H_2)}{V_N(T_2) - V_N(D_2)} = \frac{m(T_2) [m(D_2) - m(H_2)]}{m(H_2) [m(T_2) - m(D_2)]} = 3.005 \quad (5)$$

Table IV summarizes experimental values of the left-hand side of eq 5. There does not seem to be any systematic variation with temperature, but the average value is only 1.5, only half the value predicted. Thus this simple approach may be discarded forthwith.

Table IV: Retention Volume Ratios (Left-Hand Side of Eq 5) at Different Temperatures

Temp, °K	Ratio
219	1.2
211	1.3
203	1.7
197	1.3
189	1.2
181	1.7
174	1.8
169	1.7
	Av 1.5 ± 0.2

Jenkins²⁴ showed that the next higher term in the K-W expansion should be negligible at the temperatures involved in the present experiment. However, Yaris and Sams⁸ have made some use of it in fitting this model

to somewhat lower temperature data.² Therefore, for completeness it was attempted here, where now

$$V_N/A s_0 = B + \frac{I_1}{m s_0^2} + \frac{I_2}{m^2 s_0^4} \left(\frac{\psi'(\sigma)}{kT}, \frac{\psi''(\sigma)}{kT}, \frac{\psi^{III}(\sigma)}{kT}, \frac{\psi^{IV}(\sigma)}{kT} \right) \quad (6)$$

A somewhat more complex test of consistency analogous to eq 5, using the additional weight isomer HD, works quite well and so the data were fitted to the model, eq 6, using the integrals tabulated for interaction with a plane surface by Yaris and Sams⁸ for an attractive third power repulsive ninth power potential energy expression

$$\psi_i(\sigma) = \frac{3\sqrt{3}}{2} \epsilon_i^* \{ \sigma^9 - \sigma^3 \} \quad (7)$$

The parameter ϵ_i^* is the depth of the potential energy well for each isomer, initially taken to be all equal. The parameters of eq 6, evaluated by the method of least squares, are tabulated in Table V. Two facts emerge immediately. First, the rms deviation is rather large. Second, and more important, the collision parameter s_0 , which should certainly be between 2 and 3 Å, is unrealistically small (as indeed it must be to have I_2 contribute significantly at such high temperatures).

Table V: "Best Fit" Results to Yaris and Sams Functions, Equal ϵ_i^*

Isomers (joint fit)	A , m ² /g	ϵ^*/k , °K	s_0 , Å	Root mean square dev ^a
H_2 , D_2 , T_2	160	1290	1.189	0.29
H_2 , D_2 , T_2 , HD	171	1282	1.163	0.28
H_2 , D_2 , T_2 , HD, HT	187	1261	1.17	0.26

^a The rms deviation is to be compared to the standard deviations of the data in Table I and the maximum difference in V_N° for H_2 and T_2 of 2.44 at 169°K and the minimum difference of 0.40 at 219°K.

This approach, though not promising, could not be categorically dismissed without trying various refinements. The first change was to rederive the equations for adsorption in spherical cavities so that they more nearly correspond to the adsorption geometry in molecular sieves.²⁵ When the radius of the sphere was left as an adjustable parameter, however, the computer consistently converged to infinite radius with no

(23) H. Friedmann, *Advan. Chem. Phys.*, **4**, 225 (1962).

(24) C. Jenkins, Jr., Ph.D. Thesis, Department of Physics, University of Kentucky, Lexington, Ky., 1962.

(25) D. W. Breck, *J. Chem. Educ.*, **41**, 678 (1964).

improvement in the collision parameter s_0 . When the radius was fixed at reasonable values (2 to 3 molecular diameters), the converged value of the surface area was an order of magnitude too high (ca. 3500 m²/g) and the collision parameter smaller yet. When the model was refined further, by allowing the isomers to assume different adsorption energies to allow for the fact that the greater centrifugal force on the interatomic bonds of the lighter isotopes causes them to stretch and increase in polarizability,²⁶ no further improvement was noted. The computer made only slight adjustments in the energies of the different isomers and more often than not ordered them in the wrong sequence. Further refinements, mostly trivial reformulation attempts, met with no better success, so we are forced to the negative conclusion that an adsorption model based on the Kirkwood-Wigner partition function does not satisfactorily account for these data.

Hybrid Partition Function. Stimulated by these problems, an independent study was initiated on the role of hindered rotation in hydrogen adsorption⁹ using a rather more cumbersome approximate partition function based on the work of Hagyard.²⁷ This new partition function, fully described elsewhere,⁹ may be generated when the physical situation is sufficiently simple to allow the partition function to be factored into single particle partition functions (the case for high-temperature adsorption) and the lower few energy levels are known for the potential expression which may now include the rotational degrees of freedom. The procedure is to form the usual exponential sum over states for the known energy levels and add to that the classical partition function evaluated over all phase space, again including the rotational degrees of freedom, excluding only those lowest cells containing and corresponding in number to the known energy levels.

A single gross feature immediately emerging from this study is sufficient to explain the failure of the Kirkwood-Wigner partition function for these data. Namely, the partition functions for all isomers when logarithmically plotted *vs.* $1/T$ waver somewhat but are more or less well behaved excepting in the limited temperature range studied in this experiment (Figure 1). Here, a significant "spoon" arising entirely from the rotational contribution of the classical part of the partition function obviates conformity to the simpler K-W model. The functions plotted in Figure 1 are for the combined nuclear spin isomers and have been reduced by the respective gas-phase partition functions so as to give a function directly identifiable with the excess retention volume measurements of gas chromatography, but reduced by the capacity factor As_0 . They were generated for a depth of potential energy well of 2500 cal/mol (corresponding to a depth of well of 2167 cal/mol for spherically averaged molecules and a collision parameter of 2.2 Å ($\gamma = 1.20$) in a Morse po-

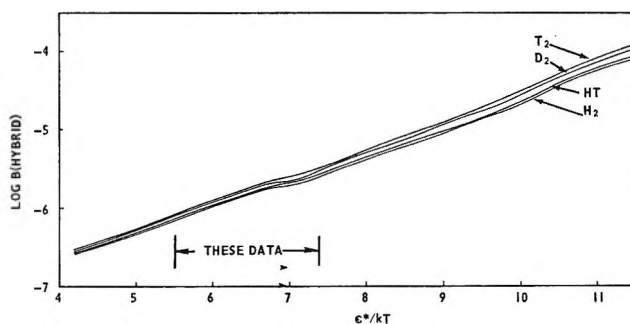


Figure 1. The revised hybrid partition functions for the weight isomers of hydrogen shown. $\epsilon^* = 2500$ cal/mol, $s_0 = 2.2$ Å ($\gamma = 1.20$).

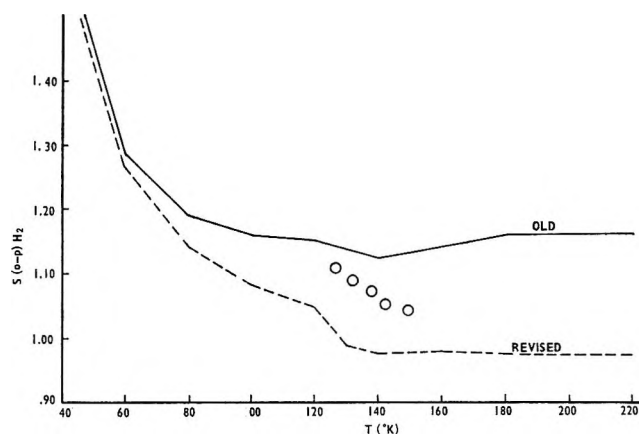


Figure 2. The measured *ortho-para* separator factors for H₂ together with theoretical separation factors derived from the hybrid partition function ($\epsilon^* = 2500$ cal/mol, $s_0 = 2.2$ Å) both old (ref 9) and revised (this work).

tential described elsewhere.^{9,12} The partition functions plotted here, the revised values, differ slightly from those published previously,⁹ called the old values, in that allowance is made for the known empty energy levels above the known filled levels for *ortho*-H₂ and T₂ and *para*-D₂. Although this change is scarcely noticeable in the plot of Figure 1, as shown below it has a rather beneficial effect on the computed spin isomer separation factors (Figure 2). Note that the increased "wavering" of the revised functions is probably due at least in part to the increased density of computed values.

For various reasons, fitting this model to the present experimental data is not straightforward. First, the hybrid function does not work for the asymmetric isotopes in that HT is almost indistinguishable from D₂ in its experimental behavior (as predicted by the K-W formulation), whereas the hybrid function says it should be indistinguishable from hydrogen in the temperature regime studied here (see a limited discussion in Conclusions, below). For this reason, only the

(26) H. F. F. Knapp and J. J. M. Beenakker, *Physica*, **27**, 523 (1961).

(27) M. S. Hagyard, Ph.D. Thesis, Department of Physics, University of Kentucky, Lexington, Ky., 1967.

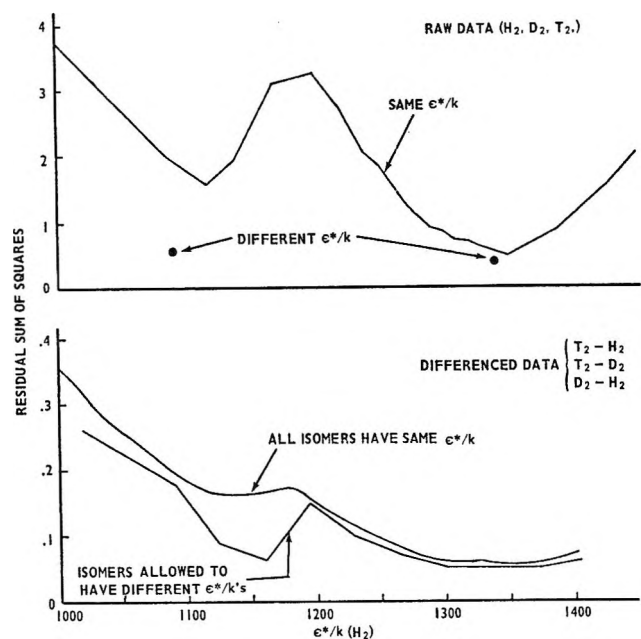


Figure 3. Sections of the sum of squares surfaces (fitting the best capacity parameter at each energy) for data both raw and differenced.

symmetric isomers could be considered. Second, the energy levels were evaluated for a particular depth of potential energy well and collision parameter,⁹ so that the partition function cannot be rigorously used to evaluate independently all the parameters available with the KW models. The area is of course still available as a capacity factor and, as a compromise measure, the partition function is incorrectly expressed as a function of reduced reciprocal temperature factor ϵ^*/kT to permit the estimation of an energy parameter. However, it must be understood that the resulting fit is only accurate for $\epsilon^* = 2500$ cal/mol; the larger the departure from this figure, the greater the uncertainty in the parameters evaluated. Further, as mentioned before, the plane geometry implicit in the model is inappropriate for adsorption in molecular sieves where adsorption in spherical cavities would be a more meaningful model. A somewhat subtle test of the importance of this consideration is to fit (1) the data as measured, which we will call the raw data, and differencing the partition functions, (2) to fit the differences in retention volumes for the three isomers. Differencing should subtract out the classical contribution (and thus the "spoon") which should be most strongly a function of surface curvature because it involves functions that decay less rapidly with separation from the surface than the quantum effects which are important only when the molecule is close to its potential energy minimum. If there is no bias caused by failure of the classical part of the model and all error is random, it is easy to show that the residual error of the curve-fitting process for the differenced data should be bigger than that for the raw data by a factor of $\sqrt{2}$.

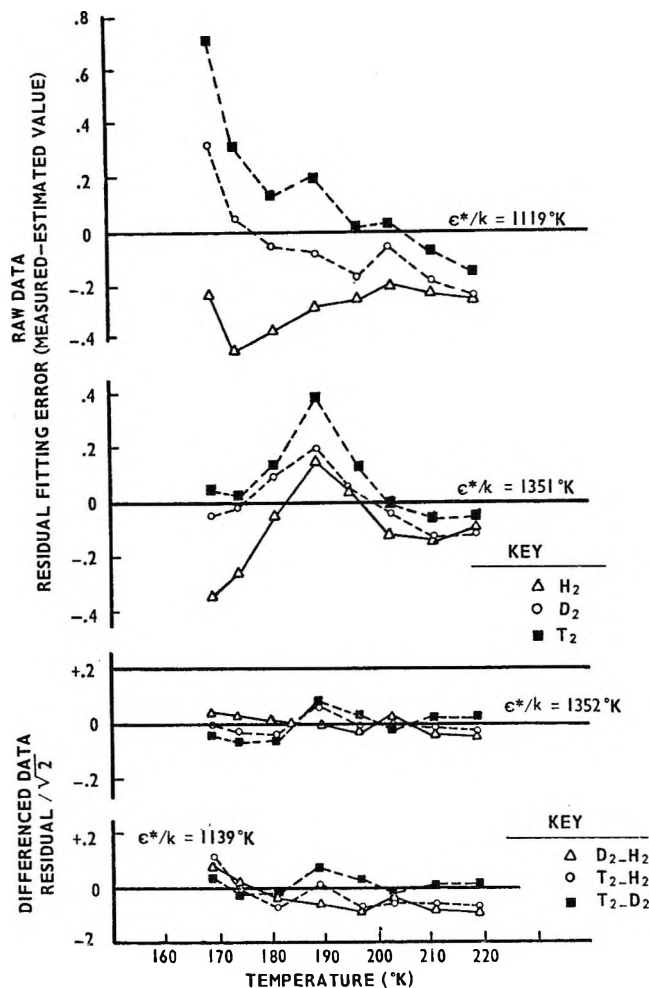


Figure 4. Residuals of the best fits to the raw and differenced data shown for both minima (all isomers same energy).

The model was fitted to the raw data for the three symmetric isomers and the differenced model to the differenced data using the redundant set of all three differences so as to weight the isomers equally. In each case this was done for the same value of ϵ^* for each of the isomers and then again, allowing the energies to vary independently. In every case a double minimum was found in the sum of squares surface. Table VI shows the fitted parameters together with their asymptotic marginal 95% confidence limits and estimated standard deviation of fit. As anticipated, the fit of the differenced data has but one-third the standard deviation of the best fits of the raw data (instead of being $\sqrt{2}$ times as great) so that bias in the fit of the raw data is clearly demonstrated even though the parameters obtained are essentially the same as those obtained for the difference fits. (Note that the standard deviations of the differenced data are on the order of $\sqrt{2}$ times the standard deviations of Table I, indicating optimum conformity to model.) The double minima may in fact arise from this surface curvature, but it seems more probable that it is the result of incorrectly treating the partition function as a func-

Table VI: Best Fits of the Hybrid Partition Function to the Symmetric Isomer Retention Time Data

Case	A , m^2	$\epsilon^*/k(H_2)$, $^\circ K$	$\epsilon^*(D_2)/\epsilon^*(H_2)$	$\epsilon^*(T_2)/\epsilon^*(H_2)$	Estd std dev
Raw Data					
High energy	148 ± 10	1351 ± 15	0.155
minimum	$(151 \pm 9)^a$	(1339 ± 15)	(1.007 ± 0.006)	(1.009 ± 0.005)	(0.131)
Low energy	367 ± 140	1119 ± 88	0.271
minimum	(385 ± 90)	(1089 ± 52)	(1.018 ± 0.009)	(1.027 ± 0.009)	(0.165)
Differenced Data					
High energy	177 ± 40	1351 ± 40	0.052
minimum	(173 ± 40)	(1352 ± 62)	(1.001 ± 0.006)	(1.001 ± 0.006)	(0.051)
Low energy	548 ± 26	1139 ± 92	0.086
minimum	(595 ± 33)	(1157 ± 3)	(0.994 ± 0.002)	(0.992 ± 0.002)	(0.051)

^a Parenthetical values are those obtained when the energies were allowed to vary independently.

tion of reduced temperature. One of these minima is certainly spurious. However, picking either of these alternatives as the correct one would be at best arbitrary. Refitting the raw and differenced data, allowing the isomers to have independently adjustable adsorption energies, improves the fit somewhat but makes no appreciable difference otherwise, as shown by the sections through the sum of squares surfaces shown in Figure 3 and the energy ratios in Table VI. One might note, however, that examination of the residuals (Figure 4) shows that for both raw and differenced data the residuals for the lower energy minimum demonstrate a more systematic departure from model. Furthermore, the capacity factor is somewhat more nearly the expected value for the high energy surface in that it is about one-third the known area of these adsorbents²⁵ and this is probably about right for these mildly heterogeneous surfaces.²⁸

It remains to compare the spin isomer separation factors predicted by this model with those observed for H₂ at lower temperatures. The measured separation factors are in Figure 4, together with separation-factor functions derived from the previously published hybrid partition functions⁹ and these revised functions (Figure 1). No attempt has been made to adjust the energy parameters. Clearly the agreement is satisfactory to within the degree of ambiguity and precision of calculation of the functions.

Conclusions

It is at once clear that carefully done gsc techniques are indeed suitable for the detailed study of high temperature physical adsorption phenomena on the one hand, and that hydrogen adsorption in this tempera-

ture regime importantly involves hindered rotation on the other, a conclusion reached previously.⁹ Although the ambiguity and approximate nature of the partition function, together with the compromises made in its application, preclude an exact or even unique assignment of the adsorption parameters, the functional form is more nearly correct than that of the Kirkwood-Wigner formulation for spherically symmetric molecules. Note that this latter formulation may only be applied to data encompassing a much wider temperature range than is usually experimentally convenient, and then only with reservation.⁹

The conclusion found before when analyzing other data,⁹ that the polarizability differences of the different molecules is inconsequential, is borne out in the present analysis. In only one of the four fitting procedures where the energies were allowed to vary independently did they differ by more than 1% and in three of the four cases they were ordered in the wrong direction (*i.e.*, H₂ was the least energetic).

Finally, the dilemma of the asymmetric isomers remains. These data strongly reaffirm that for these isomers the hybrid partition function is wrong. This probably reflects back to the potential energy expression, albeit apparently quite reasonable, used to find the energy levels.¹² No serious attempt at an explanation has as yet been proposed, but it is probably somehow related to the effect of the constraint of the surface on the librational mode. This might be expected to cause the angular motion to center more nearly about the center of the molecule than about the center of mass as it does in free rotation.

(28) M. P. Freeman and K. Kolb, *J. Phys. Chem.*, **67**, 217 (1963).

Reactions Involving Electron Transfer at Semiconductor Surfaces.¹

I. Dissociation of Nitrous Oxide over n-Type Semiconductors at 20°

by Joseph Cunningham, John J. Kelly, and A. L. Penny

Chemistry Department, University College, Belfield, Dublin 4, Ireland (Received December 2, 1969)

Dissociation of nitrous oxide at 20° has been observed over surfaces of zinc oxides or ferric oxide activated *in vacuo* at 400°. Extent of dissociation over various zinc oxides varied in a manner agreeing with boundary layer theory. Kinetics of N₂O dissociation over the oxides were identical with those obtained for changes in conductivity of oxide films contacted with N₂O. A mechanism in which localization of an electron at the oxide surface is the rate-determining step accounts for the results and for changes in reactivity produced by prior exposure of the oxide to hydrogen or oxygen. Evaporated zinc films also dissociated N₂O readily at 20° and different kinetics were observed at different N₂O pressures.

Introduction

Transfer and sharing of electrons between semiconducting solids and molecules adsorbed on their surfaces are important steps in proposed mechanisms for many reactions catalyzed by such surfaces^{2,3} and are frequently referred to as the "electronic factor" in chemisorption. Recent studies on zinc oxide, using difficult ac Hall effect techniques, supports the importance of such an 'electronic factor'^{4,5} in chemisorption and reaction on that material. Thus a correlation was found between the number of oxygen species chemisorbed on the surface of zinc oxide and the number of mobile conduction band electrons trapped during chemisorption.

This paper presents the results of attempts to use nitrous oxide gas as a chemical indicator of electron availability at "dark" surfaces of n-type oxide semiconductors (pure and doped zinc oxides and ferric oxide). Subsequent papers will deal with the use of N₂O and other molecules to study the availability of electrons and holes at illuminated semiconductor surfaces.

Choice of N₂O as the probe gas was influenced by reports of its extensive use as an efficient electron "scavenger" in radiolysis^{6,7} and by the importance placed on the electronic mechanism of its catalyzed decomposition over semiconducting surfaces.⁸⁻¹⁰

There is general agreement among workers using N₂O for such experiments that the important primary dissociative step is rupture of the N-O bond, produced by interaction of N₂O molecules with low-energy electrons.¹¹⁻¹⁵

Electron capture by N₂O in the gas phase may occur either by an apparent three-body process or by a two-body process,¹⁶ and lifetimes of 10⁻⁷ to 10⁻³ sec have been estimated for the gaseous molecular anion, N₂O⁻.^{14,17}

This extensive background information suggested that N₂O could be used to study the electronic proper-

ties of various semiconductors by measuring dissociation of the gas occurring at the semiconductor surface.

Experimental Section

1. *Materials.* The zinc oxides used in the present study were powdered samples obtained by courtesy of the New Jersey Zinc Co. Material here referred to as ZnO was their high-purity grade, labeled SP 500. Lithium-doped zinc oxide (Li-ZnO) contained 463 ppm of lithium and the indium-doped sample (In-ZnO) contained 110 ppm of indium.

Ferric oxide (Fe₂O₃) was Speepure grade powder supplied by Johnson Matthey and Co. Ltd.

(1) This work is supported in part by the Air Force Office of Scientific Research through the European Office of Aerospace Research, OAR, United States Air Force under Contract AF 61(052)-67C-0044.

(2) (a) K. Hauffe, *Advan. Catal.*, **9**, 187 (1957); (b) Th. Wolkenstein, "The Electron Theory of Catalysis on Semiconductors," Pergamon Press, 1963.

(3) F. Garcia Moliner, *Catal. Rev.*, **2**, 1 (1968).

(4) H. Chon and C. D. Prater, *Discussions Faraday Soc.*, **41**, 380 (1966).

(5) H. Chon and J. Pajares, *J. Catal.*, **14**, 257 (1969).

(6) J. M. Warman, *Nature*, **213**, 381 (1967).

(7) J. T. Sears, *J. Phys. Chem.*, **73**, 1143 (1969).

(8) K. Hauffe, R. Glang, and H. J. Engell, *Z. Phys. Chem. (Leipzig)*, **201**, 223 (1952).

(9) Y. Saito, Y. Yoneda, and S. Makishima, *Actes Congr. Int. Catal.*, **2nd**, **2**, 1937 (1960).

(10) W. D. Schulz and J. Scheve, *Z. Anorg. Allg. Chem.*, **366**, 231 (1969).

(11) R. D. Iyengar and A. C. Zettlemoyer, *J. Colloid. Sci.*, **20**, 857 (1965).

(12) G. Scholes and M. Simic, *Nature*, **202**, 895 (1964).

(13) N. H. Sargent, R. W. Robinson, and A. C. Blair, *Can. J. Chem.*, **46**, 3511 (1968).

(14) J. H. Warman, K-D. Asmus, and R. E. Schuler, *Advances in Chemistry Series*, No. 82, Vol. II, American Chemical Society, Washington, D. C., 1968, p 25.

(15) V. Pravdic, A. E. Wilcox, and A. C. Zettlemoyer, *Surface Sci.*, **13**, 280 (1968).

(16) A. V. Phelps and R. E. Voshall, *J. Chem. Phys.*, **49**, 3246 (1968).

(17) G. Porter and M. W. Windsor, *Proc. Roy. Soc.*, **A245**, 238 (1958).

Table I: Comparison of Boundary-Layer-Limited Depletive Chemisorption, θ_{\max} , with Observed Dark Dissociation of N_2O , θ_{exptl} , over n-Type Oxides

	Li-ZnO	ZnO	In-ZnO	Fe ₂ O ₃
Surface area, m ² /g	1.1	4.0	0.1	3.2
Extent of dissocn, V_N , (ml at STP)/m ² of oxide	8.4×10^{-5}	4.4×10^{-4}	15.6×10^{-3}	11.7×10^{-3}
n_e , concn of mobile carriers ^a	2.7×10^{14}	3×10^{16}	1.8×10^{18}	...
n_D , donor concn ^b	3×10^{18} (8.1×10^{14})	9×10^{16}	4.0×10^{18}	...
θ_{\max} ^c	0.009 (0.008)	0.086	0.90	...
θ_{exptl} ^d	0.016	0.090	3.3	2.5

^a Values from ref 4. ^b Estimated values using data quoted, respectively, in ref 18, R. Glemza and R. J. Kokes, *J. Phys. Chem.*, **69**, 3254 (1965), and ref 21, P. B. Weisz, *J. Chem. Phys.*, **21**, 1531 (1953), and ref 23, M. A. Seitz and D. H. Whitmore, *J. Phys. Chem. Solids*, **29**, 1033 (1968). ^c Calculated from eq IIb for In-ZnO + ZnO. See text for Li-ZnO calculation. ^d $\theta_{\text{exptl}} = (\text{no. of } O^- \text{ ions on surface}) \times (\text{area per ion}) \times 100 / (\text{total surface area})$, assuming $(\text{no. of } O^- \text{ on surface}) = (\text{no. of } N_2 \text{ observed in gas phase})$.

Surface areas as determined by the conventional BET method and equipment, using krypton adsorption at liquid nitrogen temperature, are listed in Table I.

Commercially available high-purity gases (Grade X N_2O , H_2 , O_2 supplied by British Oxygen Co.) were used throughout. Purity of N_2O was maintained by trap-to-trap distillation using acetone-Dry Ice and liquid nitrogen traps. H_2 and O_2 were introduced to the system through liquid nitrogen traps. Immediately prior to their use in kinetic studies, oxide samples were "activated" by evacuation at 400° for 16 hr on a mercury-free vacuum rack and then cooled *in vacuo* to room temperature, being at all times protected from grease and pump vapors by liquid nitrogen traps. Total residual gas pressures in the reaction system after activation and before admitting reactant gases were 2×10^{-5} Torr at 400° and 2×10^{-6} Torr at 20°.

Zinc films were laid by evaporating the Analar metal at 400° onto the Pyrex walls of a cylindrical vessel, of geometric surface area *ca.* 8×10^{-2} m². Residual gas pressure during film deposition was 10^{-4} Torr. Stated levels of principal impurities in the zinc metal were cadmium (<10 ppm), iron (<20 ppm), and lead (<40 ppm). The zinc metal was supplied by B.D.H. Chemicals Ltd., Poole, England.

2. Reaction Systems. Two types of reaction system were used to study the decomposition of N_2O over newly activated surfaces. (a) *Static System.* The required quantity of N_2O for each run was obtained by passing the gas from its reservoir through a calibrated glass leak into a trap held at 77°K on the reaction system. The system was then isolated by means of a brass bellows-seal valve (Hoke).

The reaction was started by evaporating the N_2O in the closed-off system containing the activated oxide sample (30–40 g). Total gas pressure above the sample was monitored on an extended-range Pirani gauge (Ed-

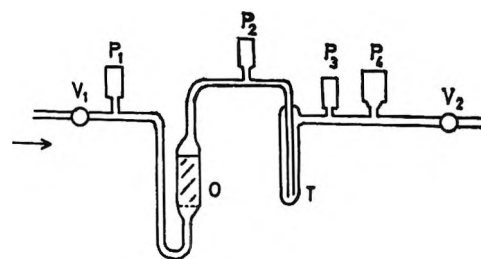


Figure 1. Flow reaction system used to follow fast formation of *nc* product over ZnO powders (O).

wards Type G-9). The reaction was followed by measuring the pressure of the noncondensable product gas (Edwards Pirani gauges G9 and G5C-2) after first condensing the unreacted N_2O at 77°K.

(b) *Flow System.* A flow system was used (Figure 1) to follow the initial rapid production of noncondensable product when N_2O was contacted with the activated oxide. N_2O was admitted through the metal valve, V_1 , and passed through the oxide powder O. The pressure differential across the sample was measured by Piranis P_1 and P_2 . Unreacted N_2O was trapped by liquid nitrogen and noncondensable (*nc*) product gas was detected by Piranis P_3 and P_4 . Output from P_4 was fed to a recorder with $1/2$ -sec response time, and a time *vs.* pressure trace obtained.

It was found that the activity of the oxide surface towards N_2O could be regenerated after each run by heating at 400° under vacuum for 16 hr. However, after a certain number of reproducible runs the original activity could not be achieved by the reactivation process whereupon the sample was discarded. It was also found that the activity of a zinc oxide sample heated in O_2 at 400° and subsequently evacuated at that temperature for 16 hr was considerably less than that of the fresh oxide. Consequently, the procedure of firing

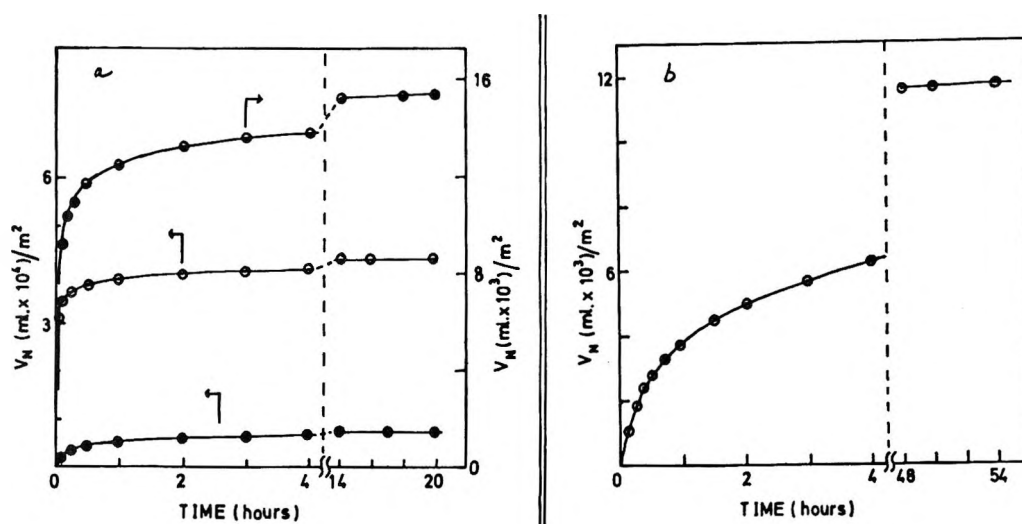


Figure 2. Growth of n c product, V_N , with contact time between N_2O and activated oxide surfaces. Data in (a) relate to ZnO (O), Li-ZnO (●), and In-ZnO (⊖). Data in (b) related to Fe_2O_3 , $P_{N_2O} = 1$ Torr in all cases.

the sample in O_2 , often adopted in the preparation of catalysts, was avoided in the present work.

3. Conductivity System. Thin oxide films (0.1 mm thick) were deposited onto gold-plated glass substrates from suspensions of the oxides in deionized water distilled from alkaline $KMnO_4$. Films, rather than pellets, were chosen for the conductivity measurements to ensure fast response to admitted gases and avoid the danger that gas diffusion through a pressed oxide pellet might determine the rate of change of conductivity. In order to avoid contamination of the films, the glass substrate with deposited gold electrodes, stainless steel contact clips, and chromel-alumel thermocouple were outgassed *in vacuo* at 400° before depositing the oxide film. Very high resistance was observed along the uncoated glass substrate across the 10 mm gap between the edges of the deposited gold electrodes, but conductivity was easily measurable after oxide deposition.

Films were first evacuated at room temperature for 4 hr and the temperature was then raised slowly to 400° . After evacuation at this temperature for 16 hr, conductivity measurements were made at 400° and during slow cooling to room temperature under a pressure of 2×10^{-6} Torr.

Two methods were employed for conductivity measurements. (a) A dc voltage (in the Ohm's law region) was applied across the film by means of a stabilized dc supply (Fluke Unit 412B) and current was measured by an electrometer (Keithley 602) with provision for a recorder output. Rapid changes in conductivity could thus be directly recorded. (b) A Wayne Kerr bridge B221 operating at 1592 cps was used to measure ac conductivity.

Good agreement between the two methods was found for all ranges of resistance encountered with the different films. For consistency, the conductivity data

here reported are dc results taken with 6 V applied across the films.

Experimental Results

Decomposition Kinetics. N_2O was found to decompose on the activated oxides at $20^\circ (\pm 2^\circ)$ and mass spectrometric analysis of the product gas showed it to be more than 95% N_2 . Thus oxygen species from dissociation remained on the surface of the oxides. The rate and extent of reaction, as measured on the static reaction system by following the increase in the pressure of the noncondensable product N_2 , differed for each oxide. Typical results showing the increase of V_N (the volume of N_2 gas in ml at stp per m^2 of oxide) with contact time are given in Figure 2.

It will be noted that after a high initial rate, the rate of dissociation over any oxide decreases almost to zero. For the range of N_2O pressures investigated (0.6–10 Torr) the rate of formation of noncondensable product over the zinc oxides did not vary by more than 10%. A much lower initial rate of dissociation of N_2O was observed over the Fe_2O_3 (see Figure 2).

Previous work^{9–11} on N_2O decomposition over n -type oxides was carried out at high temperatures ($>500^\circ$) where desorption of oxygen product occurred and extended reaction was reported. In contrast, the maximum extents of decomposition obtained in the present work at 20° were very slight (see Table 1) *e.g.*, at an initial N_2O pressure of 5 Torr less than 2% of the gas was dissociated over ZnO. These data were obtained by maintaining N_2O in contact with zinc oxide samples for extended periods as indicated on the abscissas of Figure 2.

The kinetics of the initial rapid formation of product were also studied for each zinc oxide sample, and typical data obtained with the flow system (see Figure 1) are illustrated in Figure 3 for an In-ZnO sample.

Factors Modifying Surface Reactivity. When O_2 was admitted to an activated zinc oxide surface at 20° and subsequently pumped off to a pressure of less than 5×10^{-6} Torr, the activity of the oxide surface for the decomposition of N_2O was destroyed. On the other hand, when the zinc oxide was heated in H_2 (40 Torr) at 200° for approximately 2 hr, then cooled to room temperature and evacuated, its activity was greatly enhanced. An eightfold increase in the maximum extent of N_2O dissociation over In-ZnO was obtained by this reducing treatment, which increases the concentration of surface donors.

The reactivity toward N_2O of a surface containing a much higher concentration of un-ionized zinc was investigated by use of *vacuum-deposited zinc films*. Extensive dissociation of the gas occurred over these films at 20°. Figure 4a shows the decomposition of N_2O to $N_2(g)$ on such a film. At low pressures (0.102 and 0.050 Torr shown) the reaction was first order in N_2O pressure and complete decomposition of reactant gas occurred. Figure 4b, lower graph, shows a first-order plot of these two runs where V_0 is the initial volume of N_2O (ml at STP) and V_N is the volume of N_2 (ml at STP) produced at time t and measured by condensing the unreacted N_2O . The first-order rate constant was $2.25 \times 10^{-2} \text{ min}^{-1}$.

At higher pressures of N_2O , first-order kinetics no longer held (uppermost curve Figure 4a) nor was complete decomposition of N_2O effected even after prolonged contact.

Conductivity Changes. N_2O decreased the conductivity of the activated oxide films in the manner shown in Figure 5 where i/i_0 , the ratio of current at time t to that at time zero, is plotted against contact time. The effect of N_2O on the conductivity of ZnO is very similar to that reported for O_2 by Glemza and Kokes.¹⁸ Although measurements of the electrical conductivity of some powders by dc and low-frequency ac methods may yield mainly information on their surface conductivity, the results of a previous detailed investigation of the frequency dependence of the conductivity of ZnO samples¹⁹ indicated that, for this material, information on bulk conductivity could be obtained from our conductivity measurements. Saltsburg and Snowden found that increasing the frequency 10^3 – 10^{10} cps increased the conductivity of ZnO powders by $>10^4$ indicating greater participation of bulk carriers. Adsorbed oxygen sharply decreased the conductivity and they observed qualitatively similar decreases by dc as by ac measurements at all frequencies. The magnitude of these relative conductivity changes varied only slowly with frequency and decreased by less than one order of magnitude when frequency increased 10^3 – 10^{10} cps, thus indicating similarity between behavior of surface and bulk carriers. Chon and Prater showed more recently⁴ that measurements of the Hall effect of ZnO samples by an ac technique yielded information

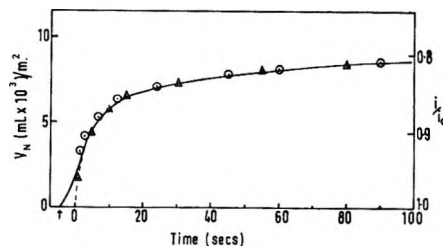


Figure 3. Plot showing initial rapid reaction when N_2O was contacted with In-ZnO. The continuous curve is an experimental trace of pressure of nc gas vs. time, obtained with the flow system shown in Figure 1. Open circle points were calculated from an Elovich plot fitted to data taken at longer contact time. Triangular points define the manner in which conductivity of a film of In-ZnO varied when contacted with the same pressure of N_2O .

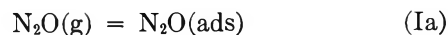
on bulk carriers. They report a 1:1 correspondence between the number of oxygen atoms chemisorbed (as O^-) and the number of electrons removed from the bulk by this chemisorption. It thus seems reasonable to expect conductivity data as in Figure 5 to yield qualitative information on variations in bulk conductivity, as also in surface conductivity.

The change in conductivity of the zinc oxides was very rapid on introduction of N_2O , whereas for Fe_2O_3 the change was much slower. Comparison of Figures 2 and 5 shows the parallel features between the kinetics of the decomposition of N_2O and those for changes in conductivity. Previous workers have shown that oxygen, at room temperature, reduced the conductivity of zinc oxide¹⁸ and that hydrogen at 200° increased its conductivity.²⁰ Similar results were obtained for the zinc oxides used in the present investigation; e.g., exposing an In-ZnO film to 20 Torr H_2 at 200° for 30 min increased its conductivity, observed at room temperature, by a factor of 3, whereas exposure of a similar In-ZnO film to 50 Torr dry air at 20° reduced the conductivity by a factor of 7.

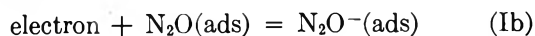
Discussion

Our observations that nitrous oxide reduced the conductivity of these n-type oxides is consistent with mechanisms proposed by other workers for its dissociation over semiconducting surfaces.⁸⁻¹¹ Five processes can be distinguished

weak chemisorption



electron localization



(18) R. Glemza and R. J. Kokes, *J. Phys. Chem.*, **69**, 3254 (1965).

(19) H. Saltsburg and D. P. Snowden, *ibid.*, **68**, 2734 (1964).

(20) A. Cimino, E. Molinari, F. Cramarossa, and G. Ghersini, *J. Catal.*, **1**, 275 (1962).

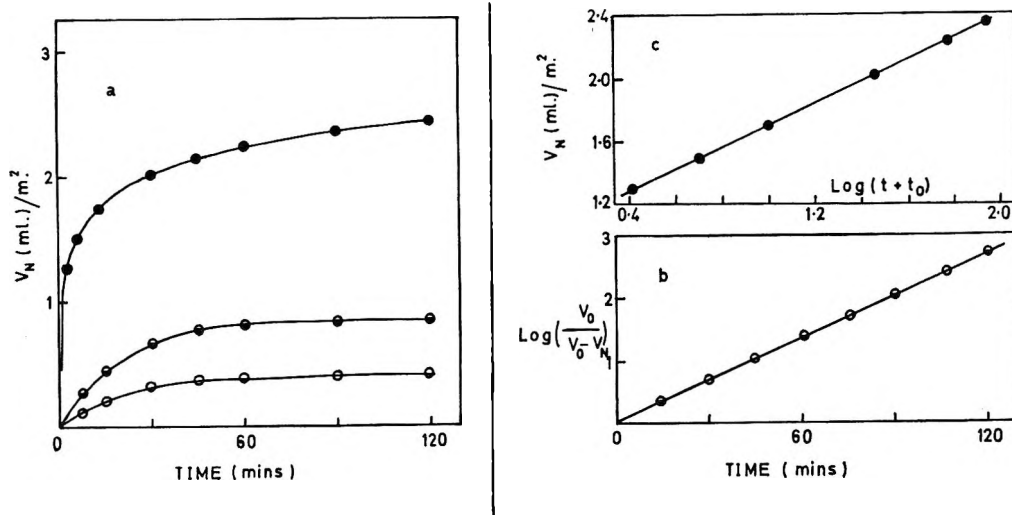


Figure 4. Growth of nc product with time when N_2O at various pressures was contacted with evaporated zinc films: (a) plots of product vs. time for $P_{N_2O} = 0.05$ Torr (O), 0.1 Torr (◐), and 1 Torr (●); (b) first-order type plot of data at $P_{N_2O} = 0.05$ and 0.1 Torr; (c) Elovich type plot of data taken at $P_{N_2O} = 1$ Torr.

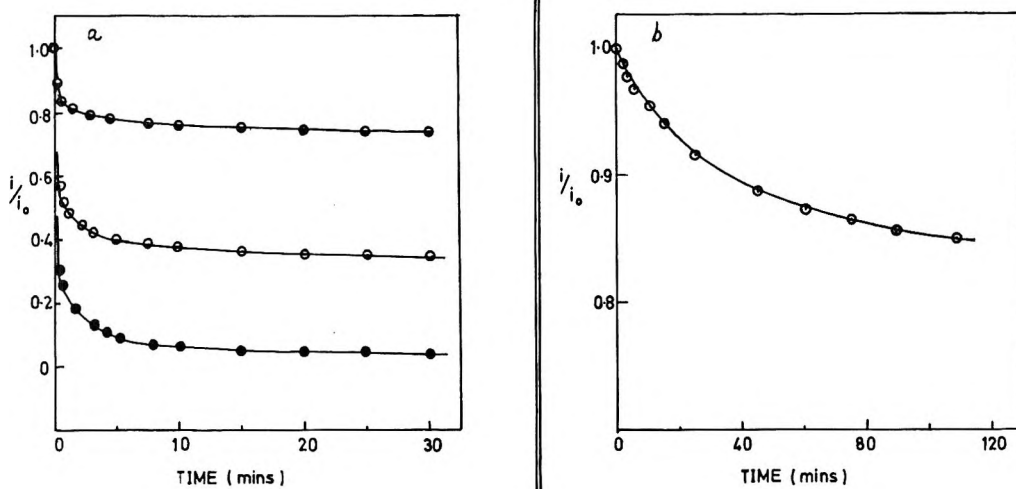
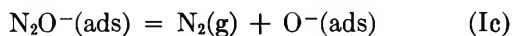
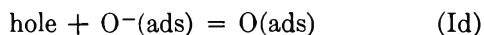


Figure 5. Variation of conductivity of oxide films with time after exposure to nitrous oxide at 20° : (a) variations observed for various zinc oxides at $P_{N_2O} = 0.6$ Torr; data for ZnO (O), for Li-ZnO (●), and In-ZnO (◐); (b) variation observed for Fe_2O_3 at $P_{N_2O} = 2$ Torr.

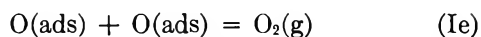
dissociation



neutralization of surface charge



desorption



The very low concentrations of holes in n-type semiconductors in the dark means that the rates of step Id, and consequently of Ie, are greatly reduced relative to steps Ia, b, and c—indeed this interpretation has been advanced to account for the much higher temperatures ($500\text{--}700^\circ$) needed to achieve extensive

catalytic dissociation of N_2O over n-type oxides than over p-type oxides ($200\text{--}300^\circ$).^{8,9} Discussion of the present results obtained over n-type oxides in the dark at 20° may therefore be restricted to steps Ia, b, and c. These result in one electron being localized at the surface for each N_2O strongly chemisorbed by Ib or dissociated *via* Ic. Such a process should reduce the conductivity and this result was here observed experimentally (Figure 5). Weisz,²¹ and later Barry and Stone,²² have shown that boundary layer theory can be used to calculate the extent to which processes dependent upon such depletive chemisorption may pro-

(21) P. B. Weisz, *J. Chem. Phys.*, **21**, 1531 (1953).

(22) T. I. Barry and F. S. Stone, *Proc. Roy. Soc.*, **A255**, 124 (1960).

ceed over semiconductor surfaces. It is therefore of interest to compare the predictions of their boundary layer theories with the extent of N_2O dissociation here observed over the various zinc oxides.

In such boundary layer considerations, the number of surface chemisorbed species, each bearing a negative charge, is set to correspond to the total positive charge produced by depletion of electrons in a layer extending to depth D within the solid. The electrical potential in this boundary layer, denoted by $E(x)$ at depth x , takes a maximum value of E_0' at the surface. It is generally considered that no further appreciable depletion chemisorption can occur when the surface potential attains a limiting value.

In the Weisz treatment of an n-type semiconductor with a density of donor levels, n_D , located at depth $2Q$ below the conduction band, two main cases are distinguished.

Case A. $E_0 \gg Q$, $Q \sim kT/e$ or $Q > kT/e$. Values estimated in the literature indicate that these conditions may be applicable to ZnO ($E_0' \sim 1.0$ eV, $2Q \sim 0.03$ eV),²¹ and In-ZnO ($E_0' \sim 1.5$ eV, $2Q \sim 0.057$ eV)⁴ at room temperature ($kT/e \sim 0.03$ eV). The limiting number of molecules chemisorbed at saturation, N_0 , may be derived from (IIa), and the corresponding percentage coverage of the surface at saturation, θ_{max} , is given by (IIb), assuming a site area of 9 \AA^2

$$N_0 = 10^3(\epsilon E_0' n_D)^{1/2} \quad (\text{IIa})$$

$$\theta_{max} = 3 \times 10(\epsilon E_0' B)^{1/2} \quad (\text{IIb})$$

Here ϵ is the dielectric constant (8.6); B , the ratio of the concentration of active donor sites relative to total lattice sites $\sim n_D/10^{23}$; and E_0' is the maximum electrical potential in the boundary layer. Using the above-mentioned literature estimates of E_0' , and values of n_D calculated from reported values of free electron concentrations, n_e , in ZnO and In-ZnO samples, from the same source as ours,⁴ expression IIb yields calculated values of θ_{max} as listed in Table I. For pure ZnO there is excellent agreement between this calculated boundary-layer-limited coverage and the coverage by O^- corresponding to the observed dissociation of N_2O . For In-ZnO, agreement is not so good but the theory does predict a greater coverage over In-ZnO than over ZnO, in qualitative agreement with the N_2O dissociation results (Table I).

Case B. $E_0 < Q$, $Q > kT/e$. These conditions may be approached in Li-ZnO since trap depths are known to be much greater ($2Q \sim 0.3\text{--}0.4$ eV)²³ and values of E_0' are expected to be smaller than for pure ZnO. In the Weisz treatment,²¹ the saturation coverage in these conditions (for the case $E_0 \sim kT/e$) will be lower than that for case A conditions by approximately the factor $(n_e/n_D)^{1/2}$. Table I gives values of n_D , the donor concentration, and n_b , the concentration of mobile carriers. The calculated factor is 9.5×10^{-2}

when for internal consistency, an n_e value of 2.4×10^{14} electrons/cm⁻³, reported for Li-ZnO in the same study as that on ZnO and In-ZnO,⁴ was used. A limiting θ_{max} value of only 0.009% may thus be estimated for Li-ZnO which agrees well with θ_{exp} observed for this sample. The agreement may, however, be fortuitous since lithium doping would be expected to yield a much lower (*ca.* 10^8) carrier concentration. However, if the high reported value of 2.4×10^{14} cm⁻³ be attributed to zinc donors introduced in the lithium doping treatment, then the Q value appropriate to such donors would be the same as for pure ZnO, so that θ_{max} for Li-ZnO should then be calculated as for case A above. This yields the values shown in brackets for Li-ZnO in Table I where θ_{max} is seen to be comparable to that calculated for case B conditions. Boundary layer calculations thus can account only semiquantitatively for the variations in θ_{exp} for the different zinc oxides, but the extent of agreement between θ_{max} and θ_{exp} is sufficient to lend support to our hypothesis that the reaction-limiting process in N_2O dissociation is a buildup of surface charge *via* (Ia), (Ib), and (Ic).

Similar boundary layer considerations were not applied to Fe_2O_3 because estimates of n_D were not available. There is the further complication that pure Fe_2O_3 has a very low conductivity (6×10^{-7} ohm⁻¹ cm⁻¹) compared with ZnO (10^{-3} ohm⁻¹ cm⁻¹). This, at first hand, seems to contradict boundary layer theory and the high observed value of $\theta_{exp,ptl}$. However, conductivity studies have shown that the mobility of electrons in pure Fe_2O_3 is very low (10^{-5} to 10^{-1} cm²/V sec)^{24,25} compared with the zinc oxides (Li-ZnO 2–8 cm²/V sec,²³ ZnO 5–40 cm²/V sec).²⁶ This low mobility means that the donor concentration may still be large despite the low conductivity. A large value of n_D would explain the large value of $\theta_{exp,ptl}$ observed.

Our kinetic results can be used to further test the validity of the proposed mechanism Ia, b, and c.

(a) *Comparison of the Kinetics of Dissociation and Conductivity.* The chemisorption step, Ib, which involves localization of an electron at a surface position reduces the number of free carriers and contributes to growth of a charged boundary layer. If this is the rate-determining step then identical kinetics should be observed for the decrease in conductivity and increase in product $N_2(g)$. The following analysis of the kinetic data in Figures 2 and 5 shows that this requirement is satisfied in striking fashion for dissociation over both ZnO and Fe_2O_3 .

(23) M. A. Seitz and D. H. Whitmore, *J. Phys. Chem. Solids*, **29**, 1033 (1968).

(24) F. J. Morin, *Phys. Rev.*, **93**, 1195 (1954).

(25) R. F. G. Gardner, F. Sweett, and D. W. Tanner, *J. Phys. Chem. Solids*, **24**, 1183 (1963).

(26) G. Heiland, E. Mollwo, and F. Stockmann, *Solid State Phys.*, **8**, 191 (1959).

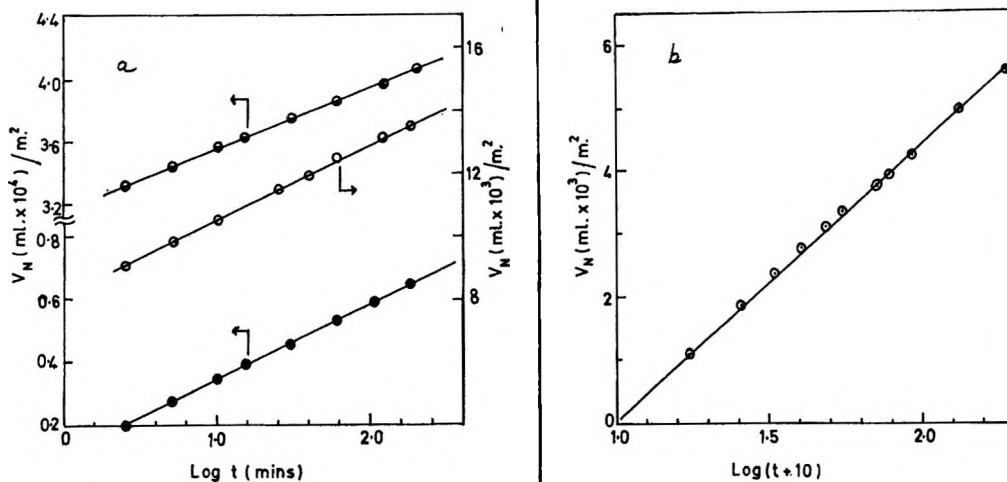


Figure 6. Plots showing that data for N_2O dissociation over different oxides obey the Elovich Equation: (a) data for three different zinc oxides: pure ZnO (○), Li-ZnO (●), and In-ZnO (◐); (b) data for Fe_2O_3 .

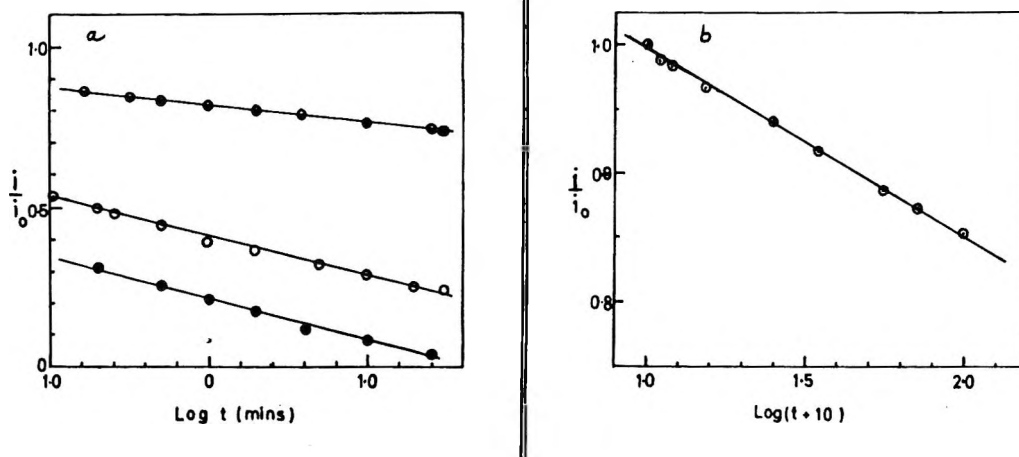


Figure 7. Plots showing that the changes in conductivity with time, after films of various oxides were contacted with N_2O , obey the Elovich equation: (a) data for different zinc oxides: pure ZnO (○), Li-ZnO (●), In-ZnO (◐); (b) data for Fe_2O_3 .

Weisz has shown that for the buildup of a boundary layer of the type just described the rate of adsorption should depend on an exponential function of the amount adsorbed. Barry and Stone, from similar considerations, have derived an expression for depletive chemisorption of the type $dq/dt = a \exp(-bq)$, where q is the amount of gas chemisorbed at time t . Processes with kinetics obeying a differential rate expression of this form, or an equivalent integrated rate expression, are often said to exhibit Elovich kinetics and this convention will be followed here.

In the present case q , the volume of N_2O strongly chemisorbed should be equal to V_N , the volume of N_2 in the gas phase, provided that step Ib is the rate-determining step. Therefore the equation

$$\frac{dV_N}{dt} = a \exp(-bV_N)$$

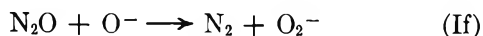
should hold. An integrated form of this expression is

$$V_N = C \log(t + t_0) + D$$

where V_N is the volume of N_2 in gas phase at time t , C and D are constants, and t_0 is a parameter with dimensions of time which does not change during a particular run but whose absolute magnitude can vary markedly from one gas-solid system to another. When the kinetic data for growth of N_2 product over ZnO were plotted as V_N vs. $\log(t + t_0)$, straight lines were obtained provided that the value of t_0 was set as zero (see Figure 6a). The kinetics of decrease of conductivity of ZnO likewise gave straight lines on such plots, again provided that $t_0 = 0$ (see Figure 7a). Neither the data for kinetics of N_2O dissociation over Fe_2O_3 nor the kinetics of change in conductivity produced in Fe_2O_3 films by exposure to N_2O gave straight lines

when t_0 was set equal to zero. A value of $t_0 = 10$ min did, however, yield straight lines for kinetic data from the N_2O dissociation and from the conductivity studies on Fe_2O_3 (Figures 6b and 7b).

(b) *Possible Contributions of Other Reactions.* There has been controversy in the literature^{7,14} as to the importance of another reaction



for dissociation of N_2O . Since this reaction does not involve additional charge localization, it is clear that addition of this reaction to the dissociation scheme Ia, Ib, and Ic could cause deviations from Elovich kinetics and discrepancies between the kinetics of N_2O dissociation and those of changes in conductivity. Figure 3 shows a detailed comparison between (a) experimental data for changes in conductivity on admitting N_2O to In-ZnO, (b) experimental data from flow system for N_2 product formation in the first 100 sec contact of N_2O with In-ZnO, and (c) points from an Elovich plot based on kinetic data taken at long times with the static system and then extrapolated back toward zero time. The three sets of data are in excellent agreement, which does not support any significant role of reaction If in the dissociation at 20°.

(c) *Limiting Case When Availability of Electrons Is No Longer Rate Determining.* Electron availability and transport are important factors in the oxidation of metals²⁷ and many workers^{28,29} have argued that transfer of electrons from the metal through the oxide to the oxide-gas interface can be the rate-controlling step in oxidation of some metals.

The concentration of electrons is greater and the electronic work function is smaller for zinc metal than for its oxide. Consequently, the availability, of electrons at the surface of a zinc film, even one oxidized to some extent during deposition at 10^{-4} Torr, is expected to be much greater than at a zinc oxide surface. So it can be argued that for low pressures of N_2O , with the surface electron concentration regarded as constant, step Ia may become the rate-determining step instead of Ib. First-order kinetics should result³⁰ and these are observed experimentally (Figure 4b).

As the thickness of the oxide layer on the zinc film increases, the availability of electrons at the oxide- N_2O interface is expected to decrease. Subsequent kinetics may then be determined by the rate at which electrons pass through the oxide layer. It has been shown that such a mechanism can yield a logarithmic growth law.^{28,29} Our data fit such a law as shown by upper graph Figure 4c, where V_N , the volume of N_2 at STP produced at time t (= volume oxygen left on the film), is plotted against $\log(t + t_0)$.

Nature of the Reactive Surface. Bevan, Shelton, and Anderson³¹ reported evidence for equilibration of the surfaces of ZnO and Fe_2O_3 in *vacuo* at temperatures

above *ca.* $0.25 T_m$ (where T_m is the mp in °K) and this would occur at *ca.* 220° for ZnO.

More recent conductivity studies³² on thick ZnO layers at temperatures 20–400° show discontinuities in conductivity vs. temperature plots at 330°, which the authors have interpreted as evidence for onset of migration of interstitial zinc to the surface where it reacts with adsorbed oxygen.¹⁸ Surface equilibration by such processes provides a reasonable hypothesis for the apparent ability of our activation procedure (16 hr at 400°) to give reproducible surface activity. Present results are, however, insufficient to reject the alternative hypothesis that such activation thermally removed surface oxygen and so produced surface layers with an equilibrium concentration of donors.

Each N_2O dissociated upon the equilibrated surface according to Ia, Ib, and Ic contributes a unit negative charge to the surface layer. Since the maximum accumulated negative charge at the surface is limited in accordance with boundary layer theory, the amount of N_2O dissociation (V_N) attainable on a ZnO surface should be decreased by prior chemisorption of another gas which also localized electrons at the surface. Oxygen is reported to chemisorb onto ZnO as O_2^- or O^- with the proportion of O^- increasing with temperature.^{4,5}

Our observations that prior treatment of the ZnO surface with oxygen at room temperature decreased the attainable N_2O dissociation and the conductivity were thus fully consistent with oxygen-induced formation of a negatively charged surface layer of O_2^- or O^- .

Furthermore, they led to the prediction that if a ZnO surface were first "titrated" with known quantities of oxygen and then exposed to nitrous oxide, an "end-point" corresponding to accumulation of the maximum permissible number of O_2^- or O^- ions at the surface, would be indicated by failure of the oxygen-treated surface to promote any dissociation of N_2O . The results of such "titration" experiments are shown in Table II for ZnO powder which was reactivated at 350° before each new addition of oxygen. Chemisorption of these quantities of oxygen on the activated ZnO surfaces at room temperature was effectively completed in less than the 10 sec response time of the pressure-measuring system. Formation of noncondensable product when known amounts of N_2O were subsequently added (column 2) was not completed so rapidly but after 2 hr contact time product was >90% of that

(27) W. Roberts, *Quart. Rev. Chem. Soc.*, **16**, 71 (1962).

(28) A. Fromhold, *Nature*, **200**, 1309 (1963).

(29) V. O. Nwoko and H. H. Uhlig, *J. Electrochem. Soc.*, **112**, 1181 (1965).

(30) I. M. Ritchie and G. L. Hunt, *Surface Sci.*, **15**, 524 (1969).

(31) D. J. M. Bevan, J. P. Shelton, and J. S. Anderson, *J. Chem. Soc.*, 1729 (1948).

(32) E. Segal and M. Teodorescu, *Rev. Roum. Chim.*, **12**, 75 (1967).

obtained in 24 hr contact and these are the values listed in column 3. Entries in the first two rows establish that the activated surface was capable of dissociating $9 \pm 1 \mu\text{l}$ of N_2O . Subsequent rows show that $11 \mu\text{l}$ or more of O_2 was needed to cause a 90% reduction in ability of the surface to dissociate N_2O . This "end point" is much closer to the value of $9 \mu\text{l}$ expected if each O_2 , like each N_2O , contributed to localizing one electron, than to the value of $4 \mu\text{l}$ which would result if each O_2 chemisorbed as two O^- ions. It is thus in agreement with recent views that at low temperatures and pressures oxygen chemisorbs onto ZnO mainly as O_2^- and O_2 .⁵ The electron affinity of O_2 (0.5 eV) is greater than that of N_2O (ca. 0.1 eV) and electrons localized as O_2^- are therefore not "available" for rapid reaction with N_2O molecules subsequently admitted.

Table II: Effect of Preadsorbed Oxygen in Reducing the Ability of a ZnO Surface (56.8 m^2) to Dissociate N_2O at 20°

Amt of oxygen preadsorbed μl at STP	amt of N_2O added, μl at STP	amt of "fast" product, μl at STP	% N_2O dissociated
0	13.2	8.8	66
0	13.2	9.2	70
3.4	13.2	5.9	45
6.8	16.0	4.0	25
11.0	17.5	0.95	5
14.0	16.0	0.33	2

At elevated temperatures, the chemisorption of H_2 on ZnO introduces donors, increasing n_D .³³ The ionization of these donors provides the electrons to account for the increased conductivity²⁰ and the greater dissociation of N_2O .

Conclusions

The results with various zinc oxides indicate that extent of N_2O dissociation can be used as a chemical method for indicating the relative availability of electrons at the surfaces of these powdered materials. The kinetics of N_2O dissociation over ZnO and Fe_2O_3 , and their similarity to kinetics of conductivity changes produced in films of ZnO and Fe_2O_3 by N_2O , identify electron localization at the surface as the rate-determining step for N_2O dissociation over these semiconductors.

Electron localization at the surface was not rate determining in deposits made by evaporating zinc metal in a moderate vacuum of ca. 10^{-4} Torr. Rates of N_2O dissociation over these deposits were first order in N_2O at low pressures. Nitrous oxide would therefore seem to deserve wider consideration as a reagent for the study of metal oxidations at low temperatures. No large activation energy is needed (as for $\text{O}_2 \rightarrow 2\text{O}$ dissociation) and the course of reaction is easily followed even at high N_2O pressures by measuring the noncondensable product.

(33) A. R. Hutson, *Phys. Rev.*, **108**, 222 (1957).

Stokes' Principle of Reversion and the Optical Measurement of Soap Film Thickness

by J. B. Rijnbout

Van 't Hoff Laboratory, Sterrenbos 19, Utrecht, The Netherlands (Received November 10, 1969)

A general equation is derived for the reflection of light by a soap film as a function of its thickness, without assuming any model for the surface layers. It is also shown how the thickness of the aqueous core of the film may be obtained from experimental data. The results agree with Corkill's infrared absorption measurements.

Introduction

The intensity of monochromatic light reflected by a soap film (as found in soap bubbles) is often used to calculate its thickness. The connection between the coefficient for the reflected intensity, R^2 , and the thickness, d , is given by Airy's formula¹

$$R^2 = \frac{4r^2 \sin^2 \beta}{(1 - r^2)^2 + 4r^2 \sin^2 \beta} \quad (1)$$

where r^2 is the coefficient for the intensity reflected by a single surface and $\beta = kd \cos \theta$ with k the wave number ($2\pi n/\lambda$) within the film and θ the angle of refraction in the film. This equation applies to a plane-parallel homogeneous layer.

We know, however, that a soap film is in fact not homogeneous but that its surfaces are covered with a layer of soap molecules. To take this into account, Duyvis,² Lyklema, Scholten, and Mysels,³ and Frankel and Mysels⁴ considered a film consisting of three homogeneous layers, *i.e.*, two soap layers and an aqueous core. An interesting result of their calculations is that the difference between the thickness so calculated and that calculated from eq 1 is independent of the core thickness.

In order to check if this is valid for any model of the surface layer, a more general derivation would be desirable. In searching for such a proof I found that in principle it was given already by Stokes in his 1849 paper⁵ on the perfect blackness of the central spot in Newton's rings.

I propose to give this derivation in modified and extended form and to apply the resulting equation to some model systems.

General Formulation of Reflection and Transmission at an Interface

Consider the interface between two media, called 1 and 3. Let the nonabsorbing transition layer from medium 1 to medium 3 be included between two mathematical planes situated in the homogeneous parts of 1 and 3 (see Figure 1). If a light beam of unit ampli-

tude, polarized either parallel or perpendicular to the plane of incidence, is incident on O, the reflected amplitude may be written as

$$r = |r| \exp(-i\rho) \quad (2)$$

where ρ is the phase change on reflection and $i = \sqrt{-1}$, and the transmitted amplitude is likewise given by

$$t = |t| \exp(-i\tau) \quad (3)$$

The phase change ρ refers to O, the point where the incident beam meets the first boundary plane, and τ refers to O', the point opposite to O on the other boundary plane; this convention about the phase reference points applies throughout this paper. For a beam which is incident from medium 3 and makes the same angle with the normal as the transmitted beam of Figure 1, the reflection and transmission coefficients are called r' and t' .

Now according to Stokes, in the absence of absorption the time may be reversed in Figure 1 without effect on the amplitudes. So in a thought experiment all arrows may be reversed and r and t replaced by their complex conjugates r^* and t^* , as the amplitude which is leading in phase when time goes forward, becomes the lagging one when time goes backward. (Compare Figure 1 with Figure 2A.)

But the situation of Figure 2A can also be obtained by superposition of the separate beams r^* and t^* and their respective reflected and transmitted beams (Figures 2B and 2C). In mathematical form

$$r^*r + t^*t' = 1 \quad (4)$$

$$r^*t + t^*r' = 0 \quad (5)$$

(1) See, for instance, M. Born and E. Wolf, "Principles of Optics," Pergamon Press, London, 1959, p 324.

(2) E. M. Duyvis, "The Equilibrium Thickness of Free Liquid Films," Thesis, Utrecht, 1962.

(3) J. Lyklema, P. C. Scholten, and K. J. Mysels, *J. Phys. Chem.* **69**, 116 (1965).

(4) S. P. Frankel and K. J. Mysels, *J. Appl. Phys.*, **37**, 3725 (1966).

(5) G. G. Stokes, "Mathematical and Physical Papers," Vol. II, Cambridge University Press, 1883, p 89.

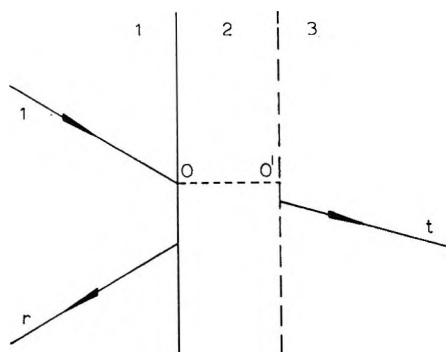


Figure 1. Reflection and transmission at an interface: *i*, incident beam; *r* reflected beam; *t*, transmitted beam; *0*, phase reference point for medium 1; *0'*, phase reference point for medium 3.

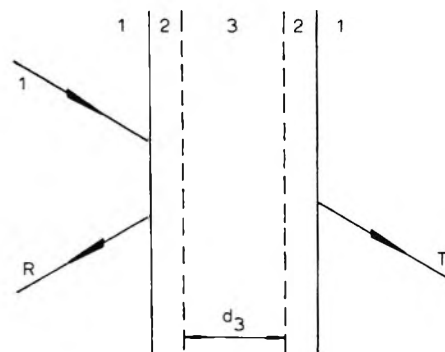


Figure 3. Reflection and transmission by a film: 1, external medium; 2, surface layer; 3, core.

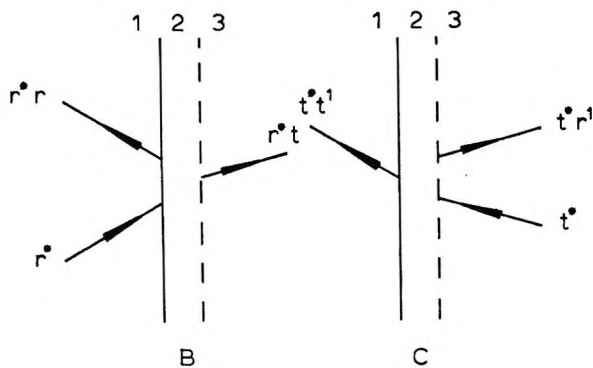
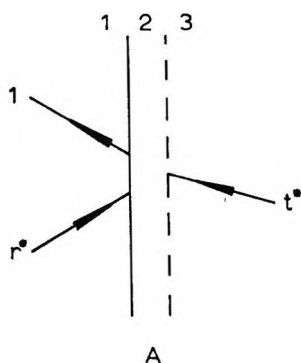


Figure 2. A, the beams of Figure 1 after time inversion; B, C, the separate contributions of r^* and t^* to the beams of Figure 2A.

These equations give

$$r' = \frac{-r^*t}{t^*}; \quad t' = \frac{1 - r^*r}{t^*} \quad (6)$$

We find r and t in terms of r' and t' by starting with a primary beam incident from the other side or by solving eq 4 and 5 for r and t (via r^* and t^*). In the latter case we notice that from eq 4 t^*t' is real, thus $t^*t' = tt'^*$ or $t/t^* = t'/t'^*$ meaning that the phase shift on transmission is the same in both directions, and that by multiplying the first eq 6 by its complex conjugate we obtain the result $r'r'^* = rr^*$ meaning that the in-

tensity reflection coefficient is the same in both directions. So we find

$$r = \frac{-r'^*t'}{t'^*}; \quad t = \frac{1 - r'^*r'}{t'^*} \quad (7)$$

These general relations are valid for a layer of arbitrary thickness and refractive index profile and may now be used in the calculation of film reflectivity.

General Formulation of Reflection by a Film

We consider a soap film, consisting of an optically homogeneous central layer of thickness d_3 with two identical surface layers (Figure 3). By summation of amplitudes⁶ we find for the amplitude reflection coefficient of the film

$$R = r + \frac{tr't' \exp(-2i\beta_3)}{1 - (r')^2 \exp(-2i\beta_3)} \quad (8)$$

where $\beta_3 = k_3 d_3 \cos \theta_3$ with k_3 = wave number in the central layer, d_3 = thickness of the central layer, and θ_3 = angle of refraction in the central layer.

Converting in this equation r and t to r' and t' by eq 7, remembering that from eq 6 r'^*r' equals r^*r and defining ρ' by

$$r' = |r'| \exp(-i\rho') \quad (9)$$

we find for the reflected intensity, multiplying R by its complex conjugate

$$RR^* = \frac{4rr^* \sin^2(\beta_3 + \rho')}{(1 - rr^*)^2 + 4rr^* \sin^2(\beta_3 + \rho')} \quad (10)$$

This conforms to eq 1, with β replaced by $\beta_3 + \rho'$. Again rr^* is the intensity reflection coefficient of a single surface which may be measured separately or obtained from the maximum value of RR^* which equals $4rr^*/(1 + rr^*)^2$.

From the argument of the sine in eq 1 one obtains a film thickness $d = \beta/k \cos \theta$. If one uses the bulk refractive index n_3 for the calculation of $k \cos \theta$ this thickness is the so-called equivalent water thickness

(6) See, for instance, ref 1, p 323.

d_w of the film. So we have for a film with known reflectivity, equating the right-hand members of eq 1 and 10

$$k_3 d_w \cos \theta_3 = \beta_3 + \rho' \pm m_1 \pi$$

$$d_w = d_3 + \frac{\rho' \pm m_1 \pi}{k_3 \cos \theta_3} \quad (11)$$

where m_1 is an as yet unknown whole number. Since ρ' is independent of d_3 , we find indeed a constant difference between d_3 and d_w . The magnitude of this difference, however, can only be calculated by the introduction of a model for the surface layer.

Application to Films with Thin Homogeneous Surface Layers. We take first the model of a thin homogeneous surface layer 2, between an external medium 1 and a central layer 3. The phase shift ρ' for reflection from the inside against such a layer is given by⁷

$$\tan \rho' = \frac{r_{21}(1 - r_{32}^2) \sin(2k_2 d_2 \cos \theta_2)}{r_{32}(1 + r_{21}^2) + r_{21}(1 + r_{32}^2) \cos(2k_2 d_2 \cos \theta_2)} \quad (12)$$

where r_{ij} is the amplitude reflection coefficient for light going from medium i to medium j . As we are interested in surface layers having a thickness small compared to the wavelength of light, we expand eq 12 up to the first power of $k_2 d_2$ putting the tangent and the sine equal to their arguments and the cosine equal to one. Furthermore, in order to calculate r_{ij} we now have to make a choice with respect to the state of polarization of the incident light. We limit the treatment to the situation more commonly encountered in practical measurements because any other choice disturbs the simplicity of the resulting equations, and substitute the Fresnel expressions for light polarized with its electric vector perpendicular to the plane of incidence

$$r_{ij} = \frac{n_i \cos \theta_i - n_j \cos \theta_j}{n_i \cos \theta_i + n_j \cos \theta_j} \quad (13)$$

where n_i is the refractive index of medium i . Then we find

$$\rho' = 2d_2 \frac{n_2^2 - n_1^2}{n_3^2 - n_1^2} k_3 \cos \theta_3 \pm m_2 \pi \quad (14)$$

where m_2 is a whole number, and substituting this in eq 11

$$d_w = d_3 + 2d_2 \frac{n_2^2 - n_1^2}{n_3^2 - n_1^2} \quad (15)$$

In order that $d_w - d_3$ goes to zero with d_2 , m_1 , and m_2 must satisfy the condition $m_1 + m_2 = 0$. If for a homogeneous film ($d_2 = 0$, $d_w = d_3$) we have $\rho' = 0$, then $m_2 = 0$ (eq 14) and $m_1 = 0$ (eq 11). So for a thin homogeneous surface layer and perpendicular polarization of the light, the difference between the core thickness and the equivalent water thickness of

the film is the same for all angles of incidence and has the form given by Duyvis² and by Frankel and Mysels⁴ for normal incidence.

Extension to Films with Heterogeneous Surface Layers. Equation 15 can be written as

$$(n_3^2 - n_1^2)d_w = \sum (n_i^2 - n_1^2)d_i \quad (16)$$

where the summation extends over all layers. The form of this equation suggests that it will apply to any number of layers, which can indeed be proved by evaluating ρ' from the characteristic matrix⁸ of a multilayer surface, again assuming that the thickness of this compound surface layer is small with respect to the wavelength of the light used. Frankel and Mysels obtained the same result in another way, restricted to the case of normal incidence.

To make further use of eq 16 we need pairs of values for n_i and d_i which are generally unknown and difficult to estimate. In the simplest and practically most important case the external medium is air with $n_1 = 1$. In that case we need values of $n_i^2 - 1$ which may be obtained from the specific refraction A_i of the substance of layer i as defined in the Lorentz-Lorenz equation

$$\frac{n_i^2 - 1}{n_i^2 + 2} = A_i \rho_i \quad (17)$$

where ρ_i is the density of the i th layer. (The applicability of this equation to thin layers instead of homogeneous bulk material may be doubted, but it probably is not far from the truth and a better approximation is not available.)

We substitute $n_i^2 - 1$ from eq 17 into eq 16 and for $\rho_i d_i$ we write m_i , the mass of layer i per cm² of surface area. Then we obtain

$$d_3 = d_w - \frac{1}{n_3^2 - 1} \sum' (n_i^2 + 2) A_i m_i \quad (18)$$

where the prime indicates that the central layer is excluded from the summation.

As a reasonably accurate value of $n^2 + 2$ can be obtained from a carefully estimated value of n , the second term in eq 18 may now be evaluated when the composition of the surface layer is known, without need for an accurate knowledge of its thickness and refractive index.

Comparison with Absorption Measurements

To determine the water content of very thin soap films, Corkill, *et al.*,⁹ measured their infrared absorption at 2.93 μ m, a method which avoids the difficulties due to the presence of surface layers, but which is subject to uncertainty as to the value of the molar extinction coef-

(7) See ref 1, p 61.

(8) See ref 1, p 54.

(9) J. M. Corkill, J. F. Goodman, and C. P. Odgen, *Trans. Faraday Soc.*, **61**, 583 (1965).

ficient of water in these thin layers. The reflectances and the amount of soap per cm² of surface area of these films of decyltrimethylammonium decyl sulfate (C₁₀C₁₀) are known so we can also apply our method to them and compare the results.

From tracer measurements and surface tension *vs.* concentration curves Corkill, *et al.*,¹⁰ found that the surface concentration in these films corresponds to one molecule of C₁₀C₁₀ per (58 ± 3) Å², which means a mass m_i of (1.25 ± 0.06)10⁻⁷ g/cm².

Now we need an estimate of the refractive index of the surface layer to calculate $n_i^2 + 2$. We may think of this layer as consisting of a paraffinic part containing the hydrocarbon chains and a part containing the ionized groups in an aqueous environment. The refractive index of the hydrocarbon part will be lower than that of bulk decane which equals 1.41 at a density of 0.73. The lowest possible density of the hydrocarbon layer is obtained if the 14.5 Å long decyl chains are extended perpendicularly to the surface. This would give a density of 0.56 and a refractive index of 1.31. The aqueous part containing the ionized groups will have a refractive index larger than 1.33 but presumably not larger than that of a 40% ammonium sulfate solution (containing about four water molecules per ion) which equals 1.39. So it does not seem necessary to differentiate between the paraffinic layer and the layer of head groups and it is reasonable to assume that the refractive index of the surface layer is between 1.31 and 1.41 and $n^2 + 2 = 3.85 ± 0.14$. Here we consider the head groups as components of the surface layer whereas the water which is present in the layer of head groups is excluded from the surface. This is possible because the components in a layer contribute additively to the specific refraction of the mixture, and so may be thought of as contributing additively to $n^2 - 1$ (eq 17), whereas $n^2 + 2$ is determined by the refractive index of the mixture as a whole. If we want to exclude a component from the surface layer, we should exclude its contribution to $n^2 - 1$, but not that to $n^2 + 2$. This is in accordance with the meaning of these factors: $n^2 - 1$ is built up additively from the polarizabilities of the molecules and $(n^2 + 2)/3$ is the Lorentz correction factor for the internal field, which depends on the average polarizability of the surroundings of a molecule.

Further, we need the specific refraction of C₁₀C₁₀. As we do not have data on the density and refractive index of C₁₀C₁₀ solutions we have to derive its specific refraction from data on related compounds. The molar refraction of C₁₀C₁₀ which equals its specific refraction times its molecular weight is obtained by adding the molar refraction of C₁₂H₂₅OSO₃Na (sodium dodecyl sulfate) to that of C₁₂H₂₅(CH₃)₃NBr (dodecyltrimethylammonium bromide) and subtracting four times the molar refraction of a CH₂ group and that of aqueous NaBr.

To calculate the specific refraction of a solute we

write the Lorentz-Lorenz equation for a two-component system

$$(n^2 - 1)/(n^2 + 2) = A_0g_0 + A_1g_1 \quad (19)$$

where A_0 and A_1 are the specific refractions of solvent and solute and g_0 and g_1 their masses per unit volume of solution.

By differentiation we obtain

$$A_1 = \frac{6n}{(n^2 + 2)^2} \frac{dn}{dg_1} + A_0 \left(1 - \frac{d\rho}{dg_1}\right) \quad (20)$$

when the solution density ρ equals $g_0 + g_1$. For micellar solutions of sodium dodecyl sulfate, $dn/dg_1 = 0.1257$ cm³/g¹¹ and $d\rho/dg_1 = 0.111$.¹²

For dodecyltrimethylammonium bromide, $dn/dg_1 = 0.1542$ cm³/g¹¹ and $d\rho/dg_1 = 0.046$.¹³ This gives for sodium dodecyl sulfate $A = 0.2539$ cm³/g and a molar refraction of 69.2 cm³ and for dodecyltrimethylammonium bromide $A = 0.2833$ cm³/g and a molar refraction of 87.4 cm³. The molar refraction of a CH₂ group is 5.17 cm³ and for aqueous NaBr it is given as 12.8 in Landolt-Börnstein.¹⁴ So the molar refraction of C₁₀C₁₀ becomes 69.2 + 87.4 - 20.7 - 12.8 = 123.1 cm³ and $A = 0.2812$ cm³/g.

If we put these values of A , m , and $n^2 + 2$ into eq 18 and take for n_3 the refractive index of a 0.5 M NaBr solution as used by Corkill, which equals 1.342, we get

$$d_3 = d_w - (33.8 ± 3.5) \text{ \AA} \quad (21)$$

We obtain d_w from the reflectance of the film. For the films used in their absorption measurements, Corkill, *et al.*,⁹ give the ratio of the reflection intensity of the film to that of the last bright band. From eq 1, substituting $\beta = k_3d_w$ for normal incidence and approximating $\sin \beta = \beta$ for these thin films we obtain

$$d_w = \frac{1}{k_3} \left(\frac{1 - r^2}{1 + r^2} \right) \sqrt{\frac{R^2}{R_{\text{max}}^2}} \quad (22)$$

In the calculation of k_3 we use $n_3 = 1.342$ and $\lambda_0 = 5461$ Å, r^2 is calculated from the Fresnel expression (eq 13) with $n = 1.342$ as it is hardly modified by the presence of a very thin surface layer; this gives $r^2 = 0.021$. The values of d_w and d_3 thus obtained are given in Table I. The maximum error of 5 Å in d_3 is composed of a variable error of at most 1.5 Å in d_w and a constant error of at most 3.5 Å in the second term of eq 21.

(10) J. M. Corkill, J. F. Goodman, C. P. Odgen, and J. R. Tate, *Proc. Roy. Soc.*, **A273**, 84 (1963).

(11) H. V. Tartar and A. L. M. Lelong, *J. Phys. Chem.*, **59**, 1185 (1955).

(12) K. A. Wright and H. V. Tartar, *J. Amer. Chem. Soc.*, **61**, 544 (1939).

(13) A. B. Scott and H. V. Tartar, *ibid.*, **65**, 692 (1943).

(14) Landolt-Börnstein, "Physikalisch-Chemische Tabellen," 5. Aufl. Eg IIIb, Julius Springer, Berlin, 1935, p 1701.

These values for d_3 may be compared with those given in the last column, which were derived from infrared absorption at $2.93 \mu\text{m}$ as reported by Corkill, *et al.*⁹ As a $0.5 M$ NaBr solution contains about 50 g of NaBr and 990 g of $\text{H}_2\text{O}/\text{l.}$, their values of the thickness were multiplied by 1.01 to obtain the equivalent thickness of a $0.5 M$ NaBr solution. All values of d_3 from eq 21 are seen to be higher than the corresponding values

Then these quantities will be related by an equation of the form: $A \times d_3(\text{ir}) = d_3(\text{eq 21}) + B$. Assuming that $d_3(\text{ir})$ and d_3 (eq 21) are of about equal precision we find by the usual methods of least squares

$$(1.01 \pm 0.03)d_3(\text{ir}) = d_3(\text{eq 21}) - (2.6 \pm 0.9) \text{ \AA} \quad (23)$$

The standard deviation from this straight line amounts to 1.0 \AA for one observation.

Due to the fact that the values reported for R^2/R_{max}^2 are grouped in classes with a half-width corresponding to about 1.5 \AA we expect a standard deviation of $1.5/\sqrt{3} = 0.87 \text{ \AA}$ already from this source only, so there is no reason to look for a better fit. That A is not greatly different from unity indicates that the molar extinction coefficient at $2.93 \mu\text{m}$ of water in these films is close to 133, the value used by Corkill, *et al.*⁹ The agreement between the two sets of core thicknesses may be improved by changing the second term at the right-hand side of eq 21 to -36.4 \AA which is still within the range of expectations, and suggests that the surface concentration and refractive index could be a few per cent higher than we assumed.

As the sets of values in the last two columns of the table represent completely independent estimates of the water core thickness, their agreement may be considered very satisfactory.

Acknowledgment. Thanks are due to Professor J. Th. G. Overbeek and Professor A. Vrij, whose interest stimulated this publication and who contributed to its final form by many helpful suggestions.

Table I: Comparison of Core Thicknesses Obtained from Reflectivity and from Infrared Absorption

$10^4 \frac{R^2}{R_{\text{max}}^2}$	Number obsd	d_w , eq 22, Å	d_3 , eq 21, Å	d_3 , ir, Å
85	1	57.3	23.5	22.2
95	6	60.5	26.7	24.3
105	11	63.6	29.8	27.1
115	4	66.6	32.8	29.9
125	6	69.4	35.6	32.7
135	2	72.2	38.4	34.3
145	2	74.8	41.0	35.6
155	3	77.3	43.5	39.7
165	1	79.7	45.9	44.4
175	2	82.2	48.4	48.0
± 5		± 1.5	± 5.0	

of d_3 from infrared absorption. Systematic differences between the two may be caused on one side by an incorrect second term in eq 21 which leads to a constant absolute error in d_3 (eq 21) and on the other side by an incorrect molar extinction coefficient of water which leads to a constant relative error in d_3 (ir).

Electrokinetic Flow in Fine Capillary Channels¹

by Douglas Hildreth

Department of Mechanical Engineering, Polytechnic Institute of Brooklyn, Brooklyn, New York 11201
(Received November 26, 1969)

A study is made of electroosmotic flow and streaming potential generation in fine capillary slits, taking into account the presence of a distributed conductance across the capillary channel and the effect of the differences in the ionic mobilities of the co-ions and counterions. A comparison of the theoretical results obtained in the present analysis, with experimental data obtained by previous investigators, shows good agreement. The apparent increase in viscosity that is observed in experiments with fine capillaries, is shown to be a natural flow retardation that is obtained from equilibrium-continuum considerations in ultrafine capillary systems. The analysis indicates the possibility of obtaining large flow retardations in capillary systems with small electrokinetic radii. As a consequence, high efficiencies are obtainable for electroosmotic pumping and for streaming potential generation. The results are presented graphically in a form that permits their direct application for the evaluation or the design of electrokinetic systems.

Introduction

The problem of electrokinetic flow through fine capillaries has been studied by a number of authors in recent years. Burgreen and Nakache^{2a} investigated electrokinetic flow in capillary slits and obtained results that predicted high flow retardation and high efficiencies in capillary systems having small electrokinetic radii (ratio of width of capillary slit to Debye length). Morrison and Osterle^{2b} investigated electroosmotic flow and streaming potential generation in ultrafine capillary channels of circular cross section. Dresner³ analyzed electrokinetic flow in fine capillary tubes but restricted his analysis to systems with electrokinetic radii sufficiently small to preclude the presence of co-ions. He calculated high flow retardations for fluids pumped through ultrafine capillaries; his results are in good agreement with the experimental data of Henniker.⁴

While these studies represent important contributions to electrokinetics, each of the analyses contains certain restrictions which limit the usefulness of the results. The article by Burgreen and Nakache^{2a} assumes a lumped or mean conductivity, thereby avoiding some of the analytical difficulties of a distributed conductivity, but leaves open to question the error that such an approximation introduces. Morrison and Osterle^{2b} include in their analysis the distributed conductivity, but do not obtain solutions in a closed form. They make the simplifying assumption that the electrochemical ionic mobilities of each of the dissociated ions is the same (which is often not the case). Dresner³ introduces the approximation of complete co-ion exclusion, which simplifies the analysis but limits the generality of the solution.

In the present paper these restrictions are removed and a more general analysis of electrokinetic flow in slits is developed, with particular emphasis on electrokinetic flow in ultrafine capillary elements. Linear

coupled equations describing the mass and electrical current transport as a function of voltage differences and pressure forces, are derived. The terminology and the nondimensional parameters defined by Burgreen and Nakache^{2a} are utilized in the present study, and in addition, two new parameters are defined which account for the variation of conductivity across the capillary channel and the differences in the ionic mobilities.

The lateral variation of local charge in the capillary channel is obtained from the Boltzmann distribution which relates the charge density to the local potential; and the Poisson equation, which defines the spatial potential variation in terms of the charge density in which body forces proportional to the electric field are present, is coupled with electric charge transport equations to obtain a solution yielding the volumetric flow rate and the flow of electrical current. The net electric current flow is obtained by the superposition of charges moving with the fluid and the charges moving relative to the fluid, *via* electrolytic conduction.

An expression is then derived for the surface conductance of capillaries with a moderate or a large electrokinetic radius. The generated streaming potential and the associated flow retardation is shown to be strongly dependent upon the differences in ionic mobilities of the constituents, as well as upon the other well-known parameters of electrokinetic flow. Finally, a comparison is made of the analytical results that are obtained with experimental data that are available.

(1) This work was supported by a grant from the National Science Foundation.

(2) (a) D. Burgreen and F. Nakache, *J. Phys. Chem.*, **68**, 1084 (1964); (b) F. A. Morrison, Jr., and J. F. Osterle, *J. Chem. Phys.*, **43**, 2111 (1965).

(3) L. Dresner, *J. Phys. Chem.*, **67**, 1635 (1963).

(4) J. C. Henniker, *J. Colloid Sci.*, **7**, 443 (1952).

Nomenclature

b_+	Mobility of the positive ion
b_-	Mobility of the negative ion
B	$M^2\mu\omega^2/K_0$
D	Dielectric constant of the fluid
e	Electron charge
$E(\theta, t)$	Elliptic integral of the second kind
$F(\theta, t)$	Elliptic integral of the first kind
h	Half-channel separation
I	Total electrical current
$I(\eta)$	Local electrical current
$I_+(\eta)$	Local current of positive ions
$I_-(\eta)$	Local current of negative ions
k	Boltzmann constant
K	System conductivity
K_0	Specific conductivity of the fluid
K_s	Surface conductance
M	Electrokinetic mobility
\bar{n}	Average number of positive or negative ions per unit volume
\bar{n}_i	Average number of ions of the i th kind per unit volume
n_i	Number of ions of the i th kind per unit volume
P	Pressure
T	Absolute temperature
u	Local fluid velocity
V	Volumetric flow rate
x	Axial coordinate
Y	Axial electric field
Y_0	Streaming potential field
Y_e	Applied axial electric field
z	Number of charges on an ion when both ions present carry the same number of charges
z_i	Number of charges on anion of the i th type
α	Ratio of surface ionic to thermal energy = $\frac{ez\psi_0}{KT}$
γ	Ratio of the difference in ionic mobilities to the sum = $\frac{b_- - b_+}{b_+ + b_-}$
η	Lateral coordinate
μ	Fluid viscosity
μ_a	Apparent fluid viscosity
ρ	Local charge density
ψ	Local potential
ψ_0	Surface ionic potential
ψ_c	Potential at the center of the channel
ω	Inverse Debye length
Ω	Electrokinetic radius = $2\omega h$

Distribution of Potential and Charge

At a solid-liquid interface, an electrical potential is observed to exist between the fluid close to the surface and the bulk of uncharged fluid at some distance from it. The mechanism by which this potential is generated is not clearly understood. However, it is generally attributed to a preferential surface adsorption of ions. In order to simplify the analysis of electrokinetic flow in capillaries, consideration of surface phenomena will be minimized by assuming that the surface ionic potential, ψ_0 , is the potential of the fluid at some small distance from the wall.⁵ At this distance from the wall, which is of the order of molecular dimensions, the fluid is assumed to be stationary.

The surface ionic potential is taken to be a fundamental quantity dependent upon the particular fluid

and the capillary wall with which it is in contact. Since mass and charge transport normal to capillary wall is prevented, the lateral equilibrium of forces due to the distributed charge and osmotic pressure produces a Boltzmann distribution of ionic concentration expressed as

$$n_i = \bar{n}_i e^{-ez_i\psi/kT}$$

For a completely dissociated solute containing ions of two types with charges $z_+ = -z_- = z$ and ionic concentration densities $\bar{n}_+ = \bar{n}_- = n$, the concentration of each ion above a potential ψ is

$$\begin{aligned} n_+ &= \bar{n} e^{-ez\psi/kT} \\ n_- &= \bar{n} e^{ez\psi/kT} \end{aligned} \quad (1)$$

The local charge density, ρ , is the excess of positive over negative charge, or

$$\rho = ez(n_+ - n_-) = -2\bar{n}ez \sinh \frac{\alpha\psi}{\psi_0} \quad (2)$$

In the foregoing equation α is the ratio of surface ionic energy to thermal energy, namely $\alpha = ez\psi_0/kT$. The Poisson equation in the lateral dimension η , relates the spatial charge and potential distribution. It is

$$\frac{d^2\psi}{d\eta^2} = \frac{-4\pi}{D} \rho \quad (3)$$

with D equal to the dielectric constant of the fluid. Combining the foregoing eq 2, and using the inverse Debye length ω , defined as

$$\omega = \sqrt{\frac{8\pi\bar{n}ez\alpha}{D\psi_0}}$$

one obtains

$$\frac{d^2\left(\frac{\alpha\psi}{\psi_0}\right)}{d(\omega\eta)^2} = \sinh \frac{\alpha\psi}{\psi_0}$$

The integration of this equation subject to the boundary conditions

$$\frac{d\psi}{d\eta} = 0; \quad \psi = \psi_c \text{ at } \eta = 0$$

(wherein the subscript c denotes the center of the channel ($\eta = 0$)) gives⁶

$$d(\omega\eta) = \frac{d\left(\frac{\alpha\psi}{\psi_0}\right)}{\left(\cosh^2 \frac{\alpha\psi}{2\psi_0} - \cosh^2 \frac{\alpha\psi_c}{2\psi_0}\right)^{1/2}} \quad (4)$$

(5) A. J. Rutgers, "Physical Chemistry," Interscience Publishers, New York, N. Y., 1954.

(6) I. S. Gradshteyn and I. M. Ryzhik, "Table of Integrals, Series and Products," Academic Press, New York, N. Y., 1965.

The integration of eq 4 yields $\omega\eta$, as

$$\omega\eta = F(\theta_\eta, t) / \cosh \frac{\alpha\psi_c}{2\psi_0} \quad (5)$$

where $F(\theta_\eta, t)$ is the elliptic integral of the first kind

$$\theta_\eta = \sin^{-1} \left[\frac{\left(\cosh^2 \frac{\alpha\psi}{2\psi_0} - \cosh^2 \frac{\alpha\psi_c}{2\psi_0} \right)^{1/2}}{\sinh \frac{\alpha\psi}{2\psi_0}} \right]$$

and

$$t = \left(\cosh \frac{\alpha\psi_c}{2\psi_0} \right)^{-1}$$

Equation 5 relates the local potential ψ , to the distance from the center of the slit, η . When the integration is carried out to the capillary wall, the result is

$$\frac{\Omega}{2} = \omega h = F(\theta_h, t) / \cosh \frac{\alpha\psi_c}{2\psi_0} \quad (6)$$

The foregoing expression defines the center potential, ψ_c , in terms of the fluid properties, capillary radius, and the surface ionic potential, ψ_0 . Ω is the electrokinetic radius defined^{2a} as twice the product of the channel area and the inverse Debye length, divided by the wetted perimeter, *i.e.*, the ratio of hydrodynamic radius to Debye length. In the case of axial laminar flow, the above equations are valid, since the lateral charge distribution is not disturbed. The variation of the ratio of center ionic potential to surface ionic potential with electrokinetic radius is plotted in Figure 1 for several values of α . Note that for an electrokinetic radius greater than 10, the potential at the center of the channel is essentially zero; that is, it is at a level ψ_0 below the potential at the surface. This approximation is useful as it permits a simplified expression for the flow when the electrokinetic radius is large.

Mass Transport

For incompressible steady-state electrokinetic flow, the one-dimensional Navier-Stokes equation, with an electrical body force term, applies. It is, as given in ref 1

$$\mu \frac{d^2 u}{d\eta^2} - \frac{dP}{dx} - \rho Y = 0$$

with Y the constant axial electric field equal to dE/dx . The velocity u is expressed as the sum of a pressure-induced velocity and an electrically induced velocity, or $u = u_p + u_e$. We have, with the use of eq 3

$$\frac{d^2 u_e}{d\eta^2} = \frac{-DY}{4\pi\mu} \frac{d^2 \psi}{d\eta^2}$$

$$\frac{d^2 u_p}{d\eta^2} = \frac{1}{\mu} \frac{dP}{dx}$$

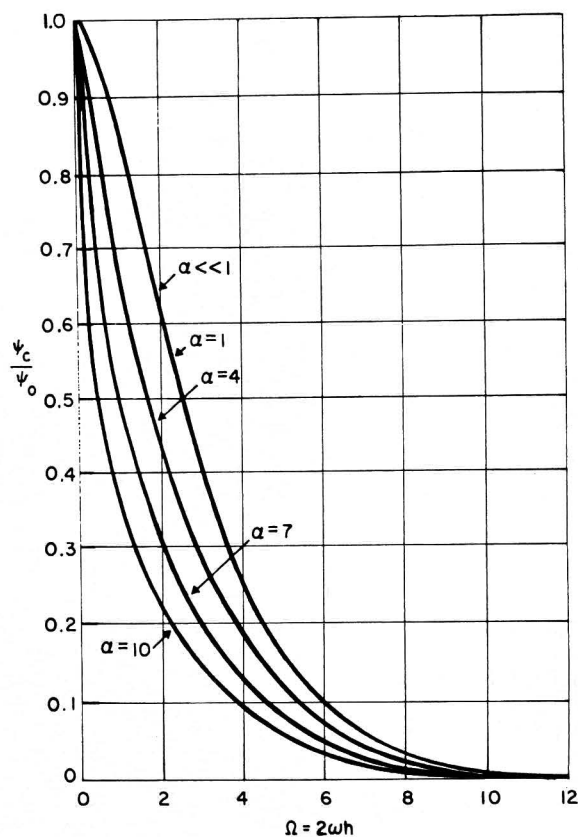


Figure 1. Variation of ψ_c/ψ_0 with electrokinetic radius.

The applicable boundary conditions are

$$\frac{du_p}{d\eta} = \frac{du_e}{d\eta} = \frac{d\psi}{d\eta} = 0 \text{ at } \eta = 0$$

and

$$u_p = u_e = 0 \text{ at } \eta = h$$

The electroosmotic and mechanically generated flows, obtained by the integration of the above equations, are, respectively

$$u_e = MY \left(1 - \frac{\psi_0}{\psi} \right) \quad (7)$$

and

$$u_p = \frac{1}{2\mu} (\eta^2 - h^2) \frac{dP}{dx} \quad (8)$$

The quantity M in eq 7 is the electrokinetic mobility, defined as

$$M = \frac{D\psi_0}{4\pi\mu}$$

The net velocity is the sum of the pressure-induced flow and the electrically generated flow, or

$$u = \frac{1}{2\mu} (\eta^2 - h^2) \frac{dP}{dx} + MY \left(1 - \frac{\psi_0}{\psi} \right)$$

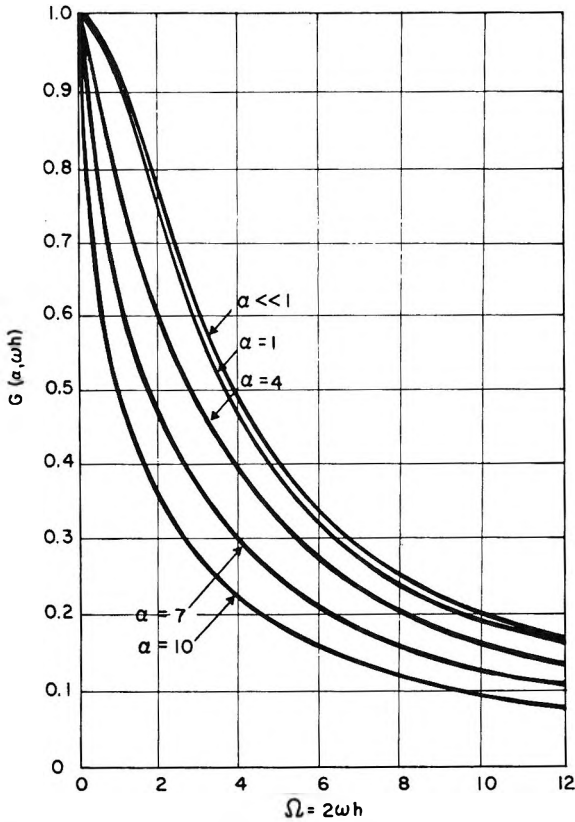


Figure 2. Variation of G with electrokinetic radius, Ω .

The mean velocity V is obtained through integration of the velocity over the slit. It is

$$V = \frac{1}{2\mu} \frac{dP}{dx} \frac{1}{h} \int_0^h (\eta^2 - h^2) d\eta + \frac{MY}{h} \int_0^h \left(1 - \frac{\psi}{\psi_0}\right) d\eta$$

or

$$V = \frac{-h^2}{3\mu} \frac{dP}{dx} + MY(1 - G) \tag{9}$$

The function $G = G(\alpha, \omega h)$ is defined as

$$G = \frac{1}{\omega h} \int_0^{\omega h} \left(\frac{\psi}{\psi_0}\right) d(\omega\eta)$$

Substitution of the expression for $d(\omega\eta)$, from eq 4 into the foregoing yields

$$G = \frac{1}{\left(\frac{\alpha}{2}\right)\omega h} \int_{\psi_c}^{\psi_0} \frac{\left(\frac{\alpha\psi}{2\psi_0}\right) d\left(\frac{\alpha\psi}{2\psi_0}\right)}{\left(\cosh^2 \frac{\alpha\psi}{2\psi_0} - \cosh^2 \frac{\alpha\psi_c}{2\psi_0}\right)^{1/2}} \tag{10}$$

The function G is obtained by numerical integration, and its variation with electrokinetic radius is plotted in Figure 2. When the electrokinetic radius becomes larger than about 10 the approximation that $\psi_c = 0$ is permissible, and the integral is reduced to a function of α alone. That is

$$G = \frac{1}{\omega h \left(\frac{\alpha}{2}\right)} \int_0^{\psi_0} \frac{\left(\frac{\alpha\psi}{2\psi_0}\right) d\left(\frac{\alpha\psi}{2\psi_0}\right)}{\sinh \frac{\alpha\psi}{2\psi_0}}$$

or

$$G = \frac{F(\alpha)}{\omega h} \tag{11a}$$

with

$$F(\alpha) = \frac{1}{\frac{\alpha}{2}} \int_0^{\psi_0} \frac{\left(\frac{\alpha\psi}{2\psi_0}\right) d\left(\frac{\alpha\psi}{2\psi_0}\right)}{\sinh \frac{\alpha\psi}{2\psi_0}} \tag{11b}$$

The variation of $F(\alpha)$ with α is plotted in Figure 3. For moderate-to-large electrokinetic radii, the mean velocity becomes

$$V = \frac{-h^2}{3\mu} \frac{dP}{dx} + MY \left(1 - \frac{F(\alpha)}{\omega h}\right) \tag{12}$$

Equations 9 and 12 together with the graphs of $F(\alpha)$ and G , which are plotted in Figures 2 and 3, permit the calculation of the mean velocity or the volumetric flow through a capillary slit. There are two separate velocity components; the first, as seen in equations 9 and 12 is a pressure-generated flow and the second is the flow that is generated by the electric field $Y = dE/dx$. When the electric field Y is controlled externally, the foregoing equation can be used directly to determine the mass transport. In most of the problems of interest, the electric field Y is self-induced and is termed the streaming potential.

Axial Transport of Electric Charge

There are two modes of transport of charge in electrokinetic flow in capillaries. They are: the motion of

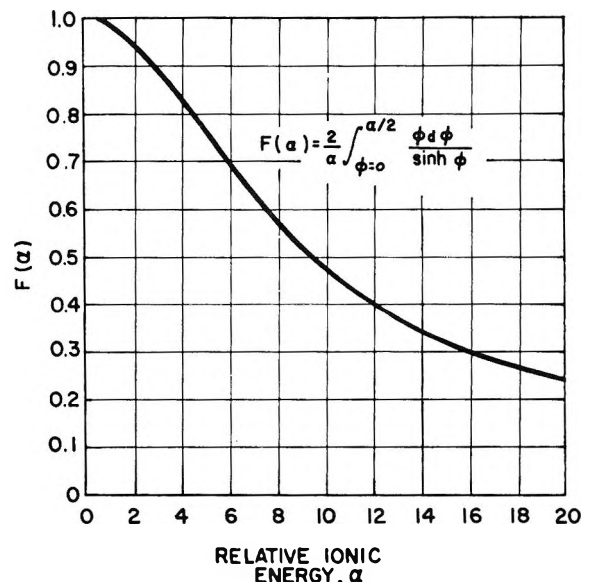


Figure 3. Variation of $F(\alpha)$ with α .

ions with the bulk of the fluid moving with a velocity, u ; the motion of ions relative to the fluid, as in electrolytic conduction. These effects are superposed and are expressed as a positive ion current density and a negative ion current density with transport and conduction components. Thus $I_+(\eta) = n_+ ezu - n_+ ez b_+ Y$ and $I_-(\eta) = -n_- ezu - n_- ez b_- Y$ where b_+ and b_- are the electrochemical conduction mobilities of the positive and negative ions. The addition of the above equations and substitution from eq 1, yields the net current density as

$$I(\eta) = I_+(\eta) + I_-(\eta) =$$

$$\bar{n}ez(\epsilon^{-\alpha\psi/\psi_0} - \epsilon^{\alpha\psi/\psi_0})u - \bar{n}ez(b_+\epsilon^{-\alpha\psi/\psi_0} + b_-\epsilon^{\alpha\psi/\psi_0})Y$$

With the use of eq 2 the current density can be expressed as

$$I(\eta) = \rho u - \bar{n}ezY \left[(b_+ + b_-) \times \cosh \frac{\alpha\psi}{\psi_0} + (b_- - b_+) \sinh \frac{\alpha\psi}{\psi_0} \right]$$

It is noted that K_0 , in simple electrolytic conduction, is equal to $\bar{n}ez(b_+ + b_-)$. Integration over a unit capillary cross section area yields the net current density

$$I = \frac{1}{\omega h} \int_0^h \rho u d(\omega\eta) - K_0 Y \left[\frac{1}{\omega h} \int_0^h \cosh \times \frac{\alpha\psi}{\psi_0} d(\omega\eta) + \frac{(b_- - b_+)}{(b_- + b_+)} \frac{1}{\omega h} \int_0^h \sinh \frac{\alpha\psi}{\psi_0} d(\omega\eta) \right]$$

The velocity, u , is given by eq 7 and 8. Substitution into the foregoing equation gives

$$I = \frac{1}{\omega h} \int_0^h \frac{\rho}{2\mu} (\eta^2 - h^2) d(\omega\eta) \frac{dP}{dx} - Y K_0 \left[\frac{1}{\omega h} \int_0^h \cosh \frac{\alpha\omega}{\psi_0} d(\omega\eta) + \frac{(b_- - b_+)}{(b_- + b_+)} \frac{1}{\omega h} \int_0^h \sinh \frac{\alpha\psi}{\psi_0} d(\omega\eta) - \frac{M}{K_0 \omega h} \int_0^h \rho \left(1 - \frac{\psi}{\psi_0} \right) d(\omega\eta) \right] \quad (13)$$

The integral $(1/\omega h) \int_0^h (\rho/2\mu)(\eta^2 - h^2) d(\omega\eta)$ can be put into another form by using eq 3 and integrating by parts. It is

$$\frac{1}{\omega h} \int_0^h \frac{\rho}{2\mu} (\eta^2 - h^2) d(\omega\eta) = M(1 - G) \quad (14)$$

The phenomenological coefficient $M(1 - G)$ appears as a cross coupling coefficient in both eq 9 and 14. This is as it should be in accordance with the Onsager reciprocal theorem.⁷

The remaining terms in eq 13 can be evaluated analytically. The integral

$$\frac{1}{\omega h} \int_0^h \cosh \frac{\alpha\psi}{\psi_0} d(\omega\eta)$$

represents the mean conductance of the fluid in the capillary channel when the mobilities of both ions are identical. It is defined as the conductivity distribution ratio, K_r/K_0 . With the use of eq 4 we obtain

$$\frac{K_r}{K_0} = \frac{1}{\omega h} \left[\omega h + 2 \int_{\psi_c}^{\psi_0} \frac{\sinh^2 \frac{\alpha\psi}{2\psi_0} d\left(\frac{\alpha\psi}{2\psi_0}\right)}{\left(\cosh^2 \frac{\alpha\psi}{\psi_0} - \cosh^2 \frac{\alpha\psi_c}{2\psi_0}\right)^{1/2}} \right]$$

This can be expressed in terms of elliptic integrals⁶ as

$$\frac{K_r}{K_0} = 1 + \frac{2}{\omega h} \left[\cosh \frac{\alpha}{2} \left(\cosh^2 \frac{\alpha}{2} - \cosh^2 \frac{\alpha\psi_c}{2\psi_0} \right)^{1/2} + \frac{\sinh^2 \frac{\alpha\psi_c}{2\psi_0}}{\cosh \frac{\alpha\psi_c}{2\psi_0}} F(\theta_h, t) - \cosh \frac{\alpha\psi_c}{2\psi_0} E(\theta_h, t) \right] \quad (15)$$

where θ_h denotes evaluation of θ_η at $\eta = h$. The variation of K_r/K_0 with electrokinetic radius is plotted in Figure 4. As the electrokinetic radius becomes large the ratio approaches unity and the fluid in the capillary can be assumed to possess the specific conductance of the bulk fluid. When the electrokinetic radius approaches zero, K_r/K_0 becomes equal to $\cosh \alpha$. For moderate or large values of electrokinetic radius, *i.e.*, $\psi_c = 0$, eq 15 becomes

$$\frac{K_r}{K_0} = 1 + \frac{2}{\omega h} \left(\cosh \frac{\alpha}{2} - 1 \right) \quad (16)$$

The term

$$\frac{(b_- - b_+)}{(b_- + b_+)} \frac{1}{\omega h} \int_0^h \sinh \frac{\alpha\psi}{\psi_0} d(\omega\eta)$$

which is designated as the variable ionic mobility conduction ratio, K_b/K_0 , modifies the distributed conductance to account for differences in electrochemical ionic mobility. When the ionic mobilities are unequal it can make a significant alteration in the net current. For example, in a dilute aqueous solution of hydrochloric acid the mobility of the hydronium ion is about four and one-half times that of the chloride ion, and the ratio $(b_- - b_+)/ (b_- + b_+)$, defined as γ , is equal to -0.636 . γ takes on values between minus and plus one, and its value can be obtained from tables of equivalent conductances. Integration of the foregoing expression yields

(7) S. R. De Groot, "Thermodynamics of Irreversible Processes," Interscience Publishers, New York, N. Y., 1966.

$$\frac{K_b}{K_0} = \frac{2\gamma}{\omega h} \left(\cosh^2 \frac{\alpha}{2} - \cosh^2 \frac{\alpha\psi_c}{2\psi_0} \right)^{1/2} \quad (17)$$

K_b/K_0 is an odd function of α . When K_b/K_0 applies to a capillary element with a moderate to large electrokinetic radius the expression for K_b/K_0 degenerates to

$$\frac{K_b}{K_0} = \frac{2\gamma}{\omega h} \sinh \frac{\alpha}{2} \quad (18)$$

The hyperbolic sine is an odd function of the argument $\alpha/2$, and a change in the sign of α will change the sign of K_b/K_0 . This property of K_b/K_0 is important because through a proper selection of electrolyte the average conductivity of the fluid in the capillary can be made less than that of the bulk fluid, thereby increasing generated voltages and flow retardations.

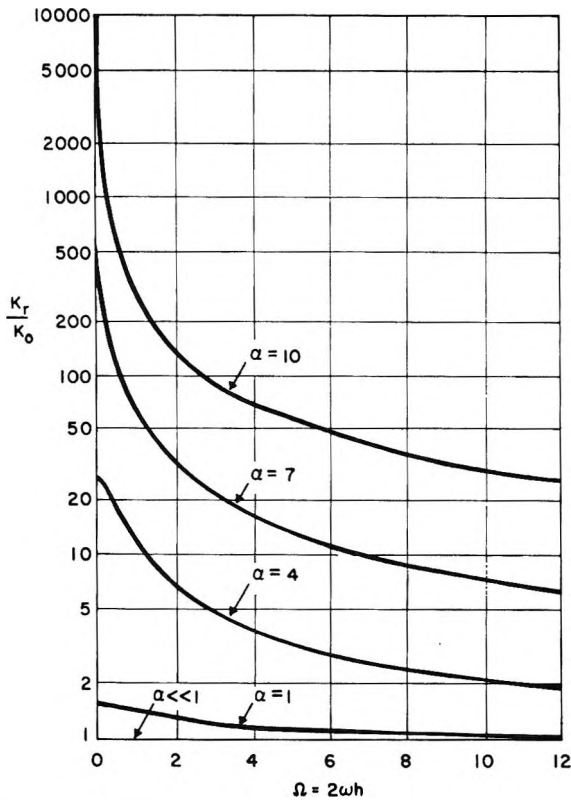


Figure 4. Variation of K_r/K_0 with electrokinetic radius, Ω .

The effect of the distributed conductance upon the current flowing in the capillary is determined by the terms K_r/K_0 and K_b/K_0 . The derivation of the expressions for these terms is based upon the assumption that the ionic mobilities are constant everywhere in the capillary. It precludes interionic attractions that may contribute to the motions of the ions relative to the fluid. Although this approximation is adequate for dilute solutions, a high surface ionic potential which can increase the concentration near the wall by several orders of magnitude may cause the ionic mobilities to vary significantly over the cross section.

The last term in eq 13 is

$$-\frac{M}{K_0 h} \int_0^h \rho \left(1 - \frac{\psi}{\psi_0} \right) d(\omega\eta)$$

It accounts for the transport of charge due to the fluid velocity induced by the axial electric field, and is designated I_t . With the use of eq 2 and 4 it becomes

$$I_t = \frac{-M}{K_0 h} \int_0^h \rho \left(1 - \frac{\psi}{\psi_0} \right) d(\omega\eta) = \frac{M^2 \mu \omega^2}{\left(\frac{\alpha}{2} \right)^2 \omega h} \int_{\psi_c}^{\psi_0} \times \frac{\sinh \frac{\alpha\psi}{2\psi_0} \cosh \frac{\alpha\psi}{2\psi_0} \left(\frac{\alpha}{2} - \frac{\alpha\psi}{2\psi_0} \right) d \left(\frac{\alpha\psi}{2\psi_0} \right)}{\left(\cosh^2 \frac{\alpha\psi}{2\psi_0} - \cosh^2 \frac{\alpha\psi_c}{2\psi_0} \right)^{1/2}}$$

Integration and use of the nondimensional parameter^{2a} $B = M^2 \mu \omega^2 / K_0$ yields

$$\frac{I_t}{BI_c} = \frac{1}{\left(\frac{\alpha}{2} \right)^2 \omega h} \left[\cosh \frac{\alpha}{2} \left(\cosh^2 \frac{\alpha}{2} - \cosh^2 \frac{\alpha\psi_c}{2\psi_0} \right)^{1/2} - \cosh \frac{\alpha\psi_c}{2\psi_0} E(\theta_h, t) \right] \quad (19)$$

where $I_c = K_0 Y$ represents the conduction current in undisturbed fluid, and I_t/I_c denotes the normalized electrical transport. I_t/BI_c is plotted against electrokinetic radius in Figure 5. It can be shown that it approaches zero as the electrokinetic radius becomes either large or approaches zero. For moderate values of electrokinetic radius, say $2\omega h > 10$, it becomes

$$\frac{I_t}{BI_c} = \frac{1}{\left(\frac{\alpha}{2} \right)^2 \omega h} \left(\cosh \frac{\alpha}{2} - 1 \right) \quad (20)$$

The expression for the current in the capillary, eq 13, becomes

$$I = M(1 - G) \frac{dP}{dx} - K_0 Y \left(\frac{K_r}{K_0} + \frac{K_b}{K_0} + \frac{I_t}{I_c} \right) \quad (21)$$

In the case of an ultrafine slit the parameters G , K_r/K_0 , and I_t/I_c can be obtained from Figures 2, 4, and 5. When the electrokinetic radius is large the electrical current, using eq 11, 16, 18, and 20, becomes

$$I = M \left(1 - \frac{F(\alpha)}{\omega h} \right) \frac{dP}{dx} - K_0 Y \left[1 + \frac{2}{\omega h} \left(\cosh \frac{\alpha}{2} - 1 \right) + \frac{2\gamma}{\omega h} \sinh \frac{\alpha}{2} + \frac{B}{\left(\frac{\alpha}{2} \right)^2 \omega h} \left(\cosh \frac{\alpha}{2} - 1 \right) \right] \quad (22)$$

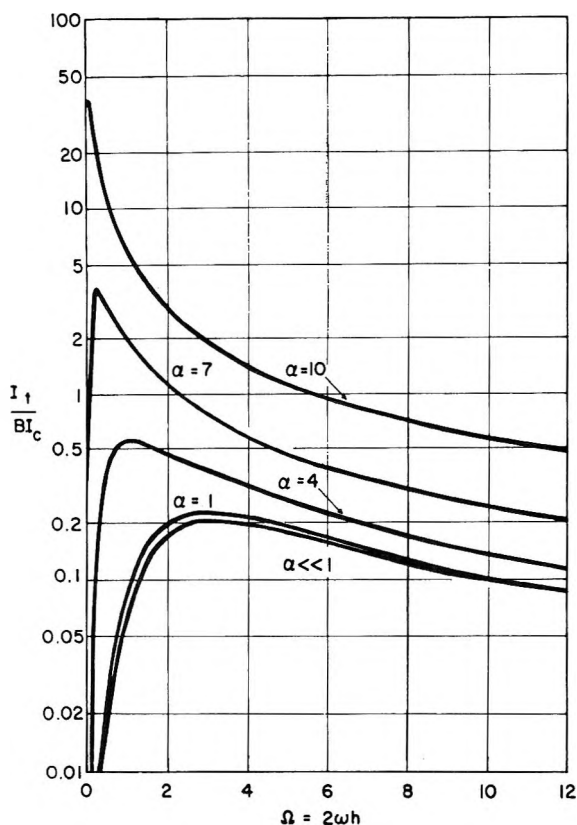


Figure 5. Variation of I_t/BI_c with electrokinetic radius, Ω .

with $F(\alpha)$ given in Figure 3. The foregoing equation can be written in terms of a surface conductance as

$$I = M \left(1 - \frac{F(\alpha)}{\omega h} \right) \frac{dP}{dx} - K_0 Y \left[1 + \frac{K_s^-}{K_0 h} \right] \quad (23)$$

where the surface conductance is

$$K_s = \frac{K_0}{\omega} \left[\left(2 + \frac{B}{\left(\frac{\alpha}{2} \right)^2} \right) \left(\cosh \frac{\alpha}{2} - 1 \right) + 2\gamma \sinh \frac{\alpha}{2} \right] \quad (24)$$

The terminology "surface conductance" is often used in descriptions of the increased conductivity that is present in relatively large capillaries, in which the modified lateral ion distribution increases the conductivity of the fluid near the surface. For moderate and large size capillaries, expressions in terms of surface conductance are convenient because K_s , as defined by eq 24, is invariant with respect to the size of the capillary. It should also be noted, in eq 24, that the surface conductance contains the electroosmotic transport term, I_t/I_c , and is not solely due to the increased electrolytic conduction in the fluid near the interface. A further examination of eq 24 reveals the possibility, in certain cases, of achieving a negative surface conductance. This would occur when there is good ion exclusion in the capillary and the ion that forms the

spatial charge distribution has a low mobility in comparison with the ion that is excluded from the capillary.

Cole⁸ has derived a formula for surface conductance applicable to capillaries with relatively large electrokinetic radii, that is equivalent to eq 24, and his calculated values of surface conductance are found to be in good agreement with experimental data obtained by Urban and White.⁹ Fricke and Curtis¹⁰ measured the conductance of suspensions of small glass spherules (diameter = 1.7 μ), and found that Cole's formula adequately predicted surface conductance in solutions of potassium chloride and hydrochloric acid, providing the solution is not too dilute. This restriction is required since small particles in a dilute solution corresponds to a system with small electrokinetic radius.

The surface conductance is descriptive of the increased conductivity due to the presence of a high density of counterions in the fluid near the wall of a relatively large capillary channel, and is independent of the width of the capillary channel. However, in fine capillaries, such as those considered in the present analysis, the counterions are distributed over the channel cross section so that the change in conductivity is no longer due to ions near the surface, and therefore becomes a function of channel width. In fine capillaries the basic conductivity of the fluid is modified by three factors: the distributed conductivity factor; the nonuniform ionic mobility factor; the transport current factor. It is therefore a "modified conductance" rather than a "surface conductance."

Electrokinetic Systems

Figure 6 shows a schematic arrangement of a general electrokinetic system. It includes an external voltage source, an external resistance, R_0 , which is the sum of the load resistance and internal resistance of the voltage source, as well as components of the capillary element. The equation for the external circuit is simply $E_1 + E_0 + R_0 I = E_2$, from which

$$\frac{E_2 - E_1}{L} = \frac{E_0}{L} + \frac{R_0 I}{L} \text{ or } Y = Y_e + \frac{R_0}{L}$$

where Y_e is the applied electric field equal to E_0/L and $Y = E_2 - E_1/L$ is the electric field over the length of the capillary element. Substitution for I from eq 21 into the foregoing yields

$$Y = \frac{Y_e \frac{L}{R_0} + M(1 - G) \frac{dP}{dx}}{\frac{L}{R_0} + K_0 \left(\frac{K_r}{K_0} + \frac{K_b}{K_0} + \frac{I_t}{I_c} \right)} \quad (25)$$

(8) K. S. Cole, "Surface Conductance," Cold Spring Harbor Symposia on Quantitative Biology, Vol. 1, 1933.

(9) F. Urban and H. L. White, *J. Phys. Chem.*, **36**, 3157 (1932).

(10) H. Fricke and H. Curtis, *ibid.*, **40**, 715 (1936).

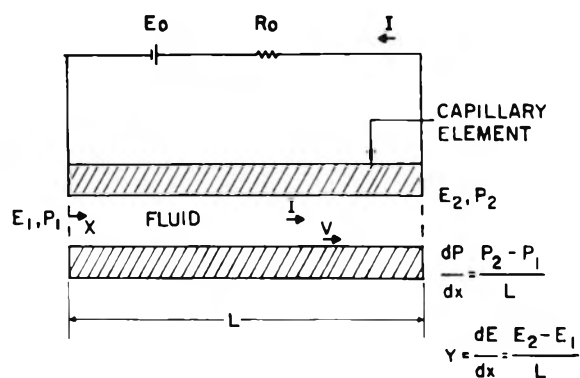


Figure 6. Electrokinetic system.

If a system conductance K is defined as $K = K_0 + L/R_0A$, and this is used to eliminate L/R_0 from eq 25, the axial electric field becomes

$$Y = \frac{Y_0 \left(\frac{K}{K_0} - 1 \right) + \frac{M}{K_0} \frac{dP}{dx} (1 - G)}{\left(\frac{K}{K_0} - 1 \right) + \left(\frac{K_r}{K_0} + \frac{K_b}{K_0} + \frac{I_t}{I_c} \right)} \quad (26)$$

Equation 26 is applicable to both electroosmotic pumping and streaming potential generation. In the case of electroosmotic pumping the quantity dP/dx is zero in both eq 12 and 26. To determine the electroosmotic velocity, Y is found from eq 26 and its value is set into eq 12.

In the case of streaming potential generation, fluid is forced by a pressure difference through a capillary. The transport of the distributed ions within the capillary generates a potential over the length of the capillary that is sufficient to maintain electrical equilibrium. When there is no external voltage source, this voltage is the streaming potential. If there is no path, external to the capillary, through which an electrical current can flow, the current in the capillary will be equal to zero. Then, eq 21 becomes

$$I = M(1 - G) \frac{dP}{dx} - K_0 Y_0 \left(\frac{K_r}{K_0} + \frac{K_b}{K_0} + \frac{I_t}{I_c} \right)$$

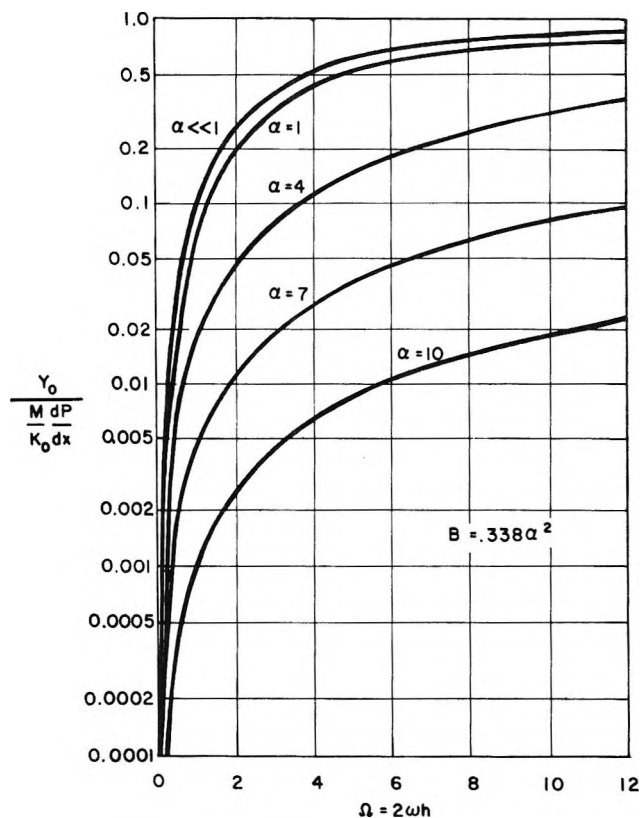
where Y_0 denotes the conventional open circuit streaming potential.

Solving for Y_0 and normalizing with respect to $M/K_0 dP/dx$ gives

$$\frac{Y_0}{\frac{M}{K_0} \frac{dP}{dx}} = \frac{(1 - G)}{\left(\frac{K_r}{K_0} + \frac{K_b}{K_0} + \frac{I_t}{I_c} \right)} \quad (27)$$

The same result is obtained by allowing R_0 to approach infinity, ($K/K_0 = 1$) in eq 26.

The normalized open circuit streaming potential is plotted in Figure 7 against electrokinetic radius, for several values of α . The parameter γ is chosen as

Figure 7. Normalized streaming potential vs. electrokinetic radius, Ω ($\gamma = 0$).

zero, implying identical ionic mobilities, and B is taken to be equal to $0.338\alpha^2$ (a typical value that is obtained for B in a dilute aqueous solution in which $K_0 = 0.1 \text{ C (ohm-cm)}^{-1}$). The curves of Figure 7 show the modification in the basic double-layer streaming potential, $Y_0 = M/K_0 dP/dx$, that is introduced by taking into consideration the retarding velocity induced by the generated electric field, the true lateral distribution of charge, and the transport of charge associated with the mass flow. It is observed that as the ionic energy, which is proportional to α , is decreased, and the electrokinetic radius, which is the ratio of hydraulic radius to Debye length, is increased, the open circuit streaming potential approaches the double-layer value of $M/K_0 dP/dx = 1$. That is, the curves are all asymptotic to $M/K_0 dP/dx = 1$. It is clear then that the inclusion of the aforementioned refinements is of value only in fine capillaries.

In order to illustrate the pronounced effect that differences in co-ion and counterion mobilities can have on the streaming potential, Figure 8 shows $Y_0 K_0 / M dP/dx$ plotted against electrokinetic radius for $\alpha = 4$, $B = 5.3$, and several values of γ between the limits of plus and minus one. The curves of Figure 8 show that negative values of K_b/K_0 enhance the magnitude of generated streaming potential while positive value of K_b/K_0 to diminish the streaming potential. In fine capillaries the effect can be quite large. For example,

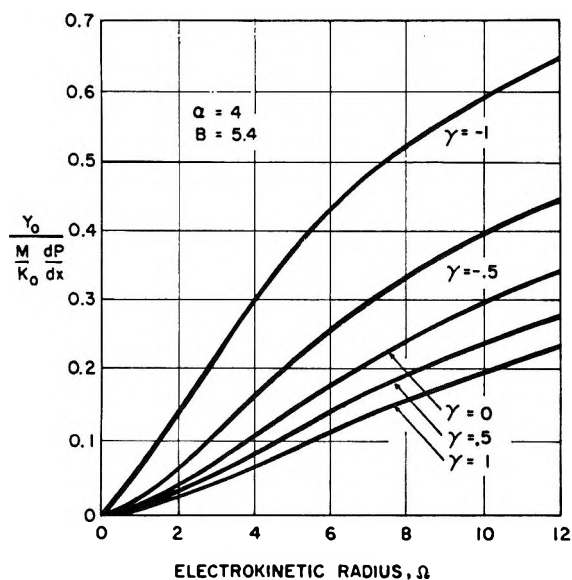


Figure 8. Normalized streaming potential vs. electrokinetic radius, Ω , with variable γ .

when the electrokinetic radius, Ω , is equal to 6, the magnitude of the streaming potential can increase by a factor of 4 over the range of complete conduction by the co-ions to complete conduction by the counterions.

Flow Retardation

The streaming potential produces electrical body forces which act primarily on the fluid near the capillary wall. These forces set up an electroosmotic countercurrent of mass flow which retards the pressure-induced flow. In ultrafine capillary elements this retarding flow can be a very significant portion of the total flow.

With the use of eq 9, the negative ratio of electroosmotic induced flow to pressure induced flow can be written as

$$\frac{V_r}{V_p} = \frac{MY(1-G)}{\frac{h^2 dP}{3\mu dx}} \quad (28)$$

Substitution for Y_0 from eq 27 yields

$$\frac{V_r}{V_p} = \frac{3M^2\mu}{K_0 h^2} \frac{(1-G)^2}{\left(\frac{K_r}{K_0} + \frac{K_b}{K_0} + \frac{I_t}{I_c}\right)}$$

or

$$\frac{V_r}{V_p} = \frac{3B}{(\omega h)^2} \frac{(1-G)^2}{\left(\frac{K_r}{K_0} + \frac{K_b}{K_0} + \frac{I_t}{I_c}\right)} \quad (29)$$

The retarding flow ratio, V_r/V_p , is plotted in Figure 9 as a function of the electrokinetic radius for several values of α . The constituent ionic mobilities are taken to be equal ($\gamma = 0$), and as before B is equal to

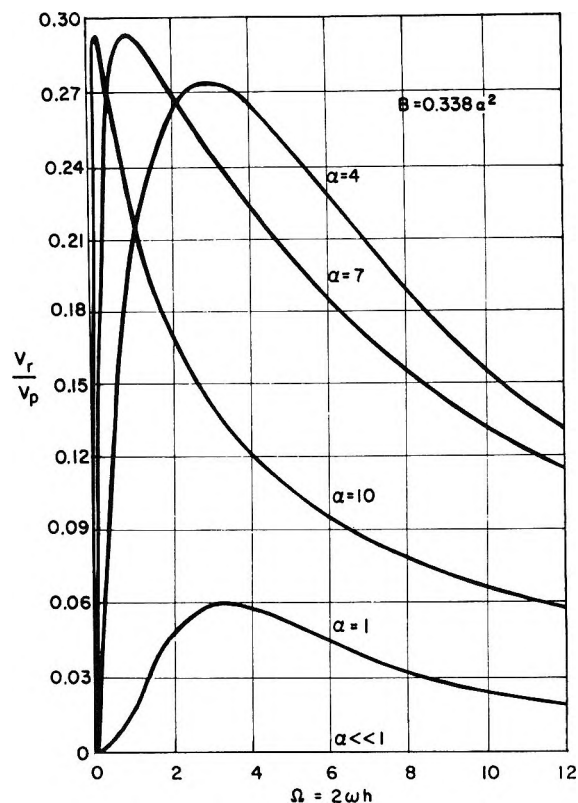


Figure 9. Variation of flow retardation ratio, V_r/V_p with electrokinetic radius, Ω ($\gamma = 0$).

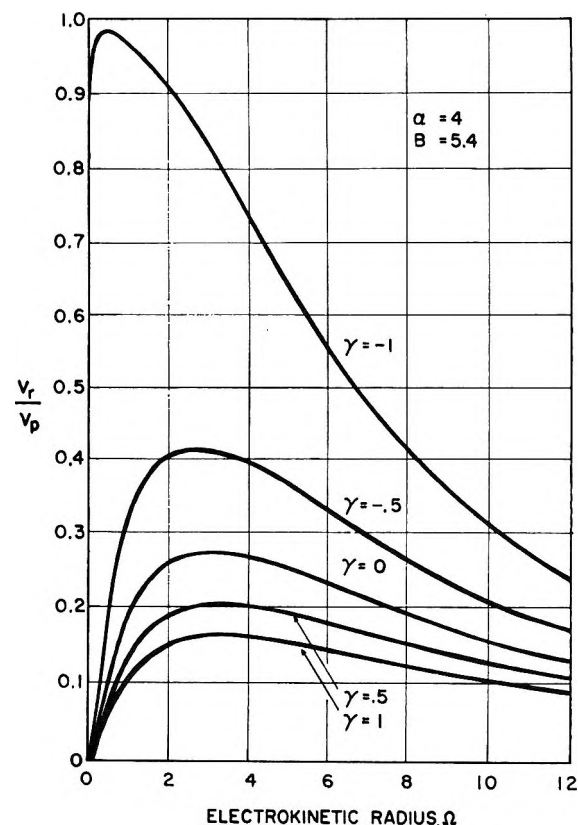


Figure 10. Variation of flow retardation ratio, V_r/V_p , with electrokinetic radius, Ω ; γ , variable.

$0.338\alpha^2$. Note that beyond $\alpha = 4$, further increases in α have little effect upon the maximum attainable flow retardation. It should also be observed that for many small values of electrokinetic radius the ratio of retarding flow to pressure-induced flow can be increased by reducing α , provided that α is greater than 4.

Differences in ionic mobility have a surprisingly strong influence upon the retarding flow. Figure 10 contains a set of curves showing the variation of V_r/V_p with electrokinetic radius for $\alpha = 4$ and $B = 5.4$, and for several values of γ between the limits of plus and minus one. When the charge distribution in the capillary has a relatively low ionic mobility the capillary element would apparently seem to be impermeable. An exceptionally low streaming potential is, however, associated with this high flow retardation, as can be seen by a comparison of Figures 9 and 10 with Figures 7 and 8. The large flow retardations that are shown by curves of Figure 10 could possibly account for some large increases in the apparent viscosity of fluids in very fine channels, that has been observed experimentally.⁴ Electroosmotic pumping and electrokinetic power generation efficiencies have been shown to be dependent upon the ratio of the retarding electroosmotic flow component to the pressure-induced flow component.¹¹ If this is indeed the case, the possibility presents itself that with a proper choice of electrolyte, *i.e.*, one for which the value of γ would cause K_b/K_0 to be negative, the efficiencies of electrokinetic systems may be increased substantially.

Analytical expressions and graphical representations of the flow retardation are now compared with experimental measurements of the so-called electroviscous effect. By definition $V = V_p - V_r$ or

$$V/V_p = 1 - V_r/V_p \quad (28)$$

V_p is inversely proportional to the viscosity of the fluid, μ . An apparent viscosity, μ_a , can be defined so that the flow in the capillary satisfies the Poiseuille law, or

$$V = \frac{-h^2 dP}{3\mu_a dx}$$

Equation 28 then becomes

$$\frac{\mu}{\mu_a} = 1 - \frac{V_r}{V_p}$$

or

$$\frac{\mu_a}{\mu} = \frac{1}{1 - V_r/V_p} \quad (30)$$

This expression shows the simple relationship that exists between the ratio of apparent viscosity to equal and the flow retardation ratio V_r/V_p .

A comparison of flow retardations calculated for slits with those observed experimentally is complicated by the fact that slits of sufficient fineness have not, as yet, been constructed. High retardations have generally been observed to occur only in fine porous elements such as bacteriological filters.

Henniker⁴ and Rideal¹² have observed anomalously high retardations by flowing dilute salt solutions through a microporous porcelain bacteriological filter. Experimental values of μ_a/μ as high as 1.2 have been reported by Henniker; this corresponds to a V_r/V_p , flow retardation ratio, of 1.67, a magnitude well within the range of retardations predicted here for fine slits. An exact prediction of the flow retardation in a microporous element of this type would be difficult as the geometry of the capillary is unknown.

The favorable comparison of the analytically computed apparent viscosity with experimental measurements is encouraging since it serves to eliminate the inference of phenomena other than those which are due to the basic electrokinetic parameters. The reduced flow in fine capillaries need not be attributed to an apparent increased viscosity. Rather, it is a flow retardation which is due primarily to the induced streaming potential which acts upon the charged fluid and produces forces that are directed opposite to the pressure flow. There can, of course, be real changes in physical properties such as changes in viscosity and dielectric constant at points of very high ion concentration. Additional experimental data and comparisons with analyses are necessary to determine at which point the derived analytical expressions are no longer valid.

Acknowledgment. The author is grateful to the National Science Foundation for providing the support that made this study possible. The author is also indebted to Professor David Burgreen of the Polytechnic Institute of Brooklyn for his advice and guidance.

(11) D. Burgreen and F. Nakache, *J. Appl. Mech.*, 675 (1965).

(12) J. J. Davies and E. K. Rideal, "Interfacial Phenomena," Academic Press, Inc., New York, N. Y., 1963.

The Ionization of Clusters. I. The Dicarboxylic Acids

by S. L. Dygert, Giovanna Muzii,¹ and H. A. Saroff

National Institute of Arthritis and Metabolic Diseases, National Institutes of Health, Public Health Service,
U. S. Department of Health, Education and Welfare, Bethesda, Maryland 20014 (Received June 30, 1969)

A method for extracting values for the intramolecular hydrogen bonding constants and the factor E ("electrostatic factor") for symmetrical dicarboxylic acids is presented. This method is applied to several series of symmetrical dicarboxylic acids from the literature. The structural factors correlated with changes in E and the intramolecular hydrogen-bonding constants are pointed out. It is concluded that large values of $K_1/4K_2$ (over 300) usually indicate intramolecular hydrogen bonding, and that it is possible for a strong intramolecular hydrogen bond to exist in aqueous solution. Sodium binding to malonic acid is found to be approximately equal to the binding of sodium to diethylmalonic acid. This contrasts with the much stronger intramolecular hydrogen bond found for the diethyl derivative as compared to malonic acid.

Studies on the binding of hydrogen and other ions to proteins have resulted in a number of interpretations invoking localized interactions between charged sites on protein molecules. In the case of serum albumin,² β -lactoglobulin,^{3a} and myosin,^{3b} pairing of carboxylate and ammonium ions was invoked. In ribonuclease,⁴ clusters of positive charges interacted with both internal carboxylate ions and other anions in solution. Such clustering of positive and negative charges was demonstrated in the models constructed from the X-ray data for both ribonuclease⁵ and ribonuclease-S.⁶

In this communication we consider, as a possible model for the clustering of charged groups in proteins, the symmetrical dicarboxylic acids. The model includes charge effects and intramolecular hydrogen bonding. A technique for evaluating the charge effect and hydrogen-bonding constants is presented and the implications of the analysis are discussed.

I. Explanation of Model

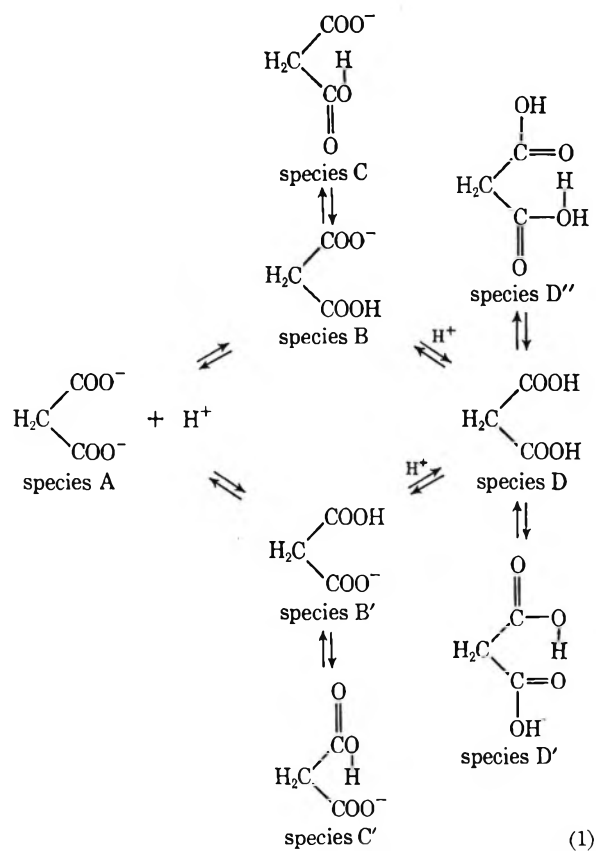
Ratios of the two macroscopic association constants for the malonic acids and other symmetrical dibasic acids have been the subject of considerable study emphasizing both charge effects⁷ and the intramolecular hydrogen bond.⁸ The model considered in this paper includes both hydrogen bonding and the effect of the charge of the neighboring carboxyl group (factor E) on the hydrogen ion association constant.

Consider the reactions in eq 1. The microscopic association constants (eq 2-5) can be defined from this scheme, where brackets refer to activities.

$$k_H = \frac{[D]}{[B][H^+]} = \frac{[D]}{[B'][H^+]} \quad (2)$$

$$k_{HE} = \frac{[B]}{[A][H^+]} = \frac{[B']}{[A][H^+]} \quad (3)$$

$$k_{DC} = \frac{[D'']}{[D]} = \frac{[D']}{[D]} \quad (4)$$



(1) Visiting Fellow, National Institutes of Health, 1964-1965; present address: Stazione Zoologica, Acquario, Naples, Italy.

(2) H. A. Saroff and M. S. Lewis, *J. Phys. Chem.*, **69**, 1211 (1963); H. A. Saroff, *ibid.*, **61**, 1364 (1957).

(3) (a) H. P. Baker and H. A. Saroff, *Biochemistry*, **4**, 1670 (1965); (b) M. S. Lewis and H. A. Saroff, *J. Amer. Chem. Soc.*, **79**, 2112 (1957).

(4) G. I. Loeb and H. A. Saroff, *Biochemistry*, **3**, 1819 (1964).

(5) G. Kartha, J. Bellow, and D. Harker in "Structural Chemistry and Molecular Biology," A. Rich and N. Davidson, Ed., W. H. Freeman and Corp., San Francisco, Calif., 1968, p 36.

(6) H. W. Wyckoff, K. D. Hardman, N. M. Allewell, T. Inagami, L. N. Johnson, and F. M. Richards, *J. Biol. Chem.*, **242**, 3984 (1967).

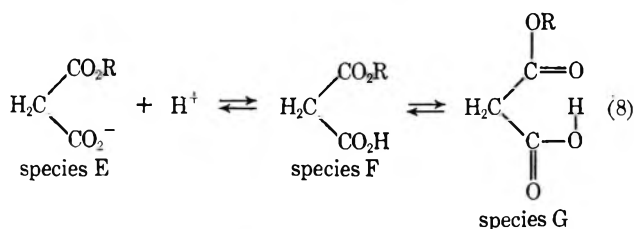
$$k_D = \frac{[C]}{[B]} = \frac{[C']}{[B']} \quad (5)$$

The macroscopic association constants are

$$K_{1, \text{assoc}} = \frac{[B + C + B' + C']}{[A][H^+]} = 2k_H E(1 + k_D) \quad (6)$$

$$K_{2, \text{assoc}} = \frac{[D + D' + D'']}{[B + C + B' + C'][H^+]} = \frac{k_H(1 + 2k_{DO})}{2(1 + k_D)} \quad (7)$$

It is assumed that the ester and monoprotonated species have the same microscopic association constant and that the microscopic intramolecular hydrogen bonding constant for the diacid and ester are equivalent.⁹ Thus, k_H and k_{DO} can also be defined from the association reaction of the ester



$$k_H = \frac{[F]}{[E][H^+]} \quad (9)$$

$$k_{DO} = \frac{[G]}{[F]} \quad (10)$$

The macroscopic association constant $K_{E, \text{assoc}}$ is given by

$$K_{E, \text{assoc}} = \frac{[F + G]}{[E][H^+]} = \frac{k_H[E][H^+](1 + k_{DO})}{[E][H^+]} = k_H(1 + k_{DO}) \quad (11)$$

The four microscopic constants k_H , E , k_D , and k_{DO} are thus related to the three macroscopic constants by eq 6, 7, and 11. Figure 1 shows the perturbations of a titration curve resulting from variations in the values of E , k_D , and k_{DO} . [It is *not* implied that the four microscopic constants can be determined by fitting the experimental curve for a symmetrical dibasic acid. In fact, the curves are completely determined by the two macroscopic constants K_1 and K_2 .]

Since these three equations contain four unknowns, it is evident that a solution can be obtained only through added information. One way to obtain such a solution is to assign a value to one of the parameters, such as assuming $k_{DO} = 0$.⁹ Obviously, it is also possible to solve for the four microscopic parameters if a fourth equation can be introduced.

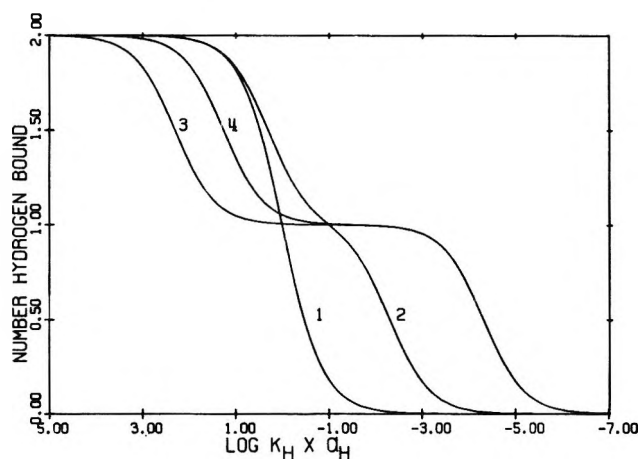


Figure 1. Theoretical titration curves for a dibasic acid: curve 1, unperturbed, $E = 1$, $k_D = k_{DO} = 0$; curve 2, $E = 100$, $k_D = k_{DO} = 0$; curve 3, $E = 100$, $k_D = 100$, $k_{DO} = 0$; curve 4, $E = 100$, $k_D = 100$, $k_{DO} = 10$.

We write the fourth equation

$$R = k_D/k_{DO} \quad (12)$$

where R is simply the ratio of the intramolecular hydrogen-bonding association constant for the monoprotonated species to the comparable constant for the diprotonated species. There is evidence, in some cases at least, that k_D is greater than k_{DO} .^{10,11} Thus, one can specify a reasonable range of values for R and calculate a corresponding range of values for the microscopic constants k_H , k_D , k_{DO} , and E . Figures 2, 3, and 4 show that the calculated range of values for the microscopic constants will often be small if one assumes $R \geq 10$.

A. Significance of k_H and E . k_H is the microscopic association constant for the association of the monoprotonated species with hydrogen ion. It thus includes the inductive effect of the neighboring protonated carboxyl group. The microscopic association constant for an unprotonated carboxyl in the presence of another unprotonated carboxyl is $k_H \cdot E$. Since we are dealing with symmetrical dibasic acids, the factor E represents the total effect of the ionized carboxyl as compared to the un-ionized carboxyl on the association constant. Thus E may include inductive and solvent effects as well as an electrostatic effect.

(7) (a) N. Bjerrum, *Z. Phys. Chem.*, **106**, 219 (1923); (b) J. G. Kirkwood and F. H. Westheimer, *J. Chem. Phys.*, **6**, 506 (1938). For additional references see L. Ebersson, *Acta Chem. Scand.*, **13**, 211 (1959).

(8) H. C. Brown, D. H. McDaniel, and O. Häfiger in "Determination of Organic Structures by Physical Methods," E. A. Braude and F. C. Nachod, Ed., Academic Press, Inc., New York, N. Y., 1955, p 628; see also, D. H. McDaniel and H. C. Brown, *Science*, **118**, 370 (1953).

(9) F. H. Westheimer and O. T. Benfey, *J. Amer. Chem. Soc.*, **78**, 5309 (1956).

(10) R. E. Dodd, R. E. Miller, and W. F. K. Wynne-Jones, *J. Chem. Soc.*, 2790 (1961).

(11) L. Ebersson, *Acta Chem. Scand.*, **13**, 224 (1959).

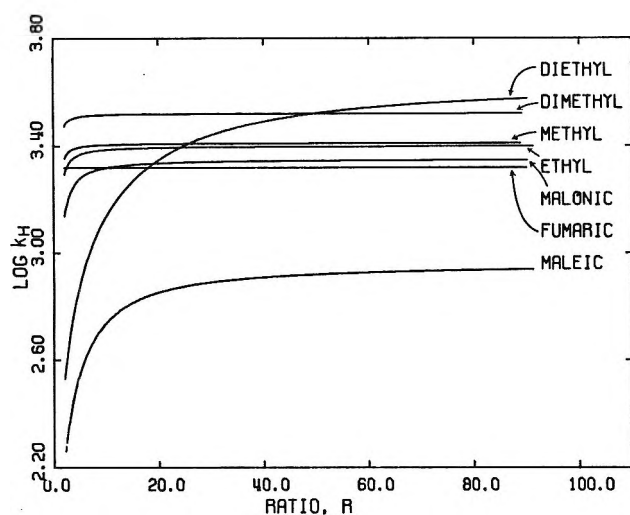


Figure 2. Variation of the microscopic association constant, k_H , for maleic, fumaric, malonic, ethylmalonic, methylmalonic, dimethylmalonic, and diethylmalonic acids as a function of the ratio k_D/k_{D0} .

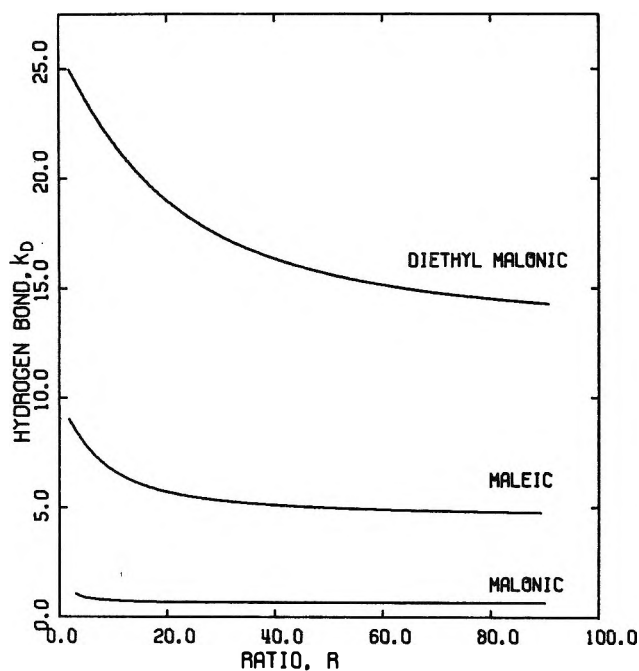


Figure 3. Hydrogen-bonding association constant, k_D , as a function of k_D/k_{D0} for malonic, maleic, and diethylmalonic acids.

It is possible to find dicarboxylic acids in which hydrogen bonding is not possible, such as *trans*-carboxyl groups on a rigid ring structure or separated by a double bond. In such compounds one can solve for the factor E directly. Although not all shapes of molecules nor all possible charge separations can be included, such a procedure gives a general idea of the order of magnitude to be expected from the factor E in some cases and should help provide a check on the assumptions in the present analysis. These data are shown in Table I.

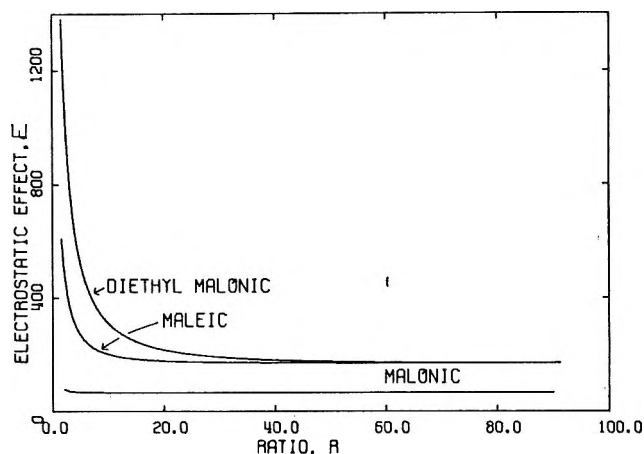


Figure 4. Electrostatic effect, E , as a function of k_D/k_{D0} for malonic, maleic, and diethylmalonic acids.

Table I: Ratio of Hydrogen Ion Association Constants for Symmetrical Dicarboxylic Acids in Which Intramolecular Hydrogen Bonding Is Not Possible^{a,b}

Acid	$K_1/4K_2$
<i>trans</i> -Cyclopropane-1,2-DCA ^c (24°)	7.5
<i>trans</i> -Cyclobutane-1,2-DCA (20°)	16.5
<i>trans</i> -Cyclopentane-1,2-DCA (25°)	19.6
<i>trans</i> -Cyclopentane-1,3-DCA (25°)	3.2
<i>trans</i> -Cyclohexane-1,2-DCA (19°)	14.0
<i>trans</i> -Cyclohexane-1,3-DCA (19°)	6.6
<i>trans</i> -Cyclohexane-1,4-DCA (16–19°)	4.3
<i>trans</i> -Cyclohexene-4-1,2-DCA (20°)	18.1
<i>trans</i> -Cyclohexyl-1,2-diacetic acid (20°)	2.7
<i>trans</i> -Tetrahydronaphthalin-2,3-DCA (20°)	12.5
<i>trans</i> -Hexahydro-3,6-endomethylene- <i>o</i> -phthalic acid (20°)	9.7
<i>trans</i> - Δ^4 -Tetrahydro-3,6-endomethylene- <i>o</i> -phthalic acid (20°)	12.0
<i>trans</i> -Hexahydro-3,6-endoethylene- <i>o</i> -phthalic acid (20°)	28.7
<i>trans</i> - Δ^4 -Tetrahydro-3,6-endoethylene- <i>o</i> -phthalic acid (20°)	21.8
<i>trans</i> -C ₁₄ H ₁₈ O ₄ -DCA (20°)	10.9
<i>trans</i> -Caronic acid (25°)	7.9
<i>trans</i> -Norpin acid (21.8°)	11.6
<i>cis</i> -Norpin acid (21.8°)	12.9
<i>trans</i> -Ethyleneoxy-DCA (19°)	5.2
Isophthalic acid (25°)	2.4
Terephthalic acid (25°)	2.1
Fumaric acid (25°)	5.8

^a Values of association constants taken from G. Kortüm, W. Vogel, and K. Andrussow, "Dissociation Constants of Organic Acids in Aqueous Solution," Butterworths, London, 1961. Temperature given in parentheses. ^b The ratio $K_1/4K_2$ is equal to the factor E for these diacids. ^c DCA = dicarboxylic acid.

The magnitude of the factor E ($K_1/4K_2$ in these compounds) is seen to fall between 2.1 and 28.7.

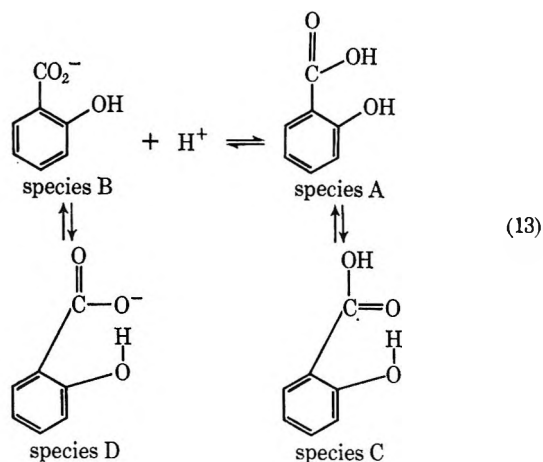
One further point can be made about k_H . If a series is studied in which the only difference between one compound and the next is an increased amount of

alkyl substituent, one expects k_H to increase slightly in analogy with the monocarboxylic acid series. This additional information will further help to reduce the range of possible R values in certain cases.

B. Significance of R . It is difficult to say *a priori* what the ratio k_D/k_{DO} should be, since the formation of the intramolecular hydrogen bond is undoubtedly from a species hydrogen bonded to water. Thus the solvent would be expected to play an important role, and any assumption that k_{DO} must necessarily be zero or much less than k_D is open to question.

Because of this uncertainty concerning the value of R , we make "minimal" assumptions about R . The following arguments, the first based on the hydrogen ion association constants of salicylic acid and *o*-methoxybenzoic acid and the second and third on ir spectral evidence, are intended to show that the assumption, $R \geq 10$, is a reasonable one.

1. A lower limit can be put on the ratio of k_D/k_{DO} for salicylic acid as follows, with the assumption that OCH_3 is equivalent to OH with regard to the dissociation of the carboxyl group. Consider



$$k_H = \frac{[A]}{[B][H^+]} \quad (14)$$

$$k_{DO} = \frac{[C]}{[A]} \quad (15)$$

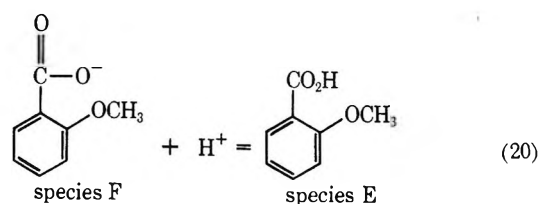
$$k_D = \frac{[D]}{[B]} \quad (16)$$

$$K_1 = \frac{[A + C]}{[H^+][B + D]} = \frac{[1 + k_{DO}]k_H}{[1 + k_D]} \quad (17)$$

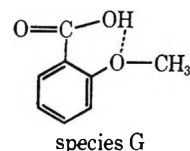
$$\frac{k_H}{K_1} = \frac{1 + k_D}{1 + k_{DO}} \quad (18)$$

Now assume that k_H is given by

$$k_H = \frac{[E]}{[F][H^+]} \quad (19)$$



(This involves ignoring the intramolecular hydrogen-bonded species



which will have little effect on k_H/K_1 as long as the hydrogen-bonded species in which the OH donates the hydrogen predominates over species G.)

Let

$$Z = \frac{k_H}{K_1} = \frac{1 + k_D}{1 + k_{DO}} \quad (21)$$

Then

$$R = \frac{k_D}{k_{DO}} = \frac{(Z - 1)}{k_{DO}} + Z \quad (22)$$

As $k_{DO} \rightarrow 0$, $R \rightarrow \infty$, and as $k_{DO} \rightarrow \infty$, $R \rightarrow Z$. Thus Z (*i.e.*, k_H/k_1) gives a minimum value of R . For salicylic acid and *o*-methoxybenzoic acid the hydrogen ion association constants are 9.55×10^2 and 1.22×10^4 , respectively,¹² which results in a value for Z of approximately 13. This means that, for salicylic acid, the intramolecular hydrogen-bonding association constant for hydrogen bonding to the dissociated carboxyl is at least 13 times that for hydrogen bonding to the protonated carboxyl group.








2. Dodd, *et al.*,¹⁰ have reported the ir spectra of maleic acid and potassium hydrogen maleate in aqueous solution. They were not able to detect an intramolecular hydrogen bond in maleic acid, but they reported a stable intramolecular hydrogen bond in the monoprotonated maleate ion.

3. Ebersson¹¹ studied the ir spectra in methanol of highly alkylated succinic acids. In the case of tetraethylsuccinic acid, the monohydrogen salt showed evidence of an intramolecular hydrogen bond, whereas the diacid showed none. (The racemic forms of three symmetrically substituted acids showed evidence of intramolecular hydrogen bonding in both the mono- and diprotonated species.)

Thus there are at least three cases, two of which are in aqueous solution, in which the intramolecular hydrogen bond formed by the monohydrogen salt would appear to be much stronger than that formed by the diacid.

(12) C. E. K. Branch and D. L. Yabroff, *J. Amer. Chem. Soc.*, **56**, 2568 (1934).

Table II: Experimental Hydrogen Ion Association Constants and Calculated Parameters for Six "Series" of Symmetrical Dicarboxylic Acids

Acid	log K_1	log K_2	log K_E	$K_1/4K_2$	R_{min}	k_{D0}	k_D	log k_H	E	$(1 + kd)^2 / (1 + 2k_{D0})$
Malonic Acid Series in Water; 25°										
Malonic ^{a,b}	5.69	2.83	3.35	181	10	0-0.077	0.775-0.656	3.32-3.35	66.1-66.4	2.73-2.74
Methylmalonic ^{a,b}	5.76	3.05	3.41	128	10	0-0.016	0.145-0.164	3.40-3.41	97.7	1.31
Ethylmalonic ^{a,b}	5.83	2.99	3.40	173	10	0-0.033	0.285-0.326	3.38-3.40	104.7-104.8	1.65
Dimethylmalonic ^{a,b}	6.06	3.17	3.52	194	10	0-0.0134	0.119-0.134	3.51-3.52	154.9	1.25
Methyllethylmalonic ^{a,c}	6.41	2.86	3.58	1,000	10	0-0.25	1.92-2.51	3.48-3.58	116-121	8.6-8.3
Diethylmalonic ^{a,b}	7.29	2.21	3.64	30,100	50	0-0.31	12.5-15.7	3.52-3.64	166-176	181-171
Butyl(1-ethylvinyl)malonic ^d	8.40	2.91	3.65	77,300	10	0-0.23	1.75-2.25	3.56-3.65	10,200-10,600	7.58-7.29
Succinic Acid Series in Water; 25 ^{oa,e}										
Succinic	5.48	4.19	4.52	4.9	10	0-0.0077	0.069-0.077	4.52	4.37	1.14
Tetramethylsuccinic	7.28	3.50	4.91	1,510	20	0-0.90	11.9-17.9	4.63-4.91	9.1-11.7	166-129
Acids Studied by McCoy ^f in Water; 25 ^{oi}										
1. 	7.63	1.12	3.32	809,000	60	0-2.21	78-133	2.81-3.32	129-245	6,271-3,706
2. 	8.00	1.32	3.19	1.2 × 10 ⁶	40	0-1.45	36-58	2.80-3.19	871-1,341	1,378-895
3. 	7.77	1.32	3.02	705,000	50	0-0.685	24-34	2.79-3.02	1,122-1,344	628-525
4. 	7.27	1.64	2.94	223,000	30	0-0.39	9.0-11.8	2.80-2.94	1,071-1,164	208-192
5. 	6.23	1.92	2.96	5,100	10	0-0.67	4.48-6.68	2.74-2.96	170-202	30-25
6. 	7.84	1.44	3.75	628,000	10	0-19.8	101-198	2.43-3.75	60-643	10,467-3,172
7. 	5.41	2.95	3.26	72	10	0-0.0023	0.021-0.023	3.26	69.1	1.04
Malonic Acid Series in 7 M Urea; 37 ^{oo}										
Malonic	5.83	3.19	3.74	110	10	0-0.092	0.77-0.92	3.70-3.74	34.7-34.9	3.17-3.15
Dimethylmalonic	6.16	3.49	3.93	117	10	0-0.043	0.38-0.43	3.91-3.93	61.7-61.8	1.90-1.89
Diethylmalonic	7.42	2.85	4.16	9,330	20	0-0.66	9.2-13.3	3.94-4.16	89-106	105-88
Ethylisopropylmalonic	8.33	2.51	4.22	7,940	30	0-0.78	15.9-23.4	3.94-4.18	275-341	28.9-23.3
Succinic Acid Derivatives in 50% Ethanol; 20 ^{oa}										
<i>rac</i> - α,α' -Dimethylsuccinic	8.17	5.04	5.98	338	10	0-0.48	3.35-4.76	5.81-5.98	17.8-19.8	19-17
<i>meso</i> - α,α' -Dimethylsuccinic	7.58	4.97	5.92	103	10	0-0.30	3.46-4.93	5.74-5.92	5.13-5.76	20-18

<i>rac</i> - α,α' -Diethylsuccinic	9.22	4.76	6.01	7,250	20	0-0.55	7.9-11.1	5.82-6.01	91-104	79.7-69.7
<i>meso</i> - α,α' -Diethylsuccinic	7.43	5.37	6.04	29	10	0-0.17	1.34-1.67	5.97-6.04	5.2-5.4	5.6-5.4
<i>rac</i> - α,α' -Diisopropylsuccinic	11.44	3.66	6.63	1.5×10^7	155	0-5.56	466-861	5.81-6.63	69-245	2.2×10^6 - 6.1×10^4
<i>meso</i> - α,α' -Diisopropylsuccinic	8.10	5.98	6.40	33	10	0-0.036	0.32-0.36	6.38-6.40	19.1	1.73
<i>rac</i> - α,α' -Di(<i>t</i> -butyl)succinic	13.12	3.58	7.44	8.75×10^8	170	0-0.42	3,621-7,159	5.80-7.44	66-1,440	1.3×10^7 - 6.1×10^6
<i>meso</i> - α,α' -Di(<i>t</i> -butyl)succinic	8.29	6.43	6.83	18	10	0-0.029	0.26-0.29	6.82	11.5	1.57
Tetramethylsuccinic	10.13	4.84	6.80	5.0×10^4	10	0-8.5	44.6-83.4	5.82-6.80	23-118	2,200-420
Tetraethylsuccinic	11.42	4.78	7.35	1.1×10^6	10	0-36	185-366	5.77-7.35	31-602	35,000-1,800

Highly Substituted Malonic Acids in 50% Ethanol^{a,i}

1. -CH ₂ C ₆ H ₅	10.20	3.53	4.90	1.18×10^6	10	0-1.83	10.7-18.3	4.45-4.90	8,500-23,700	138-49.6
2. -C(C ₆ H ₅) ₂ C=CH ₂	10.22	3.33	5.30	1.9×10^6	10	0-8.8	45.7-87.5	4.3-5.3	890-4,580	2,180-424
3. -C ₂ H ₅	10.39	3.32	5.14	2.95×10^6	10	0-6.0	32.0-80.4	4.3-5.7	2,691-10,200	1,096-289
4. -CH(CH ₃) ₂	10.70	3.25	5.22	7.0×10^6	10	0-8.8	45.6-87.5	4.2-5.2	16,600-1,070	422-3,972
5. -CH(C ₆ H ₅)C ₂ H ₅	10.88	3.65	5.75	4.25×10^6	10	0-12.0	62-120	4.6-5.7	1,070-7,300	3,972-582
6. -C(CH ₃) ₃	11.15	3.39	5.34	14.4×10^6	10	0-8.3	43.6-83.4	4.4-5.3	7,200-35,700	2,000-403

^a Reference 14 (K_1 and K_2 : extrapolated to zero ionic strength). ^b Reference 13 (K_E : 0.0009-0.1 *M*). ^c No value for log K_E has been determined. The value in the table represents a linear interpolation between values for the dimethyl and diethyl derivatives. ^d References 20 and 21 (apparently 0.002-0.003 *M*). ^e Reference 16 (0.003-0.06 *M*). ^f Reference 17 (0.005-0.009 for K_E and K_1 , $K_{1,assoc}$; 0.05-0.09 for K_2 , $K_{2,assoc}$ with activity coefficient corrections). ^g Reference 18 (probably 0.02 *M*). ^h Reference 19 (0.004-0.005 *M*). ⁱ The side-chain groups listed here represent R in the structure H₂C₂(CO₂H)C(R)=CH₂. ^j Values in parentheses represent distance in ångströms between two carboxyl groups.

It does not seem obvious that this need be the case if one considers the competition from a hydrogen-bonding solvent. Also, this evidence does not prove that R is large for all diacids, since the examples include only cases with a large amount of hydrogen bonding. (It might be, for instance, that a dicarboxylic acid with strong intramolecular hydrogen bonding is distinguished from one with weak intramolecular hydrogen bonding by its large value of R .)

However, in this analysis we assume that $R \geq 10$ for all of the symmetrical dicarboxylic acids. The above discussion makes this a "reasonable" assumption only. The internal consistency of the analysis lends further support to this assumption.

C. Calculation of Microscopic Parameters. The assumption is made for all of the symmetrical dicarboxylic acids analyzed that $R \geq 10$. This establishes a base line value of log k_H for a series. It is then assumed that addition of aliphatic substituents to a dicarboxylic acid must increase the value of log k_H in analogy to the general trend of the monocarboxylic acid series. Using these two assumptions one can often limit the values of the microscopic constants to quite small ranges.

As an example of the use of this technique, consider the malonic acid series reported by Walker¹³ and by Gane and Ingold¹⁴: malonic, methylmalonic, ethylmalonic, dimethylmalonic, and diethylmalonic acids. (A discussion of the calculation of the thermodynamic constants $K_{1,assoc}$ and $K_{2,assoc}$ from the titration data for this series will be found in section III.) The association constants of these acids and their esters are given in Table II. Figure 2 shows a plot of log k_H as a function of R for each of the diacids of this series, calculated from eq 6, 7, 11, and 12. (From eq 12, $k_D = Rk_{D0}$ is substituted into eq 7. Equations 7 and 11 are solved for k_{D0} using the quadratic formula with a plus sign for the square root. Then $k_D = Rk_{D0}$, $k_H = 2K_2(1 + k_D)/(1 + 2k_{D0})$, and $E = K_1/2k_H(1 + k_D)$. The hydrogen-bonding contribution to $K_1/4k_2$ is simply $K_1/4K_2E$. For the special case of $k_{D0} = 0$, eq 6, 7, and 11 are easily solved for k_H , k_D , and E .) For malonic acid and its methyl, ethyl, and dimethyl derivatives very narrow ranges of log k_H are obtained from assuming $R \geq 10$ (refer to Table II). Note that log k_H increases progressively as the aliphatic substitution is increased. In the case of the diethyl derivative, a larger value for R_{min} is established by requiring that log k_H be greater than for the dimethyl derivative. This is true only for $R \geq 50$, so R_{min} for the diethyl derivative is 50.

D. Functional Dependence of Calculated Parameters. The four calculated parameters have the following functional dependence on the three macroscopic association constants and R

(13) J. Walker, *J. Chem. Soc.*, 61, 696 (1892).

(14) R. Gane and C. K. Ingold, *ibid.*, 2153 (1931).

$$k_D = f(R, K_2/K_E) \quad (23)$$

$$k_{DO} = f(R, K_2/K_E) \quad (24)$$

$$k_H = f(R, K_2, K_E) \quad (25)$$

$$E = f(R, K_2/K_E, K_1/K_E) \quad (26)$$

Note in particular that (1) only k_H depends on the actual values of the macroscopic association constants (the three constants k_D , k_{DO} , and E depend only on ratios of these constants (and of course, R)) and that (2) k_D and k_{DO} depend only on R and the K_2/K_E ratio, *i.e.*, there is no dependence on K_1 .

For $\log K_E/K_2$ equal to 0.4, k_D has the range 0.256–0.291 (for $R = 10$ to ∞). Since $\log K_E/K_2$ should be approximately 0.3 when k_D and k_{DO} equal zero, an error in $\log K_E/K_2$ of 0.1 (due to failure to extrapolate to zero concentration, for instance) would produce a k_D value of only about 0.3. Thus one can assume that a value of k_D greater than 0.3 or 0.4 is not due to experimental error.

II. Discussion

Bjerrum^{7a,15} explained the ratio $K_1/4K_2$ for symmetrical dibasic acids by considering the electrostatic effect of the charge on the neighboring carboxyl group acting through the solvent of dielectric constant D_{solv} . The factor $\log K_1/4K_2$ was then equal to e^2/Dr , which is just the charge of the hydrogen ion times the potential, at the point of protonation, resulting from the adjacent charged group. The distance between the charges on the symmetrical dibasic acid is r .

Bjerrum's theory gave reasonable values for the dibasic acids of formula $\text{HO}_2\text{C}-(\text{CH}_2)_m-\text{CO}_2\text{H}$ where $m \geq 2$. However, for malonic acid ($m = 1$) and for aliphatically substituted malonic, succinic, and glutaric acids, the calculated values were too small; *i.e.*, the actual effect was larger than predicted by the theory. Kirkwood and Westheimer^{7b} modified the Bjerrum theory to include the effect of the low dielectric bulk of the dibasic acid. Using the formalism of Bjerrum, they set $\log K_1/4K_2$ equal to $e^2/D_e r$, where D_e , the effective dielectric constant, is greatly decreased over that of the pure solvent, and thus consistent with the fact that Bjerrum's calculated value for r is too small.

Neither Bjerrum nor Kirkwood and Westheimer took hydrogen bonding into account. Brown, McDaniel, and Häfliger⁸ emphasized the importance of hydrogen bonding. Since the presence of hydrogen bonding may increase the value of $K_1/4K_2$, the possibility existed that hydrogen bonding might have been the reason for the failure of Bjerrum's theory. Westheimer and Benfey,⁹ introducing the assumptions cited above concerning the ester, showed that by further assuming $k_{DO} = 0$, a *maximum* effect of hydrogen bonding on the $K_1/4K_2$ ratio could be calculated. Since this effect is small in some cases where Bjerrum's calculated value of r is too small (*e.g.*, methylmalonic acid), the failure

to take into account hydrogen bonding cannot account for all cases in which Bjerrum's theory does not work.

Using the technique and assumptions outlined in this paper, it is possible to determine, usually within fairly narrow limits, the actual values of k_{DO} , k_H , k_D , E , and the effect of hydrogen bonding on the $K_1/4K_2$ ratio. It should thus be possible to determine the relative importance of various parameters (*e.g.*, the structure of the acid and the composition of the solvent) in influencing especially k_D and E . This would seem to be a valuable first step in attempting to understand the factors responsible for the strength of the intramolecular hydrogen bond and the value of E .

Table II lists acids of several series which will be discussed below. The range of values for the microscopic constants corresponds to the range of R values for $R = R_{\text{min}}$ to infinity. The experimental ratio $K_1/4K_2$ is partitioned between the charge factor E and the hydrogen-bonding factor $(1 + k_D)^2/(1 + 2k_{DO})$.

Each series is analyzed similarly to the analysis outlined for the malonic acid series above. The two assumptions used to fix the largest possible R_{min} value are (1) $R_{\text{min}} \geq 10$ for all diacids analyzed, and (2) addition of aliphatic substituents must increase $\log k_H$.

From Table II one sees that there are several examples where the hydrogen-bonding effect is dominant over the factor E in determining the $K_1/4K_2$ ratio. In fact, it is apparent that a large increase in $K_1/4K_2$ within a series is usually due to increased intramolecular hydrogen bonding. The values of k_D cover a wide range and demonstrate that it is possible for a high percentage of the monoprotonated species to be intramolecularly hydrogen bonded, even when the solvent is water. A more detailed discussion of each series follows.

A. Malonic Acid Series in Water.^{13,14} The malonic acid series consists of data determined by Walker¹³ and by Gane and Ingold,¹⁴ and analyzed as stated below, with two exceptions: ethylmethylmalonic acid and butyl(1-ethylvinyl)malonic acid.²⁰ For these two compounds no activity coefficient corrections have been made, and for the ethyl methyl derivative the $\log K_{E,\text{assoc}}$ value for the ester has been estimated from the values for the dimethyl- and diethylmalonic acids.

The first important and obvious result is that the factor E does not dramatically increase between dimethylmalonic and diethylmalonic acid. The increase in the $K_1/4K_2$ ratio is instead due to the large increase in the strength of the hydrogen bond. The actual magnitude of E is too large to be consistent with Bjerrum's theory. This could easily be rationalized on the basis of an inductive effect and thus does not in itself provide evidence for Kirkwood and Westheimer's argument. However, the gradual increase in E as the degree of aliphatic substitution is increased does

(15) J. Greenspan, *Chem. Rev.*, 12, 339 (1933).

show clearly the ability of the aliphatic side chains to increase E . The interpretation is still somewhat clouded by the possibility that the aliphatic groups might operate on the inductive effect. Thus the substituted succinic and especially the glutaric acid series, where the inductive effect should be minimal, might be important in confirming this trend.

Intramolecular hydrogen bonding appears to be fairly insignificant for the first four members of the malonic acid family. There is then a factor of 10 increase in k_D from dimethylmalonic to methylethylmalonic and another factor of 10 increase in going to diethylmalonic. As shown in Table V, sodium binding does not show this sudden jump between malonic and diethylmalonic acid. (Discussion of sodium binding to malonic acid and diethylmalonic acid is presented in section IV.)

Addition of the butyl-1-ethylvinyl derivative to the series disrupts the trend evident in previous members of the series. One might expect the very large increase in the $K_1/4K_2$ ratio to be the result mainly of a strong intramolecular hydrogen bond with a modest increase in E . Instead, there is a very large increase in E and an actual decrease in k_D .

B. Succinic Acid Series in Water.^{14,16} This series includes only two compounds. The tetramethyl substitution is assumed to increase $\log k_H$ by at least 0.1. The four methyl groups increase the value of k_D by a factor of approximately 150. E is increased by a factor of 2. The magnitude of E is entirely reasonable on the basis of the previous discussion and Table I.

*C. Acids Studied by McCoy.*¹⁷ Five compounds of this group are reasonably similar in regard to the electronic environment of the carboxyl groups and opportunity for resonance to allow comparison as a "series." They are essentially symmetrical dibasic acids with the two carboxyl groups separated by a double bond and with various degrees of aliphatic substituents added. They are the first five compounds listed under "McCoy series" in Table II and are in the order of decreasing distance between the oxygen atoms making up the hydrogen bond.

Maleic acid is considered the "parent" compound and $R = 10$ establishes a minimum value of $\log k_H$ for maleic acid of 2.74. It is assumed that the $\log k_H$ value for the other members of the "series" will be at least 2.80.

We note that the strength of the hydrogen bond increases with an increase in distance between the oxygen atoms, as concluded by McCoy. It is, however, uncertain, due to an overlap of k_D ranges, if a maximum is present in the curve of k_D vs. O...O distance as suggested by McCoy.

The value of E tends to increase with decreasing distance between the oxygen atoms which would be consistent with a Bjerrum-type electrostatic effect. However, there is a very notable exception in that maleic

acid, with the closest oxygen atoms, also has a small E value. If we line the E values up in terms of the amount of aliphatic bulk, *i.e.*, 5, 1, 4, 2, 3, we note a fairly progressive increase in E with increase in aliphatic bulk. This again points to the ability of aliphatic substituents to increase E . The actual magnitude of E is somewhat larger for 2, 3, and 4 than for the compounds shown in Table I.

*D. Malonic Acid Series in 7 M Urea.*¹⁸ The experimental values for this series were determined at 37° so direct comparison with the water series is not strictly correct. However, it would appear, as concluded by Levy, *et al.*,¹⁶ that the 7 M urea does not appreciably affect the intramolecular hydrogen bond. The large increase in k_D between the dimethyl and the diethyl derivatives is present as in water, with a further increase for ethylisopropyl. The E values again show a progressive increase with increasing size of the aliphatic substituents, with a particularly marked increase between diethyl and ethylisopropyl. It is not surprising that E values for the malonic acid series are somewhat higher than for diacids of Table I, since the inductive effect is greater and the carboxyl groups are closer together.

*E. Succinic Acid Derivatives in Ethanol.*¹⁹ The dimethyl derivatives are used to establish the base-line $\log k_H$ values: 5.75 for the *meso* acid and 5.80 for the racemic acid. The first eight compounds constitute four symmetrically substituted *meso*-racemic pairs with increasing aliphatic substitution from dimethyl to di-*t*-butyl.

Consider the eclipsed conformation of these symmetrically disubstituted succinic acids, with one carboxyl group eclipsed by the other. In the *meso* acid, one alkyl group eclipses the other, whereas in the racemic acid, the alkyl groups are eclipsed by hydrogen atoms. Assuming an unfavorable interaction between the aliphatic groups analogous to the interaction of the hydrogens on adjacent carbons of ethane, it is not surprising that the *meso* isomers inhibit intramolecular hydrogen-bond formation and that the racemic form stabilizes the hydrogen-bond formation. Thus the *meso* forms show a progressive decrease in hydrogen bond formation with increasing substitution. The racemic diisopropyl and di-*t*-butyl acids show very large increases in the intramolecular hydrogen bonding, and one would wonder if this can be explained entirely on the basis of rotational entropy decrease due to repulsive interactions between the aliphatic groups.

The E values for the *meso* forms are entirely reasonable in light of the previous discussion. The E values

(16) W. A. Bone, J. J. Sudborough, and C. H. G. Spankling, *J. Chem. Soc.*, **85**, 534 (1904).

(17) L. L. McCoy, *J. Amer. Chem. Soc.*, **89**, 1673 (1967).

(18) M. Levy and J. P. Magoulas, *ibid.*, **84**, 1345 (1962).

(19) L. Ebersson, *Acta Chem. Scand.*, **13**, 211 (1959).

For the racemic isomers are somewhat higher than for the *meso* which is consistent with a smaller average distance between the carboxyl groups. There is no steady increase in E in the *meso* isomers with increasing size of the aliphatic substituents, which is probably due to the cancellation of the effect of a decreasing effective dielectric constant and that of the increasing average distance between carboxyl groups. There is an increase in E from dimethyl to diethyl for the racemic form, but it is not possible to narrow the range of E values enough for the diisopropyl and di-*t*-butyl compounds to determine if this trend continues.

Tetraethylsuccinic acid shows an increase in k_D over the value found for tetramethylsuccinic acid. It is not possible to determine the relative magnitude of E for these two compounds due to overlap of the ranges.

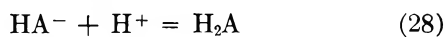
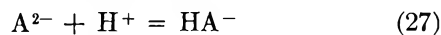
F. Highly Substituted Malonic Acids in 50% Ethanol.^{20,21} The E values are extremely large as was found also for a member of this series in water. It is interesting that the butyl(1-ethylvinyl) derivative shows a decrease in the value of E in 50% ethanol as compared to water. This is contrary to what would be expected on the basis of an electrostatic effect and to the result shown for tetramethylsuccinic acid in these two solvents. The possibility of a solvent effect is thus suggested.

The value of k_D increases in going from water to 50% ethanol for the butyl(1-ethylvinyl) derivative which is consistent with the values for tetramethylsuccinic acid. There seems to be no dramatic k_D changes within the series in 50% ethanol.

If one accepts the assumptions of this analysis, the following conclusions are evident. (1) E , which represents the effect of the ionized carboxyl compared to the effect of the unionized carboxyl, *i.e.*, includes inductive, electrostatic, and possibly solvent effects, is not, in most cases, larger than 300 for aqueous and 50% ethanol solvents. (There are exceptions to this conclusion, namely, three members of the McCoy series which have E values around 1000, and the highly substituted malonic acid derivatives of Wotiz and Merrill which have E values around 10,000.) This contrasts with the conclusion of Ebersson and Wadso²² that a $K_1/4K_2$ ratio up to 2500 is probably due *entirely* to the factor E . Our conclusion is that $K_1/4K_2$ ratios of greater than 300 are *probably* evidence for intramolecular hydrogen bonding. (2) There is in general an increase in E with increasing aliphatic substitution, but the magnitude of the change is not large. This trend is in agreement with predictions of the Kirkwood and Westheimer model, but might also be the result of interaction with solvent or inductive effects. (3) The results with regard to k_D indicate that it is possible for a very strong intramolecular hydrogen bond to exist in water solution. Particularly striking is the large increase in k_D resulting from an increase in aliphatic substitution in the malonic acid and succinic acid series.

III. Evaluation of the Apparent Constants K_1 and K_2 for the Malonic Acid Series

Consider the following reactions



$$K_1 a_H = \frac{a_{HA^-}}{a_{A^{2-}}} \quad (29)$$

$$K_2 a_H = \frac{a_{H_2A}}{a_{HA^-}} \quad (30)$$

where K_1 and K_2 represent macroscopic association constants and a refers to the activity of the species in the subscript. We define $\bar{\nu}_H$ as the average number of hydrogen ions bound per mole of total dibasic acid. It follows that

$$\bar{\nu}_H = \frac{c_{HA^-} + 2c_{H_2A}}{c_{A^{2-}} + c_{HA^-} + c_{H_2A}} = \frac{K_1 a_H \frac{f_{A^{2-}}}{f_{HA^-}} + 2K_1 K_2 a_H^2 \frac{f_{A^{2-}}}{f_{H_2A}}}{1 + K_1 a_H \frac{f_{A^{2-}}}{f_{HA^-}} + K_1 K_2 a_H^2 \frac{f_{A^{2-}}}{f_{H_2A}}} \quad (31)$$

where c and f refer to concentrations and activity coefficients, respectively, of that species in the subscript.

Equation 31 (in a different form) was used by Gane and Ingold¹⁴ for the malonic acids with activity coefficients taken as unity. The titration curves for the malonic acids were measured at concentrations varying from 0.00125 to 0.05 M and the final K_1 and K_2 values were found by extrapolation to zero concentration.

There are three concentration-dependent factors that need to be considered: (a) activity coefficients, (b) dimerization, and (c) cation binding (sodium ions in the case of Gane and Ingold's malonic acid data).

We have analyzed Gane and Ingold's data using a curve-fitting routine to obtain a least-squares fit to the data. The Debye-Hückel theory was used to obtain activity coefficients with

$$\log f_H = \frac{-0.509\sqrt{I}}{1 + 1.6\sqrt{I}} \quad (32)$$

where I is the ionic strength, $f_{A^{2-}} = f_H^4$ and $f_{HA^-} = f_H$.

Table III gives the calculated values for constants for malonic acid using activity coefficient corrections. The averages of these values, $\log K_1 = 5.67$ and $\log K_2 = 2.81$, agree well with the extrapolated values reported by Gane and Ingold ($\log K_1 = 5.69$, $\log K_2 = 2.83$).

(20) J. H. Wotiz and H. E. Merrill, *J. Amer. Chem. Soc.*, **80**, 866 (1958).

(21) H. E. Merrill, Thesis, University of Pittsburgh, 1957.

(22) L. Ebersson and I. Wadso, *Acta Chem. Scand.*, **17**, 1552 (1963).

Table III: Constants for the Association of H⁺ with Malonic Acid

Concn of malonic acid, <i>M</i>	Calculated with Debye-Hückel activity coefficients		Calculated by Gane and Ingold	
	log <i>K</i> ₁	log <i>K</i> ₂	log <i>K</i> ₁	log <i>K</i> ₂
0.05	5.71	2.79	5.38	2.75
0.02	5.66	2.84	5.59	2.80
0.01	5.70	2.83	5.62	2.82
0.01	5.70	2.81	5.62	2.81
0.004	5.68	2.78	5.68	2.82
0.00125	5.63	2.81	5.67	2.83

The constant for dimerization of the short-chain carboxylic acids, 0.2 to 0.7, already reported²³ and the value of 6.7 for the binding of sodium ion to the malonate ion reported below, indicate a minor amount of dimerization and sodium binding, respectively. The lack of consistent variation in the corrected values (Table III) as a function of concentration is in agreement with this conclusion. (No activity coefficient corrections were made on the ester compounds.)

IV. Binding of Sodium Ions to Malonic Acid

The hydrogen-bonding constant is approximately 16 for diethylmalonic acid compared to 0.12 to 0.7 for the preceding malonic acid derivatives in the series. To test the possibility of a similar pattern for sodium binding, the binding of sodium to malonic acid and diethylmalonic acid was measured. Previous estimates of the binding of sodium to malonic acid are found in ref 24.

A. Experimental Section. Binding of the sodium ion to the dianionic species of malonic acid (A²⁻) was studied by the use of two different cells, each being essentially as shown in Figure 2 of ref 25, *i.e.*, with two calomel half-cells, each connected to a solution on one side of the membrane by a density stabilized liquid junction. One cell developed a potential across a permselective negatively charged Nalfilm membrane (referred to as Nalfilm electrode) supplied by the National Aluminate Corp., Chicago, Ill. The other cell developed a potential across a sodium-sensitive glass (referred to as sodium glass electrode).²⁶

The experimental procedure consisted of first placing the same reference NaCl solution on both sides of the membrane. Under these conditions, the potential developed was usually 0.2 mV or less. Then the unknown was placed on one side of the membrane and read against two different concentrations of reference solution, one chosen to give a positive millivolt reading and the other a negative millivolt reading (usually ±5 mV). The equation for the potential developed across the membrane separating the reference and unknown solutions of activity $a_{\text{Na}^{\text{ref}}}$ and $a_{\text{Na}^{\text{un}}}$, respectively (any potential due to asymmetry between the half-cells is subtracted), is

$$\Delta E \text{ (mV)} = 59.2 \log \frac{a_{\text{Na}^{\text{un}}}}{a_{\text{Na}^{\text{ref}}}} \quad (33)$$

In terms of concentrations, the potential (assuming the concentration of the unknown solution is held constant) is given by

$$\Delta E \text{ (mV)} = \text{constant} - 59.2 \log f_{\text{Na}^{\text{ref}}} - 59.2 \log c_{\text{Na}^{\text{ref}}} \quad (34)$$

where $f_{\text{Na}^{\text{ref}}}$ and $c_{\text{Na}^{\text{ref}}}$ are the activity coefficient and concentration, respectively, of the sodium ion in the reference solution.

Thus a plot of $\log c_{\text{Na}^{\text{ref}}}$ will be approximately linear with ΔE (mV) as long as the range of $c_{\text{Na}^{\text{ref}}}$ is small enough to ensure that $f_{\text{Na}^{\text{ref}}}$ is approximately constant over this range. This was found to be true in the ±5 mV range in which the measurements were taken. Later, just two points were taken, one on each side of the unknown solution. Interpolation between these points to 0 mV gives the concentration of reference solution of NaCl that would produce a zero potential compared to the unknown solution. The activity of sodium ion in reference solution of this concentration is equal to that in the unknown solution.

B. Results. 1. Measurements with Nalfilm Electrode. Because of incomplete neutralization of the H₂A species with NaOH in this work, it is necessary to consider the HA⁻ species as well as A²⁻ and NaA⁻. Experimentally determined values for NaA⁻ can be calculated from the following equations. From the known value for the concentration of reference solution of NaCl that gives a 0 mV reading, one calculates the activity of sodium ion, which is the same on both sides of the membrane at the interpolated point of 0 mV

$$a_{\text{Na}^{\text{un}}} = a_{\text{Na}^{\text{ref}}} = f_{\text{Na}^{\text{ref}}} \cdot c_{\text{Na}^{\text{ref}}} \quad (35)$$

$$\log f_{\text{Na}^{\text{ref}}} = \frac{-0.509\sqrt{I}}{1 + 1.6\sqrt{I}} \quad (36)$$

$$I = c_{\text{Na}^{\text{ref}}} \quad (37)$$

The following equations refer to the unknown side, where Ma designates the acid

$$c_{\text{Na}^{\text{un}}} = \frac{a_{\text{Na}^{\text{un}}}}{f_{\text{Na}^{\text{un}}}} \quad (38)$$

$$c_{\text{A}^{2-}} = c_{\text{Na}^{\text{un}}} - c_{\text{Ma}^{\text{tot}}} \quad (39)$$

$$I = 2c_{\text{Na}^{\text{un}}} - c_{\text{Ma}^{\text{tot}}} \quad (40)$$

(23) A. Katchalsky, H. Eisenberg, and S. Lifson, *J. Amer. Chem. Soc.*, **73**, 5889 (1951).

(24) J. A. Barclay, M. J. Hickling, and K. White, *Biochem. J.*, **99**, 11P (1960).

(25) W. R. Carroll, J. M. Callahan, and H. A. Saroff, *J. Biol. Chem.*, **234**, 2314 (1959).

(26) The authors wish to thank Professor G. Eisenman for the sample of sodium-sensitive glass.

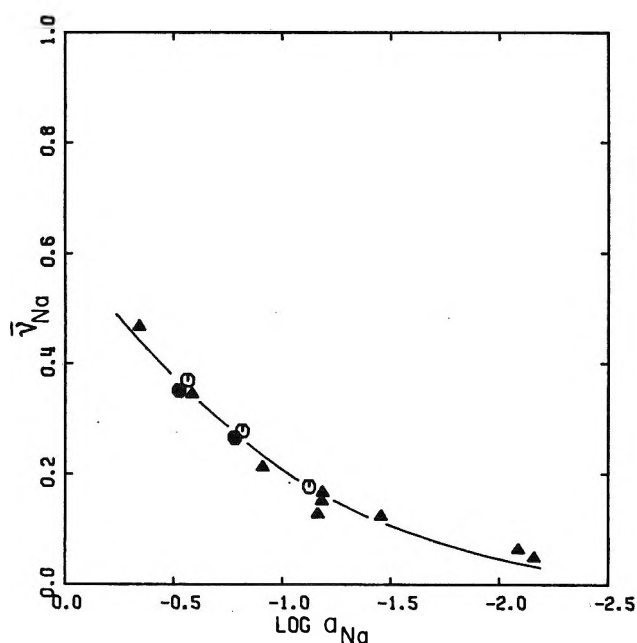


Figure 5. Average number of sodium ions bound, $\bar{\nu}_{Na}$, as a function of $\log a_{Na}$: \blacktriangle , malonic acid points using Nalfilm electrode; \circ , malonic acid points using sodium glass electrode; \bullet , diethylmalonic acid points using sodium glass electrode. Curve represents least-squares fit of Nalfilm electrode data, which results in a value for k_{Na} of 6.66.

One then solves eq 38, 39, 40, and 36 iteratively until a constant value of f is obtained. Then

$$c_{NaA}^{-\text{exptl}} = c_{Na}^{\text{tot,un}} - c_{Na}^{\text{un}} \quad (41)$$

$$\bar{\nu}_{Na}^{\text{exptl}} = \frac{c_{NaA}^{-\text{exptl}}}{c_{NaA}^{-\text{exptl}} + c_{A^{2-}}^{\text{exptl}}} \quad (42)$$

The $\bar{\nu}_{Na}^{\text{exptl}}$ can now be compared to a calculated value of $\bar{\nu}_{Na}$ for various values of k_{Na} until a best least-squares solution is found. This is accomplished by use of the following equations

$$k_{Na} = \frac{a_{NaA}^{-}}{a_{Na} \cdot a_{A^{2-}}} = \frac{c_{NaA}^{-}}{c_{Na} \cdot f_{Na}^4 \cdot c_{A^{2-}}} \quad (43)$$

$$c_{Na} = c_{Na}^{\text{tot}} - c_{NaA}^{-} \quad (44)$$

$$c_{HA^{-}} = c_{Ma}^{\text{tot}} - c_{NaA}^{-} - c_{A^{2-}} \quad (45)$$

$$c_{Na} = c_{HA^{-}} + c_{NaA}^{-} + 2c_{A^{2-}} \quad (46)$$

$$I = c_{HA^{-}} + 3c_{A^{2-}} + c_{NaA}^{-} \quad (47)$$

From (43), (44), and (45), one can express eq 46 as a quadratic in A^{2-} and solve for A^{2-} , then for HA^{-} and NaA^{-} and iterate to constant f_{Na} , using once again eq

36 to calculate f_{Na} . Table IV shows the results of these calculations. The calculated values of $\bar{\nu}_{Na}$ were obtained by using the k_{Na} that gives the best (least-squares) fit of the data. This value is 6.66, which agrees well with that reported by Barclay, *et al.*²⁴

Table IV: Binding of Sodium Ion to Malonate Ion Studied with Nalfilm Electrode

c_{Na}^{ref}	$c_{Na}^{\text{tot,un}}$	c_{Ma}^{tot}	$a_{Na}^{\text{un,ref}}$	$\bar{\nu}_{Na}^{\text{calcd}}$	$\bar{\nu}_{Na}^{\text{exptl}}$
0.16535	0.18926	0.100	0.124	0.238	0.204
0.08654	0.0946	0.050	0.0685	0.168	0.117
0.009005	0.009463	0.005	0.00818	0.0377	0.0667
0.6904	0.916	0.498	0.455	0.448	0.497
0.373	0.458	0.249	0.260	0.348	0.350
0.0828	0.0916	0.0498	0.0657	0.166	0.147
0.08196	0.0916	0.0498	0.0651	0.166	0.170
0.042	0.0458	0.0249	0.0351	0.112	0.127
0.0088	0.00916	0.00498	0.0080	0.0368	0.0495

2. Measurements Using Sodium Glass Electrode.

The above data were confirmed using the sodium glass electrode. Each measurement was used to calculate k_{Na} from eq 43 and c_{Na}^{exptl} from eq 44. The quantities needed are obtained from an iterative solution of the following equations plus eq 36 and 38

$$c_{NaA}^{-} = c_{Na}^{\text{tot,un}} - c_{Na}^{\text{un}} \quad (48)$$

$$c_{A^{2-}} = c_{Ma}^{\text{tot}} - c_{NaA}^{-} \quad (49)$$

$$I = 3c_{A^{2-}} + c_{NaA}^{-} \quad (50)$$

Samples of both malonic acid and diethylmalonic acid were examined for sodium binding. The results are tabulated in Table V. The calculated values of $\bar{\nu}_{Na}$ are also shown in Figure 5, although these points were not used to obtain the best fit of the equation to the experimental points.

Table V: Binding of Sodium Ion to Malonate and Diethyl Malonate Ions Studied with the Sodium Glass Electrode

c_{Na}^{ref}	$c_{Na}^{\text{tot,un}}$	c_{Ma}^{tot}	$a_{Na}^{\text{un,ref}}$	$\bar{\nu}_{Na}^{\text{exptl}}$	k_{Na}
0.096 ^a	0.109	0.0545	0.0753	0.178	6.58
0.39435 ^a	0.50	0.25	0.273	0.370	7.14
0.2078 ^a	0.25	0.125	0.153	0.279	7.10
0.435 ^b	0.5454	0.2727	0.300	0.351	6.18
0.2283 ^b	0.2727	0.1363	0.166	0.266	6.27

^a Malonic acid. ^b Diethylmalonic acid.

NOTES

Nuclear Magnetic Resonance Studies of 2-Pyridones, 2-Pyridithiones, and 2-Thioalkylpyridines¹

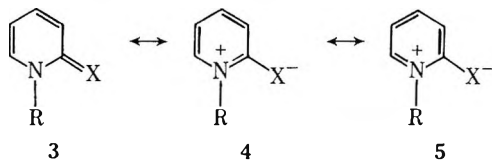
by W. E. Stewart and T. H. Siddall, III

Savannah River Laboratory, E. I. du Pont de Nemours and Company,
Aiken, South Carolina 29801 (Received November 13, 1969)

The higher barriers to rotation around the C(X)-N bond in thionamides (X = S) as compared to the corresponding amides (X = O) have been attributed to the greater contribution in the former case of resonance structure **2** to the ground state.² Upon the basis of this



proposal, the ring π -electron delocalization, or aromaticity,^{3a,3b} of 2-pyridithiones (**3**, X = S) should be greater than that of 2-pyridones (**3**, X = O) because of the greater contributions of structures **4** and **5** to the ground state of 2-pyridithiones. This line of reasoning has been used to explain the much larger dipole moment of 2-pyridithiones as compared to the corresponding 2-pyridones.⁴ Jackman and coworkers, de-



fining aromaticity as the ability to sustain a ring current, have concluded from a study of the chemical shifts of methyl protons attached to the 2-pyridone ring^{3a} and from SCF calculations^{3b} that 2-pyridones possess about 35% of the aromaticity of the benzene ring. Analyses of the pmr spectra (using computer program LAOCN3⁵) of several N-substituted 2-pyridones, 2-pyridithiones, and 2-thioalkylpyridines show that the 2-pyridithiones do indeed exhibit greater delocalization as evidenced by the trends in the pmr parameters in the series pyridone \rightarrow pyridithione \rightarrow pyridine.

Experimental Section

The compounds in this study that were not commercially available were prepared by conventional means.^{3a,6} 4-*t*-Butyl-1-methyl-2-pyridone and 1-deu-

teriomethyl-2-pyridone were prepared by the oxidation of the corresponding 1-methylpyridinium sulfates.⁷ The 2-pyridithiones were prepared by the action of P₂S₅ on the corresponding oxygen compounds.⁸ The 2-thioalkylpyridines were prepared by alkylation of the potassium salt of 2-pyridithiones in ethanolic solution.⁹ All compounds were purified by vacuum distillation, recrystallization, or both.

The samples for nmr analysis consisted of 20 wt % of the compound in a specified solvent and were degassed and sealed under vacuum. The spectra were calibrated by the usual side-band method, using TMS as internal standards on a Varian A-60 or an HR-60 nmr spectrometer at probe temperature. The reported line positions are averages of four forward and four reverse sweeps. Average deviations were always less than 0.08 cps.

Results and Discussion

The observed ring proton coupling constants and chemical shifts are listed in Table I. The values obtained for the pyridones and pyridithiones agree with previously reported first-order analyses for some of the compounds^{3a,10} and with an exact analysis reported for N-methyl-2-pyridone in CDCl₃.¹¹ The values for 2-thioalkylpyridine coupling constants are close to those reported for 2-methoxypyridine.¹¹

Coupling across the fixed double bonds C₃-C₄ and C₅-C₆ decreases, but coupling across the single bond C₄-C₅ increases in going through the series pyridone \rightarrow pyridithione \rightarrow pyridine. The decreases in J_{34} and J_{56} indicate a decrease in the double-bond character of

(1) The information contained in this article was developed during the course of work under Contract AT(07-2)-1 with the U. S. Atomic Energy Commission.

(2) R. C. Neuman, Jr., D. N. Roark, and V. Jonas, *J. Amer. Chem. Soc.*, **89**, 3412 (1967), and references therein.

(3) (a) J. A. Elvidge and L. M. Jackman, *J. Chem. Soc.*, 859 (1961); (b) G. G. Hall, A. Fardisson, and L. M. Jackson, *Tetrahedron*, **19**, 101 (1963).

(4) M. H. Krackov, C. M. Lee, and H. G. Mautner, *J. Amer. Chem. Soc.*, **87**, 892 (1965).

(5) A revised version of LAOCOON II described by S. M. Castellano and A. A. Bothner-By, *J. Chem. Phys.*, **41**, 3863 (1964).

(6) D. J. Cook, R. E. Bowen, P. Sorter, and E. Daniels, *J. Org. Chem.*, **26**, 4949 (1961).

(7) E. A. Prill and S. M. McElvain, *Org. Syn.*, **2**, 419 (1943).

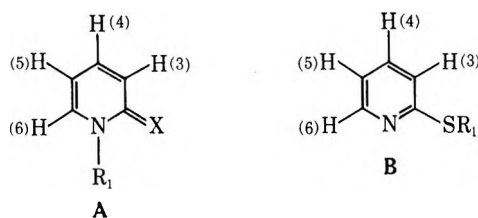
(8) R. B. Wagner and H. D. Zook, "Synthetic Organic Chemistry," John Wiley and Sons, New York, N. Y., 1953, p 827.

(9) J. Renalt, *Ann. Chim. (Paris)*, **10**, 135 (1955).

(10) C. L. Bell, R. S. Egan, and L. Bauer, *J. Heterocycl. Chem.*, **2**, 420 (1965).

(11) R. H. Cox and A. A. Bothner-By, *J. Phys. Chem.*, **73**, 2465 (1969).

Table I: Nmr Parameters of Ring Protons of Substituted 2-Pyridones (A, X = O), 2-Pyridithiones (A, X = S), and 2-Thioalkylpyridines B



Substituents	Solvent	ν_3^a	ν_4	ν_5	ν_6	J_{34}^b	J_{35}	J_{36}	J_{45}	J_{46}	J_{56}
2-Pyridones											
$R_1 = CD_3$	DMSO	385.57	445.17	372.27	462.03	9.13	1.38	0.71	6.62	2.13	6.71
	CCl_4	379.95	434.20	362.72	450.04	9.16	1.37	0.72	6.63	2.13	6.71
$R_1 = CH_3$	TFA ^c	449.68	494.95	442.03	489.22	8.72	1.25	0.65	7.40	1.76	6.55
$R_1 = Et$	DMSO	382.89	443.61	372.64	461.35	9.08	1.33	0.64	6.60	2.08	6.70
	CH_3OH	392.13	449.75	382.54	458.49	9.09	1.32	0.65	6.73	2.08	6.81
	C_6D_6	389.84	423.99	354.98	431.96	9.12	1.32	0.73	6.62	2.17	6.74
$R_1 = 2\text{-propyl}$	DMSO	383.21	442.24	375.42	462.64	9.13	1.44	0.71	6.63	2.04	6.79
$R_1 = CH_3, R_6 = CH_3^d$	C_6D_6	384.53	431.29	361.62	...	9.12	1.33	...	6.83
$R_1 = CH_3, R_4 = t\text{-butyl}$	$CDCl_3$	392.64	...	373.29	437.37	...	2.16	0.53	7.06
2-Pyridithiones											
$R_1 = CH_3$	DMSO	450.40	440.40	406.28	492.65	8.69	1.42	0.79	7.10	1.67	6.62
$R_1 = Et$	DMSO	450.04	439.55	408.72	487.64	8.68	1.50	0.75	6.98	1.72	6.54
$R_1 = 2\text{-propyl}$	DMSO	452.63	437.06	410.84	489.12	8.65	1.63	0.67	6.86	1.62	6.66
$R_1 = CH_3, R_4 = t\text{-butyl}$	DMSO	445.31	...	412.57	485.64	...	2.33	0.55	6.95
2-Thioalkylpyridines											
$R_1 = CH_3$	DMSO	436.98	457.23	425.09	507.56	8.14	1.02	0.99	7.37	1.88	4.91
$R_1 = Et$	DMSO	434.95	456.24	424.35	506.81	8.07	1.03	0.98	7.39	1.91	4.97
$R_1 = 2\text{-propyl}$	DMSO	434.02	456.49	424.81	507.21	8.04	1.05	0.98	7.36	1.93	4.92

^a In Hz from TMS at 60 MHz. ^b In Hz. ^c From ref 11. ^d $\nu_{C-CH_3} = 140.84$, $J_{H(3)-CH_3} = 0.69$, $J_{H(4)-CH_3} = 0.00$, $J_{H(5)-CH_3} = 0.74$.

the C_3-C_4 and the C_5-C_6 bonds, but the increase in J_{45} indicates an increase in the C_4-C_5 double-bond character, as would be expected for increasing delocalization.¹²⁻¹⁵

Of the four-bond coupling constants, J_{35} is the same for the pyridithiones as for the pyridones, but J_{46} is about 0.45 cps less for the pyridithiones than for the pyridones. The fact that J_{35} does not change but J_{46} does suggests that the change in J_{46} may be partly due to the increased positive charge on the nitrogen atom in the more polar pyridithiones. (J_{46} increases from 1.79 in pyridine to 1.54 in N-protonated pyridine, but J_{35} shows no significant decrease.)¹⁶

Within a series, neither solvent nor nature of the N-alkyl or S-alkyl substituent has a significant effect upon the coupling constants; however, the remaining coupling constants change when a *t*-butyl group is substituted into the 4-position in N-methyl-2-pyridone and N-methyl-2-pyridithione. The directions and magnitudes of the coupling constant changes are the same

as those for the corresponding benzene ring proton coupling constants when a *t*-butyl group is substituted.¹⁷

In the pyridones and pyridithiones with $R_1 = CH_3$ and $R_6 = H$, coupling between the N- CH_3 protons and H_6 was large enough to obscure the H_3-H_6 coupling, but was not large enough to be resolved. In these cases it was necessary to use deuterium substitution or decoupling of the N- CH_3 protons. With $R_1 = ethyl$ or 2-propyl, the only observable effect of the coupling was a slight broadening of the H_6 lines.

(12) N. Jonathan, S. Gordon, and B. P. Dailey, *J. Chem. Phys.*, **36**, 2443 (1962).

(13) W. B. Smith, W. H. Watson, and S. Chiranjeevi, *J. Amer. Chem. Soc.*, **89**, 1438 (1967).

(14) H. Günther, *Tetrahedron Lett.*, 2967 (1967).

(15) S. Castellano and R. Kostelnik, *J. Amer. Chem. Soc.*, **90**, 141 (1967).

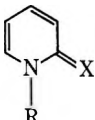
(16) J. B. Merry and J. H. Goldstein, *ibid.*, **88**, 5560 (1966).

(17) S. Castellano and R. Kostelnik, *Tetrahedron Lett.*, 5211 (1967).

The chemical shifts of the ring protons are quite dependent on concentration and solvent. Because the measurements were not extrapolated to infinite dilution, no attempts are made to rationalize the solvent shifts (with the exception of the benzene solvent shifts) or the shifts within a series. There are significant changes in the proton shifts in going from pyridones to pyridthiones, however. Protons H₃, H₅, and H₆ are shifted downfield by about 64 Hz, 34 Hz, and 30 Hz, respectively, but H₄ undergoes a slight upfield shift. Downfield shifts of the ring protons in the pyridthiones are consistent with increased ring current and the larger -C=X group anisotropy shifts to be expected in pyridthiones.¹⁸⁻²¹ The upfield shift of H₄ is not easily explained. It could arise from increased charge density on C₄, but this is unlikely. Previous studies of the magnetic anisotropy effect in amides suggest that protons in the plane of the amide group are deshielded.²² Thus, if the amide group is replaced with the more anisotropic thionamide group,²³ the H₄ resonance should shift downfield. Possible explanations of this presumably anomalous behavior are that H₄ lies in a nodal region or that the anisotropic field of the thionamide group does not have the same shape as that of the amide group.

The chemical shifts of the protons of the N-alkyl groups are given in Table II. The 19-Hz downfield

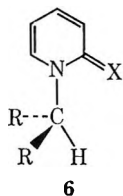
Table II: Proton Chemical Shifts of N-Substituents of



in DMSO

X	R	Hz from TMS		
		ν_{CH_3}	ν_{CH_2}	ν_{CH}
O	CH ₃	215.0		
S	CH ₃	233.7		
O	C ₂ H ₅	81	245	
S	C ₂ H ₅	80	273	
O	2-propyl	83.0		325
S	2-propyl	83.5		372

shift of the N-CH₃ protons in pyridthiones as compared to that in pyridones is consistent with a larger anisotropy in pyridthiones and with a freely rotating methyl group. The much larger downfield shifts of the α protons of the N-ethyl and N-isopropyl groups suggests that the preferred conformations in these cases are those with the β methyl groups oriented away from the carbonyl group, as in structure 6.



- (18) K. Nagarajan, M. D. Nair, and P. M. Pillai, *Tetrahedron*, **23**, 1683 (1967).
 (19) P. L. Southwick, J. A. Fitzgerald, and G. F. Milliman, *Tetrahedron Lett.*, 1247 (1965).
 (20) R. Greenhalgh and M. A. Weinberger, *Can. J. Chem.*, **43**, 3340 (1965).
 (21) H. Booth and A. H. Bostock, *Chem. Commun.*, 637 (1967).
 (22) R. F. C. Brown, L. Radom, S. Sternhell, and I. D. Rae, *Can. J. Chem.*, **46**, 2577 (1968), and references therein.
 (23) P. V. Demarco, D. Doddrell, and E. Wenkert, *Chem. Commun.*, 1418 (1969).

The Dimerization of the Tetracyanoethylene Anion Radical

by Raymond Chang

Department of Chemistry, Williams College,
 Williamstown, Massachusetts 01267 (Received December 8, 1969)

In recent years the dimerization reaction of radicals in solution has been successfully studied by the electron spin resonance (esr) and optical techniques. For example, the Wurster blue perchlorate cation radical¹ and tetracyanoquinodimethan anion radical² are known to form diamagnetic dimers in solution. Aromatic ketyl radicals³ and certain pyridinyl radicals,⁴ on the other hand, dimerize to form biradical species. We report here yet another radical dimerization reaction—that between the tetracyanoethylene (TCNE) anion radicals to form the diamagnetic dimer. The existence of this dimer has recently been postulated by Freed, *et al.*, in their study of Heisenberg spin exchange processes.⁵

At room temperature the esr spectrum of the TCNE anion radical prepared by the reduction with sodium in 2-methyltetrahydrofuran shows the expected nine lines. The intensity of the lines increased with decreasing temperature, reaching a maximum at about -60°. Below this temperature the integrated intensity decreased with decreasing temperature, in contrast to Curie's law. The line shape did not vary appreciably between -90 and -140°, however, and the hyperfine splitting constant remained virtually unchanged throughout. Following Kawamori, *et al.*,¹ we write the equilibrium constant for the dimerization $2\text{TCNE}^- \rightleftharpoons (\text{TCNE}^-)_2$ as $K = K_0 \exp(-\Delta H/RT) = (1 - \alpha)/$

- (1) A. Kawamori, A. Honda, N. Joo, K. Suzuki, and Y. Ooshika, *J. Chem. Phys.*, **44**, 4363 (1966).
 (2) R. H. Boyd and W. D. Phillips, *ibid.*, **43**, 2927 (1965).
 (3) N. Hirota and S. I. Weissman, *J. Amer. Chem. Soc.*, **86**, 2538 (1964).
 (4) M. Itoh and E. M. Kosower, *ibid.*, **89**, 3655 (1967).
 (5) M. P. Eastman, R. G. Kooser, M. R. Das, and J. H. Freed, *J. Chem. Phys.*, **51**, 2690 (1969).

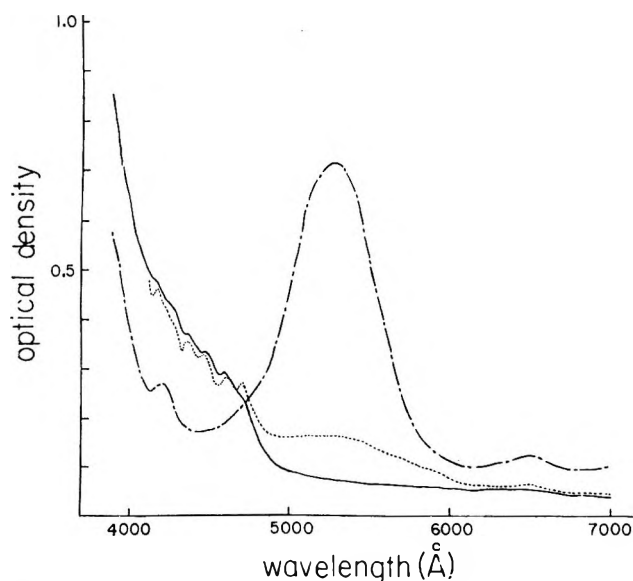


Figure 1. Temperature dependence of the absorption spectra of the tetracyanoethylene anion radical in 2-methyltetrahydrofuran: concentration, approximately $1 \times 10^{-3} M$; light path length, 0.2 cm; —, at room temperature; — —, at -90° ; - · - ·, at -195° .

$2c\alpha^2$, where c is the stoichiometric concentration of the radical anion and α is the fractional concentration of the monomer which is given by IT/c where I is the relative intensity. The extent of dimerization depends strongly on the radical concentration, and using values of c between $2 \times 10^{-4} M$ and $1 \times 10^{-3} M$ we obtain a value of $-8 \text{ kcal mol dimer}^{-1}$ for the heat of dimerization. No rigid media esr spectra could be detected at liquid nitrogen temperature. This suggests that the dimer is most probably diamagnetic. The visible spectra of TCNE^- at 25, -90 , and -195° are shown in Figure 1. The bright yellow color of the monomer has no absorption band between 5000 \AA and 7000 \AA whereas the dimer, which is pink, has an ϵ_{max} at 5300 \AA . Changes in both the esr and optical spectra are reversible with temperature.⁶

Acknowledgment. The author is pleased to acknowledge funds made available as part of a grant to Williams College by the Alfred P. Sloan Foundation.

(6) NOTE ADDED IN PROOF. After this paper was submitted, M. Itoh [*J. Amer. Chem. Soc.*, **92**, 886 (1970)] reported a similar dimerization reaction of the TCNE anion radical.

COMMUNICATIONS TO THE EDITOR

Proposed Temperature Effects on the Phosphorescence Lifetime of Benzene in Glasses at 77°K ^{1a,b}

Sir: Leubner^{1b} has obtained phosphorescence lifetime (τ) data for benzene- h_6 (H6) as a function of temperature in three glassy media.^{1b} At 77°K , τ increases rapidly as T decreases. We found that τ rose slowly (over hours) for benzene at 77°K , an effect we related to relaxation of the glassy solvents.² The measurement of the temperature dependence of τ (which we abbreviate as $\tau(\text{temp})$) led Leubner to suggest that $\tau(\text{temp})$ (and not glass relaxation) effects accounted for the phenomena we reported. The central issue involves the time needed for the system to equilibrate with respect to temperature. As we will show below, temperature effects of the kind proposed^{1b} are incapable of accounting for the observations.²

Our earlier note concerned changes in τ observed over extended periods of time (\sim hours) for both benzene- d_6 (D6) and H6 in glasses having T_g near 77°K . No such changes in τ were found for other kinds of sol-

vents, whether crystalline, amorphous, or glassy—with T_g not near 77°K . Taken together, these comprise four cases which were examined to test the consistency of the results with the idea of a "relaxation effect." Of these four cases, only one has been considered in ref 1b: H6 in solvents that form glasses which relax around 77°K .

First some clarifications of our note² are in order.³ The relaxation effect has been observed for degassed, sealed (partially evacuated), and open (corked) samples with no systematic differences in τ , τ_E (the time the sample takes to equilibrate, as indicated by a constant τ), or the character of the decay (which was generally

(1) (a) Supported in part by The National Research Council of Canada. (b) This communication is in reply to a communication by I. H. Leubner, *J. Phys. Chem.*, **73**, 2088 (1969). The editor regrets his error in not arranging to have the two communications published in the same issue.

(2) T. E. Martin and A. H. Kalantar, *J. Phys. Chem.*, **72**, 2265 (1968).

(3) Some corrections are also necessary: the solvents were transparent to 2500 \AA and the uv cutoff (1.0 optical density) was at no greater wavelength than 2200 \AA (except for EPA). The quartz sample tubes were 0.8 cm (not mm) o.d. The intensity ratios used for the τ measurements were 0.48 and 0.048. We also note that the τ reported are the observed values, uncorrected for instrumental error ($<1\%$) or, for example, for any C_6HD_5 in D6.

nonexponential). Lamp intensity made no difference either. We found no differences between relaxation effects as indicated by D6 or H6 (or several other deuteriobenzenes). The effect as shown in Figure 1 and the τ_E listed in the tables of ref 2 are typical but not invariant because the effect is irregular even for the same sample: sometimes τ_E is considerably shorter; occasionally τ leveled out at lifetimes $< \tau_{m_2}$ for a period. Extreme irregularities (*e.g.*, very short τ_E) occurred for less than 10% of the more than 50 runs made on a score of 3-methylpentane (3MP) samples. Repeated efforts, under carefully controlled conditions, to ascertain the exact form of the τ vs. time curve over the first hour were unavailing because of irregularities. (This irregular behavior may be related to the attainment of the final (random) glassy configuration in which the solvent settles.) Likewise, we have been unsuccessful in cracking the strained glass at will to test whether this strain-relieving event is accompanied by a sudden jump in τ to τ_m , as we once chanced to observe for D6 in 3MP. Notwithstanding the irregularities, however, the observed lifetimes increased with time in solvents whose T_g is near 77°K. Lifetimes never decreased over time for any environment, glass or otherwise.

We now present two considerations that cast doubt on the generality of the proposal of ref 1b. 1. It has been implicitly assumed^{1b} that $\tau(\text{temp})$ for D6 is approximately the same as for H6, *i.e.*, that the slopes at 77°K are quite comparable (even though it is stated^{1b} that $\tau(\text{temp})$ curves cannot be predicted). Given the data^{1b,2} this must be the case if Leubner's hypothesis^{1b} is correct. Nieman, *et al.*, have shown^{4,5} that the $\tau(\text{temp})$ curves for D6 are considerably displaced from those of H6 in three different environments. In particular, the region in which τ changes most for D6 appears⁵ to lie $\sim 25^\circ\text{K}$ higher than the corresponding region for H6. We therefore regard it as quite probable that the $\tau(\text{temp})$ curves for D6 in at least one (if not all) of the three glasses examined^{1b} will be such that τ for D6 will be relatively temperature insensitive near 77°K, as is the case for D6 in stable cyclohexane-*h*₁₂⁴ or -*d*₁₂⁵.

2. We have found a "relaxation effect" on the lifetime for all three of the glasses in which $\tau(\text{temp})$ for H6 was examined.^{1b} We feel some solvent in which no such effect has been found (*e.g.*, isopropyl alcohol (IPOH)^{2,6}) should also have been used for a $\tau(\text{temp})$ study for H6. The proposal of ref 1b requires the lifetimes to be essentially temperature independent at 77°K in such a system, provided the cooling procedures and rates are substantially the same for these solvents (they are, see below).

When Nieman's data for H6 in stable cyclohexane⁵ are replotted on the figure of ref 1b, it is found that they fall between the EPA and 3MP curves. The slope for the cyclohexane data at 77°K is distinctly not zero, being essentially equal to those of the glasses, namely

about 0.3 sec/deg. However, we have observed *no* relaxation effect for H6 in stable (or for D6 in metastable) cyclohexane.^{2,7}

The two points above merely suggest ways of testing the proposal^{1b} by extending $\tau(\text{temp})$ measurements to crucial test cases. The results of such measurements could either be consistent with (though not prove) or disprove the hypothesis.^{1b} It is unfortunate that we are not equipped to make such checks.

There is, however, a third test that can be made: this involves determination of the length of time it takes the sample, immersed⁸ in liquid nitrogen, to reach the bath temperature. Crude measurements⁸ were referred to in ref 2; however, the error was $\pm 1^\circ$. We have since increased the sensitivity of the measurements and extended them to several other solvents including (N means no "relaxation effect" is observed): cyclohexane (N), isooctane (N), methylcyclohexane (as glass⁷), IPOH (N), EPA, 3MP, 3-methylhexane, 3-methylheptane (N), and the 2,4- and 2,5-dimethylhexane mixture. A type K-3 potentiometer and 14-mm o.d. tubes were used. A centered, four-junction iron-constantan thermopile (with the reference taped to the outside of the sample tube) was also used. Thin (AWG No. 63) wire was used to minimize heat flow through the thermopile.

The temperature difference was monitored as a function of time. The temperature fell nearly exponentially over the range from more than 100° to less than 1° above the bath temperature for all solvents and for the empty tube. Then the cooling rate slowed. The temperature at the sample's center is 1° higher than the liquid nitrogen bath after 3–4.5 min. It is 0.1° higher after only 5–8 min depending upon the solvent.⁹ The results varied nearly as much for a given solvent as they did for the different glassy solvents irrespective of whether they show "relaxation effects" on τ or not.¹⁰ Cooling times measured in a 9-mm o.d. tube are 1–2 min shorter. These times are very much shorter than those required by combining the proposal of ref 1b with our figure² (*e.g.*, 0.5° difference in EPA after 1 hr). In an independent experiment, the temperature of the

(4) G. F. Hatch, M. D. Erlitz, and G. C. Nieman in "Molecular Luminescence," E. Lim, Ed., W. Benjamin, Inc., New York, N. Y., 1969, p 21.

(5) G. F. Hatch, M. D. Erlitz, and G. C. Nieman, *J. Chem. Phys.*, **49**, 3723 (1968).

(6) T. E. Martin and A. H. Kalantar, *ibid.*, **48**, 4996 (1968).

(7) T. E. Martin and A. H. Kalantar, *ibid.*, **49**, 244 (1968).

(8) The sample tubes (1 mm thick walls) were immersed in liquid nitrogen, as we stated² in Table I at the outset of the Results section. Moreover, we said² "The temperature at the center of the sample reached 77°K within ~ 3 min of immersion."

(9) Cooling in the "empty" tube slowed after 4 min and took ~ 12 min to reach within 0.1° of the bath. After 4 min the condensed air within the tube reached the thermopile.

(10) The crystalline solvents (cyclohexane and isooctane) cooled a little faster than the glassy solvents. Although the thermal conductivities are comparable for all the solvents, the fast cooling of cyclohexane vitiates our second point above, of course.

nitrogen (*vs.* ice) was also monitored while measuring τ for H6 in EPA. The temperature fluctuated $<0.1^\circ$ (the error for a single thermocouple) while the lifetime increased over a 6.5 hr period during which time ~ 40 -ml quantities of liquid nitrogen were added to the dewar every ~ 0.25 hr.

There remains one point to examine. In an indirect check of the proposal,^{1b} no change in τ with time was found for some thin (quickly cooled) samples. McGlynn, *et al.*, have also reported¹¹ the same negative result. We had found the effect in tubes down to 4 mm i.d., but upon receipt of a thin sample (H6 in EPA) from McGlynn, *et al.*, we, too, found no change in τ , having checked lifetimes for a mere ~ 0.5 hr after immersion in an initial attempt. However, such negative experiments prove little, and, to be meaningful, must be repeated for reasonable periods and with sufficient readings of high precision.^{2,6,7} Upon repeating the experiment, we found increases in τ both in their¹¹ degassed (3 mm o.d.) and our open (4 mm o.d.) sample tubes (using a fresh H6/EPA solution), there being gradual and statistically significant τ changes over a 5-hr period.

If we combine the τ (temp) data^{1b} and the above ΔT *vs.* time data, we conclude that after ~ 6 min, thermal equilibration can *not* account for the effects of Figure 1 of our note² *via* τ (temp) effects. (Naturally (gross) temperature changes are important: without them our observations² and obviously glass relaxation could not be observed.) Thus it appears that the conclusions of ref 1b resulted from misleading experimental coincidences.

We now comment on the puzzling problem of the rather different lifetimes reported,^{1b,11} as compared with our larger ($\sim 20\%$ or 1–2 sec) τ values for the same systems.^{2,12} We find no dependence (*i.e.*, $\pm 1\%$) of τ on degassing, concentration, or tube diameter. At our altitude, nitrogen boils at $76.6 \pm 0.1^\circ\text{K}$ (for a ± 10 mm pressure change), so the effect on τ , although in the correct direction, is too small (<0.2 sec). The only other factors (short of errors¹³) that could explain our longer τ values require that the decay be nonexponential.⁷ We use a later³ portion of the decay curve for τ , but this accounts for only a portion of the differences. Moreover, our toluene¹² decays are fairly exponential. If their^{1b,11} illumination of the samples is of short duration ($\sim <\tau$),⁷ this could shorten the observed τ considerably.¹⁴ When more experimental detail becomes available, the differences may be resolved. Admittedly, however, this problem involving absolute lifetimes is somewhat academic since only self-consistent *relative* lifetimes have been necessary for the work of references 2, 11, and 12.

To conclude, we summarize the present status of the relation between glass relaxation and observed phosphorescence lifetimes: in these systems glass relaxation occurs, accompanied by changes in strain.² It is

known that benzene's lifetime is sensitive to the environment and can even vary within one solvent at some temperature.^{7,15} A variety of experiments has shown that these observations might be causally linked, but this is not proved unambiguously. There presently appears to be no hypothesis, other than one involving glass relaxation, that is consistent with the experimental observations.

Acknowledgment. We acknowledge, with thanks, useful correspondence with I. H. Leubner.

(11) J. W. Rabalais, H. J. Maria, and S. P. McGlynn, *Chem. Phys. Lett.*, **3**, 59 (1969).

(12) T. E. Martin and A. H. Kalantar, *ibid.*, **1**, 623 (1968); **4**, 235 (1969).

(13) This may be the case since lifetimes of naphthalene-*d*₈ in EPA at 77°K have been variously reported by the same group as ~ 21 sec (B. N. Srinivasan, M. Kinoshita, J. W. Rabalais, and S. P. McGlynn, *J. Chem. Phys.*, **48**, 1924 (1968), and more recently, the 20% lower value of 16.8 ± 0.25 sec (J. W. Rabalais, H. J. Maria, and S. P. McGlynn, *ibid.*, **51**, 2259 (1969)).

(14) The illumination times of ref 1b are apparently $\sim \tau$ sec, but it is uncertain how nonexponential these decays are at 77°K (I. H. Leubner and J. E. Hodgkins, *J. Phys. Chem.*, **73**, 2545 (1969)). In any case, nonexponential character is difficult to detect unless the decays are followed for about two orders (base 10) of intensity change or for 4–5 lifetimes (*e.g.*, G. F. Hatch and G. C. Nieman, *J. Chem. Phys.*, **48**, 4166 (1968) or ref 7).

(15) Thus the statement,^{1b} "The incoherence of reported phosphorescence lifetimes for a single substance at 77°K in the same solvent must be attributed to temperature dependent effects," is inapplicable.

DEPARTMENT OF CHEMISTRY
UNIVERSITY OF ALBERTA
EDMONTON, ALBERTA, CANADA

T. E. MARTIN
A. H. KALANTAR

RECEIVED AUGUST 11, 1969

Comments on "Thermodynamics of Micellization of Some Zwitterionic N-Alkyl Betaines"

Sir: In a recent paper under the above title, Swarbrick¹ concluded that "Some workers^{2,3} have computed values for ΔS_m° that changed from positive to negative as the temperature was raised. However, the entropy change was calculated on the unlikely assumption that ΔG_m° was zero and therefore ΔS_m° could be regarded as equal to $\Delta H_m^\circ/T$. Under these conditions, ΔS_m° necessarily had the same sign and changed in the same manner as ΔH_m° ."

As these two papers are principally along with my theory,^{4–6} I feel that I have to defend the correctness

(1) J. Swarbrick and J. Daruwala, *J. Phys. Chem.*, **73**, 2627 (1969).

(2) M. J. Schick, *ibid.*, **67**, 1796 (1963).

(3) E. H. Crook, G. F. Trebbi, and D. B. Fordyce, *ibid.*, **68**, 3598 (1964).

(4) K. Shinoda, *et al.*, "Colloidal Surfactants," Academic Press, Inc., New York, N. Y., 1963, p 30.

(5) K. Shinoda and E. Hutchinson, *J. Phys. Chem.*, **66**, 577 (1962).

(6) K. Shinoda, *Bull. Chem. Soc. Jap.*, **26**, 101 (1953).

of these papers. The notation that Dr. Swarbrick used is the hypothetical standard free energy, entropy, and enthalpy, but the enthalpy and entropy of micellization discussed in these papers are the real enthalpy and entropy change accompanied at the micellization. The chemical potentials (partial molal Gibbs free energy) of any component in the two phases in equilibrium at constant T and P are equal. Namely, the Gibbs free energy change of surfactant at the micellization, ΔG_m , is zero. Therefore, the thermodynamics described on these two papers^{2,3} are correct.

In this occasion, I would like to emphasize that it is identical, in principle, to treat micelle formation either as a mass action equilibrium or as a pseudo-phase.⁴ If the aggregation number of micelle is small, the mass action model may be used, while if the aggregation number is large, the phase separation model may be applied.^{4,5} Two approaches are not incompatible, but are compatible.

DEPARTMENT OF CHEMISTRY
YOKOHAMA NATIONAL UNIVERSITY
OOKA-2, MINAMIKU
YOKOHAMA, JAPAN

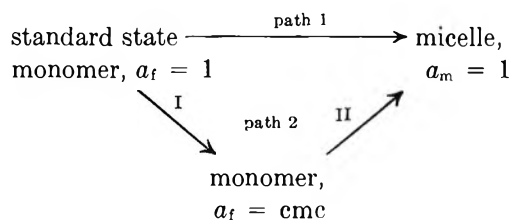
Kōzō SHINODA

RECEIVED OCTOBER 8, 1969

Entropy Changes Associated with Micellization

Sir: Comments by Shinoda¹ on a recent paper from this group² are indicative of certain differences which exist with regard to the presentation of thermodynamic data on micellization.

One may regard micellization as taking place along either of two paths



where a_f and a_m refer to the activities of the surfactant in the free and micellized forms, respectively.

Path 1 describes the conversion of monomer in its hypothetical standard 1 m state to micelle in its hypothetical "pure" hydrocarbon state. The association thermodynamics have been described as^{3,4}

$$\Delta G_m^\circ = RT \ln cmc \quad (1)$$

$$\Delta H_m^\circ = \delta(\Delta G_m^\circ/T)/\delta(1/T) \quad (2)$$

$$\Delta S_m^\circ = (\Delta H_m^\circ - \Delta G_m^\circ)/T \quad (3)$$

where ΔS_m° is defined as (molar entropy in the micelle) - (molar entropy in the standard state.)

Path 2 must describe precisely the same changes since the initial and final states are identical with those of path 1. Step I represents a change in concentration, in which case

$$\Delta G_m^I = RT \ln a_{cmc} \quad (4)$$

Under ideal conditions of mixing, eq 4 becomes

$$\Delta G_m^I = RT \ln cmc \quad (5)$$

Additionally, ideal mixing requires that

$$\Delta H_m^I = 0 \quad (6)$$

The entropy change, ΔS_m^I , is given by

$$\Delta S_m^I = (\Delta H_m^I - \Delta G_m^I)/T \quad (7)$$

On substituting eq 5 and 6 into eq 7, one obtains

$$\Delta S_m^I = -R \ln cmc \quad (8)$$

Step II of path 2 is simply the difference between path 1 and step I of path 2. Thus

$$\Delta G_m^{II} = \Delta G_m^\circ - \Delta G_m^I \quad (9)$$

From eq 1 and 5

$$\Delta G_m^{II} = 0 \quad (10)$$

Equation 10 is the criterion for a state of equilibrium, presumably that of a phase change. In a similar fashion, the enthalpy change for step II is given by

$$\Delta H_m^{II} = \Delta H_m^\circ - \Delta H_m^I \quad (11)$$

which, through eq 6, reduces to

$$\Delta H_m^{II} = \Delta H_m^\circ \quad (12)$$

The enthalpy change is then given, by using either eq 3 and 8 or eq 10 and 12, as

$$\Delta S_m^{II} = \Delta H_m^\circ/T \quad (13)$$

where ΔS_m^{II} is defined as (molar entropy in the micelle) - (molar entropy at the cmc).

The literature reveals that the entropy of micellization is calculated in one of two ways: either through the use of eq 3 or eq 13. While the latter is more definitive in describing the entropy changes occurring upon micellization, actual data on this phenomenon are scarce, due to the fact that calorimetric ΔH_m° values suffer from various uncertainties, especially when the alkyl chain contains more than about ten carbon atoms.^{4,5} To circumvent this problem, a number of workers derive a ΔH_m according to eq 2, and immediately introduce this term into eq 13. The entropy values thus obtained are

(1) K. Shinoda, *J. Phys. Chem.*, to be published.

(2) J. Swarbrick and J. Daruwala, *ibid.*, **73**, 2627 (1969).

(3) P. Molyneux, C. T. Rhodes, and J. Swarbrick, *Trans. Faraday Soc.*, **61**, 1043 (1965).

(4) D. G. Hall and B. A. Pethica, "Nonionic Surfactants," M. J. Schick, Ed., Marcel Dekker, Inc., New York, N. Y., 1967, Chapter 6.

(5) L. Benjamin, *J. Phys. Chem.*, **68**, 3575 (1964).

quite misleading, since they include a cratic term which is of little significance in describing the events taking place during the formation of a micelle. On the other hand, use of eq 3 provides entropy values which more closely resemble unitary functions, since it excludes the entropy of mixing. This procedure would appear to offer more advantage, at least until such time as precise calorimetric data become available.

Finally, it should be pointed out that the compatibility of the mass action and phase separation approaches is not in dispute. As previous work showed,² the data for the N-alkyl betaines support the view, widely held, that the longer the alkyl chain of the amphiphile, the better the agreement between the two models.

DIVISION OF PHARMACEUTICS
SCHOOL OF PHARMACY
UNIVERSITY OF CONNECTICUT,
STORRS, CONNECTICUT 06268

RICHARD E. LINDSTROM
JAMES SWARBRICK

RECEIVED NOVEMBER 5, 1969

Molecular Mobility in Simple Glasses

Sir: In a recent paper, one of us¹ proposed a picture of viscous flow and the glass transition that suggested that secondary relaxations in the glassy state could arise solely from intermolecular processes, thus leading to the prediction that such molecular relaxations could be a universal feature of the glassy state.

Argon² made a similar conjecture on the basis of a description of viscous flow due to Orowan,³ whose ideas were also used as the basis of the picture referred to earlier.¹

To test this hypothesis we have studied, by dielectric relaxation measurements, molecular mobility in glasses formed from molecules lacking obvious internal degrees of freedom capable of giving relaxations due to intramolecular processes. We studied the fused-salt glasses $\text{Ca}(\text{NO}_3)_2 \cdot 4\text{H}_2\text{O}$ and a 45 mol % $\text{Ca}(\text{NO}_3)_2$ - KNO_3 mixture; simple molecular glasses of 10–15 mol % solutions of several mono- and di-halogen substituted benzenes and naphthalenes in the nonpolar solvent decalin; 50–60 mol % mixtures of pyridine with several halogen-substituted benzenes and naphthalenes and several pure aromatic hydrocarbons and aliphatic alcohols. We used a General Radio 1615A capacitance bridge and a parallel plate guarded electrode assembly as the dielectric cell. Measurements were made in the frequency range 50 Hz to 200 kHz and at several temperatures near and below the respective glass transition temperature, T_g .

We may summarize our results by stating that almost all of these glasses show a secondary relaxation below T_g . Figure 1 shows the dielectric loss factor ($\tan \delta$) at 1 kHz plotted on a logarithmic scale against tem-

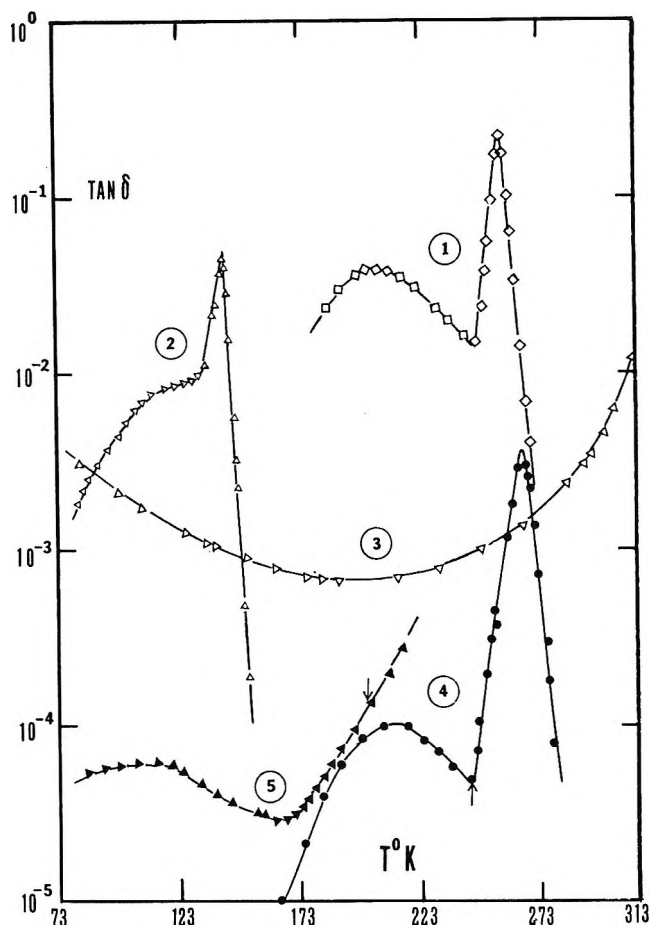


Figure 1. Dielectric loss factor of (1) 63.2 mol % pyridine in 1-chloronaphthalene (scale has been shifted to the right by 100°); (2) 16.5 mol % chlorobenzene in decalin; (3) 45 mol % $\text{Ca}(\text{NO}_3)_2$ - KNO_3 mixture; (4) o-terphenyl; and (5) $\text{Ca}(\text{NO}_3)_2 \cdot 4\text{H}_2\text{O}$ (scale has been shifted downwards by two logarithmic cycles) at 1 kHz as a function of temperature. Arrows indicate the literature values for T_g when known.

perature for five of the systems studied. The $\text{Ca}(\text{NO}_3)_2$ - KNO_3 glass is atypical in that the secondary relaxation does not appear near T_g (60°) but instead $\tan \delta$ shows a rise below 200°K, indicative of a maximum below the boiling point of liquid nitrogen. The behavior of most other systems we studied is more like that of the other four shown in the figure in that: (1) A secondary transition (peak in $\tan \delta$) appears some 30–50° below T_g at a measuring frequency of 10^3 Hz. (2) The “activation energy” of the main transition is much greater than that of the secondary peak, so that the two relaxations must either cross in a temperature–frequency diagram or else merge into a single loss region above T_g at higher frequencies. (3) Neither relaxation is described by a single relaxation

(1) M. Goldstein, *J. Chem. Phys.*, **51**, 3728 (1969).

(2) A. S. Argon, *J. Appl. Phys.*, **39**, 4080 (1968).

(3) E. Orowan, “Creep in Metallic and Non-Metallic Materials,” *Proceedings of the First National Congress of Applied Mechanics*, American Society of Mechanical Engineers, New York, N. Y., 1952, pp 453–472.

time. (4) The relaxation time spectra are markedly temperature dependent, broadening as temperature is lowered. The similarity to behavior in many polymer glasses is striking.

One alternative explanation that could be given to some of our results is that phase separation occurs in glasses formed from mixtures of simple molecules and that the appearance of secondary relaxation peaks (below T_g) is an artifact due to this. But the near universality of this behavior both in a wide variety of mixtures, and in pure substances as well, leads us to exclude this possibility.

Most molecular explanations for the presence of molecular mobility (indicated by secondary relaxation regions below T_g) have been in terms of internal molecular motions involving hindered rotation around chemical bonds.^{4,5} In this view these relaxations are extrinsic to the glassy state and arise from intramolecular modes of motion that remain active even when the molecule as a whole is frozen in the glassy matrix. On the basis of our studies, we suggest that relaxations in the glassy state need to be reexamined from the point of view of intermolecular rather than intramolecular degrees of freedom.

We are continuing these studies on additional simple glass forming systems and will report this work in detail and discuss implications of this picture on dielectric relaxation in liquids later.

Acknowledgment. We are grateful to the Owen-Illinois Foundation and to the Department of Defense (Grant No. N00014-69-A-0411) for the support of this research.

(4) N. G. McCrum, B. E. Read, and G. Williams, "Anelastic and Dielectric Effects in Polymeric Solids," John Wiley and Sons, New York, N. Y., 1967.

(5) A. E. Woodward and J. A. Sauer in "Physics and Chemistry of the Organic Solid State," Vol. II, Interscience Publishers, New York, N. Y., 1965, p 638.

BELFER GRADUATE SCHOOL OF SCIENCE
YESHIVA UNIVERSITY
NEW YORK, NEW YORK 10033

GYAN P. JOHARI
MARTIN GOLDSTEIN

RECEIVED NOVEMBER 20, 1969

Dehydration and Polymerization of Barium Methacrylate Monohydrate¹

Sir: The thermal degradation of barium methacrylate monohydrate has recently been reported by Bowden and O'Donnell.^{2a} An understanding of this process can play an important role in defining the mechanisms of the solid-state polymerizations of acrylate and methacrylate salts. We report here some additional observations on the dehydration phenomenon.

The salt of barium methacrylate has been previously reported by Lando and Morawetz to be a di-

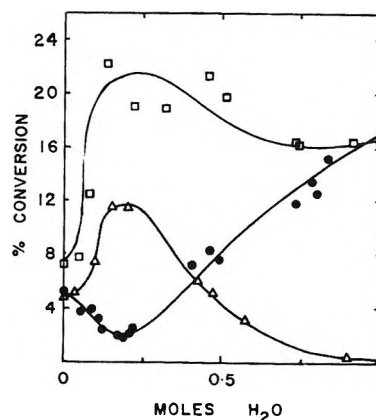


Figure 1. Postirradiation polymerization of hydrated barium methacrylate at 35°. Dose 0.86 Mrad at -78° ; *in vacuo*: Δ , 0.6 days; \square , 27.6 days; *in air*: \bullet , 34 days.

hydrate.^{2b} Our studies have shown it to be a monohydrate and this observation is in agreement with the recent report of Bowden and O'Donnell.^{2a} These workers, however, have studied the dehydration process *in air*, for comparison with polymerization studies, believing the polymerization to be unaffected by the presence of oxygen. Results obtained in our laboratory indicate that this conclusion is valid only for the monohydrate and anhydrate. At all intermediate states of hydration, the polymerization is observed to be extremely sensitive to the presence of oxygen. In Figure 1 the yields of polymer on postirradiation polymerization *in vacuo* at 35° for 0.6 and 27.6 days are shown as a function of water content. (The loss of water from the crystal hydrates, under the experimental conditions used, is negligible even at the longest polymerization times.³ Therefore, the quoted level of hydration is the correct one at any time.) A maximum in the polymerization rate is observed at the 0.25 hydrate. In the presence of air, however, while the rates at the zero and monohydrate compositions are unchanged, those at all other compositions show an inversion relative to the vacuum polymerizations. We have therefore examined the dehydration process *in vacuo* at 47°. The results show that dehydration proceeds with no loss in crystallinity. Infrared spectra and X-ray powder diffraction measurements were identical with those reported by Bowden and O'Donnell. In addition, density measurements of monohydrate, anhydrate and intermediate compositions show that there is no collapse of the lattice upon removal of the water of crystallization. A minor expansion (3%) along the C axis was observed.

(1) Paper presented in part at the 15th Canadian High Polymer Forum, Kingston, Ontario, Sept 3-5, 1969.

(2) (a) M. J. Bowden and J. H. O'Donnell, *J. Phys. Chem.*, **73**, 2871 (1969); (b) J. B. Lando and H. Morawetz, *J. Poly. Sci., C*, **4**, 789 (1964).

(3) F. M. Costaschuk, D. F. R. Gilson, and L. E. St. Pierre, to be published.

The oxygen inhibition is rationalized on the basis of increased permeability of crystals rich in defects^{3,4} and will be treated more fully in a paper which will follow.

Further evidence of the nonessential role of water in maintaining the crystal structure of barium methacrylate is obtained from infrared spectra. The O-H stretch occurs as a sharp strong absorption at 3562 cm^{-1} , indicative of free O-H stretching, rather than a broad peak at longer wavelengths which would indicate a hydrogen-bonded species. These results are in contrast to those found for calcium acrylate dihydrate³ where the water of hydration plays an important function in maintaining the crystalline structure.

(4) G. Adler, *J. Poly. Sci.*, **C16**, 1215 (1967).

DEPARTMENT OF CHEMISTRY
MCGILL UNIVERSITY
MONTREAL, CANADA

F. M. COSTASCHUK
D. F. R. GILSON
L. E. ST. PIERRE

RECEIVED DECEMBER 3, 1969

Comment on "Electron Spin Resonance of Perfluorocyclobutanone Ketyl. Long-Range Fluorine Coupling," by J. A. Gerlock and E. G. Janzen. The Angular Dependence of β -Fluorine Hyperfine Splitting

Sir: Branching at a carbon attached to a radical site normally reduces the hyperfine splitting (hfs) of the remaining β protons, as referenced to the methyl-substituted radical. This result stems from an increased population of conformers in which the β protons are at dihedral angles greater than 45° . The maximum β proton hyperfine splitting is expected at a 0° dihedral angle with a minimum value at a 90° angle.^{1,2} Perfluorobranched at a trifluoromethyl group, however, increases the hfs of the remaining β fluorines. The fluorine splitting in ditrifluoromethyl nitroxide is 8.2–8.6 G,³ while the β -fluorine splittings in symmetrical nitroxides substituted with ClCF_2CF_2 and $\text{MeOCO-CF}_2\text{CF}_2$ groups are 10.1⁴ and 13.8 G,⁵ respectively. Similar effects have been noted in perfluoroalkyl-*t*-butoxy nitroxides⁶ and perfluoronitroalkane anion radicals.^{7,8} If the conformational properties of perfluoroalkyl groups are similar to those of alkyl groups (an assumption), then the dihedral dependence of β -fluorine hfs might be exactly opposite to that of β protons.

Recently, Gerlock and Janzen studied the esr spectrum of perfluorocyclobutanone ketyl.⁷ In this radical, the β hfs was 82.9 G and the γ hfs was 37.3 G, as compared to the 34.7-G splitting found in hexafluoroacetone ketyl,⁹ where the average dihedral angle is 45° . Since the dihedral angle of the β fluorines in the cyclic ketyl is $25\text{--}30^\circ$, Gerlock and Janzen concluded the β fluorine

splitting might follow the same angular dependence as β proton splitting. This conclusion, however, is not forced on one by the evidence of the β fluorine splitting. In symmetrical ketals of this type, there is no independent means of monitoring the spin distribution unless the carbonyl ^{13}C hfs is measured. Cyclization to a perfluorocyclobutyl ring may well affect the spin distribution within the carbonyl group. Nevertheless, the 37.3-G splitting from the γ -fluorines, which are at a 0° dihedral angle with the spin site, lends plausibility to their conclusion.

Elementary bonding arguments can be used to rationalize maximum β -fluorine hfs at either the 90° or 0° dihedral angles. If the fluorine atom is at a 90° angle to the p orbitals containing the odd electron, spin transfer can occur by a 1,3 p- π mechanism, *i.e.*, overlap of the + and - lobes of the fluorine p orbital with the corresponding + and - lobes of the radical system. (The orthogonal fluorine p orbital is in the nodal plane of the π system. Note, however, that it can interact with the lone-pair electrons on the oxygen.) This situation is shown in I for the specific case of a nitroxide. On the other hand, if the dihedral angle is 0° , spin transfer can be achieved by a 1,3 p- σ overlap, *i.e.*, interaction of + lobe with + lobe as shown in II. Recent INDO calculations predict a maximum β -fluorine hfs at 0° .¹⁰ If both p- π and p- σ spin transfer mechanisms are operative, the dihedral angle dependence could be complicated.



A definitive answer to the question of the angular dependence of β -fluorine splitting must await experiments in rigid cyclic systems in which the fluorine atoms are at reasonably well-known dihedral angles and in which the spin densities can be monitored. However, if the angular dependence for fluorine splitting is the same as that for proton splitting, it follows from the experimental results cited above that the conformer population in perfluoroalkyl substituted radicals of the above type

(1) (a) M. C. R. Symons, *J. Chem. Soc.*, 277 (1959); (b) H. C. Heller and H. M. McConnell, *J. Chem. Phys.*, **32**, 1535 (1960).

(2) For a thorough review, David H. Geske in *Progr. Phys. Org. Chem.*, **IV**, 125 (1967).

(3) (a) W. D. Blackley and R. R. Reinhard, *J. Amer. Chem. Soc.*, **87**, 802 (1965); (b) I. V. Miroshnichenko, G. M'. Larin, S. P. Makarov, and A. F. Videnko, *Zh. Strukt. Khim.*, **6**, 776 (1965).

(4) W. D. Blackley, *J. Amer. Chem. Soc.*, **88**, 480 (1966).

(5) E. T. Strom and A. L. Bluhm, *Chem. Commun.*, 115 (1966).

(6) A. L. Bluhm and E. T. Strom, unpublished research.

(7) J. L. Gerlock and E. G. Janzen, *J. Phys. Chem.*, **72**, 1832 (1968).

(8) In the radicals cited, changes in nitrogen hfs were minor.

(9) E. G. Janzen and J. L. Gerlock, *J. Phys. Chem.*, **71**, 4577 (1967).

(10) K. Morokuma, *J. Amer. Chem. Soc.*, **91**, 5412 (1969).

must be opposite to that in the analogous alkyl substituted radicals. The difference in polarities of the C-H and C-F bonds as well as the presence of lone pair electrons on fluorine might play a part in such a reversal.

MOBIL RESEARCH AND
DEVELOPMENT CORPORATION
FIELD RESEARCH LABORATORY
DALLAS, TEXAS 75221

E. THOMAS STROM

PIONEERING RESEARCH LABORATORY
U. S. ARMY NATICK LABORATORIES
NATICK, MASSACHUSETTS 01760

AARON L. BLUHM

RECEIVED DECEMBER 5, 1969

On the Angular Dependence of β -Fluorine Electron Spin Resonance Hyperfine Coupling in Fluoro-Substituted Nitroxide Radicals¹

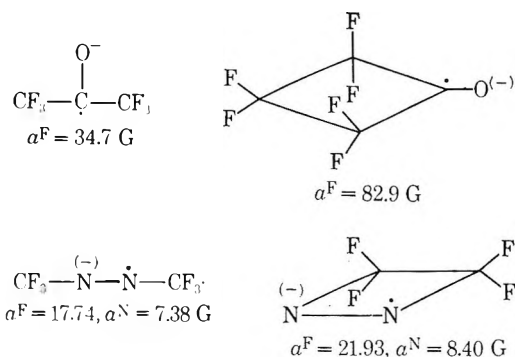
Sir: In connection with an esr study of photolysis products of nitrosoperfluoroalkanes, Strom and Bluhm² found that the magnitude of β -fluorine coupling in the nitroxide produced *increases* with substitution. This observation appeared unusual in light of the many known examples where the magnitude of β -hydrogen coupling *decreases* with substitution.³ It was thus suggested that fluorine coupling might be enhanced by p - π overlap which was thought to be favored at larger dihedral angles. This suggestion was based on the assumption that the probable average conformation of the perfluoroalkyl group was the same as for normal alkyl groups. An alternate assumption, however, might have been that the angular dependence of the β -fluorine coupling was normal (*i.e.*, the same as for hydrogen) but that the average conformation of the perfluoroalkyl group was different from that of normal alkyl groups.⁴

Table I: Temperature Dependence of Nitrogen and β -Fluorine Hyperfine Coupling in R-N \dot{O} -C(Me)₃^a

Temp, °C	—R = CF ₂ -CF ₂ —			—C ₆ H ₅ -CF ₂ —		—(CF ₂) ₂ CF—		
	A _N	A β^F	A γ^F	A _N	A _F	A _N	A β^F	A γ^F
40	11.33	20.80	0.39	11.66	19.06 ^b	12.10	2.30	2.30
25	11.25	21.16	0.43	11.66	19.26 ^c	12.11	2.27	2.27
-30	11.28	22.27	0.34	11.54	20.69	12.13	1.59	2.33
-60	11.31	22.65	0.22			12.15	1.32	2.29
-90	11.32	23.15	<0.20			12.14	0.76	2.31

^a In gauss. ^b At 35°. ^c At 26°; A_N = 11.6, A_F = 20.38 G, at -7°.

Recently, INDO^{5,6} and extended Hückel⁷ calculations show that β -fluorine coupling should be at a maximum when the dihedral angle $\theta = 0^\circ$. A comparison of the following pairs of radical anions provides the same apparent conclusion at least for $\theta \cong 25$ -45°.^{8,9}



The criticism of Strom and Bluhm¹⁰ regarding the possible difference in spin density distribution in the hexafluoroacetone and perfluorocyclobutanone ketyls is a valid one and could be checked by obtaining C-13 data. Although such data have been obtained for the former radical anion,¹¹ we were unable to detect C-13 splitting for the latter compound because of low radical concentrations, and the unavailability of more starting material has hindered further attempts. However, a comparison of the perfluoroazoalkane radical anions is more dependable since the spin densities on the nitrogen atoms must remain the same in both compounds and the nitrogen coupling should indicate gross differences in hybridization about nitrogen. Taking into account that in perfluoroazoethane radical anion $a^N = 7.72$ G ($a^F = 35.23$ G),⁹ it is clear that the nitrogen coupling does not change appreciably (~ 0.7 G) when a perfluoroazoalkane radical anion is constrained into the shape of a four-membered ring. However, β -fluorine coupling still *increases* with *decrease* in dihedral angle.

If it is concluded that the angular dependence of the β -fluorine coupling resembles hydrogen, the possibility that the average conformation of the perfluoroalkyl group is different from that assumed by normal alkyl groups should be investigated. The limiting conforma-

(1) This work is being supported by AFOSR-(SRC)-OAR, U. S. Air Force Grant No. 1069-66 and the Petroleum Research Fund administered by the American Chemical Society.

(2) E. T. Strom and A. L. Bluhm, *Chem. Commun.*, 115 (1966).

(3) (a) D. H. Geske, *Prog. Phys. Org. Chem.*, **4**, 125 (1967), and references therein; (b) M. D. Sevilla and G. Vincow, *J. Phys. Chem.*, **72**, 3647 (1968).

(4) A third alternative might have been to consider the effect of substituting a strongly electronegative group for fluorine in the trifluoromethyl group. However, a comparison of the coupling constants obtained from perfluoroethyl and α,α -difluorobenzyl-*t*-butylnitroxide (Table I) shows that such substitution has no detectable effect on the β -fluorine coupling.

(5) K. Morokuma, *J. Amer. Chem. Soc.*, **91**, 5412 (1969).

(6) G. R. Underwood, V. L. Vogel, and I. Krefting, unpublished; see acknowledgment with appreciation the receipt of a preprint of this work.

(7) J. L. Meyer and E. G. Janzen, in preparation.

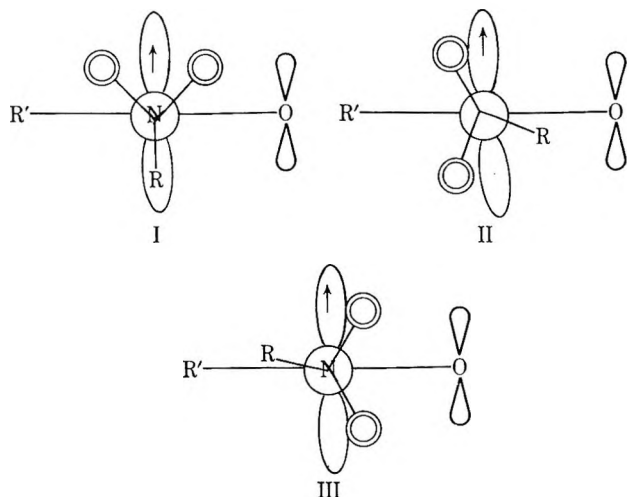
(8) E. G. Janzen and J. L. Gerlock, *J. Phys. Chem.*, **71**, 4577 (1967); J. L. Gerlock and E. G. Janzen, *ibid.*, **72**, 1832 (1968).

(9) J. L. Gerlock, E. G. Janzen, and J. K. Ruff, *J. Amer. Chem. Soc.*, **92**, 2558 (1970).

(10) E. T. Strom and A. L. Bluhm, *J. Phys. Chem.*, **74**, 2036 (1970).

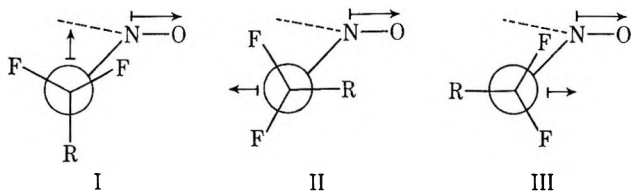
(11) W. R. Knolle and J. R. Bolton, *J. Amer. Chem. Soc.*, **91**, 5411 (1969).

tions for hindered alkyl nitroxides are I, II, and III.



The β -hydrogen coupling in numerous examples indicates that I is the most probable conformation. Inspection of space-filling models of the analogous β,β -difluoro derivatives indicates that I is *not* obviously better than II or III. This result is due mainly to the increased size of the fluorine atom which causes significant steric interaction with the oxygen atom and the R' group in I.¹² Conformations II and III appear at least equally favorable since the fluorine atoms interact less with R' or oxygen, respectively, in spite of the fact that R eclipses oxygen or R', respectively.

Further consideration of the probable dipole-dipole interaction existing in such compounds leads to the conclusion that II should be the most probable conformation for the difluoro nitroxide derivatives. Thus when R = phenyl



On the basis of the combined effect of steric and dipole-dipole interactions it is our prediction that the limiting conformation preferred will be II in β,β -difluoroalkyl nitroxides.¹³

This prediction should be testable. Thus if one assumes that the freedom of rotation of the substituent will increase with increase in temperature so that eventually the apparent average NCF dihedral angle will be 45° as in the freely rotating trifluoromethyl group, the average dihedral angle will become smaller in I and larger in II with increase in temperature. Furthermore, if the angular dependence of β -fluorine coupling approximately follows a $\cos^2 \theta$ relationship, as for β -hydrogen coupling, the fluorine coupling should increase in I and decrease in II with increase in temperature. The β -fluorine temperature dependence for the

perfluoroethyl and the α,α -difluorobenzyl-*t*-butylnitroxide is found to *decrease* with increase in temperature for both radicals (Table I). This observation thus supports the conclusion that II is the preferred limiting conformation for β,β -difluoroalkylnitroxide derivatives and that it is for this reason that the β -fluorine coupling increases with substitution as first observed by Strom and Bluhm.

The β -fluorine coupling situation when $\theta = 90^\circ$ is by no means clear. From INDO calculations Morokuma⁵ concluded that the coupling should be near zero when $\theta = 90^\circ$ whereas Kosman and Stock¹⁴ as well as Underwood, *et al.*,⁶ show that a residual coupling should be present at this angle. Experimental data differ for each system studied. Perfluoroisopropyl-*t*-butylnitroxide shows a relatively small β -fluorine coupling which decreases in magnitude to a very small value when the temperature is lowered (Table I). This result is consistent with β -fluorine coupling decreasing to zero as $\theta \rightarrow 90^\circ$. In triptycene semiquinone,¹⁴ however, the bridgehead fluorine coupling is appreciable (approximately one-third of the value found for the freely rotating trifluoromethyl group) and a very large value for the β -fluorine coupling is found in 2-perfluoroazopropane radical anion⁹ ($\alpha_\beta^F = 62.45$ G).

(12) In β,β -dichloro nitroxide derivatives this interaction very clearly makes I the *least* probable conformation shown: E. G. Janzen, B. R. Knauer, L. T. Williams, and W. B. Harrison, submitted for publication.

(13) The same conclusion has been reached by Underwood, *et al.*,⁶ based on a comparison of literature data on the preferred conformations of alkyl aldehydes and ketones with nitroxides of similar structure.

(14) D. Kosman and L. M. Stock, *J. Amer. Chem. Soc.*, **92**, 409 (1970).

DEPARTMENT OF CHEMISTRY
UNIVERSITY OF GEORGIA
ATHENS, GEORGIA 30601

EDWARD G. JANZEN
BRUCE R. KNAUER
JOHN L. GERLOCK

DEPARTMENT OF CHEMISTRY
UNIVERSITY OF IOWA
IOWA CITY, IOWA 52240

KENNETH J. KLABUNDE

RECEIVED FEBRUARY 16, 1970

Electrical Conductivity of Bromine Trifluoride^{1a}

Sir: Karl Christe^{1b} has recently commented on the report by Toy and Cannon² of the preparation and identification of difluorobromium tetrafluoroborate $\text{BrF}_2^+ \text{BrF}_4^-$. We were indeed skeptical of Toy and Cannon's report for the reasons Christe has outlined and are inclined to accept his conclusion, but his paper includes comments on the conductivity of bromine trifluoride that appear to be incorrect and may prove mis-

(1) (a) Work performed under the auspices of the U. S. Atomic Energy Commission; (b) K. O. Christe, *J. Phys. Chem.*, **73**, 2792 (1969).

(2) M. S. Toy and W. A. Cannon, *ibid.*, **70**, 2241 (1966).

leading to workers in the field. The conductivity of bromine trifluoride has been studied by several groups on separate batches of material purified by their individual techniques and in apparatus constructed of diverse materials. The observations of Banks, Emeleus, and Woolf³ and Quarterman, Hyman, and Katz⁴ are in excellent agreement both qualitatively and quantitatively and involve authentic bromine trifluoride samples of reasonably high purity. We have recently been studying the bromine trifluoride-hydrogen fluoride system which will be discussed elsewhere. Like bromine and bromine pentafluoride, whose effects were studied by Quarterman, *et al.*, hydrogen fluoride acts to reduce the electrical conductivity of bromine trifluoride (Table I). For distilled material these three

Table I: Conductivity of Dilute Solutions of Volatile Impurities in Bromine Trifluoride

Impurity	Concn, mol %	Cond $\times 10^{-3}$, ohm ⁻¹ cm ⁻¹ (at 25°)	Impurity	Concn, mol %	Cond $\times 10^{-3}$, ohm ⁻¹ cm ⁻¹ (at 25°)
None		8.03	BrF ₃	3.0	7.30
Br ₂	3.99	7.21	HF	8.1	7.52

volatile materials are the most likely impurities in bromine trifluoride.

We believe that the high conductivity of this reagent is associated with a high mobility of the parent ions, perhaps *via* a chain conducting mechanism. For this reason we suspect that the effect of any impurity, whether an inert diluent or any solute other than a strong acid or base, will lead to a net reduction in the specific conductivity. After Christie's communication appeared, we reexamined a new batch of carefully distilled bromine trifluoride. We found as expected that removing volatile impurities led to a small increase in conductivity. Various batches showed values between 7.94 and 8.04×10^{-3} ohm⁻¹ cm⁻¹ with a mean of 8.01×10^{-3} ohm⁻¹ cm⁻¹ at 25°. In a single case where a distilled bromine trifluoride sample was refractionated by a simple trap-to-trap distillation the distillate showed a conductivity of 7.89, the residue of 8.03×10^{-3} ohm⁻¹ cm⁻¹. In exploring the specific conductivity as a function of temperature the negative temperature coefficient was confirmed over the range 10.5–50.0° (Table II) in quite good agreement with the 1957 measurements.

At this time we are not prepared to speculate on the nature of the impurities that either Toy or Cannon and/or Christie were dealing with. We simply suggest that anyone working with bromine trifluoride with an electrical conductivity substantially below 8×10^{-3} at 25° must be presumed to be working with a mixture and bears the burden of a more complete identification of his material.

Table II: Temperature Dependence of the Specific Conductivity of BrF₃

Temp, °C	Cond $\times 10^{-3}$, ohm ⁻¹ cm ⁻¹	Cond, ref 4	Temp, °C	Cond $\times 10^{-3}$, ohm ⁻¹ cm ⁻¹	Cond, ref 4
10.5	8.34		35.0	7.82	7.80
18.0	8.20		40.0	7.71	7.65
25.0	8.03	8.01	45.0	7.49	7.47
30.0	7.97	7.92	50.0	7.31	7.27

Electrical conductivities were measured using polychlorotrifluoroethylene cells with bright platinum electrodes essentially as described in ref 4 and a Wayne Kerr autobalance precision bridge Model B331.

(3) A. A. Banks, H. J. Emeleus, and A. A. Woolf, *J. Chem. Soc.*, 2861 (1949).

(4) L. A. Quarterman, H. H. Hyman, and J. J. Katz, *J. Phys. Chem.*, 61, 912 (1957).

CHEMISTRY DEPARTMENT
ARGONNE NATIONAL LABORATORY
ARGONNE, ILLINOIS 60439

HERBERT H. HYMAN
TERRY SURLS
LLOYD A. QUARTERMAN

DEPARTMENT OF CHEMISTRY
MICHIGAN STATE UNIVERSITY
EAST LANSING, MICHIGAN 48823

ALEXANDER POPOV

RECEIVED DECEMBER 16, 1969

Electrical Conductivity of Bromine Trifluoride

Sir: The discrepancy between our previously reported¹ conductivity values of BrF₃ and those of Hyman and coworkers² has successfully been resolved. A re-investigation of the BrF₃ system showed that the BrF₃ samples used in our study were of high purity and that the difference in conductivity could not be attributed to impurities as suggested by Hyman.² Using the same conductivity cell as in our original experiments, our previously reported data¹ could be reproduced. However, it was found that the measured resistance was dependent on the applied ac voltage indicating interfering reactances. When a new conductivity cell (having larger electrode surface areas and a much higher cell constant) was used, no detectable interferences were encountered and values were obtained which differed by less than one per cent from those obtained by Hyman.² Consequently, the values given in the preceding paper² are confirmed.

(1) K. O. Christie, *J. Phys. Chem.*, 73, 2792 (1969).

(2) H. H. Hyman, T. Surlis, L. A. Quarterman, and A. Popov, *ibid.*, 74, 2038 (1970).

ROCKETDYNE, A DIVISION OF NORTH
AMERICAN ROCKWELL CORPORATION
CANOGA PARK, CALIFORNIA 91304

KARL O. CHRISTE

RECEIVED FEBRUARY 24, 1970

The Kinetics of Spreading

Sir: In a recent paper, Yin^{1,2} has derived equations for the spreading of a liquid droplet on a smooth, rigid surface. In it he obtained an equation for the equilibrium value of contact angle that appears to be inconsistent with the Young equation. This inconsistency will be shown to be the result of defects in the mathematical formulism used to obtain the equation for steady-state spreading.

Yin's eq 17 for equilibrium is

$$I_2/I_1 = -S_0/\gamma_l$$

where I_1 and I_2 are integrals that were evaluated numerically by computer, and $S_0 = \gamma_s - \gamma_{sl} - \gamma_l$. In the notation used by Yin, the Young equation requires that

$$\gamma_s - \gamma_{sl} = \gamma_l \cos \theta$$

Substitution of the Young equation into Yin's eq 17 gives

$$I_2/I_1 = 1 - \cos \theta$$

However, Yin's Figure 5, giving I_2/I_1 as a function of θ , shows that I_2/I_1 cannot satisfy this equation, since, for example, I_2/I_1 does not equal zero when the equilibrium contact angle θ is zero.

In his derivation, Yin used ϕ to mean both the angle of the liquid surface with the horizontal, an angle that varies with height above the interface, and the value of this angle at the interface (the instantaneous contact angle), and he used h to mean both the varying height above the interface and its value at the top of the droplet. In order to distinguish the variables from these respective limits, let us use φ and z for the variables and retain ϕ and h for the limits mentioned. The geometrical relations involved are shown in our Figure 1. From these one can find that the variables satisfy the equations

$$z = h - \rho \tan \frac{\varphi}{2} \quad \rho = R \sin \varphi$$

where ρ is the radius of any horizontal cross section of the droplet, another variable dependent on the height z .

Yin set the spreading force at the interface equal to the viscous retarding force to get his eq 4 for steady-state spreading. In our modified notation we would write

$$2\pi r S_\phi = -\pi r^2 \eta \frac{dv}{dz} \quad (z = 0)$$

where

$$S_\phi = \gamma_s - \gamma_{sl} - \gamma_l \cos \phi$$

However, the integration of the right-hand side of eq 4 was then carried out as if the balance of forces

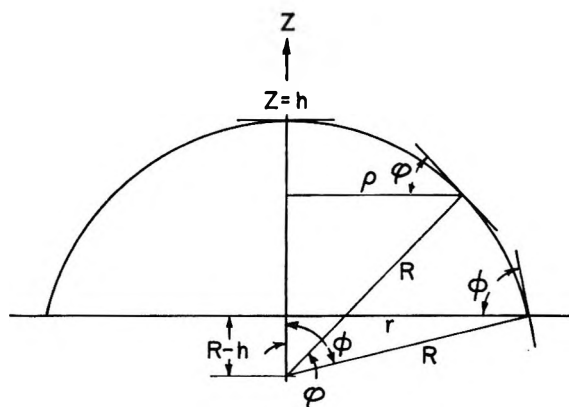


Figure 1. Vertical cross section of liquid droplet on smooth, rigid surface.

applied at all levels from the interface to the top of the droplet, that is, in our notation

$$2\pi r S_\phi = -\pi r^2 \eta \frac{dv}{dz} \quad (0 \leq z \leq h)$$

where

$$S_\phi = \gamma_s - \gamma_{sl} - \gamma_l \cos \phi$$

but if such a balance can be written for the liquid layers above the interface it would be of the form

$$2\pi \rho S_\varphi = -\pi \rho^2 \eta \frac{dv}{dz} \quad (0 < z \leq h)$$

where S_φ would contain no terms dependent on the properties of the solid surface. Furthermore, in changing the integral $\int S_\phi dz$ to one of the form $\int F(\varphi) d\varphi$, Yin used relations, given by his eq 5 and 8, which hold for the limiting values of ϕ and h but do not hold for the variables φ and z . Lastly, in the integration of his eq 14 to get eq 15, $\langle dA/dt \rangle$ which is a function of ϕ was treated as a constant independent of ϕ .

In addition to satisfying the Young equation at equilibrium, any solution must also be self-consistent. That is, since

$$\left\langle \frac{dA}{dt} \right\rangle = 2\pi r v_r$$

where v_r is independent of time and

$$r = \left(\frac{3V_0}{\pi} \right)^{1/3} \left(\frac{2 \sin^2(\phi/2)}{3 - 2 \sin^2(\phi/2)} \right)^{1/3} \cot(\phi/2)$$

from Yin's eq 5 and 9, any steady-state solution for $\langle dA/dt \rangle$ must be of the form

$$\left\langle \frac{dA}{dt} \right\rangle = K \left(\frac{2 \sin^2(\phi/2)}{3 - 2 \sin^2(\phi/2)} \right)^{1/3} \cot(\phi/2).$$

(1) T. P. Yin, *J. Phys. Chem.*, **73**, 2413 (1969).

(2) EDITOR'S NOTE. Dr. Yin was killed earlier this year in an automobile accident, and was therefore unable to reply to this communication. The reviewer to whom the manuscript was sent for examination feels that Dr. Dyba's remarks are justified.

Yin's form of the balance of forces equation, when integrated correctly, does not satisfy either of these criteria. Several simple alternatives that we have considered do not give a self-consistent result, although any using our S_{ϕ} will satisfy the Young equation.

TEXTILE RESEARCH INSTITUTE
PRINCETON, NEW JERSEY 08540

RAYMOND V. DYBA

RECEIVED JANUARY 16, 1970

Absorption Spectrum of the Pyrene Excimer

Sir: Since their detection by Förster and Kasper,¹ the study of excimers has been based on emission spectroscopy. This limited the available experimental information to the lowest excited singlet² or triplet states^{3,4} of the molecular pair. Recently, using a nanosecond laser photolysis technique, it has been possible to observe absorption bands due to the fluorescing state of the anthracene-N,N-diethylaniline hetero excimer.⁵ The same technique is now being applied to pyrene, for which excimer formation has been extensively studied.⁴

Concentrated (0.5 M) solutions of pyrene in toluene, or dilute (2×10^{-5} M) solutions in cyclohexane, were deaerated and excited by means of the 3371-Å line of an Avco-Everett pulsed N₂ laser. This particular choice of solvents was due to the high solubility of pyrene in toluene as well as to the relatively low excimer yield in cyclohexane. A pulsed Xe lamp was employed as the monitoring light source in an absorption setup described elsewhere.⁵ In dilute solutions, laser excitation is followed by the formation of an absorption transient whose lifetime (200 nsec) matches the decay of the pyrene 400-nm fluorescence (Figure 1a, insert). The absorption is thus assigned to pyrene's lowest excited singlet state. The complete spectrum of the transient, obtained after introducing appropriate corrections for the contribution of fluorescence to the absorption traces, is plotted in Figure 1a. The data in the figure are based on measurements 20 nsec after triggering the laser, when only a small fraction of excited singlets have decayed. Thus, the contribution of T → T absorption to the excited singlet → singlet spectrum may be considered as negligible. These results are in qualitative agreement with previous data.^{6,7}

Laser excitation experiments were also carried out in 0.5 M pyrene solutions where excimerization is completed within less than 1 nsec.⁸ Under the usual conditions of steady-state fluorescence measurements, the excimer at such concentration is the predominant excited species, exhibiting a lifetime of ~50 nsec. However, at our very high intensities of excitation^{5,9} (the focused 5×10^{-4} J laser beam is absorbed within a volume of less than 5×10^{-7} cm³) the excimer decay is no longer exponential, being shortened by excimer-

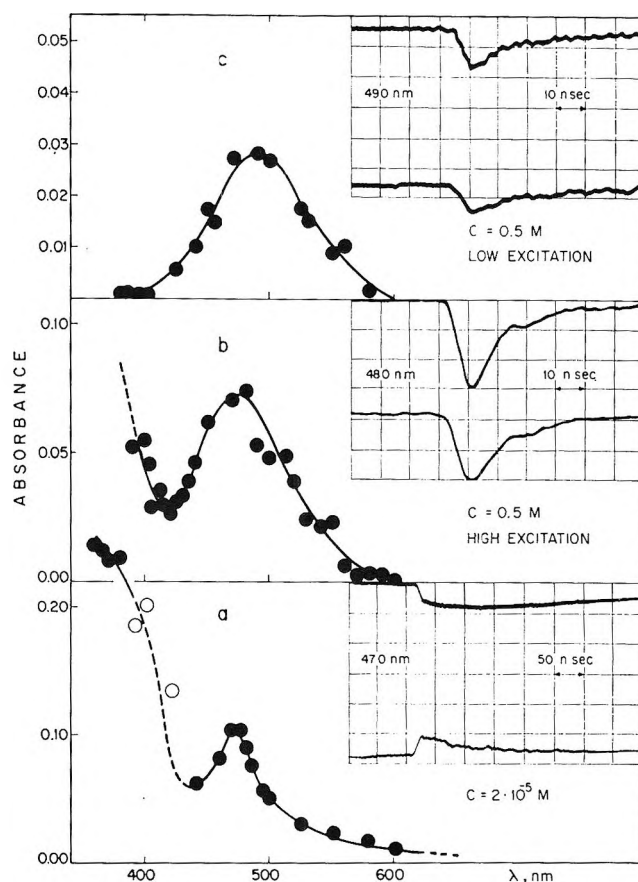


Figure 1. Spectra of transients in the laser photolysis of pyrene solutions. Inserts are representative oscillograms from which each of the corresponding spectra was derived. (Vertical sensitivity: 50 mV/division; load impedance: 50 ohms.). Lower traces in each oscillogram are in presence of monitoring light. Upper traces are with monitoring light off, representing the contribution of fluorescence to the lower traces. All experiments were carried out at room temperature. (Empty circles and broken line in curve a refer to the region of high fluorescence intensity, implying lower accuracy of the absorbance data).

excimer interaction⁹ to less than the 10-nsec laser profile. It is therefore impossible to look for excimer absorption after the decay of the exciting pulse; thus, use was made of a technique allowing the detection of transient absorptions closely following the flash pro-

- (1) Th. Förster and K. Kasper, *Z. Phys. Chem. (Frankfurt am Main)*, **1**, 275 (1954).
- (2) J. B. Birks and L. G. Christophorou, *Proc. Roy. Soc.*, **A277**, 571 (1964).
- (3) H. C. Lim and S. K. Chakrabarti, *Mol. Phys.*, **13**, 293 (1967).
- (4) Th. Förster, *Angew. Chem. Int. Ed. Engl.*, **8**, 333 (1969).
- (5) C. R. Goldschmidt and M. Ottolenghi, *Chem. Phys. Lett.*, **4**, 570 (1970).
- (6) Y. Nakato, N. Yamamoto, and H. Tsubomura, *ibid.*, **2**, 57 (1968).
- (7) G. Porter and M. R. Topp, *Nature*, **220**, 1228 (1968).
- (8) C. R. Goldschmidt, Y. Tomkiewicz, and A. Weinreb, *Spectrochim. Acta*, **25A**, 1471 (1969).
- (9) C. R. Goldschmidt, Y. Tomkiewicz, and I. B. Berlman, *Chem. Phys. Lett.*, **2**, 520 (1968).

file.^{5,6,10} The results for the 0.5 M pyrene solution are shown in Figure 1b, insert. As in previous cases,^{5,10} due to the intense superposed fluorescence, the presence of an absorbing transient could be detected only by subtracting the emission profile in the presence of the monitoring beam from that recorded in the absence of the analyzing light. The complete difference spectrum is plotted in Figure 1b. (Using a light guide, control experiments were carried out in which the fluorescence excited by the laser pulse in one solution was superposed, close to the monochromator's entrance slit, on the analyzing light beam passed through a second solution which was not excited by the laser. At all wavelengths the pulse profile with no monitoring light was found identical with that containing the superposed analyzing beam.) Examination of the spectra in Figures 1b and 1c shows a considerable similarity between the corresponding curves, suggesting a non-negligible contribution of the excited monomer absorption to the curve in Figure 1b. This should in fact be expected since the half-life of the excited monomer, under the present conditions of high-excitation intensity, was of the same order of magnitude as that of the excimer. In order to increase the relative concentration of the excimer and thus its contribution to the spectrum, we have carried out experiments in which the laser intensity was reduced by a factor of ~ 10 . At this reduced intensity the excimer decay time is increased, reaching a half-width value of ~ 20 nsec. (See Figure 1c, insert). Further reduction of the excitation intensity, leading to even longer excimer lifetimes, was prevented by signal to noise ratio considerations. The spectrum recorded under the low-intensity conditions is shown in Figure 1c. Lacking the steep rise below 410 nm (the maximum in the visible being shifted to 490 nm), it may be considered to be practically free of any excited monomer absorption (see Figure 1a) and is thus assigned to the pyrene excimer.

It is interesting to establish to what extent the experimental spectrum, presented in Figure 1c, agrees with the available theoretical calculations of the pyrene excimer energy levels. The present approaches to the theory of excimer binding are based on the interaction between molecular exciton and charge resonance states.^{11,12} Azumi, Armstrong, and McGlynn¹³ have carried out configuration interaction calculations assuming that the D_{2h} symmetry of the pyrene monomer is retained by the dimer.¹³ The lowest resulting excimer states are B_{3g}^- , B_{2u}^- , B_{2u}^+ , and B_{3g}^+ . Their energy relative to the unstable A_g ground state has been evaluated as a function of the interplanar distance (D) in the dimer. An effective nuclear charge $Z = 3.18$ has been chosen in the evaluation of AO integrals. Three different computational devices (A, B, C) for evaluation of diagonal terms in the secular equation were em-

ployed, leading to three sets of energy levels for the D_{2h} excimer. However, the calculated results giving for a chosen Z the energy levels as function of D , could not be directly tested by comparison with the observed energy (2.3 eV) of the $A_g \leftarrow B_{3g}^-$ fluorescent transition. This is due to the lack of independent information concerning the equilibrium distance, D . For each of the three computational methods, a different D value in the 3–4 Å range is required in order to obtain agreement between calculations and experiment. A more critical test of the theoretical calculations can now be carried out by means of the spectrum in Figure 1c showing, within the 370–1000-nm (1.2–3.2 eV) range of our experiments, a single excimer band with onset around 2.2 eV. The computational method A yields agreement with the 2.3 eV onset of the $A_g \leftarrow B_{3g}^-$ fluorescence at $D = 3.2$ Å. The two symmetry-allowed transitions in absorption, $B_{3g}^- \rightarrow B_{2u}^-$ and $B_{3g}^- \rightarrow B_{2u}^+$, are then predicted at 1.3 eV and 2.3 eV, respectively. Assuming an oscillator strength of the same order of magnitude for the two transitions, then our failure to observe any additional excimer band in the 600–1000-nm range means that the experimental data are not in full agreement with the predictions of method A. Method C yields agreement with fluorescence at $D = 3.6$ Å. The two allowed absorption transitions at this interplanar value are predicted at 0.4 eV and 1.5 eV. Neither agrees with the observed value at 2.2 eV. Turning finally to method B, one finds that at $D = 3.8$ Å, calculations predict 2.3 eV for the $A_g \leftarrow B_{3g}^-$ fluorescence and 2.1 eV for the $B_{3g}^- \rightarrow B_{2u}^+$ absorption, in agreement with experiment. The low-energy absorption $B_{3g}^- \rightarrow B_{2u}^-$ is predicted at 0.5 eV which is far beyond the limit of our detection range. It may therefore be concluded that the combined excimer absorption and emission data favor the computational mode B and the interplanar value of 3.8 Å. It should, however, be recalled that such conclusions may be altered by allowing for excimer structures which are less symmetrical than the D_{2h} sandwich configuration.^{14,15}

(10) D. S. Kliger and A. C. Albrecht, *J. Chem. Phys.*, **50**, 4109 (1969).

(11) T. Azumi and S. P. McGlynn, *ibid.*, **41**, 3131 (1964).

(12) J. N. Murrell and J. Tanaka, *Mol. Phys.*, **7**, 363 (1964).

(13) (a) T. Azumi, A. T. Armstrong, and S. P. McGlynn, *J. Chem. Phys.*, **41**, 3839 (1964); (b) S. P. McGlynn, A. T. Armstrong, and T. Azumi in "Modern Quantum Chemistry," O. Sinanoglu, Ed., Academic Press, Inc., New York, N. Y., 1965, p 203.

(14) T. Azumi and S. P. McGlynn, *J. Chem. Phys.*, **42**, 1675 (1965).

(15) T. Azumi and H. Azumi, *Bull. Chem. Soc. Jap.*, **39**, 1829, 2317 (1966).

DEPARTMENT OF
PHYSICAL CHEMISTRY
THE HEBREW UNIVERSITY
JERUSALEM, ISRAEL

CHMOUEL R. GOLDSCHMIDT
MICHAEL OTTOLENGHI

RECEIVED JANUARY 26, 1970